



AFRL-PR-WP-TR-2006-2076

**SCIENTIFIC PRESENTATIONS ON
SUPERCONDUCTIVITY FROM 2002-2005**

Paul N. Barnes and Lt. Brandon Craig Harrison

Power Generation Branch (AFRL/PRPG)

Power Division

JANUARY 2006

Final Report

Approved for public release; distribution unlimited.

See additional restrictions described on inside pages

STINFO COPY

**AIR FORCE RESEARCH LABORATORY
PROPULSION DIRECTORATE
WRIGHT-PATTERSON AIR FORCE BASE, OH 45433-7251
AIR FORCE MATERIEL COMMAND
UNITED STATES AIR FORCE**

NOTICE

Using Government drawings, specifications, or other data included in this document for any purpose other than Government procurement does not in any way obligate the U.S. Government. The fact that the Government formulated or supplied the drawings, specifications, or other data does not license the holder or any other person or corporation; or convey any rights or permission to manufacture, use, or sell any patented invention that may relate to them.

This report was cleared for public release by the Air Force Research Laboratory Wright Site (AFRL/WS) Public Affairs Office (PAO) and is releasable to the National Technical Information Service (NTIS). It will be available to the general public, including foreign nationals.

PAO Case Number: AFRL/WS-06-0325, 07 Feb 2006

THIS TECHNICAL REPORT IS APPROVED FOR PUBLICATION.

/s/

BRANDON C. HARRISON 2d Lt, USAF
Research Chemist
Power Division, AFRL/PRPG

/s/

C. SCOTT RUBERTUS
Branch Chief
Power Division, AFRL/PRPG

/s/

RICHARD FINGERS
Deputy for Technology
Power Division, AFRL/PRP

This report is published in the interest of scientific and technical information exchange and its publication does not constitute the Government's approval or disapproval of its ideas or findings.

REPORT DOCUMENTATION PAGE				<i>Form Approved</i> OMB No. 0704-0188	
The public reporting burden for this collection of information is estimated to average 1 hour per response, including the time for reviewing instructions, searching existing data sources, gathering and maintaining the data needed, and completing and reviewing the collection of information. Send comments regarding this burden estimate or any other aspect of this collection of information, including suggestions for reducing this burden, to Department of Defense, Washington Headquarters Services, Directorate for Information Operations and Reports (0704-0188), 1215 Jefferson Davis Highway, Suite 1204, Arlington, VA 22202-4302. Respondents should be aware that notwithstanding any other provision of law, no person shall be subject to any penalty for failing to comply with a collection of information if it does not display a currently valid OMB control number. PLEASE DO NOT RETURN YOUR FORM TO THE ABOVE ADDRESS.					
1. REPORT DATE (DD-MM-YY) January 2006		2. REPORT TYPE Final		3. DATES COVERED (From - To) 01 January 2001 – 31 October 2005	
4. TITLE AND SUBTITLE SCIENTIFIC PRESENTATIONS ON SUPERCONDUCTIVITY FROM 2002-2005				5a. CONTRACT NUMBER In-house	
				5b. GRANT NUMBER	
				5c. PROGRAM ELEMENT NUMBER 62203F	
6. AUTHOR(S) Paul N. Barnes and Lt. Brandon Craig Harrison				5d. PROJECT NUMBER 3145	
				5e. TASK NUMBER 32	
				5f. WORK UNIT NUMBER 314532Z9	
7. PERFORMING ORGANIZATION NAME(S) AND ADDRESS(ES) Power Generation Branch (AFRL/PRPG) Power Division Air Force Research Laboratory, Propulsion Directorate Wright-Patterson Air Force Base, OH 45433-7251 Air Force Materiel Command, United States Air Force				8. PERFORMING ORGANIZATION REPORT NUMBER AFRL-PR-WP-TR-2006-2076	
9. SPONSORING/MONITORING AGENCY NAME(S) AND ADDRESS(ES) Air Force Research Laboratory Propulsion Directorate Wright-Patterson Air Force Base, OH 45433-7251 Air Force Materiel Command United States Air Force				10. SPONSORING/MONITORING AGENCY ACRONYM(S) AFRL/PRPG	
				11. SPONSORING/MONITORING AGENCY REPORT NUMBER(S) AFRL-PR-WP-TR-2006-2076	
12. DISTRIBUTION/AVAILABILITY STATEMENT Approved for public release; distribution unlimited.					
13. SUPPLEMENTARY NOTES PAO Case Number: AFRL/WS-06-0325; Clearance Date: 07 Feb 2006. Document contains color.					
14. ABSTRACT <p>This program addresses the basic scientific and engineering issues related to the development of the second-generation high- temperature superconducting (HTS) coated conductor for use in magnet and generator coil windings of power applications relevant to the Air Force (AF).</p> <p>Current work focuses on the development of an ac YBCO-coated conductor and enhancement of the current dc coated conductor. The dc coated conductor development is done as part of an overall AF program that includes industry and academic research facilities. This program is coordinated with the Department of Energy's Coated Conductor Program to ensure integration with no redundancy. Flux pinning in the conductor is a significant focus of the overall coated conductor work to improve in-field critical currents. The ac loss issues as well as stability (and quench protection) ultimately must be considered for study, and work has commenced in this area within the in-house program. In order for the conductor to be ready for projected power generation requirements (for directed energy weapons), the superconductivity group is determining the unique AF requirements of the conductor and investigating ac loss and flux pinning issues.</p>					
15. SUBJECT TERMS YBCO, superconductor, coated conductor, flux pinning, nanoparticles, thin films, high critical current, ac loss, MOD, MOCVD					
16. SECURITY CLASSIFICATION OF:			17. LIMITATION OF ABSTRACT: SAR	18. NUMBER OF PAGES 416	19a. NAME OF RESPONSIBLE PERSON (Monitor) 2d Lt Brandon Craig Harrison 19b. TELEPHONE NUMBER (Include Area Code) N/A
a. REPORT Unclassified	b. ABSTRACT Unclassified	c. THIS PAGE Unclassified			

TABLE OF CONTENTS

Section	Page
Introduction 1.1: Cryogenic Power Research	1
1.1.1 Program Goal	1
1.1.2 Technical Objectives.....	1
1.1.3 Challenges & Approach.....	2
1.1.4 Relevance.....	2
1.1.5 Reports	6
Introduction 1.2: HTS Coated Conductor Development Issues.....	23
1.2.1 HTS Conductor Applications.....	23
1.2.2 Conductor Environment.....	23
1.2.3 Semi-realistic Holy Grail	24
1.2.4 Proprietarily Speaking	24
1.2.5 The Basics	24
1.2.6 Standard Process	25
1.2.7 Fabrication Pathways	26
1.2.8 Substrate.....	26
1.2.9 Buffer – Seed Layer	27
1.2.10 Buffer – Diffusion Barrier	27
1.2.11 Buffer – Cap Layer	28
1.2.12 HTS – YBCO Deposition	28
1.2.13 HTS – AC Loss Issues	28
1.2.14 HTS – AC Loss Issues	29
1.2.15 Passivation	29
1.2.16 Passivation	30
1.2.17 Stabilization	30
1.2.18 Insulation.....	31
1.2.19 The Non-cryogenic Connection.....	31
1.2.20 HTS Conductor	32
1.2.21 Summary – Suggestions.....	32
Chapter 2A: Layered Nanoparticulate Dispersions	33
2a.1 Advantages of $\text{YBa}_2\text{Cu}_3\text{O}_{7-\delta}$ Multilayer (211~2nm/123~10nm)xN Thin Film Architecture for Coated Conductor Applications	33
2a.1.1 Outline.....	33
2a.1.2 Flux Pinning.....	34
2a.1.3 Flux Pinning Theory	34
2a.1.4 Y-211 Advantages.....	34
2a.1.5 Multilayer Particulate Defects.....	35
2a.1.6 ‘Soft’ Flux Pinning.....	36
2a.1.7 Experimental Layers Deposited by PLD.....	36
2a.1.8 Surface Nanoparticles	37
2a.1.9 TEM Planar View	39
2a.1.10 XRD Two-theta.....	40
2a.1.11 T_c by AC Susceptibility.....	41
2a.1.12 T_c Transition.....	41

2a.1.13 Transport Properties	42
2a.1.14 60 K Specific Improvement	42
2a.1.15 Magnetic J_c	43
2a.1.16 Temperature Dependence of J_c	43
2a.1.17 Surface Smoothness	44
2a.1.18 Surface Defect Particulates	45
2a.1.19 Multilayer on RABIT's Substrates.....	48
2a.1.20 RABIT's Transport J_{cs}	48
2a.1.21 Conclusions	49
2a.2 Flux Pinning Effects of Y_2O_3 in YBCO Multi-layer ($Y_2O_3 \sim 0.2-1.4nm/Y123 \sim 7-50nm$)xN Thin Films	49
2a.2.1 Objectives.....	49
2a.2.2 Magnetic Flux Pining Theory	49
2a.2.3 Experimental	49
2a.2.4 T_c Reduction vs. Y_2O_3 Thickness (Y123~ 9.9nm/layer).....	50
2a.2.5 χ Measurements.....	50
2a.2.6 Y_2O_3 Layer	51
2a.2.7 Transport and Magnetic J_c Measurements	52
2a.2.8 XRD 2 Theta Scan	55
2a.2.9 Summary	55
2a.3 PLD Parameters of $YBa_2Cu_3O_{7-\delta}$ and Alternating Nanolayers for Flux Pinning	55
2a.3.1 Introduction	55
2a.3.3 Comparison of Conditions	57
2a.3.4 O_2 Pressure Effect On Plume	57
2a.3.5 Deposition Rate vs. O_2 Pressure.....	58
2a.3.6 AC susceptibility data	58
2a.3.7 T_c Onset vs. O_2 Pressure.....	60
2a.3.8 Transport J_c vs. O_2 Pressure.....	60
2a.3.9 Room Temp. Resistivity vs. O_2 Pressure	61
2a.3.10 Surface Effects	61
2a.3.11 Additional Results	62
2a.3.12 Stacked Layer Approach Comparison	62
2a.3.13 70K Specific Improvement	62
2a.3.14 Conclusions	63
2a.3.15 Room Temp. Resistivity vs. J_c	64
2a.4 Nanoparticle Formation from $Y_1Ba_2Cu_3O_{7-\delta}$ for Potential Flux Pinning Mechanism	64
2a.4.1 Introduction	64
2a.4.2 Nanoparticles and Flux Pinning	65
2a.4.3 Comparative PLD System.....	65
2a.4.4 PLD YBCO Characterization.....	67
2a.4.5 Surface Effects	67
2a.4.6 Synthesis of Nanoparticles From YBCO	68
2a.4.7 Experimental Conditions.....	68
2a.4.8 AFM Micrographs.....	69
2a.4.9 TEM Images	69
2a.4.10 Formation Mechanisms	70

2a.4.11 Emission Intensity	70
2a.4.12 Electronic Temperature	71
2a.4.13 Ion/Neutral Ratios	71
2a.4.14 Summary	72
2a.5 FLUX PINNING and PROPERTIES OF (Y,RE)Ba ₂ Cu ₃ O ₇ -Z THIN FILM	
SUPERCONDUCTORS: RE = Eu, Er	72
2a.5.1 Flux Pinning Methods	72
2a.5.2 OUTLINE	73
2a.5.3 Properties of Pinning Agents	73
2a.5.4 J _c (H) Optimization	74
2a.5.5 Pinning Layer Optimization	75
2a.5.6 Ultra-high Resolution SEM.....	75
2a.5.7 SEM Micrographs	76
2a.5.8 Surface Nanoparticles	76
2a.5.9 (211/123)xN on Single Crystals.....	77
2a.5.10 T _c by AC susceptibility.....	77
2a.5.11 J _c by VSM.....	78
2a.5.12 Sm123 multilayers	78
2a.5.13 Sm123 Addition	79
2a.5.14 Transport J _c	79
2a.5.15 Transport J _c	80
2a.5.16 Pinning Force Studies	81
2a.5.17 J _{cm} Ramp Rate Studies.....	81
2a.5.18 U ₀ Pinning Potentials.....	82
2a.5.19 TEM Cross-Sections	83
2a.5.20 CONCLUSIONS	84
2a.5.21 Flux Pinning Questions	84
2a.5.22 Film Surface Defects.....	85
2a.5.23 J _{cm} by VSM.....	85
2a.5.24 TEM Diffraction Patterns.....	86
2a.5.25 TEM X-Section	87
2a.5.26.....	87
2a.5.27 J _{ct} (H,θ)	88
2a.5.28 F _p studies	88
2a.5.29 X-sections.....	89
2a.5.30.....	90
2a.6 Controlled nanoparticulate flux pinning structures in YBCO.....	91
2a.6.1 Magnetic Flux Pinning	91
2a.6.2 Pinning by Nanoparticulates	91
2a.6.3 Experimental	92
2a.6.4 Critical Transition Temperature	92
2a.6.5 X-Ray Diffraction	92
2a.6.7 Transport J _c Comparison	94
2a.6.8 Micrographs of Nanoparticles.....	95
2a.6.9 TEM of CeO ₂ Layered Structure.....	95
2a.6.10 Y ₂ O ₃ and CeO ₂ Nano-inclusions.....	96

2a.6.11 Y2O3 Nanoparticulate Performance	96
2a.6.12 CeO2 Nanoparticulate Performance	97
2a.6.13 Properties of Pinning Agents	98
2a.6.14 High Resolution Planar SEM	98
2a.6.15 J_{cm} Comparison by VSM	99
2a.6.16 Special Considerations	100
2a.6.17 Rare Earth Pinning Nd-doped YBCO Films	101
2a.6.18 Minute CeO2 Doping (0.1%)	102
2a.6.19 Conclusions	103
2a.7 Controlled nanoparticulate flux pinning structures in YBCO	103
2a.7.1 Outline	103
2a.7.2 (Insulator/123)xN Flux Pinning	103
2a.7.3 Properties of Pinning Agents	104
2a.7.4 Film Surface Defects	105
2a.7.5 Experimental	105
2a.7.6 TEM X-Section	106
2a.7.7 TEM Cross-Sections	106
2a.7.8 TEM Cross-Sections	106
2a.7.9 TEM – Planar View	107
2a.7.10 Surface Nanoparticles	107
2a.7.11 Surface Smoothness	108
2a.7.12 X-Ray Diffraction	108
2a.7.13 TEM Diffraction Patterns	109
2a.7.14 T_c Transition	110
2a.7.16 Transport J_c s	111
2a.7.17 Temperature Dependence of J_c	111
2a.7.18 Scaling Up: Multilayer on RABiTs™	112
2a.7.19 Multilayer on RABIT's Ni	112
2a.7.20 Multilayer on RABiTs™ Substrates	113
2a.7.21 J_c Comparison	113
2a.7.22 Increased Film Thickness	114
2a.7.23 J_c vs Layer Thickness	114
2a.7.24 SUMMARY	115
2a.8 Increased Flux-Pinning of YBa ₂ Cu ₃ O _{7-δ} Thin Films by Addition of Y ₂ BaCuO ₅ Nano- dimensional Multilayers	115
2a.8.1 Flux Pinning Theory	115
2a.8.2 Y-211 Advantages	116
2a.8.3 Transport J_c vs. Y(3d5/2) FWHM	116
2a.8.4 T_c FWHM " χ " vs. Y(3d5/2) FWHM	117
2a.8.5 T_c vs. Y(3d5/2) FWHM	117
2a.8.6 J_c vs. Cu(2p)/Ba(3d) Intensity Ratio	117
2a.8.7 T_c FWHM " χ " vs. Cu(2p)/Ba(3d) Intensity Ratio	118
2a.8.8 T_c vs. Cu(2p)/Ba(3d) Intensity Ratio	118
2a.8.9 Zr Diffusion Issue	119
2a.8.10 Summary	119
2a.8.11 Stacked Layer Approach Comparison	120

2a.8.12 T_c	121
2a.8.13 Architecture for Pinning.....	121
2a.8.14 Varying Y123 Thickness.....	122
2a.8.15 60K Specific Improvement	122
2a.8.16 70 K Specific Improvement	123
2a.8.17 Stacked Layer Properties.....	123
2a.8.18 Summary	124
Chapter 2B: Randomized Non-Layered Nanoparticulate Dispersions	125
2b.1 Novel method of introducing particulate pinning centers in $YBa_2Cu_3O_{7-x}$ films during pulsed laser deposition.....	126
2b.1.1 Introduction.....	126
2b.1.2 Experimental.....	126
2b.1.3 PLD Target.....	127
2b.1.4 AC Susceptibility Curves.....	127
2b.1.5 AFM Data	128
2b.1.6 VSM Data	129
2b.1.7 Transport Current Data	132
2b.1.8 J_c Angular Dependence.....	133
2b.1.9 High Resolution SEM.....	133
2b.1.10 Focused Ion Beam Cross Sectional SEM	134
2b.1.11 Conclusions.....	134
2b.2 Studies on Flux Pinning Properties of $YBa_2Cu_3O_{7-\delta}$ Thin Films with Nano Particulate Dispersions.....	135
2b.2.1 Experimental	135
2b.2.2 Gas Phase nano particulate dispersion.....	135
2b.2.3 Ca Doped 211 nano particulate dispersion on Bi-crystals	135
2b.2.4 Transition Temperature data	136
2b.2.5 J_c vs Bi-crystal angle.....	136
2b.2.6 Y211 vs Ca5% Y211	137
2b.2.7 X-TEM OF Y123/YCa5%211 multilayers	137
2b.2.8 Surface of Y123/(Y,Ca)211multilayers	139
2b.2.9 Comparison of $Y_2O_3/Y211/Y123$ (PPMS DATA)	141
2b.2.10 Y211 vs Ca5% Y211	141
2b.2.11 AC Susceptibility of $Y_{1.8}Ca_{0.2}BaCuO_5$ film on STO substrate	142
2b.2.12 Summary	142
2b.2.13 Future scope of this work.....	143
2b.3 Studies on flux pinning properties of $Y_{2-x}Ca_xBaCuO_5$ nano-particulates in $YBa_2Cu_3O_{7-x}$ coated conductors.....	143
2b.3.1 Ca doping in Y123 films.....	143
2b.3.2 Experimental	144
2b.3.3 XRD Pattern of Y123 film with Ca 5% doped Y211 nano-particles.....	144
2b.3.4 T_c Comparison of Y123 films with and without $Y_{2-x}Ca_xBaCuO_5$ ($x = 0, 0.1$ and 0.2) nano-particulates	145
2b.3.5 XRD of $Y_{1.9}Ca_{0.1}BaCuO_5$ film deposited on $LaAlO_3(100)$ substrate	146
2b.3.6 XRD of 10 % Ca doped Y211 film deposited on $LaAlO_3(100)$ substrate	146
2b.3.7 AC Susceptibility of the 10% Ca doped Y211 film deposited on LAO substrate ...	146

2b.3.8 Raman Spectrum of the 10% Ca doped Y211 film deposited on LaAlO ₃ (100) substrate	147
2b.3.9 Cross Sectional Transmission Electron Microscope image (prepared using FIB method) of Ca 10% doped Y211 film.....	148
2b.3.10 Conclusions.....	148
2b.4 Fundamental studies of magnetic flux pinning mechanisms	149
2b.4.1 Pinning by Ca Doped Y2BaCuO ₅ Nanoparticles.....	149
2b.4.2 Fp of 5% & 10% Ca-doped Y211 Nanoparticles.....	150
2b.4.3 Minute Additions of Tb, Ce, Pr Dopants in Y1-xRExBa ₂ Cu ₃ O _{7-z}	151
2b.4.4 Ce-Doped YBCO Films.....	151
2b.4.5 Pr-Doped YBCO Films.....	152
2b.4.6 Tb-Doped YBCO Films.....	153
2b.4.7 Grooved Substrate for Filamentary YBCO.....	154
2b.4.8 Filamentary Current Sharing.....	155
2b.4.9 Summary	156
Chapter 2C: Rare Earth Substitutions	157
2c.1 Characterization of Nd Doped YBa ₂ Cu ₃ O _{7-x} films	157
2c.1.1 Abstract	157
2c.1.2 Objectives.....	157
2c.1.3 Theory	158
2c.1.4 Experimental (Powder Processing)	158
2c.1.5 Experimental (PLD)	158
2c.1.6 Measurements*	159
2c.1.7 Results	159
2c.1.8 Transition temperature of the bulk superconducting volume fraction	160
2c.1.9 Maximum critical current density estimated from M-H loops.....	160
2c.1.10 Normalized (J_c/J_{c-max}) for Ba = 2.0 and varying Nd content	161
2c.1.11 Conclusions	161
2c.2 Tb and Ce Doped YBa ₂ Cu ₃ O _{7-x} Films Processed by Pulsed Laser Deposition	162
2c.2.1 Objectives.....	162
2c.2.3 Experimental – PLD.....	162
2c.2.4 Magnetic J_c 's of Tb doped Y-123 at 77K	163
2c.2.5 Magnetic J_c 's of Tb doped Y-123 at 65K	164
2c.2.6 Summary of (Y,Tb)-123 Films	165
2c.2.7 Magnetic J_c 's of Ce doped Y-123 at 77K	166
2c.2.8 Magnetic J_c 's of Ce doped Y-123 at 65K	167
2c.2.9 Summary of (Y,Ce)-123 Films	168
2c.2.10 Conclusions	168
2c.3 Nd doped YBa ₂ Cu ₃ O _{7-x} Films Deposited by Pulsed Laser Ablation	169
2c.3.1 Introduction	169
2c.3.2 Experimental	170
2c.3.3 AC susceptibility of Nd _{0.2} Y _{0.8} Ba ₂ Cu ₃ O _{7-x} films	170
2c.3.4 T_c comparison between different composition films (AC susceptibility curves)	171
2c.3.5 XPS data summary on films grown using Nd _{0.6} Y _{0.4} Ba ₂ Cu ₃ O _{7-x} target.....	172
2c.3.6 Raman Spectra	172
2c.3.7 Scanning electron micrograph of a Nd _{0.4} Y _{0.6} Ba ₂ Cu ₃ O _{7-x} film on LAO substrate....	174

2c.3.8 X-ray diffraction data on a Nd doped YBCO film.....	175
2c.3.9 Transport current measurement on $\text{Nd}_{0.4}\text{Y}_{0.6}\text{Ba}_2\text{Cu}_3\text{O}_{7-x}$ film	176
2c.3.10 Magnetization J_c data of an $\text{Nd}_{0.2}\text{Y}_{0.8}\text{Ba}_2\text{Cu}_3\text{O}_{7-x}$ film at different temperatures ...	177
2c.3.11 Conclusions	177
2c.4 Flux Pinning of YBCO with Rare Earth Substitutions	177
2c.4.1 Rare Earth Substitution $(\text{Y,RE})_{1+x}\text{Ba}_{2-x}\text{Cu}_3\text{O}_{7-d}$	178
2c.4.2 Experimental	178
2c.4.3 J_c vs. H_{appl} – Air Anneal Only	178
2c.4.4 J_c Norm. vs. H_{appl} – Air Anneal Only	179
2c.4.6 J_c vs. H_{appl} – 1% O_2 Anneal	180
2c.4.7 J_c Norm. vs. H_{appl} – 1% O_2 Anneal.....	181
2c.4.8 Primary Objective	181
2c.4.9 XRD of $(\text{Y}_{0.5},\text{RE}_{0.5})\text{Ba}_2\text{Cu}_3\text{O}_{7-d}$	182
2c.4.10 XRD of $(\text{Y}_{0.5},\text{RE}_{0.6})\text{Ba}_{1.9}\text{Cu}_3\text{O}_{7-d}$	183
2c.4.11 $J_c/J_{c-\text{max}}$, 65K, $(\text{Y}_{0.5},\text{RE}_{0.5})\text{Ba}_2\text{Cu}_3\text{O}_{7-d}$	183
2c.4.12 $J_c/J_{c-\text{max}}$, 65K, $(\text{Y}_{0.5},\text{RE}_{0.6})\text{Ba}_{1.9}\text{Cu}_3\text{O}_{7-d}$	184
2c.4.13 J_c vs. Ionic Radius	184
2c.4.14 Measurement Technique	185
2c.4.15 AC Susceptibility Data - χ'	185
2c.4.16 AC Susceptibility Data - χ''	185
2c.4.17 ΔT of AC Susceptibility Data	187
2c.4.18 Critical Transition Temperature	187
2c.4.19 χ'' Peak to Peak Comparison	188
2c.4.20 Results	188
2c.4.21 χ'' Peak to Peak.....	189
2c.4.22 Results	190
2c.4.23 Conclusions	190
2c.5 Minute RE Doping for YBCO flux pinning.....	191
2c.5.1 $(\text{Y}_{1-x}\text{RE}_x)\text{Ba}_2\text{Cu}_3\text{O}_{7-z}$	191
2c.5.2 $(\text{Y}_{1-x}\text{RE}_x)\text{Ba}_2\text{Cu}_3\text{O}_{7-z}$	191
2c.5.3 Experimental	191
2c.5.4 Tb-doped, 77 K	192
2c.5.5 Tb-doped, 65 K	192
2c.5.7 Ce-doped, 65 K	193
2c.5.8 Nanoparticle Pinning.....	194
2c.5.9 Nanoparticulate Pinning.....	194
2c.5.10 Y_2O_3 Nanoparticles.....	195
2c.5.11 Defect Propagation.....	195
2c.5.12 Ouch!.....	196
2c.5.13 Pinning Potential	196
2c.5.14 Nanoparticle Pinning.....	197
2c.5.15 Summary	198
2c.6 Sm and Nd Substitutions in YBCO Films Produced Through Metal Organic Deposition	198
2c.6.1	198
2c.6.2 Sample Compositions.....	199

2c.6.3 X-Ray Diffraction Data.....	199
2c.6.4 X-ray Diffraction Data	200
2c.6.5 X-ray Diffraction Data	200
2c.6.6 Tc by AC susceptibility.....	201
2c.6.7 Tc by Transport	201
2c.6.8 Jc by VSM.....	202
2c.6.9 Jc by VSM.....	202
2c.6.10 SEM Micrographs	203
2c.6.11 Surface Nanoparticles	204
2c.6.12 Surface Nanoparticles	204
2c.6.13 Nanoparticle Comparison.....	205
2c.6.14 CONCLUSIONS.....	205
2c.7 Properties of $(Y_{1-x}RE_x)_{1+y}Ba_{2-y}Cu_3O_{7-z}$ Bulk Superconductors for Flux Pinning	206
2c.7.1 Objectives.....	206
2c.7.2 THEORY.....	206
2c.7.3 EXPERIMENTAL	206
2c.7.4 EXPERIMENTAL	207
2c.7.5 EXPERIMENTAL	207
2c.7.6 EXPERIMENTAL	208
2c.7.7 MEASUREMENTS	208
2c.7.8.....	209
2c.7.9.....	209
2c.7.10.....	210
2c.7.11.....	210
2c.7.12.....	211
2c.7.13.....	211
2c.7.14.....	212
2c.7.15.....	212
2c.7.16.....	213
2c.7.17 RESULTS	213
2c.7.18 CONCLUSIONS.....	213
2c.7.19 COMMENTS	213
Chapter 3: AC Loss.....	214
3.1 Striated YBCO	214
3.1.1 Introduction.....	214
3.1.2 Striated YBCO-VSM.....	214
3.1.3 Striated YBCO-Resistive Barriers	215
3.1.4 Striated YBCO-Techniques	215
3.1.5 Low Loss Substrates	216
3.1.6 Low Loss Substrates-Non-magnetic	216
3.1.7 Coil Testing.....	216
3.1.8 AC Loss Minimization.....	216
3.1.9 Susceptibility Data	218
3.1.10 Hysteretic Loss.....	219
3.1.11 Loss Reduction.....	219
3.1.12 Effective Filament Width.....	220

3.1.13 Validity of Hysteretic Loss Equation.....	221
3.1.14 Hysteric Loss Normalized to Width	221
3.1.15 Effect of ablation on YBCO	222
3.1.16 Conclusions.....	223
3.2 Magnetization losses in multiply connected coated superconductors	224
3.2.1 Motivation for introduction of multiply connected coated superconductors	224
3.2.2 Objectives	224
3.2.3 Experimental	224
3.2.4 Role of defects	225
3.2.5 Magnetization losses (L2,L3,L4,	226
3.2.6 Control sample	226
3.2.7 20-filament without current sharing.....	227
3.2.8 Fishnet Pattern	228
3.2.9 Brickwall Pattern	229
3.2.10 Summary	231
3.3 Reduction of Coupling Losses in Superconductor – Resistor –Superconductor (Hybrid)	
Wires	232
3.3.1 Outline.....	232
3.3.2 Sweep rate dependence of power loss	232
3.3.3 Specific Loss	233
3.3.4 Coupling Loss	233
3.3.5 Break-even sweep rate and twist pitch.....	234
3.3.6 Copper wire vs superconductor	234
3.3.7 Armature coil	234
3.3.8 Hyperconductor - superconductor hybrid	235
3.3.9 Goals	235
3.3.10 Superconductor Parameters	236
3.3.11 Hybrid conductors.....	236
3.3.12 Toy Model.....	237
3.3.13 Conjugate conductors.....	237
3.3.14 Power Losses	238
3.3.15 Conclusions.....	240
3.4 AC losses in multifilament coated conductors; Hybrid conductor option	241
3.4.1 Outline.....	241
3.4.2 Reduction of Hysteresis Loss by Striation.....	241
3.4.3 Power Loss	242
3.4.4 Summary	242
3.4.5 Advantages of Hybrid Armature.....	242
3.4.6 Conclusions.....	242
3.5 Properties of Resistive Barriers Produced by Laser Micromachining in Coated	
Superconductors.....	243
3.5.1 Architecture of Coated Superconductors	243
3.5.2 Hysteretic Losses in AC Magnetic Field	244
3.5.3 Hysteretic Losses in AC Magnetic Field	244
3.5.4 Mechanism of Dissipation	245
3.5.5 Origin of Electric Field	246

3.5.6 Magneto-optical images.....	246
3.5.7 Striated Samples.....	246
3.5.8 Post-mortem images.....	247
3.5.9 Barrier resistance	248
3.5.10 Profile of the barrier.....	248
3.6 AC Loss Reduction: AFRL In-house Research	249
3.6.1 Substrate Induced Striations	249
3.6.2 Test Bridges	249
3.6.3 Weakly Linked Filaments	249
3.6.4 Scratched Substrate.....	250
3.6.5 M-H loops at 20K	251
3.6.6 M-H loops at 77K	251
3.6.7 Current Sharing.....	252
3.6.8 SC Weakly Linked Relation	252
3.6.9 Metallic vs. SC Connection	252
3.6.10 Conclusions.....	253
3.7 Filamentary YBCO Coated Conductors	254
3.7.1 AC-Tolerant YBCO Conductor	254
3.7.2 Substrate Induced Striations	254
3.7.3 Metallic vs. SC Connection	255
3.7.4 Filamentary Samples.....	256
3.7.5 List of measured samples.....	257
3.7.6 Q_m vs. $m_0 H_m$	258
3.7.7 Filamentary Bridging.....	260
3.7.8 I-V Curves for Filaments	260
3.7.9 Summary	261
3.7.10 AC Losses	261
3.7.11 Estimated AC Losses	262
3.8 The Integration of YBCO Coated Conductors into Magnets and Rotating Machinery....	264
3.8.1 Outline.....	264
3.8.2 DC application of YBCO coated conductors.....	264
3.8.3 Double pancake field coil; YBCO coated conductor.....	264
3.8.4 Double pancake field coil; YBCO coated conductor.....	265
3.8.5 Double pancake field coil; YBCO coated conductor.....	265
3.8.6 Double pancake field coil; YBCO coated conductor.....	266
3.8.7 Reduction of ac losses in YBCO conductors	266
3.8.8 Two types of twist.....	267
3.8.9 Race-track pattern (made by laser ablation.....	267
3.8.10 Patterned substrate (made by photolithography)	268
3.8.11 Making of twisted conductor	268
3.8.12 Demonstration model.....	269
3.8.13 Layered coil	269
3.8.14 Layered coil	270
3.8.15 Layered coil	270
3.8.16 Layered coil	270
3.8.17 "Transformer"?	271

3.8.18 Armature winding	271
3.8.19 Gramme ring	271
3.8.20 Diamond winding.....	272
3.8.21 Diamond winding.....	272
3.8.22 Diamond winding.....	273
3.8.23 Sheep propulsion.....	273
3.8.24 Diamond winding.....	274
3.8.25 Summary	274
3.8.26 Double pancake field coil: 1 st and 2 nd generation hybrid.....	274
Chapter 4: XPS Study of YBCO Coated Conductors	275
4.1 Chemical Depth Profiling by XPS of YBCO Coated Conductor	275
4.1.1 Introduction.....	275
4.1.2 XPS Depth Profiling	276
4.1.3 Sample Fabrication	276
4.1.4 Surface of Conductor	276
4.1.5 YBCO Layer	277
4.1.6 Yttrium Peaks.....	278
4.1.7 YBCO Near Buffer Layer.....	280
4.1.8 Zirconium Presence	280
4.1.9 Possible Diffusion.....	280
4.1.10 Conclusions.....	281
4.2 Correlation Between the Y(3d) XPS Peak Shape of $Y_1Ba_2Cu_3O_{7-x}$ and Film Quality: XPS Depth Profiling Comparison	282
4.2.1 Introduction.....	282
4.2.2 Y(3d) Peak Comparison.....	282
4.2.3 Transport J_c vs. Y(3d _{5/2}) FWHM	283
4.2.4 T_c FWHM χ'' vs. Y(3d _{5/2}) FWHM	284
4.2.5 T_c vs. Y(3d _{5/2}) FWHM.....	285
4.2.6 J_c vs. Cu(2p)/Ba(3d) Intensity Ratio	286
4.2.7 T_c FWHM χ'' vs. Cu(2p)/Ba(3d) Intensity Ratio	287
4.2.8 T_c vs. Cu(2p)/Ba(3d) Intensity Ratio	288
4.2.9 Zr Diffusion Issue	289
4.2.10 Summary	290
4.3 XPS Depth Profiling Comparison #2.....	292
4.3.1 Sample Preparation	292
4.3.2 Sputtering of Surface	292
4.3.3 Parameters vs. Y(3d _{5/2}) FWHM	293
4.3.4 Comparison with Y(3d _{3/2}) FWHM	293
4.3.5 Cu(2p _{3/2}) vs. Y(3d _{5/2}) Intensity	294
4.3.6 T_c vs. Y(3d _{5/2}) FWHM.....	293
4.3.7 Transport J_c vs. Y(3d _{5/2}) FWHM	294
4.3.8 T_c FWHM χ'' vs. Y(3d _{5/2}) FWHM	295
4.3.9 Transport J_c vs. Y(3d _{3/2}) FWHM	296
4.3.10 Transport J_c vs. Y(3d _{3/2}) FWHM	297
4.3.11 XPS Depth Profiling	299
4.3.12 Zr Diffusion Issue	300

4.3.13 Summary	300
4.4 Photoelectron Spectroscopy of Superconducting Tapes	301
4.4.1 X-Ray Photoelectron Spectroscopy (XPS)	301
4.4.2 Spectroscopic Peaks Before and After Sputtering	302
4.4.3 Microstructural Study	303
4.4.4 Films grown on Polycrystalline substrates show Zirconium diffusion from the buffer layers into the YBCO layer	304
4.4.5 XPS And Electrical Data For Different Samples	306
4.4.6 The amount of copper present may be related to the grain boundary density in these films	306
4.4.7 Summary	306
Chapter 5: Substrates and Buffer Layers	308
5.1 Biaxially Textured Copper and Copper Alloy Substrates for use in HTS Coated Conductors	308
5.1.1 High Temperature Superconductor Wire Architecture	308
5.1.2 Biaxially Textured Metallic Substrates	309
5.1.3 Copper and Copper Alloy Substrates	309
5.1.4 Experimental	309
5.1.5 Results: Copper Substrate	310
5.1.6 Results: Cu-Fe substrate	313
5.1.7 Mechanical Properties	315
5.1.8 Magnetization Measurements	317
5.1.9 Results: Resistivity Data	317
5.1.10 Results: SEM of Annealed Cu- Fe Alloy Substrates	318
5.1.11 Ni-Cr Buffer Layer	318
5.1.12 Ni-Cr coatings on Cu-Fe Substrates at different temperatures	319
5.1.13 Buffer Layers: Pt coating	321
5.1.14 Pt buffer layers on Textured Cu	322
5.1.15 Buffer Layers: YSZ by Pulsed laser Ablation on Insitu Annealed Copper	323
5.1.16 Conclusions	324
5.2 Textured Copper Metallic Substrates for HTS Coated Conductors	325
5.2.1 Objectives	325
5.2.2 Ni vs. Cu Comparison	325
5.2.3 Approach	325
5.2.4 Starting Material	325
5.2.5 Material Processing	326
5.2.6 Thermomechanical Processing	326
5.2.7 Copper As-Received	327
5.2.8 Copper After Rolling Deformation	328
5.2.9 Copper Rod After Annealing	328
5.2.10 Copper Alloy After Annealing	330
5.2.11 Discussion	331
5.2.12 Conclusions	332
5.3 Studies on YBa_2NbO_6 and $\text{YBa}_2\text{Cu}_{3-x}\text{Nb}_x\text{O}_y$ Buffer Layers	333
5.3.1 Objective	333
5.3.2 Present Work	334

5.3.3 Experimental	334
5.3.4 YBa ₂ Cu _{3-x} Nb _x O _y films deposited at 750 °C.....	334
5.3.5 YBa ₂ Cu _{3-x} Nb _x O _y films deposited at 800 °C.....	335
5.3.6 YBa ₂ Cu _{3-x} Nb _x O _y films deposited at 850° C	336
5.3.7 YBa ₂ Cu ₂ NbO _y films on various substrates	337
5.3.8 YBa ₂ Cu ₂ NbO ₈ on MgO deposited at 850 °C	338
5.3.9 Highly C-axis oriented Y123 on YBCNO/IBADMgO/Inconel.....	339
5.3.10 Texture of YBCNO films.....	339
5.3.11 YBa ₂ NbO ₆ thin films	340
5.3.12 YBNO deposited on IBAD MgO/Inconel.....	341
5.3.13 AC Susceptibility of Y123/YBCNO/INCONEL	342
5.3.14 Transport results of Y-123 films.....	343
5.3.15 AFM micrographs of YBa ₂ Cu _{3-x} Nb _x O _y and analysis.....	345
5.3.16 XPS Studies of YBa ₂ Cu _{3-x} Nb _x O _y (x = 0.25, 0.5, 0.75, 1) thin films	346
5.3.17 Cu-2p binding energy of YBCNO films.....	347
5.3.18 Raman Microscopy Studies	348
5.3.19 Cross sectional TEM of YBa ₂ Cu ₂ NbO ₈ film on STO deposited at 800 °C	351
5.3.20 EDS SPECTRA OF YBCNO FILM.....	352
5.3.21 Stoichiometry of YBa ₂ Cu ₂ NbO _y	352
5.3.22 TEM S.A.D Micrograph of YBa ₂ Cu ₂ NbO _x	353
5.3.23 Summary Notes.....	353
5.4 Growth of oxide and metal buffer layers for coated conductor applications.....	354
5.4.1 BYNO films	354
5.4.2 AC susceptibility results	354
5.4.3 BYNO thickness variation on IMgO	355
5.4.4 Texture Analysis from Sandia National Lab	356
5.4.5 Rocking curve of MgO	356
5.4.6 BYNO(220) Phi-scan.....	357
5.4.7 Sample information and summary	357
5.4.8 FIB cross section- tilted at 45°	358
5.4.9 RBS Analysis of BYNO film.....	359
5.4.10 Cross sectional TEM Image of YBCO/BYNO/IMgO/Hastelloy.....	361
5.4.11 Ag and Ca doped YBCO films	361
5.4.12 Ba ₂ YNbO ₆ film deposited on Textured Ni	361
5.4.13 YBa ₂ NbO ₆ films on RABiTS Cu-alloy.....	362
5.4.14 Micro-Raman Studies of YBNO films	363
5.4.15 SEM images of YBa ₂ NbO ₆ films on Ni substrate	365
5.4.16 Oxidation of RABiTS Cu Substrates	365
5.4.17 IBAD system for coated conductor applications	366
5.4.18 Schematic of the Experiment	367
5.4.19 Substrate Holder.....	368
5.4.20 YSZ Film on Si (6" dia) Substrate	369
5.4.21 Ru film on Si substrate.....	369
5.4.22 Mg Film using ISD	370
5.4.23 Ru Film on Cu substrate	370
5.5 COATED CONDUCTORS ON FLEXIBLE SUBSTRATES	371

5.5.1 Our Team	371
5.5.2 ACKNOWLEDGEMENTS.....	371
5.5.3 Out Line of Talk.....	371
5.5.4 What is the Present Status.....	372
5.5.5 Objective of our Work	372
5.5.6 Why Copper Substrate???	372
5.5.7 IBAD SYSTEM FOR CERAFLEX	373
5.5.8 Schematic of the Experiment	374
5.5.9 IBAD SYSTEM DETAILS	373
5.5.10 Substrate Holder (stationary substrates)	374
5.5.11 Reel to reel	374
5.5.12 Double side coating.....	374
5.5.13 Work Progress on Cera-flex substrates.....	374
5.5.14 EFFORTS ON CERAFLEX	375
5.5.15 IBAD OF Mg Films	375
5.5.17 IBAD Ru Films on Cu substrate	376
5.5.18 Pulsed Laser Deposition Parameters.....	377
5.5.19 Rh films on Bi-axially textured Ni-W alloy deposited at RT	378
5.5.20 Rh films deposited at 700 C.....	378
5.5.21 FIB X-section of Rh/Ni-W.....	379
Appendix.....	380
A.1 References	380

List of Figures

Figure	Page
Figure 1.2.1.1	23
Figure 1.2.2.1	24
Figure 1.2.3.1	25
Figure 1.2.4.1	26
Figure 1.2.5.1	27
Figure 1.2.6.1	27
Figure 1.2.7.1	27
Figure 1.2.8.1	28
Figure 1.2.9.1	28
Figure 1.2.10.1	29
Figure 1.2.11.1	29
Figure 1.2.12.1	30
Figure 1.2.13.1	30
Figure 1.2.14.1	31
Figure 1.2.15.1	31
Figure 2a.1.2.1	34
Figure 2a.1.2.2	34
Figure 2a.1.2.3	34
Figure 2a.1.4.1	35
Figure 2a.1.5.1	35
Figure 2a.1.6.1	36
Figure 2a.1.7.1	36
Figure 2a.1.8.1	37
Figure 2a.1.8.2	37
Figure 2a.1.8.3	37
Figure 2a.1.8.4	38
Figure 2a.1.8.5	38
Figure 2a.1.8.6	38
Figure 2a.1.9.1	39
Figure 2a.1.9.2	39
Figure 2a.1.10.1	40
Figure 2a.1.10.2	40
Figure 2a.1.11.1	41
Figure 2a.1.12.1	41
Figure 2a.1.13.1	42
Figure 2a.1.14.1	42
Figure 2a.1.15.1	43
Figure 2a.1.16.1	43
Figure 2a.1.17.1	44
Figure 2a.1.17.2	45
Figure 2a.1.18.1	46
Figure 2a.1.18.2	47
Figure 2a.1.18.3	47
Figure 2a.1.19.1	48
Figure 2a.1.20.1	48
Figure 2a.2.4.1	50
Figure 2a.2.5.1	50
Figure 2a.2.6.1	51

Figure 2a.2.6.2	51
Figure 2a.2.6.3	51
Figure 2a.2.7.1	52
Figure 2a.2.7.2	52
Figure 2a.2.7.3	53
Figure 2a.2.7.4	53
Figure 2a.2.7.5	54
Figure 2a.2.7.6	54
Figure 2a.2.8.1	55
Figure 2.3.3.1	57
Figure 2a.3.4.1	58
Figure 2a.3.5.1	58
Figure 2a.3.6.1	59
Figure 2a.3.6.2	59
Figure 2.3.7.1	60
Figure 2a.3.8.1	60
Figure 2a.3.9.1	61
Figure 2a.3.10.1	61
Figure 2a.3.12.1	62
Figure 2a.3.12.2	62
Figure 2a.3.13.1	63
Figure 2a.3.15.1	64
Figure 2a.4.3.1	65
Figure 2a.4.3.2	66
Figure 2a.4.4.1	67
Figure 2a.4.5.1	68
Figure 2a.4.7.1	68
Figure 2a.4.8.1	69
Figure 2a.4.9.1	69
Figure 2a.4.11.1	70
Figure 2a.4.12.1	71
Figure 2a.4.13.1	72
Figure 2a.5.3.1	73
Figure 2a.5.4.1	74
Figure 2a.5.5.1	75
Figure 2a.5.6.1	75
Figure 2a.5.6.2	75
Figure 2a.5.6.3	75
Figure 2a.5.6.4	75
Figure 2a.5.6.5	75
Figure 2a.5.6.6	75
Figure 2a.5.7.1	76
Figure 2a.5.7.2	76
Figure 2a.5.7.3	76
Figure 2a.5.7.4	76
Figure 2a.5.8.1	77
Figure 2a.5.8.2	76
Figure 2a.5.9.1	78
Figure 2a.5.9.2	77
Figure 2a.5.10.1	77
Figure 2a.5.11.1	78

Figure 2a.5.11.2	78
Figure 2a.5.12.1	79
Figure 2a.5.12.2	78
Figure 2a.5.11.1	79
Figure 2a.5.12.1	79
Figure 2a.5.13.1	79
Figure 2a.5.14.1	79
Figure 2a.5.15.1	80
Figure 2a.5.16.1	81
Figure 2a.5.17.1a	81
Figure 2a.5.17.1b	82
Figure 2a.5.18.1	82
Figure 2a.5.19.1	83
Figure 2a.5.25.1	85
Figure 2a.5.25.2	85
Figure 2a.5.25.3	85
Figure 2a.5.26.1	85
Figure 2a.5.29.1	86
Figure 2a.5.30.1	87
Figure 2a.5.32.1	88
Figure 2a.5.33.1	88
Figure 2a.5.34.1	89
Figure 2a.5.34.2	89
Figure 2a.5.34.3	89
Figure 2a.5.36.1	90
Figure 2a.6.2.1	91
Figure 2a.6.4.1	92
Figure 2a.6.5.1	93
Figure 2a.6.5.2	93
Figure 2a.6.6.1	93
Figure 2a.6.7.2	94
Figure 2a.6.8.1	95
Figure 2a.6.8.2	95
Figure 2a.6.9.1	95
Figure 2a.6.10.1 and Figure 2a.6.10.3	96
Figure 2a.6.10.2 and Figure 2a.6.10.4	96
Figure 2a.6.11.1	96
Figure 2a.6.11.2	97
Figure 2a.6.12.1 and Figure 2a.6.12.2	97
Figure 2a.6.13.1 and Figure 2a.6.13.2	98
Figure 2a.6.15.1 and Figure 2a.6.15.2	99
Figure 2a.6.17.1	100
Figure 2a.6.19.1	102
Figure 2a.7.2.1 and Figure 2a.7.2.2	103
Figure 2a.7.2.3	104
Table 2a.7.3.1	104
Figure 2a.7.3.1	104
Figure 2a.7.4.1 and Figure 2a.7.4.2 and Figure 2a.7.4.3	105
Figure 2a.7.5.1	105
Figure 2a.7.6.1	106
Figure 2a.7.6.2	106

Figure 2a.7.7.1 and Figure 2a.7.7.2	106
Figure 2a.7.8.1 and Figure 2a.7.8.2	106
Figure 2a.7.9.1	107
Figure 2a.7.10.1 and Figure 2a.7.10.2	107
Figure 2a.7.11.1	108
Figure 2a.7.12.1	108
Figure 2a.7.13.1	109
Figure 2a.7.15.1	110
Figure 2a.7.16.1 and Figure 2a.7.16.2	111
Figure 2a.7.17.1 and Figure 2a.7.17.2	111
Figure 2a.7.18.1 and Figure 2a.7.18.2	112
Figure 2a.7.19.1 and Figure 2a.7.19.2 and Figure 2a.7.19.3.....	112
Figure 2a.7.20.1 and Figure 2a.7.20.2	113
Figure 2a.7.21.1	113
Figure 2a.7.22.1	114
Figure 2a.7.23.1	114
Figure 2a.8.1.1	115
Figure 2a.8.2.1	116
Figure 2a.8.3.1	116
Figure 2a.8.4.1 and Figure 2a.8.4.2	117
Figure 2a.8.5.1	117
Figure 2a.8.6.1	118
Figure 2a.8.7.1 and Figure 2a.8.7.2	118
Figure 2a.8.8.1	119
Figure 2a.8.9.1	119
Figure 2a.8.11.1	120
Figure 2a.8.11.2	120
Figure 2a.8.12.1 and Figure 2a.8.12.2	121
Figure 2a.8.13.1	121
Figure 2a.8.14.1. (Y211/Y123) _n multilayer, total film thickness ~ 0.25 to 0.3 micron, n = 26 to 35, Y211 thickness = 1.1 nm constant.....	122
Figure 2a.8.15.1	122
Figure 2a.8.16.1	123
Figure 2a.8.17.1	124
Figure 2b.1.3.1	127
Figure 2b.1.4.1.....	127
Figure 2b.1.4.2.....	128
Figure 2b.1.5.1	128
Figure 2b.1.5.2.....	129
Figure 2b.1.6.1	129
Figure 2b.1.6.2.....	130
Figure 2b.1.6.3.....	130
Figure 2b.1.6.4.....	131
Figure 2b.1.6.5.....	131
Figure 2b.1.7.1	132
Figure 2b.1.7.2.....	132
Figure 2b.1.8.1	133
Figure 2b.1.9.1	133
Figure 2b.1.10.1	134
Figure 2b.1.10.2.....	134
Figure 2b.2.2.1	135

Figure 2b.2.4.1	136
Figure 2b.2.5.1	136
Figure 2b.2.6.1	137
Figure 2b.2.7.1	137
Figure 2b.2.7.2	138
Figure 2b.2.7.3	138
Figure 2b.2.8.1	139
Figure 2b.2.8.2	139
Figure 2b.2.8.3	140
Figure 2b.2.8.4	140
Figure 2b.2.9.1	141
Figure 2b.2.10.1	141
Figure 2b.2.11.1	142
Figure 2b.3.2.1	144
Figure 2b.3.3.1	144
Figure 2b.3.4.1	145
Figure 2b.3.4.2	145
Figure 2b.3.5.1	146
Figure 2b.3.6.1	146
Figure 2b.3.7.1	147
Figure 2b.3.8.1	147
Figure 2b.3.9.1	148
Figure 2b.4.1.1	149
Figure 2b.4.1.2	150
Figure 2b.4.2.1	150
Figure 2b.4.2.2	151
Figure 2b.4.4.1	152
Figure 2b.4.5.1	153
Figure 2b.4.6.1	154
Figure 2b.4.7.1 and Figure 2b.4.7.2 and Figure 2b.4.6.4	155
Figure 2b.4.6.3	155
Figure 2b.4.8	155
Figure 2c.1.8.1	160
Figure 2c.1.9.1	160
Figure 2c.1.10.1	161
Figure 2c.2.4.1	163
Figure 2c.2.4.2	164
Figure 2c.2.5.1	164
Figure 2c.2.5.2	165
Figure 2c.2.6.1	165
Figure 2c.2.7.1	166
Figure 2c.2.7.2	166
Figure 2c.2.8.1	167
Figure 2c.2.8.2	167
Figure 2c.2.9.1	168
Figure 2c.3.3.1	170
Figure 2c.3.3.2	171
Figure 2c.3.4.1	171
Figure 2c.3.5.1	172
Figure 2c.3.6.1	172
Figure 2c.3.6.2	173

Figure 2c.3.6.3	173
Figure 2c.3.6.4	174
Figure 2c.3.6.5	174
Figure 2c.3.7.1	175
Figure 2c.3.8.1	175
Figure 2c.3.8.2	176
Figure 2c.3.9.1	176
Figure 2c.3.10.1	177
Figure 2.12.3.1	179
Figure 2c.4.4.1	180
Figure 2c.4.6.1	180
Figure 2c.4.7.1	181
Figure 2c.4.8.1	182
Figure 2c.4.9.1	182
Figure 2c.4.10.1	183
Figure 2c.4.11.1	183
Figure 2c.4.12.1	184
Figure 2c.4.13.1	184
Figure 2c.4.15.1	185
Figure 2c.4.16.1	186
Figure 2c.4.17.1	187
Figure 2c.4.18.1	187
Figure 2c.4.19.1	188
Figure 2c.4.21.1	189
Figure 2c.4.21.2	189
Figure 2c.5.4.1	192
Figure 2c.5.5.1	192
Figure 2c.5.6.1	193
Figure 2c.5.7.1	193
Figure 2c.5.8.1	194
Figure 2c.5.9.1 and Figure 2c.5.9.2	195
Figure 2c.5.10.1	195
Figure 2c.5.11.1	196
Figure 2c.5.13.1	197
Figure 2c.6.2.1	199
Figure 2c.6.3.1	199
Figure 2c.6.4.1	200
Figure 2c.6.5.1	200
Figure 2c.6.6.1	201
Figure 2c.6.7.1	201
Figure 2c.6.8.1	202
Figure 2c.6.9.1	202
Figure 2c.6.10.1	203
Figure 2c.6.11.1	204
Figure 2c.6.12.1	204
Figure 2c.6.13.1 and Figure 2c.6.13.2	205
Figure 2c.7.5.1	207
Figure 2c.7.6.1	208
Figure 2c.7.8.1	209
Figure 2c.7.9.1	209
Figure 2c.7.10.1	210

Figure 2c.7.11.1	210
Figure 2c.7.12.1	211
Figure 2c.7.13.1	211
Figure 2c.7.14.1	212
Figure 2c.7.15.1	212
Figure 2c.7.16.1	213
Figure 3.1.8.1	217
Figure 3.1.8.2	217
Figure 3.1.8.3 and Figure 3.1.8.4	217
Figure 3.1.9.1	218
Figure 3.1.9.2	218
Figure 3.1.10.1	219
Figure 3.1.13.1	220
Figure 3.1.12.1	220
Figure 3.1.13.1	221
Figure 3.1.14.1	222
Figure 3.1.15.1	223
Figure 3.2.3.1 and Figure 3.2.3.2	225
Figure 3.2.4.1	225
Figure 3.2.6.1	226
Figure 3.2.7.1	227
Figure 3.2.7.2	227
Figure 3.2.8.1	228
Figure 3.2.8.2	228
Figure 3.2.8.3	229
Figure 3.2.9.1	229
Figure 3.2.9.2	230
Figure 3.2.9.3	230
Figure 3.2.9.4	230
Figure 3.3.2.1	232
Figure 3.3.3.1	233
Figure 3.3.4.1	233
Figure 3.3.6.1	234
Figure 3.3.7.1	234
Figure 3.3.8.1	235
Figure 3.3.13.1	236
Figure 3.3.12.1	237
Figure 3.3.13.1	237
Figure 3.3.14.1	238
Figure 3.3.14.2	238
Figure 3.3.14.3	239
Figure 3.3.14.4	239
Figure 3.3.14.5	240
Figure 3.3.14.6	240
Figure 3.4.2.1	241
Figure 3.5.3.1	243
Figure 3.5.2.1	244
Figure 3.5.3.1	244
Figure 3.5.4.1	245
Figure 3.5.5.1	245
Figure 3.5.6.1	246

Figure 3.5.7.1	246
Figure 3.5.8.1	247
Figure 3.5.8.2	247
Figure 3.5.9.1	248
Figure 3.5.10.1	248
Figure 3.6.2.1	249
Figure 3.6.3.1	250
Figure 3.6.5.1	251
Figure 3.6.6.1	251
Figure 3.7.2.1	255
Figure 3.7.4.2	256
Figure 3.7.4.3	257
Figure 3.7.6.1	258
Figure 3.7.6.2	258
Figure 3.7.6.3	259
Figure 3.7.6.4	259
Figure 3.7.8.1	260
Figure 3.7.8.2	261
Figure 3.7.13.1	262
Figure 3.7.13.2	262
Figure 3.7.13.3	263
Figure 3.8.3.1 and Figure 3.8.3.2	264
Figure 3.8.4.1 and Figure 3.8.4.2	265
Figure 3.8.5.1	265
Figure 3.8.6.1	266
Figure 3.8.7.1	266
Figure 3.8.8.1 and Figure 3.8.8.2	267
Figure 3.8.9.2	267
Figure 3.8.9.1 and Figure 3.8.9.3	267
Figure 3.8.10.1	268
Figure 3.8.11.1 and Figure 3.8.11.2	268
Figure 3.8.12.1 and Figure 3.8.12.2	269
Figure 3.8.13.1 and Figure 3.8.13.2	269
Figure 3.8.14.1 and Figure 3.8.14.2	270
Figure 3.8.17.1 and Figure 3.8.17.2	271
Figure 3.8.19.1 and Figure 3.8.19.2	271
Figure 3.8.20.1	272
Figure 3.8.21.1	272
Figure 3.8.22.1	273
Figure 3.8.23.1 and Figure 3.8.23.2	273
Figure 3.8.24.1	274
Figure 3.8.26.1	274
Figure 4.1.3.1	276
Figure 4.1.4.1	277
Figure 4.1.4.2	277
Figure 4.1.5.2	278
Figure 4.1.6.1	279
Figure 4.1.8.1	280
Figure 4.2.2.1	282
Figure 4.2.3.1	283
Figure 4.2.4.1	284

Figure 4.2.5.1	285
Figure 4.2.6.1	286
Figure 4.2.7.1	287
Figure 4.2.8.1	288
Figure 4.2.9.1	289
Figure 4.3.2.1	291
Figure 4.3.3.1	292
Figure 4.3.4.1	292
Figure 4.3.5.1	293
Figure 4.3.6.1	293
Figure 4.3.7.1	294
Figure 4.3.7.2	295
Figure 4.3.8.1	296
Figure 4.3.8.2	296
Figure 4.3.9.1	297
Figure 4.3.10.1	298
Figure 4.3.11.1	299
Figure 4.3.12.1 and Figure 4.3.12.2	300
Figure 4.4.1.1	301
Figure 4.4.1.2	302
Figure 4.4.3.1	303
Figure 4.4.3.2	303
Figure 4.4.4.1	305
Figure 4.4.5.1	306
Figure 5.1.1.1	308
Figure 5.1.5.1 Two Theta scan of a textured Copper substrate.....	310
Figure 5.1.5.2 (111) PHI scan on a textured Copper substrate. FWHM 4.7°	310
Figure 5.1.5.3 PSI scan on (111) peak of a textured copper substrate.	311
FWHM 6.2 °	311
Figure 5.1.5.4 (200) Omega scan parallel to rolling FWHM 6.3 °	311
Figure 5.1.5.2	312
Figure 5.1.5.3	312
Figure 5.1.6.2 (111) Phi scan on a textured Cu-Fe alloy substrate FWHM is 5.1 °	313
Figure 5.1.6.1 Two Theta scan of a textured Cu-Fe substrate	313
Figure 5.1.6.3 PSI scan on (111) peak of textured Cu-Fe substrate. Average FWHM 6.8 °	314
Figure 5.1.6.4 (200) Omega Scan. Parallel to rolling, FWHM=6.2o.....	314
Figure 5.1.6.2	315
Figure 5.1.7.1 and Figure 5.1.7.2	315
Figure 5.1.7.4.....	316
Figure 5.1.7.3	316
Figure 5.1.8.1	317
Figure 5.1.8.2	317
Figure 5.1.9.1	317
Figure 5.1.10.1	318
Figure 5.1.12.1	319
Figure 5.1.12.2	319
Figure 5.1.22.3	320
Figure 5.1.12.5	321
Figure 5.1.13.1	321
Figure 5.1.14.1	322

Figure 5.1.14.2	323
Figure 5.115.1	324
Figure 5.2.3.1	325
Figure 5.2.7.1	327
Figure 5.2.9.1	328
Figure 5.2.9.2	329
Figure 5.2.9.3	329
Figure 5.2.9.4	330
Figure 5.2.10.1	330
Figure 5.2.10.2	331
Figure 5.2.10.3	331
Figure 5.3.1.1	333
Figure 5.3.3.1	334
Figure 5.3.4.1	335
Figure 5.3.5.1	336
Figure 5.3.6.1	337
Figure 5.3.7.1	338
Figure 5.3.8.1	338
Figure 5.3.9.1	339
Figure 5.3.10.1	339
Figure 5.3.10.2	340
Figure 5.3.10.3	340
Figure 5.3.11.1	341
Figure 5.3.12.1	341
Figure 5.3.12.2	341
Figure 5.3.13.1	342
Figure 5.3.13.2	342
Figure 5.3.13.4	343
Figure 5.3.14.1	343
Figure 5.3.14.2	344
Figure 5.3.15.1	345
Figure 5.3.15.2 and Figure 5.3.15.3	345
Figure 5.3.16.1	346
Figure 5.3.16.2	347
Figure 5.3.17.1	348
Figure 5.3.18.1	349
Figure 5.3.18.2	350
Figure 5.3.19.3	351
Figure 5.3.19.1	351
Figure 5.3.19.2	351
Figure 5.3.20.1	352
Figure 5.3.21.1	352
Figure 5.3.22.1	353
Figure 5.4.2.1	354
Figure 5.4.3.1	355
Figure 5.4.4.1	356
Figure 5.4.5.1	356
Figure 5.4.6.1	357
Figure 5.4.7.1	357
Figure 5.4.8.1	358
Figure 5.4.8.2	358

Figure 5.4.8.3	359
Figure 5.4.9.1	359
Figure 5.4.9.2	360
Figure 5.4.9.3	360
Figure 5.4.10.1	361
Figure 5.4.12.1	362
Figure 5.4.12.2	362
Figure 5.4.13.1	363
Figure 5.4.14.1	364
Figure 5.4.15.1	365
Figure 5.4.16.1	365
Figure 5.4.17.1	366
Figure 5.4.17.2	366
Figure 5.4.18.1	367
Figure 5.4.19.1	368
Figure 5.4.20.1	369
Figure 5.4.21.1	369
Figure 5.4.22.1	370
Figure 5.4.23.1	370
Figure 5.5.4.1	372
Figure 5.5.5.1	372
Figure 5.5.7.1	373
Figure 5.5.8.1	373
Figure 5.5.10.1	374
Figure 5.5.11.1	374
Figure 5.5.12.1	374
Figure 5.5.15.1 and Figure 5.5.15.2	375
Figure 5.5.15.3	375
Figure 5.5.16.1 and Figure 5.5.16.2	376
Figure 5.5.17.1	376
Figure 5.5.17.2	377
Figure 5.5.18.1	377
Figure 5.5.19.1	378
Figure 5.5.20.1	378
Figure 5.5.20.2	378
Figure 5.5.21.1 and Figure 5.5.21.2	379

Introduction 1.1: Cryogenic Power Research

Investigators: Dr Paul N. Barnes, Dr. Timothy Haugan

Start and Completion Date: 1 AUG 2002 - 15 Jun 2005

1.1.1 Program Goal

This program addresses the basic scientific and engineering issues related to the development of the second generation high temperature superconducting (HTS) coated conductor for use in magnet and generator coil windings of power applications relevant to the Air Force.

1.1.2 Technical Objectives

Previously, YBCO has been determined to best meet the needs of the AF in the current circumstances. This determination was based on the overall capabilities of the conductor as well as its ability to be manufactured in a usable form. Some of the criteria included critical current density (J_c) $> 10^5$ A/cm², engineering critical current density (J_e) $> 10^4$ A/cm², magnetic fields of 0-4 T, operating temperatures of 65-80 K, potential long length production, commercial product viability, etc.

The current objectives of the in-house program are:

- Develop properties of the YBCO superconductor for optimal performance as a coated conductor in HTS generators and magnets (category FLUX PINNING):
 - In-field performance (up to 5 T)
 - High temperatures (65-80 K)
- Determine and minimize ac losses experienced by the conductor in a high power generator with consideration of stability issues(category AC LOSS):
 - Analytical analysis of expected ac losses
 - Material properties and conductor configurations
- Understand and improved HTS epitaxial templates along with conductor processing and architectures (category YBCO COATED CONDUCTOR):
- Work with other programs world-wide on issues that support HTS wire development and prove beneficial for future AF needs to include (category COLLABORATIONS):
 - Substrate
 - Buffer layers
 - YBCO
 - Processing issues

The inclusion of the category COLLABORATIONS is not meant to imply that the other three categories will not involve collaborations. It includes efforts both initiated by us and initiated by the collaborative group that have been deemed important to support HTS conductor development but do not fall into the other three categories.

1.1.3 Challenges & Approach

Current work focuses on the development of an ac YBCO coated conductor and enhancement of the current dc coated conductor. The dc coated conductor development is done as part of an overall AF program that includes industry and academic research facilities. This program is coordinated with the Department of Energy's Coated Conductor Program to ensure integration with no redundancy. Flux pinning in the conductor will be a significant focus of the overall coated conductor work to improve in-field critical currents. AC loss issues as well as stability (and quench protection) must be ultimately considered for study and work has commenced in this area within the in-house program. In order for the conductor to be ready for projected power generation requirements (for directed energy weapons), the superconductivity group is determining the unique, AF requirements of the conductor and investigating ac loss and flux pinning issues. Having determined the impact of ac losses, the effectiveness of ac-tolerant YBCO conductor must be addressed relevant to a viable manufacturing process for producing it in long lengths, since reel to reel YBCO coated conductor development has been established in industry (via Air Force Dual Use Science & Technology Programs and DOE Industrial Programs).

1.1.4 Relevance

A variety of future military systems will depend on high electrical power input at the Multimegawatt level. As is typical for airborne, seaborne, and ground-mobile platforms, the power generation subsystems must often be packaged in a limited space and within strict weight limits. Conventional generators that provide high electrical power have been developed and optimized over the past several decades, but these generators cannot provide the multimegawatt levels of power necessary for advanced mobile or airborne military systems without paying a significant penalty in size, weight, and efficiency. Efficiency, thermal management, and fatigue life are typically sacrificed as conventional generators are given high rotational speeds to reduce their size and weight while maintaining the high power output. Thermal management dictates that as the required power increases to megawatt levels, simple scaling of conventional airborne power generators is not a plausible solution.

The development of more efficient airborne generators is of critical importance. While the systems that use this power are being intensely developed, the greater power needed to make these systems function is often assumed. Only proactive efforts on novel power systems such as HTS generators will address these concerns. Several fundamental roadblocks prevented widespread incorporation of LTS-based generators. HTS conductors can allow these limits to be circumvented, however, HTS conductors may have their own set of difficulties to be addressed. The following is an outline of the application niche for near-term military and governmental use of such generators, which may occur before large-scale commercial uses are feasible.

Perhaps the earliest use for the superconducting technologies will be non-lethal weapons. Future military applications will likely broaden the range of situations in which military force can be used as a first strike option with non-lethal technologies. One specific technology being developed for such situations is Active Denial Technology (ADT). ADT is a non-lethal directed energy weapon (DEW) which employs high power electromagnetic radiation. To make this system airborne will require the benefits of superconducting generators. Also, the required gyrotron magnet is made with LTS. If this magnet could be replaced with HTS conductor operating at 60–77 K (as opposed to 4.2 K) it would result in a significant reduction in weight, size, and electrical power requirements of the associated cryocooler.

There are other applications for the US Air Force, Navy, and Army requiring large amounts of power. The US Air Force is also considering airborne DEW such as the Airborne Tactical Laser (ATL). Even chemically driven directed energy weapons such as the ATL will require greater electrical power to pump the chemicals through the laser. Similarly, the Army has a technological need for compact, lightweight power systems for DEW applications on mobile platforms such as Ground Tactical Lasers. Development is also ongoing with both homopolar and synchronous superconducting motors to drive the US Navy's future all-electric ship. HTS wire technology can be used in many of the system components for these military applications such as motors, power generators, transformers, power converters/inductors, primary power cabling, and high field magnets.

Technologies such as electromagnetic launch or railguns require pulsed power, but often overlooked is the fact that the required average power of these applications may extend into the megawatt range. This would require a continuous electrical power generation system to charge the energy storage system, whether capacitor banks, pulse forming networks, etc. as an alternative to pulsed alternators. Command and control operations are also demanding more power such as with the E-10A Multi-Mission Command and Control aircraft (MC2A). The MC2A would be capable of serving as an intelligence, surveillance and reconnaissance platform with a broader range of capabilities in a single package.

Another potential application is in the arena of Homeland Defense. It is clear that commercial airports, power utility generation, and power distribution grids are vulnerable to terrorist attack. Solutions to counter these possible attacks would make use of small Multimegawatt turbogenerators which can be permanently located or rapidly deployed to these areas in the event of an attack. In the case of airports, a highly mobile superconducting power generation system could be employed to power advanced protective measures. For the transmission grid, these mobile high power generators can be deployed to critical nodes if power is disrupted. The system could simply be an aeroderivative turboshaft engine coupled to a HTS generator to produce the required megawatts of power; the system could be contained in a trailer for transport to its needed location.

Commercial Uses. Establishing industrial manufacturing capability for the YBCO conductor leads to commercialization in electric power applications such as transformers, transmission cables, motors, fault current limiters, and generators. The overall advantages of using HTS conductor are: significant reduction in size and weight with the associated increase in power density, significant reduction in energy usage due to low electrical losses, noise reduction in HTS machinery and transformers.

HTS Transmission Cables

An HTS power cable is a wire-based transmission line that carries large amounts of electrical current. Liquid nitrogen flows through the cable cooling the HTS wire to the zero resistance state. HTS transmission cables would be used for power transmission and distribution in urban areas throughout the United States and the world. The benefits include: provides capability to meet increasing power demands in urban areas using the existing duct systems, eliminates need to acquire new rights of way, replaces overhead transmission lines when environmental and other concerns prohibit their installation, enhanced overall system efficiency due to exceptionally low losses, increased utility system operating flexibility, reduced electricity costs. With an estimated 80,000 miles of existing underground cable throughout the world, HTS cables will provide enormous benefits to a utility industry that is faced with an ever rising

demand for electricity and tightening constraints on siting flexibility. Conventional underground power transmission cables are utilized to transmit large amounts of power to congested urban areas through integrated underground duct systems. Existing duct systems limit the size of the conventional cables and the amount of power that can be transmitted through them but replacement HTS cables can deliver 4 times the power through the same conduits.

HTS Transformers

Transformers convert generation-level voltage to transmission-level voltage, which reduces the amount of energy lost in the transmission of power over long distances. Transformers are also needed to reduce the voltage back to a distribution level. Small, quiet, lightweight and efficient HTS transformers will be used primarily at substations within the utility grid. Environmentally friendly and oil-free, they will be particularly useful where transformers previously could not be sited, such as in high density urban areas or inside buildings. The benefits include: improved energy efficiencies, 50% smaller/lighter transformers, reduced environmental concerns from elimination of fire and environmental hazards of cooling oil, significant electrical power system improvements including more real and reactive power and improved voltage regulation, and quieter operation. Significant energy losses occur in conventional transformers due to the iron in the core (no-load losses) and the copper in the windings (load losses). If all transformers in the United States equal to or greater than 100 MVA were replaced with HTS transformers, the lifetime energy savings from conventional transformer losses could account for 340 billion kWh's or \$10.2 billion dollars. Further, conventional transformers can be overloaded for only short periods of time (200 per cent for 30 minutes. HTS transformers can carry overloads with no decrease in equipment lifespan and manageable additional load losses.

HTS Fault Current Limiters (FCL)

A current limiter is designed to react to and absorb unanticipated power disturbances in the utility grid, preventing loss of power to customers or damage to utility grid equipment. Fault current limiters would be installed in transmission and distribution systems for electric utilities and large energy users in high density areas. The benefits include: increased safety, increased reliability, improved power quality, compatible with existing protection devices, greater system flexibility from adjustable maximum allowed current, and reduced capital investment because of deferred upgrades. The superconducting FCL provides the same continuous protection with no standby energy losses due to joule heating and no voltage drop. The superconducting FCL instantaneously limits the flow of excessive current by allowing itself to go above its superconducting transition temperature and into a purely resistive state, thus minimizing the available fault current that passes through it. Fault current levels can be up to 20 times the steady state current, but the superconducting FCL will limit fault current to 3 to 5 times the steady state current, reduce standby energy losses, and provide improved flexibility in the use of existing lower-rated circuit breakers and fuses. Also, no capacitive correction is needed with a superconducting FCL since it has no reactance and is passive during non-fault conditions.

HTS Motors

Superconducting AC synchronous motors employ HTS windings in place of conventional copper coils. Because HTS wire can carry significantly larger currents, these windings are capable of generating significantly stronger magnetic fields in a given volume of space. A superconducting motor can match the power output of an equally rated conventional motor with

one-third the size and weight. Because of savings in materials and labor, HTS motors will cost less to manufacture than their conventional counterparts. The smaller size will also enable them to be manufactured and shipped directly to the customer without costly disassembly and subsequent onsite re-assembly and testing. Additionally, non-resistant HTS coils result in sharply reduced electrical losses in the rotor over copper windings yielding significant savings in electricity consumption. For continuous duty cycle motors, a one percent increase in efficiency can result in thousands of dollars in annual energy savings. Further, HTS AC synchronous motors have no iron teeth in the armature (stator windings), not only contributing to their smaller size and lighter weight, but also removing a significant source of motor noise. Superconducting motors are inherently more electrically stable during transients than conventional motors because they operate at small load angles (15 degrees vs. 70 degrees for a conventional motor) and have a much higher peak torque capability (~300%). As a result, the motor can withstand large transients or oscillatory torques without losing synchronous speed. The HTS machines do not require rapid field forcing during fast load changes or transients as is often the case with conventional machines. HTS motors will compete in the large (1,000 hp and above) commercial motor market for use in pumps, fans, compressors, blowers, and belt drives deployed by utility and industrial customers, particularly those requiring continuous operation. Another use for HTS motors is in naval and commercial ship propulsion, where size and weight savings increases design flexibility and open up limited space for use.

HTS Generators

The primary application of superconducting generators would be utility generation facilities, using either new or retrofitted generators. The benefits of the commercial superconducting generator include: increased machine efficiency beyond 99% which reduces losses by as much as 50% over conventional generators, reduced pollution per unit of energy produced, lower life-cycle costs, enhanced grid stability, reduced capital cost, and reduced installation expenses. By using superconducting wire for the field windings, losses in the rotor windings and in the armature bars can be practically eliminated. Further, the fields created in the armature by the rotor are not limited by the saturation characteristics of iron. The armatures are constructed without iron teeth removing the losses experienced in the armature teeth. A 1,000 MW superconducting generator (a typical size in large power plants) could save as much as \$4 million per year in reduced losses per generator. Even small efficiency improvements produce big dollar savings. A half of one percent improvement provides a utility with additional capacity to sell with a related value of nearly \$300,000 per 100 MVA generator. An HTS generator will be 1/3 the overall volume of its conventional equivalent. In power plants where expansion is difficult (e.g. shipboard or locomotive power), superconducting generators can increase generating capacity without using additional space. Smaller, lighter HTS generators use an "air core" design, eliminating much of the structural and magnetic steel of a conventional equivalent. Construction, shipping, and installation are all simplified and less costly. HTS generators have lowered armature reactance which can profoundly impact utility stability considerations. One implication is a reduction in the amount of spinning reserve (unused but rotating generating capacity) needed to insure a stable overall power system. Also, an HTS generator has the capability of being significantly overexcited to permit power factor correction without adding synchronous reactors or capacitors to the power system.

1.1.5 Reports

Journal Articles

Nature

T. Haugan, P.N. Barnes, R. Wheeler, F. Meisenkothen, M. Sumption, *Addition of nanoparticles dispersion to enhance flux pinning of $\text{YBa}_2\text{Cu}_3\text{O}_{7-x}$ films*, Nature **430**, 867-870 (2004).

Physical Review B

G.A. Levin, Phenomenology of conduction in incoherent layered crystals, Phys. Rev. B, **70**, 064515 (2004).

Applied Physics Letters

P. N. Barnes, T. J. Haugan, C. V. Varanasi, T. A. Campbell, *Flux pinning behavior of incomplete multilayered lattice structures in $\text{YBa}_2\text{Cu}_3\text{O}_{7-d}$* , Appl. Phys. Lett., **85**, 4088 (2004).

G.A. Levin, P.N. Barnes, N. Amemiya, S. Kasai, K. Yoda, and Z. Jiang, *Magnetization Losses in Multifilament Coated Superconductors*, Appl. Phys. Lett., **86**, 72509, (2005).

J.Z. Wu, R.L.S. Emergo, J.Z. Wu, T. Haugan, T. A. Campbell, and P. Barnes, *Tuning porosity of $\text{YBa}_2\text{Cu}_3\text{O}_{7-x}$ vicinal films by insertion of Y_2BaCuO_5 nanoparticles*, accepted.

C. Varanasi, P.N. Barnes, J. Burke, J. Carpenter, T. J. Haugan, *Controlled Introduction of Flux Pinning Centers in $\text{YBa}_2\text{Cu}_3\text{O}_{7-x}$ Films During Pulsed Laser Deposition*, accepted.

Journal of Applied Physics

P.N. Barnes and M.D. Sumption, *Low loss striated $\text{YBa}_2\text{Cu}_3\text{O}_{7-d}$ coated conductor with filament current sharing*, J. Appl. Phys., **96**, 6550 (2004).

G. A. Levin, P. N. Barnes, N. Amemiya, S. Kasai, K. Yoda, Z. Jiang, A. Polyanskii, *Magnetization Losses in Multiply Connected $\text{YBa}_2\text{Cu}_3\text{O}_{7-d}$ Coated Conductors*, accepted.

Journal of Applied Physics

A.Lamouri, A.Naruka, J.Sulcs, C.V. Varanasi, T. Brumleve, Influence of electrode, buffer gas and control gear on metal halide lamp performance, **38**, 3028 (2005).

Superconductor Science and Technology

P.N. Barnes, R. M. Nekkanti, T.J. Haugan, T.A. Campbell, N.A. Yust, and J.M. Evans, *Pulsed Laser Deposition of YBCO coated conductor using Y_2O_3 as the seed and cap layer*, Supercond. Sci. Technol. **17**, 957-962 (2004).

N. Amemiya, S. Kasai, K. Yoda, Z. Jiang, G.A. Levin, P.N. Barnes, and C.E. Oberly, *AC loss reduction of YBCO coated conductors by multifilamentary structure*, Supercond. Sci. Technol., **17**, 1464 (2004).

M.D. Sumption, E.W. Collings, and P.N. Barnes, AC loss in striped (filamentary) YBCO coated conductors leading to designs for high frequencies and field-sweep amplitudes, Supercond Sci. Technol., **18**, 122 (2005).

N. Yust, R. Nekkanti, L. Brunke, R. Srinivasan, and P. Barnes, *Copper metallic substrates for HTS coated conductors*, Supercond. Sci. Technol., **18**, 9 (2005).

S. Sathiraju, P.N. Barnes Q.X. Jia, and P.N. Arendt, *Growth of $YBa_2Cu_3O_{7-x}$ films on Ba_2YNbO_6 dielectric buffer layer on a biaxially oriented MgO template for coated conductor applications*, submitted to Supercond. Sci. Technol.

Journal of Materials Research

T. Haugan, W. Wong-Ng, L.P. Cook, M.D. Vaudin, L. Swartzendruber, and P. N. Barnes, *Partial Melt Processing of Solid-Solution $Bi_2Sr_2CaCu_2O_{8+\delta}$ Thick Film Conductors with Nanophase Al_2O_3 Additions*, J. Mater. Res. **18**, 1054-1066 (2003).

T.J. Haugan,, P.N. Barnes, I. Maartense, E.J. Lee, M. Sumption, and C.B. Cobb, Island growth of Y_2BaCuO_5 nanoparticles in $(211_{\sim 1.5nm}/123_{\sim 10nm}) \times N$ composite multilayer structures to enhance flux pinning of $YBa_2Cu_3O_{7-d}$ films, J. Mater. Res. **18**, 2618-2623 (2003).

T. Aytug, M. Paranthaman, K.J. Leonard, H.Y. Zhai, M.S. Bhuiyan, E.A. Payzant, A. Goyal, S. Sathyamurthy, D.B. Beach, P.M. Martin, D.K. Christen, X. Li, T. Kodenkandath, U. Schoop, M.W. Rupich, T. J. Haugan, P. N. Barnes, H. E. Smith, *Assessment of chemical solution synthesis and properties of $Gd_2Zr_2O_7$ thin films as buffer layers for second generation high-temperature superconductor wires*, accepted.

C. V. Varanasi, N. Yust, P. N. Barnes, Biaxially Textured Copper-Iron Alloy Substrates used in YBCO Coated Conductors, submitted.

Physica C

T. Haugan, P. Barnes, I. Maartense, L. Brunke, and J. Murphy, *Pulsed Laser Deposition of $\text{YBa}_2\text{Cu}_3\text{O}_{7-d}$ in High Oxygen Partial Pressures*, Physica C, **397**, pp.47-57, (2003).

L.B. Wang, M.B. Price, J.L. Young, C. Kwon, T.J. Haugan, P.N. Barnes, Observation of uniform current transport in epitaxial $\text{YBa}_2\text{Cu}_3\text{O}_{7-x}$ film near the superconducting transition temperature, Physica C **405**, 240-244 (2004).

W. Wong-Ng, L.P. Cook, J. Suh, R. Feenstra, T. Haugan, and P. Barnes, *Phase Equilibria of Ba-R-Cu-O for Coated-Conductor Applications (R=lanthanides and Y)*, Physica C **408-410**, 20-22 (2004).

T.A. Campbell, T.J. Haugan, P.N. Barnes, I. Maartense, J. Murphy, L. Brunke, J.M. Evans, J. Kell, N. Yust, S. Sathiraju, *Flux Pinning Effects of Y_2O_3 in YBCO Thin Films as Nanoparticulate Multilayered Dispersions*, accepted.

L.B. Wang, M.B. Price, J.L. Young, C. Kwon, G.A. Levin, T.J. Haugan, and P.N. Barnes, *Mapping the Current Distribution in $\text{YBa}_2\text{Cu}_3\text{O}_{7-x}$ Thin Films with Striations*, submitted to Physica C.

T.J. Haugan, P.N. Barnes, T.A. Campbell, A. Goyal, A. Gapud, L. Heatherly, and S. Kang, *Deposition of $(\text{Y}_2\text{BaCuO}_5/\text{YBa}_2\text{Cu}_3\text{O}_{7-x})_n$ multilayer coated conductors on Ni-based textured substrates*, **425**, 21 (2005).

IEEE Transactions on Applied Superconductivity

M. D. Sumption, E. Lee, C.B. Cobb, P.N. Barnes, T. J. Haugan, J. Tolliver, C.E. Oberly, E.W. Collings, *Hysteretic Loss vs. Filament Width in Thin YBCO Films Near the Penetration Field*, IEEE Trans. on Appl. Supercond. **13**, 3553-3556 (2003).

P. N. Barnes, S. M. Mukhopadhyay, S. Krishnaswami, T.J. Haugan, J.C. Tolliver, and I. Maartense, *Correlation between the XPS peak shapes of $\text{Y}_1\text{Ba}_2\text{Cu}_3\text{O}_{7-x}$ and film quality*, IEEE Trans. on Appl. Supercond. **13**, 3643-3647 (2003).

H. Okuyucu, L. Arda, Z.K. Heiba, M.I. El-Kawni, J.C. Tolliver, P.N. Barnes, Z. Aslanoglu, Y. Akin, and Y.S. Hascicek, *Y- and Yb-123 Coated Conductor Development by PLD and Sol-Gel on $(\text{Gd}_{1-x}\text{Er}_x)\text{O}_3$ Buffered Ni Tapes*, IEEE Trans. on Appl. Superconductivity, **13**, 2677 (2003).

T.J. Haugan, P.N. Barnes, T.A. Campbell, J.M. Evans, J.W. Kell, L.B. Brunke, J.P. Murphy, J.C. Tolliver, C.V. Varanasi, I. Maartense, L. Civale, B. Maiorov, W. Wong-Ng, L.P. Cook, *Addition of Ultra-High Density Nanoparticle Dispersions to Enhance Flux Pinning of YBCO Thin Films*, **15**, 3770 (2005).

P.N. Barnes, T.J. Haugan, M.D. Sumption, B.C. Harrison, Pinning Enhancement of $\text{YBa}_2\text{Cu}_3\text{O}_{7-d}$ Thin Films with Y_2BaCuO_5 Nanoparticulates, **15**, 3722 (2005).

J.W. Kell, T.J. Haugan, J.M. Evans, P.N. Barnes, C.V. Varanasi, L.B. Brunke, J.P. Murphy, *Tb and Ce Doped $\text{YBa}_2\text{Cu}_3\text{O}_{7-x}$ Films Processed by Pulsed Laser Deposition*, **15**, 3726 (2005).

S. Sathiraju, P. N. Barnes, C. V. Varanasi, R. Wheeler, *Studies on YBa_2NbO_6 buffer layers*, **15**, 3009 (2005).

Wang L. B. ; Selby P. ; Khanal C. ; Levin G. ; Haugan T. J. ; Barnes P. N. ; Kwon C., *The Distribution of Transport Current in YBCO Coated Conductor With Zipper Striations*, **15**, 2950 (2005).

Barnes P. N. ; Levin G. A. ; Varanasi Chakrapani ; Sumption M. D., *Low AC Loss Structures in YBCO Coated Conductors With Filamentary Current Sharing*, **15**, 2827 (2005).

Majoros M. ; Glowacki B. A. ; Campbell A. M. ; Levin G. A. ; Barnes P. N. ; Polak M., *AC Losses in Striated YBCO Coated Conductors*, **15**, 2819 (2005).

Sumption M. D. ; Barnes P. N. ; Collings E. W., *AC Losses of Coated Conductors in Perpendicular Fields and Concepts for Twisting*, **15**, 2815 (2005).

N. Amemiya, K. Yoda, S. Kasai, Zhenan Jiang, G.A. Levin, P.N. Barnes, and C.E. Oberly, *AC Loss Characteristics of Multifilamentary YBCO Coated Conductors*, **15**, 1637 (2005).

G.A. Levin, P.N. Barnes, *Concept of Multiply Connected Superconducting Tapes*, **15**, 2158 (2005).

C.V. Varanasi, J. C. Tolliver, T. J. Haugan, K. W. Schmaeman, S. Sathiraju, L. B. Brunke, J. P. Murphy, I. Maartense, Jack Burke, Jason Carpenter, P. N. Barnes, *Nd doped $\text{YBa}_2\text{Cu}_3\text{O}_{7-z}$ Films Deposited by Pulsed Laser Deposition*, **15**, 3722 (2005).

M. Polak, E. Demencik, Lubomil Jansak, Elo Usak, Pavol Mozola, Cees L. H. Thieme, D. Aized, George A. Levin, Paul N. Barnes, *Properties of a YBCO pancake coil operating with AC current at frequencies up to 1000 Hz*, submitted.

IEEE Transactions on Magnetism

P.N. Barnes, G.L. Rhoads, J.C. Tolliver, M.D. Sumption, and K.W. Schmaeman, *Compact, Lightweight Superconducting Power Generators*, to be published in IEEE Trans. Mag.

ColdFacts

A. Chaney, B.C. Harrison, T. Haugan, and P. Barnes, *Educational Outreach in Air Force*, **21**, 9, 2005.

Conference Papers

Bulletin of the American Physical Society

G.A. Levin, P.N. Barnes, and M.D. Sumption, *Reduction of AC losses in striated coated superconductors*, March Meeting of the American Physical Society (2004); Bulletin of the American Physical Society **49**, p. 137 (2004).

Materials Research Society Proceedings

S. Sathiraju, J.P. Murphy, J.M. Evans, A.L. Campbell, L.B. Brunke, and P.N. Barnes, *Substrate Planarization Studies on IBAD Substrates*, Mat. Res. Soc. Symp. Proc., **EXS-3**, pp. EE5.5.1-3 (2004).

N. Yust, R. Nekkanti, L. Brunke, and P. Barnes, *Textured Copper Metallic Substrates for 2nd Generation High Temperature Superconductor Applications*, Mat. Res. Soc. Symp. Proc., **EXS-3**, pp. EE5.6.1-3 (2004).

P.N. Barnes, T.J. Haugan, S. Sathiraju, I. Maartense, A.L. Westerfield, R.M. Nekkanti, L.B. Brunke, T.L. Peterson, J.M. Evans, and J.C. Tolliver, *Correlation of AC Loss Data from Magnetic Susceptibility Measurements with YBCO Film Quality*. Mat. Res. Soc. Symp. Proc., **EXS-3**, p. EE6.4.1-3 (2004).

S. Sathiraju, N.A. Yust, R.N. Nekkanti, I. Martense, A.L. Campbell, T.L. Peterson, T.J. Haugan, J.C. Tolliver, and P.N. Barnes, *Growth Optimization of YBa₂NbO₆ Buffer Layers*, Mat. Res. Soc. Symp. Proc., **EXS-3**, p. EE8.7.1-3 (2004).

MRS-Japan Proceedings

P.N. Barnes, T.J. Haugan, M.D. Sumption, S. Sathiraju, J.M. Evans, and J.C. Tolliver, *YBa₂Cu₃O_{7-d} Films with a Nanoparticulate Dispersion of Y₂BaCuO₅ for Enhanced Flux Pinning*, Trans. MRS-J, **29(4)**, 1385-1388 (2004).

S. Sathiraju, R.A. Wheeler, P.N. Barnes, *Pulsed Laser deposited YBa₂Cu₂NbO_y thin films on SrTiO₃ Substrate*, submitted.

S. Sathiraju, R.A. Wheeler, T.A. Campbell, T.L. Peterson, and P.N. Barnes, *Phase formation of $YBa_2Cu_{3-x}Nb_xO_y$ ($x = 0.25, 0.5, 0.75$, and 1) thin films*, submitted.

Ceramic Transactions

T.J. Haugan, M.E. Fowler, J.C. Tolliver, P.N. Barnes, W. Wong-Ng, L.P. Cook, *Flux Pinning and Properties of Solid-Solution $(Y,Nd)_{1+x}Ba_{2-x}Cu_3O_{7-d}$ Superconductors*, **140** 299 (2003).

P.N. Barnes, J.C. Tolliver, T.J. Haugan, S.M. Mukhopadhyay, and J.T. Grant, *Evaluating Superconducting YBCO Film Properties Using X-Ray Photoelectron Spectroscopy*, in "Fabrication of High-Temperature Superconductors", Ceramic Transactions, edited by R. Meng, A. Goyal, W. Wong-Ng, H.C. Freyhardt, K. Matsumoto (American Ceramic Society, Westerville OH) **149**, pp. 23-31 (2004).

R.M. Nekkanti, P.N. Barnes, L.B. Brunke, T.J. Haugan, N.A. Yust, I. Maartense, J.P. Murphy, S. Sathiraju, J.M. Evans, J.C. Tolliver, and K.R. Marken, Jr., *Pulsed Laser Deposition of YBCO with Yttrium Oxide Buffer Layers*, in "Fabrication of High-Temperature Superconductors", Ceramic Transactions, edited by R. Meng, A. Goyal, W. Wong-Ng, H.C. Freyhardt, K. Matsumoto (American Ceramic Society, Westerville OH) **149**, pp. 63-72 (2004).

T.J. Haugan, J.M. Evans, J.C. Tolliver, I. Maartense, P.N. Barnes, W. Wong-Ng, L.P. Cook, R.D. Shull, *Flux Pinning and Properties of Solid-Solution $(Y,Nd)_{1+x}Ba_{2-x}Cu_3O_{7-\delta}$ Superconductors Processed in Air and Partial Oxygen Atmospheres*, in "Fabrication of High-Temperature Superconductors", Ceramic Transactions, edited by R. Meng, A. Goyal, W. Wong-Ng, H.C. Freyhardt, K. Matsumoto (American Ceramic Society, Westerville OH) Vol. **149**, 151-162 (2004).

S. Sathiraju, P. T. Murray, T. J. Haugan, R. M. Nekkanti, L. Brunke, I. Maartense, A.L. Campbell, J. P. Murphy, J. C. Tolliver, and P. N. Barnes, *Studies on Nanoparticulate Inclusions in Y123 Thin Films*, in "Fabrication of High-Temperature Superconductors", Ceramic Transactions, edited by R. Meng, A. Goyal, W. Wong-Ng, H.C. Freyhardt, K. Matsumoto (American Ceramic Society, Westerville OH) Vol. **149**, 177-183 (2004).

J.C. Tolliver, T.J. Haugan, S. Sathiraju, N.A. Yust, P.N. Barnes, and C. Varanasi, *Pulsed Laser Deposition of Nd Doped $YBa_2Cu_3O_{7-d}$ Films*, to be published in "Epitaxial Growth of Functional Oxides", **160**, 27 (2005).

S. Sathiraju, T. Campbell, I. Maartense, J.P. Murphy, J.C. Tolliver, G.A. Levin, T.J. Haugan T.L. Peterson, P.N. Barnes, *Pulsed Laser Deposition of $(Y_{1-x}Ca_x)Ba_2NbO_6$ ($x = 0.0, 0.05, 0.1, 0.2, 0.4$) Buffer Layers*, **160**, 43 (2005).

S. Sathiraju, C.V. Varanasi, N.A. Yust, L.B. Brunke, and P.N. Barnes, Growth Optimization of Ba_2YNbO_6 Buffer Layers by Pulsed Laser Deposition on Biaxially Textured Ni-alloy and Cu-alloy Substrates, **160**, 55 (2005).

J.W. Kell, T.J. Haugan, P.N. Barnes, M.F. Locke, and T.A. Campbell C.V. Varanasi and L.B. Brunke, Processing and Characterization of $(\text{Y}_{1-x}\text{Tb}_x)\text{Ba}_2\text{Cu}_3\text{O}_{7-z}$ Superconducting Thin Films Prepared by Pulsed Laser Deposition, **160**, (2005).

Functional Growth of Epitaxial Oxides: Electrochemical Society

T. Haugan, P. Barnes, R. Nekkanti, J.M. Evans, L. Brunke, I. Maartense, J.P. Murphy, A. Goyal, A. Gapud, and L. Heatherly, *Deposition of $(211_{1.0\text{nm}}/123_{10\text{nm}})_x\text{N}$ Multilayer Coated Conductors on Ni-based Substrates*, 359 (2005).

S. Sathiraju, R. Wheeler, P. Barnes, T. Peterson, I. Maartense, A. Campbell, R. Nekkanti, L. Brunke, N. Yust, K. Fields, T. Campbell, T. Haugan, J. Tolliver, S. Velmulakonda, S. Mukhopadhyay, Q. Jia, P. Arendt, *Phase Formation of $\text{YBa}_2\text{Cu}_3\text{Nb}_x\text{O}_y$ Thin Films*, 367 (2005).

T. J. Haugan, J. M. Evans, I. Maartense, P. N. Barnes, *Superconducting Properties of $(\text{Y}_{1-x}\text{Gd}_x)\text{Ba}_2\text{Cu}_3\text{O}_{7-d}$ Composites Processed in Partial Oxygen Atmospheres*, submitted.

C.V. Varanasi, G. Landis, P.N. Barnes, J. Burke, N. Yust, T. Haugan, *Ni-20%Cr Coatings on Biaxially Textured Copper and Copper-Iron Alloy Substrates for $\text{YBa}_2\text{Cu}_3\text{O}_{7-x}$ Coated Conductor Applications*, submitted.

IEEE Proceedings of the 12th Symposium on Electromagnetic Launch Technology

P.N. Barnes, G.L. Rhoads, J.C. Tolliver, M.D. Sumption, and K.W. Schmaeman, *Compact, Lightweight Superconducting Power Generators*, IEEE Proceedings of the 2004 12th Symposium on Electromagnetic Launch Technology, (2004).

Advanced X-ray Techniques in Research and Industry

S. Sathiraju and P. Barnes, Texture Analysis Using General Area Diffraction Detector System, ed. by A.K. Singh, 102 (2005).

Proceedings of the 2003 Japan-US Workshop on Superconductivity

T. Haugan, P. N. Barnes, J. M. Evans, J. C. Tolliver, L. Brunke, T. A. Campbell, I. Maartense, W. Wong-Ng, L. P. Cook, M. Sumption, *Flux pinning of $\text{YBa}_2\text{Cu}_3\text{O}_{7-\delta}$ by nanoparticle defect addition and RE substitution for Y and Ba*, in Extended Abstract: 2003 Japan-US Workshop on Superconductivity.

EUCAS 2005

M. Majoros, B. A. Glowacki, A. M. Campbell, G. A. Levin, P. N. Barnes, *Transport AC losses in striated YBCO coated conductors*, submitted.

Drafts

C. V. Varanasi, P. N. Barnes, J. Burke, G. Landis, Textured Oxidation Protection Coatings (Ni-Cr, Pt) on Textured Copper and Copper-Iron Alloy Substrates for YBa₂Cu₃O_{7-x} Coated Conductor Application

Book Chapters

T. Haugan, J.C. Tolliver, J.M. Evans, J.W. Kell, *Crystal Chemical Substitutions of YBa₂Cu₃O_{7-δ} to Enhance Flux Pinning*, in "Studies of High Temperature Superconductors", edited by A. Narlikar, Vol. 48, 49 (Nova Science Publishers, Inc., New York NY, 2004).

Books Edited

M.P. Paranthaman, P.N. Barnes, B. Holzapfel, Y. Yamanda, K. Matsumoto, J.K.F. Yau, *High-Temperature Superconductor Materials, Devices, and Applications*, **160**, 2005.

Presentations

Materials Research Society

T. J. Haugan, P. N. Barnes, J. C. Tolliver, R. M. Nekkanti, J. P. Murphy, J. M. Evans, L. Brunke, A. L. Westerfield, S. Sathiraju, I. Maartense, T. L. Peterson, M. Sumption, L. Heatherly, and A. Goyal, *Inclusion of 211 Nanoparticles by Island-growth in (211-_{1nm}/123-_{10nm})xN Multilayer Composite Structures to Enhance the Physical-Electrical-Magnetic Properties of YBa₂Cu₃O_{7-x} Thin Films*, MRS Fall Meeting (2003).

N. Yust, R. Nekkanti, L. Brunke, R. Srinivasan, and P.N. Barnes, *Textured copper metallic substrates for second generation high temperature superconductors*, MRS Fall Meeting (2003).

S. Sathiraju, J.P. Murphy, A.L. Campbell, L.B. Brunke, and P.N. Barnes, *Substrate Planarization Studies on IBAD Substrates*, MRS Fall Meeting (2003).

P.N. Barnes, T.J. Haugan, S. Sathiraju, I. Maartense, A.L. Westerfield, R.M. Nekkanti, L.B. Brunke, T.L. Peterson, J.M. Evans, and J.C. Tolliver, *Correlation of AC Loss Data from Magnetic Susceptibility Measurements with YBCO Film Quality*, MRS Fall Meeting (2003).

S. Sathiraju, K.D. Fields, N.A. Yust, R.M. Nekkanti, L.B. Brunke, A.L. Campbell, T.J. Haugan, J.C. Tolliver, and P.N. Barnes, *Growth and microstructural studies of YBa₂NbO₆ thin films*, MRS Fall Meeting (2003).

P.N. Barnes, J.W. Kell, T.J. Haugan, C.V. Varanasi, and M.F. Locke, *Rare earth doping of YBa₂Cu₃O_{7-x} films at minute levels for magnetic flux pinning*, MRS Spring Meeting (2005).

P. N. Barnes, J. Kell, T. J. Haugan, T. Campbell, C. V. Varanasi, *Studies on nanolayered flux pinning structures in YBa₂Cu₃O_{7-x} films*, MRS Spring Meeting (2005).

C. Varanasi, P.N. Barnes, N.A. Yust, A.D. Chaney, S. Sathiraju, *Textured Oxidation Protection Coatings on Copper and Copper-Alloy Substrates to be used in Coated Conductor Applications*, MRS Spring Meeting (2005).

T.J. Haugan, T.A. Campbell, I. Maartense, C.V. Varanasi, and P.N. Barnes, *Flux Pinning Properties of (Y,RE)_{1+x}Ba_{2-x}Cu₃O_{7-x} Thin Film Superconductors; RE = Eu, Er,,* MRS Spring Meeting (2005).

B.A. Maierov, T. Haugan, T.G. Holesinger, P.N. Barnes, and L. Civale, *Matching Field Effect in the Critical Current of YBa₂Cu₃O₇ Films due to Periodic Y₂BaCuO₅ Inclusions*, MRS Spring Meeting (2005).

S. Sathiraju, A.D. Chaney, T. Haugan, R. Wheeler, A. Campbell, T. Campbell, I. Maartense, P.N. Barnes, *Studies on Ca Doped Y211 Thin Films for Nanoparticulate Pinning Centers in Y123 Thin Films (Poster)*, MRS Spring Meeting (2005).

C. Kwon, L.B. Wang, P. Shelby, C. Khanal, J.L. Young, G. You, K.R. Barraca, G.A. Levin, T.J. Haugan, and P. N. Barnes, *Current Flow Characteristics in Striated Coated Conductors*, MRS Spring Meeting (2005).

106th Annual Meeting of the American Ceramic Society

T.J. Haugan, P.N. Barnes, T.A. Campbell, J.C. Tolliver, J.W. Kell, L. Brunke, S. Sathiraju, G.A. Levin, I. Maartense, T. Peterson, R. Wheeler, and F. Meisenkothen, *Recent Studies of (211_{nanoparticle}/123_{~10nm})_xN Multilayer Composite Structures to Enhance Flux Pinning Properties of YBa₂Cu₃O_{7-x} Thin Films*, 106th Annual Meeting of the American Ceramic Society (2004).

P.N. Barnes, T.J. Haugan, M. Sumption, and T. Campbell, *Pinning Enhancement and Degradation of YBa₂Cu₃O_{7-d} Films via Composite Nanolayered Architecture*, 106th Annual Meeting of the American Ceramic Society (2004).

J.W. Kell, T.J. Haugan, J.C. Tolliver, K.W. Schmaeman, T.A. Campbell, L. Brunke, J.P. Murphy, I. Maartense, P.N. Barnes, *Flux Pinning of (Y_{1-x}Tb_x)Ba₂Cu₃O_{7-z} Superconductor Thin Films Prepared by Pulsed Laser Deposition*, 106th Annual Meeting of the American Ceramic Society (2004).

C.J. Druffner, G.P. Perram, R.R. Biggers, P.N. Barnes, *Developing Optical Diagnostic Sensors to Determine $YBa_2Cu_3O_{7-x}$ Film Quality During Continuous Deposition*, 106th Annual Meeting of the American Ceramic Society (2004).

G. Levin, K.E. Hix, M.C. Rendina, L. Brunke, J.P. Murphy, S. Sathiraju, T.J. Haugan, P.N. Barnes, *Properties of Resistive Barriers Produced by Laser Micromachining in Coated Superconductors*, 106th Annual Meeting of the American Ceramic Society (2004).

J.Z. Wu, R. Emergo, T.J. Haugan, P.N. Barnes, S. Sathiraju, X. Wang, *Engineering Microstructures of HTS Thick Films for Higher Current Carrying Capability*, 106th Annual Meeting of the American Ceramic Society (2004).

S. Sathiraju, R. Wheeler, A. Campbell, I. Maartense, T.A. Campbell, G.A. Levin, J.C. Tolliver, T.J. Haugan, T. Peterson, P.N. Barnes, *Growth Optimization of $(Y_{1-x}Ca_x)Ba_2NbO_6$ ($x=0.0, 0.1, 0.2, 0.4$) Buffer Layers*, 106th Annual Meeting of the American Ceramic Society (2004).

S. Sathiraju, N.A. Yust, L. Brunke, P.N. Barnes, *Growth Optimization of YBa_2NbO_6 Layers on Highly Textured Copper-Alloy-Substrate for HTS Coated Conductor Applications*, 106th Annual Meeting of the American Ceramic Society (2004).

T.J. Haugan, P.N. Barnes, J.C. Tolliver, T.A. Campbell, I. Maartense, A. Goyal, A.A. Gapud, L. Heatherly, *Enhanced Flux Pinning of $(211/123)_xN$ Nanolayered YBCO Coated Conductors on Ni-Based Textured Substrates*, 106th Annual Meeting of the American Ceramic Society (2004).

T.A. Campbell, T.J. Haugan, L. Brunke, P.N. Barnes, J.W. Kell, I. Maartense, S. Sathiraju, J.P. Murphy, J.C. Tolliver, *Flux Pinning Effects of Y_2O_3 in YBCO Multilayer $(Y_2O_3\sim_{1nm}/Y_{123}\sim_{10nm})_xN$* , 106th Annual Meeting of the American Ceramic Society (2004).

J.C. Tolliver, C.V. Varanasi, T.J. Haugan, K.W. Schmaeman, P.N. Barnes, *Flux Pinning Induced by RE Substitution in $(Y_{1-x}Nd_x)Ba_2Cu_3O_{7-x}$ Thin Films*, 106th Annual Meeting of the American Ceramic Society (2004).

N.A. Yust, C.V. Varanasi, S. Sathiraju, P.N. Barnes, *Highly Textured Copper-Alloy-RABIT's Substrate Tapes for HTS Coated Conductor Applications*, 106th Annual Meeting of the American Ceramic Society (2004).

Applied Superconductivity Conference

N. Amemiya, S. Kasai, K. Yoda, Z. Jiang, G.A. Levin, P.N. Barnes, C.E. Oberly, *AC loss characteristics of multifilamentary YBCO coated conductors*, Applied Superconductivity Conference (2004).

P.N. Barnes, G.A. Levin, M.D. Sumption, *Weakly linked filamentary YBCO coated conductor for current sharing*, Applied Superconductivity Conference (2004).

T.J. Haugan, P.N. Barnes, T.A. Campbell, J.M. Evans, J.W. Kell, L.B. Brunke, J.P. Murphy, J.C. Tolliver, C.V. Varanasi, I. Maartense, L. Civale, B. Maiorov, W. Wong-Ng, L.P. Cook, *Addition of Ultra-High Density Nanoparticle Dispersions to Enhance Flux Pinning of YBCO Thin Films*, Applied Superconductivity Conference (2004).

T.J. Haugan, P.N. Barnes, T.A. Campbell, J.M. Evans, L.B. Brunke, J.P. Murphy, I. Maartense, A. Goyal, A. Gapud, L. Heatherly, *Deposition of (Nanoparticle/123)_xN Multilayer Films on Ni-alloy RABiTSTM for Flux Pinned YBCO Coated Conductors*, Applied Superconductivity Conference (2004).

J.W. Kell, T.J. Haugan, J.M. Evans, P.N. Barnes, C.V. Varanasi, L.B. Brunke, J.P. Murphy, *Tb and Ce Doped YBa₂Cu₃O_{7-x} Films Processed by Pulsed Laser Deposition*, Applied Superconductivity Conference (2004).

L.B. Wang, C.M. Khanal, P. Shelby, M.B. Price, C. Kwon, G. Levin, T.J. Haugan, P.N. Barnes, *Mapping the Current Flow in YBCO Thin Films with Striations*, Applied Superconductivity Conference (2004).

G.A. Levin, P.N. Barnes, *AC losses in multiply connected superconducting tapes*, Applied Superconductivity Conference (2004).

M. Majoros, B.A. Glowacki, A.M. Campbell, G.A. Levin, P.N. Barnes, *AC Losses in striated YBCO coated conductors*, Applied Superconductivity Conference (2004).

S. Sathiraju, G.A. Levin, P.N. Barnes, T.J. Haugan, T.A. Campbell, C.V. Varanasi, *Flux Pinning Properties of Ca doped YBa₂Cu₃O_{7-x} Thin Films with Y₂O₃ nanoparticulate dispersions*, Applied Superconductivity Conference (2004).

S. Sathiraju, P.N. Barnes, R. Wheeler, N.A. Yust, *Studies on YBa₂NbO₆ buffer layers*, Applied Superconductivity Conference (2004).

K.W. Schmaeman, J.M. Evans, T.J. Haugan, J.C. Tolliver, C.V. Varanasi, P.N. Barnes, *Properties of (Y_{1-x}RE_x)_{1+y}Ba_{2-y}Cu₃O_{7-z} Bulk Superconductors for Flux Pinning*, Applied Superconductivity Conference (2004).

M.D. Sumption, E. Lee, E.W. Collings, M. Tomsic, G. Levin, P. Barnes, *Loss in Striped YBCO Coated Conductors*, Applied Superconductivity Conference (2004).

M.D. Sumption, T. Haugan, P. Barnes, *Pinning from Magnetization Decay and Ramp Rate Experiments in YBCO PLD films with multilayer structures*, Applied Superconductivity Conference (2004).

C.V. Varanasi, J. C. Tolliver, T. J. Haugan, K. W. Schmaeman, S. Sathiraju, L. B. Brunke, J. P. Murphy, I. Maartense, Jack Burke, Jason Carpenter, P. N. Barnes, *Nd doped YBa₂Cu₃O_{7-x} Films Deposited by Pulsed Laser Deposition*, Applied Superconductivity Conference (2004).

J.Z. Wu, R. Emergo, T. Haugan, P. Barnes, *High J_c in porous YBCO thick films*, Applied Superconductivity Conference (2004).

C.V. Varanasi, N.A. Yust, P.N. Barnes, S. Sathiraju, *Biaxially Textured Copper Alloy Substrates for use in HTS Coated Conductors*, Applied Superconductivity Conference (2004).

C.V. Varanasi, N.A. Yust, P.N. Barnes, S. Sathiraju, *Protective Epitaxial Metallic Plating for Textured Copper and Copper Alloy Substrates*, Applied Superconductivity Conference (2004).

C.E. Oberly, F. Rodriguez, G.L. Rhoads, *Conceptual Approach to the Ultimate Low AC Loss YBCO Superconductor*, Applied Superconductivity Conference (2004).

International Conference on Applied Materials

P.N. Barnes, T.J. Haugan, S. Sathiraju, J. Evans, E.J. Lee, M.D. Sumption, R. Nekkanti, L. Brunke, and J.C. Tolliver, *YBa₂Cu₃O_{7-x} (Y123) Films with a Nanoparticulate Dispersion of Y₂BaCuO₅ (Y211) for Enhanced Flux Pinning*, International Conference on Applied Materials (2003).

Electro-Chemical Society Meeting

S. Sathiraju, P. N. Barnes, T. L. Peterson, K. D. Fields, N. A. Yust, R. M. Nekkanti, L.B. Brunke, J. P. Murphy, A. L. Campbell, and J. C. Tolliver, *Formation of YBa₂Cu_{3-x}Nb_xO_y (x = 0.25, 0.5, 0.75, 1) Phase in Thin Films*, Electro-Chemical Society Meeting (2003).

T. J. Haugan, P. N. Barnes, I. Maartense, J. M. Evans, J. C. Tolliver, L. Brunke, J. P. Murphy, and R. N. Nekkanti, *Island-growth of 211 nanoparticles in (211_{~2nm}/123_{~10nm})_xN Multilayer Thin Film Structures for Improvement of YBa₂Cu₃O_{7-x} Coated Conductors*, Electro-Chemical Society Meeting (2003).

11th US-Japan Workshop on High T_c Superconductors

T. Haugan, P.N. Barnes, J.M. Evans, J.C. Tolliver, L. Brunke, T.A. Campbell, I. Maartense, W. Wong-Ng, L.P. Cook, M. Sumption, *Flux Pinning of Y123 with multilayer composite nanosized Y211 additions and RE substitution*, 11th US-Japan Workshop on High T_c Superconductors (2003).

Air Force Office of Scientific Research HTS Coated Conductor Review

N.A. Yust, R. Nekkanti, P.N. Barnes, S. Sathiraju, T.J. Haugan, R. Srinivasan, R. Bhattacharya, *Textured copper metallic substrates for HTS coated conductors*, AFOSR HTS Coated Conductor Review (2004).

S. Sambasivan, J. Wessling, F. Niu, J. Rechner, T. Haugan, and P.N. Barnes, *Development of YBCO CC Buffer Layers by the ECONOTM Process*, AFOSR HTS Coated Conductor Review (2004).

S. Sathiraju, R. Wheeler, P.N. Barnes, T.L. Peterson, I. Maartense, A.L. Campbell, R.M. Nekkanti, L. Brunke, J. Murphy, T.A. Campbell, N.A. Yust, T.J. Haugan, Q. Jia, P. Arendt, S. Mukhopadya, and S. Vemulakonda, *Studies on YBa₂NbO₆ and YBa₂Cu_{3-x}Nb_xO_y Buffer Layers*, AFOSR HTS Coated Conductor Review (2004).

T.J. Haugan, P. N. Barnes, J. C. Tolliver, T. A. Campbell, J. Kell, J. M. Evans, N. Yust, A. L. Westerfield, L. Brunke, R. Nekkanti, J. P. Murphy, T. Peterson, I. Maartense, R. Wheeler, F. Meisenkothen, M. Sumption, E. J. Lee, A. Goyal, A. Gapud, and L. Heatherly, *YBCO Pinning by Nanoparticulate Dispersions*, AFOSR HTS Coated Conductor Review (2004).

P.N. Barnes, T.J. Haugan, J.M. Evans, J.C. Tolliver, I. Maartense, T.L. Peterson, and S. Sathiraju, *Improving in-field J_c of YBCO coated conductors using (Y,RE)BCO films*, AFOSR HTS Coated Conductor Review (2004).

R. Emergo, X. Wang, H. Zhao, Y.Y. Xie, J. Wu, T. Haugan, P. Barnes, D. Christen, T. Aytug, M. Paranthaman, T. Pollianski, and D. Larbalestier, *High T_c & J_c HTS Thick Films*, AFOSR HTS Coated Conductor Review (2004).

C. Kwon, L.B. Wang, M. Price, K. Waller, J. Rosales, J. Mahoney, J. Young, T.J. Haugan, R. Nekkanti, G. Levin, P.N. Barnes, W. Jo, R.H. Hammond, M.R. Beasley, and A. Goyal, *Latest Developments in VTSLM at CSULB*, AFOSR HTS Coated Conductor Review (2004).

P.N. Barnes, R. Nekkanti, T.A. Campbell, C.B. Cobb, G. Levin, and M.D. Sumption, *Substrate induced ac structure with current sharing in YBCO coated conductors*, AFOSR HTS Coated Conductor Review (2004).

G.A. Levin, M. Sumption, C.E. Oberly, P.N. Barnes, R. Nekkanti, T.J. Haugan, S. Sathiraju, *Concept of Multiply Connected Superconducting Tapes*, AFOSR HTS Coated Conductor Review (2004).

M. Majoros, A.M. Campbell, A. Glowacki, P.N. Barnes, G.A. Levin, C.E. Oberly, and M. Polak, *AC Losses in YBCO Coated Conductors*, AFOSR HTS Coated Conductor Review (2004).

P.N. Barnes, G. A. Levin, M. Polak, N. Amemiya, C.V. Varanasi, *AC Loss reduction of striated YBCO*, AFOSR HTS Coated Conductor Review (2005).

P.N. Barnes, J.W. Kell, T.J. Haugan, T.A. Campbell, S. Sathiraju, C.V. Varanasi, *Minute doping of YBCO with Ce and Tb for flux pinning*, AFOSR HTS Coated Conductor Review (2005).

S. Sathiraju, P.N. Barnes, *Growth of Oxide and Metallic Buffers for Coated Conductor Applications*, AFOSR HTS Coated Conductor Review (2005).

C.V. Varanasi, N. Yust, P.N. Barnes, *Biaxially textured Cu-alloy substrates Buffer Layer Growth*, AFOSR HTS Coated Conductor Review (2005).

T.J. Haugan, T. A. Campbell, J. M. Evans, J. W. Kell., C. V. Varanasi, S. Sathiraju, G. Levin, I. Maartense, T. Peterson, F. Meisenkothen, R. Wheeler, M. Sumption, C. Civale, B. Maiorov, T. Kiss, W. Wong, L.P. Cook, A. Goyal, A. Gapud, S. Kang, L. Heatherly, M. Rupich, *Nanoparticle additions to YBCO to increase $I_c(B, \theta, T)$* , AFOSR HTS Coated Conductor Review (2005).

J. Wu, T.J. Haugan, P.N. Barnes, *Alternatives to YBCO*, AFOSR HTS Coated Conductor Review (2005).

C. Kwon, G.A. Levin, T.J. Haugan, P.N. Barnes, *Scanning laser microscopy of striated CCs*, AFOSR HTS Coated Conductor Review (2005).

G. A. Levin, P. N. Barnes, S. Sathiraju, M. Sumption, A. Contractor, S. Kawabata, *Reduction of Coupling Losses in Superconductor – Resistor – Superconductor (Hybrid) Wires*, AFOSR HTS Coated Conductor Review (2005).

ASM-International Materials conference

C. V. Varanasi, Yust, D. P. N. Barnes, R. Srinivasan, *Biaxially Textured Copper and Copper Alloy Substrates for use in HTS Coated Conductors*. N. A., ASM-International Materials conference

US - Japan AC Loss Workshop

G.A. Levin, P.N. Barnes, N. Amemiya, S. Kasai, K. Yoda, and Z. Jiang, *Magnetization Losses in Multiple Coated Conductors*, US - Japan AC Loss Workshop, (2004).

N. Amemiya, S. Kasai, K. Yoda, Z. Jiang, G.A. Levin, P.N. Barnes, C.E. Oberly, *AC-Loss Measurement – III and Simulation*, US - Japan AC Loss Workshop, (2004).

P.N. Barnes, G.A. Levin, M.D. Sumption, M. Polak, *AC Loss Structures in HTS Coated Conductors*, US - Japan AC Loss Workshop, (2004).

M.D. Sumption, T. Haugan, P. Barnes, *Coated Conductors at High Frequencies*, US - Japan AC Loss Workshop, (2004).

12th Symposium on Electromagnetic Launch Technology

P.N. Barnes, G.L. Rhoads, J.C. Tolliver, M.D. Sumption, and K.W. Schmaeman, *Compact, Lightweight Superconducting Power Generators*, 12th Symposium on Electromagnetic Launch Technology, (2004).

Ohio Superconductivity Outreach Workshop Sponsored by U.S. Department of Energy

T. Haugan, *High-Temperature Superconductors: AFRL Programs and In-house Research*, (2004).

Wire Development Workshop sponsored by the DOE's Superconductivity for Electric Systems Program

P.N. Barnes, T. Haugan, *High-Temperature Superconductors: AFRL Programs and In-house Research*, (2005).

G. A. Levin, P. N. Barnes, S. Sathiraju, M. Sumption, *AC losses in multifilament coated conductors; Hybrid conductor option*, (2005).

P.N. Barnes, *Conductor Engineering for Military Applications*, (2005).

P.N. Barnes, G.A. Levin, M. Polak, N. Amemiya, and C.V. Varanasi, *AC Loss reduction of striated YBCO*, (2005).

Multi-University Research Initiative Workshop

P.N. Barnes, *AF User Challenges for the YBCO Coated Conductors*, (2004).

M.D. Sumption, E.W. Collings, P.N. Barnes, G.A. Levin, T.J. Haugan, *AC Loss Considerations for YBCO Coated Conductors*, (2004).

International Workshop on Coated Conductors for Applications

N. Amemiya, K. Yoda, S. Kasai, Z. Jiang, P. N. Barnes, G. A. Levin, C. E. Oberly, *Experimental and numerical studies on AC loss characteristics of Multifilamentary YBCO coated conductors*, International Workshop on Coated Conductors for Applications, (2004).

P.N. Barnes, T.J. Haugan, T.A. Campbell, and S. Sathiraju, *Controlled nanoparticulate flux pinning structures in YBCO*, International Workshop on Coated Conductors for Applications, (2004).

PACRIM 6 Conference

P.N. Barnes, J.W. Kell, T.J. Haugan, C.V. Varanasi, and M.F. Locke, Minute doping ($x < 0.01$) of $Y_{1-x}RE_xBa_2Cu_3O_{7-y}$ films with Ce and Tb for magnetic flux pinning, (2005).

T. Haugan, P. N. Barnes, T. A. Campbell, M. F. Locke, N. Pierce, I. Maartense, *Nanoparticle Additions to Increase $J_c(B, T, \theta)$ Performance of YBCO Films*, (2005).

T. Haugan, P. N. Barnes, T. A. Campbell, M. F. Locke, N. Pierce, S. Sathiraju, I. Maartense, F. Meisenkothen, R. Wheeler, H.E. Smith, T. Aytug, M. Paranthaman, K. J. Leonard, H. Y. Zhai, M.S. Bhuiyan, E.A. Payzant, A. Goyal, S. Sathiyamurthy, D.B. Beach, P.M. Martin, D.K. Christen, X. Li, T. Kodanthanh, U. Schoop, M. W. Rupich, *Interfacial Reactions of YBCO Coated Conductor Composites and Effects on Flux Pinning and Device Properties*, (2005).

International Cryogenic Materials Conference (ICMC)

C. V. Varanasi, C. Leon, A. D. Chaney, N. A. Yust, P. N. Barnes, Tensile Strength Testing of Copper Alloy Substrates for Use in Coated Conductors (Poster), (2005).

C. V. Varanasi, P. N. Barnes, J. Burke, T. Haugan, Particulate pinning centers in $YBa_2Cu_3O_{7-x}$ films introduced during pulsed laser deposition, (2005).

G. A. Levin and P. N. Barnes, The Integration of YBCO Coated Conductors into Magnets and Rotating Machinery, (2005).

C. Varanasi, P.N. Barnes, Jack Burke, Lyle Brunke, Harry Efstathiadis, Copper alloy substrates for coated conductors to be used in AC and DC applications, (2005).

B. Craig Harrison, H. Fang, J. Carpenter, Patrick Klenk, P. N. Barnes, C. V. Varanasi, *Sm and Nd Substitutions in YBCO Films Produced Through Metal Organic Deposition*, (2005).

J.M. Evans, B.C. Harrison, K.W. Schmaeman, M.F. Locke, T.J. Haugan, P.N. Barnes, *Properties of $(Y_{1-x}RE_x)_{1+y}Ba_2-yCu_3O_{7-z}$ Bulk Superconductors for Flux Pinning*, (2005).

N. Amemiya, K. Yoda, Z. Jiang, G.A. Levin, P.N. Barnes, C.E. Oberly, Structure of Multifilamentary YBCO Coated Conductors and their Magnetization Loss Characteristics, (2005).

P.N. Barnes, J.W. Kell, T.J. Haugan, M.F. Locke, and C.V. Varanasi, *Rare earth doping of YBCO films at minute levels for magnetic flux pinning*, (2005).

P.N. Barnes, G.A. Levin, M.D. Sumption, and M. Polak, *Striated YBCO coated conductor with filamentary current sharing*, (2005).

T.J. Haugan, P.N. Barnes, T.A. Campbell, M.F. Locke, N. Pierce, I. Maartense, M.D. Sumption, *Addition of Nanoparticle Dispersions to Enhance $J_c(B, T, \theta)$ Properties of YBCO Films*, (2005).

T.J. Haugan, T.A. Campbell, P.N. Barnes, J.W. Kell, I. Maartense, K.W. Schmaeman, *Flux Pinning Properties of $(Y_{1-x}RE_x)Ba_2Cu_3O_{7-d}$ Thin Films: $RE = Er, Eu$* , (2005).

S. Srinivas, A. Chaney, P.N. Barnes, C.V. Varanasi, *Metallic buffers for coated conductor applications*, (2005).

Korea Superconductor Society KSS2005

C. V. Varanasi, P.N. Barnes, T. Haugan, Particulate pinning centers in $YBa_2Cu_3O_{7-x}$ films during pulsed laser deposition and Biaxially Textured Copper Alloy Substrates, (2005).

DOE Peer Review 2005

P. Barnes; C.V. Varanasi, Fundamental studies of magnetic flux pinning mechanisms; Development of striated filaments of YBCO conductor, (2005).

European Conference on Applied Superconductivity

M. Polak, L. Krempasky, E. Usak, L. Jansak, E. Demencik, G. Levin, P. Barnes, D. Wehler. B. Moenter, *Coupling losses and transverse resistivity of filamentary YBCO coated conductors*, (2005).

M. Majoros, B. A. Glowackia, A. M. Campbell, G. A. Levin, P. N. Barnes, *Transport AC losses in striated YBCO coated conductors*, (2005).

International Conference on Magnet Technology

M. Polak, E. Demencik, L. Jansak, P. Barnes, G. Levin, C. Thieme, Properties of a YBCO pancake coil operating with AC current at frequencies up to 1000 Hz, (2005).

International Symposium on Superconductivity

N. Amemiya, Z. Jiang, K. Yoda, G.A. Levin and P.N. Barnes, The Effects of filament width on magnetization loss of multifilamentary YBCO coated conductors, (2005).

Introduction 1.2: HTS Coated Conductor Development Issues What's Needed vs. What's Done

1.2.1 HTS Conductor Applications

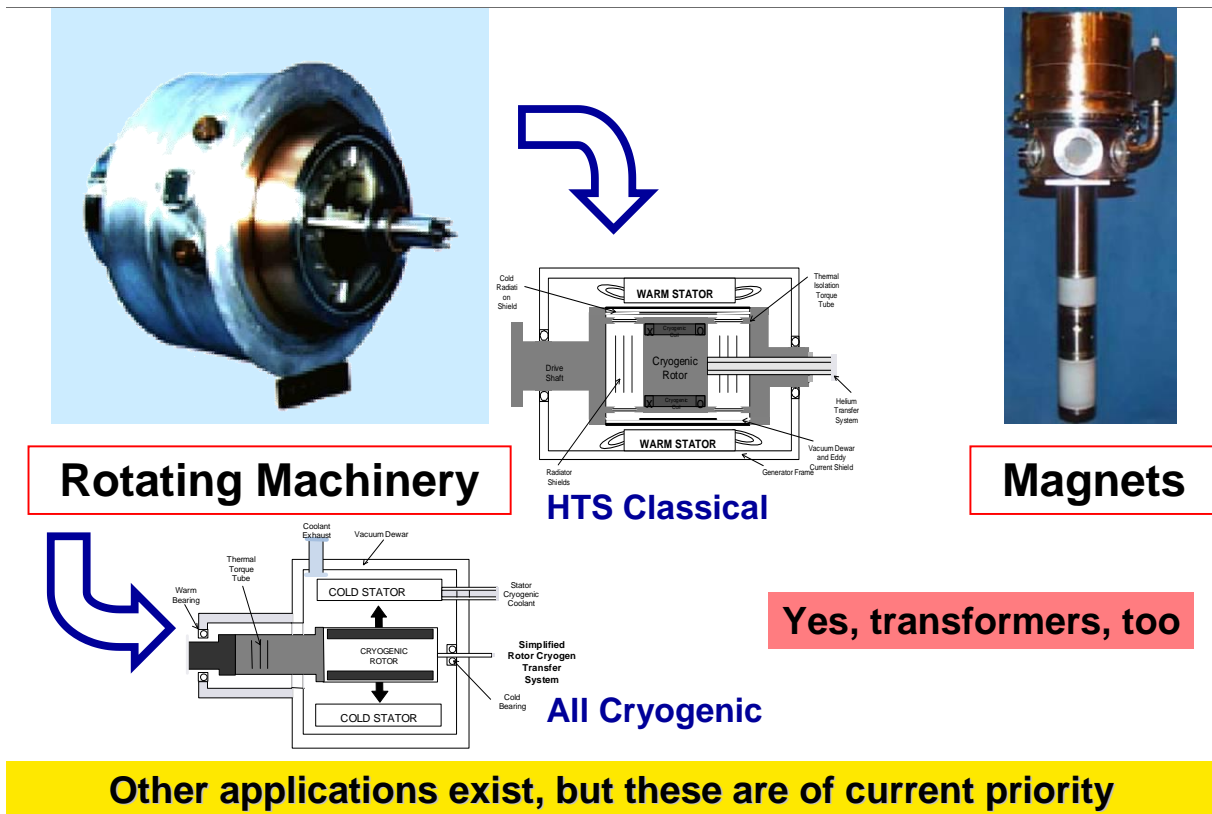


Figure 1.2.1.1

1.2.2 Conductor Environment

- Type of lengths needed 100's m to a few km length
- 100's Amps per conductor
- Rotation speeds 100's to 20,000 rpm
 - Rotor tip speeds up to couple hundred m/s
 - AC fields of 100's to a couple thousand Hz
- Magnetic fields of several Tesla
- Voltages up to kV levels
- Engineering current densities up to 10,000's A/cm²
- Losses <100 Watts/MW power
This is a sampling only

1.2.3 Semi-realistic Holy Grail

- Insulation/Passivation
- HTS layer
- Conducting Buffer
- Metallic Substrate

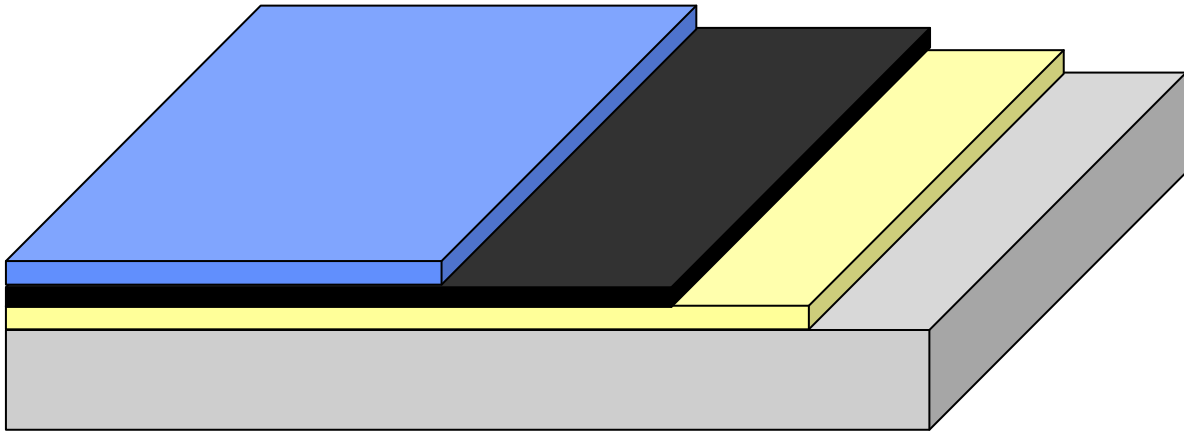


Figure 1.2.2.1

1.2.4 Proprietarily Speaking

- Companies have certain licenses and not others and this will influence choice regardless of merits
 - Must live with these choices and develop accordingly
 - Multiple methods may have unique advantages
- As long as the process remains competitive each must be developed
 - Multiple companies as opposed to a monopoly is advantageous (look at Intel vs. AMD)

1.2.5 The Basics

- The issues for HTS conductors are generally known
 - Occasionally a new issue may arise
- The questions are:
 - How to resolve the issue?
 - When to focus on it?
 - All issues can/should be worked on, but not a focus
 - Example: AC loss always known, but now a focus
 - Who should do it (never exclusive, just who is prime)?
 - Industry should concentrate on ...
 - Laboratories should concentrate on ...

1.2.6 Standard Process

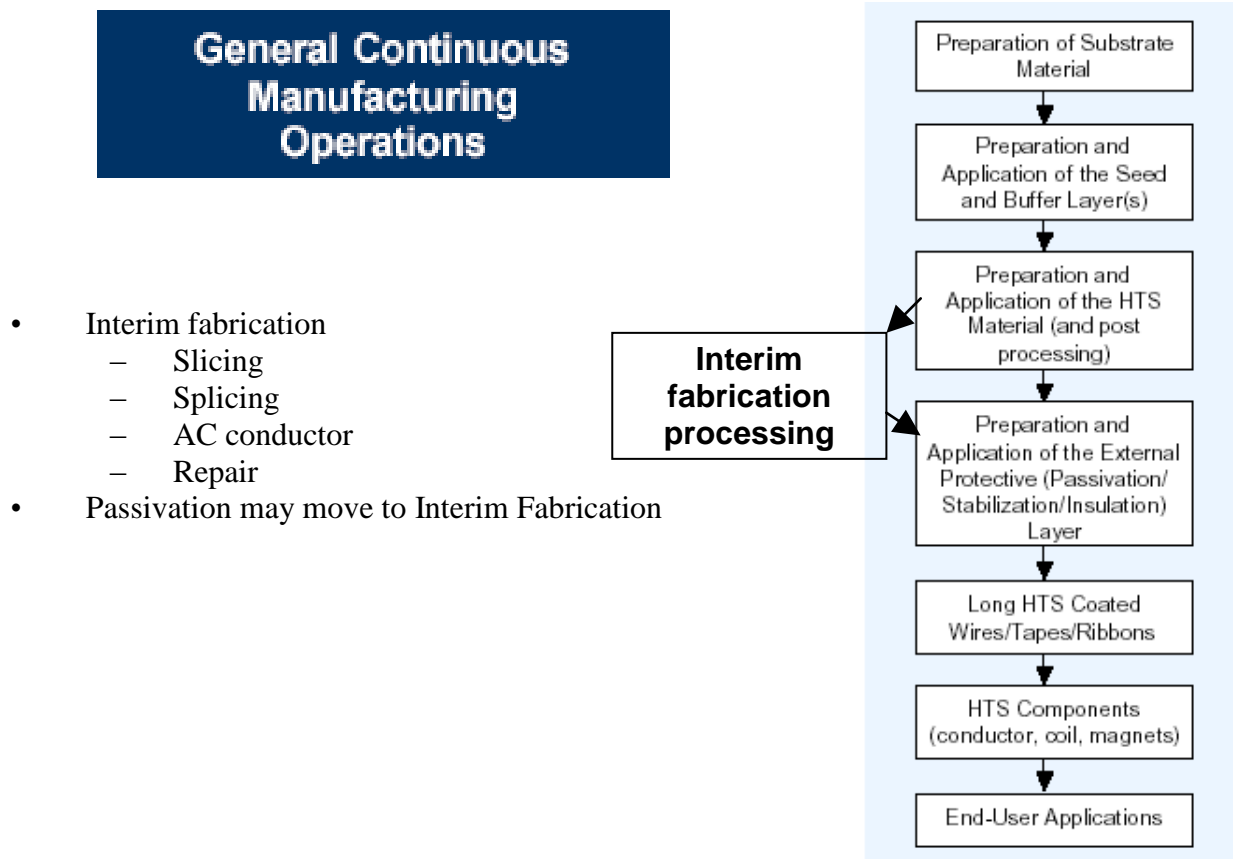


Figure 1.2.3.1

1.2.7 Fabrication Pathways

Coated Conductor Development Activities

- Process Monitoring and Control
 - Strategies/Methods are severely lacking
 - Emphasis is on real-time characterization
- When a given process is set, the time is now
- So, are we behind?

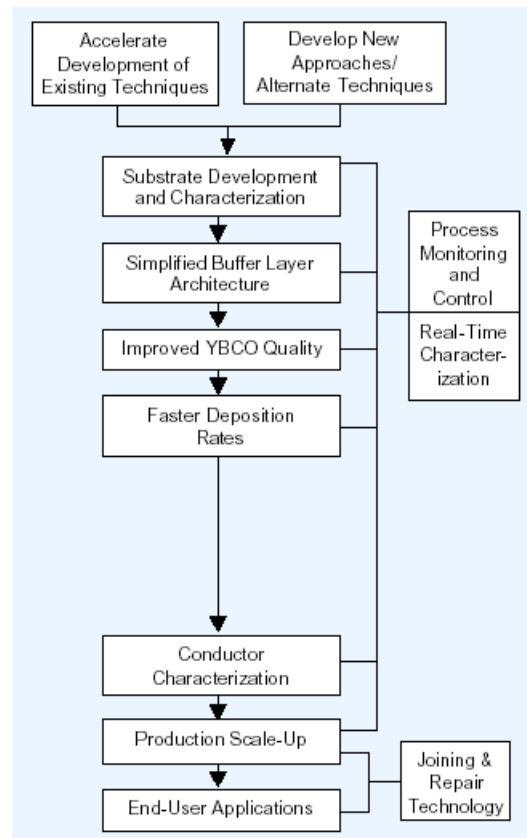


Figure 1.2.4.1

1.2.8 Substrate

- Metallic grains (deformation texturing process)
 - Minimization of high angle grain boundaries
 - Control of grain size (relation to conductor width)
- Non-magnetic
- Low eddy current losses
- Importance of surface roughness (IBAD and ISD vs. RABiTS)
- Thinner (higher J_c)
- Non-flat?

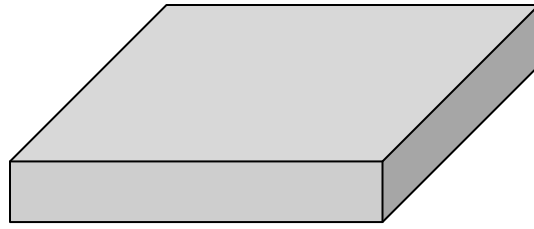


Figure 1.2.5.1

1.2.9 Buffer – Seed Layer

- Elimination is best
- Speed of deposition (if initial texture is here – IBAD or ISD)
 - Better oxide
 - Alternate for oxide (metals and nitrides)
- If metal overlayer, consideration of loss effects

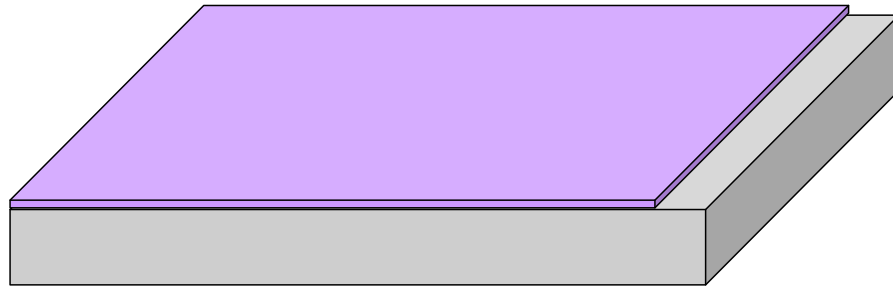


Figure 1.2.6.1

1.2.10 Buffer – Diffusion Barrier

- Conducting Buffers (both electrically and thermally)
 - Oxides or Nitrides?
 - Something else?
- Reduction in thickness (how much is enough) – cost issue
 - Increase deposition rate
 - Single buffer

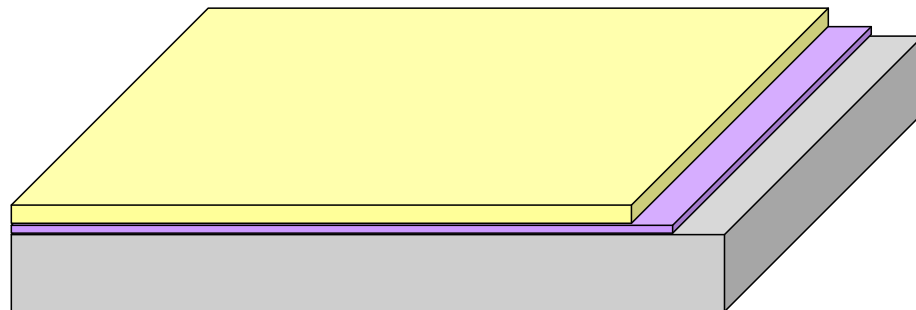


Figure 1.2.7.1

1.2.11 Buffer – Cap Layer

- Elimination is best

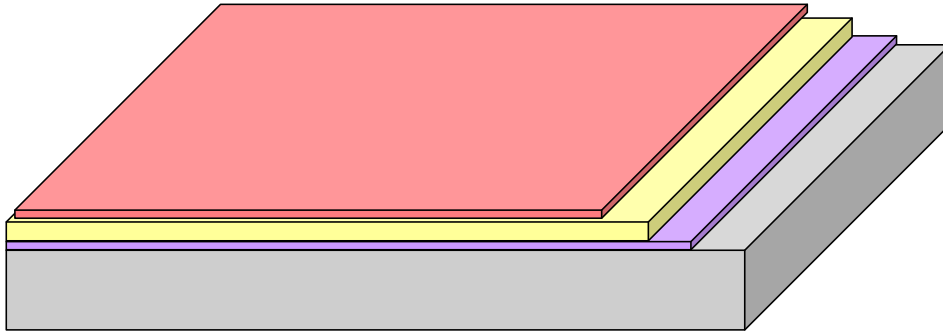


Figure 1.2.8.1

1.2.12 HTS – YBCO Deposition

- Higher J_c (for higher J_e)
 - Improved Flux Pinning (inclusions, substitutions, or voids)
 - Thicker Film
- Intergranular connectivity (minimize “weak links”)

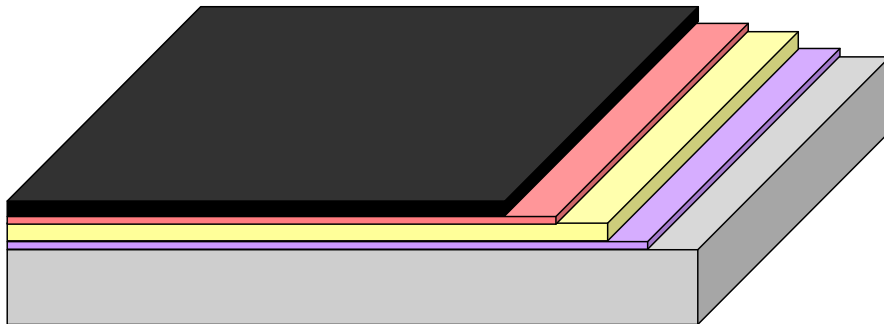


Figure 1.2.9.1

1.2.13 HTS – AC Loss Issues

- Filamentation – hysteretic loss reduction
- Coupling current losses (as a result of striated HTS layer)
 - Limit by twisting
- Barrier between filaments – conducting buffer pathways
 - High to minimize coupling current losses
 - Also a need for current sharing

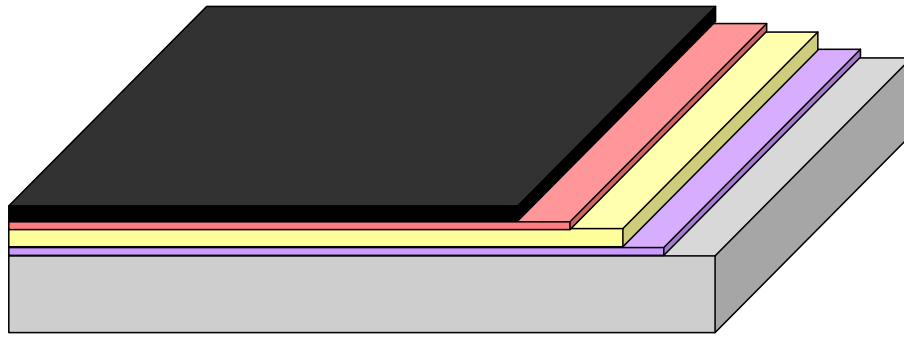


Figure 1.2.10.1

1.2.14 HTS – AC Loss Issues

- Filamentation
 - Twisting does not include interweaving the filaments
 - Sufficiently important for new methodologies?
- Self-field induced transport losses
 - Effect of high aspect ratio

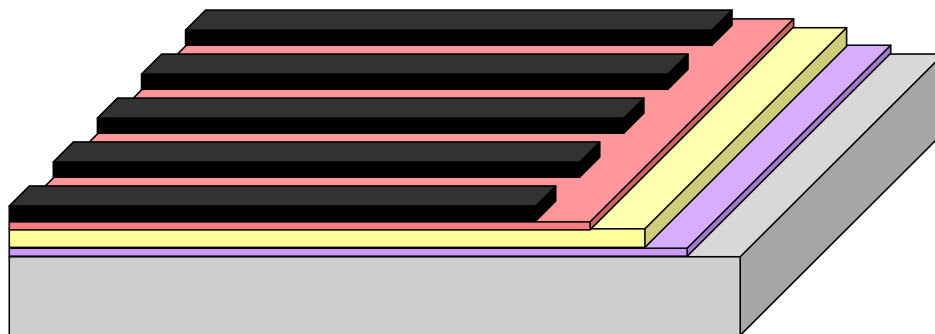


Figure 1.2.11.1

1.2.15 Passivation

- Silver only?
 - Thermally conductive

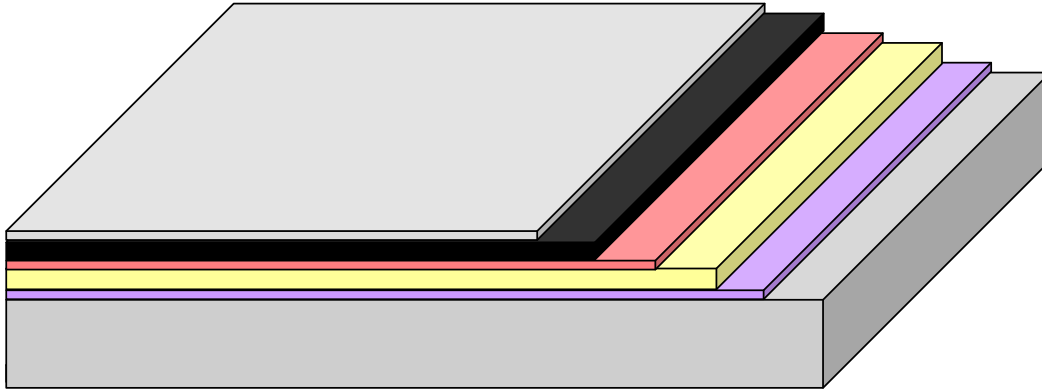


Figure 1.2.12.1

1.2.16 Passivation

- Filamentation of the Ag coating?

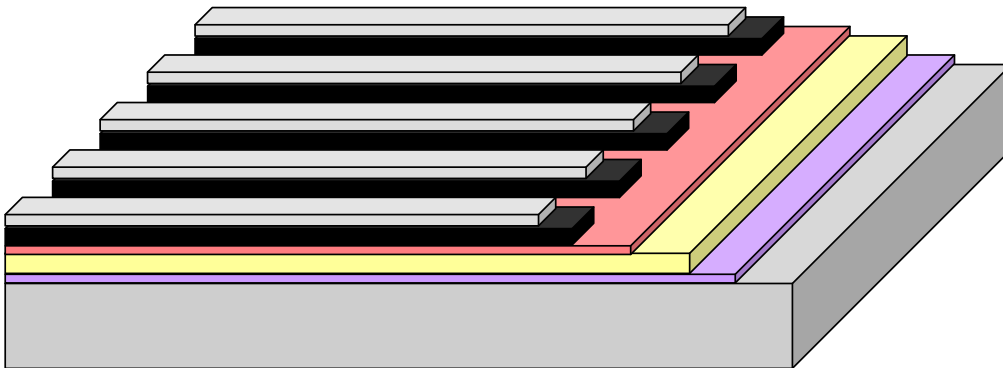


Figure 1.2.13.1

1.2.17 Stabilization

- Elimination via substrate and conducting buffers
- Other choices available?
 - Thermally and electrically conductive paths necessary

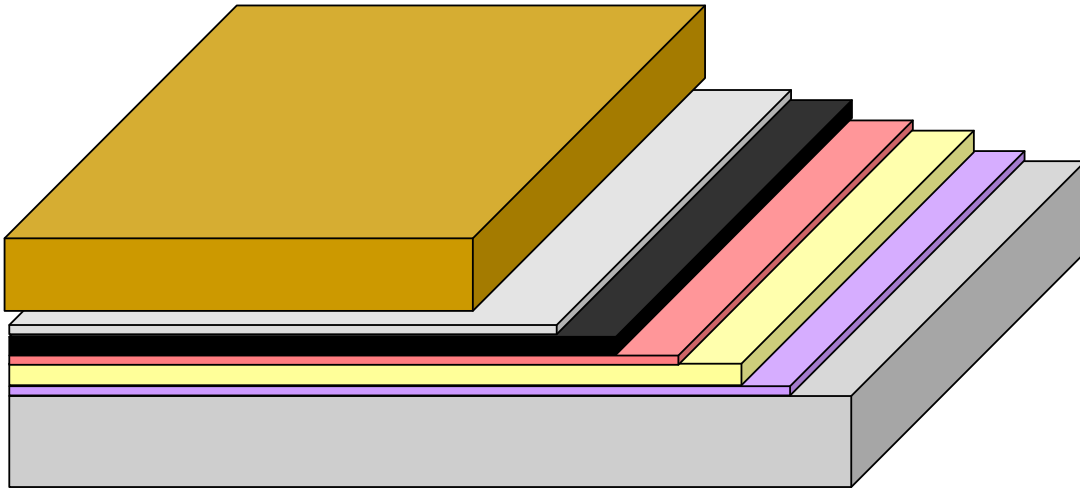


Figure 1.2.14.1

1.2.18 Insulation

- What thickness is sufficient
- Thermally conductive while electrically resistive

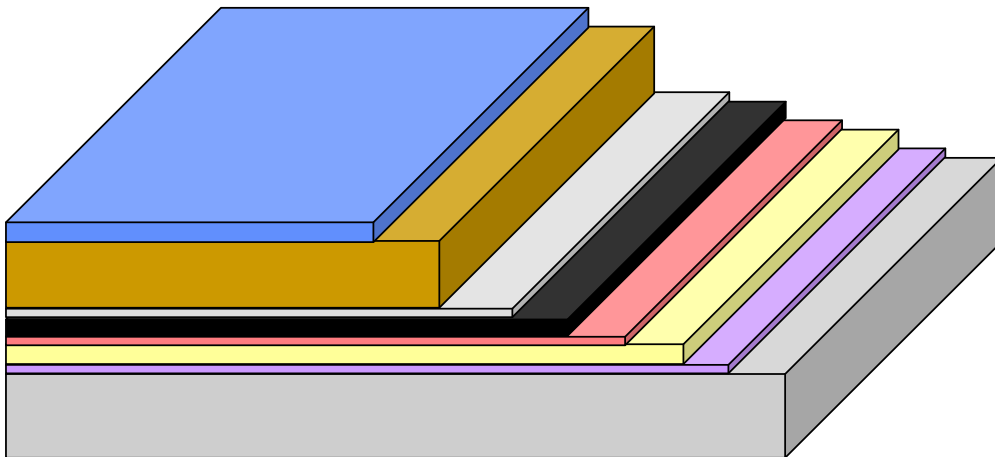


Figure 1.2.15.1

1.2.19 The Non-cryogenic Connection

- HTS coated conductor must connect to standard wire
 - low thermal diffusion desired
 - High electrical connectivity desired
- Protection of tape from centrifugal forces
 - Sufficient?
 - AMSC has steel clad BSCCO tapes
- Slitting issues
 - Minimization of damaged area

- Tape splicing issues – will this be an ultimately needed or desired technology?
- Repair– will this be an ultimately needed or desired technology?

1.2.20 HTS Conductor

- Defense examples
 - compact high field magnets (such as rf source magnets)
 - provides conductor that *enables* ground mobile and airborne high power requirements (MegaWatts)
 - naval electric drive with HTS motors and power generators
 - Transformers for power conversion
- Performance
 - AC Loss Issue much greater (at hi freq) – performance driven
 - Lightweight and compact systems requirement drives to high current density

YBCO Coated Conductor is required

1.2.21 Summary – Suggestions

- Laboratory Focus
 - High J_c -- Flux pinning mechanisms for improved in-field performance and thicker films
 - AC loss mechanisms and architectures
 - Physical architectures
 - Modeling efforts
 - Conducting buffer layers
- Industry Focus
 - Making successful lengths of YBCO coated conductor
 - Slicing of conductor
 - AC loss fabrication techniques

Chapter 2A: Layered Nanoparticulate Dispersions

The inclusion of second-phase Y_2BaCuO_5 (Y211) nanoparticles into $\text{YBa}_2\text{Cu}_3\text{O}_{7-x}$ (Y123) thin films was achieved by in-situ growth for the purpose of increasing superconducting films' magnetic pinning strength with the resultant improved in-field critical current densities. Pinning is optimized when the size of the defects approaches the superconducting coherence length ($\sim 2\text{--}4$ nm for YBCO at temperatures ≤ 77 K) and when the areal number density of defects is of the order of $(H/2) \times 10^{11} \text{ cm}^{-2}$, where H is the applied magnetic field in tesla. Such a high density has been difficult to achieve by material-processing methods that maintain a nanosize defect, except through irradiation. The Y211 particulate inclusion was accomplished by growing the Y123 layer and Y211 nanoparticles by multiple consecutive depositions with pulsed laser ablation of the respective targets on LaAlO_3 , SrTiO_3 or buffer-coated biaxially textured Ni or Ni-alloy substrates. Island growth of the Y211 was caused by lattice mismatching with the Y123 achieving a surface particle density on the order of 10^{11} cm^{-2} with typical Y211 particle size of $\sim 10\text{--}20$ nm in diameter and ~ 4 nm in height. Composite multilayer structures of (Y211 particles / Y123 layers) $\times N$ were grown with N bi-layers between 14 and 200, each bi-layer being several nanometers thick. Sufficient area of the underlying Y123 film was exposed to allow the subsequent epitaxial growth of the next Y123 deposition in the series. The Y123 phase maintained excellent epitaxy with high c -axis and good a/b in-plane orientation even with the presence of the Y211 particles. With the Y211 additions, the critical current densities increased 3 – 5 times at applied magnetic fields of 1.6 T from 30 to 77 K as compared to high quality Y123 films with no Y211 additions. The superconducting transition temperature was slightly depressed by $\sim 2\text{--}4$ K. Additionally, the investigation included observing the dependency of J_c on field strength and angle variations, as well as mechanical strength and crack resistance properties of the films.

2a.1 Advantages of $\text{YBa}_2\text{Cu}_3\text{O}_{7-\delta}$ Multilayer (211~2nm/123~10nm) $\times N$ Thin Film Architecture for Coated Conductor Applications

References: 1, 2

T. J. Haugan¹, P. N. Barnes¹, I. Maartense¹, R. M. Nekkanti¹, L. Brunke¹, J. M. Evans¹, J. P. Murphy¹, J. C. Tolliver¹, E. J. Lee², M. Sumption²

1. Air Force Research Laboratory, Wright-Patterson AFB, OH

2. Ohio State University, Columbus OH

Presented at the American Ceramic Society Annual Meeting Nashville, TN, April 2003

2a.1.1 Outline

Flux Pinning by (211/123) $\times N$ Multilayers

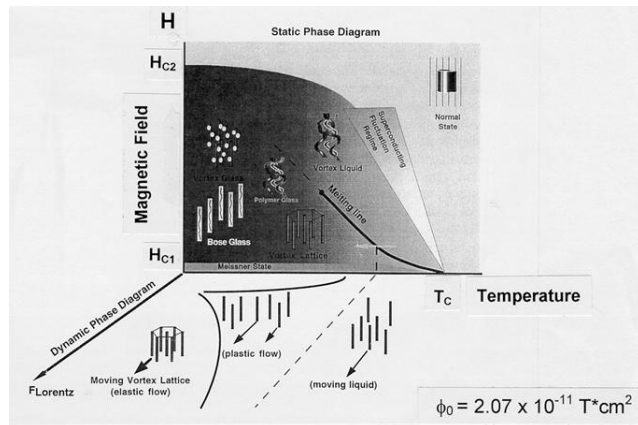
- Pinning Theory
- Experimental
- Microstructural Characterization
- Superconducting Properties
- Deposition on RABIT's substrates

Other Advantages of (211/123) $\times N$ Multilayers

- Surface Smoothness

- Isotropic Field Dependence (?)
- Crack Resistant Conductor (?)

2a.1.2 Flux Pinning



“New Research Opportunities in Superconductivity IV”,
edited by B. J. Batlogg, et al. August 1997

Figure 2a.1.2.2

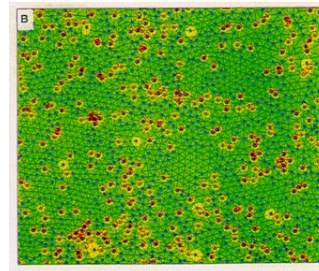


Figure
2a.1.2.1

H. Dai, S. Yoon, J. Liu, R. Budhani, C. M. Lieber,
Science 265, 1552 (1994)

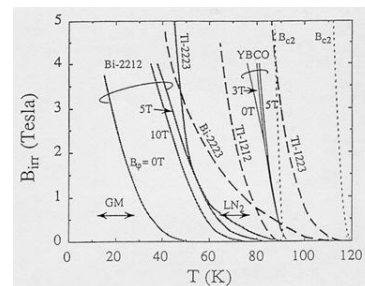


Figure
2a.1.2.3

“Processing and Properties of High-T_c Superconductors,”
edited by S. Jin, (World Scientific, Singapore, 1993).

2a.1.3 Flux Pinning Theory

The defect number density goal (surface area):

$$\approx M/2 \times 10^{11}/\text{cm}^2; \text{ for } M \text{ applied field (T)}$$

Density of Defects (linear):

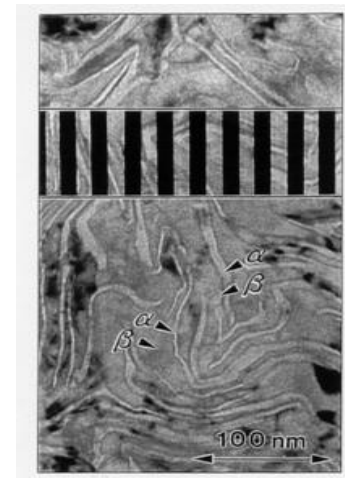
$$\approx 5 \times 10^5/\text{cm}, \approx 5 \text{ per } 100 \text{ nm spacing}$$

Size of Defects: $\xi_c \approx 2\text{nm}_{4.2\text{K}} - 4\text{nm}_{77\text{K}} < x < 10\text{--}20 \text{ nm}$

Smaller defect size allows higher superconductor volume %

2a.1.4 Y-211 Advantages

- Y-211 chemically compatible with Y-123
- no chemical diffusion or reduction of T_c,
- multilayer crystallinity expected to be maintained,
- 211/123 interface very sharp, which is best for pinning
- Y-211 deposition conditions exactly same as Y-123
- 211:123 lattice mismatch is (2-9)% which promotes island growth of 211 on 123



Flux pinning defects (~) in low temperature superconductors
(β) and optimal spacing required to pin a 5 T field (bars).
D. C. Larbalestier and M. P. Maley, MRS Bulletin Aug.
(1993) P. 50.

Figure 2a.1.4.1

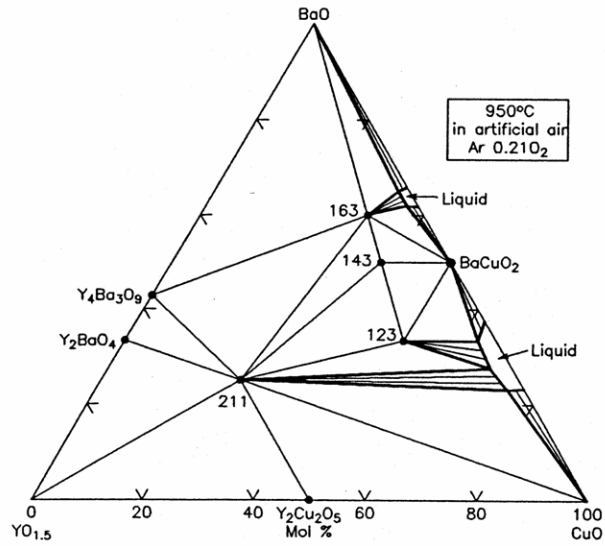


Figure 2a.1.4.1

2a.1.5 Multilayer Particulate Defects

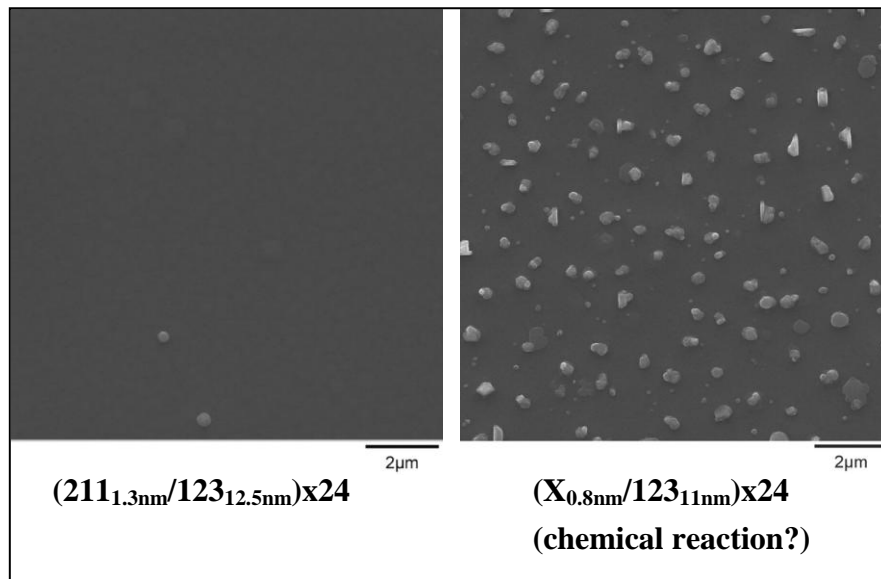


Figure 2a.1.5.1

2a.1.6 'Soft' Flux Pinning

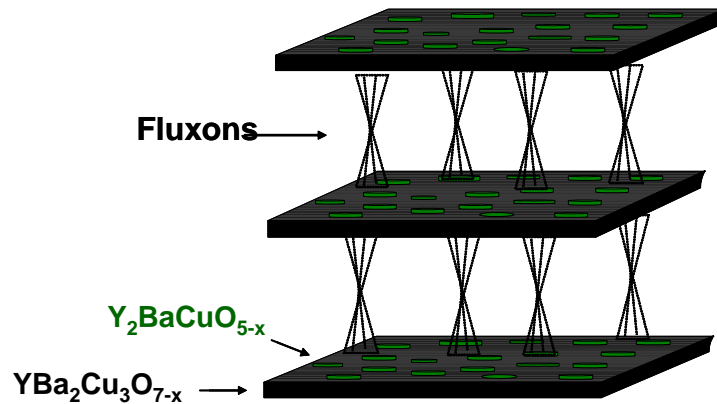


Figure 2a.1.6.1

2a.1.7 Experimental Layers Deposited by PLD

- O_2 pressure = 300 mTorr
 - Deposition rate = 15 nm/min
 - Interval of ~ 12 seconds between 211 and 123 layers
 - Laser hz = 4 to 16
- J_c by VSM magnetization and transport methods;
 - $J_{cm} = 15 \Delta M/Vol$,
 - J_{ct} by $1 \mu v/cm$ criteria.

(211/123)xN Architecture

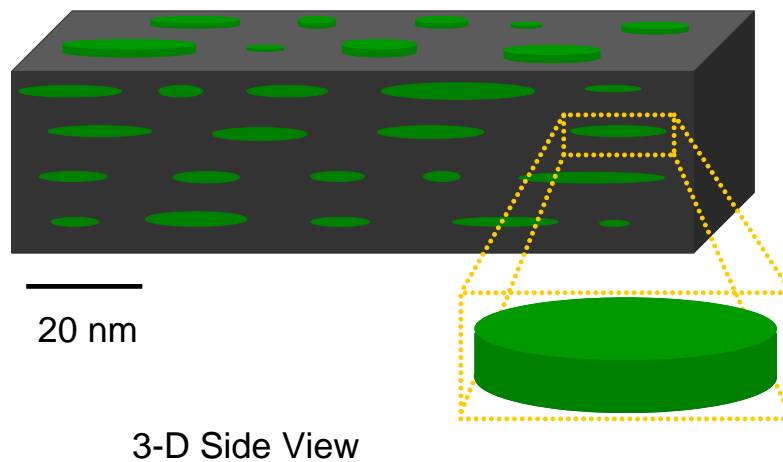
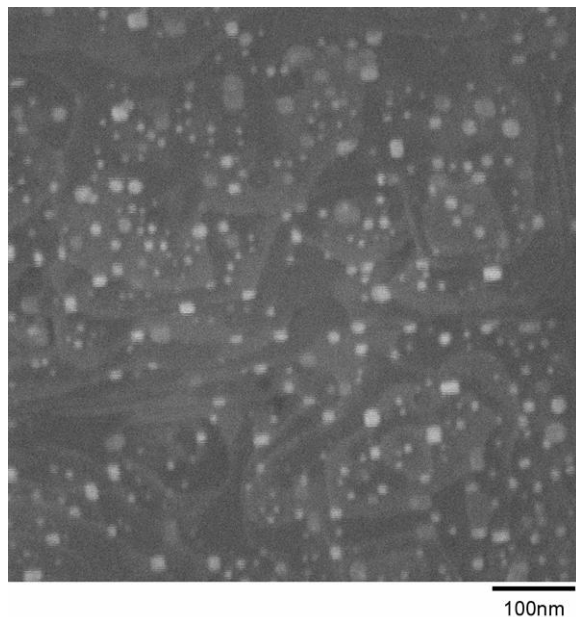


Figure 2a.1.7.1

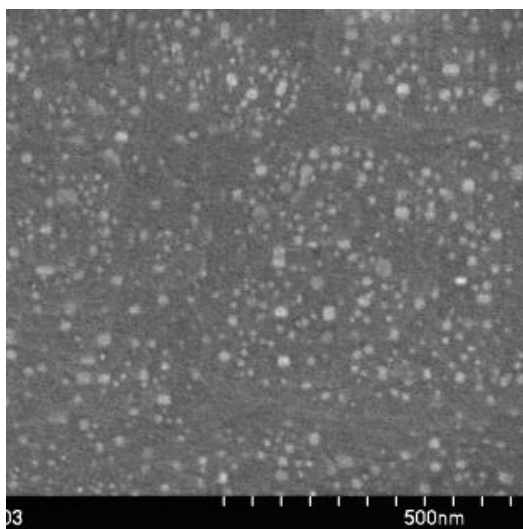
2a.1.8 Surface Nanoparticles



(211~1.2 nm/123~11 nm)x92

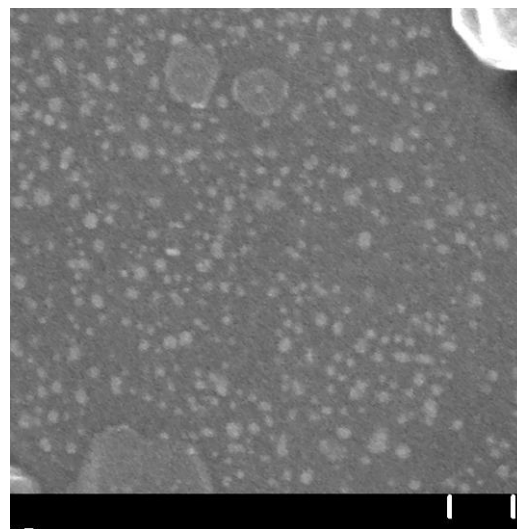
Avg. Particle Size ~ 14 nm,
Particle Density ~ $1.3 \times 10^{11} \text{ cm}^{-2}$

Figure 2a.1.8.1



(211~0.9 nm/123~5.5 nm)x35

Figure 2a.1.8.2



(211~1.6 nm/123~10 nm)x94

Figure 2a.1.8.3

TEM X-Sections



Figure 2a.1.8.4 $(X_{0.8nm}/123_{11nm}) \times 24$



Figure 2a.1.8.5 $(X_{0.8nm}/123_{11nm}) \times 24$

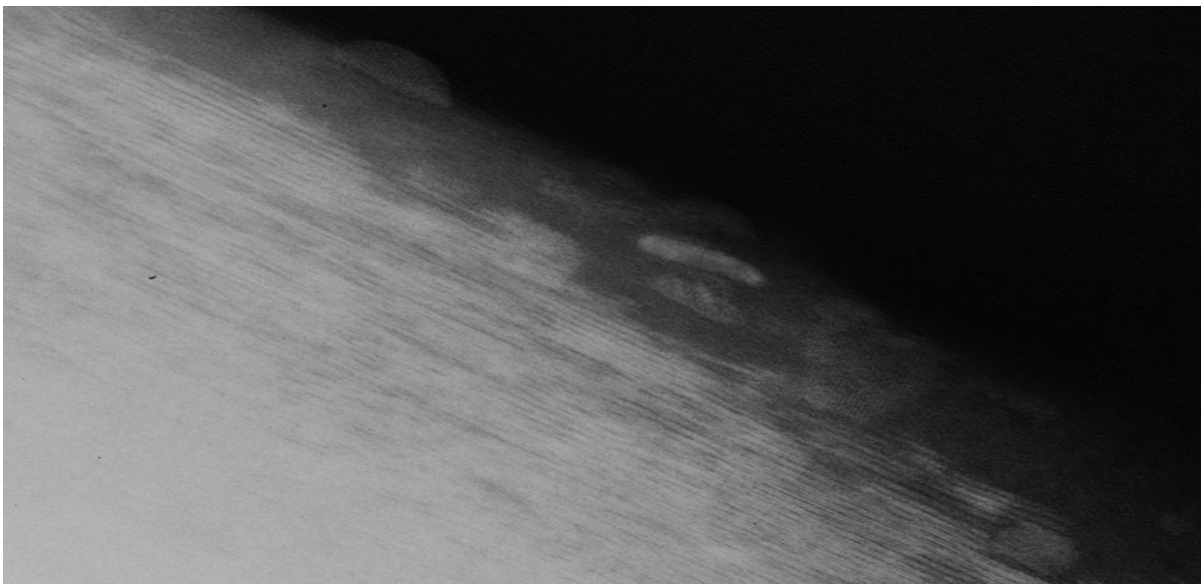


Figure 2a.1.8.6

2a.1.9 TEM Planar View

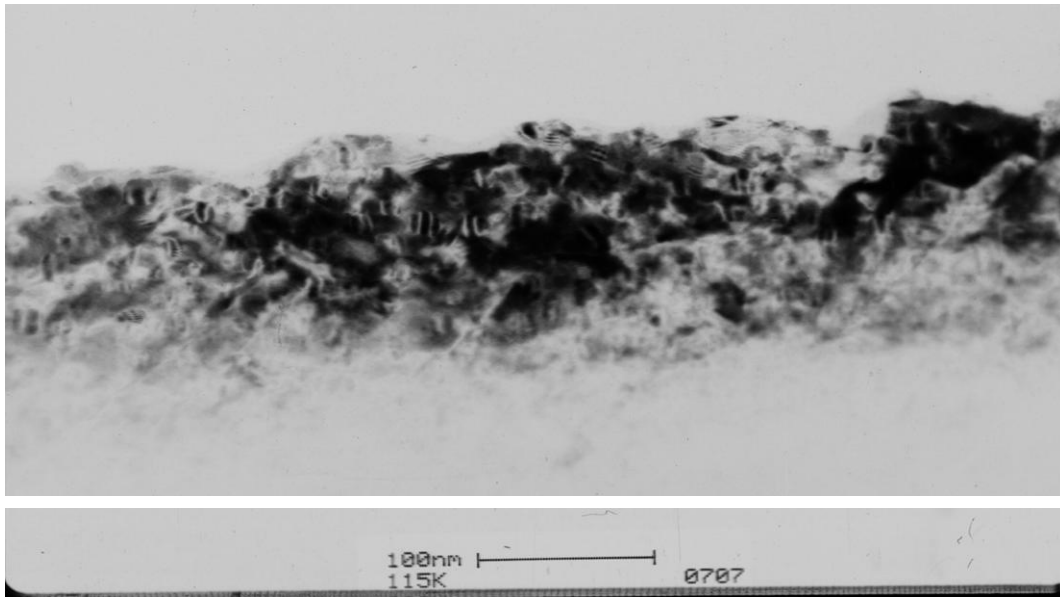


Figure 2a.1.9.1

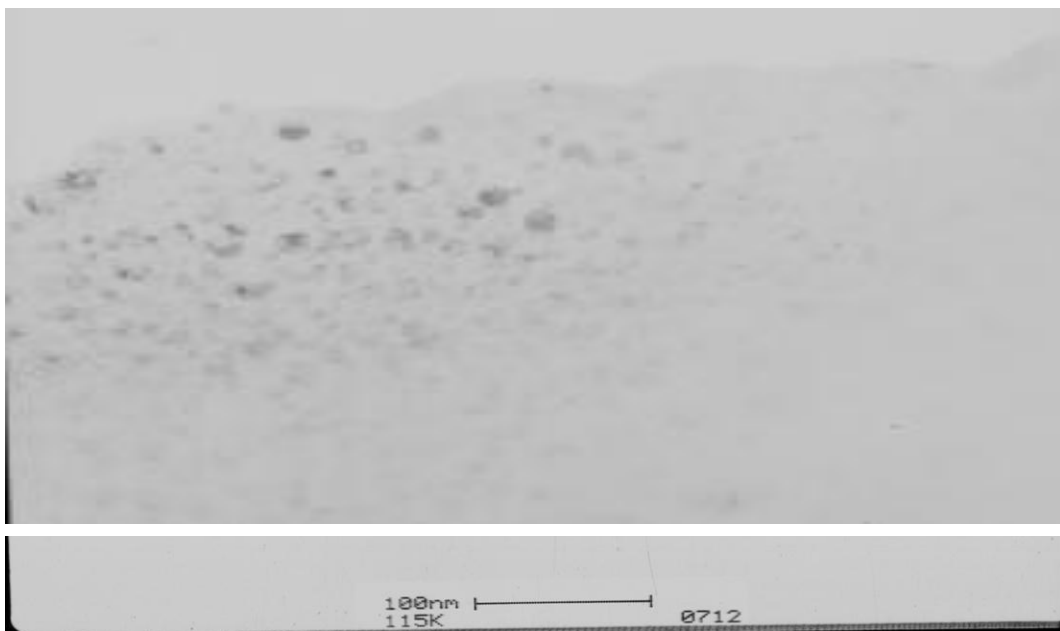
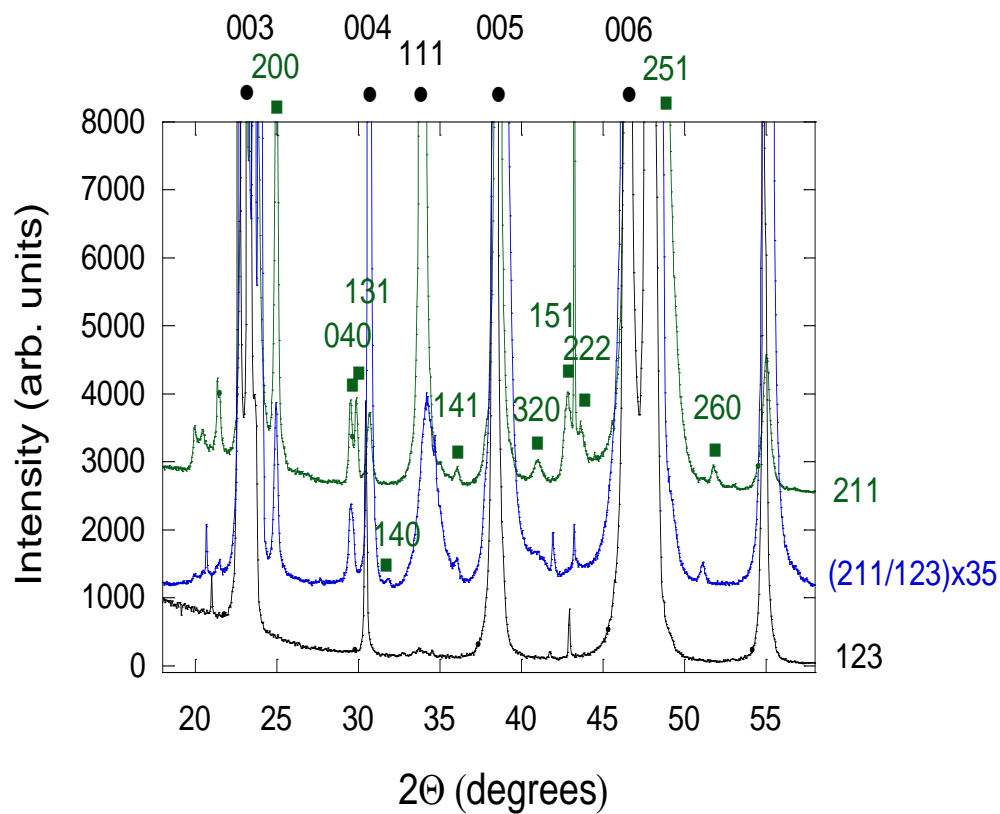


Figure 2a.1.9.2

2a.1.10 XRD Two-theta



211 in multilayers is primarily a00 or 0b0 orientation

Figure 2a.1.10.1

XRD Phi Scans

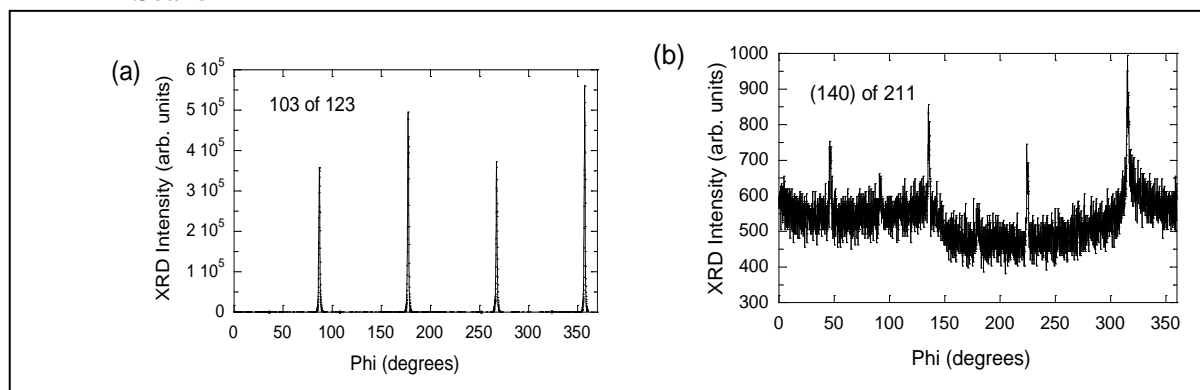


Figure 2a.1.10.2

2a.1.11 T_c by AC Susceptibility

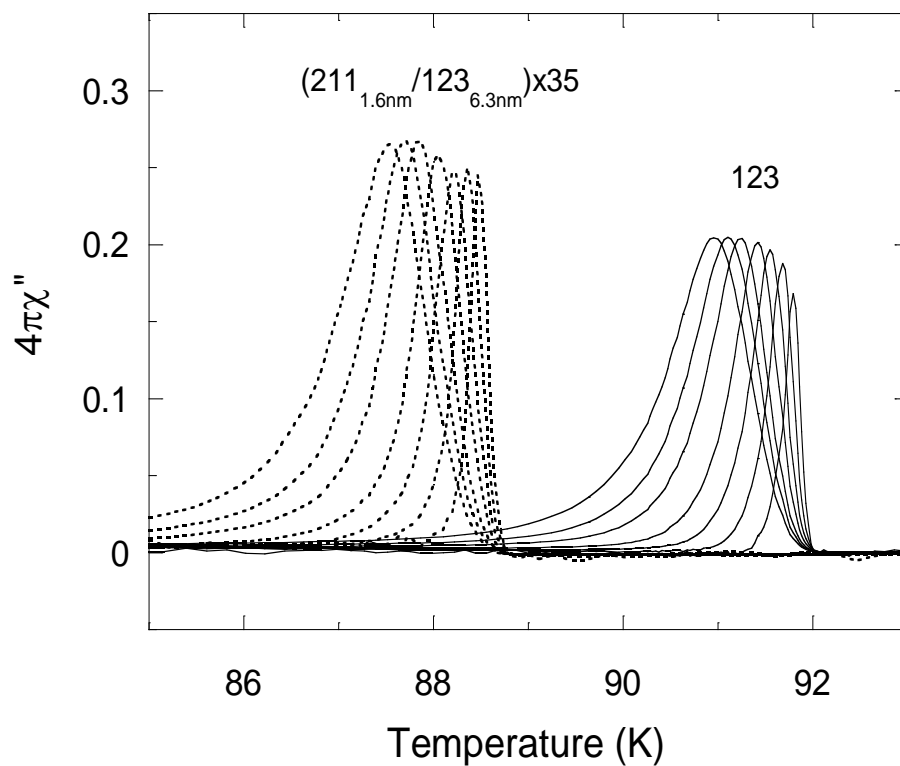


Figure 2a.1.11.1

2a.1.12 T_c Transition

For decreasing Y123 thickness or increasing Y211 thickness, the T_c was reduced and T_c FWHM ($\sim \text{const} / J_c$) was increased.

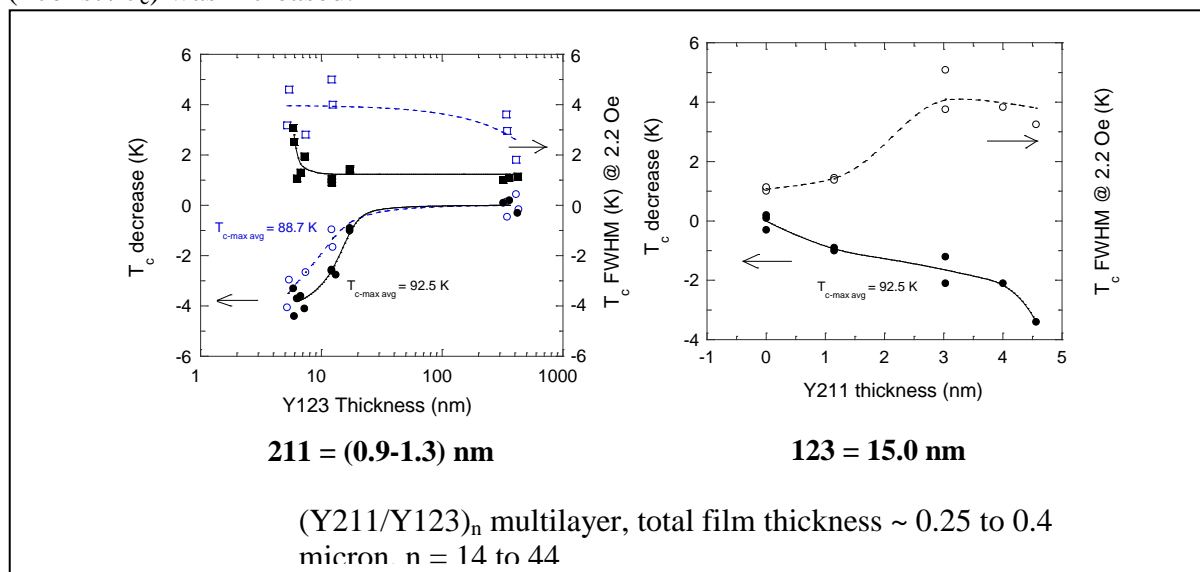
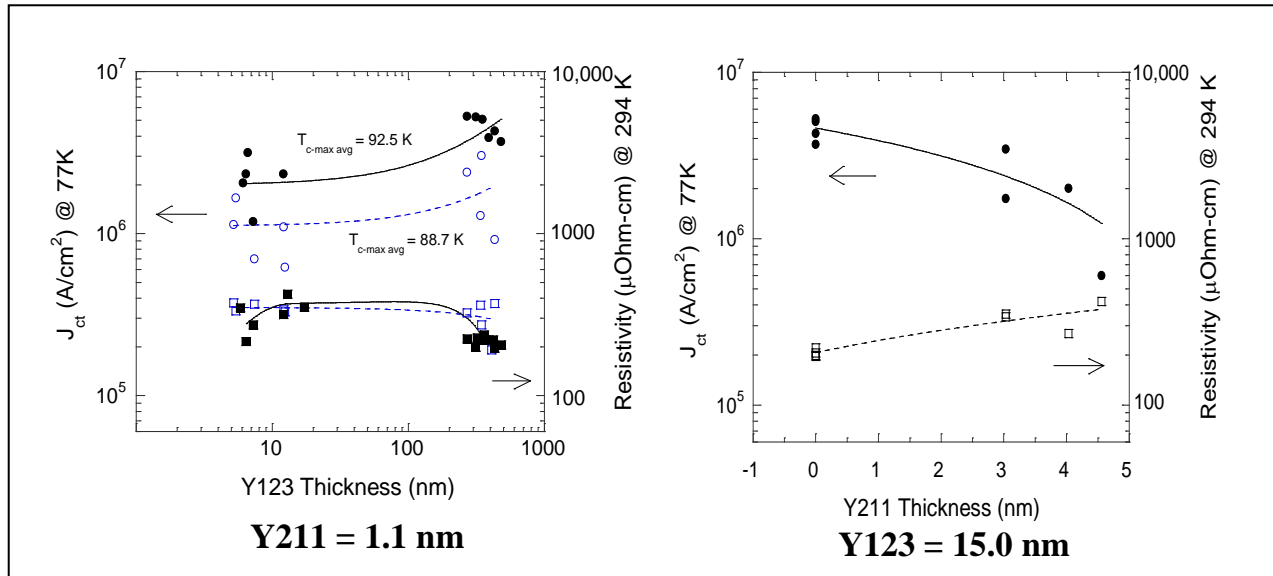


Figure 2a.1.12.1

2a.1.13 Transport Properties

For decreasing Y123 thickness or increasing Y211 thickness, the J_c and 294 K Resistivity were reduced.



$(Y_{211}/Y_{123})_n$ multilayer, total film thickness ~ 0.25 to 0.4 micron, $n = 14$ to 44

Figure 2a.1.13.1

2a.1.14 60 K Specific Improvement

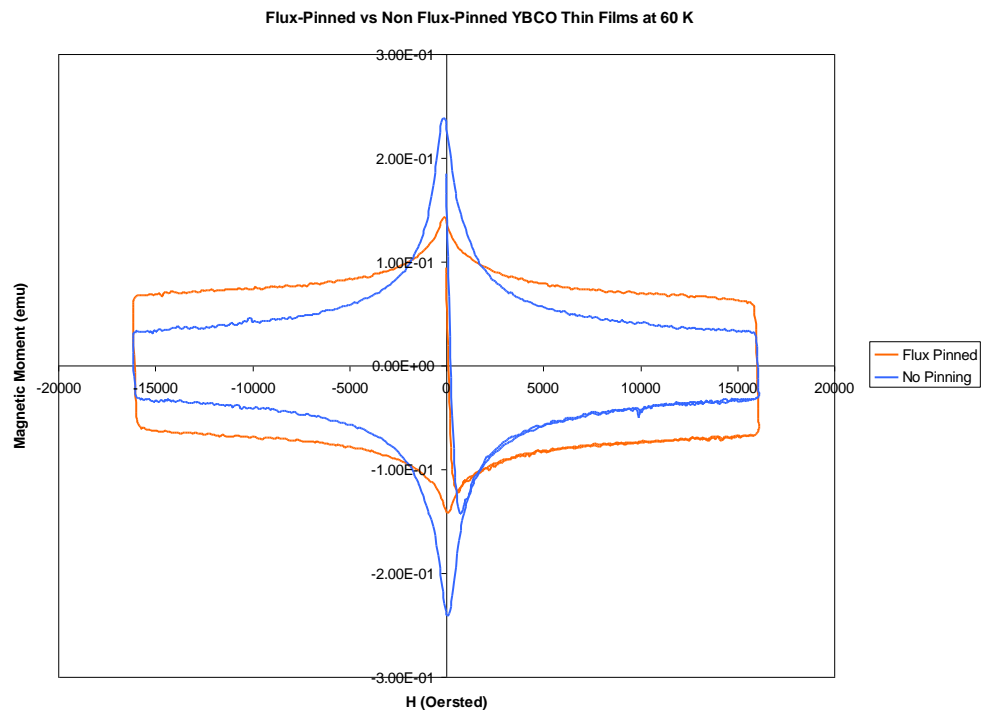


Figure 2a.1.14.1

2a.1.15 Magnetic J_c

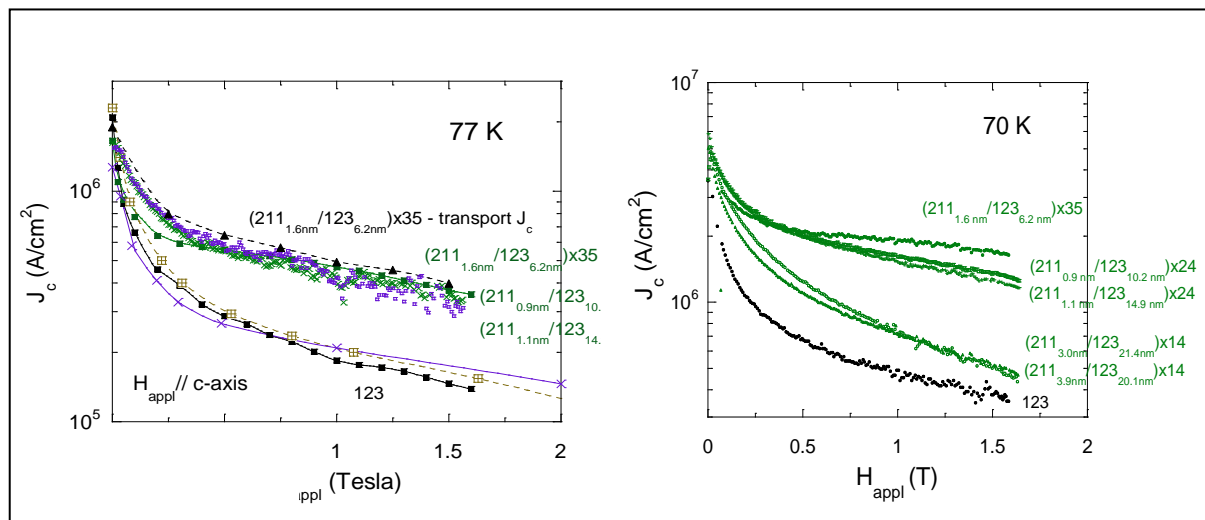


Figure 2a.1.15.1

2a.1.16 Temperature Dependence of J_c

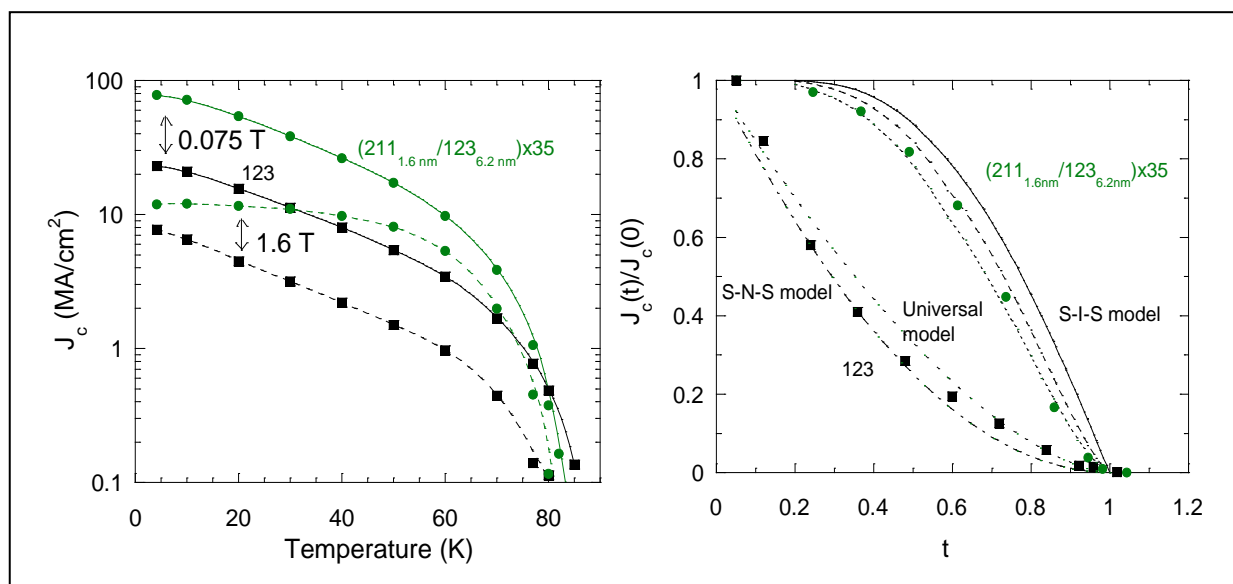
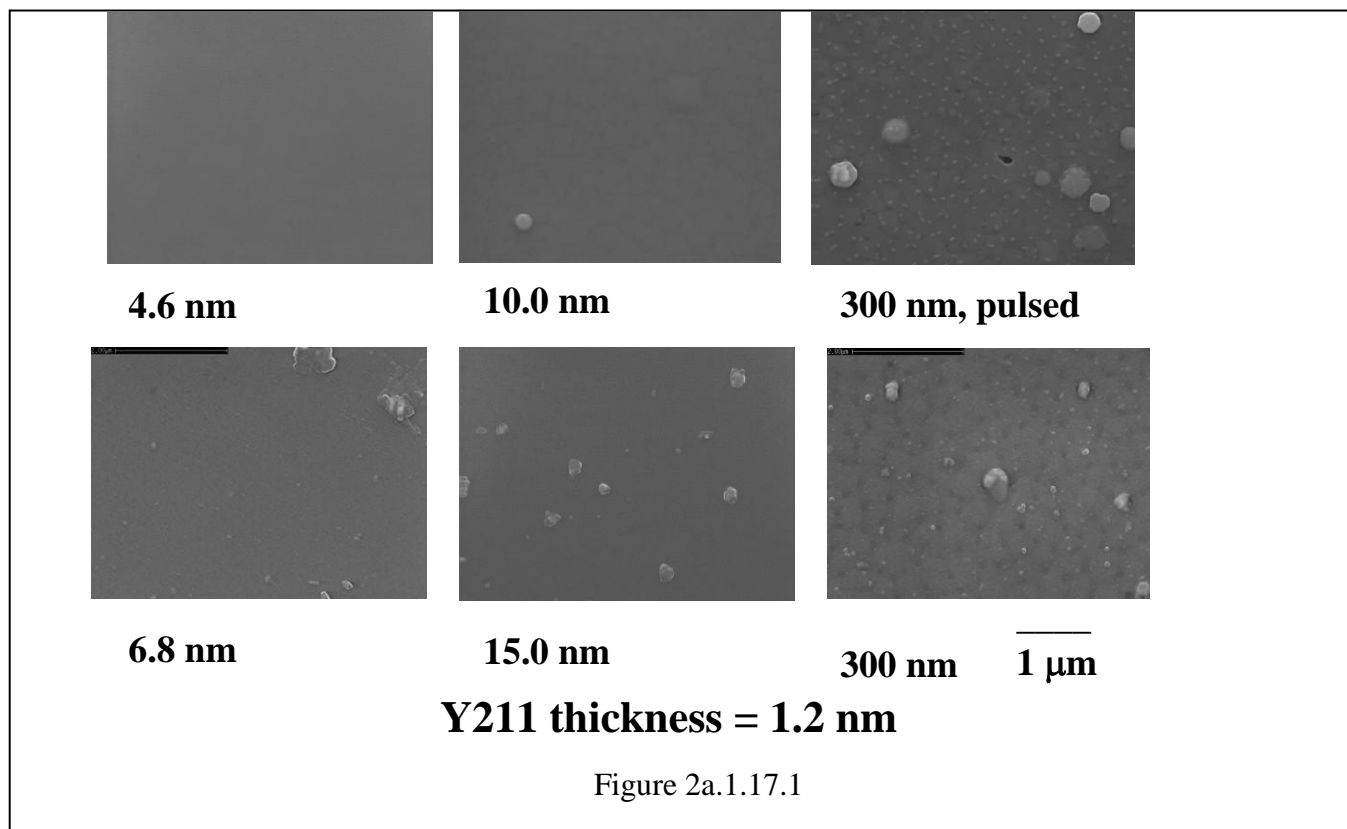
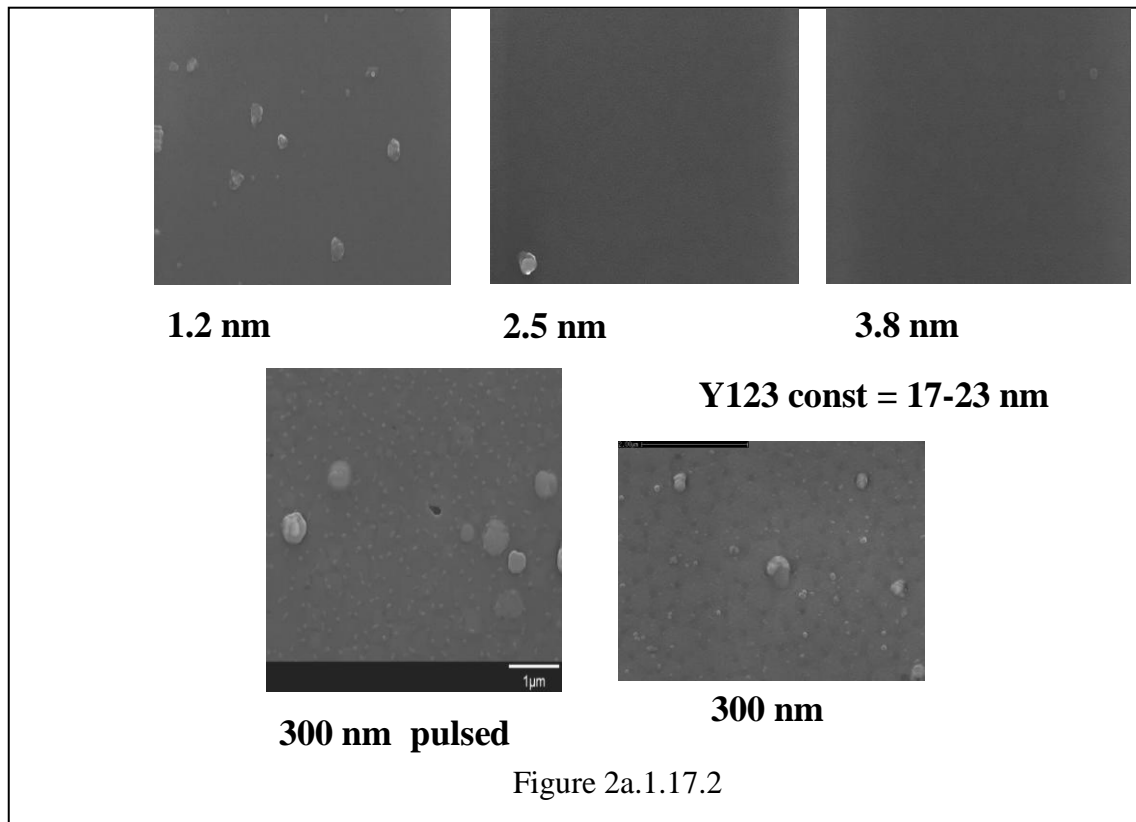


Figure 2a.1.16.1

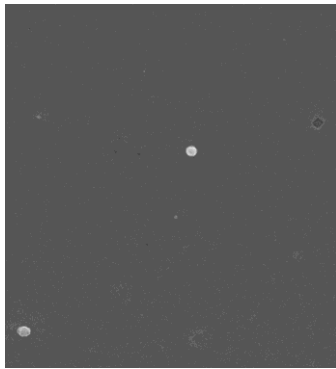
2a.1.17 Surface Smoothness



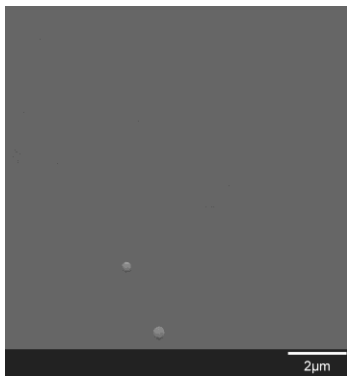


2a.1.18 Surface Defect Particulates

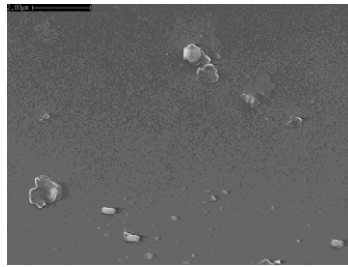
211 = 1.4±0.3 nm = constant



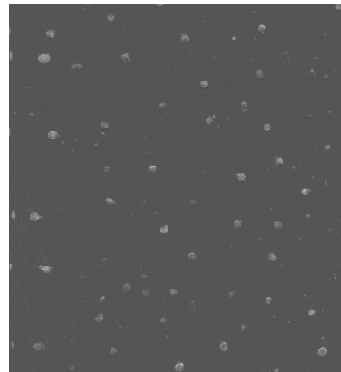
(211_{1.1nm}/123_{5.2nm})x44



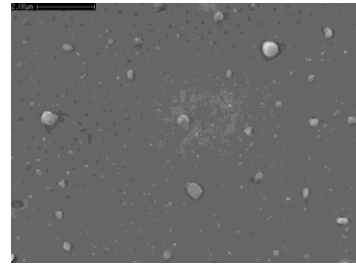
(211_{1.3nm}/123_{12.6nm})x24



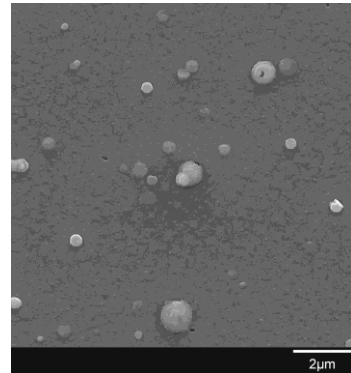
(211_{1.7nm}/123_{6.6nm})x35



(211_{1.1nm}/123_{15.9nm})x14



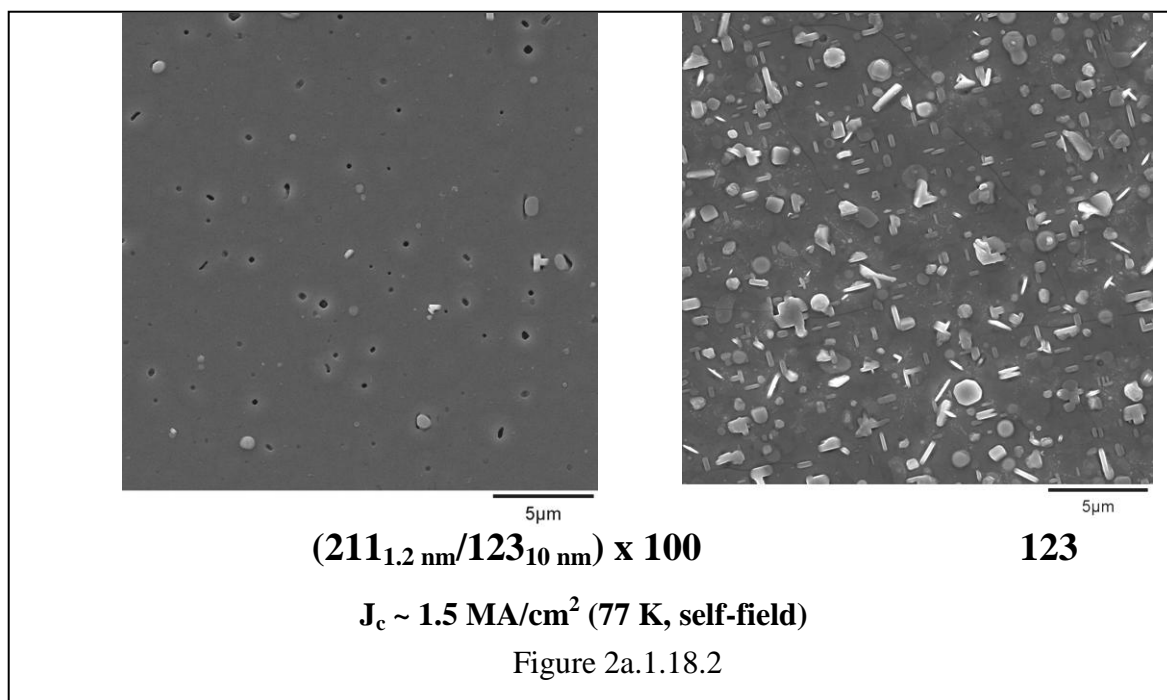
123 = 590 nm,
single layer



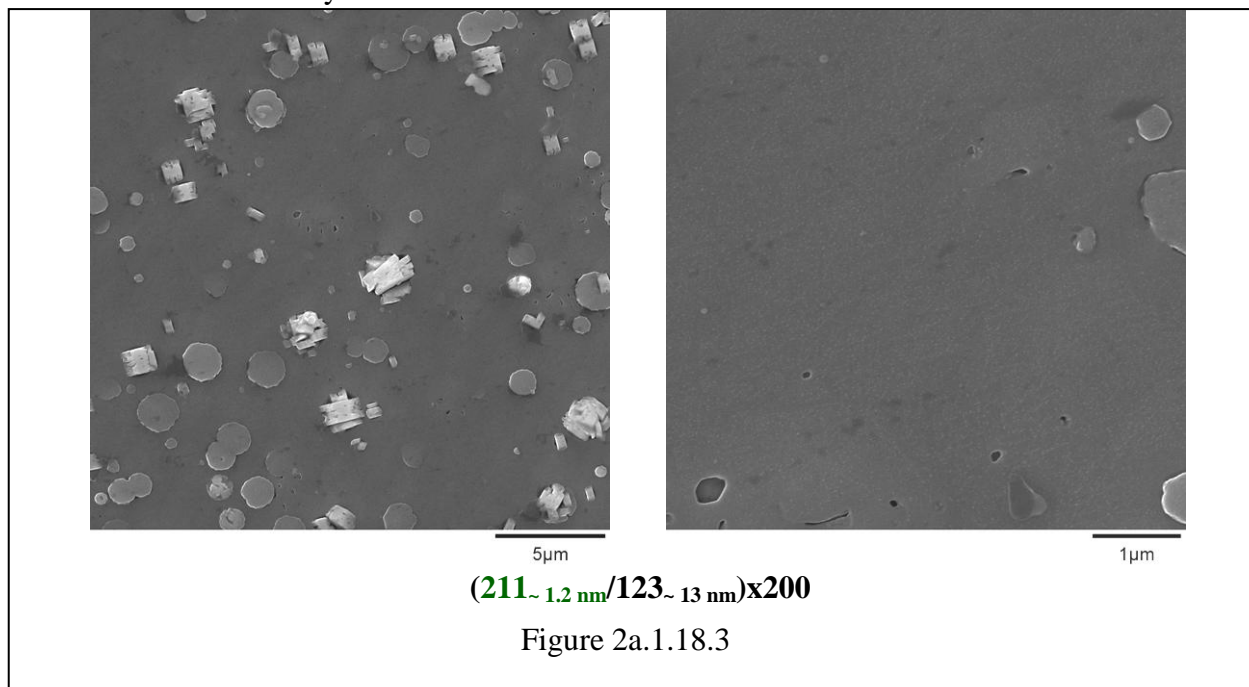
123 = 160 nm,
single layer,
pulsed deposit

~ 1 Micron thick Films

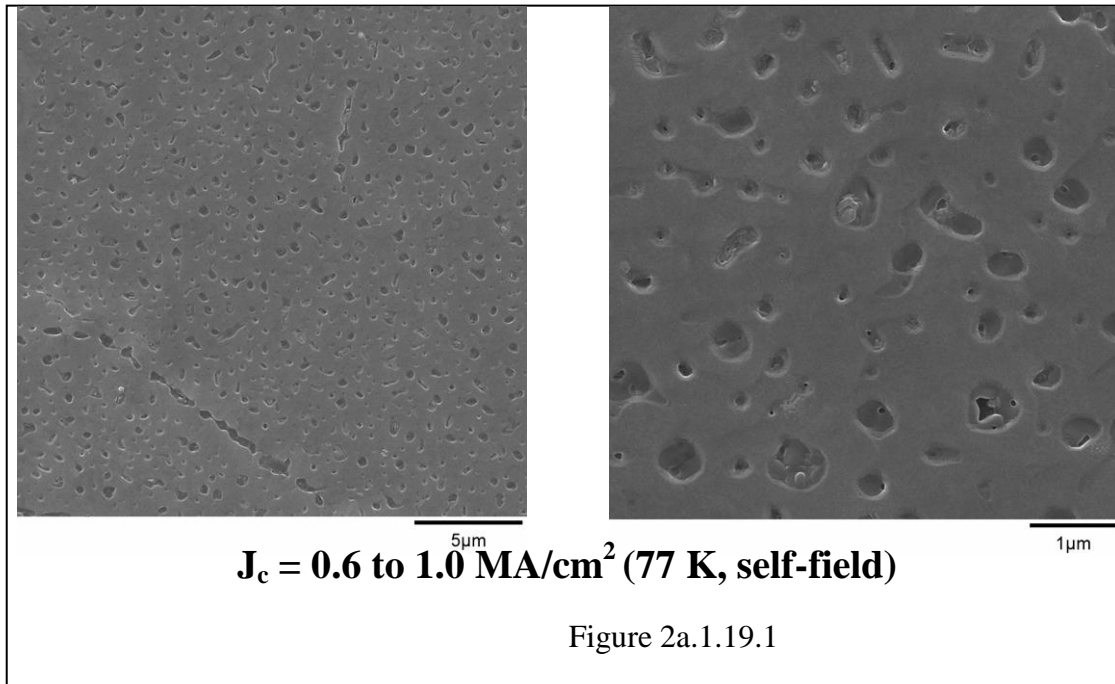
Figure 2a.1.18.1



~ 3 Micron thick Multilayer Films



2a.1.19 Multilayer on RABIT's Substrates



2a.1.20 RABIT's Transport J_c s

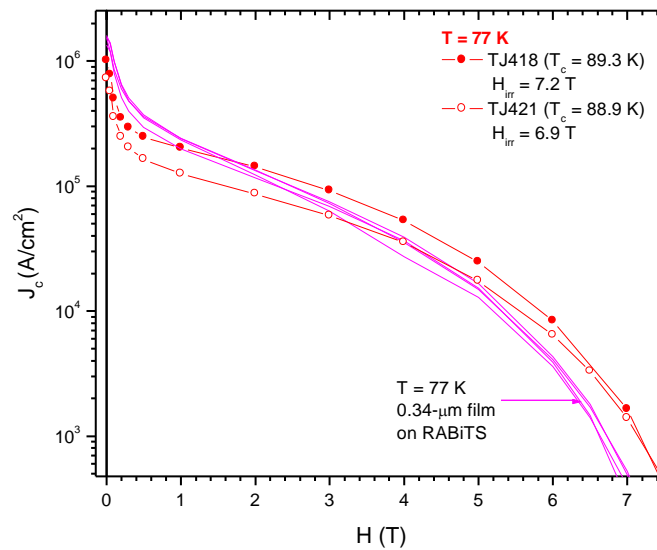


Figure 2a.1.20.1

Notes:

- I_c criterion is $1 \mu\text{V/cm}$
- H_{irr} criterion is $V(I)$ scaling exponent = 2
- Temperature is stable to within $\pm 0.008 \text{ K}$
- Used estimated width of 4.5 mm for computation of J_c , for both samples

- Comparison is with three .34- μm -thick films on RABiTS (ex-situ BaF_2) at 77 K

2a.1.21 Conclusions

5-20 nm size ‘disc-shaped’ 211 particles were incorporated into 123 films; with a 211 surface defect density $> 10^{11} \text{ cm}^{-2}$ being achieved. There was significant improvement of $J_c(H)$ from 30 K to 77 K, with J_c measured by both magnetic and transport methods. At 70-77 K, there was a 3-5 times increase of J_c at 1.5 T fields.

New type of soft flux-pinning demonstrated (?)

A slight reduction of T_c and J_c at zero-field was shown.

Other Advantages of multilayers:

- Flat film surfaces.
- Reduced surface defect particulates.
- Isotropic field dependence (?)
- Crack resistant conductor (?).

Deposition on RABIT's new study; zero-field $J_c(77\text{K})$ in the range expected.

211 and 123 conditions to optimize flux pinning not determined yet.

2a.2 Flux Pinning Effects of Y_2O_3 in YBCO Multi-layer ($\text{Y}_2\text{O}_3 \sim 0.2\text{-}1.4\text{nm}/\text{Y123} \sim 7\text{-}50\text{nm}$)xN Thin Films

References: 3

Tim Campbell¹, T. Haugan¹, P. N. Barnes¹, I. Maartense², J. Murphy², L. Brunke², J. Evans¹, J. Kell¹, N. Yust¹, Srinivas Sathiraju¹

1. Air Force Research Laboratory, Propulsion Directorate

2. University of Dayton Research Institute

2a.2.1 Objectives

- Investigate the use of Y_2O_3 nano-particulates as flux-pinning centers in 123 multi-layer thin films
- Compare results with 211/123 multi-layer thin films

2a.2.2 Magnetic Flux Pining Theory

- Desired Defect Density (area): $\sim (H/2) \times 10^{11} \text{ particles/cm}^2$, where H = applied field (T)
- Desired Defect Density (linear): ~ 5 per 100nm (5 T applied field)
- Size of Defects: $x \sim 2\text{-}4 \text{ nm} < x < 10\text{nm}$, smaller size allows high superconductor volume percentage

Flux pinning defects (a) in low temperature superconductors (b) and optimal spacing to pin a 5 T field (bars).

D. C. Larbalestier and M. P. Maley, MRS Bulletin Aug. (1993) P. 50

2a.2.3 Experimental

- Pulsed Laser Deposition of ($\text{Y}_2\text{O}_3 \sim 0.2\text{-}1.4\text{nm}/\text{Y123} \sim 7\text{-}50\text{nm}$)xN multi-layers

- SrTiO₃ substrates, 775°C, and 300 mTorr O₂ partial pressure
- 0.6 - 0.75 mm acid etched bridges
- Characterization using transport critical current (@77.2K, 1mV/cm cutoff), AC Susceptibility (T_c), VSM (@ 70 & 77K), XRD, and SEM

2a.2.4 T_c Reduction vs. Y₂O₃ Thickness (Y123~ 9.9nm/layer)

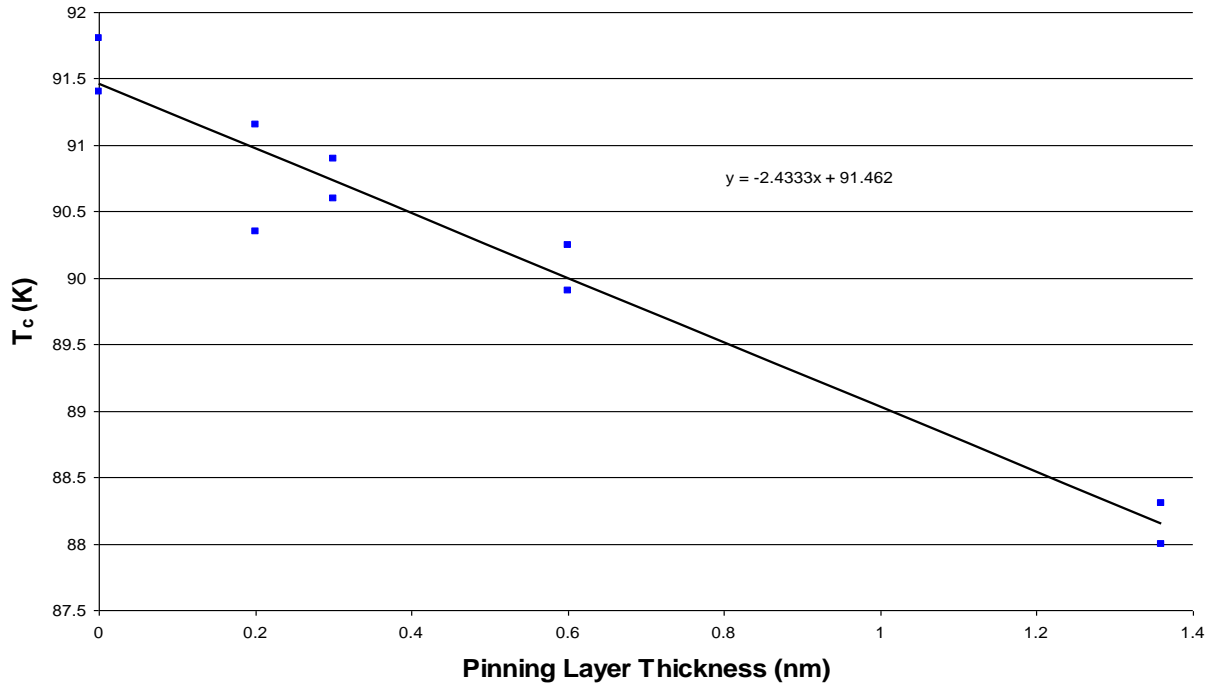


Figure 2a.2.4.1

2a.2.5 χ Measurements

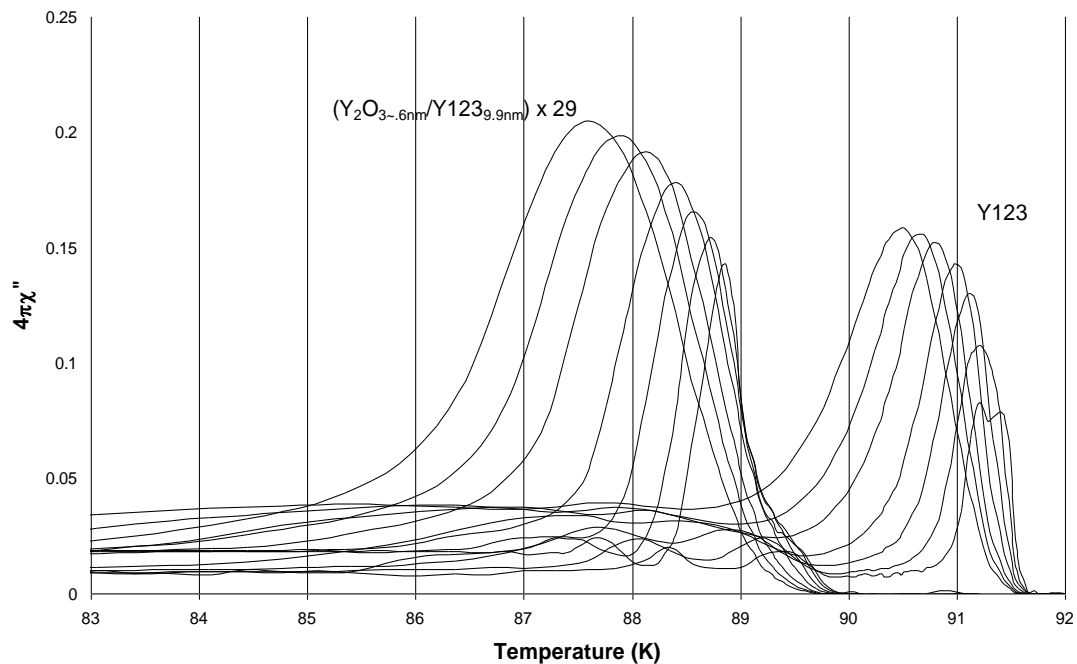


Figure 2a.2.5.1

2a.2.6 Y₂O₃ Layer

0.2nm Y₂O₃ layer (0.8×10^{11} particles/cm²)
Avg. particle diameter~ 11.2 ± 4.6 nm

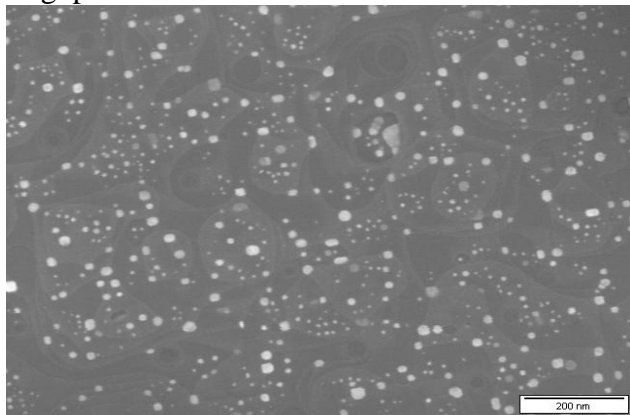


Figure 2a.2.6.1

0.48nm Y₂O₃ layer (1.25×10^{11} particles/cm²)
Avg. particle diameter~ 11.7 ± 4.3 nm

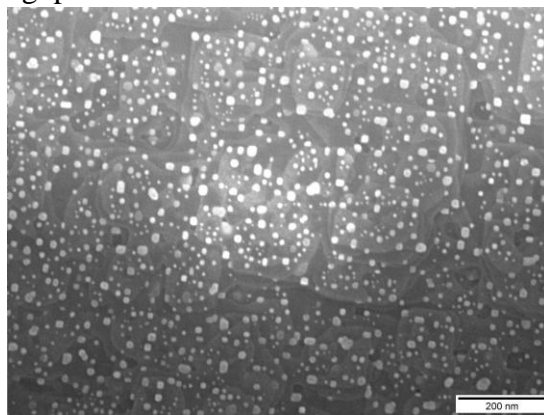


Figure 2a.2.6.2

0.9nm Y₂O₃ layer (1.6×10^{11} particles/cm²)
Avg. particle diameter~ 12.9 ± 6.2 nm

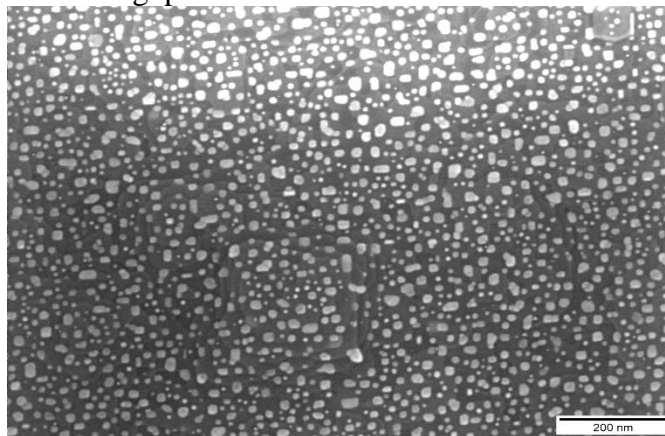


Figure 2a.2.6.3

2a.2.7 Transport and Magnetic J_c Measurements

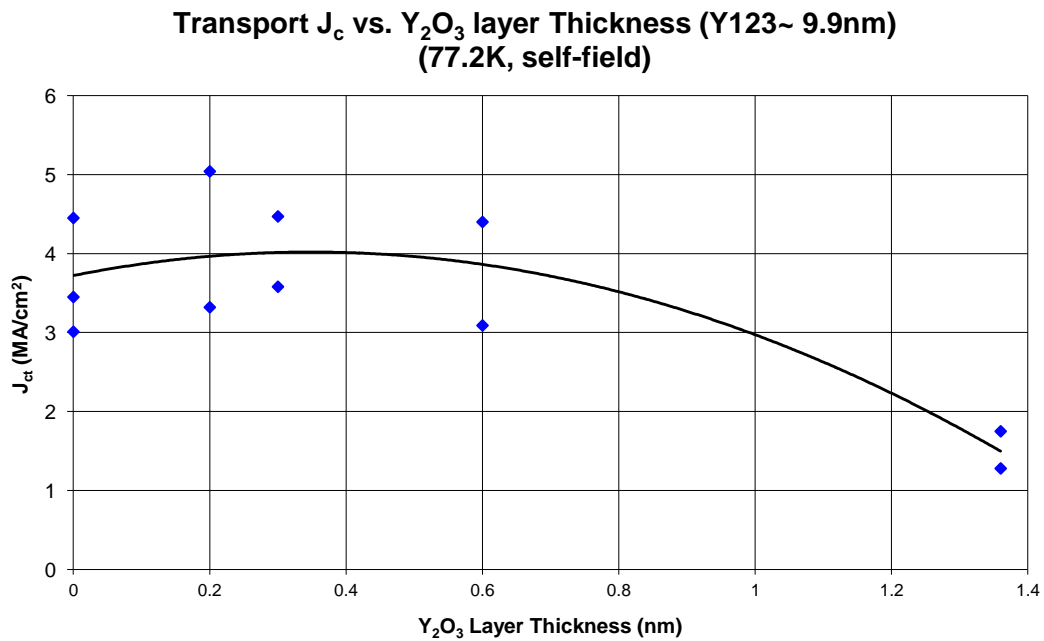


Figure 2a.2.7.1

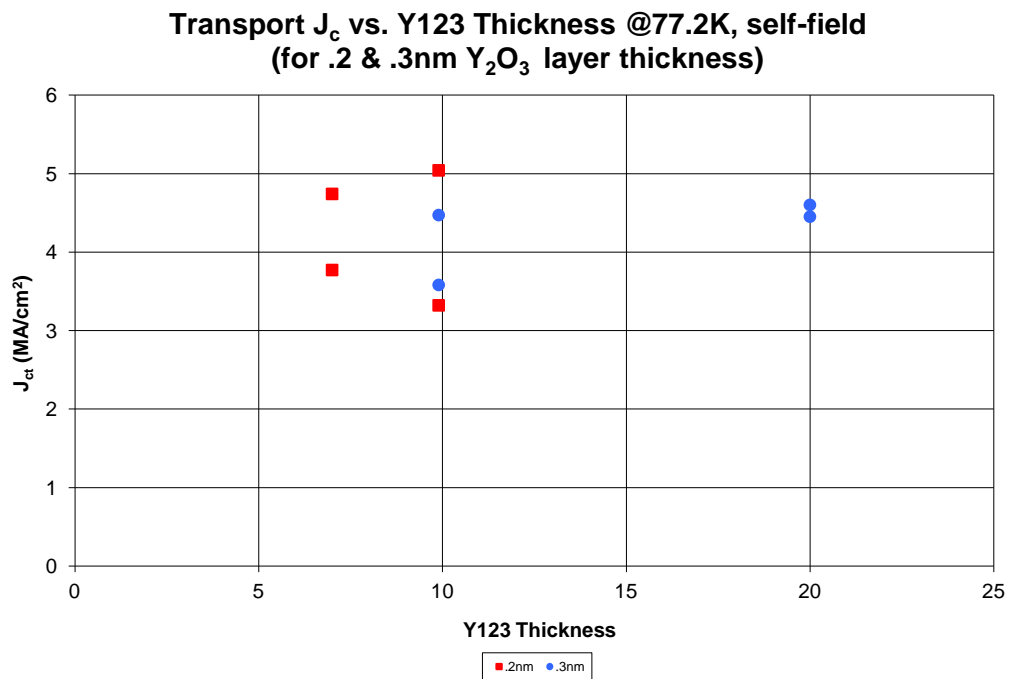


Figure 2a.2.7.2

Magnetic J_c vs. Field (T) @77K for various $Y_2O_3/Y123$ multi-layer films

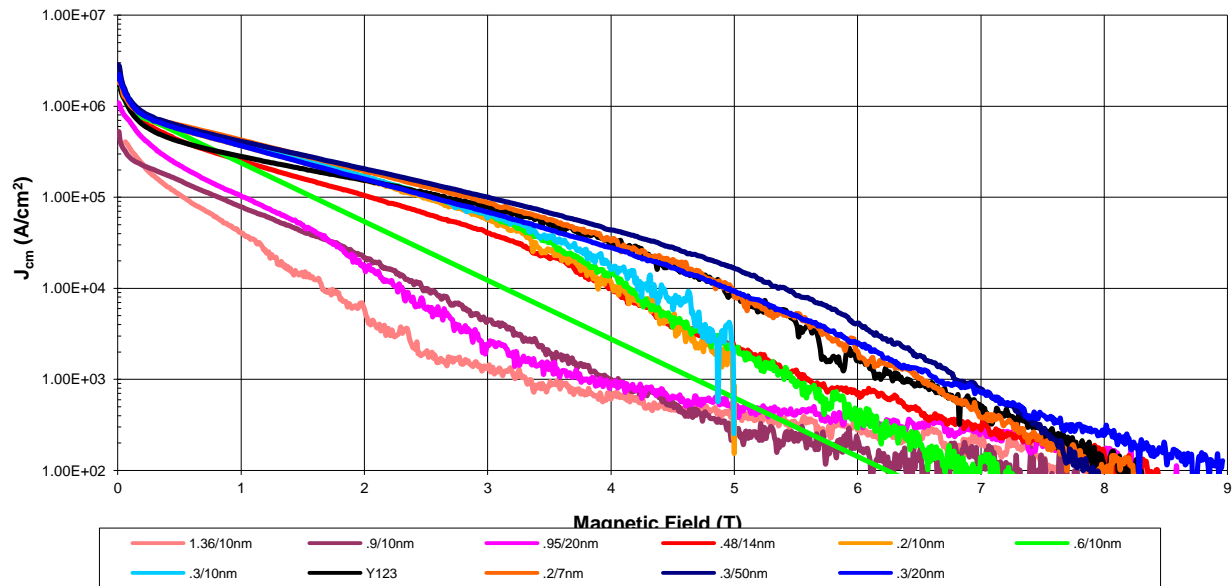


Figure 2a.2.7.3

Magnetic J_c vs. Field (T) @70K for various $Y_2O_3/Y123$ multi-layer films

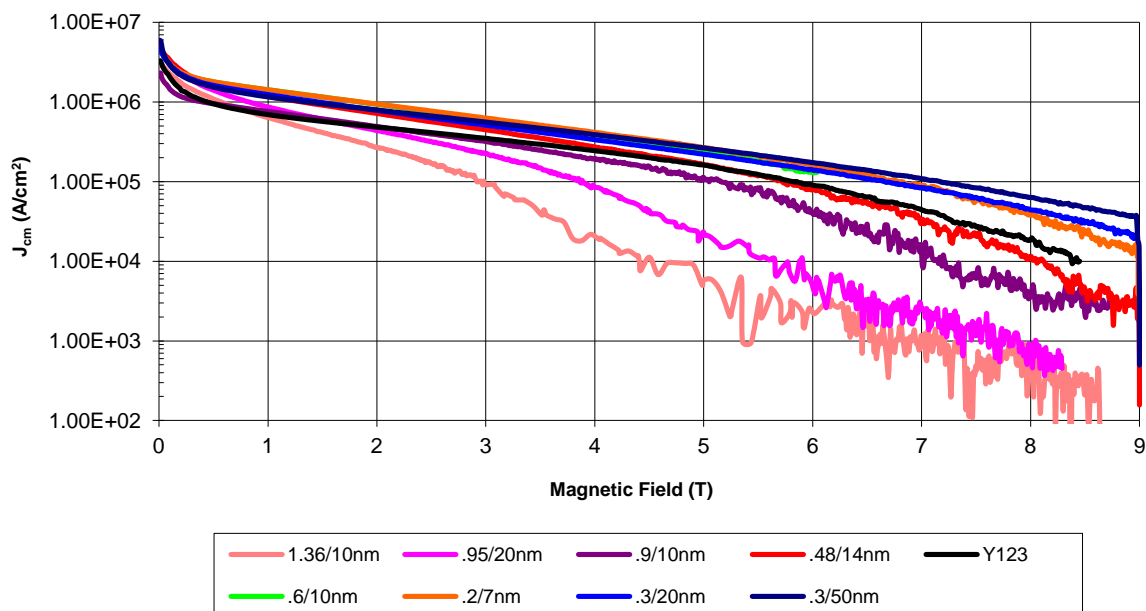


Figure 2a.2.7.4

J_{cm} for $Y_2O_3=.6nm$ vs. $Y211=.6nm$ @77K (Y123~ 9.9nm/layer)

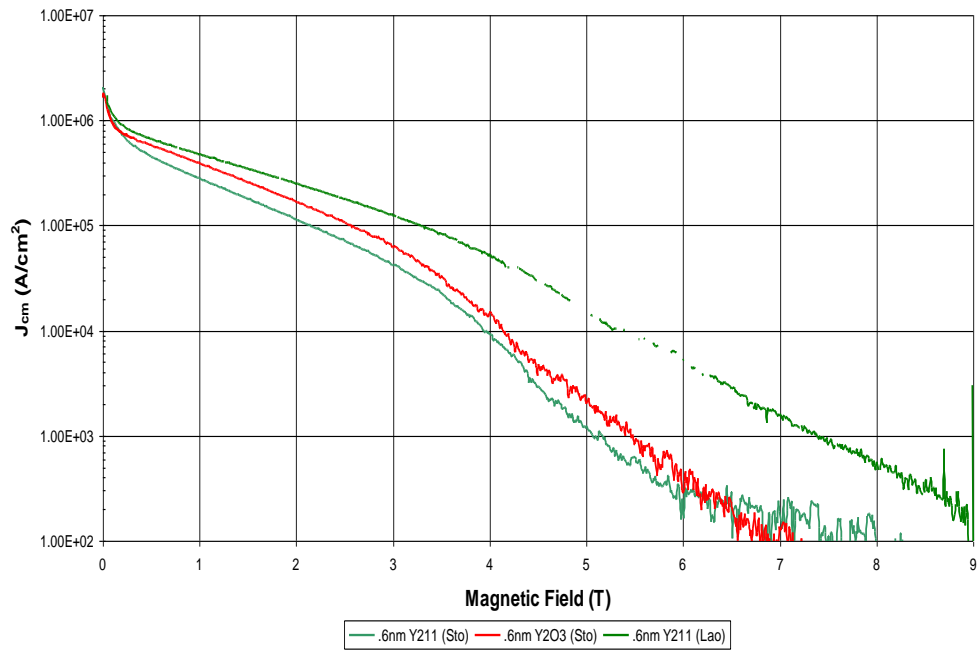


Figure 2a.2.7.5

J_{cm} for $Y_2O_3=.9nm$ vs. $Y211=.9nm$ @77K (Y123~ 9.9nm/layer)

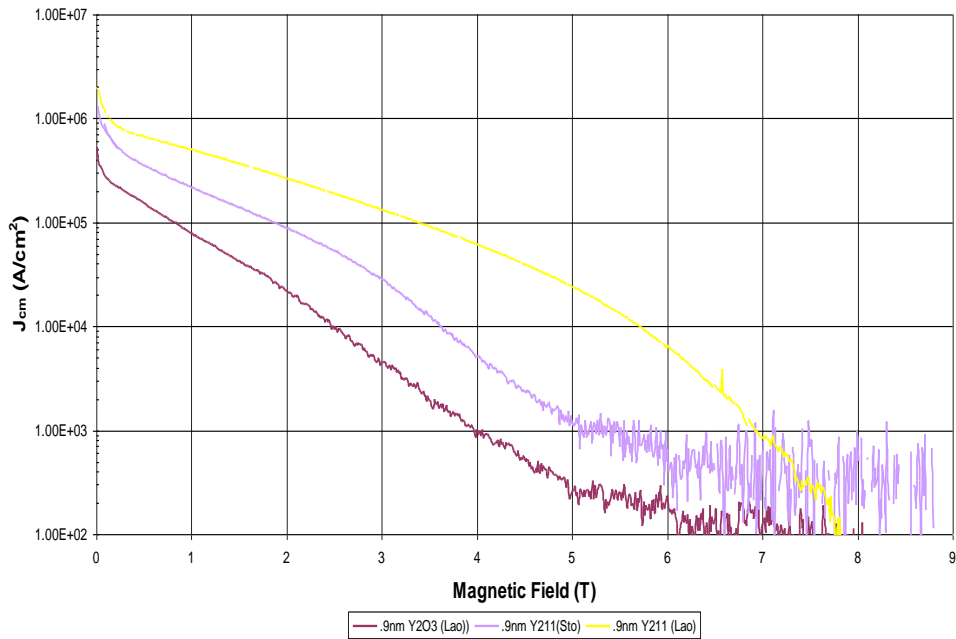


Figure 2a.2.7.6

2a.2.8 XRD 2 Theta Scan

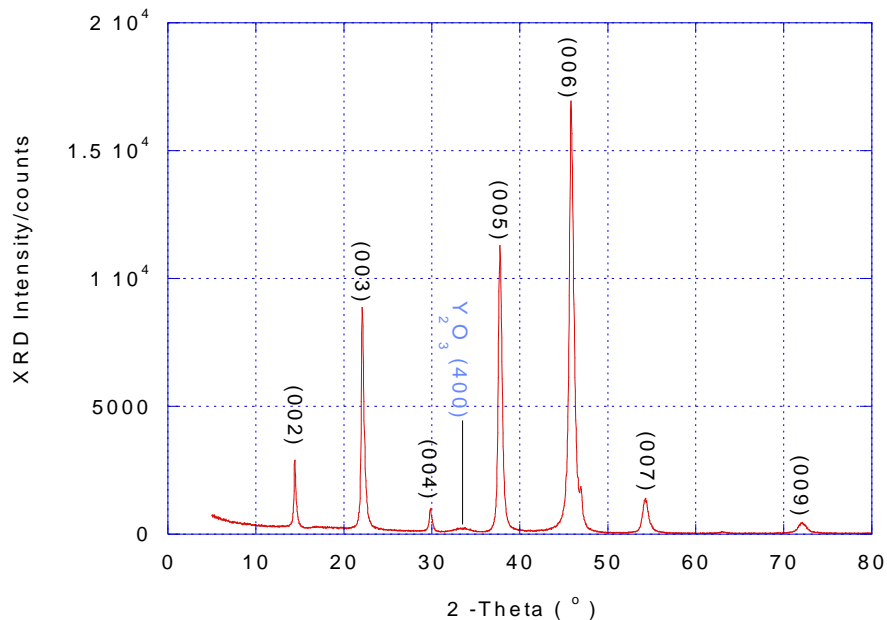


Figure 2a.2.8.1

2a.2.9 Summary

- Y_2O_3 nano-particulates show promise as pinning centers in Y123 thin Films
- Minimal reductions in critical temperature
- Good surface particle formation for varying Y_2O_3 thickness
- Transport J_{cs} over 4 MA/cm^2 for varying Y_2O_3 thickness on SrTiO_3
- Magnetic $J_{cs} \sim \text{MA/cm}^2$ at 77K & 0T
- Hrrr field improvement of $\sim 1\text{T}$ over Y123 @ 77 & 70K
- Magnetic J_{cs} for samples with the thinner Y_2O_3 layers are comparable to equivalent Y211/Y123 multi-layer films on STO

2a.3 PLD Parameters of $\text{YBa}_2\text{Cu}_3\text{O}_{7-\delta}$ and Alternating Nanolayers for Flux Pinning

References: 4

2a.3.1 Introduction

For most studies, there remains a narrow window of O_2 pressure where optimal T_c and J_c can be obtained. However, this work extends the study of O_2 deposition pressures from 120 mTorr to 1200 mTorr for a new set of deposition parameters for which T_c and J_c can be relatively insensitive to O_2 pressure. The results of this study will show:

- T_{cs} of 92 K consistently achieved for an O_2 pressure between 400 mTorr and 1200 mTorr
- J_{cs} of $6-9 \text{ MA/cm}^2$ at 77.2 K obtained for an O_2 pressure between 200 mTorr and 600 mTorr
- J_{cs} still MA/cm^2 level up to 1200 mTorr

These results are compared to previous studies where optimal quality was achieved for narrower windows of O₂ pressure.

- 2a.3.2 Experimental Conditions

- A KrF excimer laser (Lambda Physik, LPX 305i) was used.
- Oxygen pressure in the deposition chamber kept constant using downstream throttle-valve control.
- Target resurfaced periodically with SiC sandpaper, and conditioned with ~ 800 laser pulses prior to deposition.
- Target rotated during deposition with laser beam scanned across a ~ 1.5 cm length of the 5 cm diameter target.
- LaAlO₃ (100) single crystal substrates were ultrasonically cleaned using first acetone, and then dehydrated ethyl alcohol.
- After deposition, films cooled to 500 °C at 1270 °C/h, and held at 500 °C for 30 minutes, during which O₂ pressure reached 1 atm.

--Films subsequently cooled from 500 °C to 250 °C at 1270 °C/h, and from 250 °C to room temperature using the natural cooling rate of the heater block (~ 800 °C/h).

2a.3.3 Comparison of Conditions

	This work	Ref [7]	Ref [8]	Ref [9]	Ref [10]	Ref [11]
Laser Wavelength (nm)	248	193	248	308	248	308
Laser Pulsewidth (ns)	25	15	25	30	25	25
Pulse Energy (mj)	200	-	45	93	104	103
Ablation Spot Size (mm ²)	~ 1 x 6.3	-	~ 1 x 4.5	5.45	~ 2 x 4	5
Laser Fluence (J/cm ²)	3.2	3	1	1.7	1.3	2.1
Repetition Rate (Hz)	4	-	5	4	10	10
Target-to-substrate Distance (cm)	6	6	6	4.5	6.5	3.5
Laser Strike Angle (° from Target normal)	45	-	-	-	45	45
Laser Beam Uniformity	-	-	-	-	-	-
Target density (%)	92	-	-	85	high	75
Substrate	LaAlO ₃	MgO	LaAlO ₃ , MgO	SrTiO ₃ , MgO	LaAlO ₃	SrTiO ₃
Substrate Size (mm ³)	12 x 3.2-5 x 0.5	-	10 x 10	-	15 x 15	~ 1.3 x 1.3
Substrate Temperature (°C)	785	680	780 LaAlO ₃ 800 MgO	750	770	725
Film Thickness (mm)	0.2 – 0.3	-	0.1 – 0.2	-	~ 0.3	-
O ₂ In-situ Anneal	500 °C 760 Torr	-	550 °C flowing O ₂	-	470 °C 600 Torr	700 °C 760 Torr

Figure 2.3.3.1

2a.3.4 O₂ Pressure Effect On Plume

The visible plume reached the heater block at 600 mTorr. The plume was fairly uniform and “soft” around the edges. This is in contrast with another PLD system with narrower, more forward directed plumes. A transition from yellow to red in the outer edge of the plume corresponds to increased formation of YO.

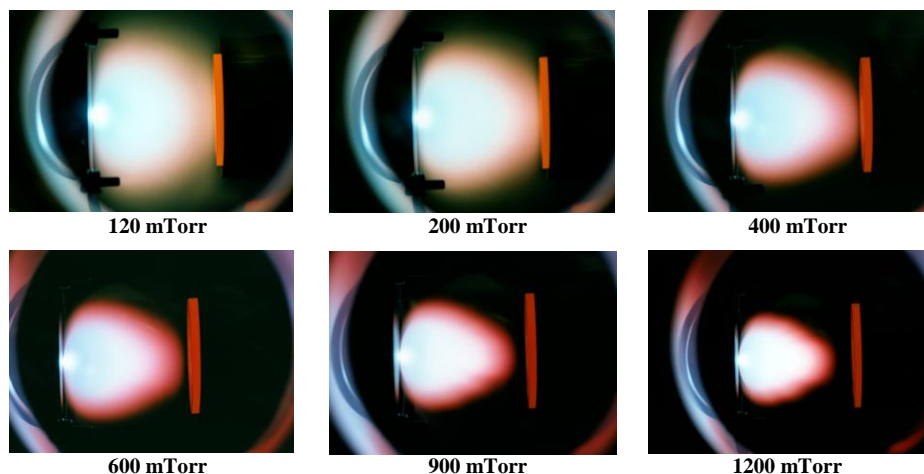


Figure 2a.3.4.1

2a.3.5 Deposition Rate vs. O₂ Pressure

The maximum deposition rate was at 600 mTorr, when the visible plume just touched the substrate, consistent with other work. When the O₂ pressure was < 600 mTorr, the plume impinges onto substrate; a potential for re-sputtering due to high energy particles. Alternatively, when the O₂ pressure was > 600 mTorr, with the substrate beyond visible plume, the amount of evaporated species dropped.

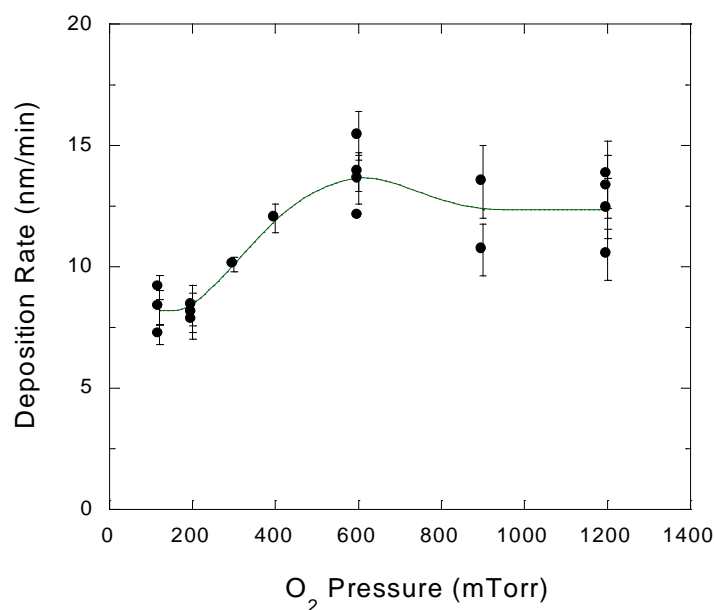


Figure 2a.3.5.1

2a.3.6 AC susceptibility data

The onset of the T_c transition is quite high at 92.3 K for 0.3 μm thick YBCO on LaAlO₃. This is near the maximum T_c for YBa₂Cu₃O_{7- δ} of 92.6 K. The transition width from T_c onset to reach X'' maximum was ~ 0.2 K for 0.1 Oe applied field, and the overall transition was ~ 0.6 K.

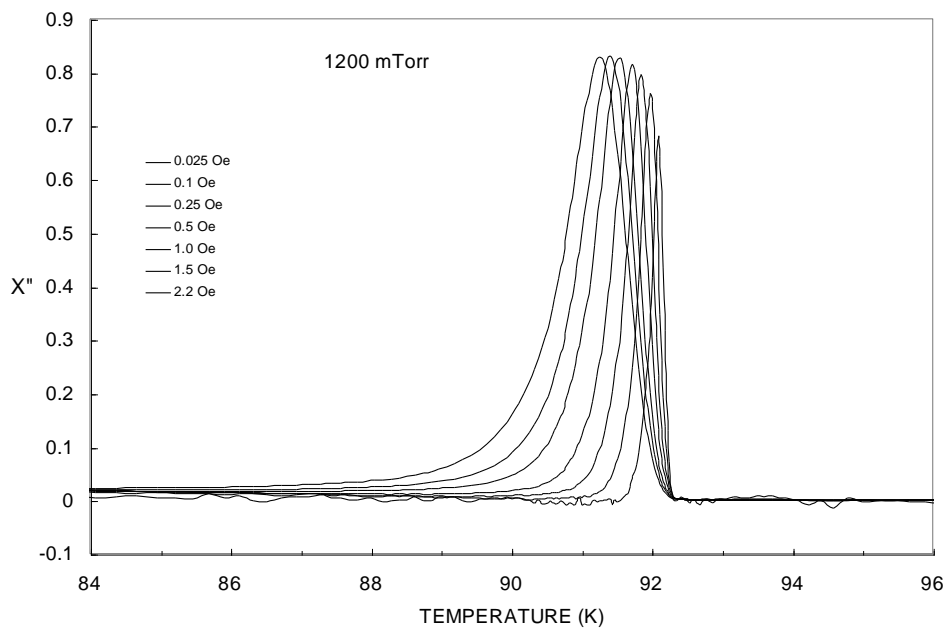


Figure 2a.3.6.1

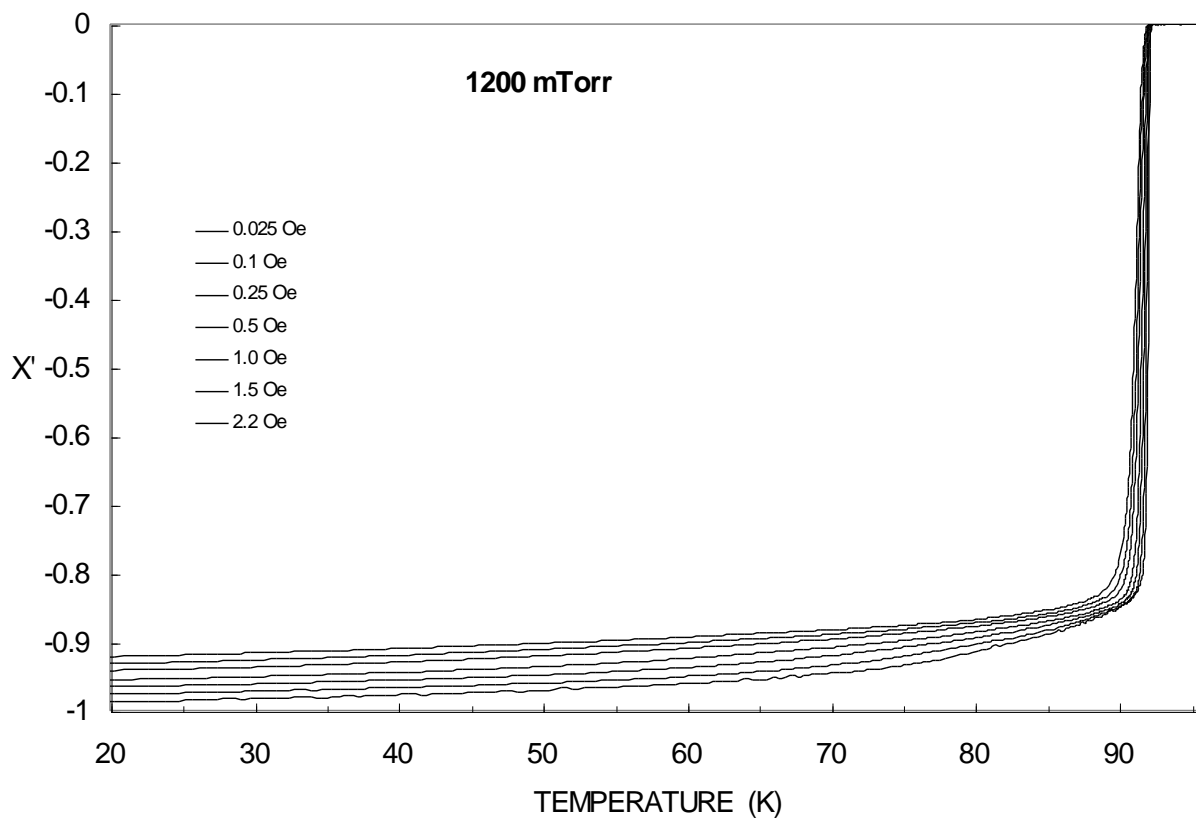


Figure 2a.3.6.2

2a.3.7 T_c Onset vs. O_2 Pressure

Obtaining T_c s of 92 K in YBCO films for such a wide range of O_2 pressure has not been reported previously. A more recent work [10] demonstrated a less narrow window. T_c was consistently measured at 92 K for films located both inside and outside the plume --partially a consequence of post-anneal treatment.

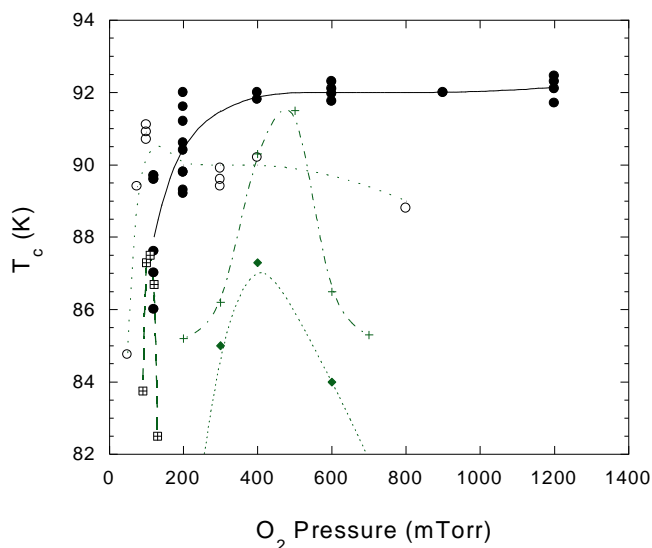


Figure 2.3.7.1

2a.3.8 Transport J_c vs. O_2 Pressure

For O_2 pressure above 200 mTorr, J_c s were consistently high from 5-9 MA/cm² at 77 K, self-field. The transport J_c s were repeatedly achieved.

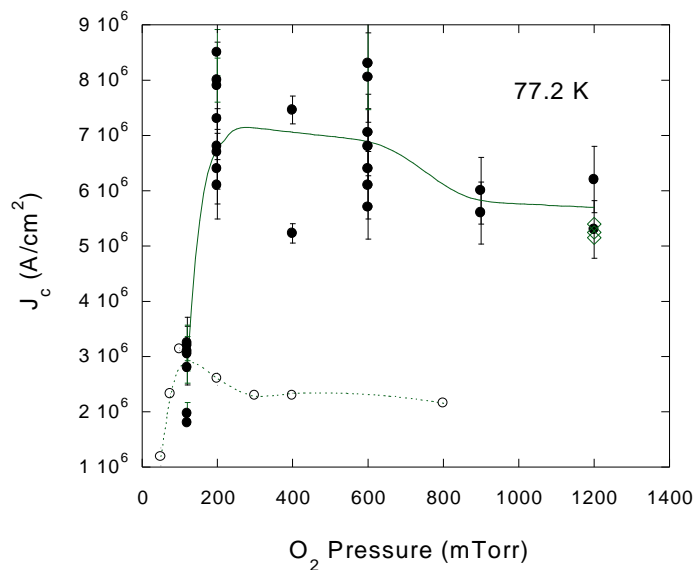


Figure 2a.3.8.1

2a.3.9 Room Temp. Resistivity vs. O₂ Pressure

The films show a slightly stronger dependence on O₂ pressure than T_c or J_c. There is obviously a different dependence than J_c.

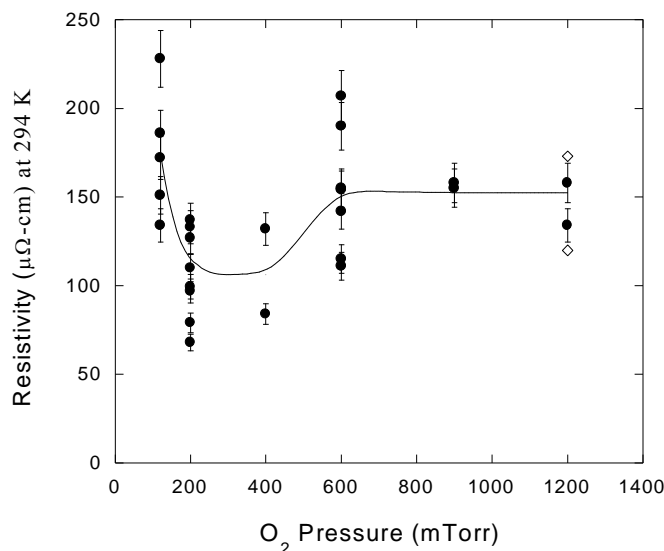


Figure 2a.3.9.1

2a.3.10 Surface Effects

All J_c's > MA/cm². At 120 mTorr, a high concentration of pinhole defects was seen. Possible selective resputtering from high translational kinetic energy particles in plume may have occurred. At 1200 mTorr, samples showed a high concentration of surface particulates. This is likely due to the formation of YBCO nano-particulates in the vapor phase.

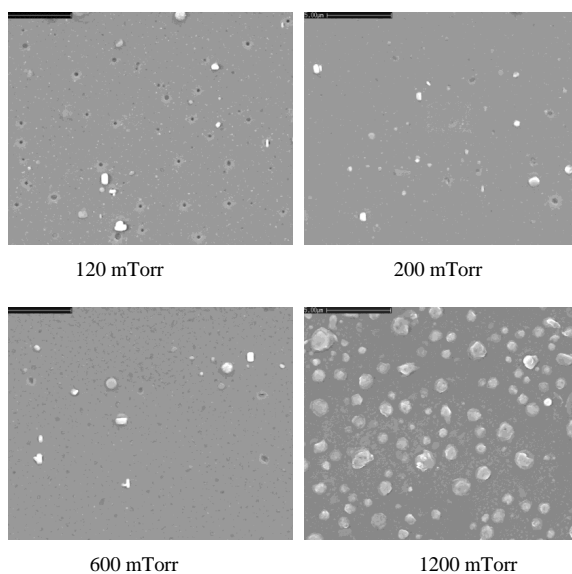


Figure 2a.3.10.1

2a.3.11 Additional Results

J_c had slightly different dependence on O_2 pressure than did T_c . At 200 mTorr, J_c s were high whereas T_c s were between 90-92 K. At 1200 mTorr, J_c s decreased slightly, even though the T_c s were consistently between 92 to 92.5 K. The decrease in J_c at 1200 mTorr may correlate with increasing surface roughness.

Oxygen content of the films was constant (measured by XRD) for all O_2 deposition pressures. However, films showed distinct differences in impurity content. At 120 mTorr (compared to 600 mTorr) measurable amounts of Al, Fe, and Cr impurities existed in films, as measured by SIMS. The impurity content is possibly from the interaction of the plume with the heater block and support structure; the heater block showed evidence of pitting.

2a.3.12 Stacked Layer Approach Comparison

Layers are epitaxially grown by pulsed laser deposition. There were 35 layers total. The total thickness of the Y123 layers is 6.7 nm, while the total of the Y211 layers is 1.0 nm thick. It is important to note that the Y211 phase is chemically stable with the Y123 phase.

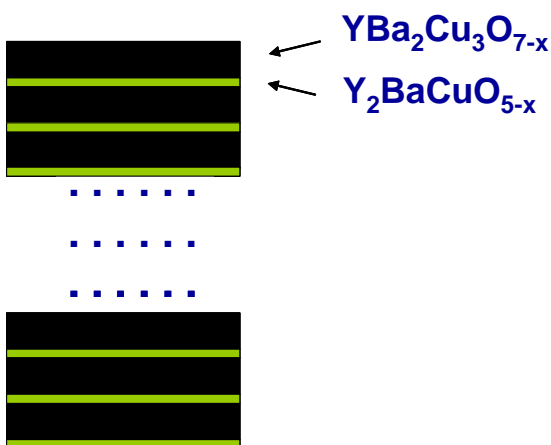


Figure 2a.3.12.1

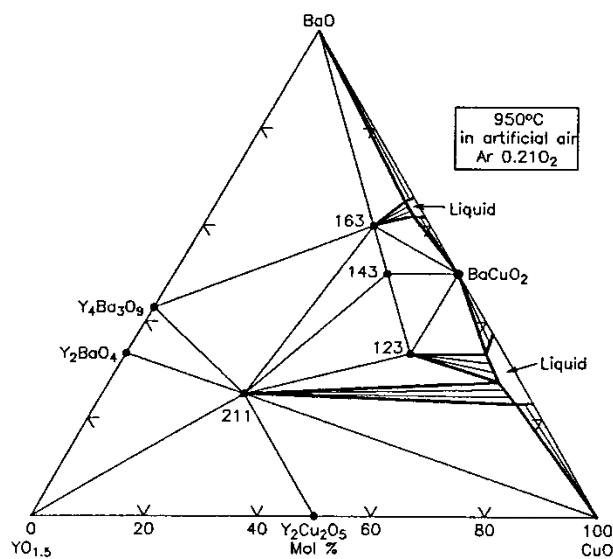


Figure 2a.3.12.2

2a.3.13 70K Specific Improvement

Although overall current density drops for very low magnetic fields, J_c is significantly enhanced for larger magnetic fields.

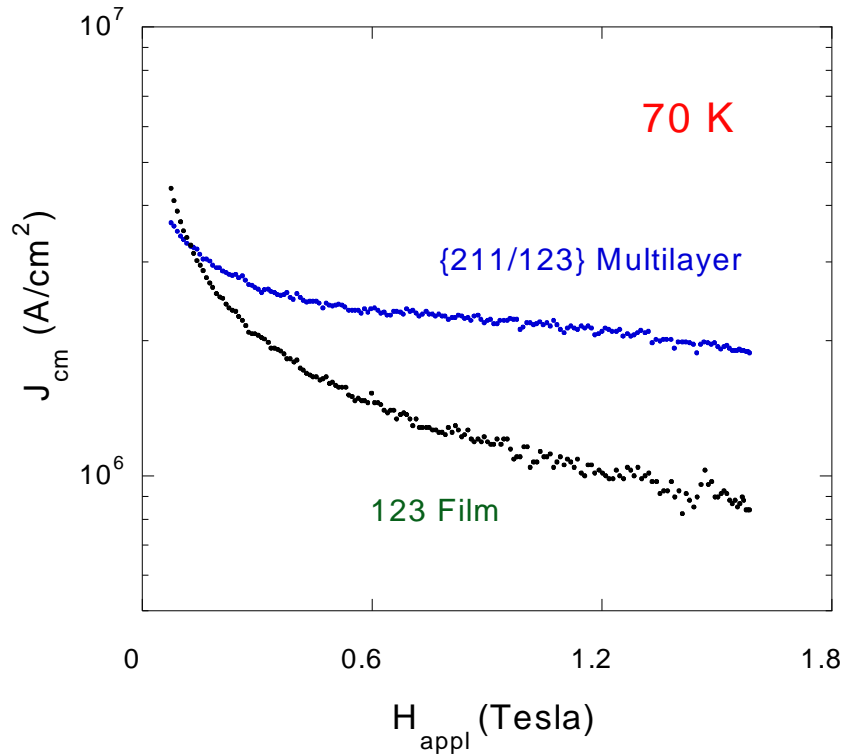


Figure 2a.3.13.1

2a.3.14 Conclusions

High quality YBCO films were deposited for a wide range of O² deposition pressure. For O₂ pressures of 400 mTorr to 1200 mTorr, T_cs were high and repeatable = 92.0 ± 0.4 K. For O₂ pressure from 200 to 600 mTorr, J_cs were in the range of 6-9 MA/cm² measured at 77 K in self-field. For O₂ pressure ≤ 200 mTorr, T_cs were lower and less stable (~ 88 K to 92 K) which is consistent with results by many other groups, and had decreasing J_c at 120 mTorr. Room temperature resistivity properties showed more dependence on O² pressure than T_c and J_c. We believe this is the first report where T_cs = 92 K have been reliably obtained in YBCO thin films for a wide range of O₂ deposition pressures. A primary difference between this work and others is a higher laser fluence used (3.2 J/cm²).

2a.3.15 Room Temp. Resistivity vs. J_c

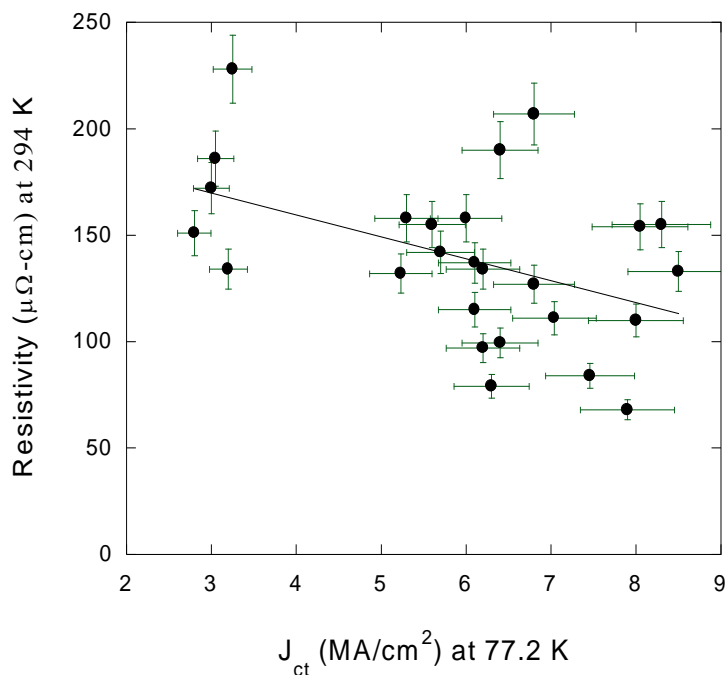


Figure 2a.3.15.1

2a.4 Nanoparticle Formation from $Y_1Ba_2Cu_3O_{7-\delta}$ for Potential Flux Pinning Mechanism

References: 5

2a.4.1 Introduction

The group continues to develop a new method for flux pinning of the YBCO coated substrate. Magnetic flux can be pinned inside high temperature superconductors (HTS) to improve current transport properties at higher fields. Samples created by this new method more than tripled the critical current density over that of a normally prepared sample at 70 K to 77 K and at 1-2 T applied field. The slight drop at lower fields is not important since it is the overall current carrying ability of the conductor that matters in rotating machinery (up to 5 T). The approach used is to deposit multilayer coatings with very thin alternating layers of a high temperature superconductor (HTS) and non-superconductor. Although the insulating layers were deposited as ultrathin layers ~ 1 nm thick, the final structure resulted in the non-superconducting material depositing as island growth clusters or globules due to preferential nucleation and growth of the non-lattice matched phase. The incorporated non-superconducting globules were disc-shaped with diameter about 10-15 nm, and height about 2-4 nm. A key element is the use of non-superconducting compounds that are not chemically reactive with the HTS compound. This requirement is more critical for nanosize defects as many compounds that otherwise would be slow to diffuse and react with the HTS material during high temperature processing can react much quicker as nanosize inclusions. One attempt to deposit nano-inclusions with a reactive material resulted in large micron-sized defects of second-phase, in contrast to results with chemically non-reactive 211 which produced no reactant phases. The pinning process was

demonstrated using pulsed laser deposition for HTS material $\text{YBa}_2\text{Cu}_3\text{O}_{7-x}$ and the non-superconducting Y_2BaCuO_5 however the process could be applied to other HTS materials and using other thin film deposition or coating techniques.

2a.4.2 Nanoparticles and Flux Pinning

Magnetic flux can be pinned inside the HTS film to minimize losses. This flux pinning occurs at defect sites in the HTS material. The defects are nanoparticles have been generated by laser ablation of Si at high pressures (several Torr), with dimensions on the order of nanometers. They are generated by ablation of primarily atomic species and the subsequent nucleation into nanometer-sized particles is due to the high background pressure.

2a.4.3 Comparative PLD System

Excellent results were achieved with 0.3 μm thick YBCO on LaAlO_3 . The T_c 's were consistent at 92 K (ac susp.) Also, J_c 's were consistent at 5-9 MA/cm^2 , now at 4-6 MA/cm^2 with the new laser.

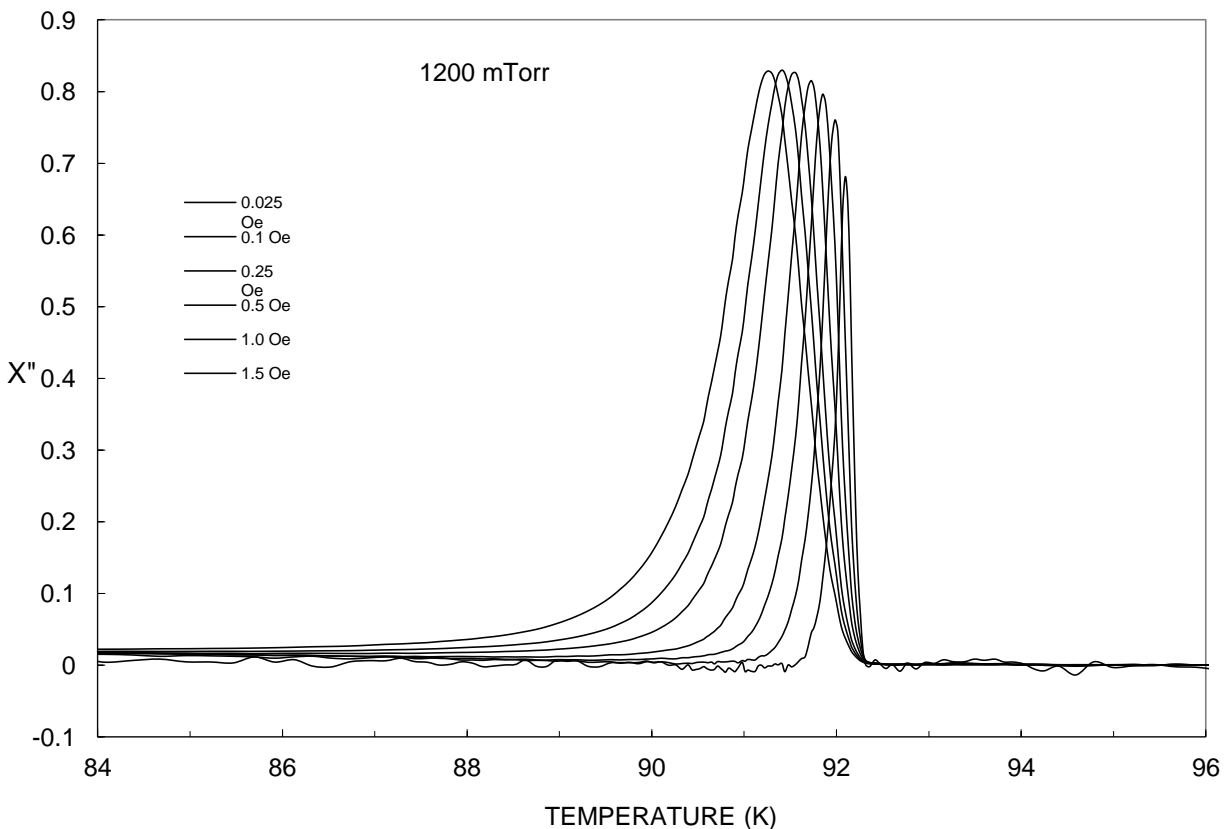


Figure 2a.4.3.1

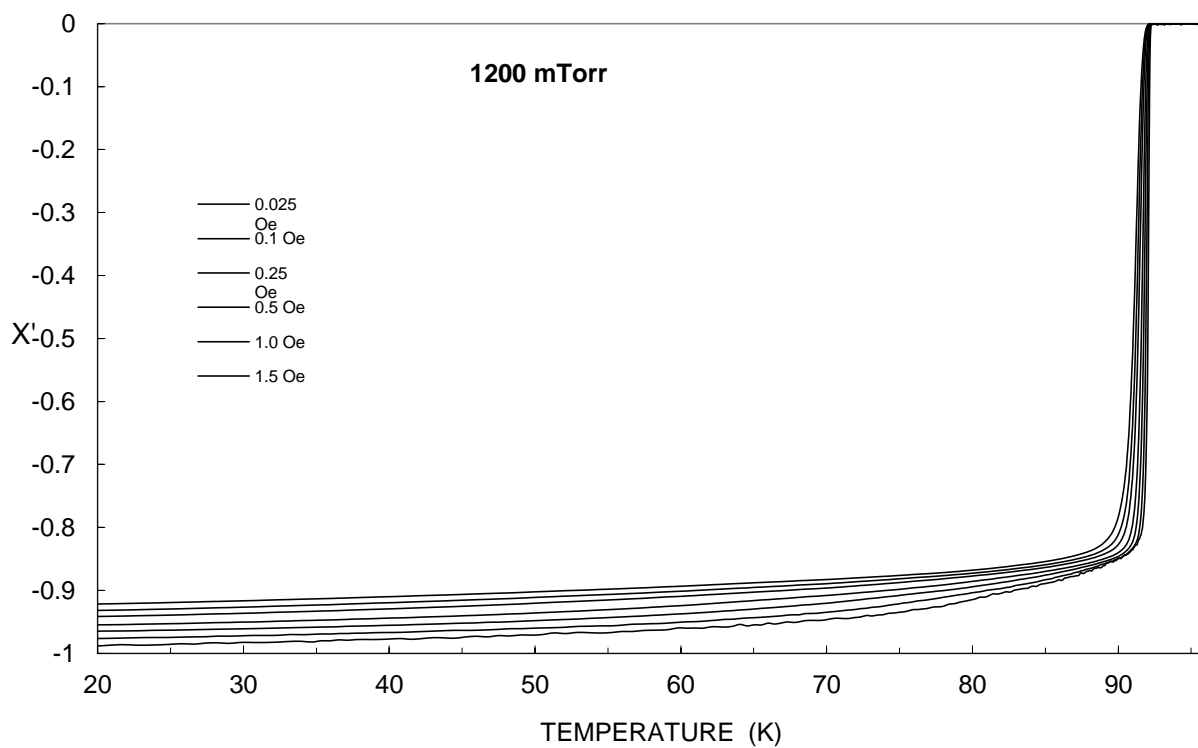
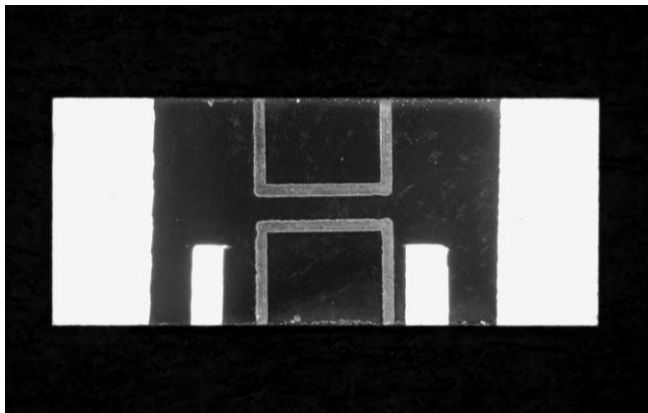


Figure 2a.4.3.2

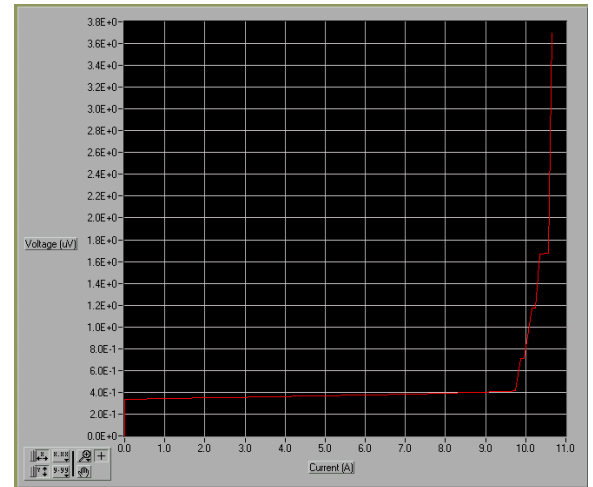
2a.4.4 PLD YBCO Characterization

Transport J_c Macrobridge



5 mm

J_c



T_c

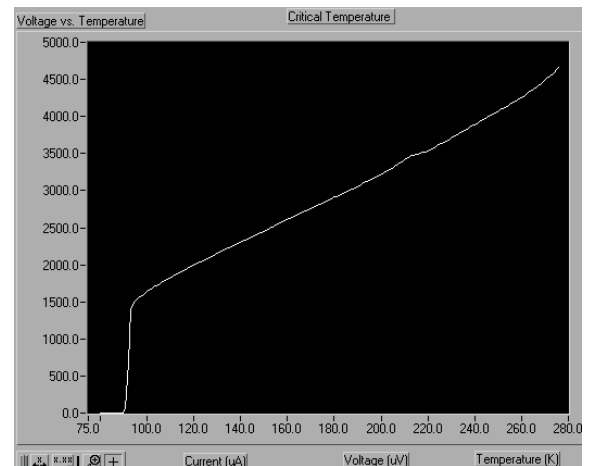


Figure 2a.4.4.1

2a.4.5 Surface Effects

J_c 's of the films remain high for varying oxygen pressure. The surface morphology is clearly different. Large particulate inclusions are formed at high pressures.

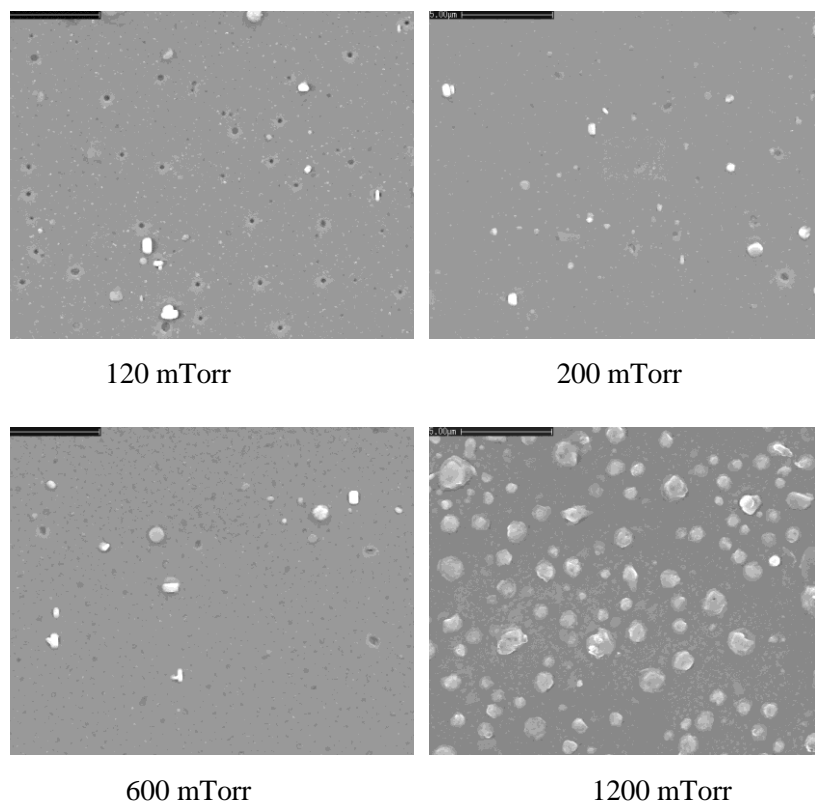


Figure 2a.4.5.1

2a.4.6 Synthesis of Nanoparticles From YBCO

Approach adopted to synthesize nanoparticles from the YBCO target *in situ*. The eventual procedure would consist of iterations of high pressure laser ablation to generate nanoparticles, followed by low pressure (120 mTorr) ablation to deposit HTS film -- the matrix for embedding the particles. Experiments were conducted to examine the possibility of generating the nanoparticles.

2a.4.7 Experimental Conditions

The deposition conditions were:

Pressure : 5 Torr (O₂)

Laser Wavelength : 248 nm

Laser energy: 50 mJ/pulse

Rep. rate: 4 Hz

Target-substrate distance: 25 mm

Deposition time: 2 min

Substrate: Single crystal Si, Target: YBCO

Substrate temperature: 25 C

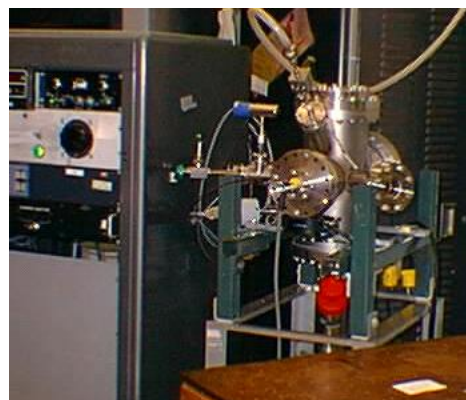


Figure 2a.4.7.1

Particles synthesized were analyzed by transmission electron Microscopy (TEM), by Atomic Force Microscopy (AFM) and by Scanning Tunneling Microscopy (STM). The TEM

measurements were made by Dr. Kevin Leedy of SN. The AFM and STM measurements were completed by Mr. Larry Grazulis of ML.

2a.4.8 AFM Micrographs

Lower laser energy density necessary for particles with a mean size of ~3-5 nm in diameter at 50 mJ/pulse. 100 mJ/pulse leads to amorphous films. Optimization may result in lower diameter particles. Higher energy may cause essentially complete dissociation of ablated material or nanoparticles with sufficient kinetic energy to dissociate on impact. May provide indication of YBCO formation in pulsed laser deposition atomic species vs. molecular globules.

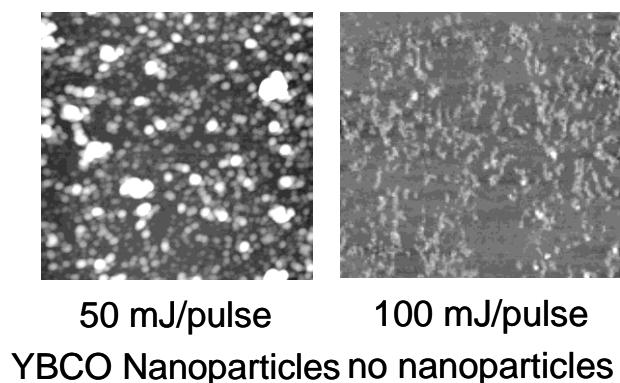


Figure 2a.4.8.1

2a.4.9 TEM Images

TEM also indicates nanoparticle creation (light spots in the micrograph.) Diffuse rings indicate very small grain sizes. The particles are on the order of 5 nm. They may not be Y123 and are probably not superconducting.

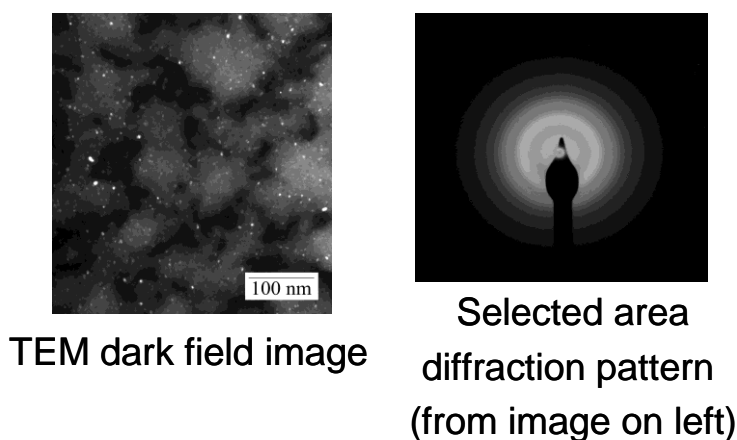


Figure 2a.4.9.1

2a.4.10 Formation Mechanisms

Using conventional PLD, the laser interacts with target resulting primarily in the ejection of neutral & singly ionized atomic Ba, Y and Cu. In high vacuum, ejected atoms leave target with hyperthermal energies (several eV's) in rectilinear trajectories until striking substrate. A thin film of the target material is formed on the substrate. At high pressure (a few Torr), the ejected species are quickly thermalized by the ambient gas allowing nucleation in the gas phase to form molecules and larger conglomerations. If residence time is sufficiently long, nanoparticles form. From results presented, the formation of the nanoparticles is a function of the higher pressure AND the laser energy. There are a couple possible explanations. The plasma generated by the higher energy laser pulse is too energetic to allow nanoparticles to be thermalized and agglomerate within the 25 mm nucleation zone. The nanoparticles that were formed under the 100 mJ conditions but were subsequently destroyed by exposure to the (higher energy) flux of ablated material or the nanoparticles themselves had sufficient kinetic energy to dissociate upon impact with the substrate.

2a.4.11 Emission Intensity

Emission intensity from neutral Ba (■) $^1P_1 \rightarrow ^1S_0$ at $\lambda = 553.5$ nm, Y(♦) $^2D_{5/2}^o \rightarrow ^2D_{5/2}$ at $\lambda = 643.5$ nm, and Cu(o) $^2P_{3/2}^o \rightarrow ^2D_{5/2}$ at $\lambda = 510.6$ nm, as a function of laser energy.

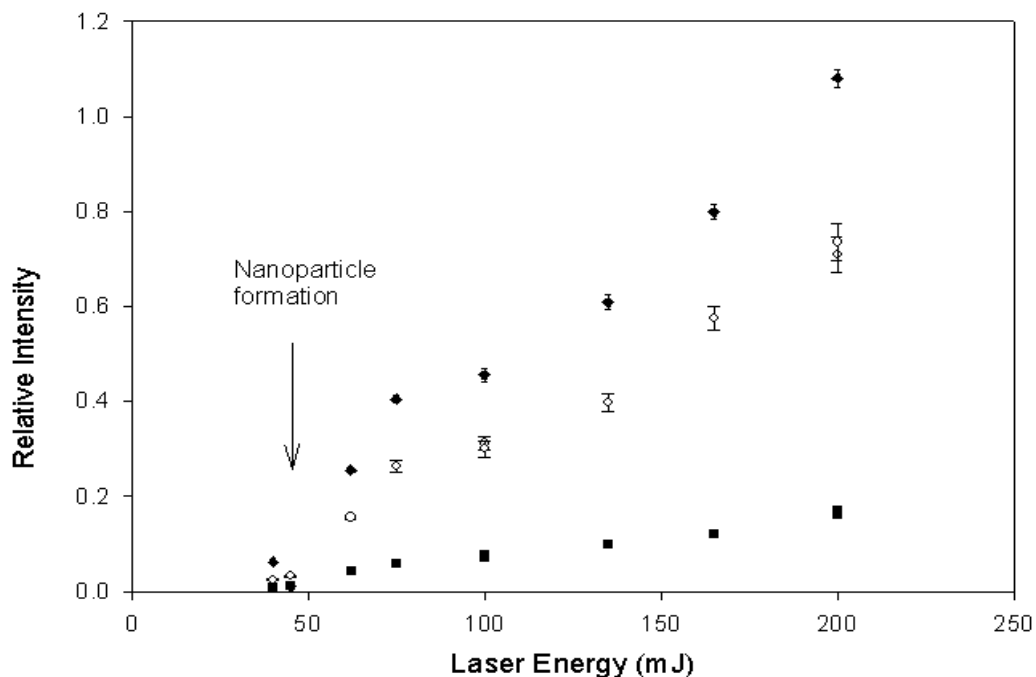


Figure 2a.4.11.1

Note that there exists a common laser energy threshold for significant emission near 40 mJ. The visible plume emission is very weak under conditions for YBCO nanoparticle formation. Apparently the plume must be depleted of most of its energy before the formation of nanoparticles can be supported. Both gas phase clustering and the survival of deposited YBCO nanoparticles would be aided by a less energized PLD plume. The relative intensity of the three atomic species is determined by the electronic state distribution and does not reflect the total

atomic content in the plume. The approximately linear dependence on laser energy suggests the emission intensity depends primarily on the total number of ablated atoms.

2a.4.12 Electronic Temperature

Electronic temperature for the PLD plume with a 5 Torr oxygen background pressure as derived from the relative intensity of the neutral yttrium $^2D^o_{5/2} \rightarrow ^2D_{5/2}$ and $^4F^o_{7/2} \rightarrow ^4F_{7/2}$ emission lines.

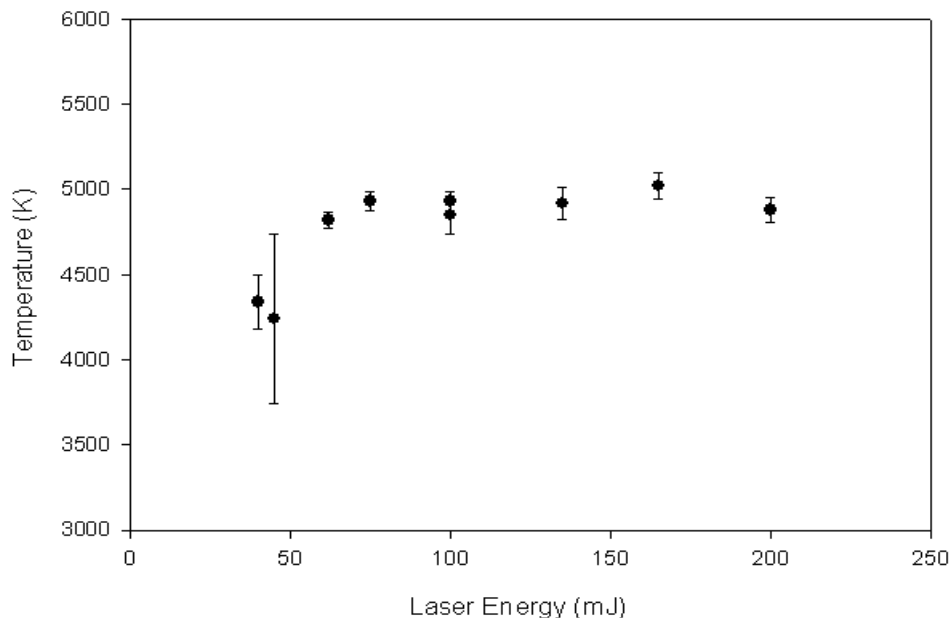


Figure 2a.4.12.1

A single electronic temperature does not adequately represent all the observed spectra, indicating that the plume is dominated by non-equilibrium kinetics. There is only a weak dependence on deposition laser energy. The plume remains collisionally dynamic even at high pressures and low laser energies.

2a.4.13 Ion/Neutral Ratios

Shown is the relative concentration of BaII $^2P^o_{1,2}$ and BaI $^1P^o_1$ as a function of ablation laser energy per pulse. The plume retains considerable excitation even when the total plume emission is low and nanoparticles are formed.

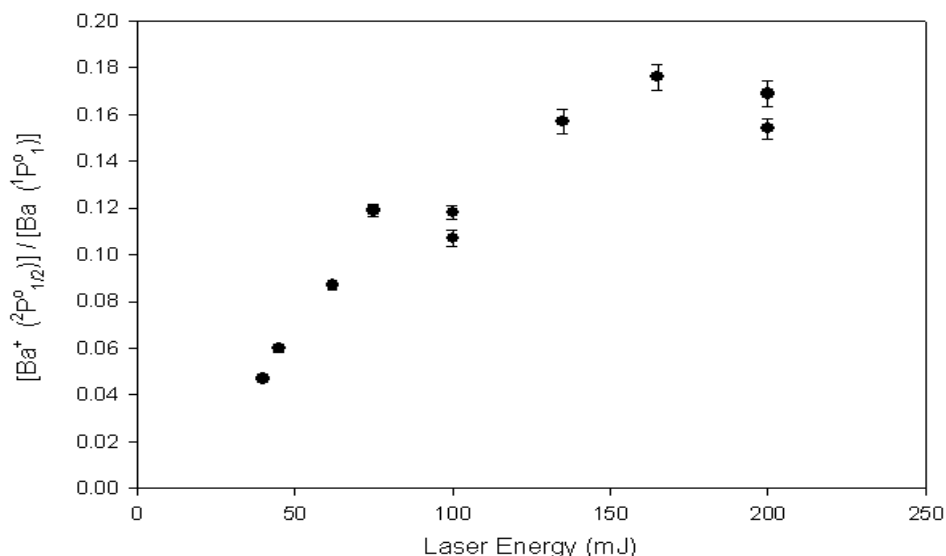


Figure 2a.4.13.1

2a.4.14 Summary

Nanoparticles were created from a YBCO target by PLD, using the typical PLD system for HTS YBCO. Some initial work was performed to understand the formation mechanisms in the PLD Plume. However, further work is necessary to test pinning ability.

2a.5 FLUX PINNING and PROPERTIES OF (Y,RE)Ba₂Cu₃O_{7-Z} THIN FILM SUPERCONDUCTORS: RE = Eu, Er

References: 21, 24

T. J. Haugan¹

1. Air Force Research Laboratory, Wright-Patterson AFB, OH 45433

Presented at MRS Spring 2005, 28 Mar 05

2a.5.1 Flux Pinning Methods

- Nanoparticle additions
 - easy route for industry to consider because of compatibility with YBCO processing (M. Rupich, AMSC)
 - AFRL by PLD: 211 or Y₂O₃
 - AMSC by MOD: (Ho,Y)O₂
 - Superpower by MOCVD: (Sm-x)
 - ORNL+UWisc by MOD: Y₂O₃
 - Rare-earth or chemical substitution/additions
 - potentially low cost, but process incompatibility issues (?)
 - Nanoscale control or engineering
 - hard to scale-up (?)
- Irradiation
- too expensive (?)

2a.5.2 OUTLINE

- Nanoparticulate Dispersions
 - Insulators
 - (Y₂BaCuO₅/123)_xN
 - (CeO₂/123)_xN
 - (Y₂O₃/123)_xN
 - (MgO/123)_xN
 - (La₂O₃/123)_xN
 - Superconductors
 - (Sm123/123)_xN
- Flux Pinning Mechanism
 - U₀ pinning potential study
 - Angular dependence of J_c(H)
 - 123 layer thickness study

2a.5.3 Properties of Pinning Agents

	Crystal Type	Lattice mismatch (X/123)%	Island Nanoparticle Shape
Y₂BaCuO₅	tetragonal	-7% to +4%*	hockey-puck
Y₂O₃	cubic	-2.5%	
CeO₂	cubic	-0.5%	monolayer
MgO	cubic	+9.6%	
La₂BaCuO₅	tetragonal	-12% to	
Sm123	tetragonal	~ +1%	

* For Y₂BaCuO₅ b-axis oriented: a* = a/2, b* = b/3, c* = cx2

Figure 2a.5.3.1

2a.5.4 J_c(H) Optimization

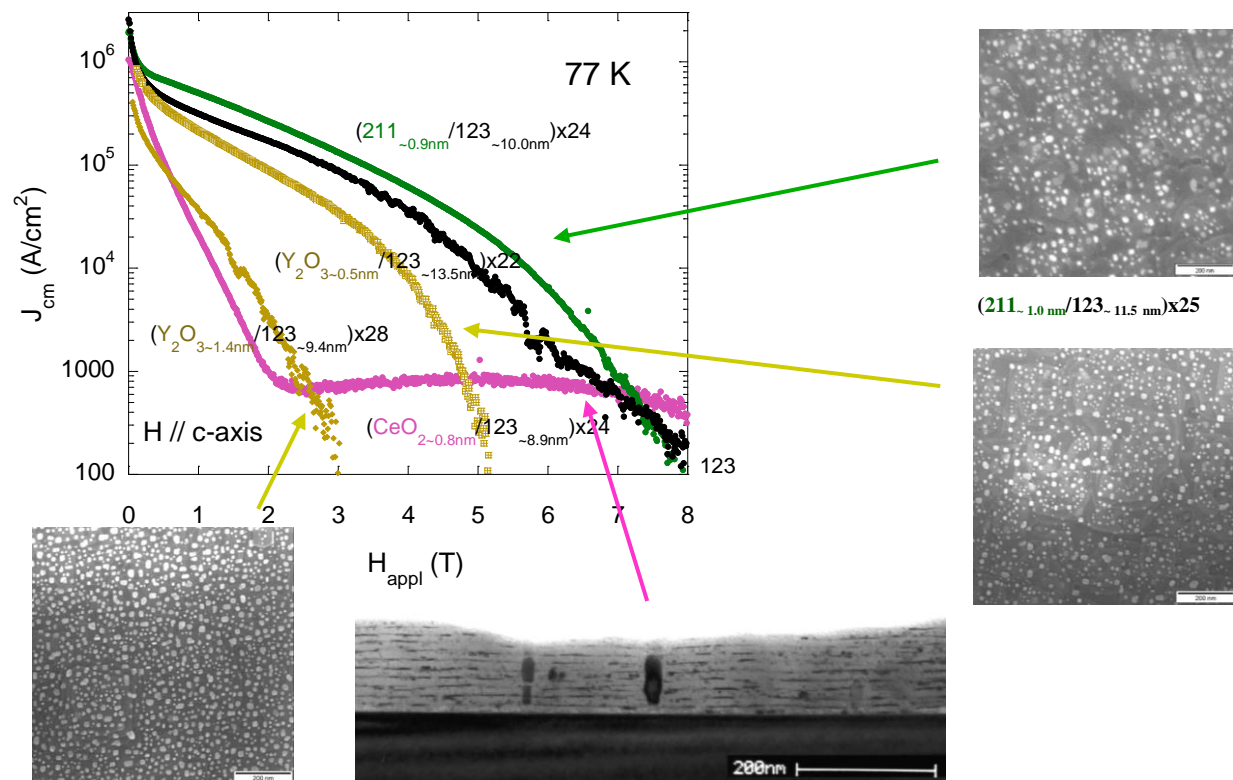


Figure 2a.5.4.1

2a.5.5 Pinning Layer Optimization

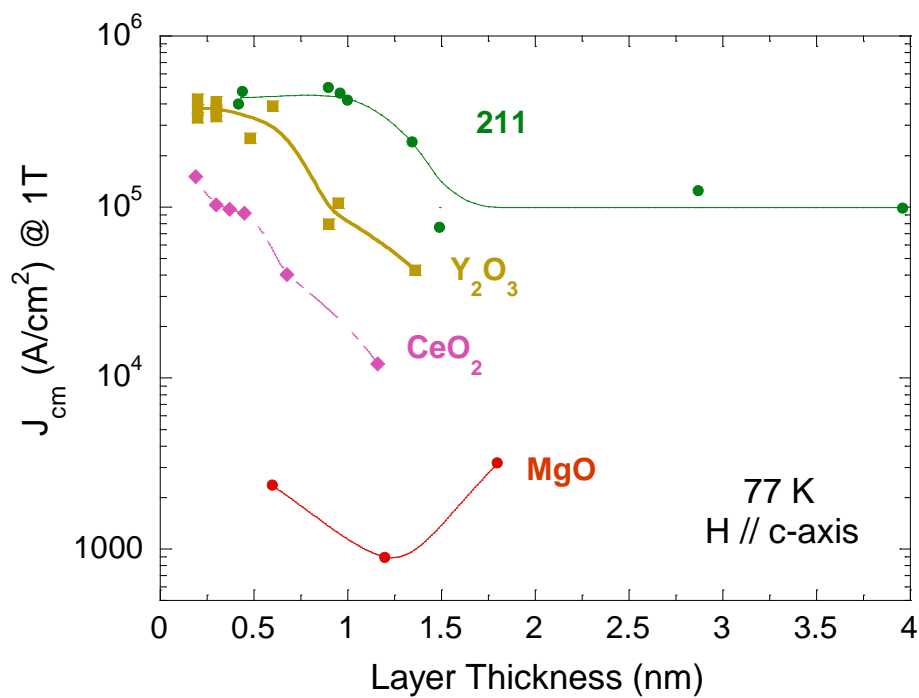
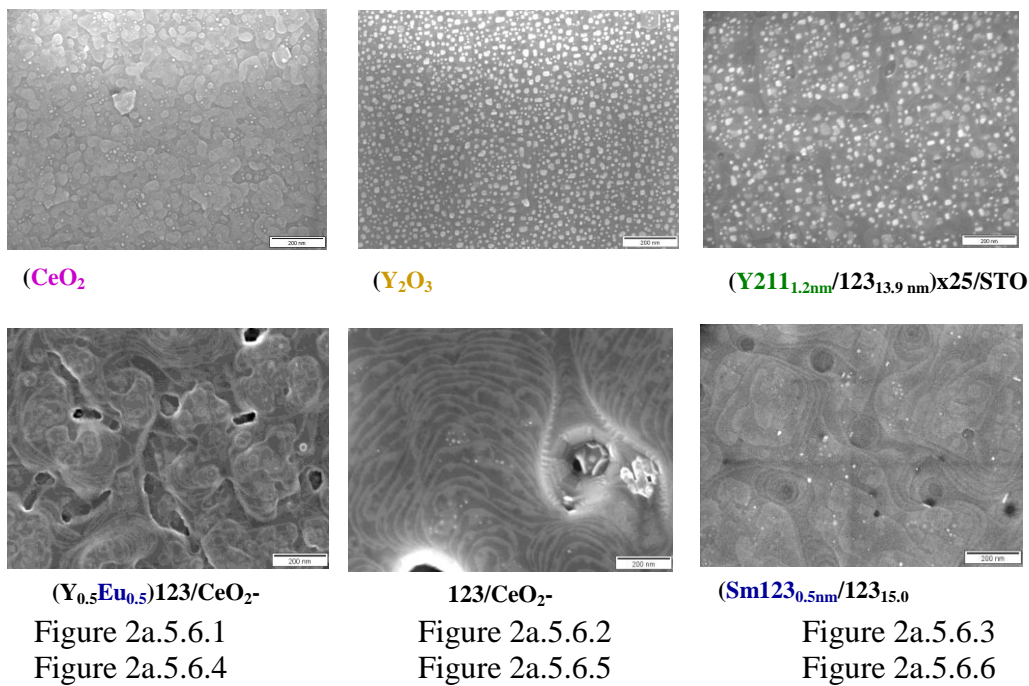


Figure 2a.5.5.1

2a.5.6 Ultra-high Resolution SEM



2a.5.7 SEM Micrographs

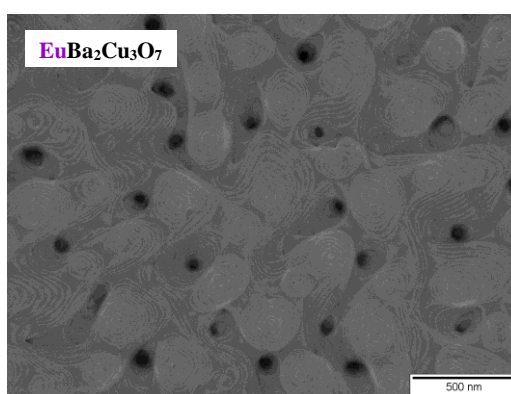
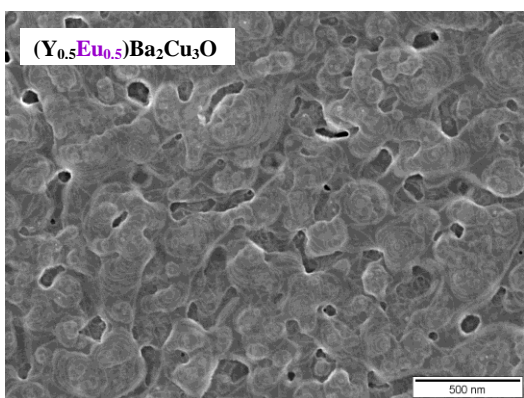
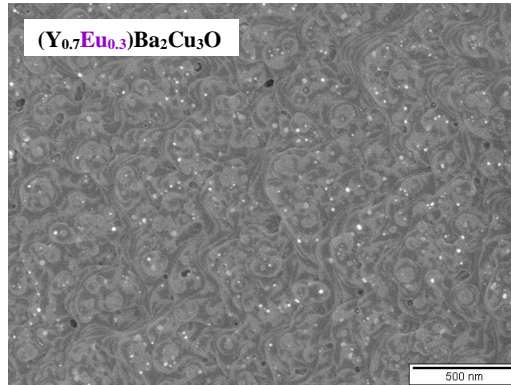
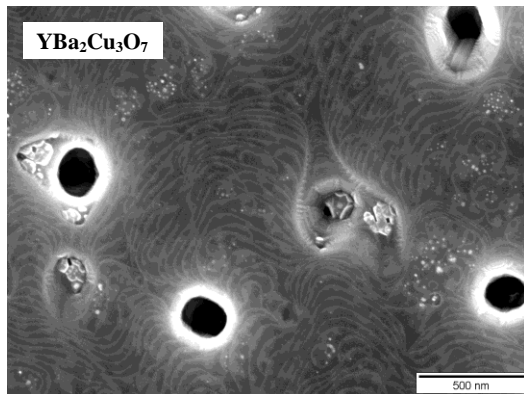


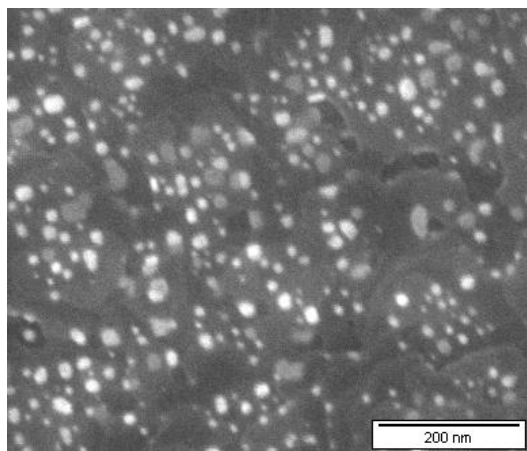
Figure 2a.5.7.1

Figure 2a.5.7.2

Figure 2a.5.7.3

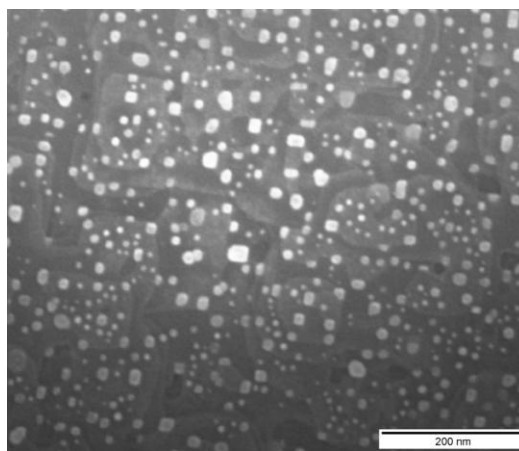
Figure 2a.5.7.4

2a.5.8 Surface Nanoparticles



Particle Density $\sim 1.2 \times 10^{11} \text{ cm}^{-2}$

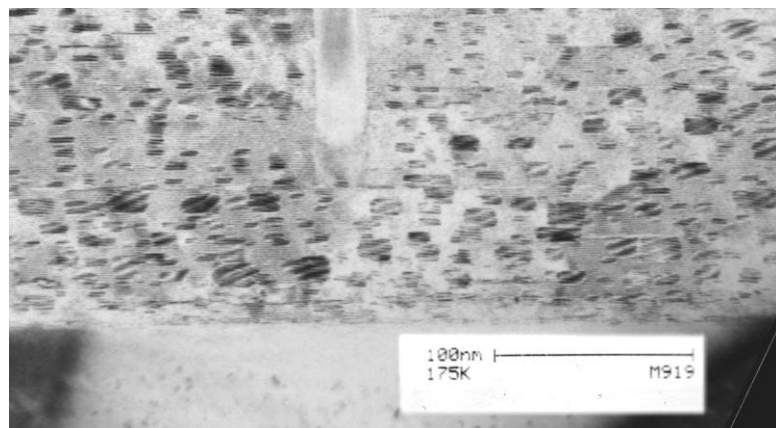
Figure 2a.5.8.1



Particle Density $\sim 1.7 \times 10^{11} \text{ cm}^{-2}$

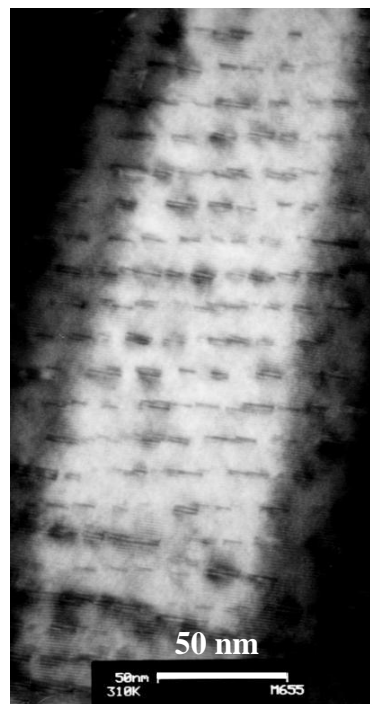
Figure 2a.5.8.2

2a.5.9 (211/123)xN on Single Crystals



(211_{1.7nm}/123_{6.6nm})x35

100 nm



(211_{0.9nm}/123_{10.4nm})x200

-T. Haugan, P. N. Barnes, et. al. *Nature* **430**, 867 (2004).

Figure 2a.5.9.1

Figure 2a.5.9.2

2a.5.10 T_c by AC susceptibility

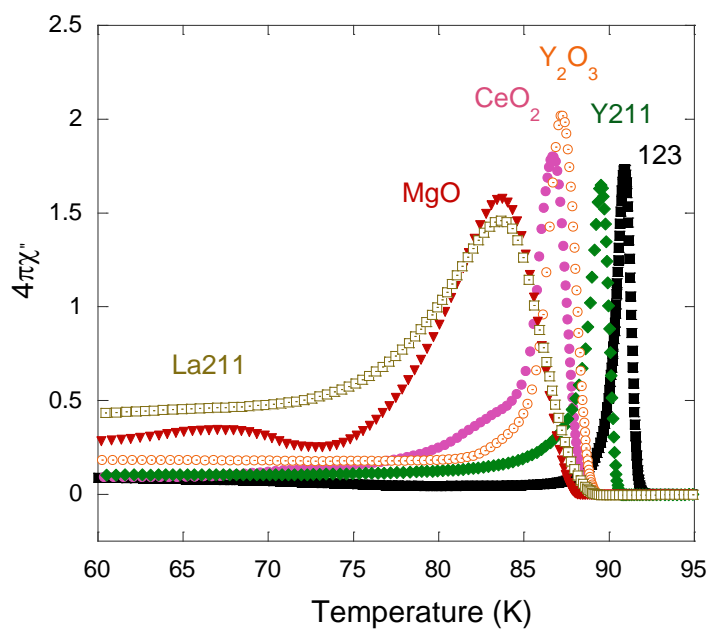


Figure 2a.5.10.1

2a.5.11 Jc by VSM

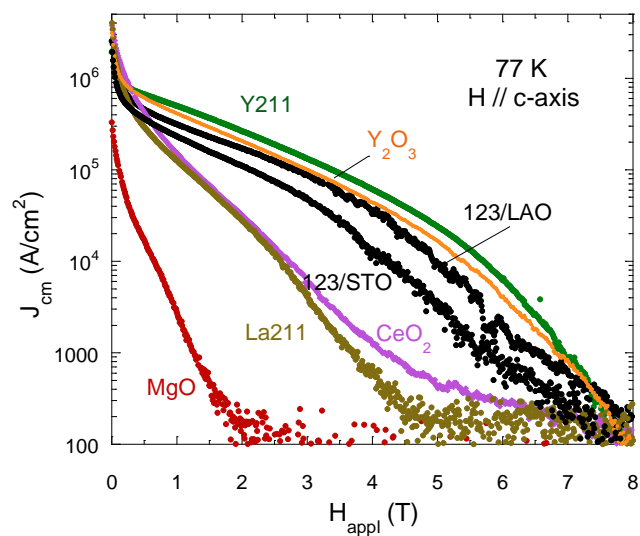


Figure 2a.5.11.1

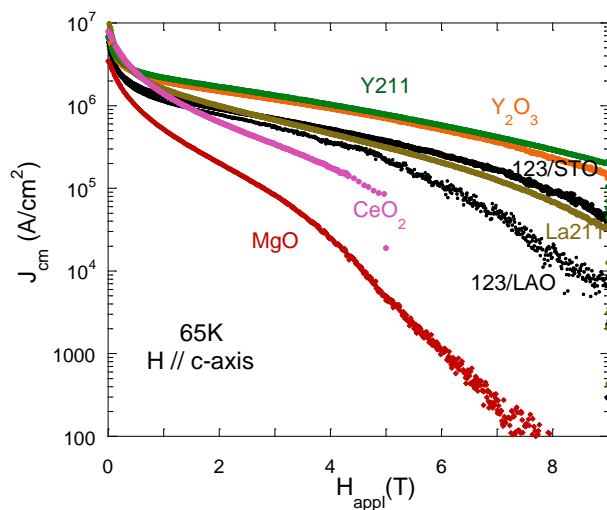
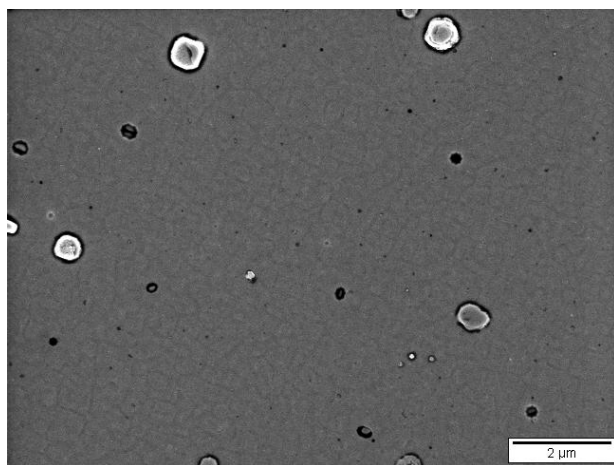


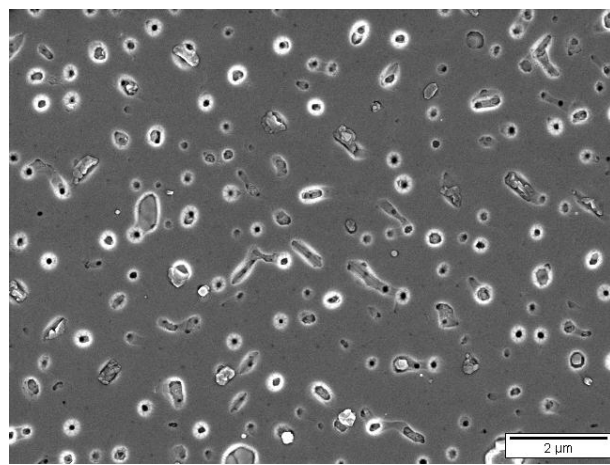
Figure 2a.5.11.2

2a.5.12 Sm123 multilayers



(Sm123)_{0.5nm}/123_{15.0}

Figure 2a.5.12.1



(Sm123)_{1.9nm}/123_{14.3 nm})x20/STO

Figure 2a.5.12.2

2a.5.13 Sm123 Addition

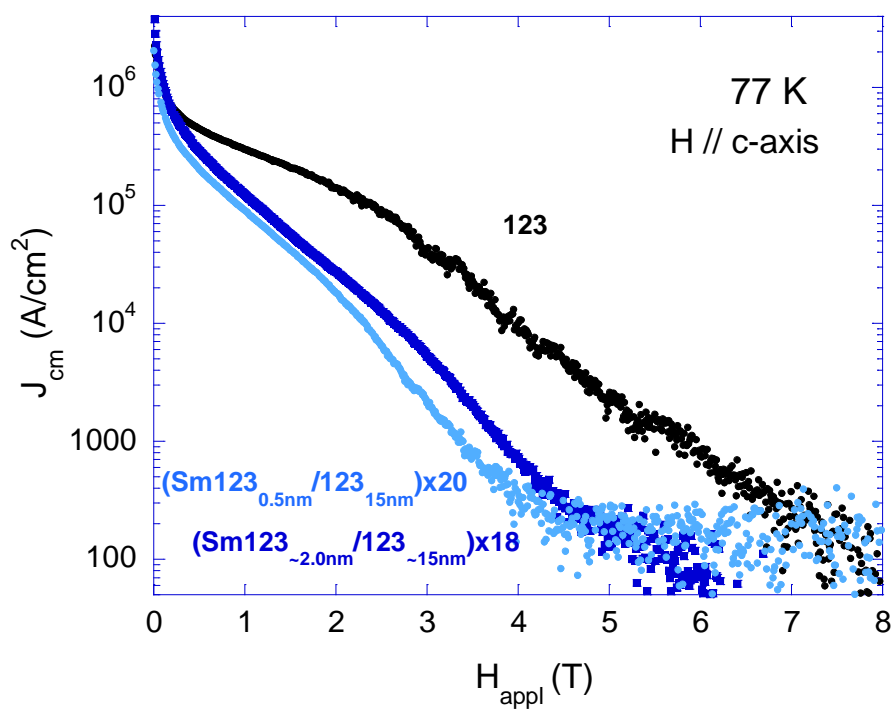


Figure 2a.5.13.1

2a.5.14 Transport Jc

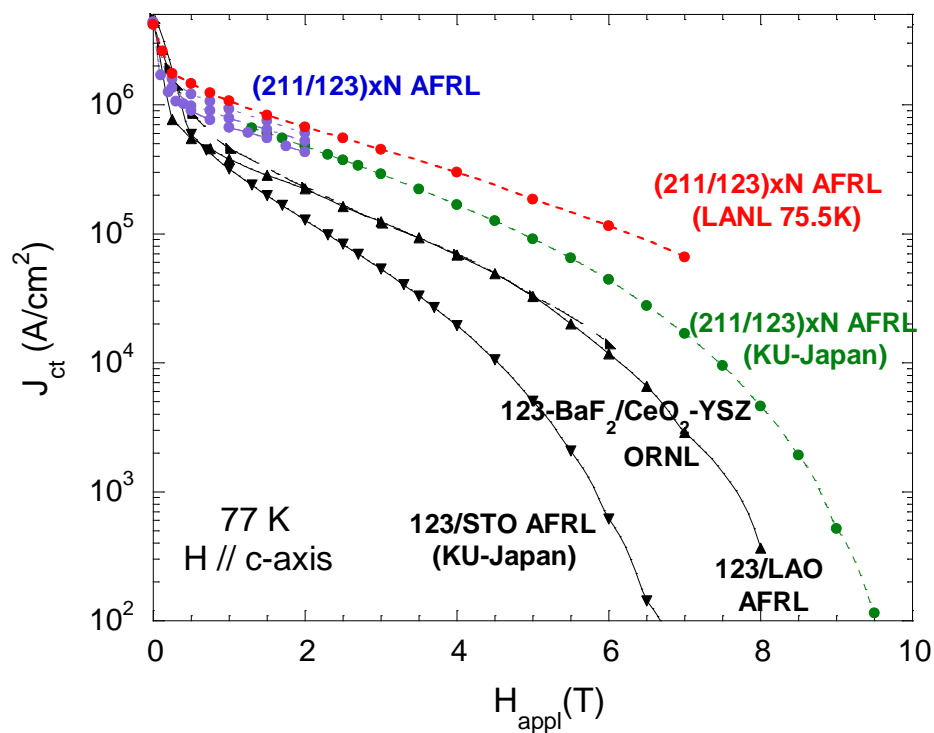


Figure 2a.5.14.1

2a.5.15 Transport Jc

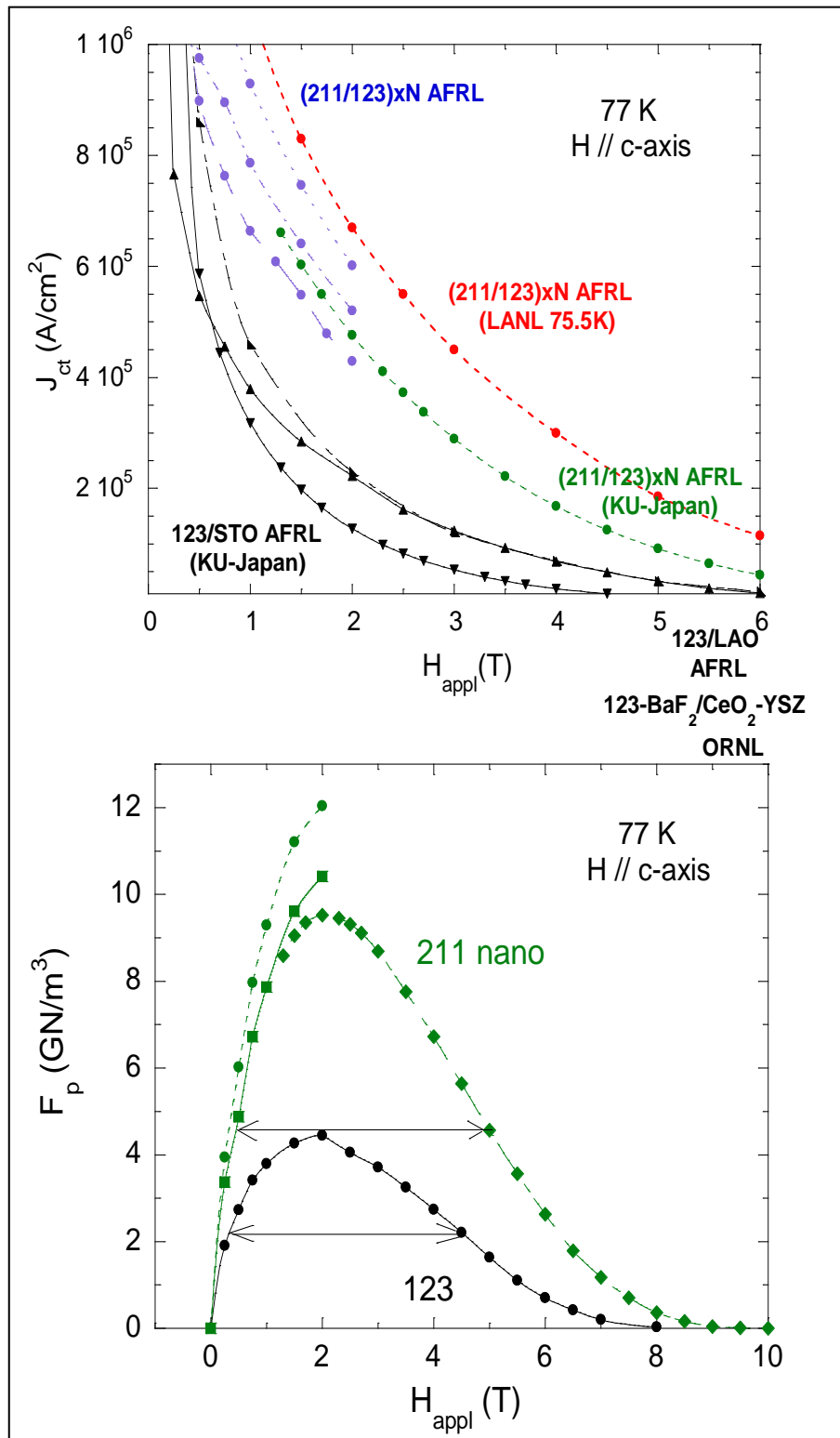


Figure 2a.5.15.1

2a.5.16 Pinning Force Studies

$F_p = Jc \times B$ (Lorentz Force)

$F_p \sim (N \cdot U_0 \beta / d)$

U_0 = pinning well potential, N = # sites, d = defect size

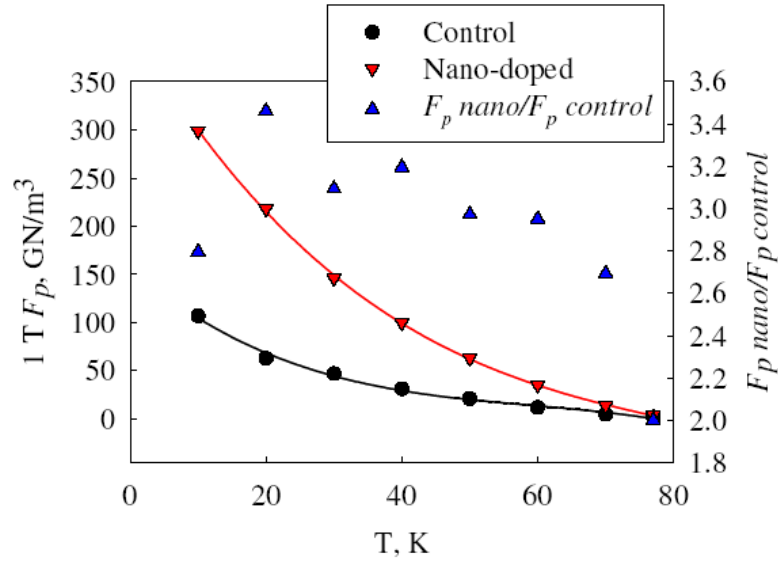


Figure 2a.5.16.1

2a.5.17 Jcm Ramp Rate Studies

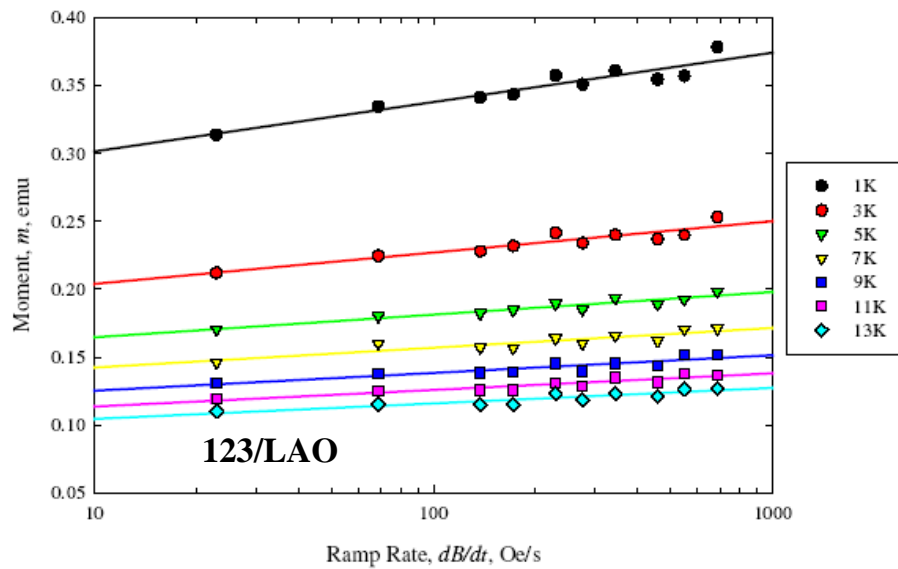
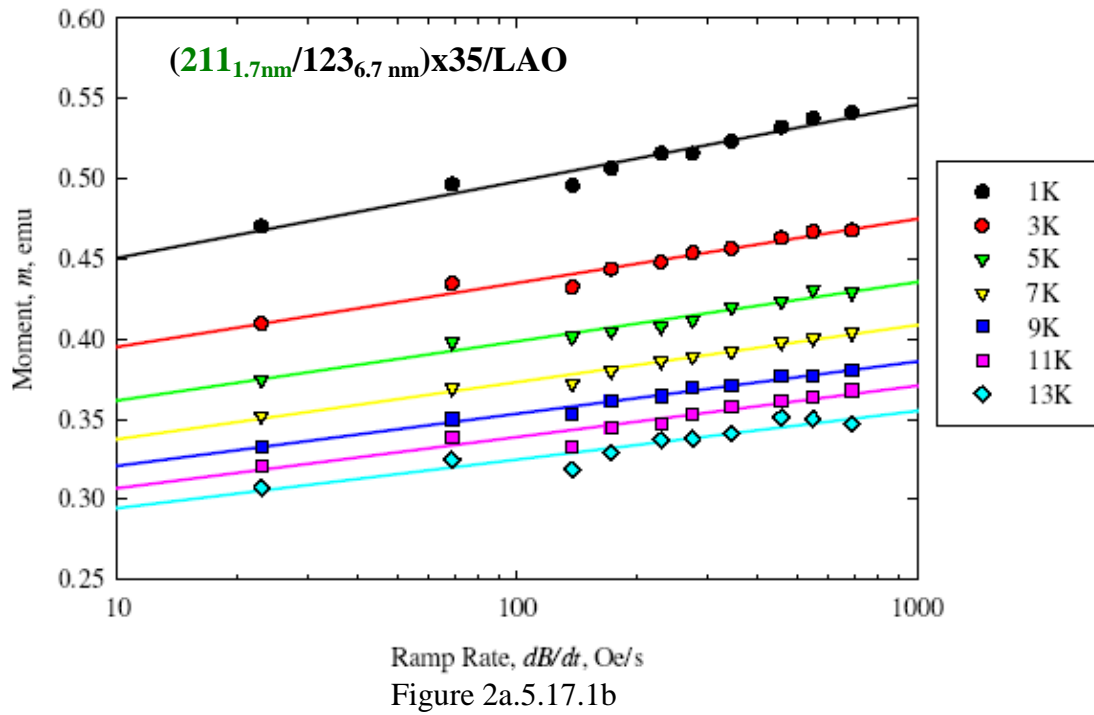


Figure 5.8. Control sample at 30 K.

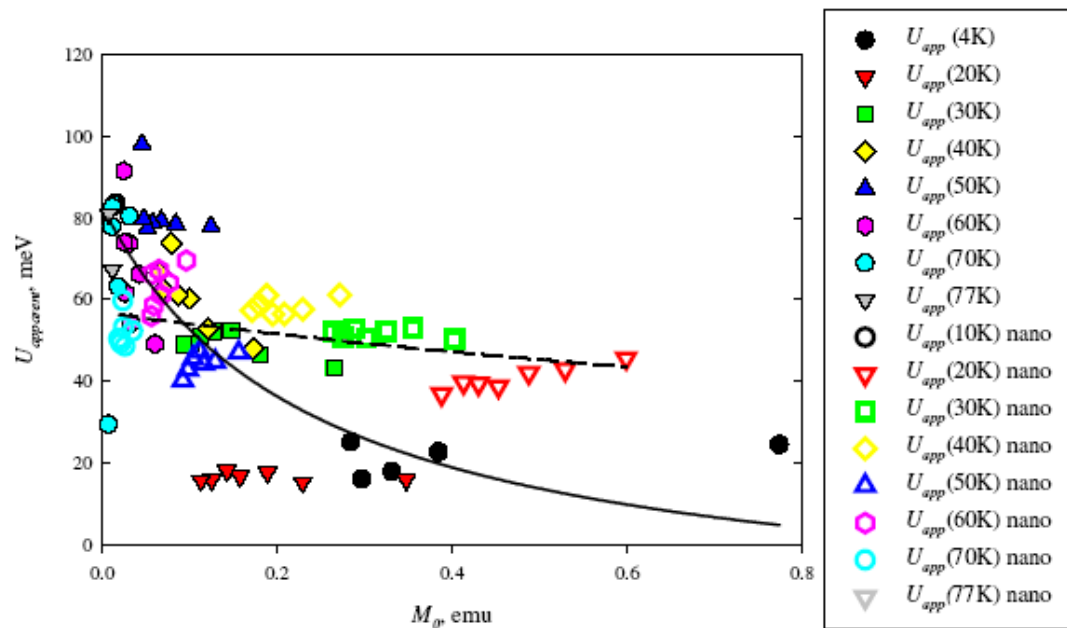
$$M = M_0 + (kTM_0/U_{\text{eff}}) \cdot \ln(dH/dt)$$

Figure 2a.5.17.1a



2a.5.18 U_o Pinning Potentials

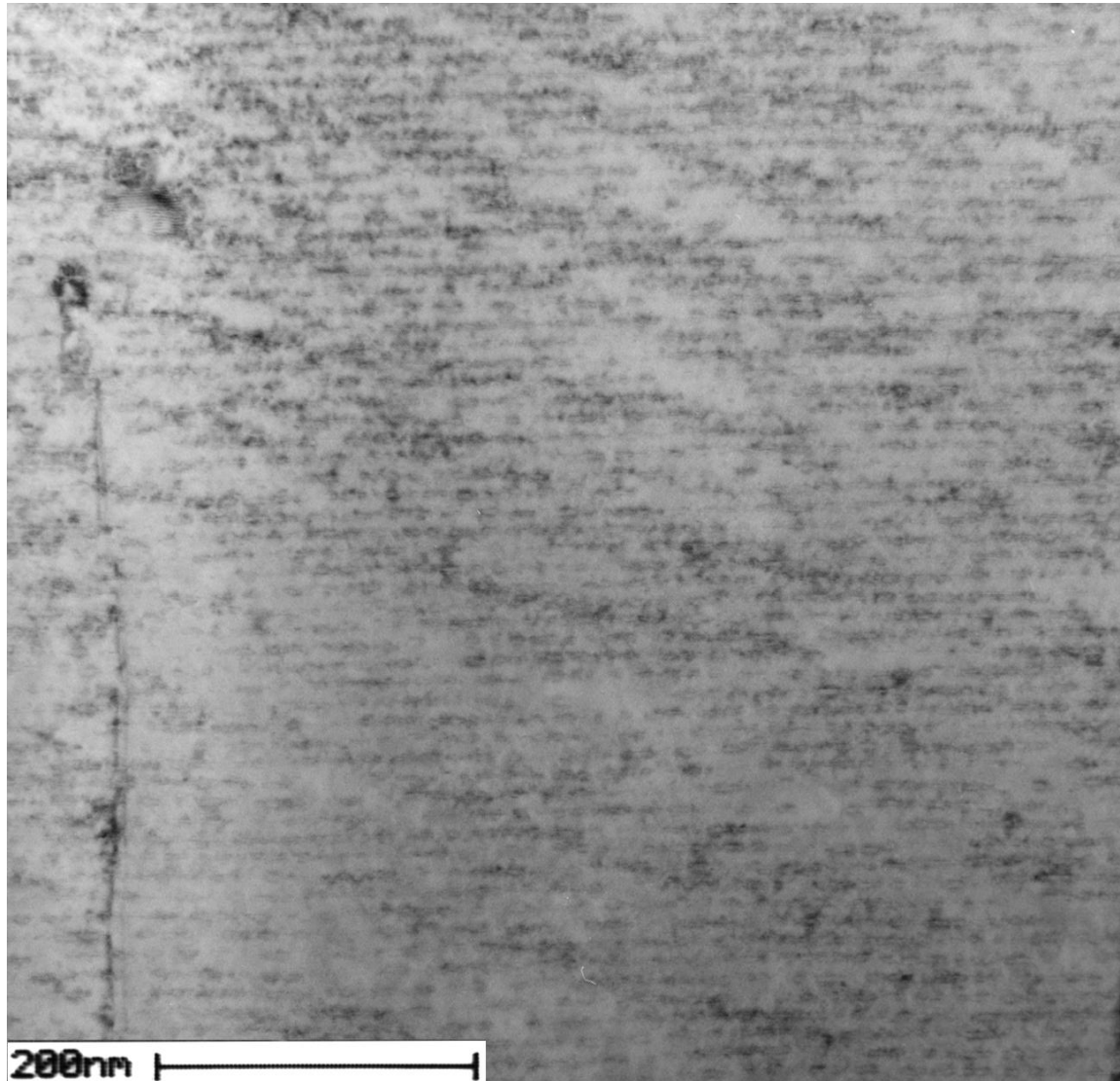
Y123
 $U_o \sim 80$
211 nano
 $U_o \sim 60$



Conclusion:

$F_p \sim (N \cdot U_o^\beta / d)$ and U_o are almost the same, so F_p is increasing for 211-nano samples by increasing the number of pinning sites N .

2a.5.19 TEM Cross-Sections



($211_{0.9\text{nm}}$ / $123_{10.5\text{nm}}$)x200

Figure 2a.5.19.1

2a.5.20 CONCLUSIONS

Nanoparticle Additions

Insulators

- ($\text{Y}_2\text{BaCuO}_5/123$)_xN strongest pinning so far
- ($\text{Y}_2\text{O}_3/123$)_xN pinning not as strong as 211 (?)
- ($\text{CeO}_2/123$)_xN, not fully optimized yet
- ($\text{MgO}/123$)_xN T_c decrease from chemical reaction
- ($\text{La}_{211}/123$)_xN poor T_c and J_c at 77K but good J_c at 65K low H

Superconductors

- ($\text{Sm}_{123}/123$)_xN surprising negative result

Flux Pinning Mechanisms

- For Y211 addition, the increase of flux pinning strength is suggested to be caused by increasing the number of pinning centers, as the pinning potential was only slightly decreased (surprising result!).
- Angular dependence indicates uniform pinning properties, except along ab plane.
- For (211/123)_xN films, a ‘matching field effect’ was observed precisely along the a-b plane, indicating enhanced pinning at specific H values that can be controlled by varying the 123 layer

2a.5.21 Flux Pinning Questions

How effective can point-defect pinning be, i.e. what is the maximum $J_c(H, \theta, T)$ that can be obtained?

Note: (H, θ , T) all critical to optimize. In many cases $\theta = 30-60^\circ$ are the weakest J_c s.

What types of second-phase particles are necessary:

lattice matched?

chemically inert?

(might be a function of $J_c(H, \theta, T)$)

What types of second-phase particle additions are compatible with industrial processing methods?

(a) MOD (Y_2O_3 , Ho_2O_3)

(b) MOCVD (Y_2O_3 , Sm-123, other?)

(c) High-rate PLD (Y_2O_3 , Sm-123 ?, Y211 ?)

What size and volume density are necessary?

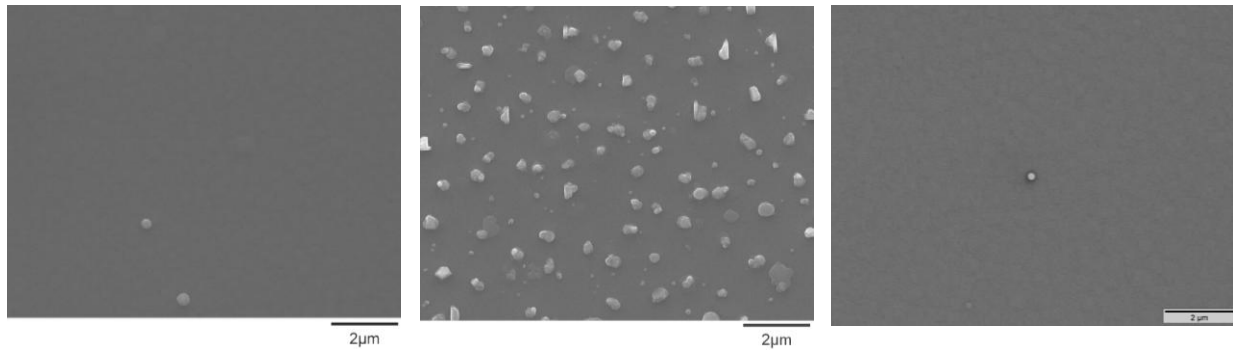
For layering of defects, what spacings are necessary?

What are secondary effects of nanoparticles:

- ΔT_c variations?
- chemical diffusion?
- extended stress effects?

Other considerations.....

2a.5.22 Film Surface Defects



($\text{211}_{1.3\text{nm}}/\text{123}_{12.5\text{nm}}$)x24

($\text{CeO}_2\sim 0.8\text{nm}/\text{123}\sim 10\text{nm}$)x24
(chemical reaction!)

($\text{Y}_2\text{O}_3\sim 0.3\text{nm}/\text{123}\sim 13.8\text{nm}$)x22

Note: at $\sim 780^\circ\text{C}$; CeO_2 reaction can be reduced/eliminated with lower substrate temperature.

Figure 2a.5.25.1

Figure 2a.5.25.2

Figure 2a.5.25.3

2a.5.23 J_c by VSM

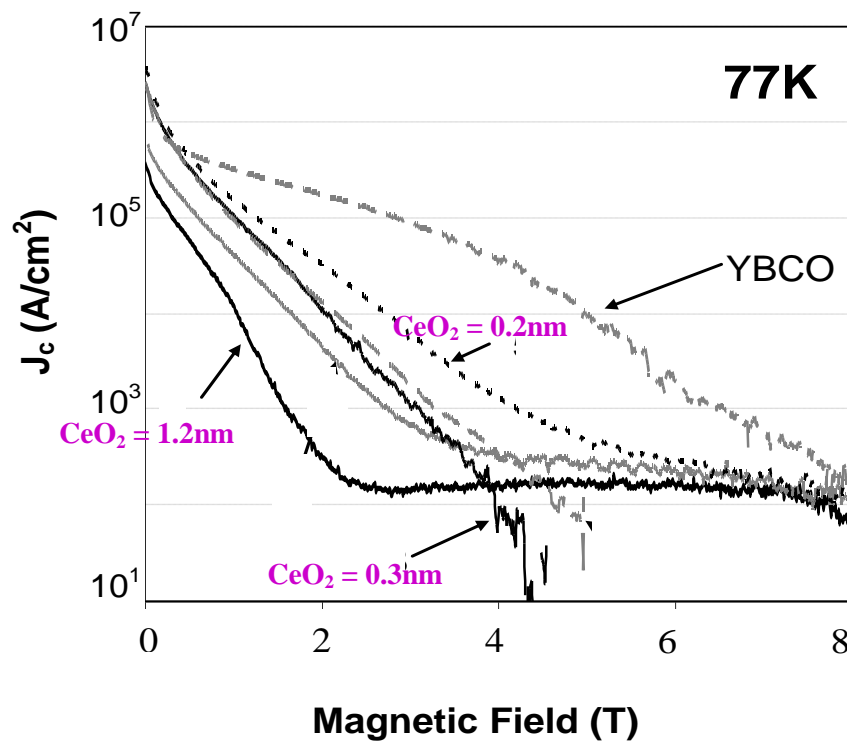
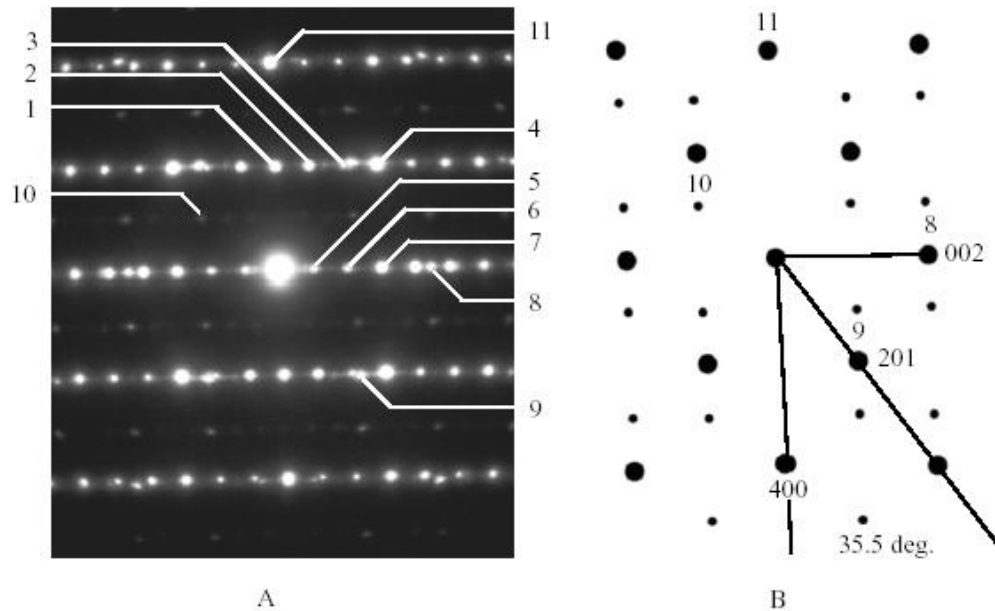


Figure 2a.5.26.1

2a.5.24 TEM Diffraction Patterns

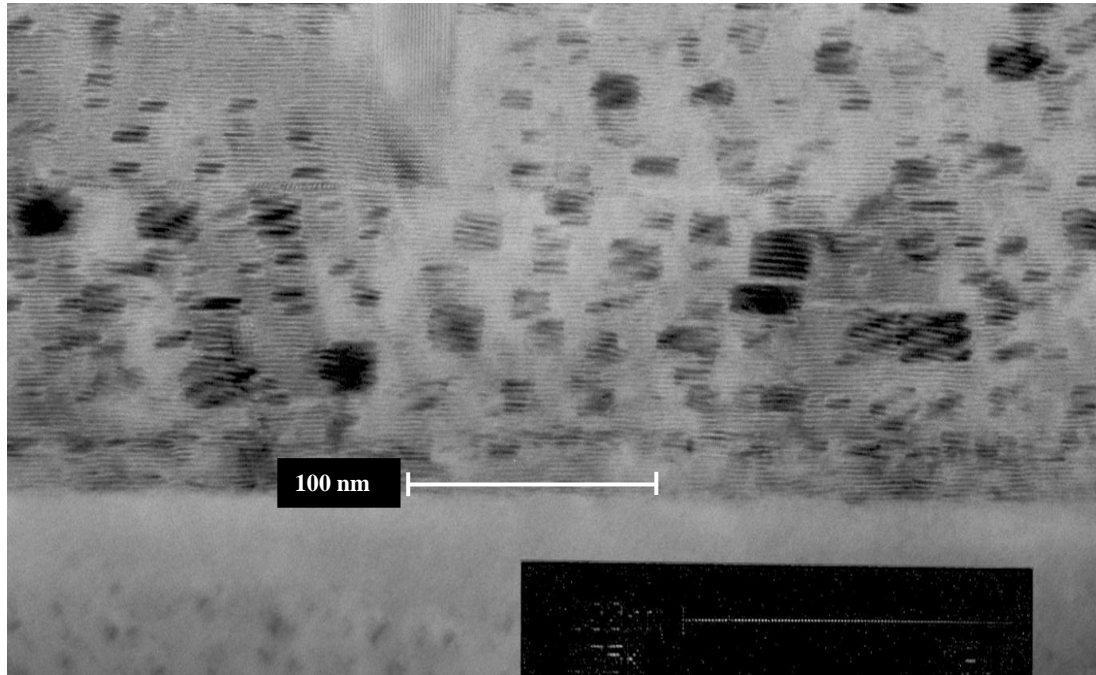


Electron diffraction pattern taken parallel to the substrate/thin film interface.
A) Selected area diffraction pattern 123-YBCO [100] zone axis pattern. B) Proposed 211-YBCO zone axis pattern. C) Pattern reflections with corresponding phase identification and indexing. Orientation relationship is $(100)_{123} // (010)_{211}$, $[010]_{123} // [100]_{211}$.

- Selected area diffraction (SAD) confirms formation of 211 and 123 phases
- 211 and 123 in relative states of strain

Figure 2a.5.29.1

2a.5.25 TEM X-Section



(211_{1.6nm}/123_{6.6nm})x35,
~ 80 sec interval

- **211 Density $\sim 5 \times 10^{11} \text{ cm}^{-2}$,**
 $H_{\text{equivalent}} \sim 10\text{T}$
- **Evidence of defects columns from**
localized stress between 211 defects ?

Figure 2a.5.30.1

2a.5.26

Problems with using chemically reactive additions:

- poor superconducting/insulating interfaces which decreases pinning strength
- diffusion creates much larger low T_c regions
- chemically reactive materials may work with much lower concentrations, or is diffusion too much of a problem (?)

T_c transitions are good indicators for flux pinning potential at 77K.

2a.5.27 Jct(H,theta)

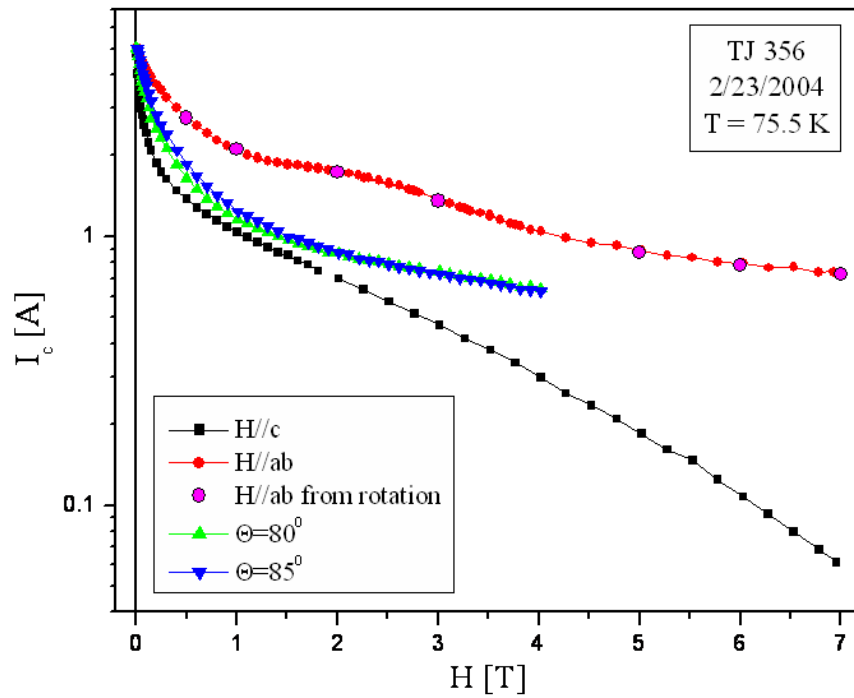


Figure 2a.5.32.1

2a.5.28 Fp studies

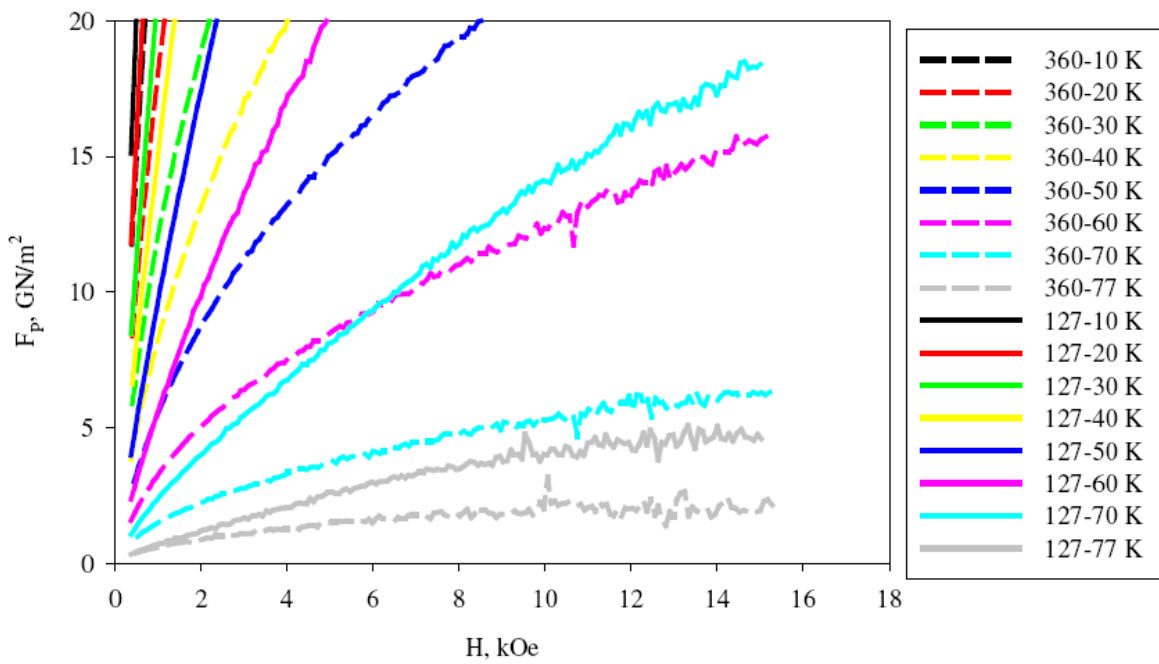
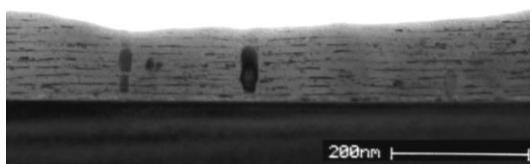
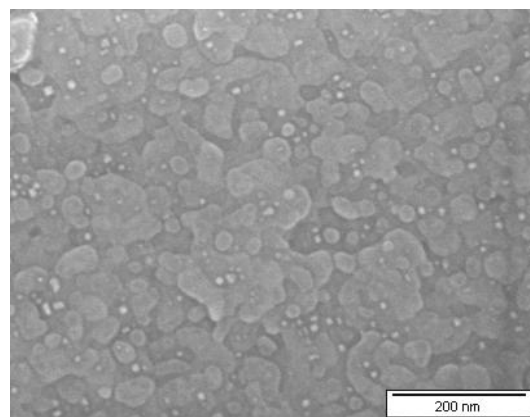


Figure 2a.5.33.1

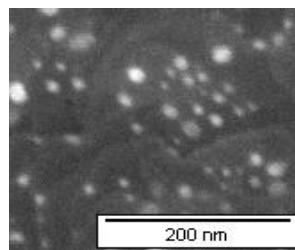
2a.5.29 X-sections



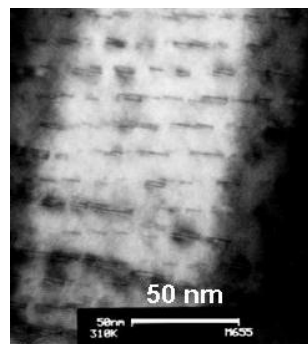
(CeO_2 1.0nm/123₁₁nm)x24

200

Figure 2a.5.34.1



(211_{0.9}nm/123_{10.4}nm)x

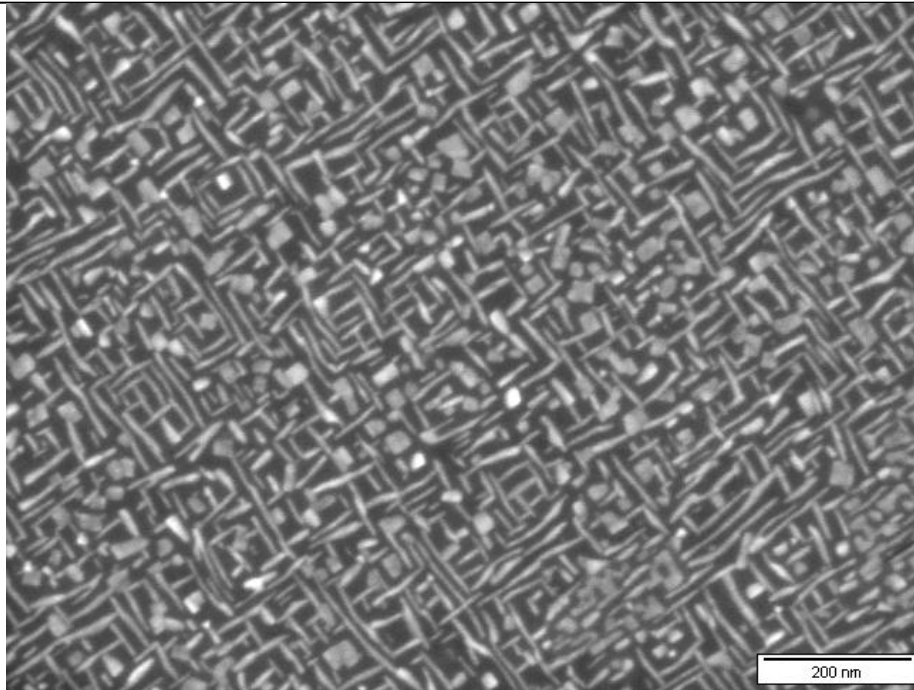


(211_{0.9}nm/123_{10.4}nm)x2

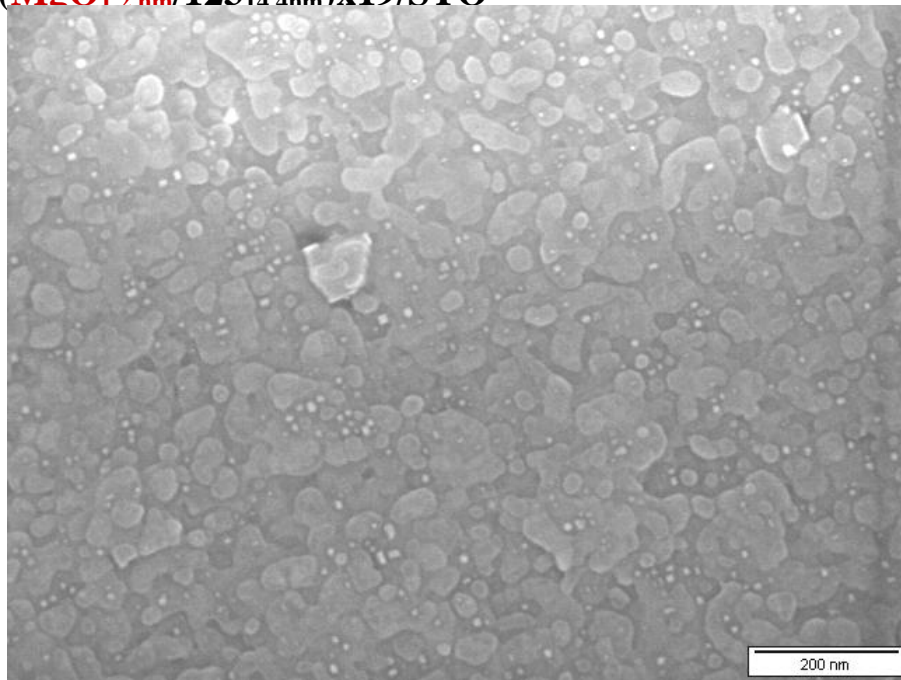
Figure 2a.5.34.2

Figure 2a.5.34.3

2a.5.30



(**MgO**_{1.2 nm}/123_{14.4 nm})x19/STO



(**CeO₂**_{1.2 nm}/123_{15.6 nm})x24/STO

Figure 2a.5.36.1

2a.6 Controlled nanoparticulate flux pinning structures in YBCO

References: 1,2,3, 6,7, 8,9 10,11,12,13,14

P. N. Barnes¹

1. Air Force Research Laboratory, Propulsion Directorate

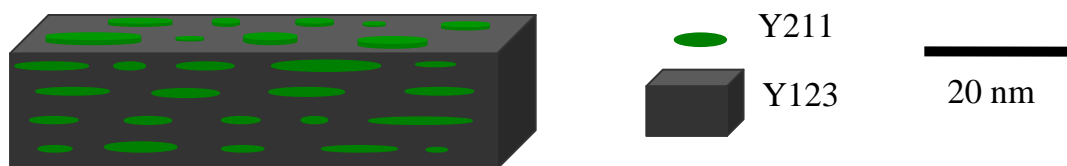
Presented at CCA 2004, 18-20 Nov 04

2a.6.1 Magnetic Flux Pinning

- Since their discovery in 1986, work has proceeded to develop the use of HTS materials for power applications.
- However, magnetic flux is not fully expelled, but contained in quantized fluxons, whose motion prevents larger supercurrents.
- The critical current of HTS conductors can be enhanced by incorporating a high density of extended defects to act as pinning centers for the fluxons which penetrate the material.
- Pinning is optimized when the defect
 - size approaches the coherence length, $\sim 2\text{-}4\text{ nm}$ for YBCO
 - number per unit area is large, $\sim (H/2) \times 10^{11} / \text{cm}^2$ $\langle H \text{ in Tesla} \rangle$
- Other than irradiation methods, the small size and high density have been difficult to achieve by material processing methods

2a.6.2 Pinning by Nanoparticulates

- New process achieving a controlled dispersion of nanoparticles in YBCO with the necessary particulate nanosize and high density
 - Places insulating nanoparticles into the YBCO by alternating, consecutive depositions of YBCO and the insulating material
 - Pulsed laser deposition of YBCO and particulate pseudo-layers
 - Particulate formation caused by lattice mismatching with the YBCO
- An advantage of the multilayered structure is the ability to have some degree of control over the nanoparticle dispersion parameters.
 - provides an excellent experimental structure to test theories of flux pinning in HTS for uniform dispersions of point-like defects



T.J. Haugan, P.N. Barnes, I. Maartense, E.J. Lee, M. Sumption, and C.B. Cobb, J. Mater. Res., **18**, 2618 (2003).

T. Haugan, P.N. Barnes, R. Wheeler, F. Meisenkothen, and M. Sumption, Nature, **430**, 867 (2004).

Figure 2a.6.2.1

2a.6.3 Experimental

- Alternate layers of nanoparticulates and YBCO were deposited by pulsed laser deposition (PLD)
 - Lambda Physik laser (LPX 305i) used operating at KrF wavelength (248 nm)
 - Laser fluence $\sim 3.2 \text{ J/cm}^2$, ablation spot size $\sim 1 \times 6.5 \text{ mm}^2$, 4 Hz rate
 - Oxygen deposition pressure 300 mTorr with O₂ flow of $\sim 1 \text{ l/min}$
 - Targets rotated and rastered during deposition
- Crystalline substrates of SrTiO₃ and LaAlO₃ used
 - Also done on buffered RABiTS
- After deposition, films were annealed in oxygen

2a.6.4 Critical Transition Temperature

- Critical transition temperature (T_c) of typical samples are shown
 - transition remains sharp and T_c reduction is minor considering operation temperature
- Critical current density (J_c) remains high in self-field
- On bi-crystals the particulate structure dramatically improved critical current flow across the interface at high angles.

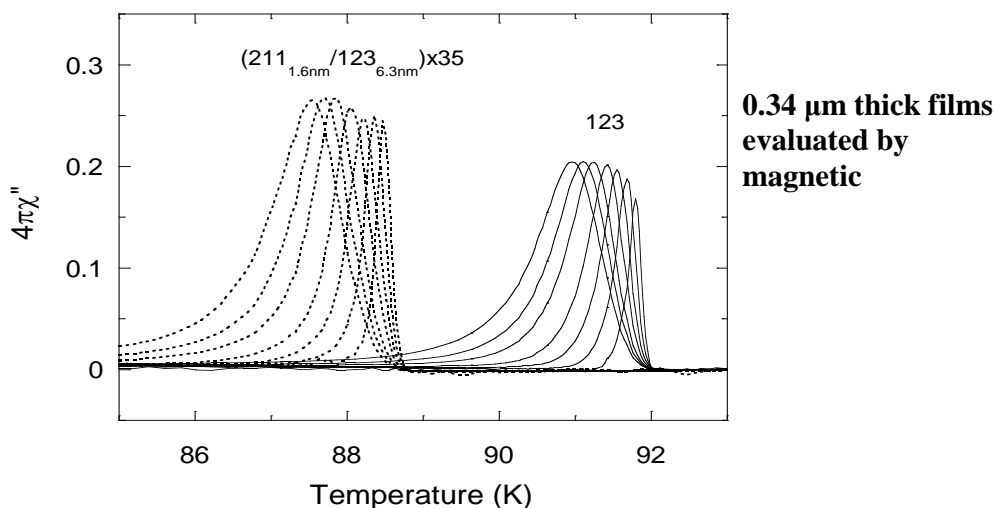


Figure 2a.6.4.1

2a.6.5 X-Ray Diffraction

- LEFT - Typical XRD θ -2 θ scans of Y211, (Y211/Y123) \times N, and Y123 films
 - Possible straining of 123 phase (lattice mismatch with 211)
 - Shift of 001 peaks in XRD to higher 2 θ values observed
- RIGHT - Typical phi scan of the (103) peak of a (2111.6nm/1236.2nm) \times 35 film
 - indicates the YBCO phase maintained excellent ab in-plane alignment in presence of nanoparticulates.

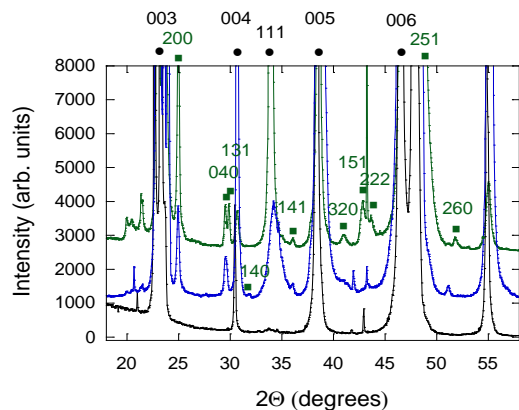


Figure 2a.6.5.1

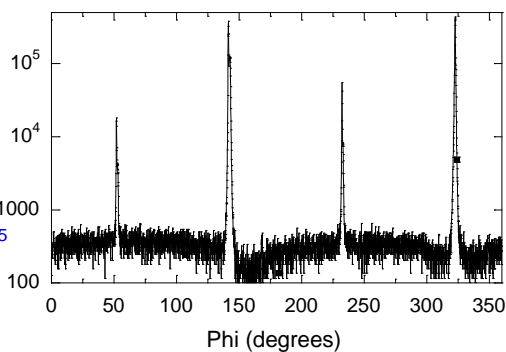


Figure 2a.6.5.2

2a.6.6 In-Field Performance

- J_c as a function of applied magnetic field for YBCO (Y123) films
 - on single crystal LaAlO_3 (AFRL and LANL), and on buffered tapes (ORNL)
- Samples of different layer spacings and particulate pseudo-layers
 - Improvement in J_c at 77 K is up to 200 – 300% at > 0.3 T
 - greater improvement at lower temperatures, 70 K shown

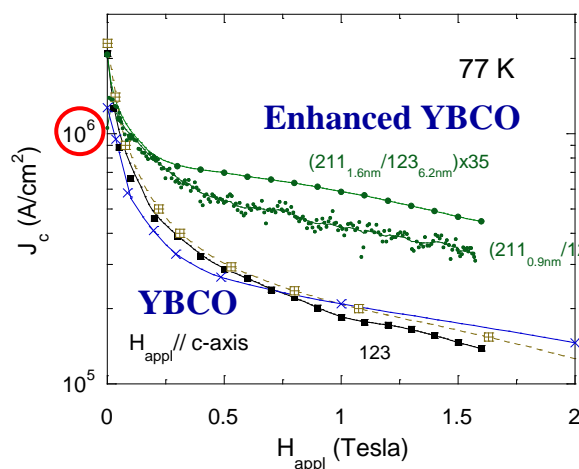


Figure 2a.6.6.1

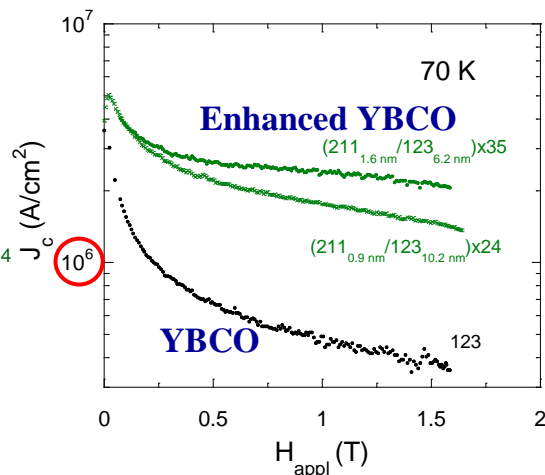


Figure 2a.6.6.2

2a.6.7 Transport J_c Comparison

- Transport J_c as a function of applied magnetic field for YBCO (Y123) films

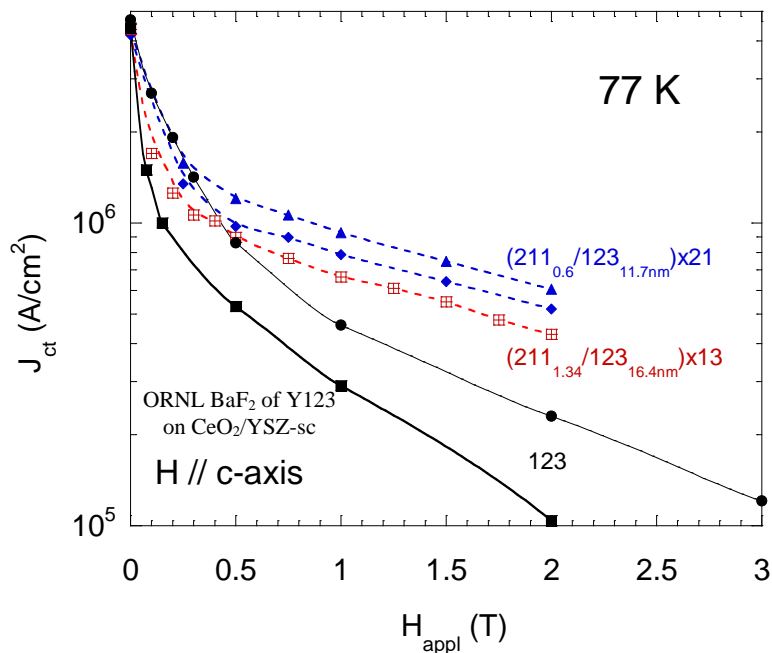
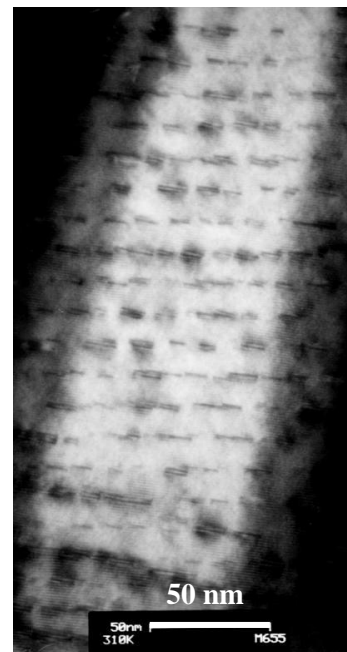


Figure 2a.6.7.1

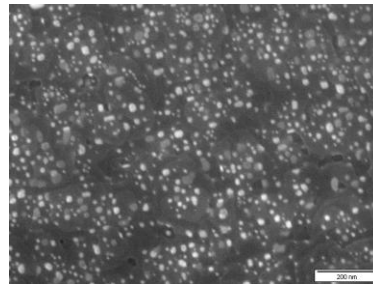


$(211_{0.9nm}/123_{10.4nm}) \times 200$

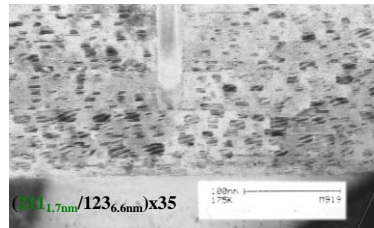
Figure 2a.6.7.2

2a.6.8 Micrographs of Nanoparticles

- Microscopy reveals a near-uniform dispersion of Y211 nanoparticles
 - Good epitaxial growth of YBCO is maintained around the Y211
- Lattice mismatching favors island growth of the nanoparticles
 - deposition is preferred on island-nucleated phases rather than the lattice-mismatched base layer
- Typical particle size is ~15 nm above and ~8 nm below and particle density about $\sim 10^{11}$ particles/cm²



Planar SEM



Cross-sectional TEM

Figure 2a.6.8.1

Figure 2a.6.8.2

2a.6.9 TEM of CeO₂ Layered Structure

- CeO₂ very closely lattice matched with Y123
 - Resulted in more of a multilayer structure than a particulate dispersion
 - Importance of lattice mismatching is underscored



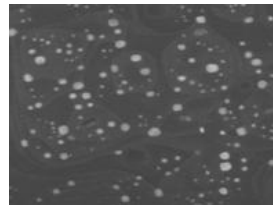
(CeO₂ 0.8nm / 123 11nm) x24

P.N. Barnes, T.J. Haugan, M.D. Sumption, S. Sathiraju, J.M. Evans, and J.C. Tolliver, Trans. MRS-J, **29**, 1385 (2004).

Figure 2a.6.9.1

2a.6.10 Y₂O₃ and CeO₂ Nano-inclusions

- **Pinning Issue of bottom images**



Y₂O₃ Nanoparticles

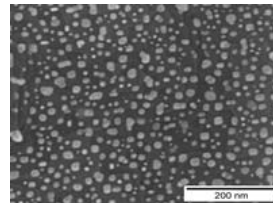
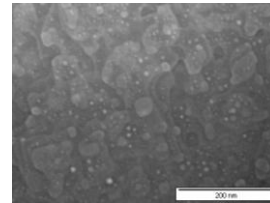


Figure 2a.6.10.1

Figure 2a.6.10.2

Shorter deposition
for inclusions
(thinner “pseudo-layer”)



CeO₂ Nanopatches

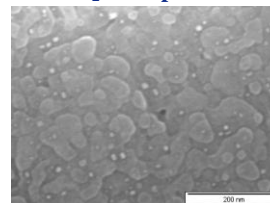


Figure 2a.6.10.3

Figure 2a.6.10.4

Longer deposition
for inclusions
(thicker “pseudo-layer”)

2a.6.11 Y₂O₃ Nanoparticulate Performance

- Note improved pinning at lower temperatures
 - Consistent in all nanoparticulate pinned samples

77 K

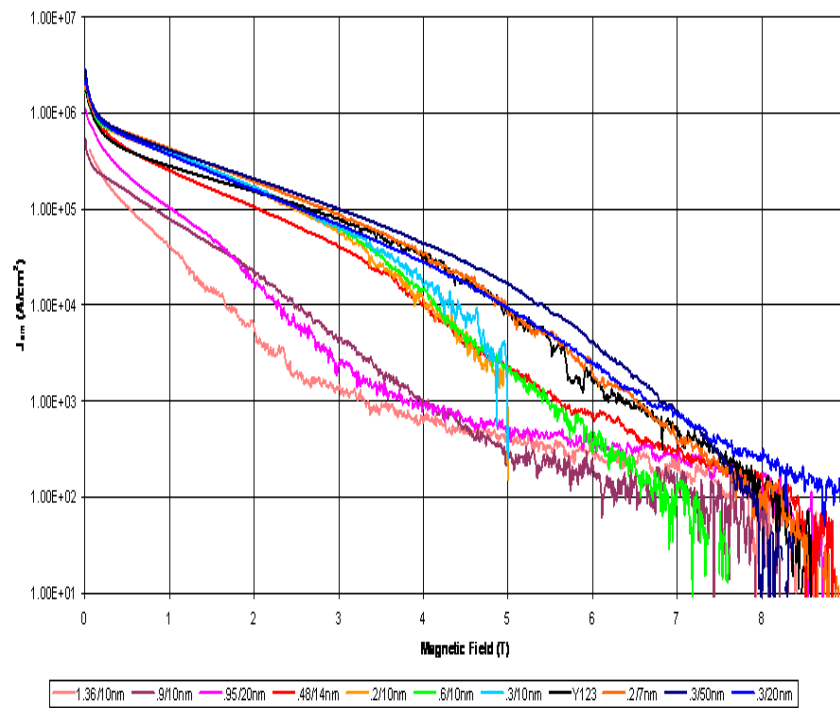


Figure 2a.6.11.1

70 K

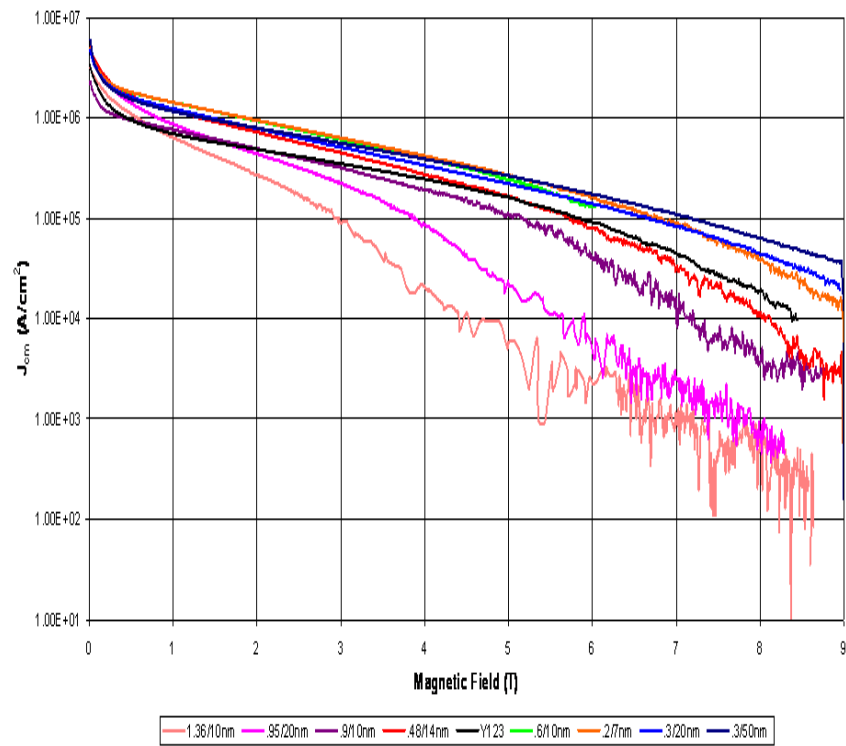


Figure 2a.6.11.2

2a.6.12 CeO2 Nanoparticulate Performance

Note peculiar behavior of CeO₂ nanopatches with more rapid convergence at ~10° lower temperature

Sample	Energy (mJ)	Rep Rate (Hz)	Dep Time (s)	Pulses (total no.)
1	511	4	3.75	15
2	511	2	4.5	9
3	196	2	4	8
4	196	4	3	12
5	196	2	2.5	5

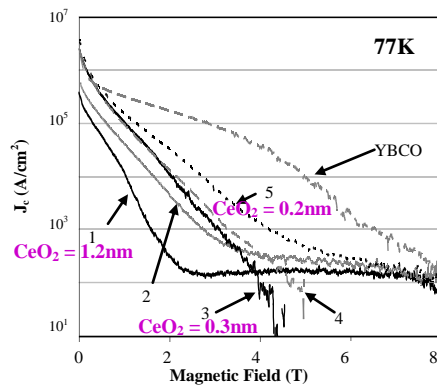


Figure 2a.6.12.1

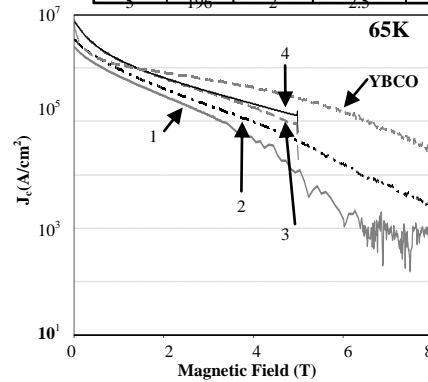


Figure 2a.6.12.2

P.N. Barnes, T.J. Haugan, C.V. Varanasi, T.A. Campbell, Appl. Phys. Lett., accepted.

2a.6.13 Properties of Pinning Agents

	Crystal Type	Lattice mismatch (X/123)%
Y_2BaCuO_5	tetragonal	-7% to +4%*
Y_2O_3	cubic	-2.5%
CeO_2	cubic	-0.5%
MgO	cubic	+9.6%
$\text{La}_2\text{BaCuO}_5$	tetragonal	-12% to +5%

* For Y_2BaCuO_5 b-axis oriented:
 $a^* = a/2$, $b^* = b/3$, $c^* = cx2$

Figure 2a.6.13.1

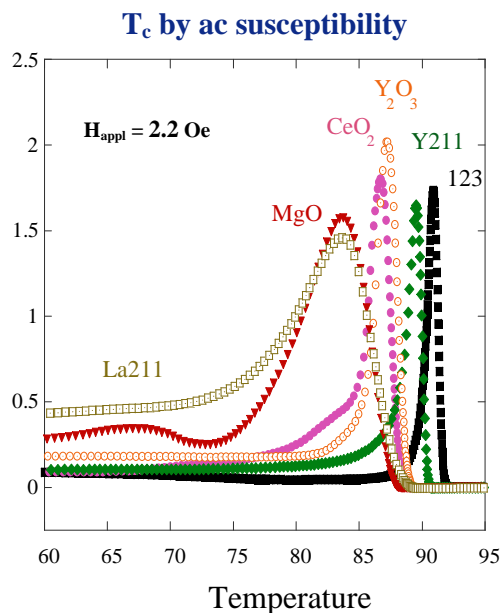


Figure 2a.6.13.2

2a.6.14 High Resolution Planar SEM

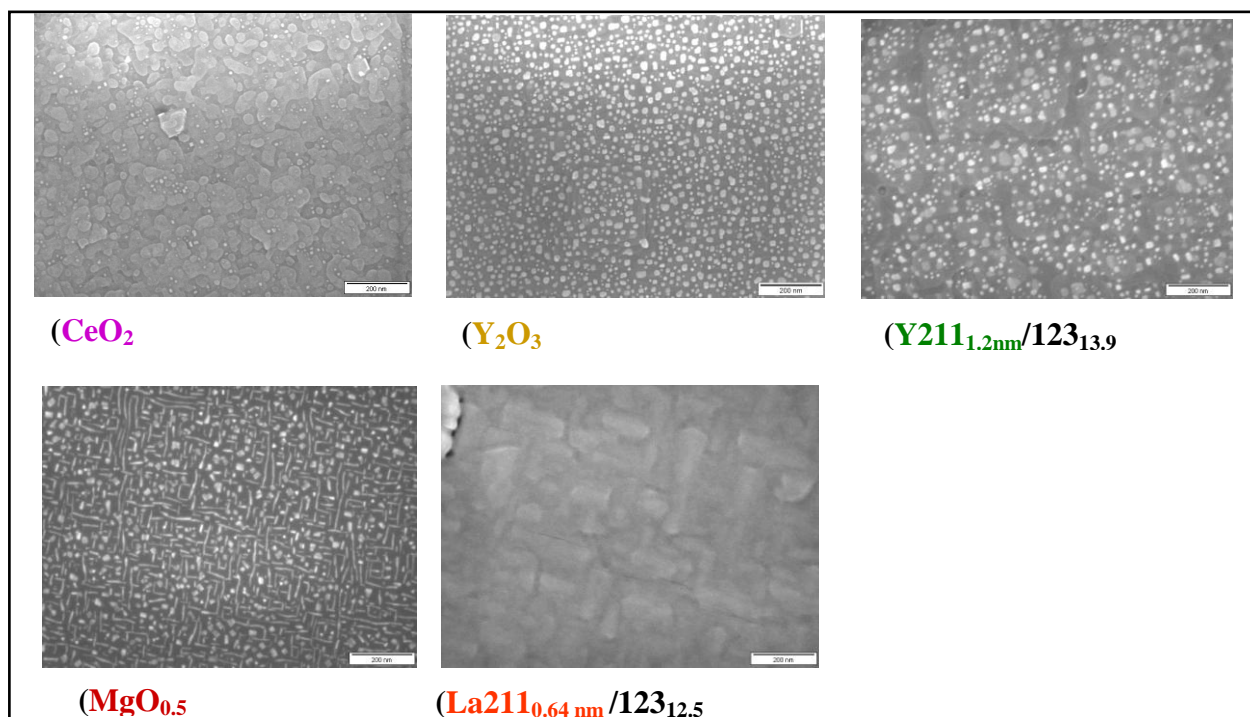


Figure 2a.6.14.1

2a.6.15 J_{cm} Comparison by VSM

- Only Y211 and Y_2O_3 are more extensively optimized
 - Others such as MgO and La211 are just initial results

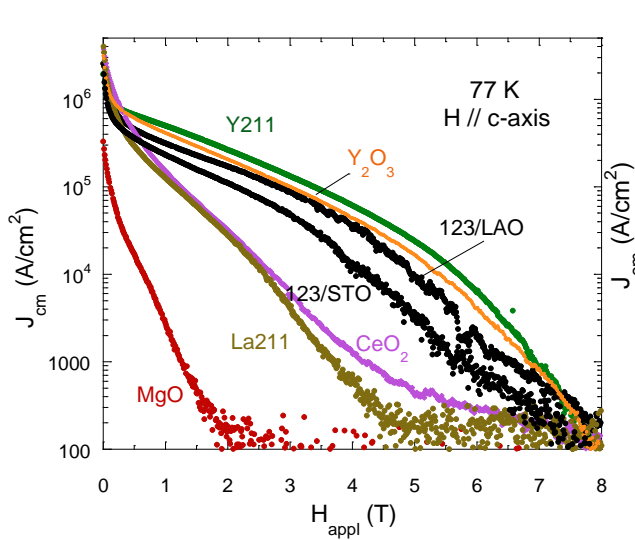


Figure 2a.6.15.1

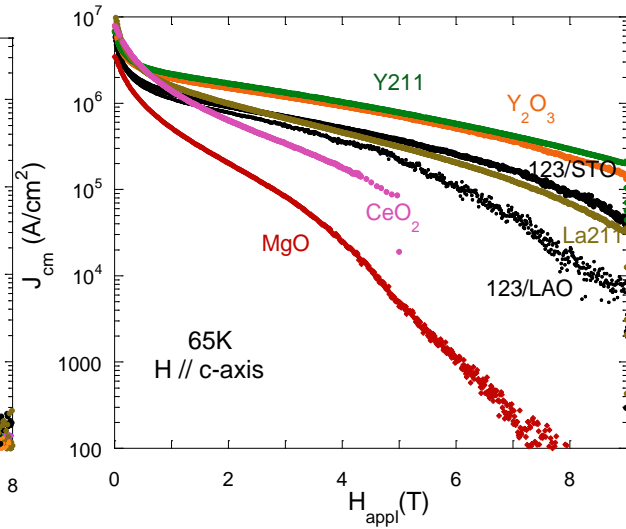


Figure 2a.6.15.2

2a.6.16 Special Considerations

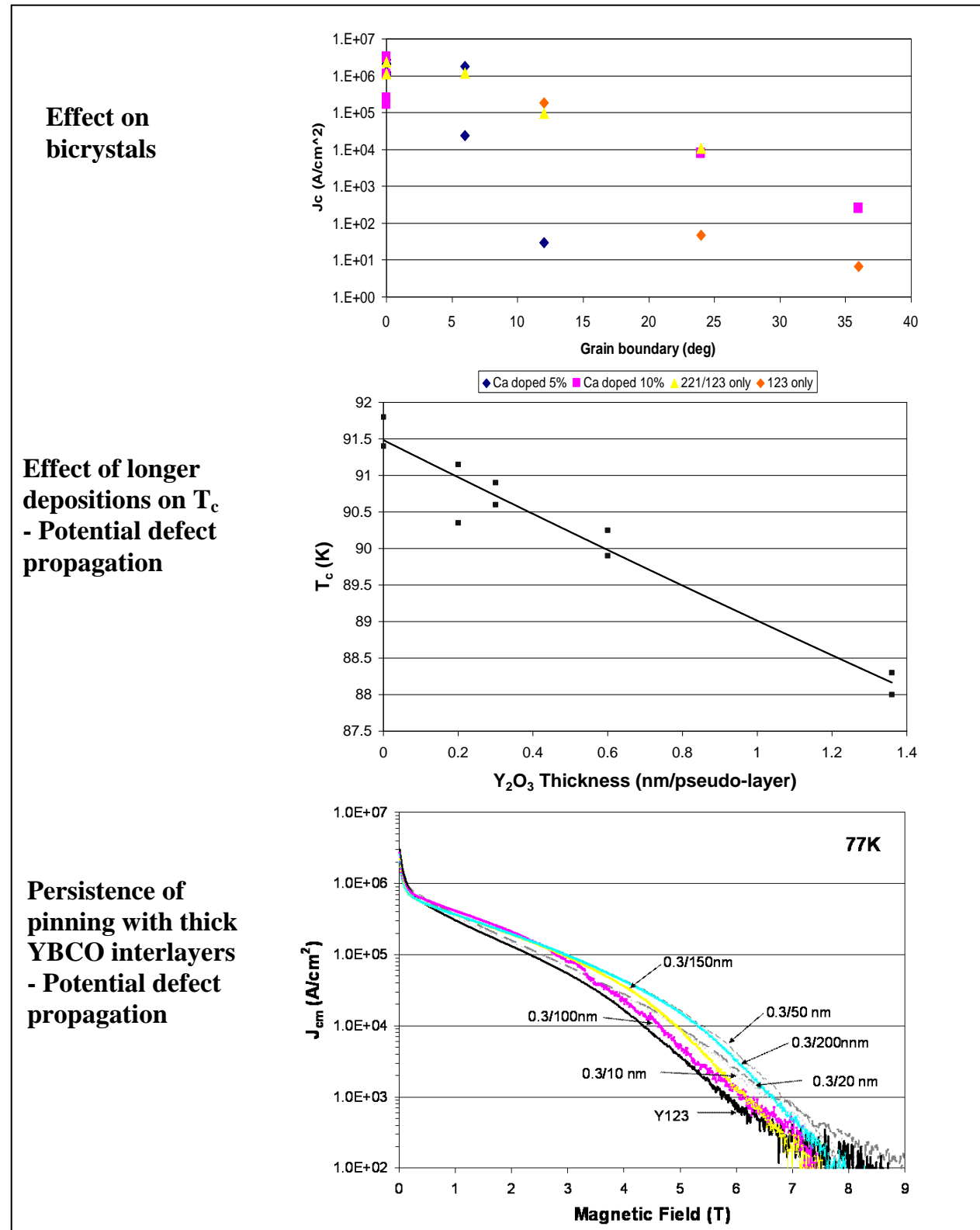
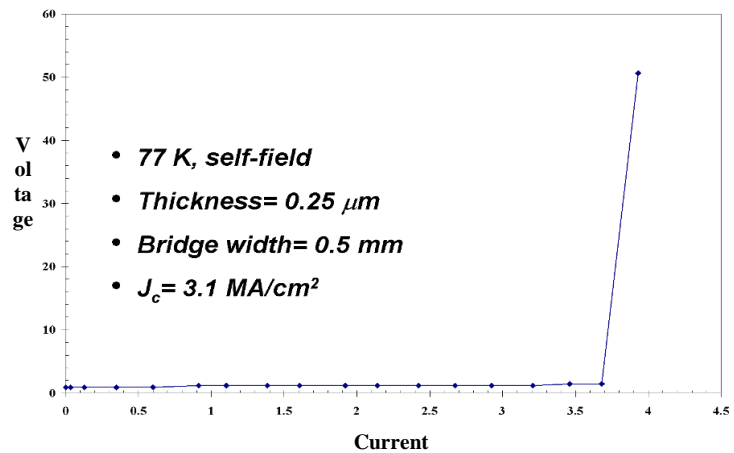
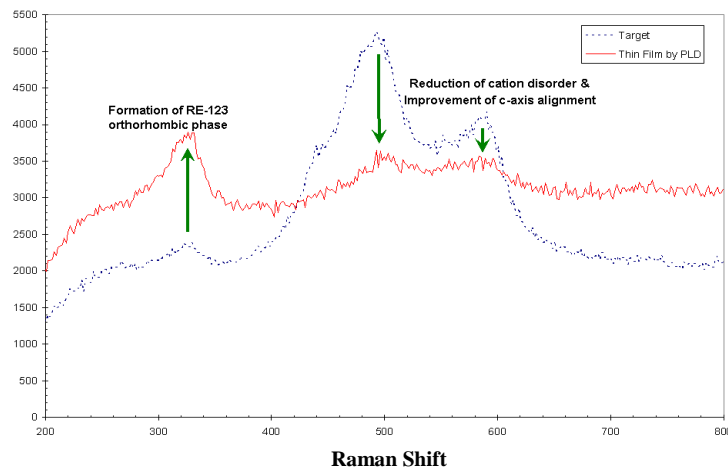
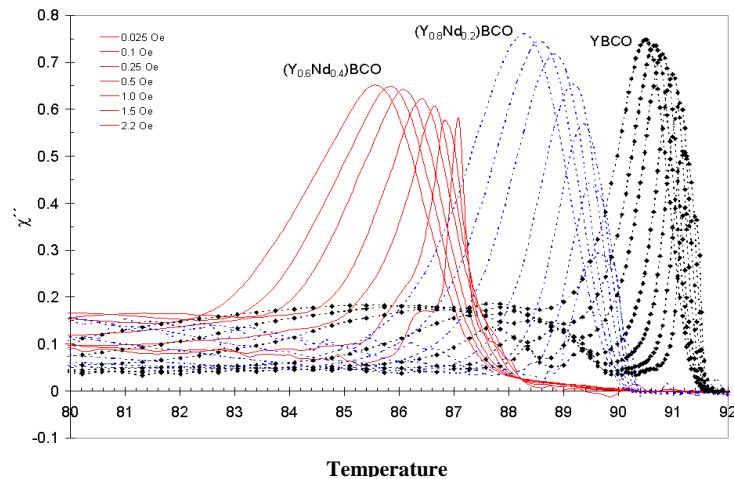


Figure 2a.6.17.1

2a.6.17 Rare Earth Pinning Nd-doped YBCO Films

- Nd doped film (40%) on right was $\sim 3 \text{ Ma/cm}^2$, 77 K (self-field)
- the in-field performance was slightly degraded from pure YBCO



C.V. Varanasi, L.B. Brunke, J.P. Murphy, I. Maartense, J.C. Tolliver, T.J. Haugan, K.W. Schmaeman, S. Sathiraju, P.N. Barnes, submitted to IEEE Trans. Appl. Supercond.

Figure 2a.6.18.1

2a.6.18 Minute CeO₂ Doping (0.1%)

- Ce-doped films at higher concentrations (e.g. 10%)
 - poor quality
 - Ce is reactive
- Minute additions ($\ll 1\%$) finely dispersed can better replicate the proper defect density

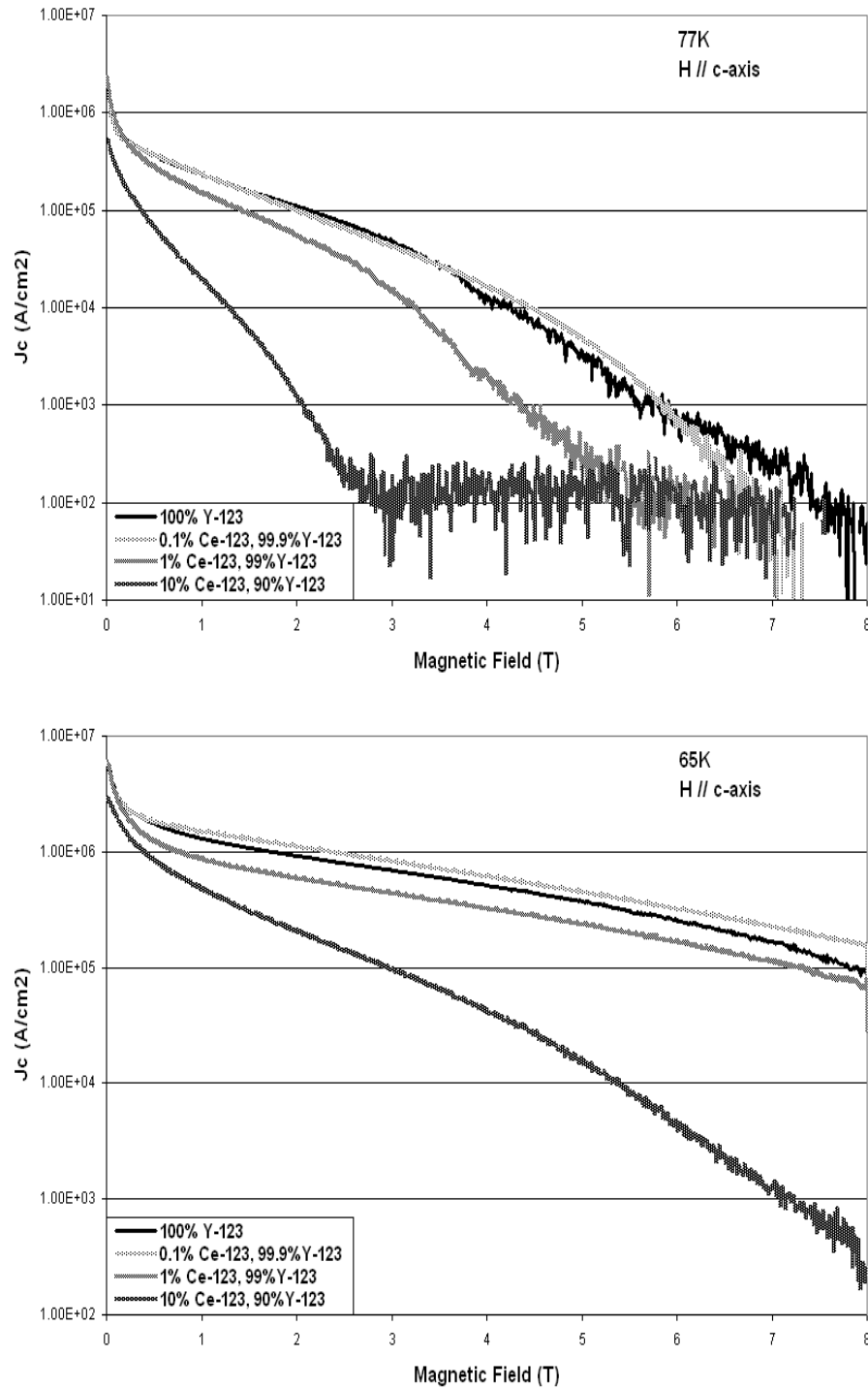


Figure 2a.6.19.1

2a.6.19 Conclusions

- Particulate inclusions (layered or non-layered) can provide substantial pinning
- Lattice mismatching is important in creating “better” nanoparticles
 - Lattice matched depositions – low deposition amounts required for sizing of particulates to coherence length
 - Lattice mismatched depositions – low deposition amounts required for appropriate particulate densities
- Currently working on non-planar particulate dispersions
- Considerations for rare earth substitution for J_c enhancement
 - Minute addition of certain rare earths (e.g. Ce, Pr, etc.)
 - Bulk addition of other (e.g. Sm, Eu, Ho; Nd avoided)
- Combine pinning methods?

2a.7 Controlled nanoparticulate flux pinning structures in YBCO

References: 1,2,3, 6,7, 8,9 10,11,12,13,14

T. Haugan ¹

1. Air Force Research Laboratory, Propulsion Directorate

Presented at AFOSR Coated Conductor Review, 20 Jan 2004

2a.7.1 Outline

- Nanoparticulate Dispersions by Multilayer Deposition
 - $(Y_2BaCuO_5/123)_xN$
 - $(CeO_2/123)_xN$
 - $(Y_2O_3/123)_xN$
- Scaling Up and Flux Pinning Mechanism
 - on RABiTs™ substrates
 - J_c vs film thickness
 - 123 layer thickness study

2a.7.2 (Insulator/123) $_xN$ Flux Pinning

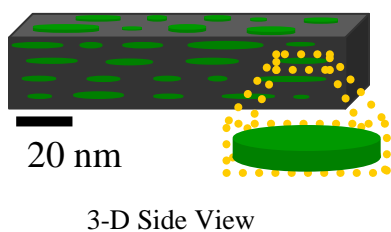


Figure 2a.7.2.1

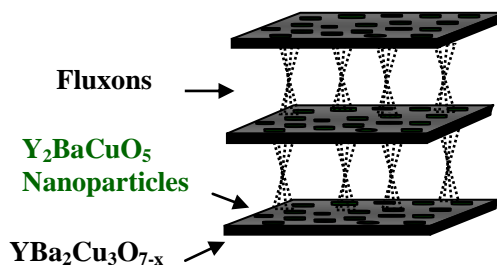
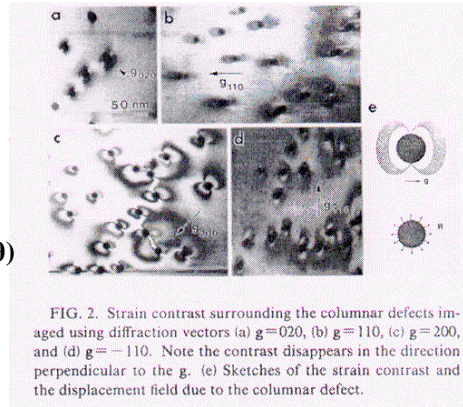


Figure 2a.7.2.2

Goals:

- Defect Density: $(H_{\text{appl}}/2) \times 10^{11} \text{ cm}^{-2}$, for H_{appl} (Tesla)
- Defect Size: $\xi_c \approx 4 \text{ nm}_{77\text{K}}$
- Reduce angular dependence of $J_c(H, \theta)$



← Strain surrounding columnar defects

Y. Zhu, Z. X. Cai, R. C. Budhani, M. Suenaga, and D. O. Welch Phys. Rev. B **48(9)** (1993) 6436.

Figure 2a.7.2.3

2a.7.3 Properties of Pinning Agents

X Insulator	Lattice Mismatch (X/123)	Island NanoParticle Height/Width Ratio	Intrinsic Stress of (X/123) composite	Chemical Reactivity of X with 123	X/123 Interface Sharpness	X PLD Compatible with 123 PLD ?
Y_2BaCuO_5	(a*/a) -6.9% (b*/b) +4.3% (c*/c) -3.2%	High	Moderate-high	None	Excellent	yes
Y_2O_3 (cubic)	-1.4% (?)	high	Moderate	Slight-none	Good (?)	Yes
CeO_2	- 0.5% (pseudo-cubic a/ $\sqrt{2}$)	low	low	moderate	Good (?)	Yes (?)

Table 2a.7.3.1

For Y_2BaCuO_5 : $a^* = a/2$, $b^* = b/3$, $c^* = cx2$

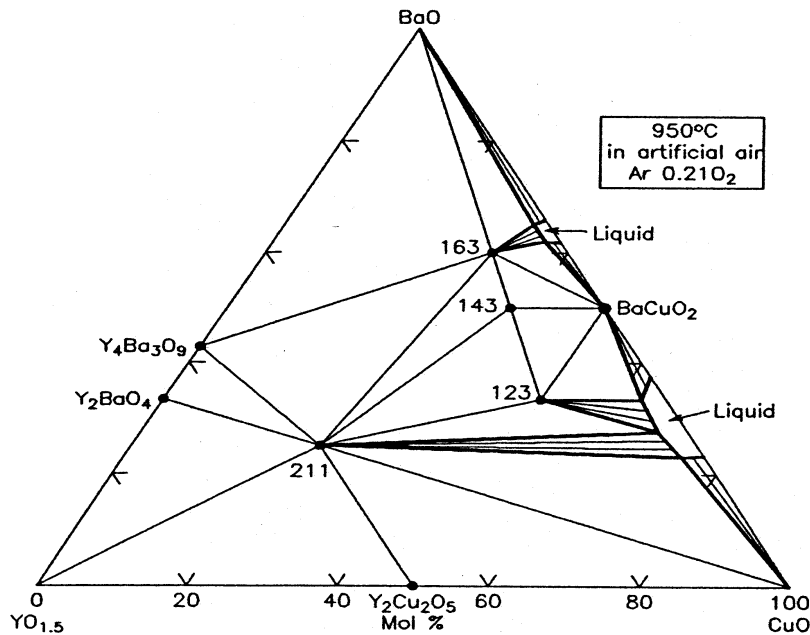
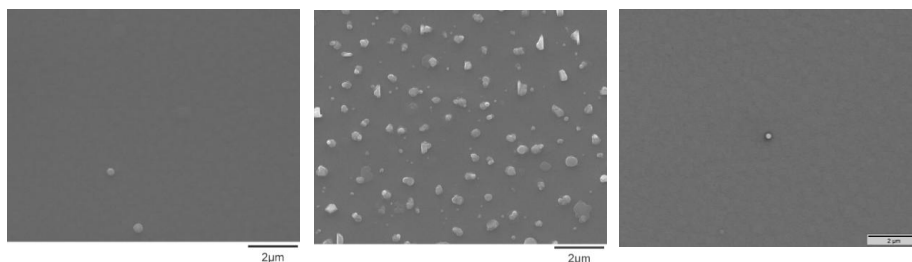


Figure 2a.7.3.1

2a.7.4 Film Surface Defects



($211_{1.3\text{nm}}/123_{12.5\text{nm}}$)x24

Figure 2a.7.4.1

($\text{CeO}_{2-0.8\text{nm}}/123_{\sim 10\text{nm}}$)x24

(chemical reaction!)

Figure 2a.7.4.2

($\text{Y}_2\text{O}_{3-0.3\text{nm}}/123_{\sim 13.8\text{nm}}$)x22

Figure 2a.7.4.3

2a.7.5 Experimental

PLD Deposition

- O₂ pressure = 300 mTorr
- Deposition rate ~ 15 nm/min
- Interval of ~ 12 sec between 123 and pinning layers
- Laser hz = 4 to 16

Jc measurements

- VSM magnetization
ramp rate = 9,000 to 40,000 (A/m*s)
- J_{cm} = 15 ΔM/Vol,
- transport currents
- J_{ct} by 1 mv/cm criteria.

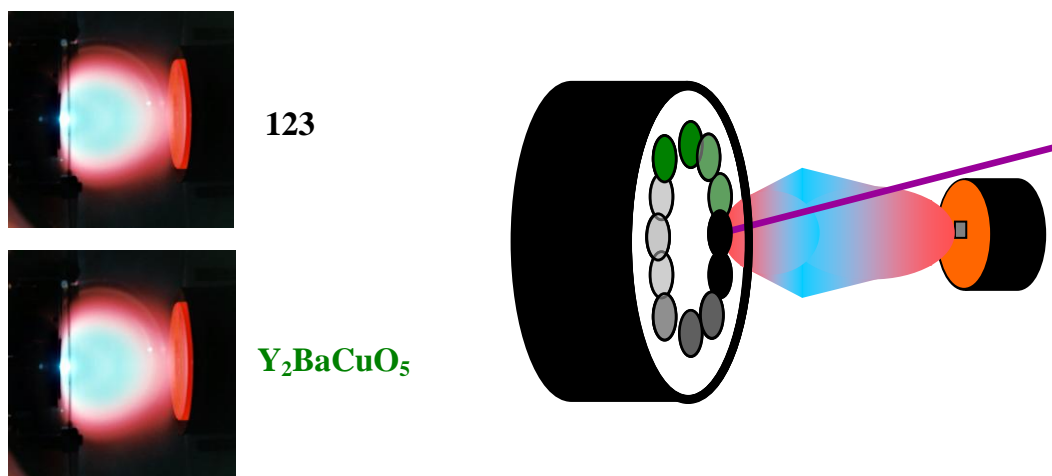
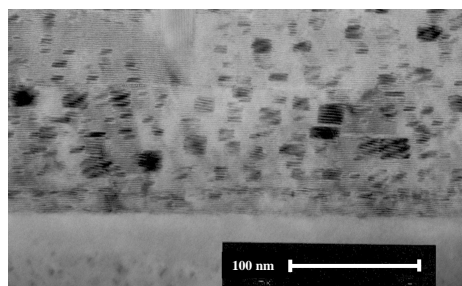


Figure 2a.7.5.1

2a.7.6 TEM X-Section



$(211_{1.6\text{nm}}/123_{6.6\text{nm}})\times 35$,
~ 80 sec interval

- 211 Density $\sim 3 \times 10^{11} \text{ cm}^{-2}$,
 $H_{\text{equivalent}} \sim 6\text{T}$
- Evidence of columnation
from localized stress

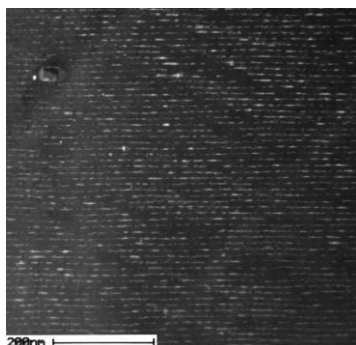


$(\text{CeO}_{2-0.8\text{nm}}/123_{11\text{nm}})\times 24$

Figure 2a.7.6.1

Figure 2a.7.6.2

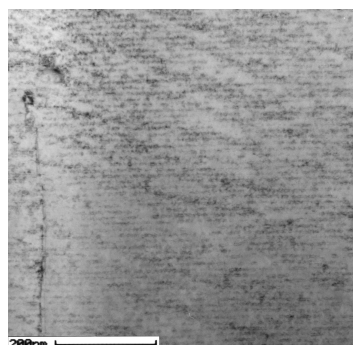
2a.7.7 TEM Cross-Sections



$(211_{0.9\text{nm}}/123_{10.5\text{nm}})\times 2$

Dark-field reflection,
using 211 diffraction vector

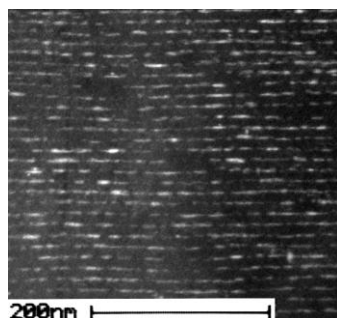
Figure 2a.7.7.1



Bright-field transmission

Figure 2a.7.7.2

2a.7.8 TEM Cross-Sections



$(211_{0.9\text{nm}}/123_{10.5\text{nm}})\times 200$

Figure 2a.7.8.1

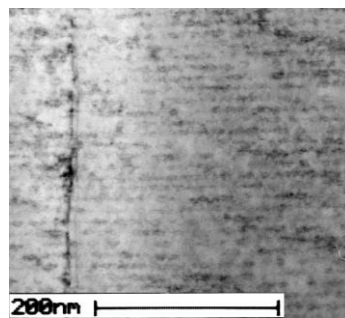
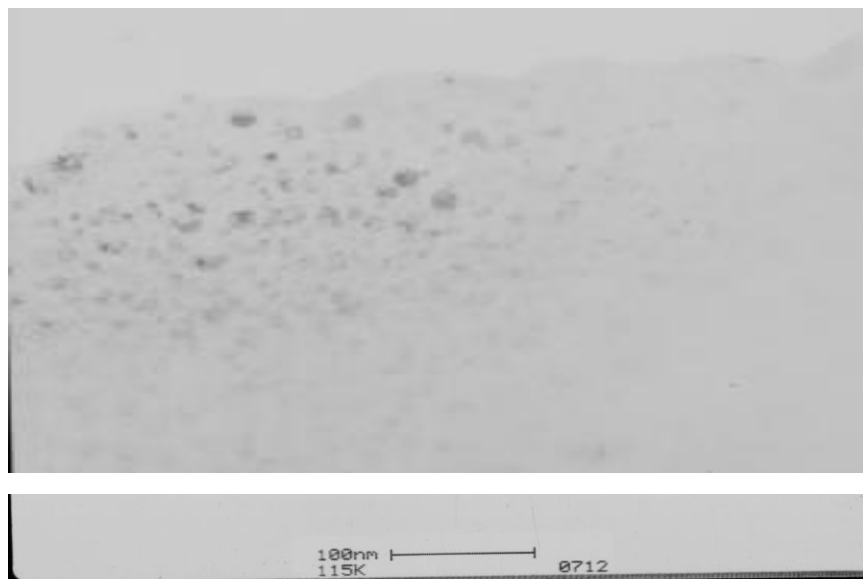


Figure 2a.7.8.2

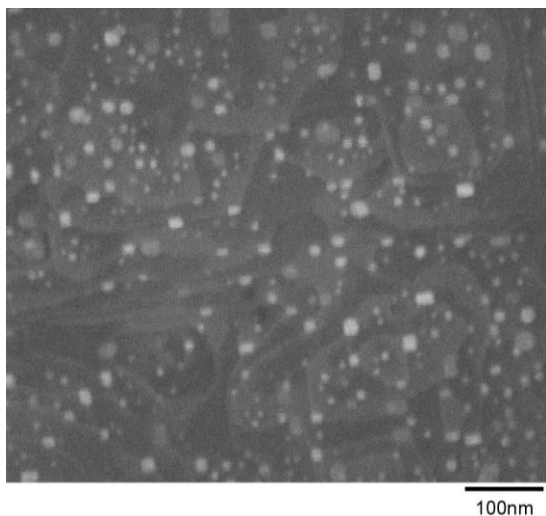
2a.7.9 TEM – Planar View



$(211_{1.6\text{nm}}/123_{6.6\text{nm}})\times 35$

Figure 2a.7.9.1

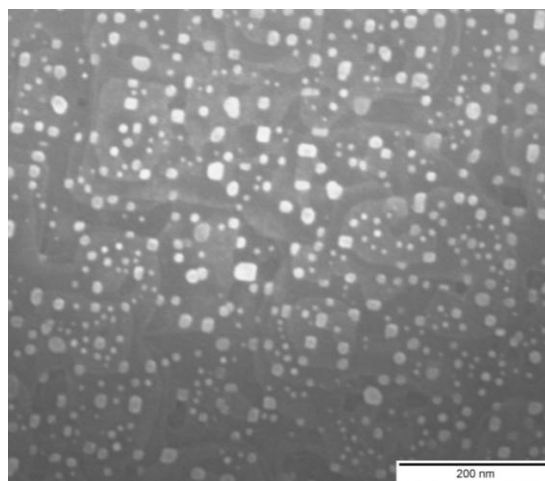
2a.7.10 Surface Nanoparticles



$(211_{\sim 1.2\text{ nm}}/123_{\sim 11\text{ nm}})\times 92$

Avg. Particle Size ~ 14 nm,
Particle Density ~ $1.3 \times 10^{11} \text{ cm}^{-2}$

Figure 2a.7.10.1



$(Y_2O_3_{\sim 0.5\text{nm}}/123_{\sim 13.5\text{nm}})\times 22$

Particle Density ~ $1.7 \times 10^{11} \text{ cm}^{-2}$

Figure 2a.7.10.2

2a.7.11 Surface Smoothness

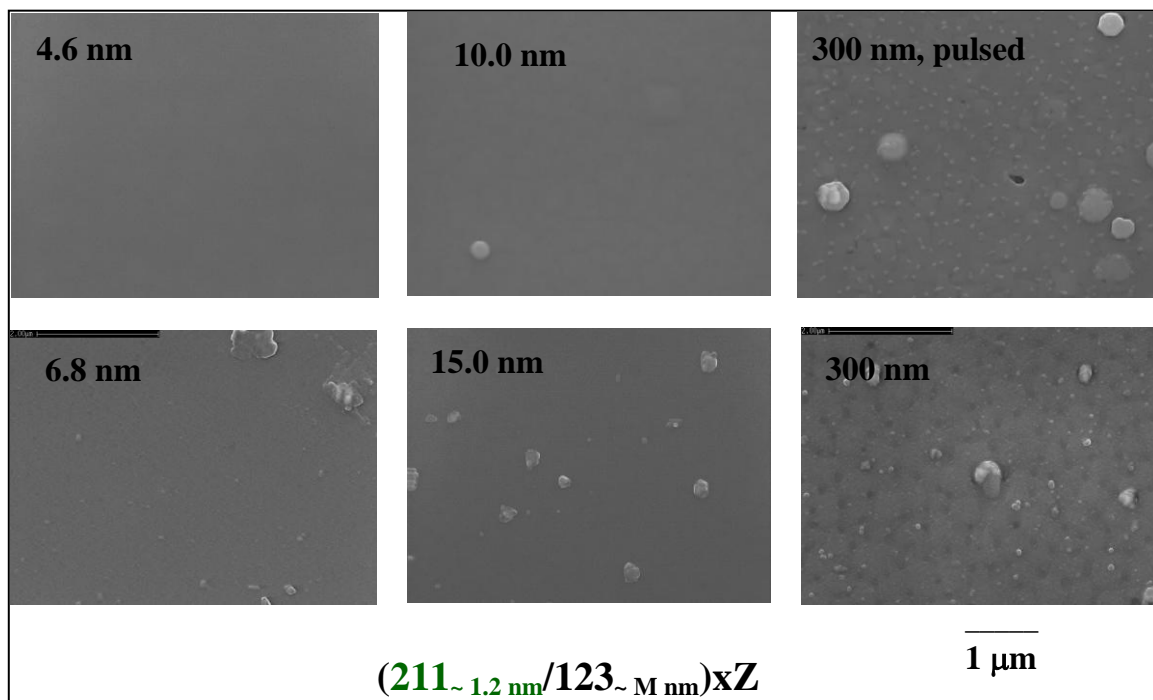


Figure 2a.7.11.1

2a.7.12 X-Ray Diffraction

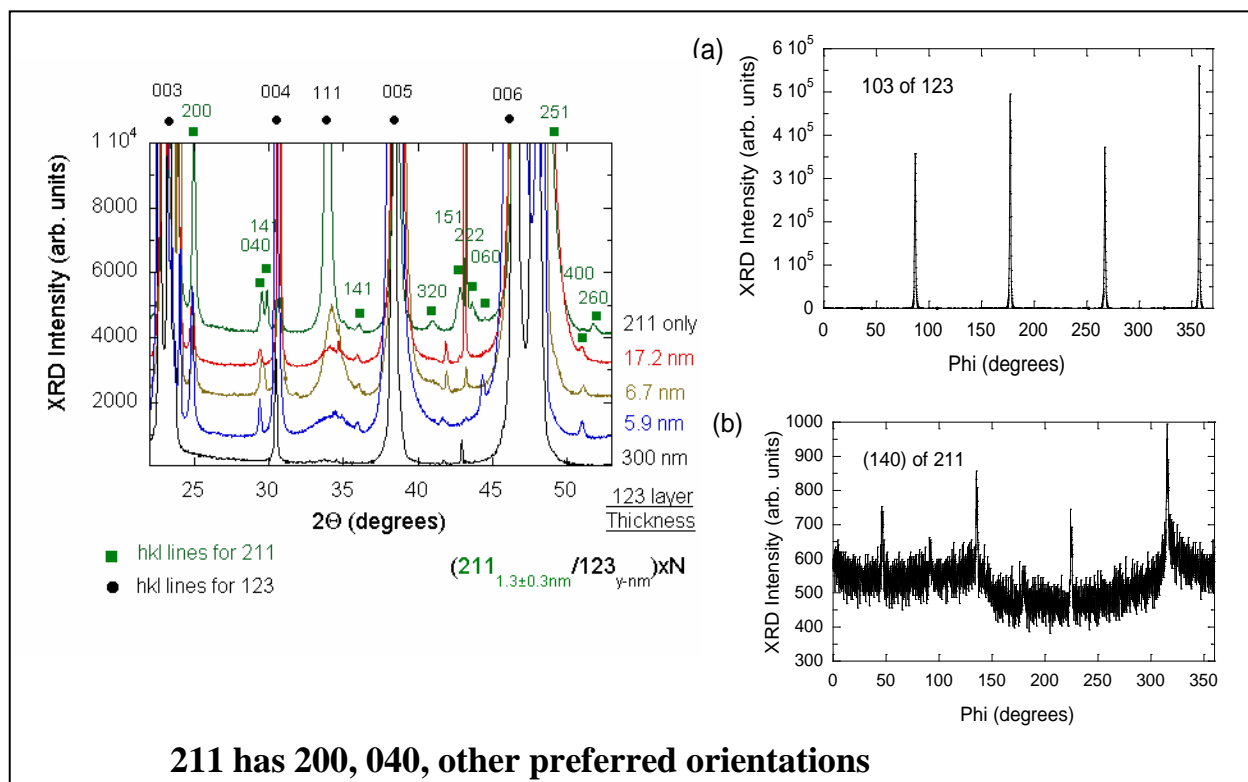


Figure 2a.7.12.1

2a.7.13 TEM Diffraction Patterns

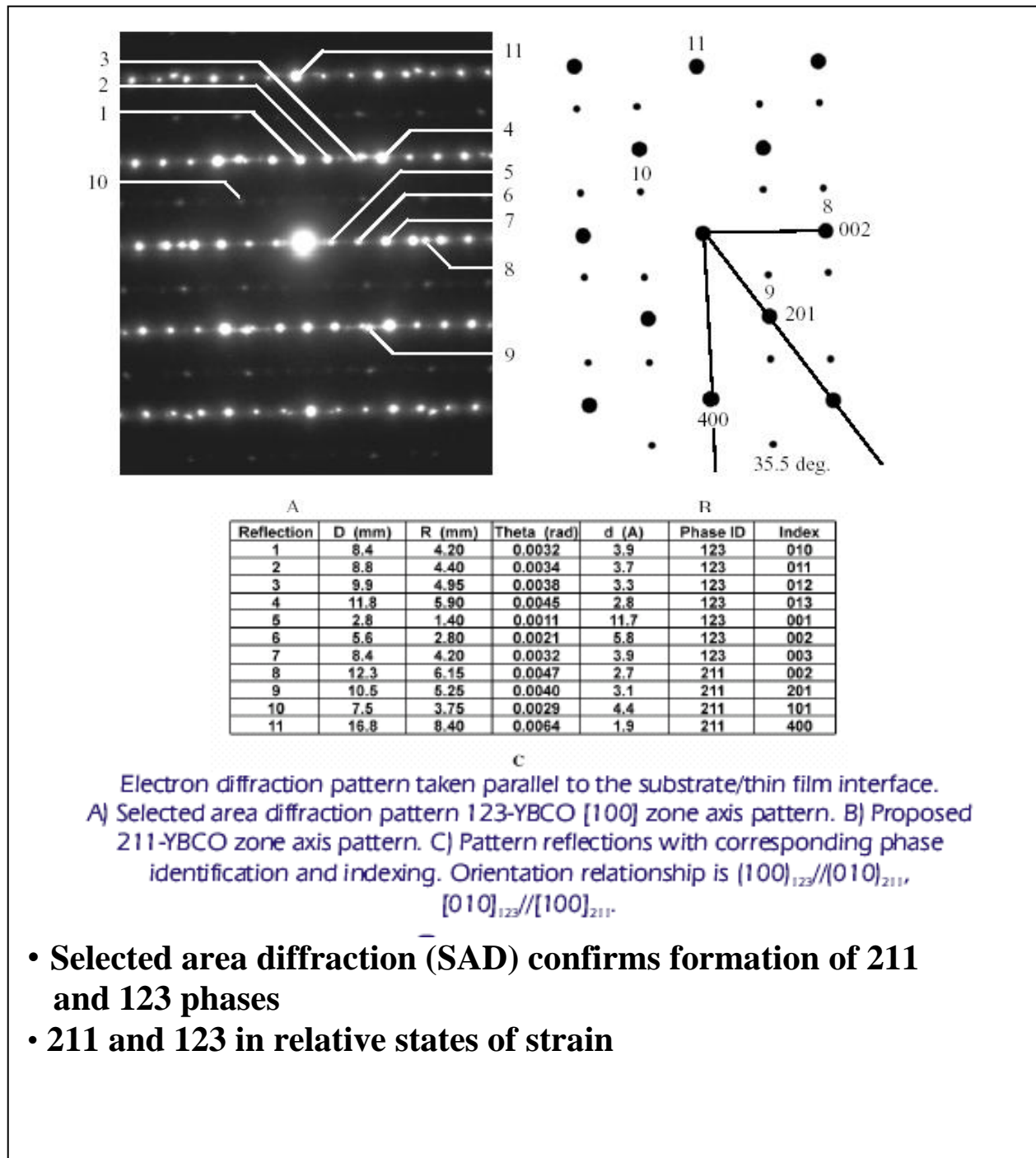


Figure 2a.7.13.1

2a.7.14 Tc Transition

T_c reduced slightly, depending on layer thickness

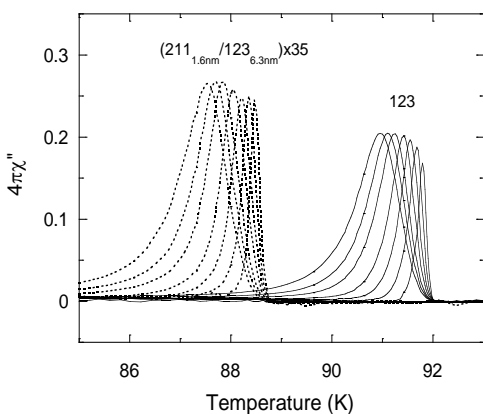
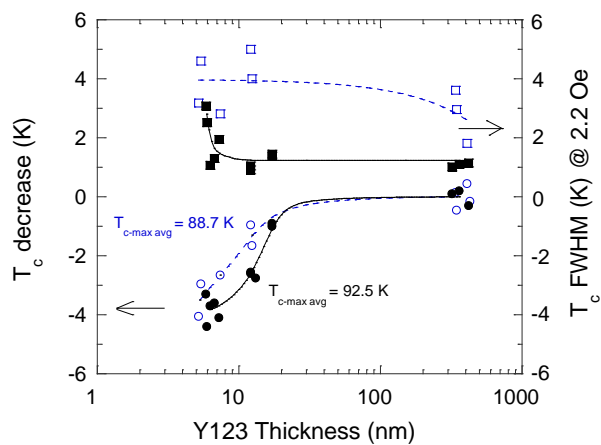


Figure 2a.7.14.1



$(211_{-1.1nm}/123_{-xnm}) \times Z$
film thickness ~ 0.25 to 0.3 micron
Figure 2a.7.14.2

2a.7.15 Critical Current Density J_c

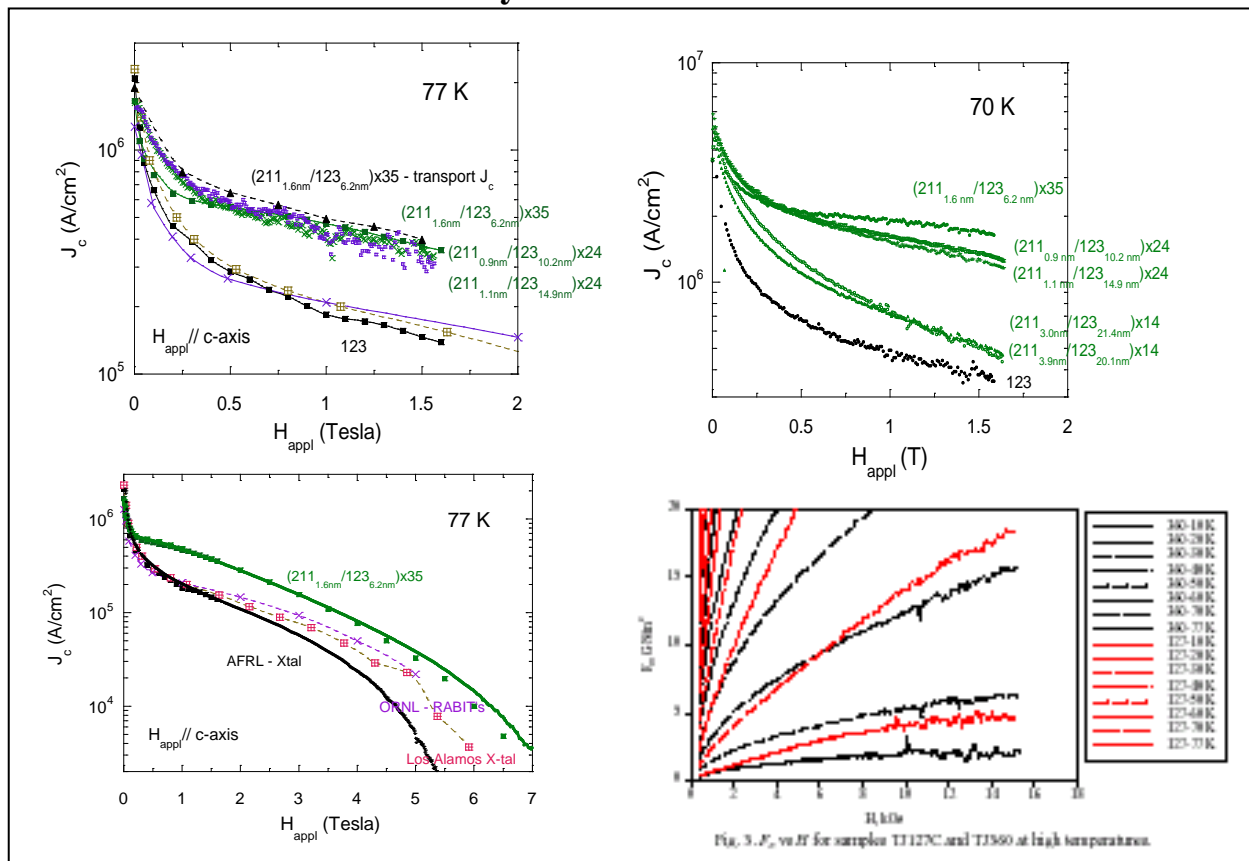
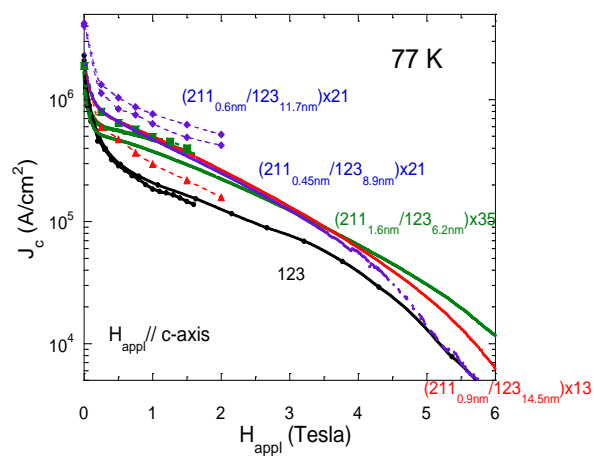


Figure 2a.7.15.1

2a.7.16 Transport J_c s



Transport J_c : dashed lines
Magnetic J_c : solid lines

Figure 2a.7.16.1

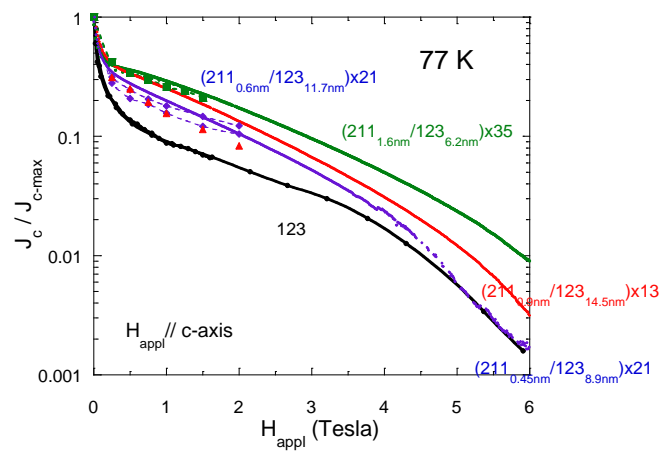


Figure 2a.7.16.2

2a.7.17 Temperature Dependence of J_c

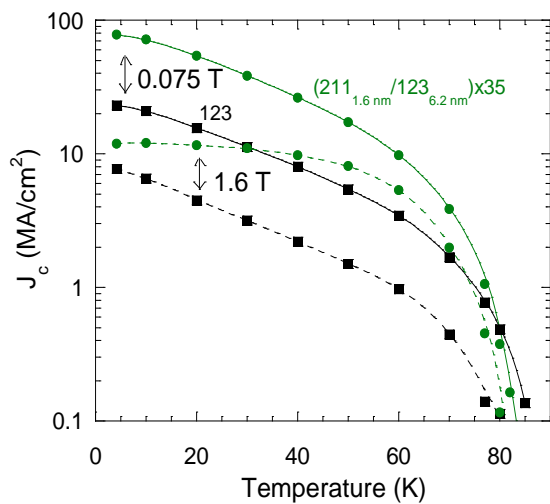
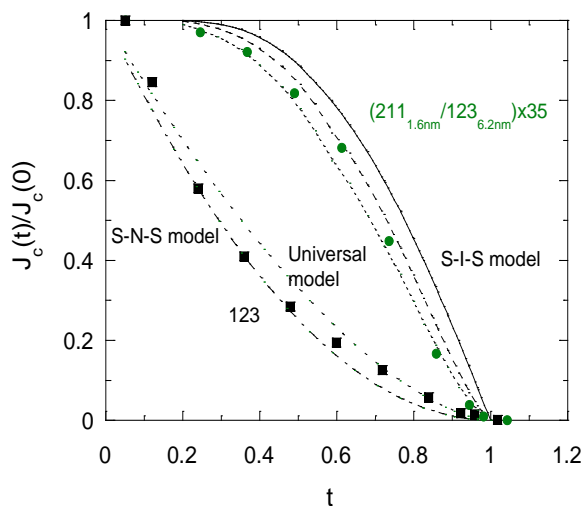


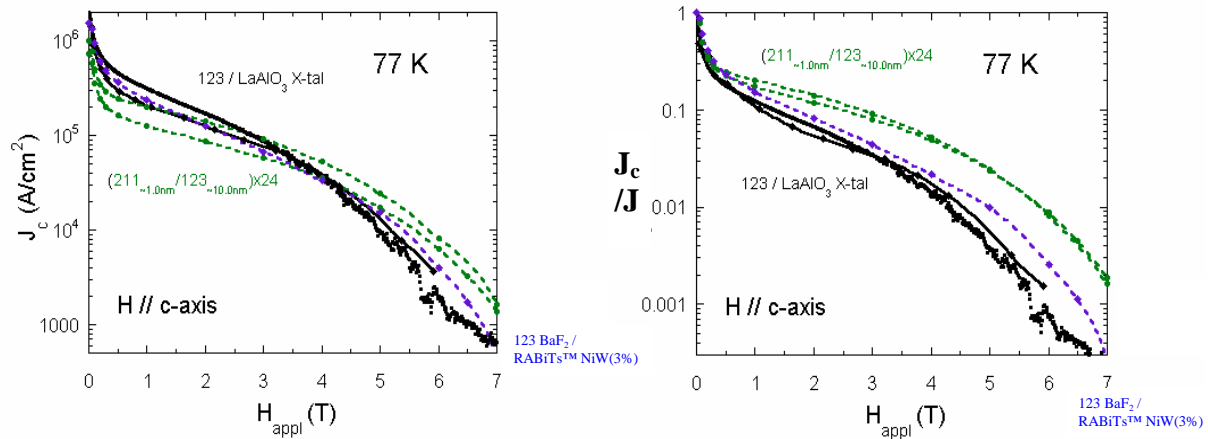
Figure 2a.7.17.1



- $t = T/T_c$
- comparing data at 1.6 T

Figure 2a.7.17.2

2a.7.18 Scaling Up: Multilayer on RABiTs™

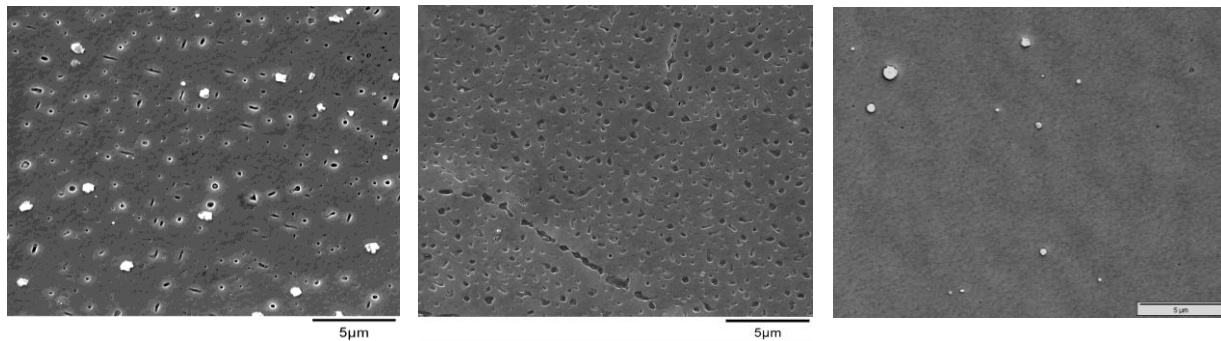


- Substrate = CeO₂/YSZ/Y₂O₃/Ni(W) by ORNL
- J_{ct} (0T) same as on CeO₂/YSZ/Y₂O₃/Ni by AFRL
- Decrease of $J_c/J_{c-max}(0.5T)$ greater than on single crystal substrates; suspect increased nucleation density of 211 at grain boundaries
- All J_{ct} data (except 123) by ORNL; J_c of 123/LaO₃ by LANL (see reference in paper below)
- “Deposition of (211_{~1.0nm}/123_{~10nm})xN Multilayer Coated Conductors on Ni-based Textured Substrates”
T. Haugan, P. Barnes, R. Nekkanti, J. Evans, J. C. Tolliver, L. Brunke, J. P. Murphy, T. A. Campbell, A. Goyal, A. Gapud, L. Heatherly, submitted to ECS 2003 Conf. Proceedings, Oct. 2003.

Figure 2a.7.18.1

Figure 2a.7.18.2

2a.7.19 Multilayer on RABIT's Ni



123

Figure 2a.7.19.1

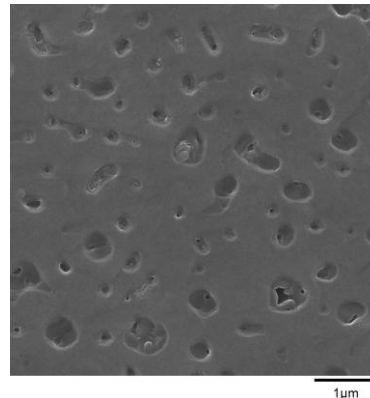
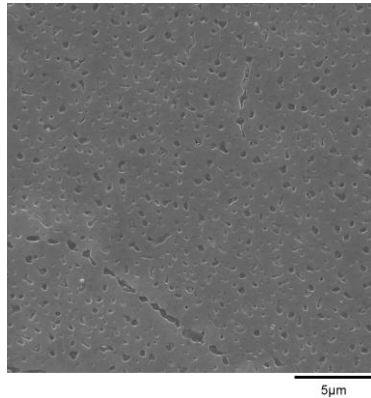
(211_{~1.0nm}/123_{~9.5nm})x27

Figure 2a.7.19.2

(211_{~0.5nm}/123_{~10.1nm})x27

Figure 2a.7.19.3

2a.7.20 Multilayer on RABiTs™ Substrates



$J_c = 0.6 \text{ to } 1.0 \text{ MA/cm}^2$ (77 K, self-field)

Figure 2a.7.20.1

Figure 2a.7.20.2

2a.7.21 J_c Comparison

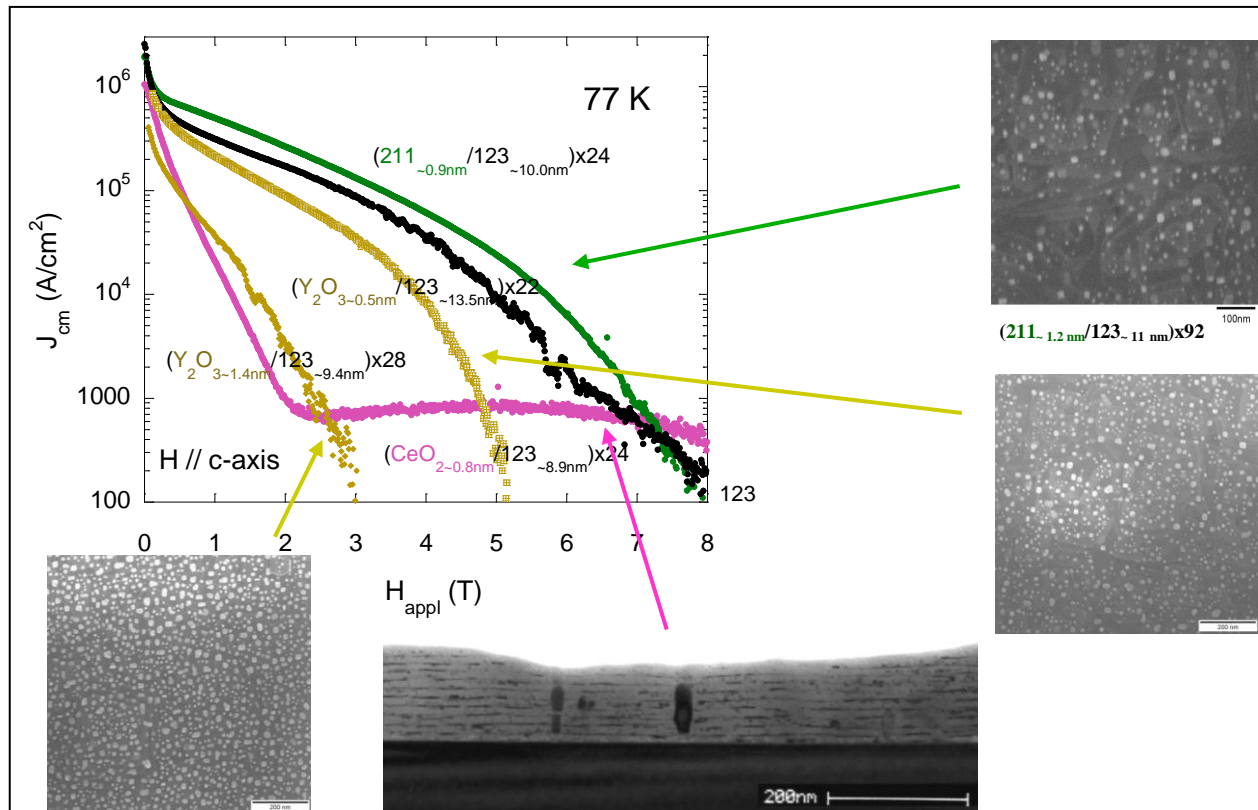


Figure 2a.7.21.1

2a.7.22 Increased Film Thickness

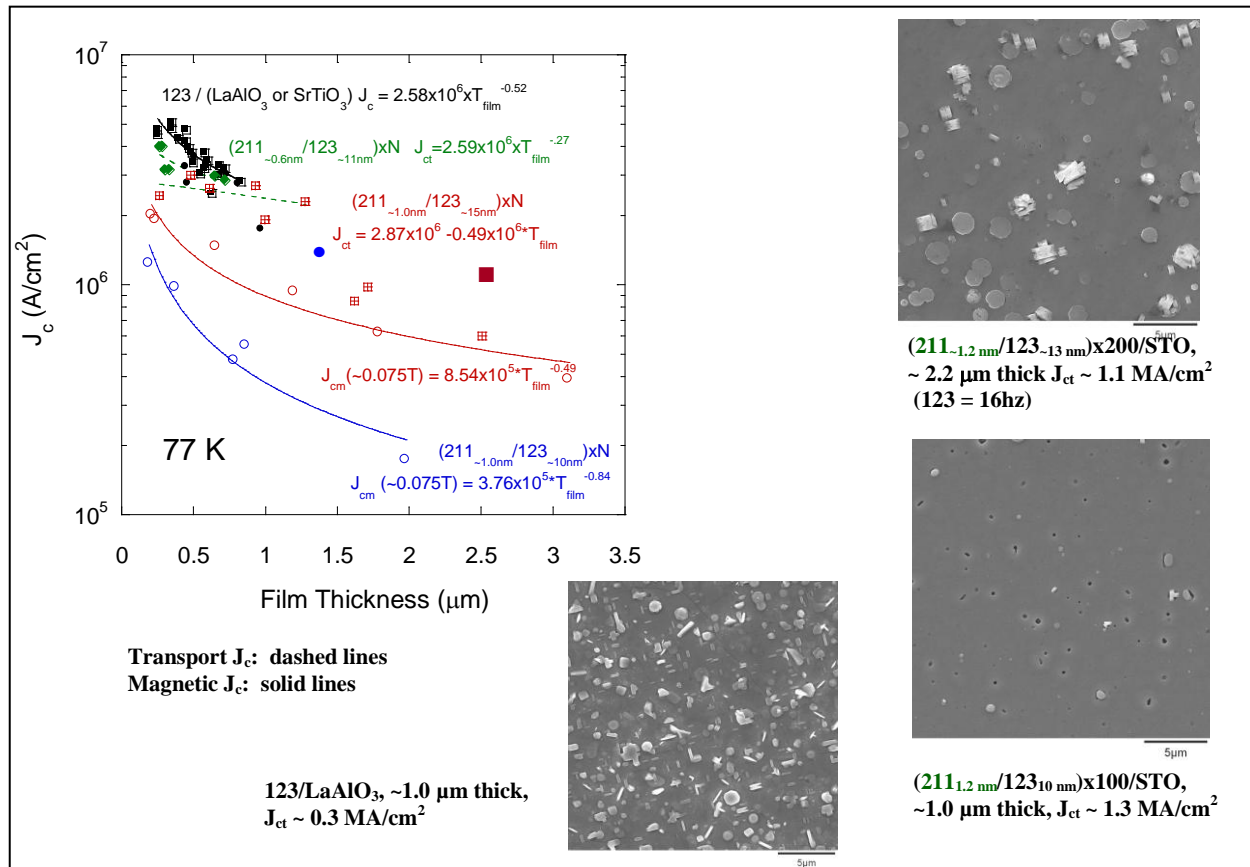


Figure 2a.7.22.1

2a.7.23 Jc vs Layer Thickness

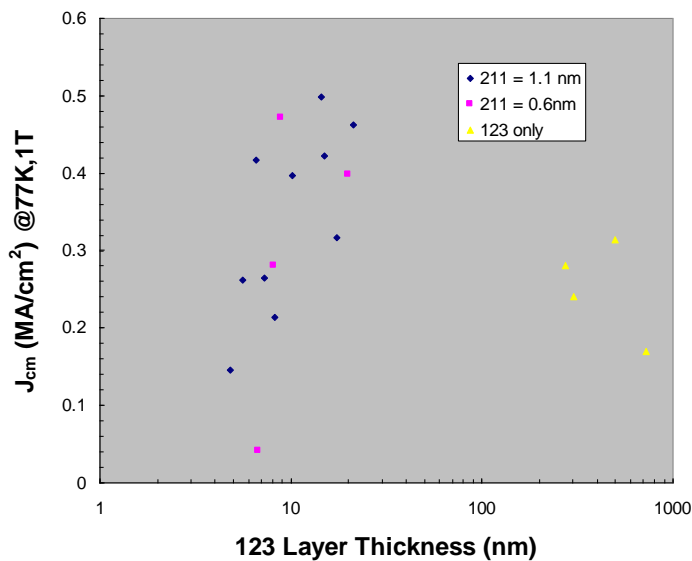


Figure 2a.7.23.1

- To determine how this affects pinning mechanism
- Upper limit for 123 layer thickness unknown yet – good for industrial application
- Increasing 123 layer thickness > 20 nm may increase anisotropy of J_c (H, 0)

2a.7.24 SUMMARY

Advantages of Multilayer Dispersions:

- J_c enhanced 2-4 times from 30-77 K, dependent on $J_c(0T)$
- Flatter film surfaces from layer renucleation
- Reduced surface defect particulates
- Evidence of increased film thickness without large J_c reduction
- Reduced dependence of $J_c(H)$ on θ (?) ; measurements needed
- Crack resistant conductor (?)

Future work:

- Experimental study of pinning mechanism and correlate to theory
- Optimization of pinning and 211 structure
- Further effort required for film thickness $> 1 \mu m$

Paper in print: T. Haugan, P. N. Barnes I. Maartense, C. B. Cobb, E. J. Lee, M. Sumption, "Island growth of Y_2BaCuO_5 nanoparticles in $(211_{-1.5nm}/123_{-10nm})_xN$ composite multilayer structures to enhance flux pinning of $YBa_2Cu_3O_{7-\delta}$ films", J. Mater. Res. **18**, p. 2618-2623 (2003) - Nov. issue.

2a.8 Increased Flux-Pinning of $YBa_2Cu_3O_{7-\delta}$ Thin Films by Addition of Y_2BaCuO_5 Nano-dimensional Multilayers

References: 1,2,7,8,9,10,12,13,14

T. J. Haugan¹, P. N. Barnes¹, C. B. Cobb¹, J. C. Tolliver¹, I. Maartense¹, J. P. Murphy¹
1. Air Force Research Laboratory, Wright-Patterson AFB, OH
Presented at the Applied Superconductivity Conference Houston, TX August 2002

2a.8.1 Flux Pinning Theory

- Density of Defects (area): $\approx 2.5 \times 10^{11}/cm^2$ (to pin 5 T field)
- Density of Defects (linear): $\approx 5 \times 10^5/cm$, ≈ 5 per 100 nm spacing
- Size of Defects: $\xi_c \approx 1-2 \text{ nm} < x < 10-20 \text{ nm}$
- Smaller defect size allows higher superconductor volume %

• Flux-pinning defects (α) in low temperature superconductors (β), and optimal spacing required to pin a 5 T field (bars).

• D. C. Larbalestier and M. P. Maley, MRS Bulletin Aug. (1993) p. 50.

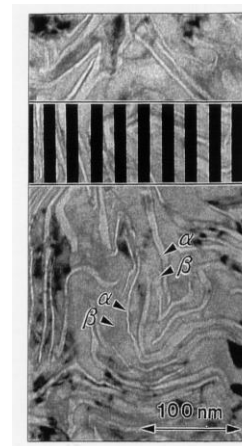


Figure 2a.8.1.1

2a.8.2 Y-211 Advantages

- Y-211 chemically compatible with Y-123, therefore no chemical reaction or unwanted diffusion and no reduction of T_c ; this is contrast to other multilayer materials.
- Can give sharp interface between the Y-211 insulating phase and Y-123 phase. The sharp interface is suggested to be best for flux pinning.
- Y-211 deposition conditions exactly compatible with Y-123 deposition conditions: no changes of O_2 pressure or laser fluence are required, which are typical for PLD of other high T_c .

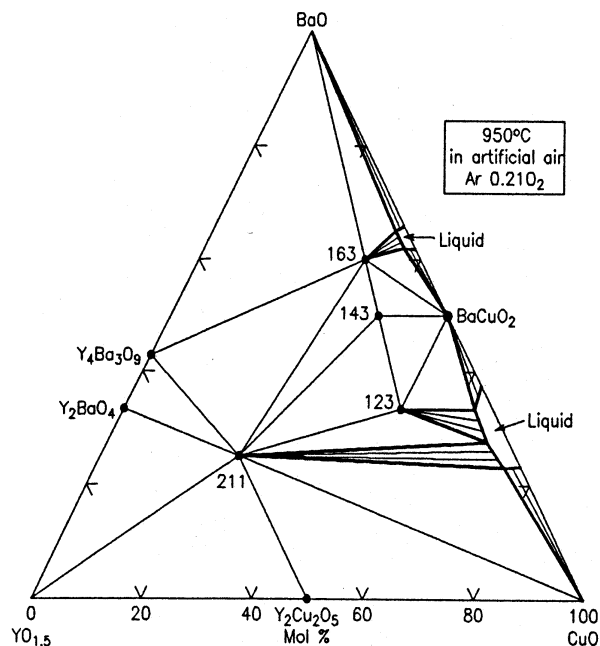


Figure 2a.8.2.1

2a.8.3 Transport J_c vs. Y(3d5/2) FWHM

- A trend to higher FWHM of Y(3d5/2) XPS peak for lower J_c samples
 - Transport J_c can be affected by physical discontinuities between contacts that will not affect XPS measurement
- Need more samples in 10^4 MA/cm² and 10^5 MA/cm² level for verification

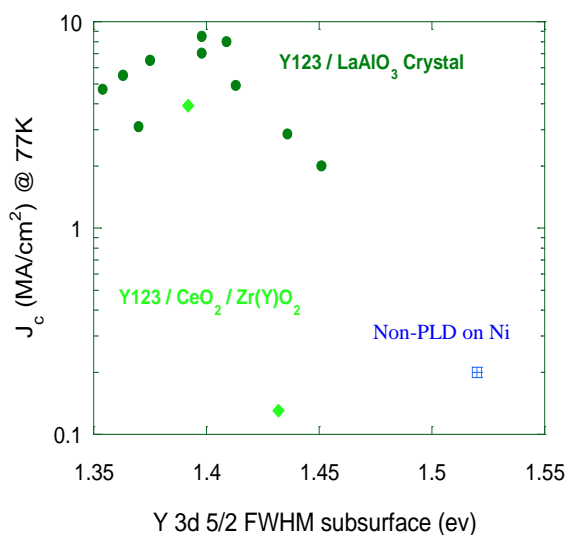


Figure 2a.8.3.1

2a.8.4 T_c FWHM χ'' vs. Y(3d5/2) FWHM

This is not as clear, but a linearly increasing (log scale) $\Delta T_c \chi''$ (susceptibility) with higher FWHM of Y(3d_{5/2}) XPS peak

Again need more lower quality samples for verification

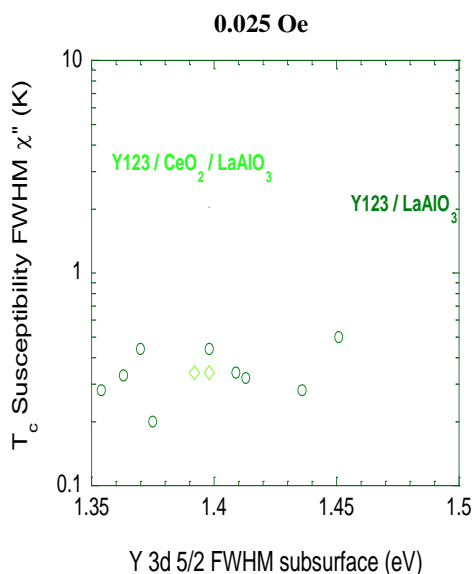


Figure 2a.8.4.1

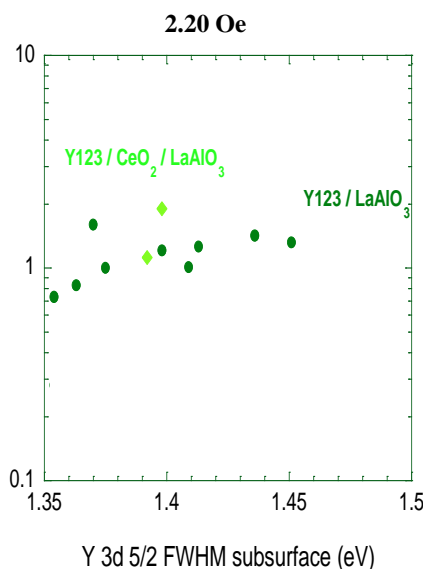


Figure 2a.8.4.2

2a.8.5 T_c vs. Y(3d5/2) FWHM

- No relation seen with T_c

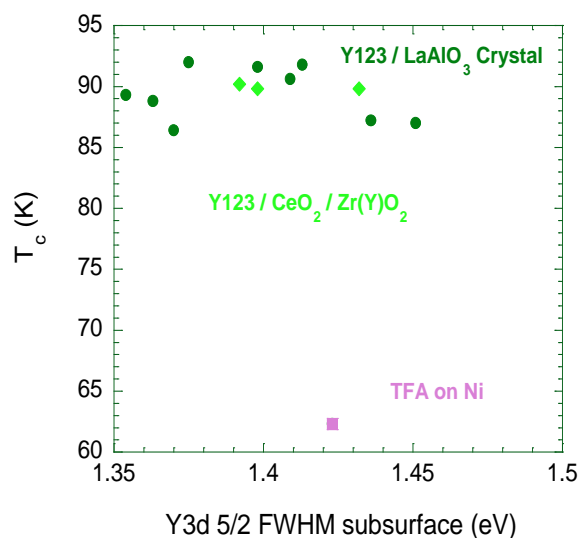


Figure 2a.8.5.1

2a.8.6 J_c vs. Cu(2p)/Ba(3d) Intensity Ratio

- Relationship is not clear for the given data
 - Transport J_c can be affected by physical discontinuities between contacts that will not affect XPS measurement

- Need more samples in 10^4 MA/cm² and 10^5 MA/cm² level for verification

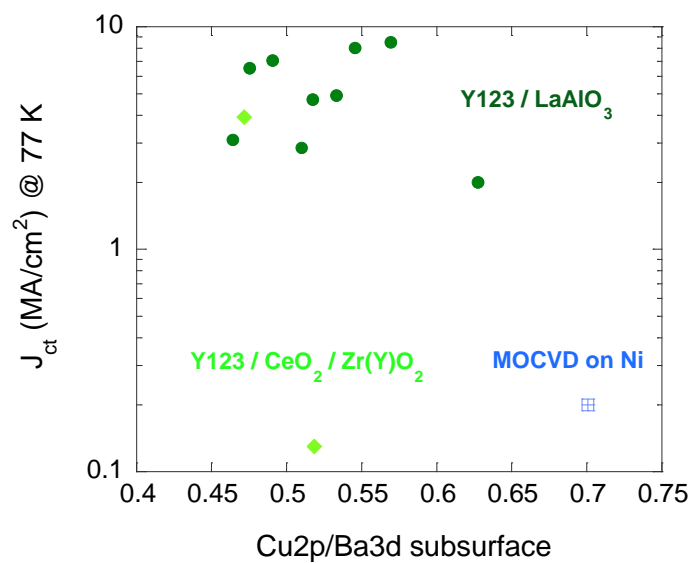


Figure 2a.8.6.1

2a.8.7 T_c FWHM "χ vs. Cu(2p)/Ba(3d) Intensity Ratio

- This appears to be the best correlation for the given points
- This correlation is not directly the same as for the Y(3d5/2) FWHM

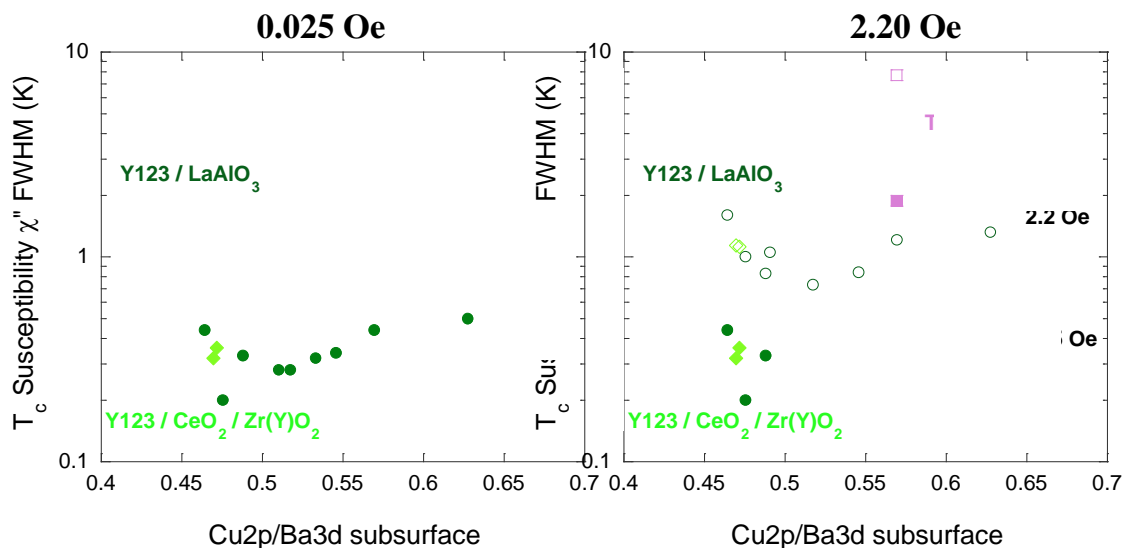


Figure 2a.8.7.1

Figure 2a.8.7.2

2a.8.8 T_c vs. Cu(2p)/Ba(3d) Intensity Ratio

- Again no real relation seen with T_c

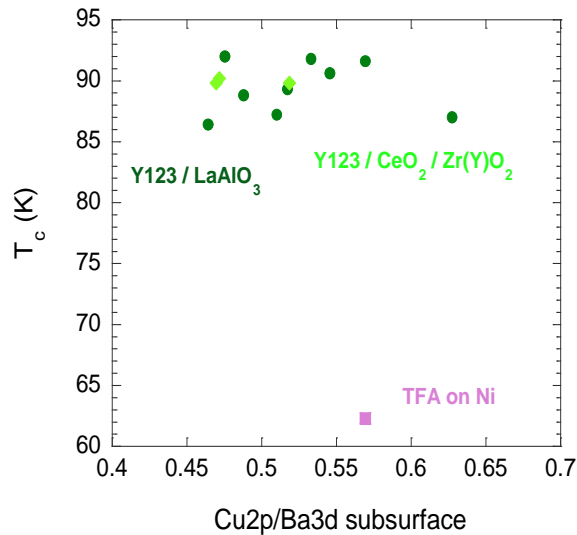


Figure 2a.8.8.1

2a.8.9 Zr Diffusion Issue

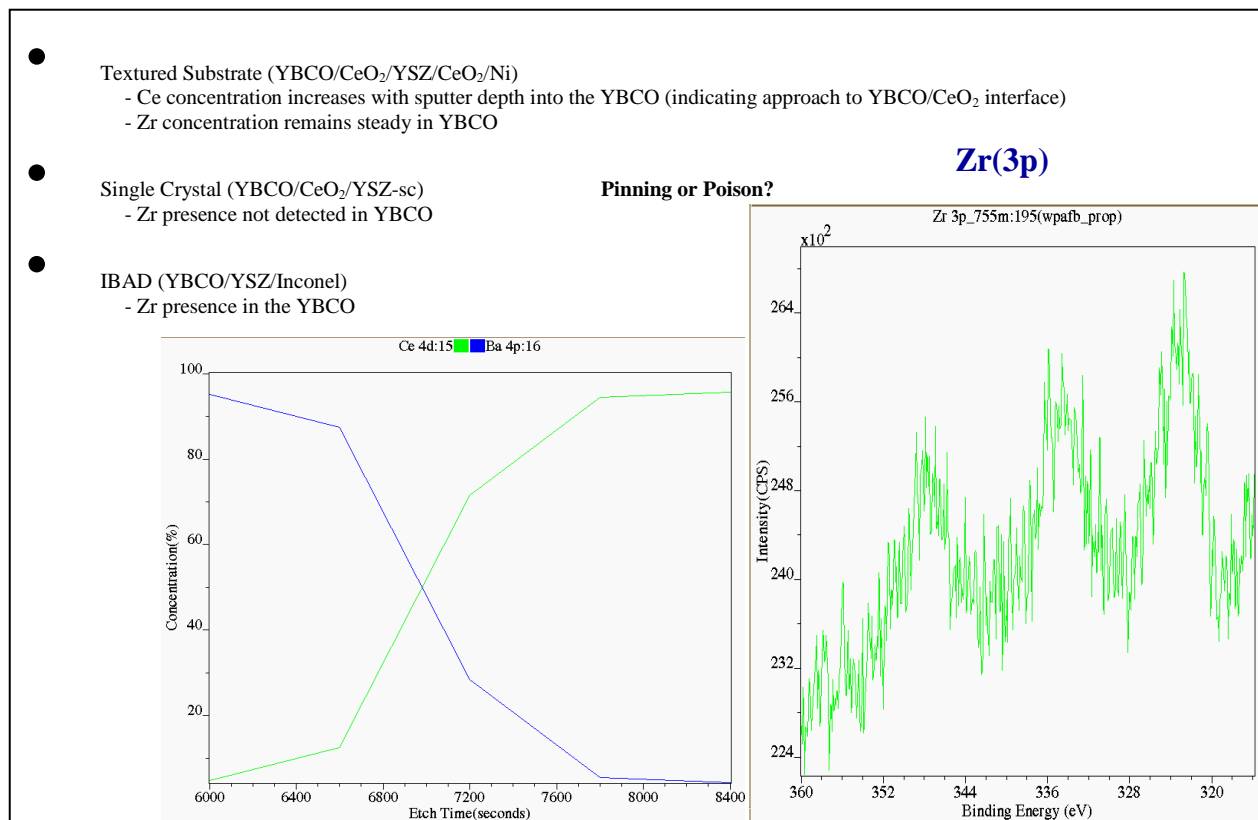


Figure 2a.8.9.1

2a.8.10 Summary

- Possible correlation of the FWHM of Y(3d5/2) XPS peak of YBCO to the film quality: Transport J_c and $\Delta T_c''\chi$
 - Need more data in the 104 MA/cm² and 105 MA/cm² range to verify

- An apparent relationship between the Tc FWHM χ vs. Cu(2p)/Ba(3d) XPS peak intensity ratio
 - More data may indicate relationship of Cu(2p)/Ba(3d) intensity ratio with the transport Jc but very unclear at this point
- Not clear now if a direct relationship exists between the FWHM of Y(3d5/2) XPS peak and Cu(2p)/Ba(3d) XPS peak intensity ratio
- Zr diffusion into lower layers of YBCO is evident but not clear how extensive without further samples

2a.8.11 Stacked Layer Approach Comparison

- Layers epitaxially grown by pulsed laser deposition
- 35 layers total
 - Y123 → 6.7 nm thick
 - Y211 → 1.0 nm thick
- Y123(Y211/Y123)₃₅

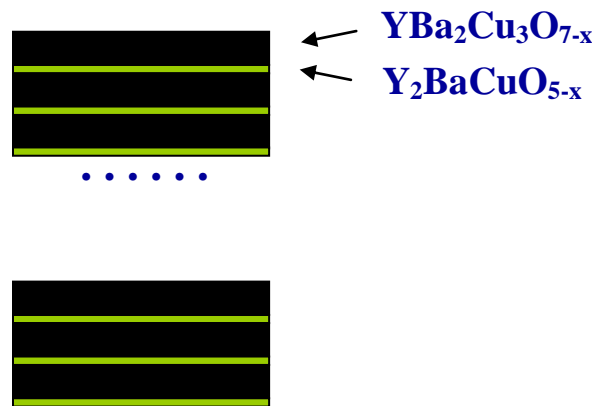


Figure 2a.8.11.1
Figure 2a.8.11.2

2a.8.12 T_c

- Lower Transition (at 77K, zero field), but very sharp transition

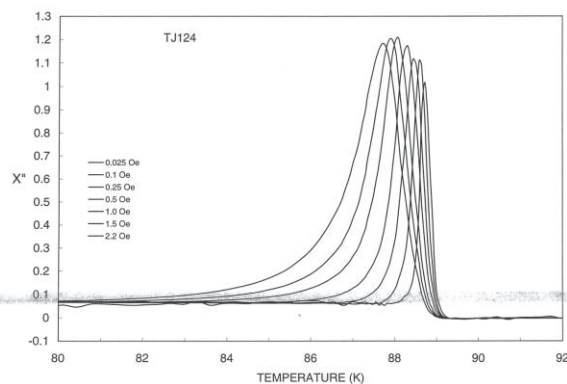


Figure 2a.8.12.1

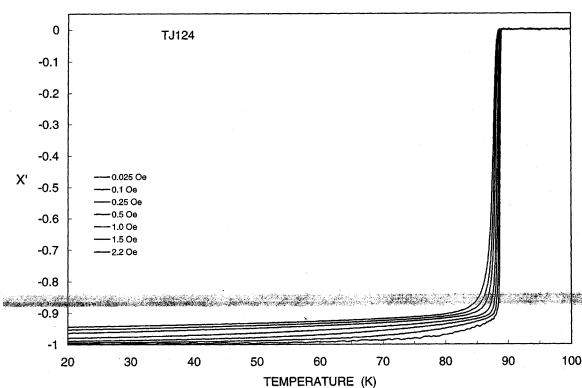


Figure 2a.8.12.2

2a.8.13 Architecture for Pinning

- Y211 phase is present

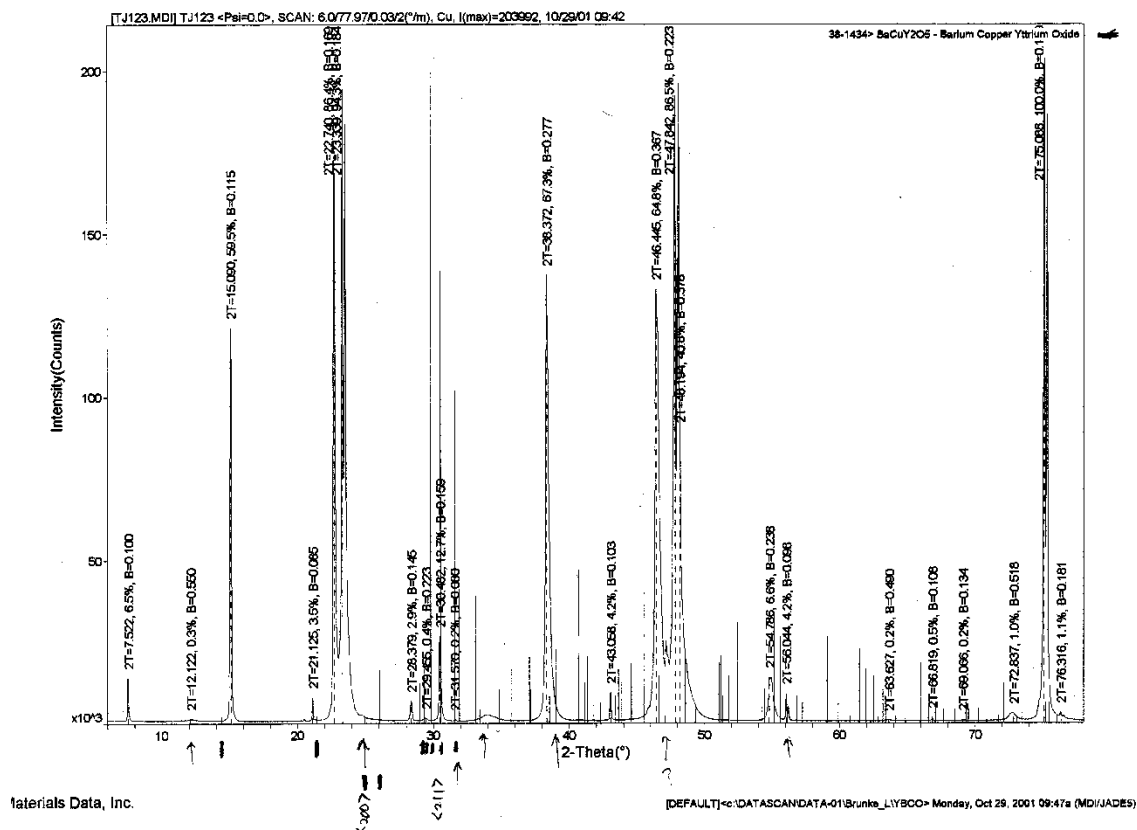


Figure 2a.8.13.1

2a.8.14 Varying Y123 Thickness

- As expected in zero magnetic field: the fewer Y211 layers, the better the sample performance

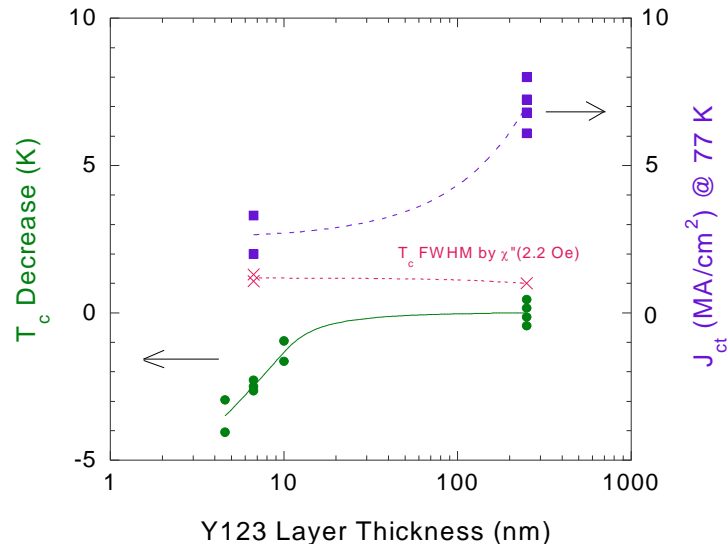


Figure 2a.8.14.1. (Y211/Y123)_n multilayer, total film thickness ~ 0.25 to 0.3 micron, n = 26 to 35, Y211 thickness = 1.1 nm constant

2a.8.15 60K Specific Improvement

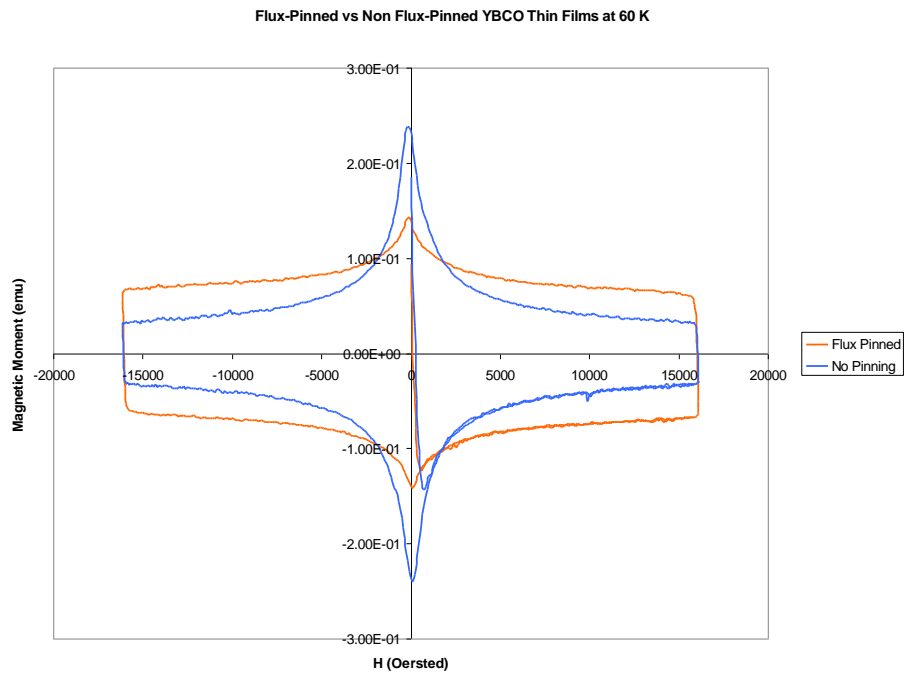


Figure 2a.8.15.1

2a.8.16 70 K Specific Improvement

- Although overall current density drops for very low magnetic fields, J_c is significantly enhanced for larger magnetic fields

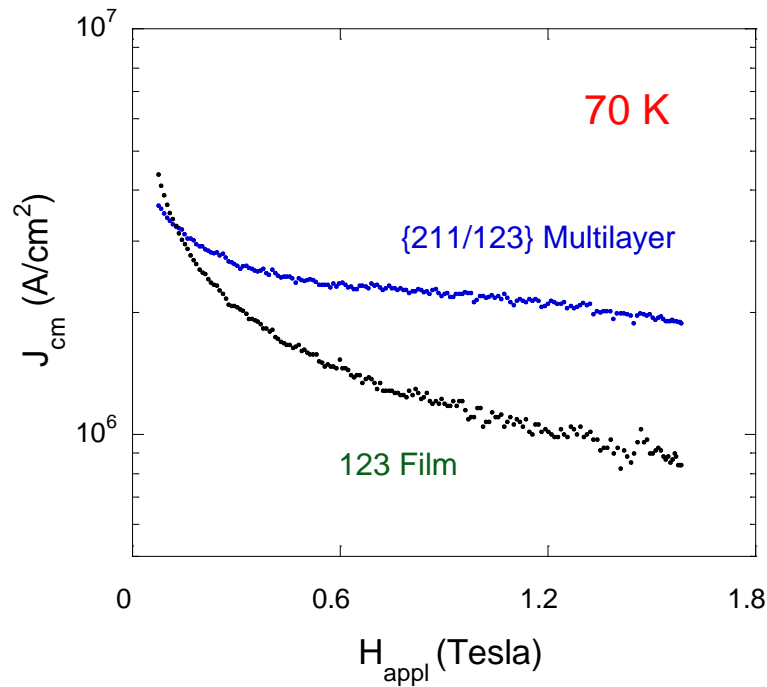


Figure 2a.8.16.1

2a.8.17 Stacked Layer Properties

- Results from vibrating sample magnetometry
- Note: J_c 's listed in this case are inferred from VSM

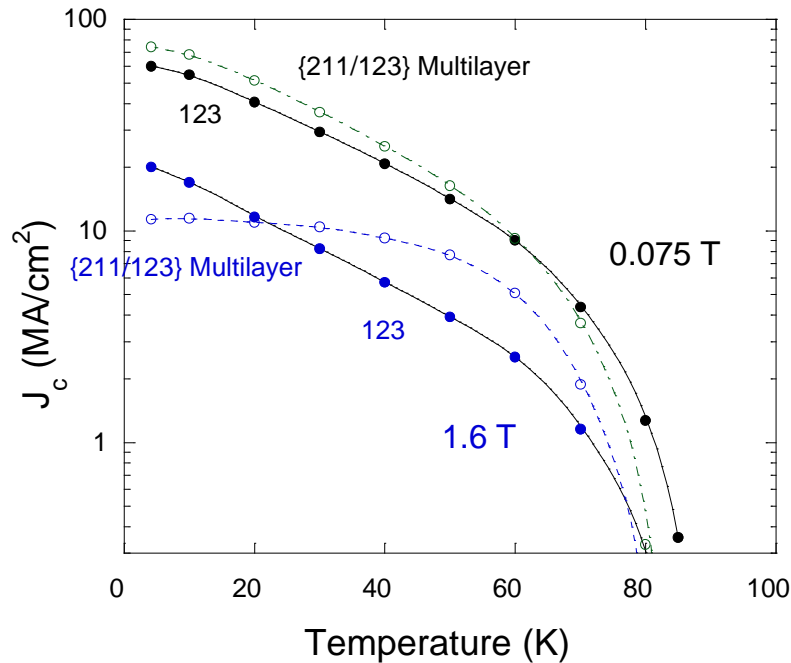


Figure 2a.8.17.1

2a.8.18 Summary

- Large improvement for in-field J_c at a few Tesla by flux pinning resulting in nanolayer additions of Y211
 - Double at 1 Tesla and even greater at higher fields
- TEM of sample in progress to determine exact structure
 - Although Y211 deposited as 1nm layers, it may be distorted from epitaxial growth on Y123
 - Do not expect pinning from smooth layers
- Further work necessary to test pinning ability of varying the layers and measurement at higher fields

Chapter 2B: Randomized Non-Layered Nanoparticulate Dispersions

Significant improvements were demonstrated in pulsed laser deposited YBCO films with Y211 and Y_2O_3 insulating particulate pseudo-layers arranged in a lamellar fashion, although these structures have a directional effect on the critical current density, controlled by the separation of the particulate pseudo-layers. However, a random distribution of pinning centers in the films which are not deposited in a layered fashion may be desired to avoid any preference for a given magnetic field orientation. This is especially relevant since in superconducting coil applications, the magnetic field will be present at a variety of angles to the coils. Work is done to develop a novel method to introduce controlled random inclusion of particulates in YBCO films during PLD growth.

A special pulsed laser ablation YBCO target with a Y_2BaCuO_5 (Y211) sector was made and used to form YBCO films with Y211 particulates on $LaAl_2O_3$ substrates. By selecting a proper laser scanning sequence, desired amount of Y 211 particles were introduced randomly into the growing YBCO films. This technique allows separation of the respective constituents for a more controlled introduction of random non-layered particulates. By introducing different materials sectors, combinations of pinning centers may be easily introduced in to the YBCO films during growth. Films were studied for microstructure by SEM, AFM and cross-sections were observed on the samples prepared by using Focused Ion Beam (FIB) technique. T_c was measured by AC susceptibility technique and a vibrating sample magnetometer (Quantum Design PPMS system) was used to obtain magnetization J_c data at various temperatures. Transport current measurements were taken on a bridged sample and thickness of the films was measured by using a profilometer. Initial angular dependency of critical current density data was obtained at 3T, 77K.

Nanometer sized particulates were found to be present in YBCO films made by using a specially made YBCO PLD target with an Y211 second phase sector. Initial results indicate improvements in magnetization J_c at both 77K and 65K especially at high fields in YBCO films made with Y211 particles. *An order of magnitude increase in the magnetization J_c at 9T at 65K was obtained in the YBCO samples made with Y_2BaCuO_5 (Y211) sector target as compared to using a regular YBCO target.* Microstructure shows uniform porosity and nm sized particles in the YBCO /films grown on La_2AlO_3 substrates using a PLD target with Y211 sector. Porosity seems to originate at the particles introduced in the films. Initial results show that YBCO films with Y211 particles can be grown on $LaAl_2O_3$ substrates with critical current density $> 3MA/cm^2$ at 77K in self-field with reduced angular dependence as compared to regular YBCO.

2b.1 Novel method of introducing particulate pinning centers in $\text{YBa}_2\text{Cu}_3\text{O}_{7-x}$ films during pulsed laser deposition

References: 15

C. Varanasi¹, Jack Burke², Jason Carpenter², T.J. Haugan², P.N. Barnes²

1. *University of Dayton Research Institute*

2. *Air Force Research Laboratory*

Presented at CEC-ICMC 2005

2b.1.1 Introduction

- Introduction of flux pinning centers into bulk $\text{YBa}_2\text{Cu}_3\text{O}_{7-x}$ (YBCO) is widely known to improve the critical current density (J_c) significantly.
- Approaches to obtain similar enhancements in YBCO films that are used in coated conductor applications are presently considered by several research groups by incorporating nm size particulates that act as flux pinning centers.
- Significant improvements were demonstrated in pulsed laser deposited YBCO films with Y211 and Y2O3 insulating particulate pseudo-layers by AFRL group.
- The films, processed in this manner with pinning centers arranged in a lamellar fashion, allow structured pinning centers with directional dependence of critical current density, controlled by the separation of the particulate pseudo-layers.
- However, a random distribution of pinning centers in the films which are not deposited in a layered fashion may be desired to avoid any preference for a given magnetic field orientation.
- This is especially relevant since in superconducting coil applications, the magnetic field will be present at a variety of angles to the coils.
- In this work a novel method to introduce controlled random inclusion of particulates in YBCO films is presented and the results obtained are discussed.

2b.1.2 Experimental

- A special pulsed laser ablation YBCO target with a Y_2BaCuO_5 (Y211) sector was made and used to form YBCO films with Y211 particulates on LaAlO_3 substrates.
- By selecting a proper laser scanning sequence, desired amount of Y 211 particles were introduced randomly in the growing YBCO films.
- This technique allows separation of the respective constituents for a more controlled introduction of random non-layered particulates.
- By introducing different materials sectors, combinations of pinning centers may be easily introduced in to the YBCO films during growth.
- Films were studied for microstructure by SEM, AFM and cross-sections were observed on the samples prepared by using Focused Ion Beam (FIB) technique.
- T_c was measured by AC susceptibility technique and a vibrating sample magnetometer (Quantum Design PPMS system) was used to obtain magnetization J_c data at various temperatures

- Transport current measurements were taken on a bridged sample and thickness of the films was measured by using a profilometer
- Initial angular dependency critical current density data obtained at 3T, 77K of the films is presented.

2b.1.3 PLD Target

Schematic of a PLD target used in the present study showing a small sector made of Y211 in a YBCO target

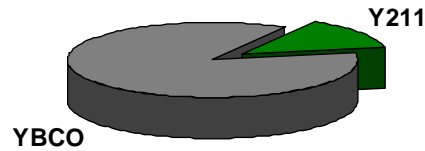


Figure 2b.1.3.1

2b.1.4 AC Susceptibility Curves

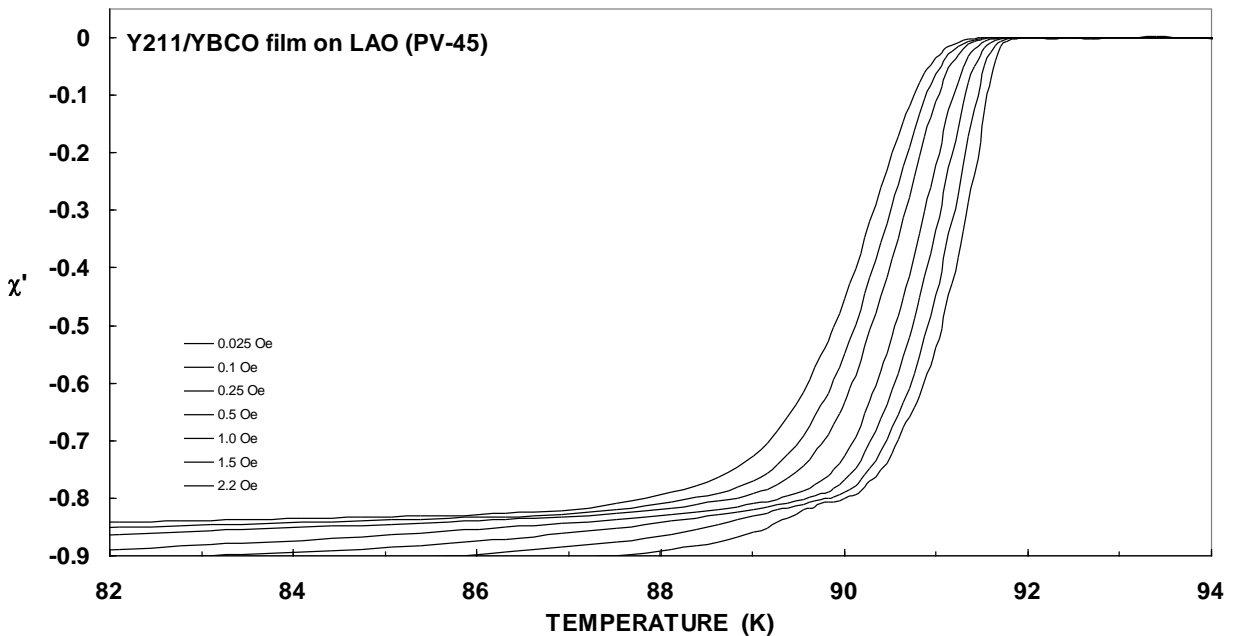


Figure 2b.1.4.1

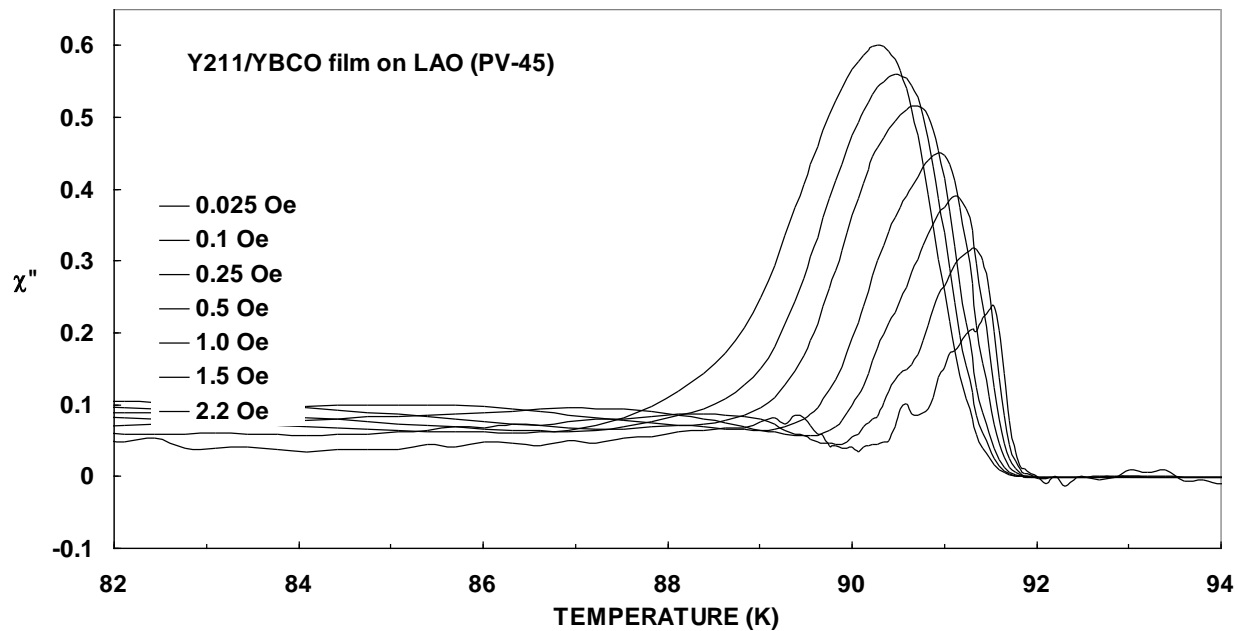


Figure 2b.1.4.2

2b.1.5 AFM Data

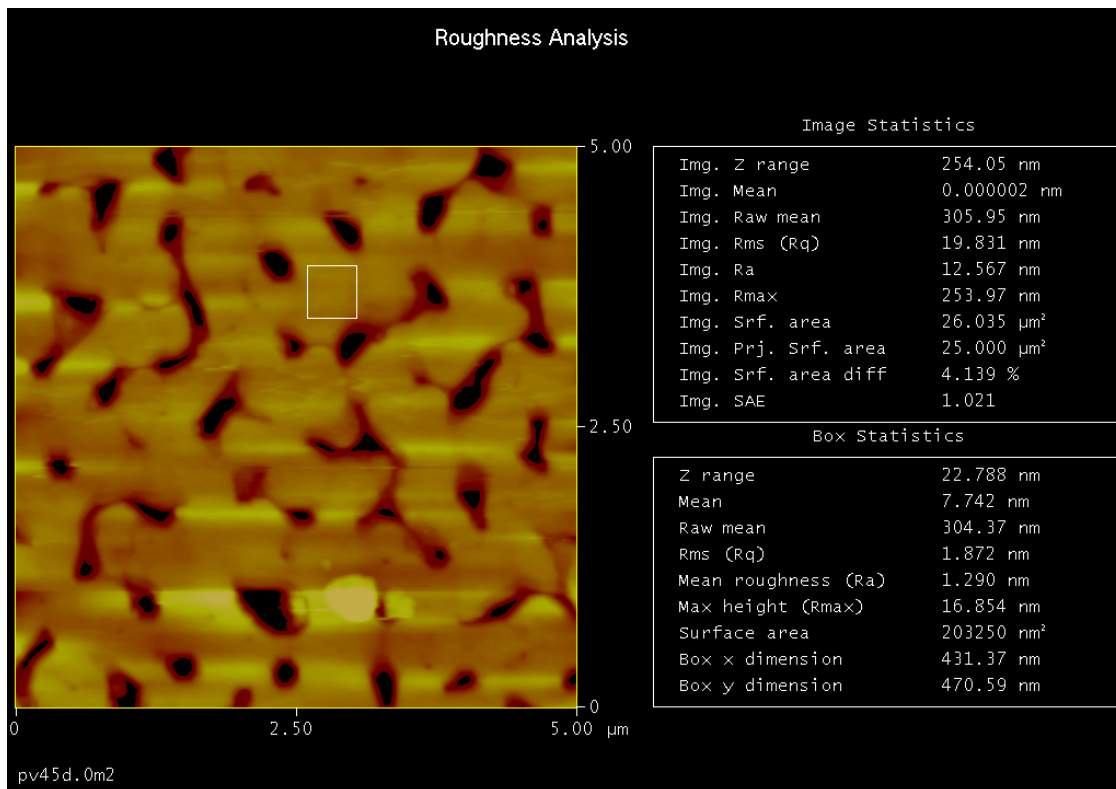


Figure 2b.1.5.1

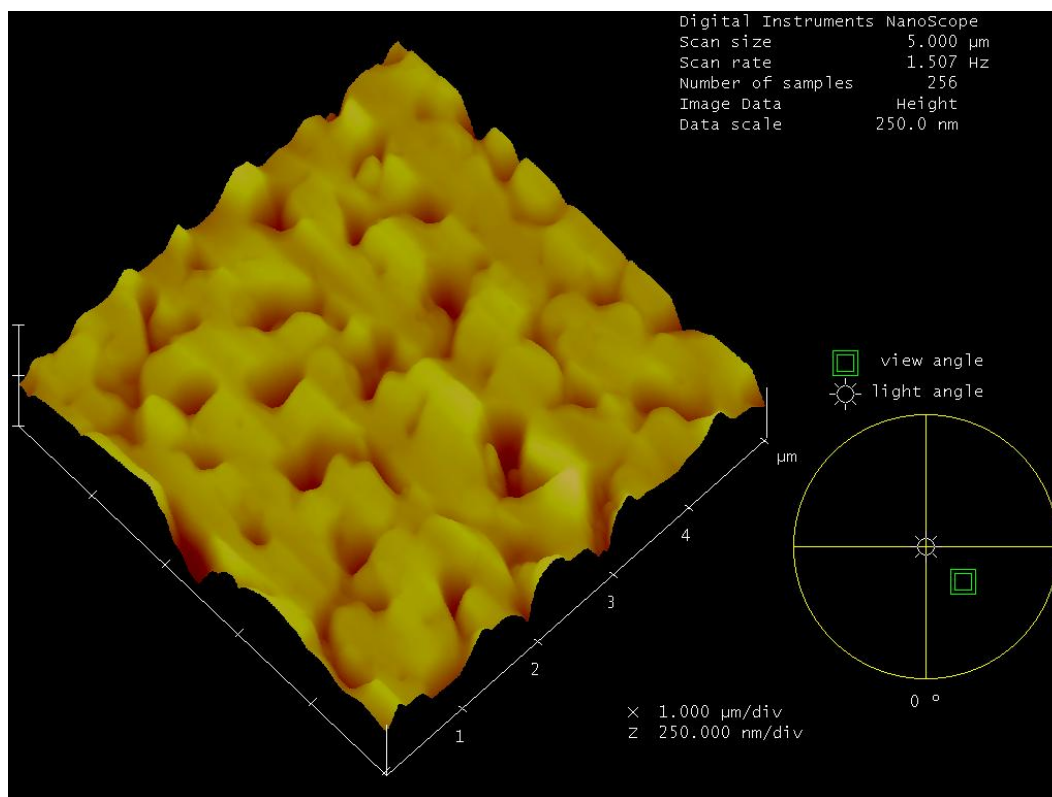


Figure 2b.1.5.2

2b.1.6 VSM Data

VSM data at 65 K

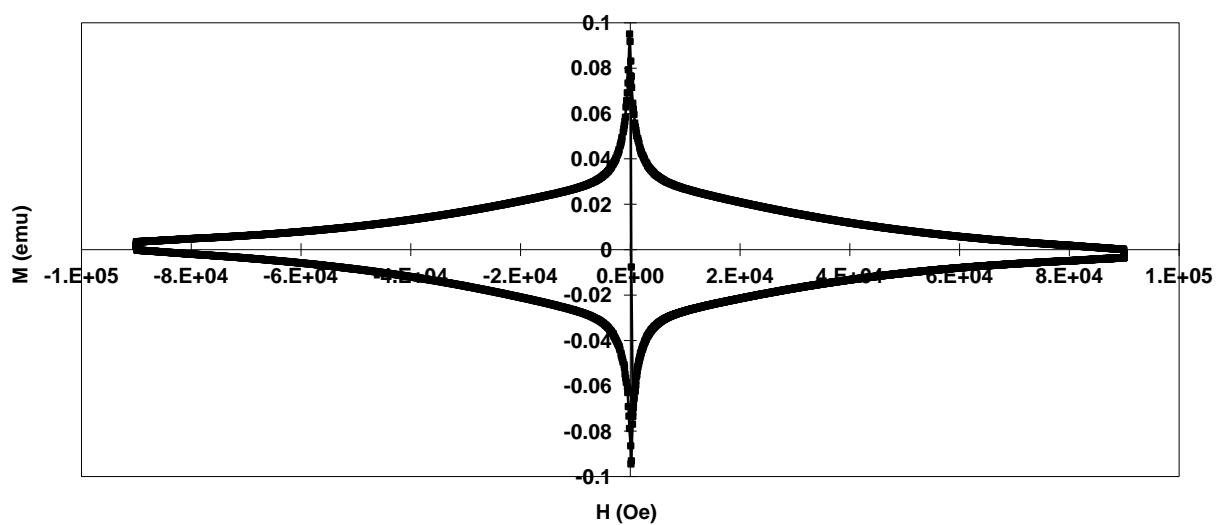


Figure 2b.1.6.1

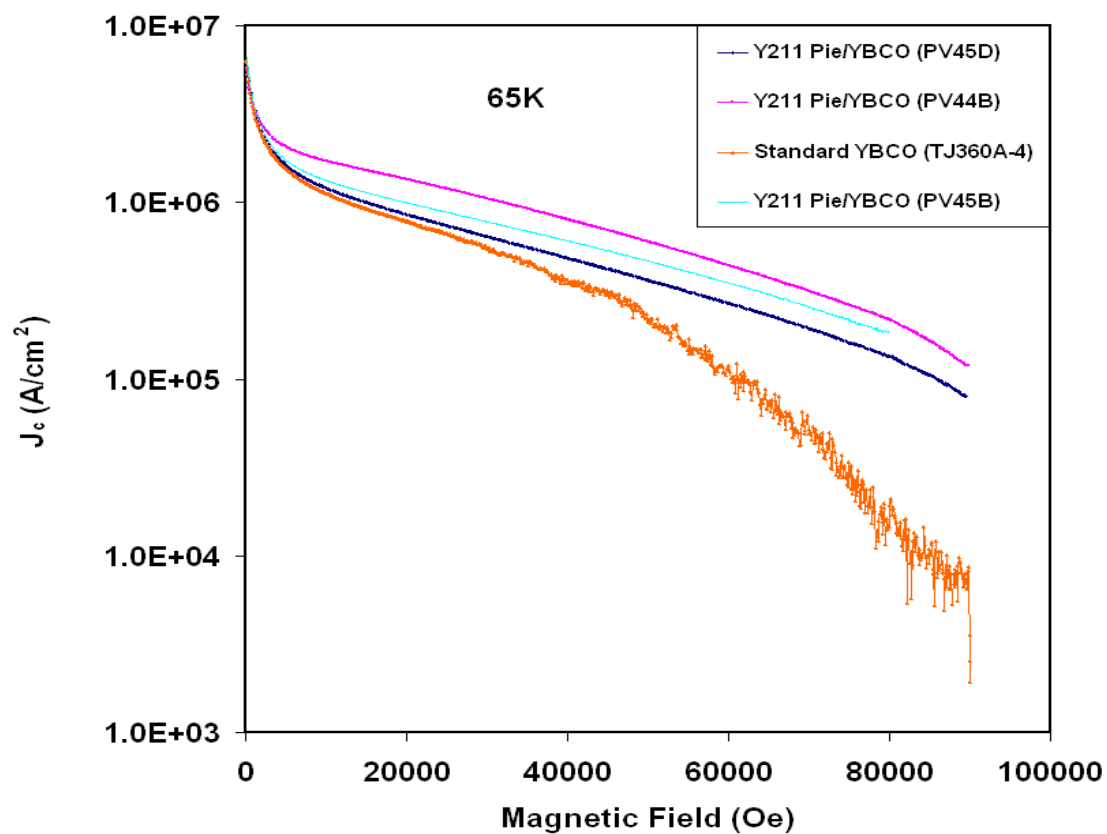


Figure 2b.1.6.2

VSM Data 77K

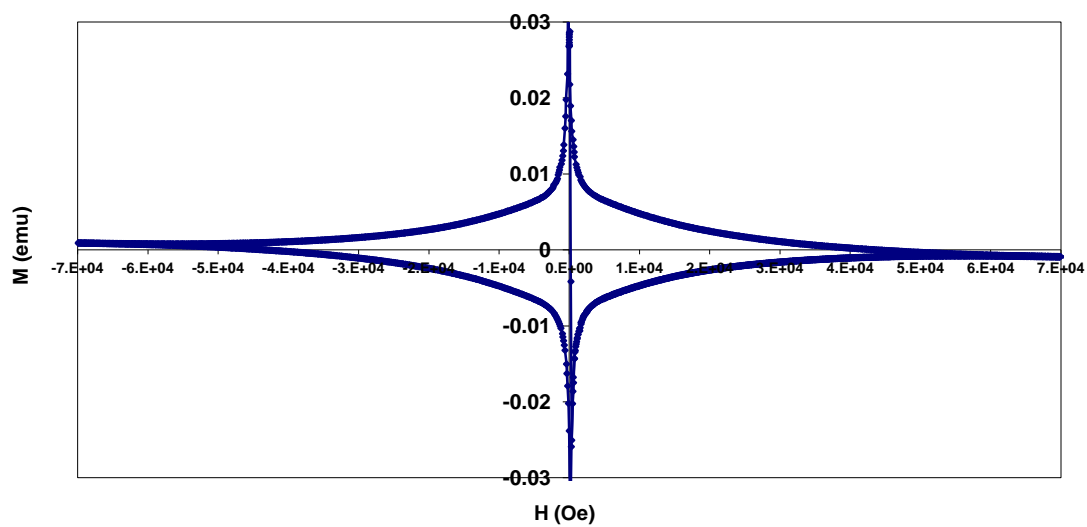


Figure 2b.1.6.3

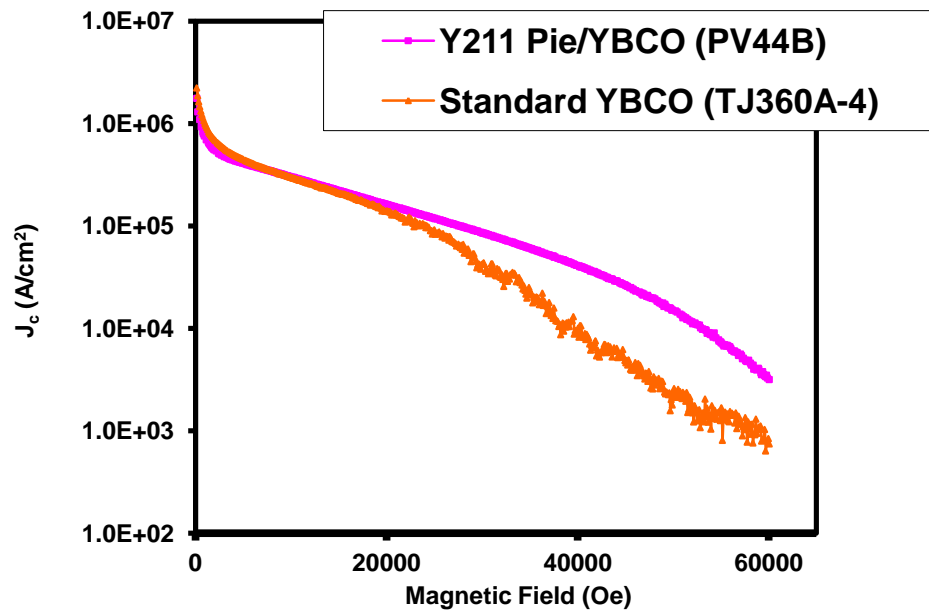


Figure 2b.1.6.4

VSM Data at Various Temperatures

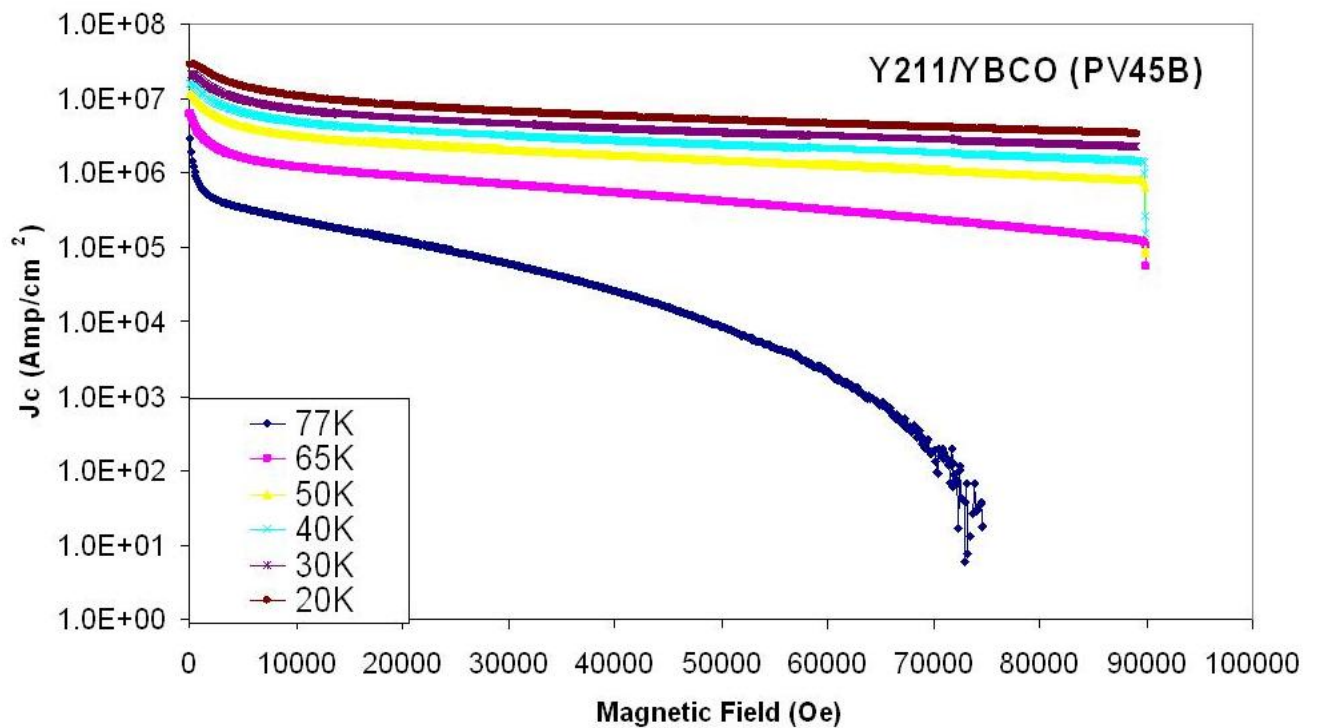


Figure 2b.1.6.5

2b.1.7 Transport Current Data

Transport Current Data

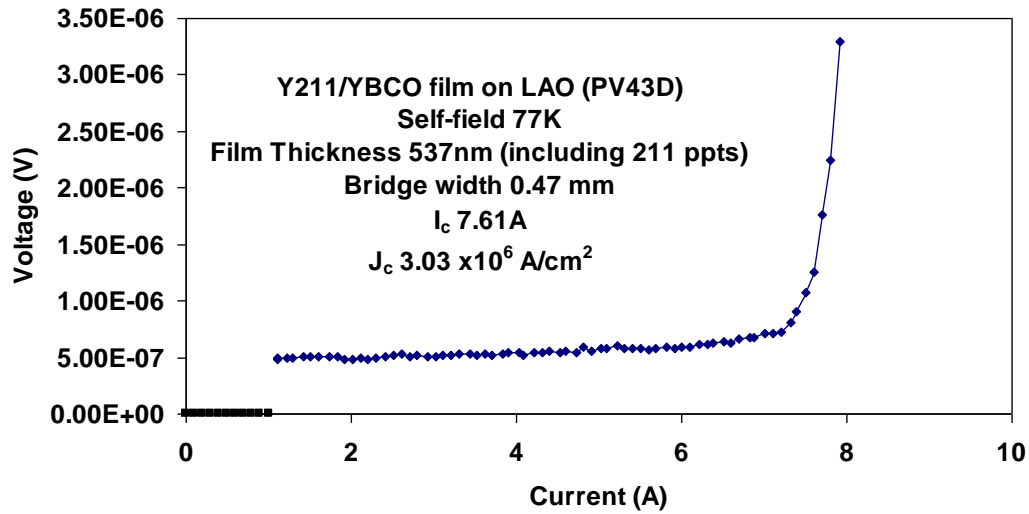


Figure 2b.1.7.1

	Thickness (μ m)	Avg. Thickness (cm)	Bridge width (mm)	Avg. Bridge width (cm)	I_c (A)	J_c (A/cm ²)
PV43D	0.597	5.37333x10-5	0.4644	0.04676	7.61	3.03x106
	0.511		0.4724			
	0.504		0.466			

Figure 2b.1.7.2

2b.1.8 J_c Angular Dependence

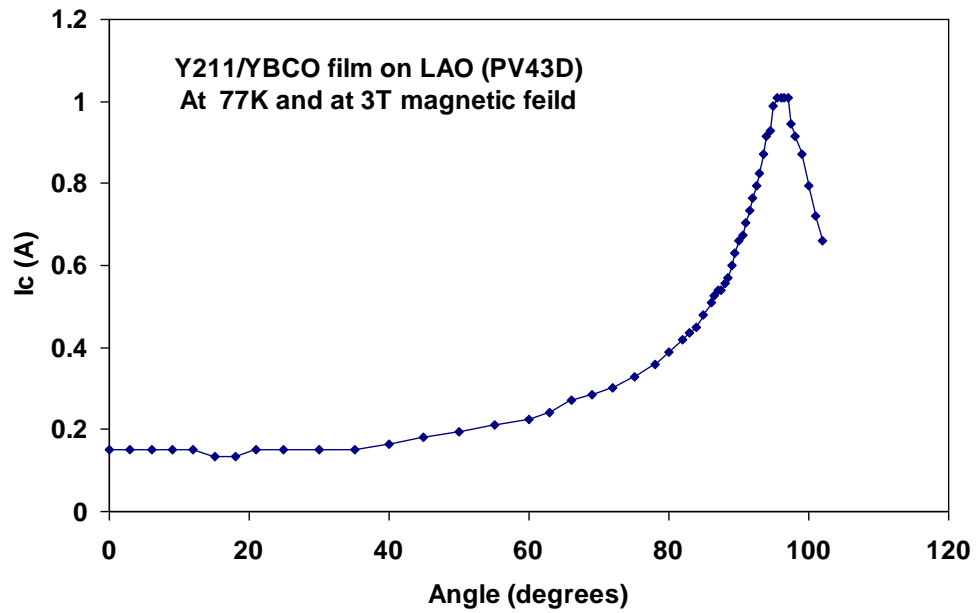


Figure 2b.1.8.1

2b.1.9 High Resolution SEM

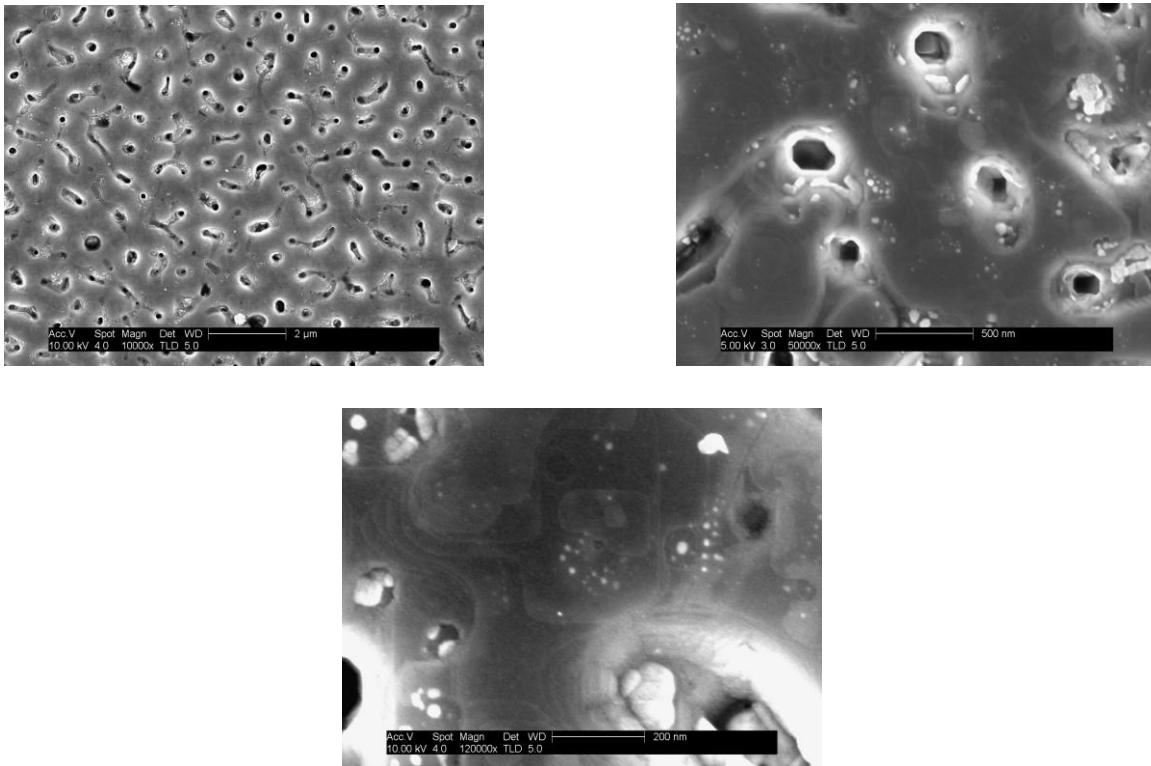


Figure 2b.1.9.1

2b.1.10 Focused Ion Beam Cross Sectional SEM

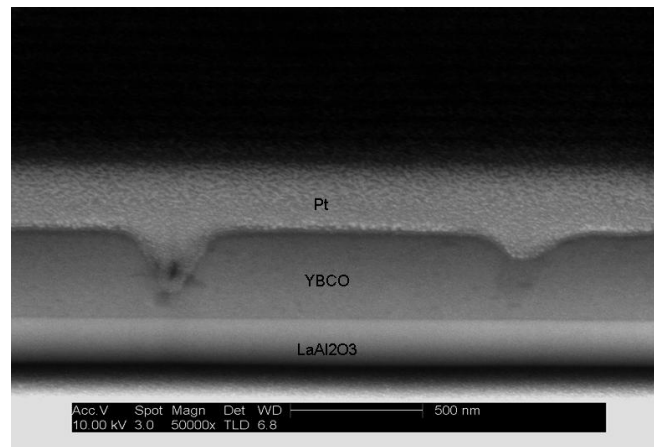


Figure 2b.1.10.1

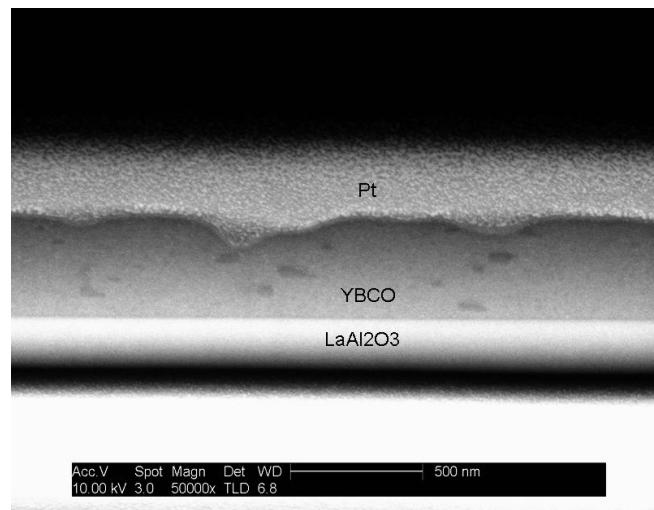


Figure 2b.1.10.2

2b.1.11 Conclusions

- Nanometer sized particulates can be introduced into YBCO films using a specially made YBCO PLD target with a second phase sector
- Initial results indicate improvements in magnetization J_c at both 77K and 65K especially at high fields in YBCO films made with Y211 particles.
- An order of magnitude increase in the magnetization J_c at 9T at 65K was obtained in the YBCO samples made with Y_2BaCuO_5 (Y211) sector target as compared to using a regular YBCO target
- Microstructure shows uniform porosity and nm sized particles in the YBCO films grown on La_2AlO_3 substrates using a PLD target with Y211 sector
- Porosity seem to originate at the particles introduced in the films.
- Initial results show that YBCO films with Y211 particles can be grown on $LaAl_2O_3$ substrates with critical current density $> 3MA/cm^2$ at 77K in self-field with reduced angular dependence as compared to regular YBCO.

- Process optimization and refinement of the particle size is presently underway and expected to improve the properties further.

2b.2 Studies on Flux Pinning Properties of $\text{YBa}_2\text{Cu}_3\text{O}_{7-\delta}$ Thin Films with Nano Particulate Dispersions

References: 5

Srinivas Sathiraju

SRA-NRC, Power Generation, Propulsion Directorate, Air Force Research Laboratory

Presented at ASC 2004 Annual Meeting, October 8, 2004

2b.2.1 Experimental

Three Methods for Flux Pinning

1. Gas Phase nano-particulate dispersion (PLD)
2. Nano particulate dispersion on Single crystals and bi crystals substrate(PLD)
3. Multilayer deposition(PLD)

Gas Phase

- Y123 Layer was deposited for 5 minutes (50nm)
- Chamber pressure increased to 1- 5 Torr and deposited 211 for 1 minute
- Y123/211/Y123 - (1 to 8 layers of 211 nano particulates having same thickness)
- Ag nano particulates
- 123 Nano particulates

2b.2.2 Gas Phase nano particulate dispersion

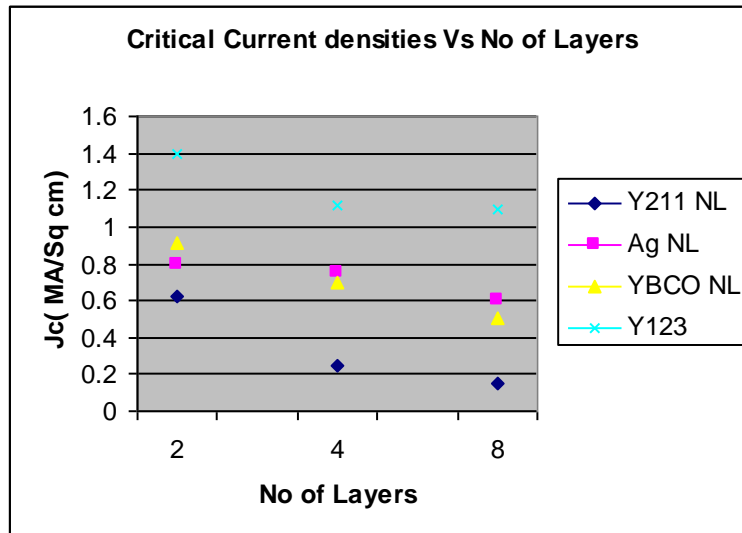


Figure 2b.2.2.1

2b.2.3 Ca Doped 211 nano particulate dispersion on Bi-crystals

WHY BI-CRYSTALS?

- Coated Conductors have large angle grain boundary misorientation problem
- Ca doping heals that problem (?)– Nature Paper
- We know that 211 doping helps flux pinning

We want to study the combination effect across bi-crystal junctions

2b.2.4 Transition Temperature data

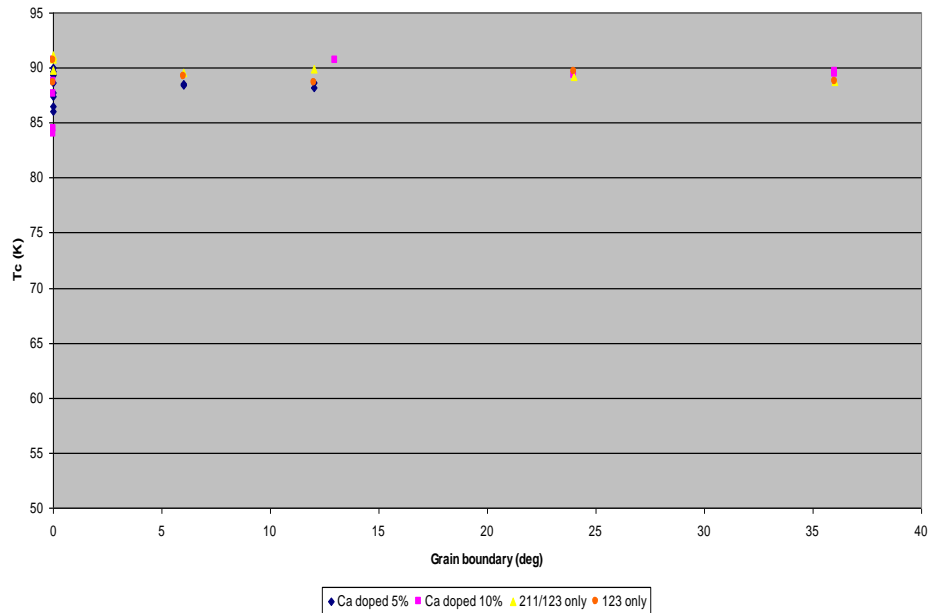


Figure 2b.2.4.1

2b.2.5 J_c vs Bi-crystal angle

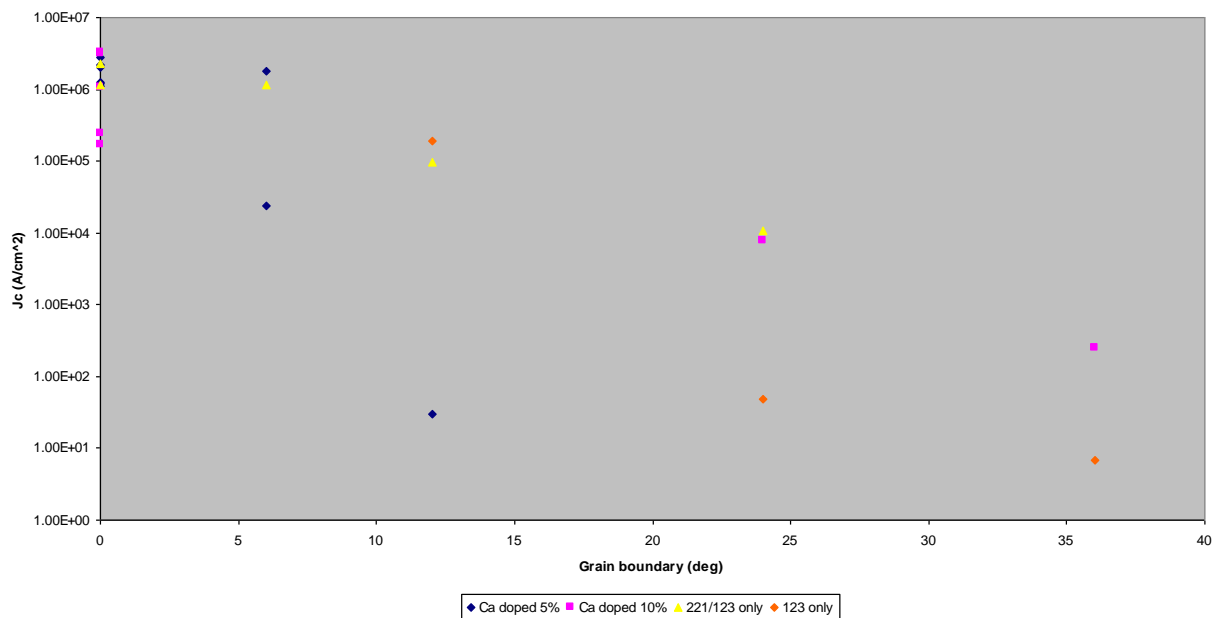


Figure 2b.2.5.1

2b.2.6 Y211 vs Ca5% Y211

OBSERVATIONS

- Y211 has better pinning than Ca 5% doped films
- Ca 10% has diluted the pinning

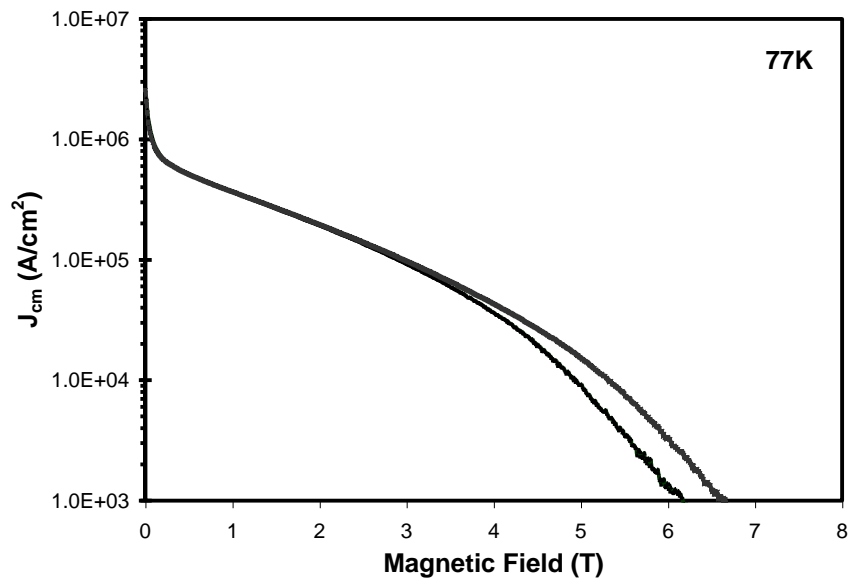


Figure 2b.2.6.1

2b.2.7 X-TEM OF Y123/YCa5%211 multilayers

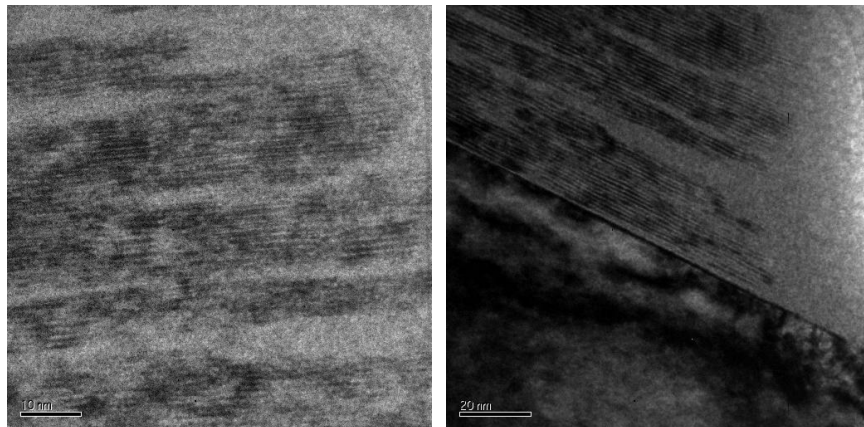


Figure 2b.2.7.1

X TEM of Y123/Ca5%211 on STO 240 bi-crystal

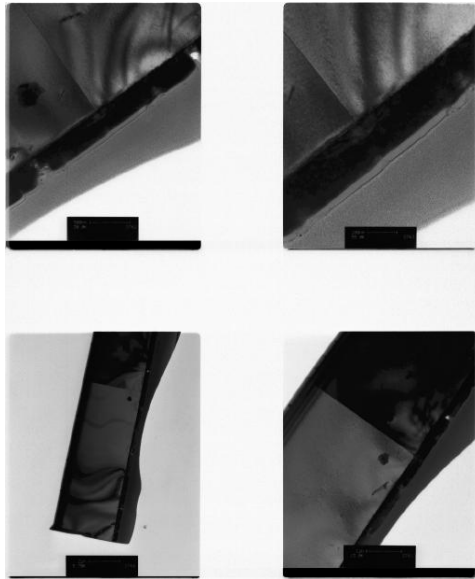


Figure 2b.2.7.2

X-TEM and SAD micrographs of Y123/Ca5%211 on STO 240 bi-crystal

Observations

1. We have noticed that our films were grown slightly out of plane with respect to the crystal plane
2. Partly C-axis and Partly a-axis oriented with the increase of Ca doping
3. Possible reason could be either quality of bi-crystal or growth optimization

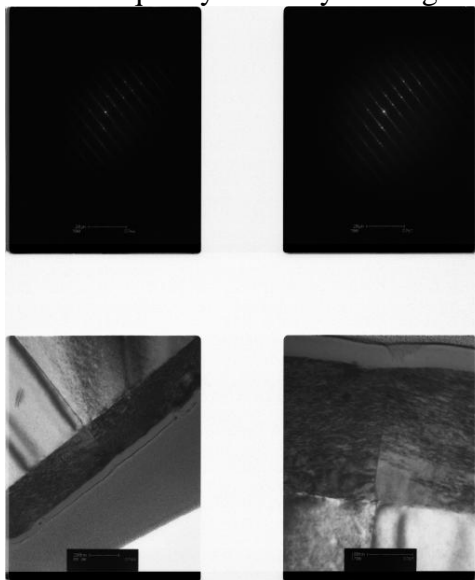


Figure 2b.2.7.3

2b.2.8 Surface of Y123/(Y,Ca)211multilayers

Surface of Y123/YCa211multilayers on 6° bi-crystal of STO

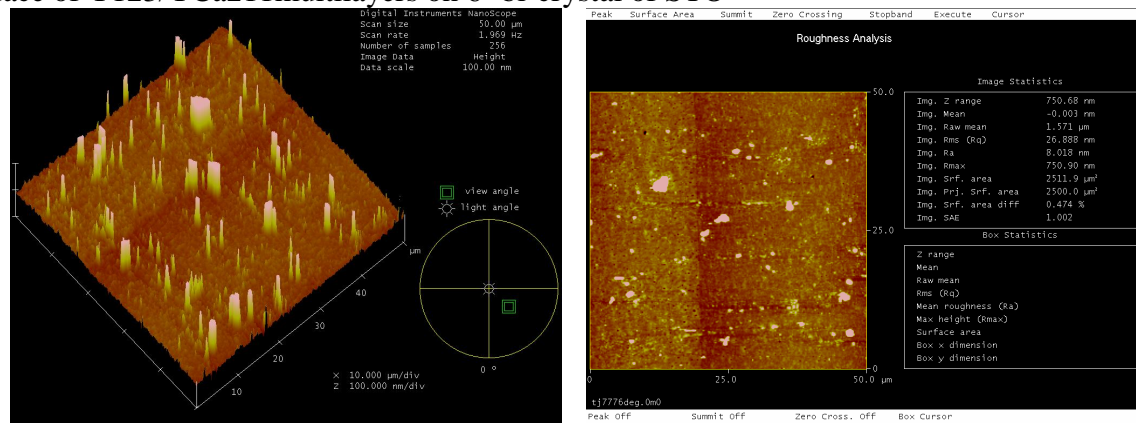


Figure 2b.2.8.1

Surface of Y123/YCa211multilayers on 12° bi-crystal of STO

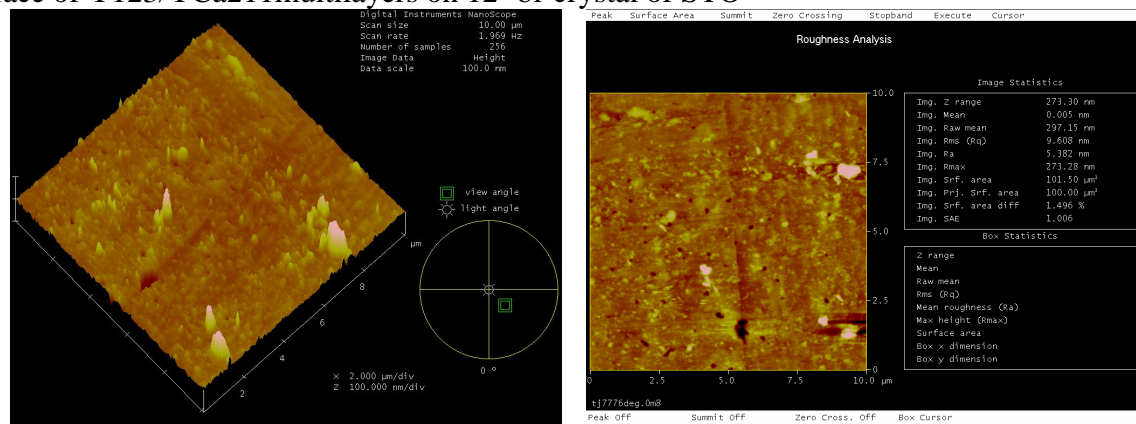


Figure 2b.2.8.2

Surface of Y123/YCa211multilayers on 24° bi-crystal of STO

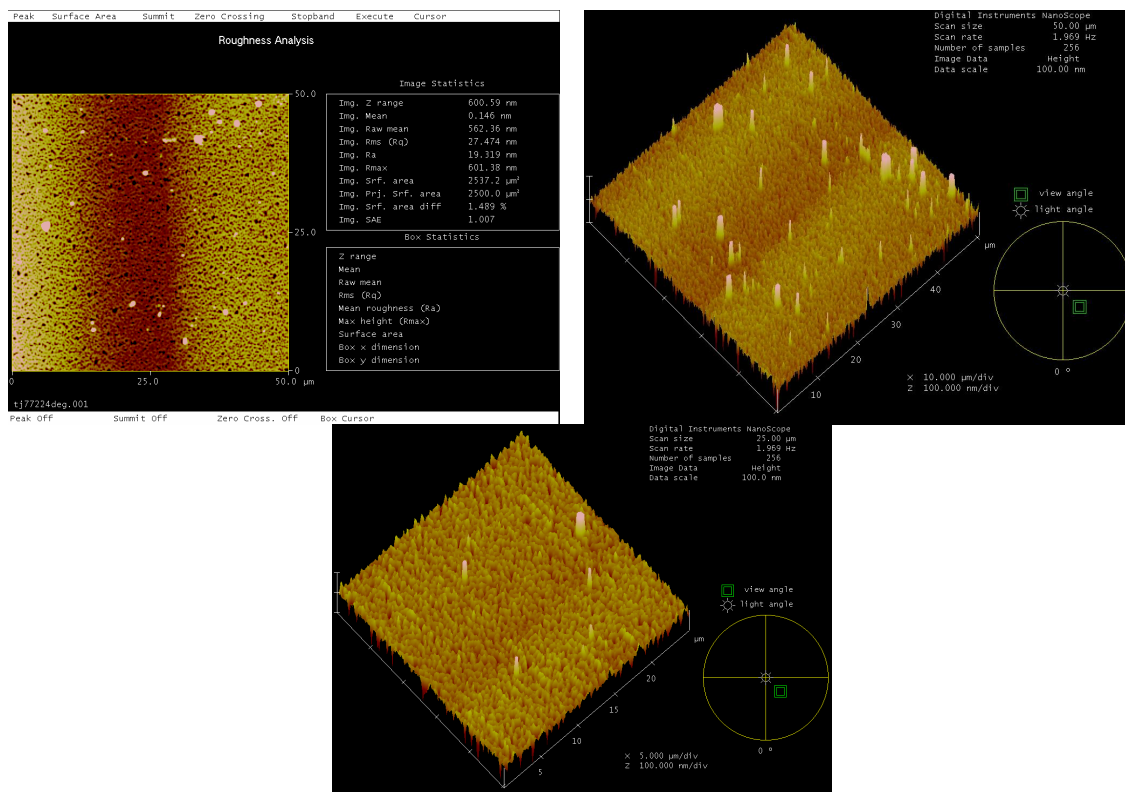


Figure 2b.2.8.3

Surface of Y123/YCa211multilayers on 36° bi-crystal of STO

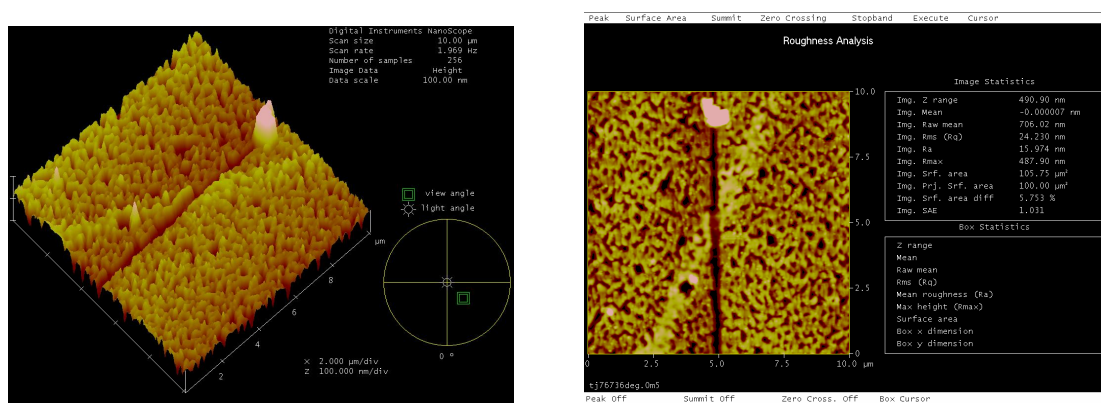


Figure 2b.2.8.4

2b.2.9 Comparison of $\text{Y}_2\text{O}_3/\text{Y211}/\text{Y123}$ (PPMS DATA)

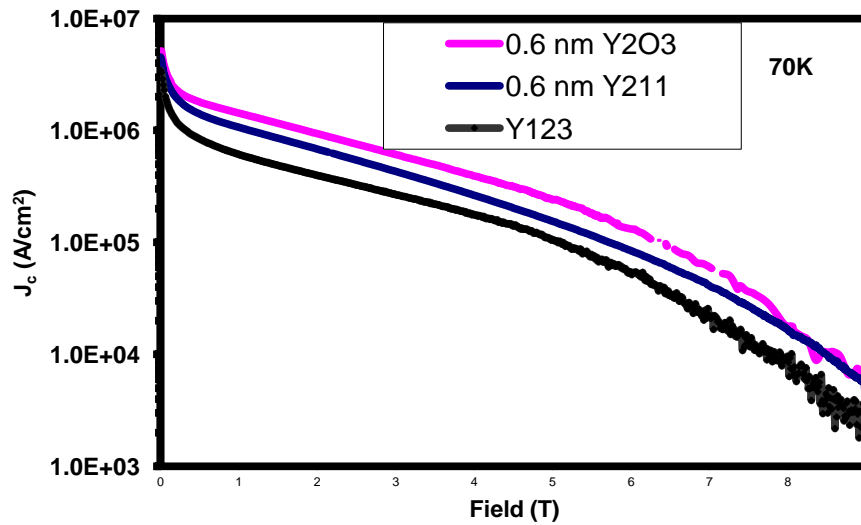


Figure 2b.2.9.1

2b.2.10 Y211 vs Ca5% Y211

- Y211 nano dispersion has better pinning than Ca doped Y211 dispersion when deposited at the same conditions
- Is Ca doping investigation is
A WRONG SELECTION
AT A WRONG SITE FOR RIGHT PINNING PROPERTIES? NO !
We have YET TO OPTIMIZE THE DEPOSITION CONDITIONS

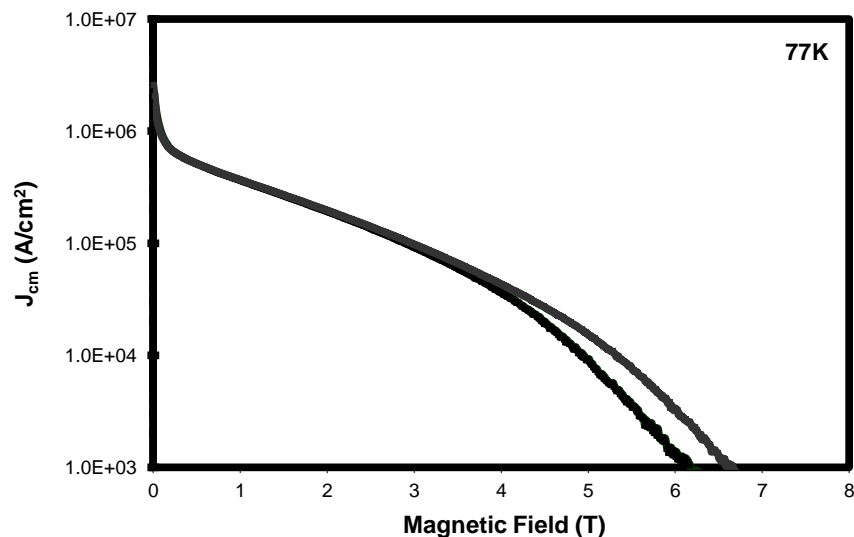


Figure 2b.2.10.1

2b.2.11 AC Susceptibility of $\text{Y}_{1.8}\text{Ca}_{0.2}\text{BaCuO}_5$ film on STO substrate

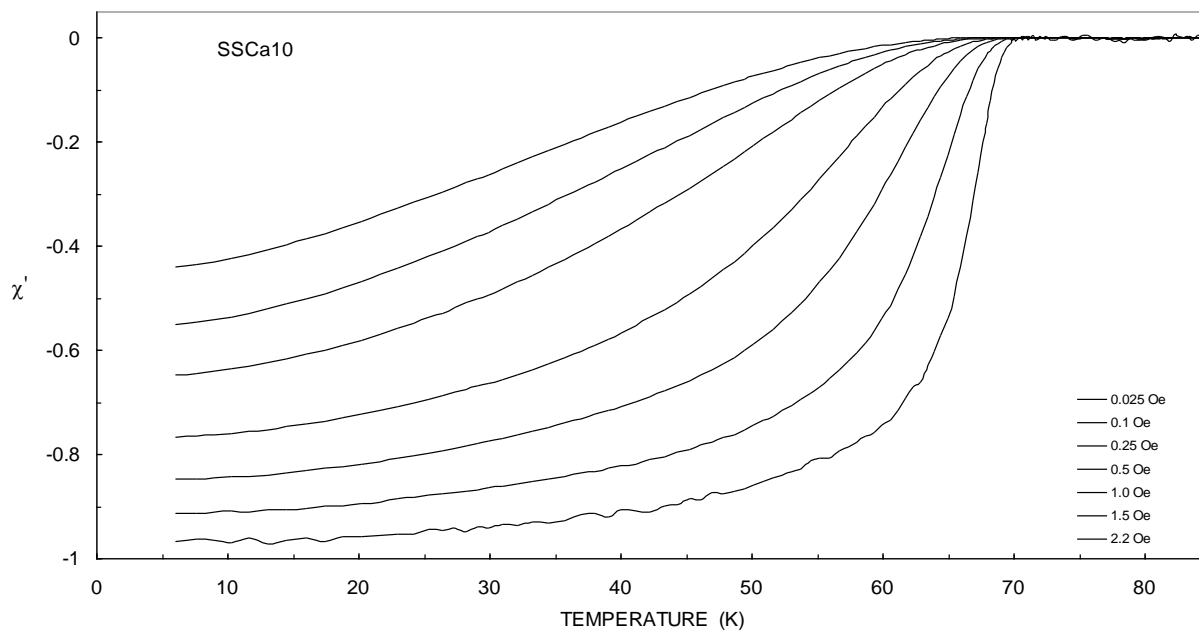
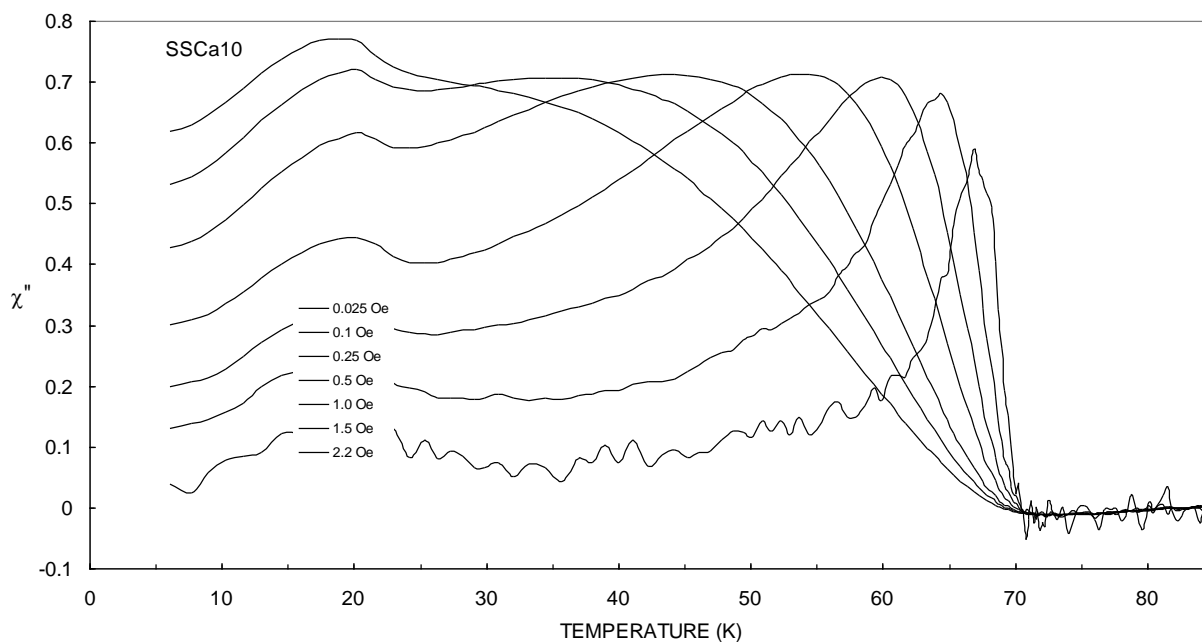


Figure 2b.2.11.1



2b.2.12 Summary

- Nano particulate dispersion in multilayers of Y123 has been investigated under similar deposition conditions
- Y_2O_3 , Ag, Y123, Y_2BaCuO_5 and $\text{Y}_{1-x}\text{Ca}_x\text{BaCuO}_5$ nano particulates were studied
- Magnetization J_c at 77K suggests that Y_2O_3 nanoparticulate dispersion has better pinning nature
- Ca 10% doped Y211 target has shown diamagnetism below 70 K

- There are much better pinning materials out there

2b.2.13 Future scope of this work

- Double Perovskites of RBa_2MO_6 WHICH DO NOT REACT WITH 123 and THEY ARE CUBIC with $a \sim 8.4 \text{ \AA}$
- Also would like to investigate effect of Conducting oxides, Insulating oxides, R_2BaMO_5 (R = Rare earth; M= Ni, Ta, Nb, W, Zr etc)

2b.3 Studies on flux pinning properties of $\text{Y}_{2-x}\text{Ca}_x\text{BaCuO}_5$ nano-particulates in $\text{YBa}_2\text{Cu}_3\text{O}_{7-x}$ coated conductors

References: 5

Paul N. Barnes

National Research Council

Propulsion Directorate, Air Force Research Laboratory

Presented at ACERS 106 annual meeting, April 20, 2004

2b.3.1 Ca doping in Y123 films

- Ca doping in Y-123 is well known to increase the population of holes in YBCO by replacing Y^{+3} with Ca^{+2} ; hence improving the superconducting coupling between the grains.
- Hammerl et al reported a 3 to 6 fold improvement of J_c for annealed Y123/Ca-123/Y123 multi-layered films where some of the Ca migrates to grain boundaries.
 G.A. Danniels et al, APL 77(2000) 3251
 G. Hammrel et al Nature, 405 (2000)162
 H.Hilgenkemp and J. Manhart, APL 73 (1998) 265
 A. Manthiram et al, J. Solid State Chem. 73 (1988)278
- Daniels et al discovered that Ca-doping increased the inter-grain critical current density in spite of a lower T_c in higher concentrations of Ca doped Y-123 films.
- Haugan et al demonstrated that Y123/211nanoparticles /Y123 multi-layers show highest magnetization J_c possible due to uniform distribution of nano-ordered pinning centers.
 G. Hammrel et al Nature, 405 (2000)162
 T. Haugan, P.N. Barnes, R. Wheeler, F. Melsenkothen and M. Sumption, Nature 430 (2004) 867
 T. Haugan, P. N. Barnes, I. Maartense, C. Cobb, E. J. Lee and M. Sumption, JMR 18 (2003) 2618.
- We would like to utilize the combined effects of Ca doping and Y211 pinning in order to improve the electrical transport properties of Y123 films. We have opted for Ca doping at Y site in Y211 since Ca doping at Y site in Y123 decreases the T_c of the films.
- In order to achieve this, one should know the structure-property relationship of Ca doped Y211films. No literature available on Ca doped Y211 films and their structure and

magnetic properties. So we would like to address both these aspects in the present research report

2b.3.2 Experimental

1	Laser Energy	2 – 3 J/cm ²
2	Substrate Temperature	800 – 820° C
3.	O ₂ Partial Pressure	250 mTorr
4.	Laser Frequency	4 - 6 Hz
5.	Thickness of the films	300 - 500 nm
6	Targets (homogeneous)	Y _{2-x} Ca _x BaCuO ₅ and YBa ₂ Cu ₃ O _{7-x}
7	Substrates	LaAlO ₃ {LAO}(100), SrTiO ₃ (100), Bicrystals of SrTiO ₃

Figure 2b.3.2.1

2b.3.3 XRD Pattern of Y123 film with Ca 5% doped Y211 nano-particles

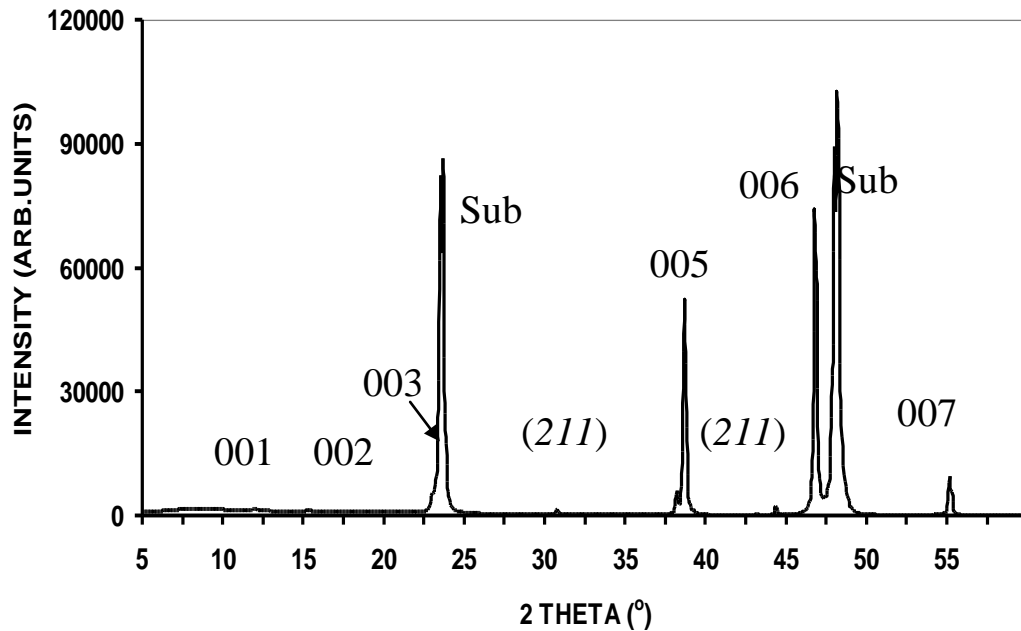


Figure 2b.3.3.1

2b.3.4 T_c Comparison of Y123 films with and without $Y_{2-x}Ca_xBaCuO_5$ ($x = 0, 0.1$ and 0.2) nano-particulates

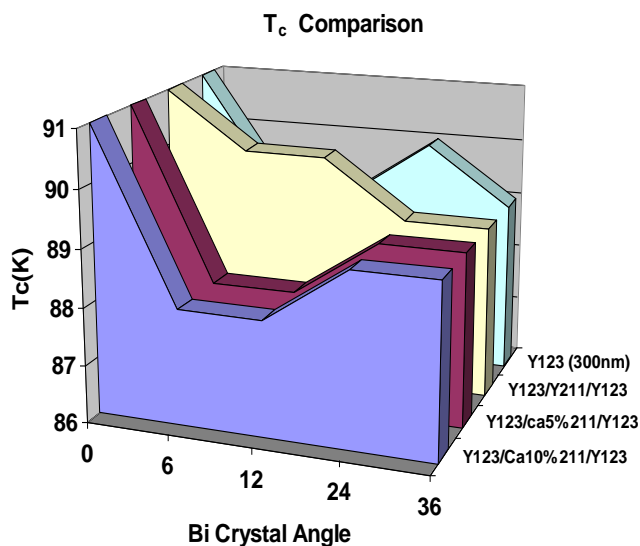


Figure 2b.3.4.1

Comparison of Transport properties in self field.

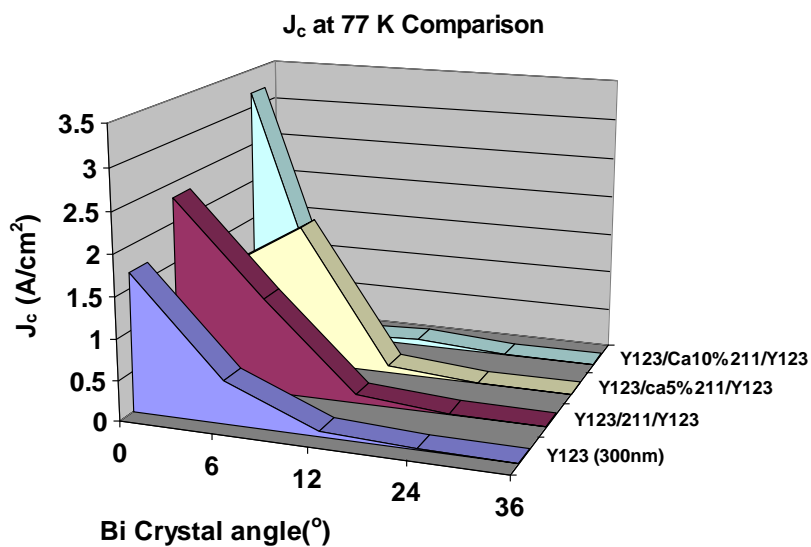


Figure 2b.3.4.2

2b.3.5 XRD of $Y_{1.9}Ca_{0.1}BaCuO_5$ film deposited on $LaAlO_3(100)$ substrate

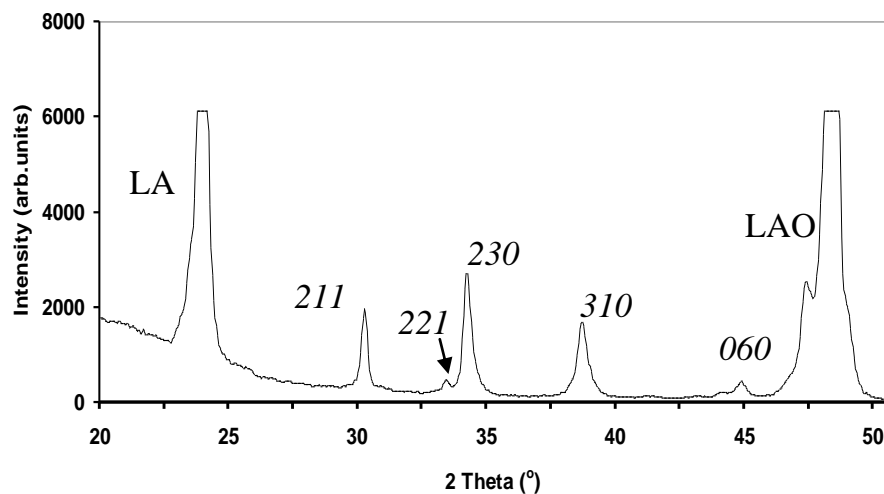


Figure 2b.3.5.1

2b.3.6 XRD of 10 % Ca doped Y211 film deposited on $LaAlO_3(100)$ substrate

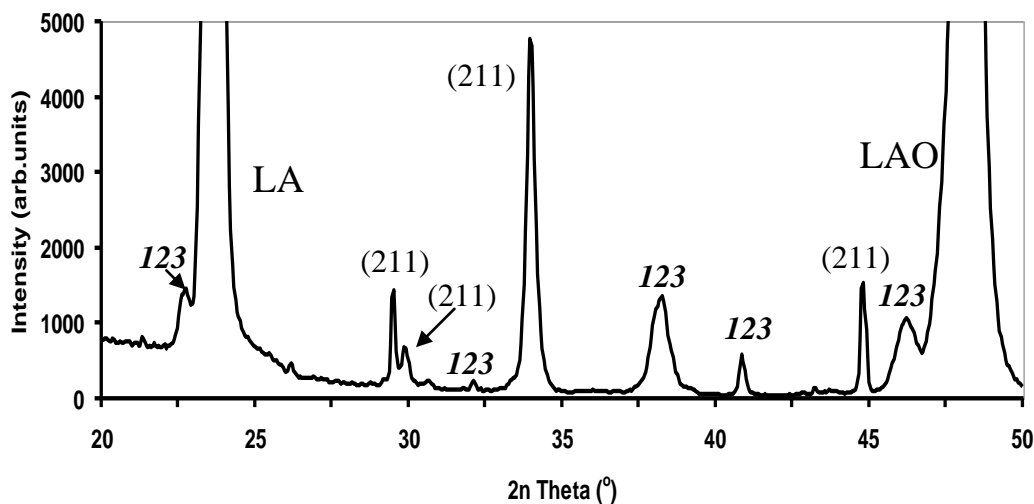


Figure 2b.3.6.1

2b.3.7 AC Susceptibility of the 10% Ca doped Y211 film deposited on LAO substrate

Shows onset T_c around 30K, however superconductivity disappears with applied field indicating a weak superconducting nature.

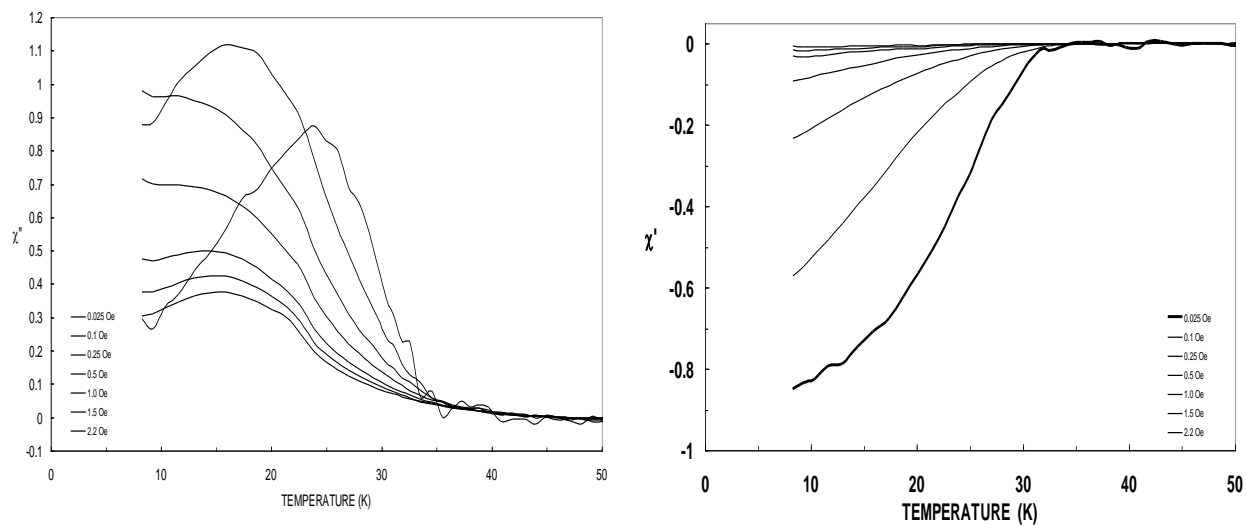


Figure 2b.3.7.1

2b.3.8 Raman Spectrum of the 10% Ca doped Y211 film deposited on LaAlO_3 (100) substrate

Indicates distorted Y123 Raman modes along with impurity phases (at 578 and 732 cm^{-1})

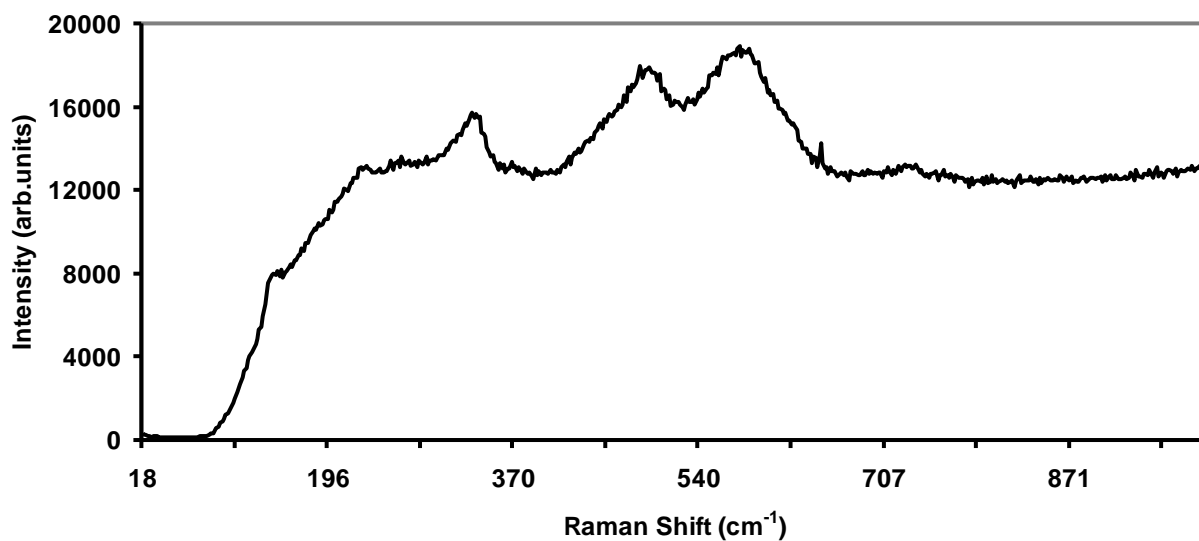


Figure 2b.3.8.1

2b.3.9 Cross Sectional Transmission Electron Microscope image (prepared using FIB method) of Ca 10% doped Y211 film

Shows columnar growth and multi-phase grains (~500 nm thick film deposited at 250 mTorr O₂ and 800 °C)

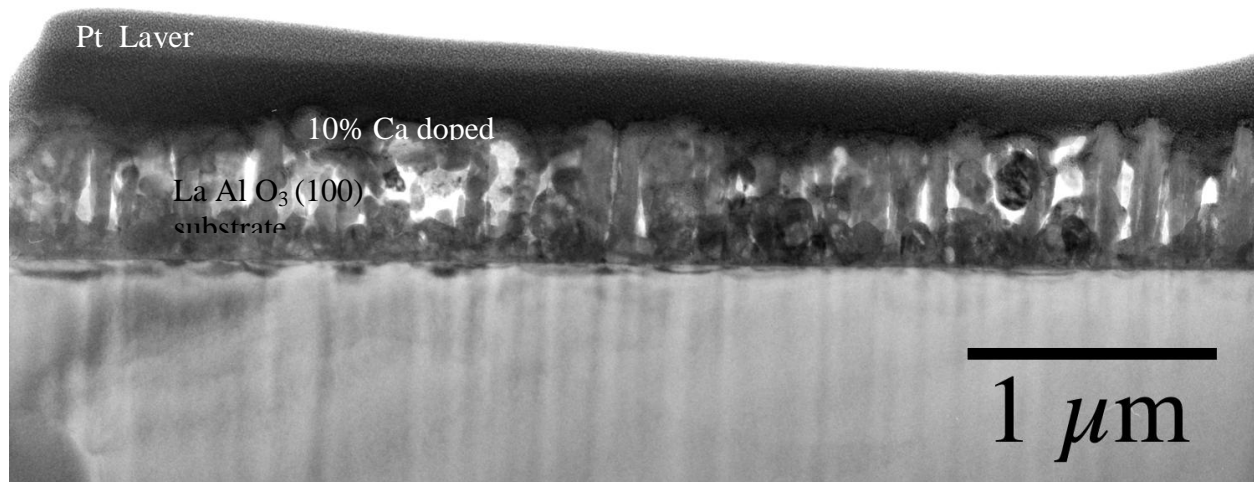


Figure 2b.3.9.1

2b.3.10 Conclusions

- Ca (5% and 10%) doped Y211 films were prepared under identical conditions using pulsed laser deposition. When Ca exceeds more than 5%, the Y211 film contains Y123 phase.
- Y123 films dispersed with Ca doped Y211 particulates have shown improvement in electrical transport properties when compared with pure Y123 and Y211 doped Y123 films when deposited on Single crystals.
- Films grown on Bi-crystal substrates indicate that Ca doping in Y211 further improves the superconducting coupling between grains and hence critical currents.
- Further studies are in progress in order to determine the optimum doping level of Ca in Y211 to achieve maximum pinning properties of Y123 coated conductors for various power applications.

2b.4 Fundamental studies of magnetic flux pinning mechanisms

Introduction of nano-sized second phase particles using PLD

Development of striated filaments of YBCO conductor

Fabrication of striated substrates using laser striation

Testing of photolithography as an approach

References: 1, 2, 25, 26, 27, 28, 29, 30, 31, 32

C. Varanasi¹, P.N. Barnes²

1. *University of Dayton Research Institute*

2. *Air Force Research Laboratory*

2b.4.1 Pinning by Ca Doped Y2BaCuO5 Nanoparticles

- Improve the transport properties of YBa2Cu3O7-y in magnetic fields via flux pinning centers of Y2-xCaxBaCuO5 (x = 0.1 and 0.2)
 - Ca-doping increases the intergrain J_c in spite of a lower T_c
 - Y211 nanoparticles improves J_c due high pinning density
- Combined the effects of Ca doping and Y211 pinning into a single step process to improve overall electrical transport in Y123 films
 - 65 K has excellent in-field J_c improvement

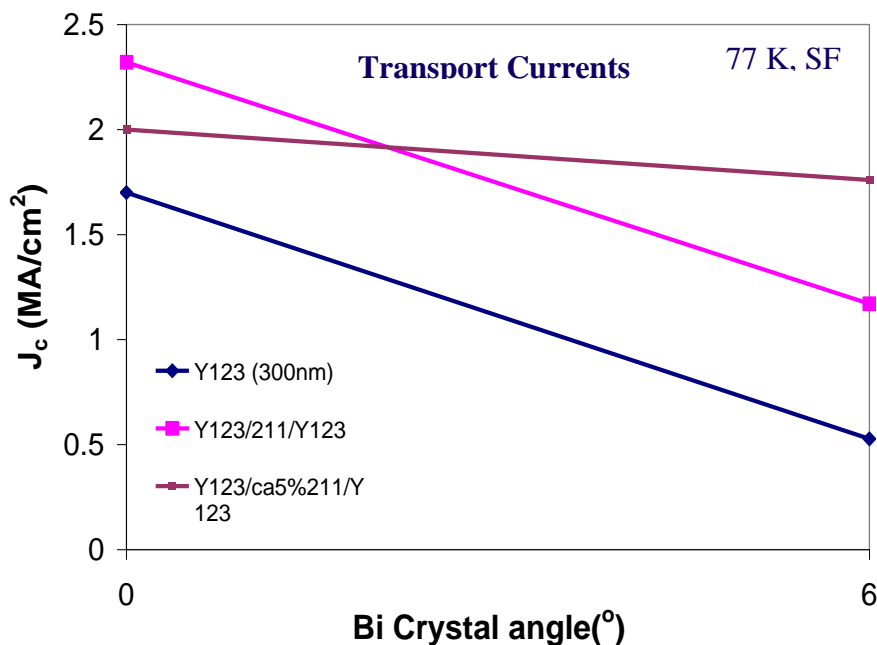


Figure 2b.4.1.1

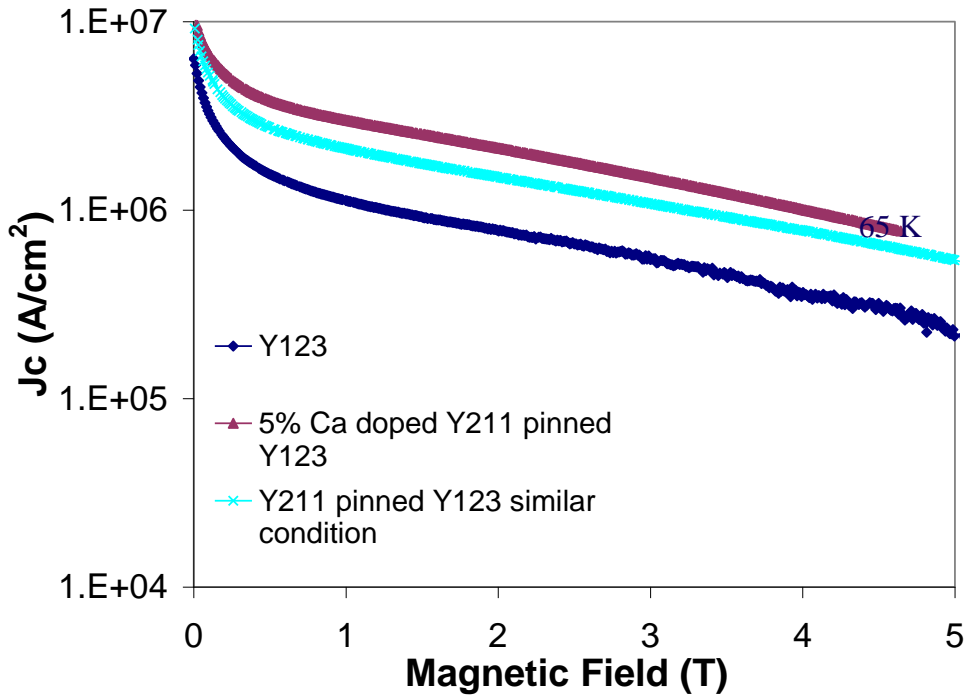


Figure 2b.4.1.2

2b.4.2 Fp of 5% & 10% Ca-doped Y211 Nanoparticles

- Note the relative reversal in peaks between 5% and 10% Ca-doping at the two different temperatures (77K and 65K)
 - University of Wisconsin research of normalized plots indicates that peak reversal is very rare (typically same or greater shift)
 - 5% doping better than 10% at 65K (raw data)
- Relationship to pinning strength and pinning density unclear

Normalized Force vs. Normalized Field

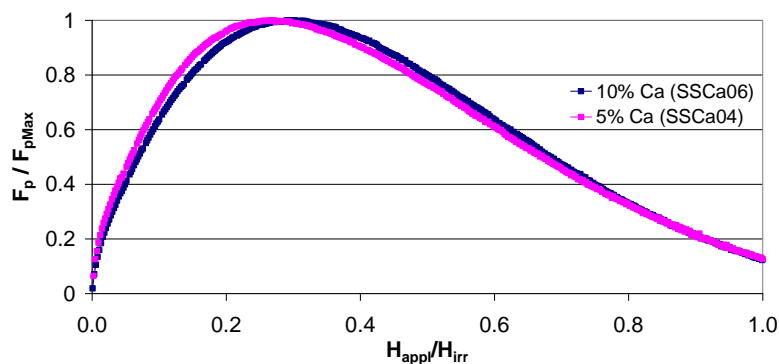


Figure 2b.4.2.1

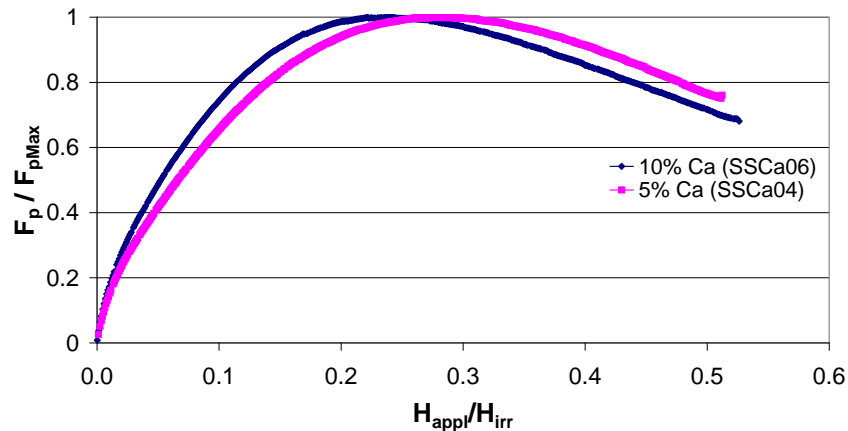


Figure 2b.4.2.2

2b.4.3 Minute Additions of Tb, Ce, Pr Dopants in $Y_{1-x}RE_xBa_2Cu_3O_{7-z}$

- Previous studies focused on RE substitution for Y in YBCO ($x \geq 0.1$)
 - Y site substitution as opposed to second phase precipitates.
- Alternate way to improve flux pinning characteristics just discussed is to introduce a high density of defects into the material
- This study focuses on substituting small quantities ($x \leq 0.1$) of Tb, Ce and Pr in YBCO films deposited by PLD
 - Tb, Ce, and Pr do not form (or difficult to form) the RE123 phase.
 - An appropriate defect density of the inclusions can be produced if these RE are sufficiently dispersed.
 - These elements are divalent, having both +3 and +4 valence states and possibly allow pinning by alternate chemical bonding.
- The literature indicates that terbium does not degrade the T_c of YBCO, but Ce significantly affects the T_c with increasing Ce content
- Small quantities of dopants potentially allow the same deposition parameters as plain YBCO

2b.4.4 Ce-Doped YBCO Films

- 0.1% Ce-doping showed J_c improvement over undoped YBCO at 65K of about 25% (2 T) to 200% (8 T)
 - Improvement at 77K is not apparent at the 0.1% level likely due to depression of T_c .
 - Further optimization is underway at different doping concentrations.
- 1% and 10% Ce doping showed typical decrease in J_c

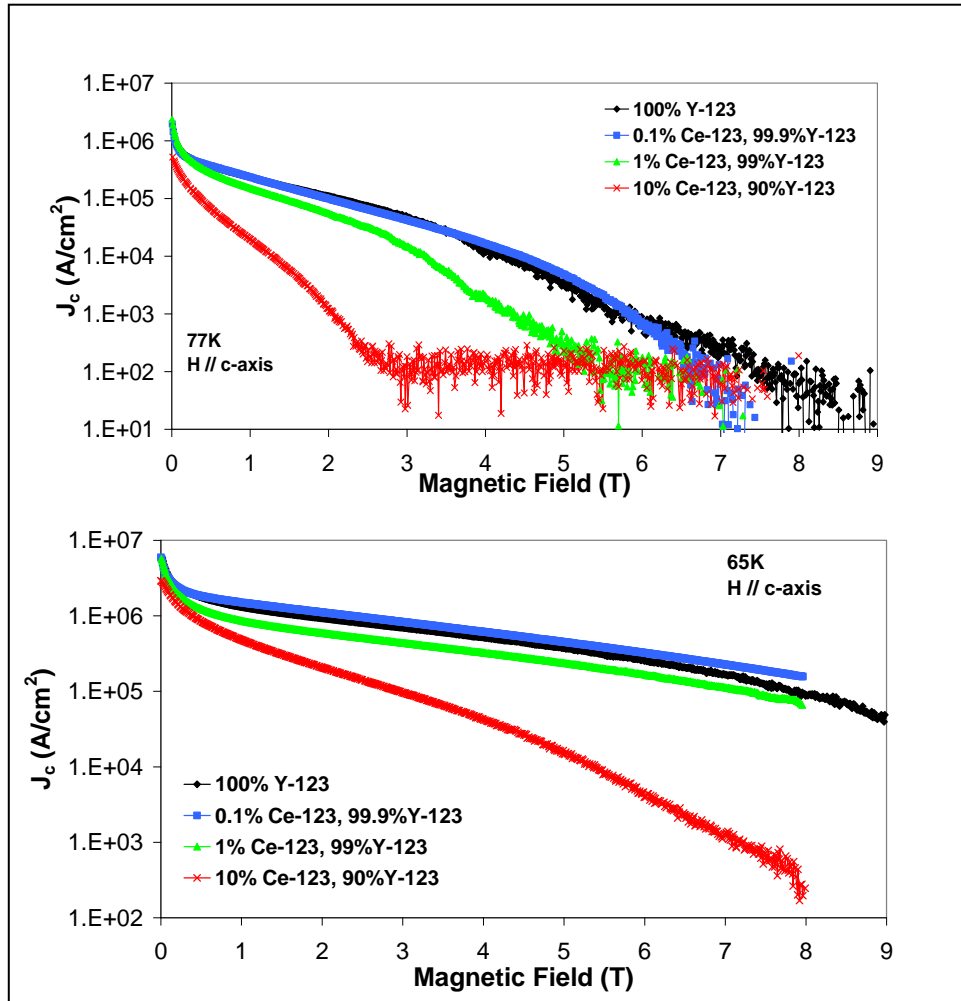


Figure 2b.4.4.1

2b.4.5 Pr-Doped YBCO Films

- 0.1% and 1% Pr doping showed a minor increase in J_c , but not significant compared to Ce minute doping
 - 65K performance is equivalent to YBCO which is contrary to Ce doping for which performance improved from 77K .
- 10% Pr doping showed J_c decrease as expected
- Pr-doping is not very effective for given parameters

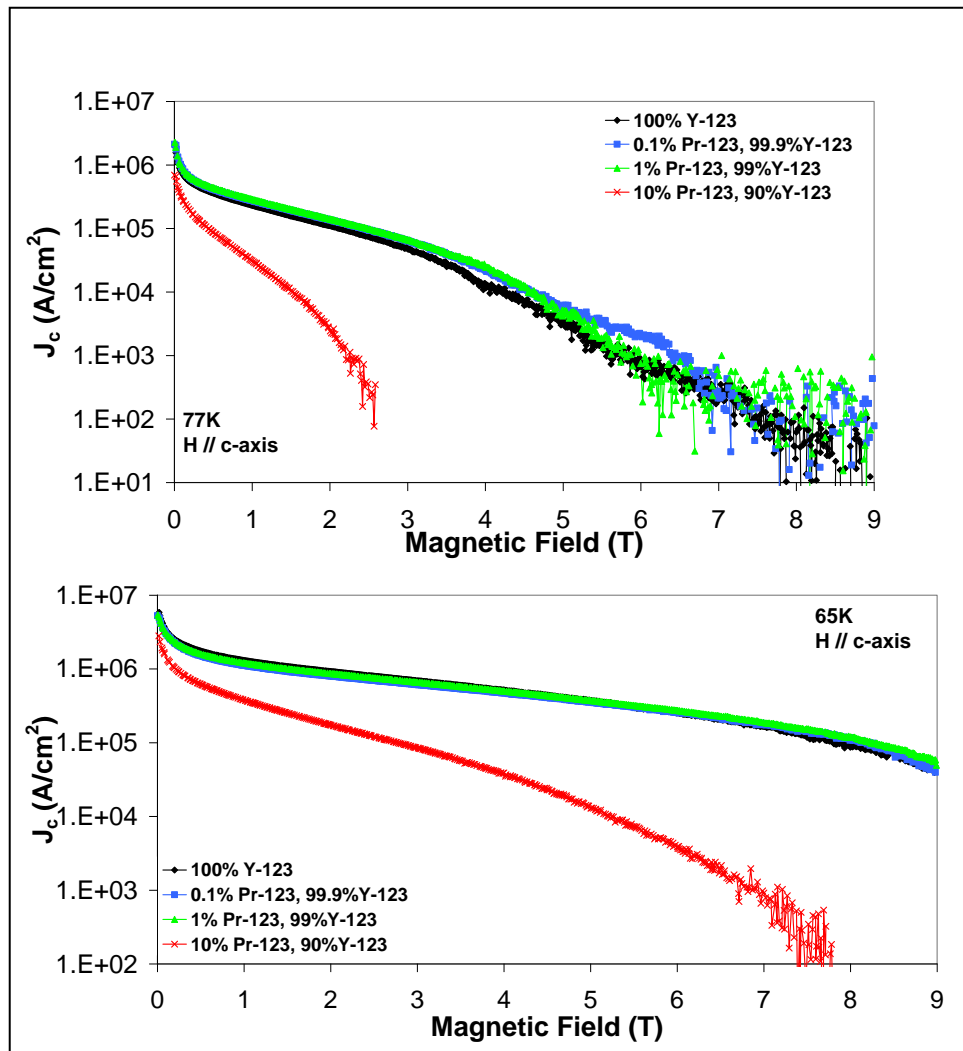


Figure 2b.4.5.1

2b.4.6 Tb-Doped YBCO Films

- 1% Tb doping showed J_c improvement over undoped YBCO at 77K
- Both 0.1% and 1% Tb doping improved J_c at 65K
 - Between 100% - 300% improvement for 1% doping > 1T.
 - Similar to nanoparticulate pinning
- Minute addition (<1%) of certain rare earths (e.g. Ce, Tb) can improve J_c by defect site induced pinning, Tb is best
 - Tb doping mechanisms is under investigation.
 - Doping is more readily accomplished by any deposition method.

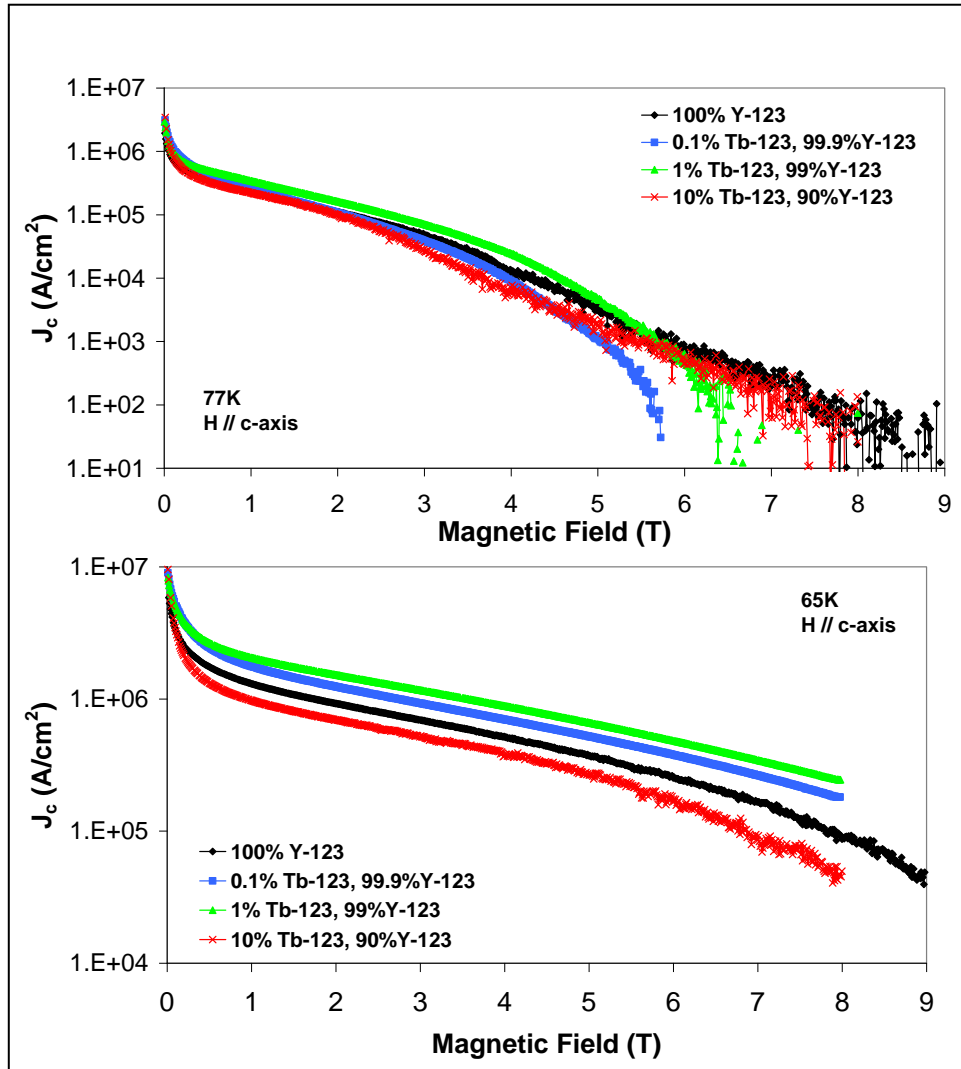


Figure 2b.4.6.1

2b.4.7 Grooved Substrate for Filamentary YBCO

- Multifilamentary YBCO has been demonstrated by the removal of YBCO via laser ablation and etching (bottom left)
- Alternatively the substrate can be grooved upon which YBCO is grown
 - Top center is laser ablated demonstrating trench depth control.
 - Bottom center is etched substrate demonstrating fine grooving.
- Grooving substrate can separate filaments in YBCO without post processing treatments (YBCO removal)

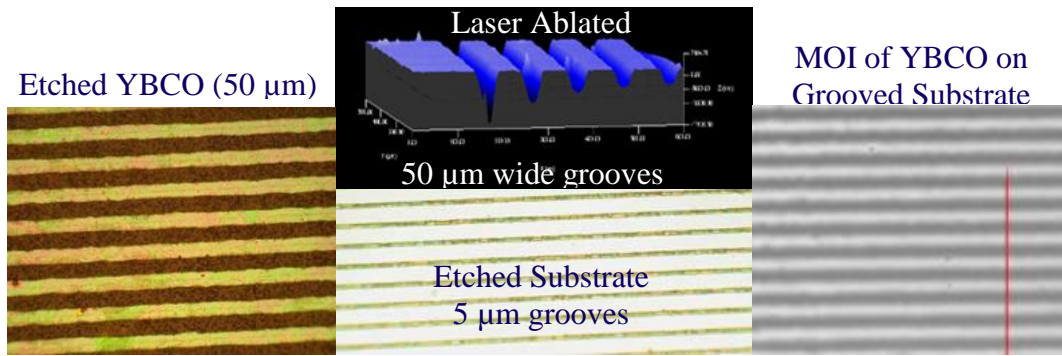


Figure 2b.4.7.1

Figure 2b.4.7.2

Figure 2b.4.6.3

Figure 2b.4.6.4

2b.4.8 Filamentary Current Sharing

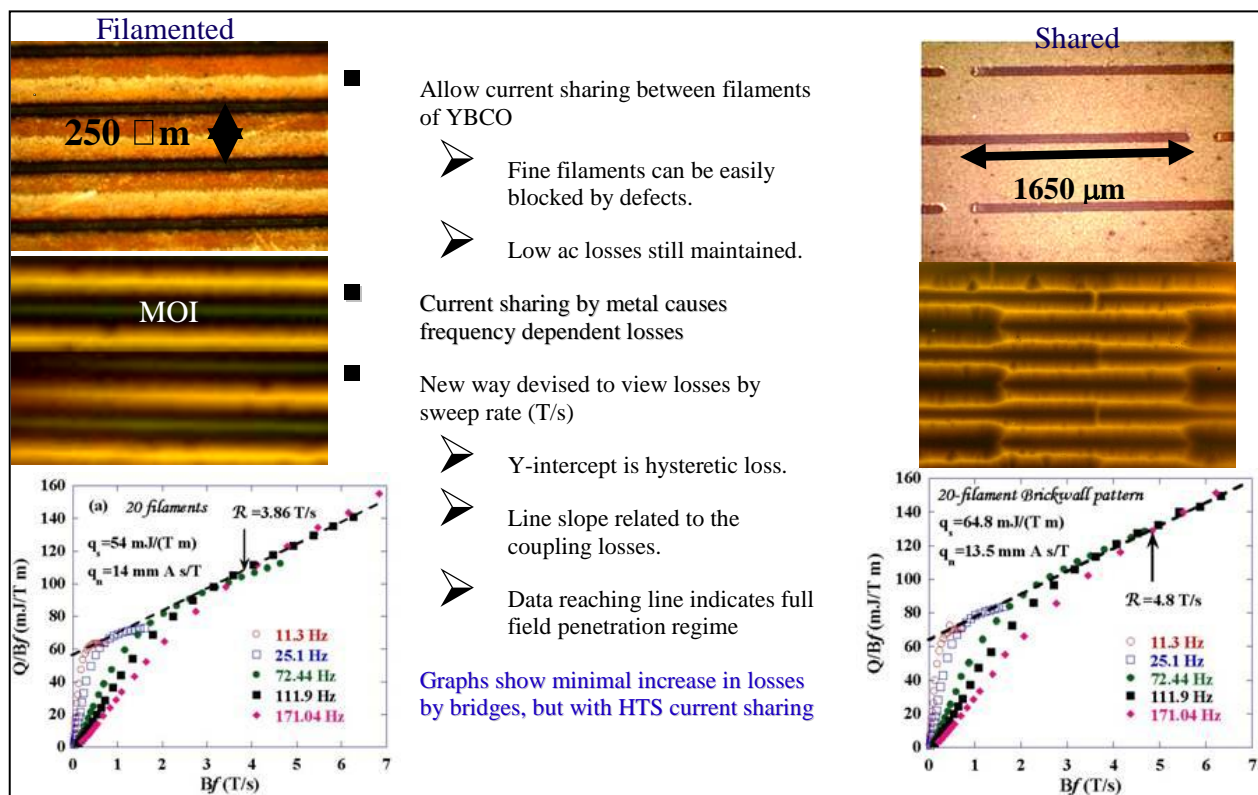


Figure 2b.4.8

2b.4.9 Summary

- Combined the effects of Ca doping and Y211 pinning into a single step process to improve overall electrical transport in Y123 films
 - Ca-doping increases the intergrain J_c in spite of a lower T_c .
 - Y211 nanoparticles improves J_c due high pinning density
- Minute addition (<1%) of certain rare earths (e.g. Ce, Tb) can improve J_c by defect site induced pinning
 - 1% Tb is best, 100% - 300% improvement for > 1 T at 65 K.
 - Similar improvements as nanoparticulate pinning.
 - Optimization required as well as additional dopants identified.
 - Minute doping technique is process independent.
- Substrate grooving provides an alternative to post YBCO treatments
 - Laser ablation provides depth control (anisotropic grooving).
 - Chemical etching provides narrow grooves but isotropic.
- Multiply connected filaments provides current sharing
 - Only a minimal increase in ac losses (hysteresis and coupling).
 - Current can circumvent blockages in fine filaments maintaining I_c .

Chapter 2C: Rare Earth Substitutions

The effect of chemical composition variations on the flux pinning and physical properties of $(Y, RE)_{1+x}Ba_{2-x}Cu_3O_{7-\delta}$ superconductors is being investigated extending previous work in this area. RE may be a single rare earth for a binary mixture but may also be dual rare earths for a ternary mixture. The goal of this research is to show that current carrying capability of HTS thin films can be improved by substituting various rare earth (RE) elements into the YBCO lattice. Nearly all RE elements have their own superconducting phase for the Y123 equivalent system, are chemically compatible with Y, and also are fairly similar in ionic radii. Differences that do exist in ionic radii may potentially strain the lattice of the superconductor and this stress field will provide greater pinning for the penetrated fluxons.

2c.1 Characterization of Nd Doped $YBa_2Cu_3O_{7-x}$ films

References: 16

J.C. Tolliver, C.V. Varanasi, J.M. Evans, T.J. Haugan, P.N. Barnes
Air Force Research Laboratory, Wright-Patterson AFB, OH 45433

2c.1.1 Abstract

YBCO superconductors are being considered for thin film coated conductors because of their high T_c (92 K) and high J_c at 77 K in magnetic fields. Because rare-earth cations have similar ionic radii, they can be considered for solid-solution substitution to vary and control physical properties such as lattice constants, T_c 's, J_c 's, and flux pinning. This paper examines the effect of solid-solution intersubstitution of Y with Nd on flux pinning and physical properties. Also examined is Ba in $(Y,Nd)_{1+y}Ba_{2-y}Cu_3O_{7-z}$. The region of single-phase crystal structures are defined and properties in that region characterized by both XRD and magnetic measurements of the bulk powder. Based on this data, a composition is selected to create a target from which a thin film is deposited on single crystal substrates by pulsed laser deposition. Results based on the correlation of the characterization of bulk powders and the resulting thin films will be presented.

2c.1.2 Objectives

- Solid-solution substitution of RE for Y and Ba in $YBa_2Cu_3O_{7-z}$ to vary and control physical properties such as lattice constants, T_c 's, J_c 's and flux pinning
- For Ba = 2.0 to 1.8, a region of single-phase crystal structures will be defined and properties in that region characterized
- Chose a representative composition and create a PLD target
- Create REBCO thin films from this target and characterize the samples and compare with bulk properties

2c.1.3 Theory

- YBCO coated conductors have great promise for commercialization due to their high T_c and J_c , which allows them to function at LN₂ temperatures (77 K). However, J_c degrades in applied magnetic fields
- Flux pinning is one way to increase J_c with increasing field
- Solid-solution intersubstitution of varying RE elements and compositions provides the pinning sites necessary—Nd was chosen in this case
- There are several possible mechanisms to increase pinning:
 - 2nd phase defects by precipitation or composition changes
 - Formation of finely-distributed, lower- T_c components from mixed solubility of RE with each other and/or Ba
 - Randomly-distributed, oxygen-deficient zones which give lower T_c 's

2c.1.4 Experimental (Powder Processing)

- Starting powders: Nd₂O₃, Y₂O₃, BaCO₃, and CuO—all ≥99.95% pure
- Powders were dehydrated at 450°C prior to weighing
- Proper ratios weighed to give 30 g of target composition (Y_{0.6}Nd_{0.4}Ba₂Cu₃O_{7-δ})
- Powders are mixed and ground with mortar and pestle
- Calcined by slow heating from 650°C to 850°C at 25°C/hr
- Annealed in air with intermediate grinding at 880°C (1) and 900°C (2)
- Annealed in 1% O₂ (balanced Ar) at 860°C
- Densification anneal in air at 910°C
- Resulting Density of PLD Target → 5.81/6.3242=91.87%

2c.1.5 Experimental (PLD)

- CT75
- O₂ Pressure
 - 350 mTorr
- Target-Substrate Distance
 - 6 cm
- Substrate Temperature
 - 750°C
- Laser Energy
 - 650 mJ at 4 Hz
- *In-situ* O₂ post-anneal
 - 500°C for 30 mins
- CT78
- O₂ Pressure
 - 400 mTorr
- Target-Substrate Distance
 - 6 cm
- Substrate Temperature
 - 735°C

- Laser Energy
 - 650 mJ at 4 Hz
- *In-situ* O₂ post-anneal
 - 500°C for 30 mins

2c.1.6 Measurements*

- XRD was performed with a Rigaku diffractometer; 2θ-scan was done at 0.03° steps
- Magnetic measurements were taken with a Quantum Design MPMS/MPMS² SQUID
- Magnetic J_c was estimated using the extended Bean critical current method: $J_c = \frac{15 \cdot \Delta M}{R}$ where ΔM is magnetic hysteresis difference in emu/cm³ and R is the radius of superconducting volume—approximated as 5x10⁻⁵ cm for finely ground powders
- Superconducting transition for each sample was determined by finding the temperature at which $\frac{d^2\chi}{dT^2} \approx 0$ upon cooling from 100 K
- T_c were accomplished by AC susceptibility and FWHM and $\sim T$'s taken from the χ'' curve

* “Certain commercial equipment, instruments, or materials are identified in this paper in order to specify the experimental procedure adequately. Such identification is not intended to imply recommendation or endorsement by the Air Force Research Laboratory or the National Institute of Standards and Technology, nor is it intended to imply that the materials or equipment identified are necessarily the best available for the purpose.”

2c.1.7 Results

- Single-phase composition was obtained for all samples excepting Y=0.3 to 0.4 for Ba=2.0, in which secondary phases such as BaCuO_{2+x} remained unreacted
 - This includes the PLD target composition of
 - Y_{0.6}Nd_{0.4}Ba₂Cu₃O_{7-δ}
- All samples showed very little fish tail effect
- With decreasing Ba content (Ba<2.0), both T_c and J_c were reduced—this is consistent with previous findings.
- Samples created by PLD gave good results
 - Depressed T_c's but promising results
 - Transitions OK, FWHM are also reasonable, indicating decent J_c
 - CT75
 - T_c of 88.2K
 - FWHM → 0.025 Oe → .451°C; 2.2 Oe → 2.82°C
 - CT78
 - T_c of 87.5K (with component above 90K)
 - FWHM → 0.025 Oe → .506°C; 2.2 Oe → 2.19°C

2c.1.8 Transition temperature of the bulk superconducting volume fraction

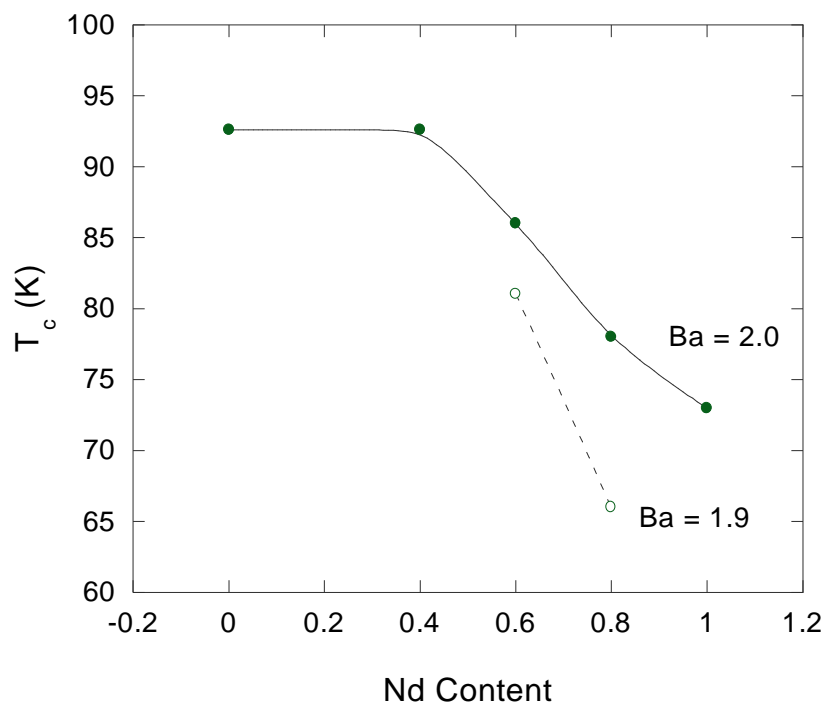


Figure 2c.1.8.1

2c.1.9 Maximum critical current density estimated from M-H loops

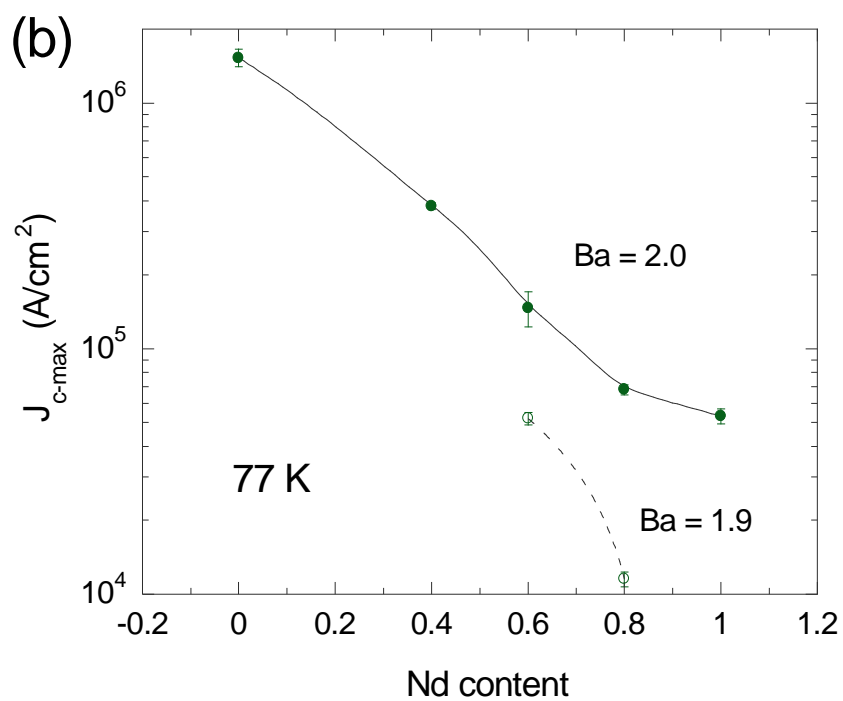


Figure 2c.1.9.1

2c.1.10 Normalized (J_c/J_{c-max}) for Ba = 2.0 and varying Nd content

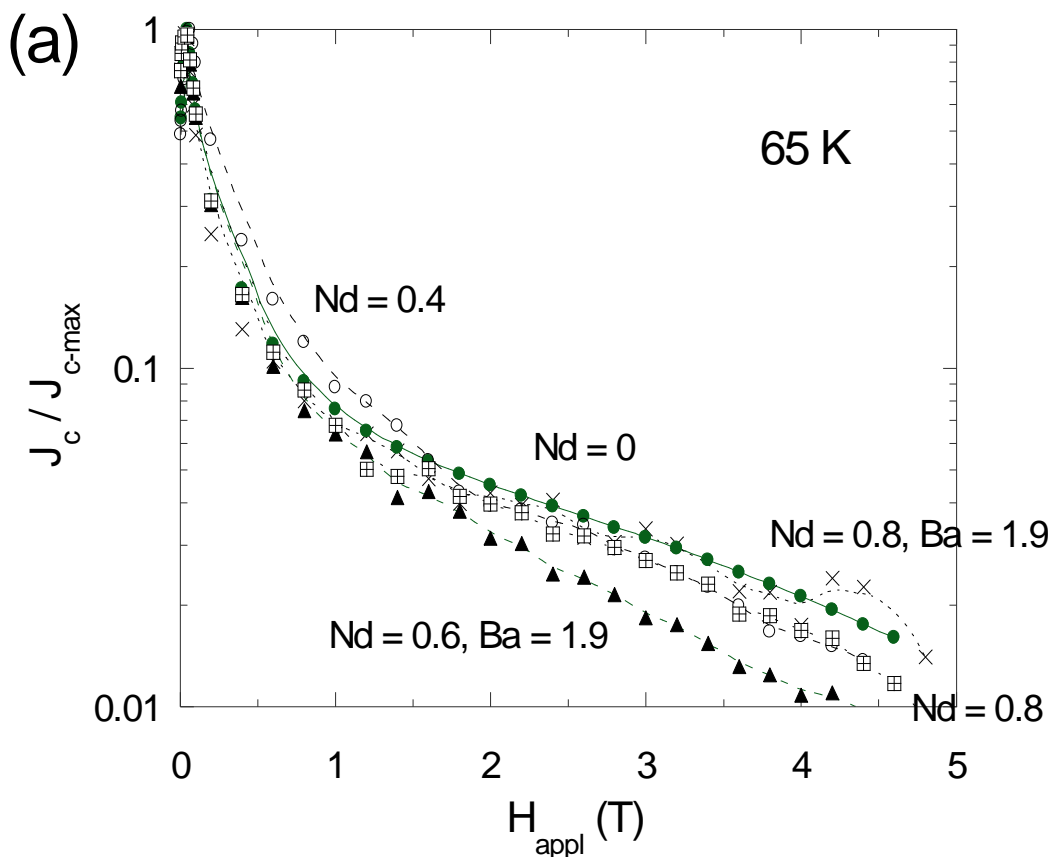


Figure 2c.1.10.1

2c.1.11 Conclusions

- $Y_{0.6}Nd_{0.4}Ba_2Cu_3O_{7-\delta}$ was created and used to create a PLD thin film. These films have not yet been fully characterized, but the initial findings indicated a good, epitaxial thin film
- T_c was depressed ($\sim 88K$), but some components can be seen above 90K. Further investigation of the actual components is necessary
- FWHM of the χ'' curves of each sample indicate a decent J_c , but the main concern of this study is J_c in-field. Results are forthcoming and we hope to report good flux pinning in PLD thin films by RE solid-solution intersubstitution

2c.2 Tb and Ce Doped $\text{YBa}_2\text{Cu}_3\text{O}_{7-x}$ Films Processed by Pulsed Laser Deposition

References: 18,24

J. W. Kell¹, T. J. Haugan¹, C. V. Varanasi², L. B. Brunke², M. F. Locke¹, J. M. Evans¹, J. P. Murphy², P. N. Barnes¹

1. Air Force Research Laboratory, Wright-Patterson AFB, OH 45433

2. University of Dayton Research Institute, Dayton, OH 45469

Presented at ASC 2004, Jacksonville, FL

2c.2.1 Objectives

- To determine if Tb and Ce can be substituted for Y in (Y,RE)-123 superconductors.
- Determine the effects of varying concentration of Tb and Ce in (Y,RE)-123 superconductors.
- Investigate how doping Y-123 with Tb-123 and Ce-123 affects the superconducting properties of thin films.

2c.2.2 Theory

- Rare earth doped $\text{YBa}_2\text{Cu}_3\text{O}_{7-x}$ (Y-123) may have beneficial flux pinning properties as compared to regular Y-123.
- Tb and Ce, which have normal valence states of +3 and +4, may substitute for Y in Y-123 superconductors.
- Tb and Y also have similar crystal ionic radii. The radius of Tb^{3+} is 1.04 Å and the radius of Y^{3+} of 1.02 Å.
- T_c 's of Tb doped Y-123 have been reported to be the same as undoped Y-123¹.
- Ce-123 however, does lower T_c in a dramatic way, but may serve as non-superconducting flux-pinning centers in Y-123 type superconductors².

1. C. R. Fincher, G. B. Blanchet, Physical Review Letters, v. 67, 2902, (1991).

2. S. Jin, T. H. Tiefel, G. W. Kammlott, R. A. Fastnacht, J. E. Graebner, Physica C, v. 173, 75 (1991).

2c.2.3 Experimental – PLD

- Targets of compositions $\text{Y}_{1-x}\text{Ce}_x\text{Ba}_2\text{Cu}_3\text{O}_{7-d}$ and $\text{Y}_{1-x}\text{Tb}_x\text{Ba}_2\text{Cu}_3\text{O}_{7-d}$ ($x = 0.1, 0.01$, and 0.001) were made using standard dry powder processing techniques
- Compositions were made using Tb_4O_7 , CeO_2 , Y_2O_3 , BaCO_3 , and CuO obtained from Alfa Aesar.
- All powders were dehydrated at 450°C and then weighed to an accuracy of $\pm 0.0005\text{g}$ before mixing. Powders were calcined by slow heating from 650°C to 850°C at 25°C/hr.
- Powders were then reground and annealed in air at 880°C.

- Powders were then pressed into a target and sintered to >80% theoretical density.
- X-ray diffraction of targets was performed to verify that all targets were of the RE123 phase. Pulsed Laser Deposition was performed using a Lambda Physik LPX 300 KrF excimer laser ($\lambda=248$ nm).
- Single crystal STO and LAO substrates were heated by contact heating using colloidal silver paste.
- Substrate temperature was measured using a pyrometer and a thermocouple mounted to the heating block. Oxygen deposition partial-pressures were maintained to 300 mTorr by downstream control.
- Scanning of the laser beam and rastering of the target was performed to provide for a more even target wear and deposition of material.
- Samples were oxygenated post deposition for 30 minutes at 500°C in 99.999% O₂ at a pressure of 1 Atm.
- T_c's were measured by DC Magnetization.
- Magnetic J_c's were measured using a Quantum Design VSM and applying a simplified Bean model with $J_c = 30 \Delta M / da^5$ where ΔM is in emu, film thickness d and lateral dimension a are in cm, and J_c is in A/cm².
- Dimensions of samples were measured on a KLA Tencor P-15 Profilometer and had a thickness of 220-280 nm and were all ~3.1 mm square.

2c.2.4 Magnetic J_c's of Tb doped Y-123 at 77K

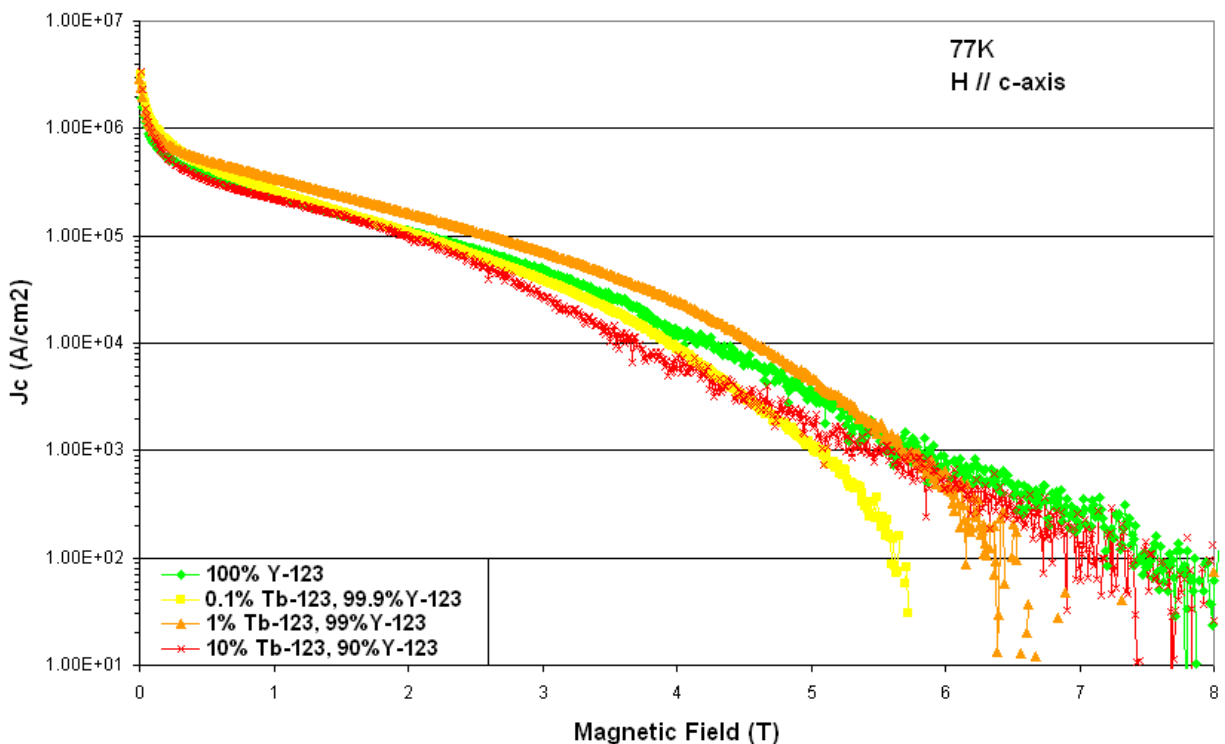


Figure 2c.2.4.1

Normalized Magnetic J_c's of Tb doped Y-123 at 77K

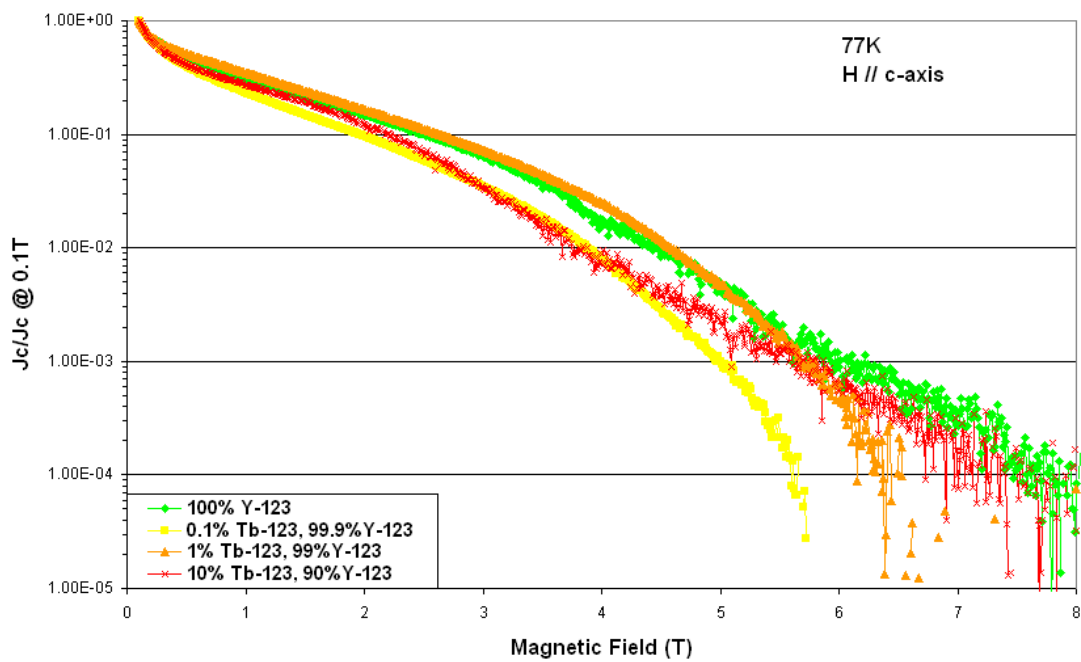


Figure 2c.2.4.2

2c.2.5 Magnetic J_c 's of Tb doped Y-123 at 65K

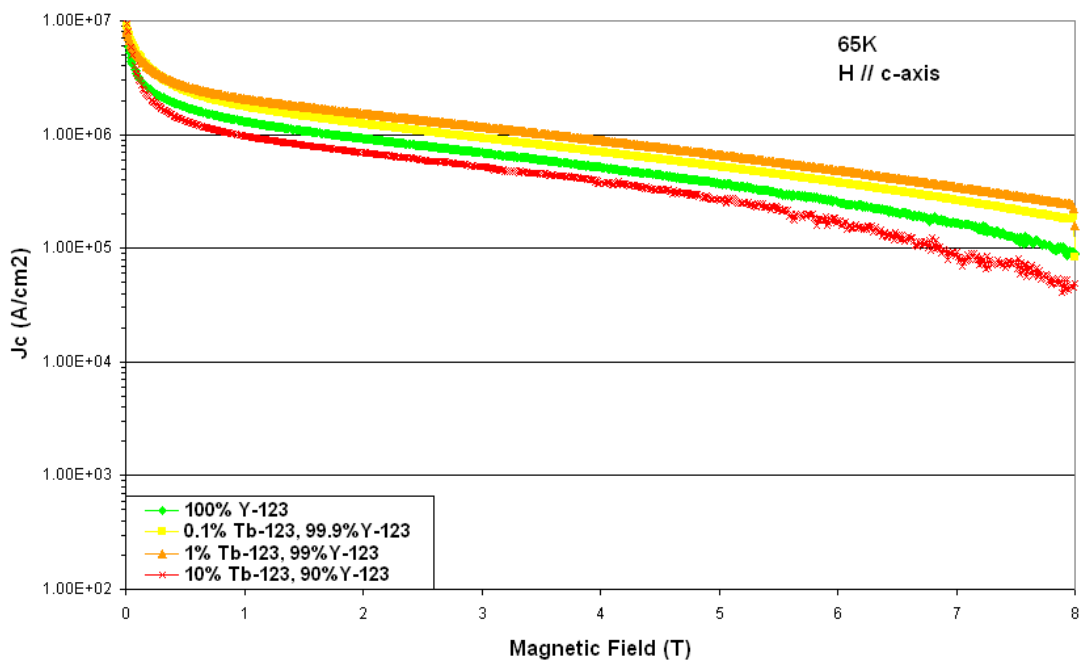


Figure 2c.2.5.1

Normalized Magnetic J_c 's of Tb doped Y-123 at 65K

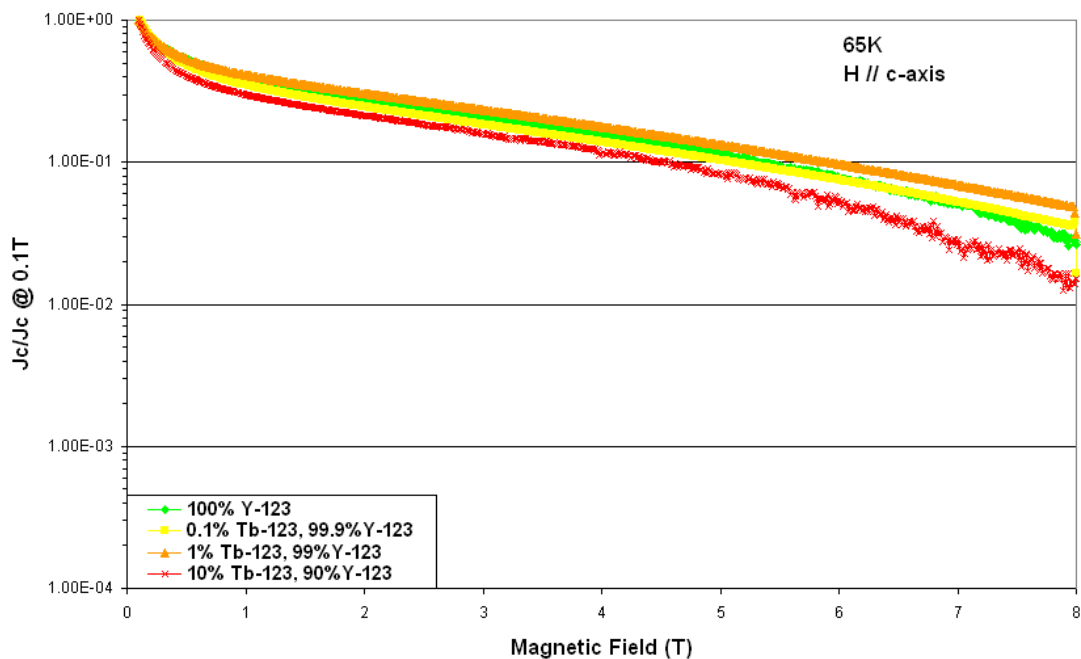


Figure 2c.2.5.2

2c.2.6 Summary of (Y,Tb)-123 Films

Film Composition	Y-123	(Y _{0.999} Tb _{0.001})-123	(Y _{0.99} Tb _{0.01})-123	(Y _{0.90} Tb _{0.10})-123
T _c (DC Magnetization)	89.2 K	88.0 K	89.0 K	89.5 K
J _c @ 77K and 0.01T Applied Field	2.23 MA/cm ²	3.13 MA/cm ²	2.68 MA/cm ²	2.123 MA/cm ²
J _c @ 65K and 0.01T Applied Field	5.87 MA/cm ²	9.01 MA/cm ²	8.29 MA/cm ²	9.54 MA/cm ²
J _c @ 77K and 2T Applied Field	0.140 MA/cm ²	0.107 MA/cm ²	0.162 MA/cm ²	0.0995 MA/cm ²
J _c @ 65K and 2T Applied Field	0.780 MA/cm ²	1.24 MA/cm ²	1.53 MA/cm ²	0.695 MA/cm ²

Figure 2c.2.6.1

2c.2.7 Magnetic J_c 's of Ce doped Y-123 at 77K

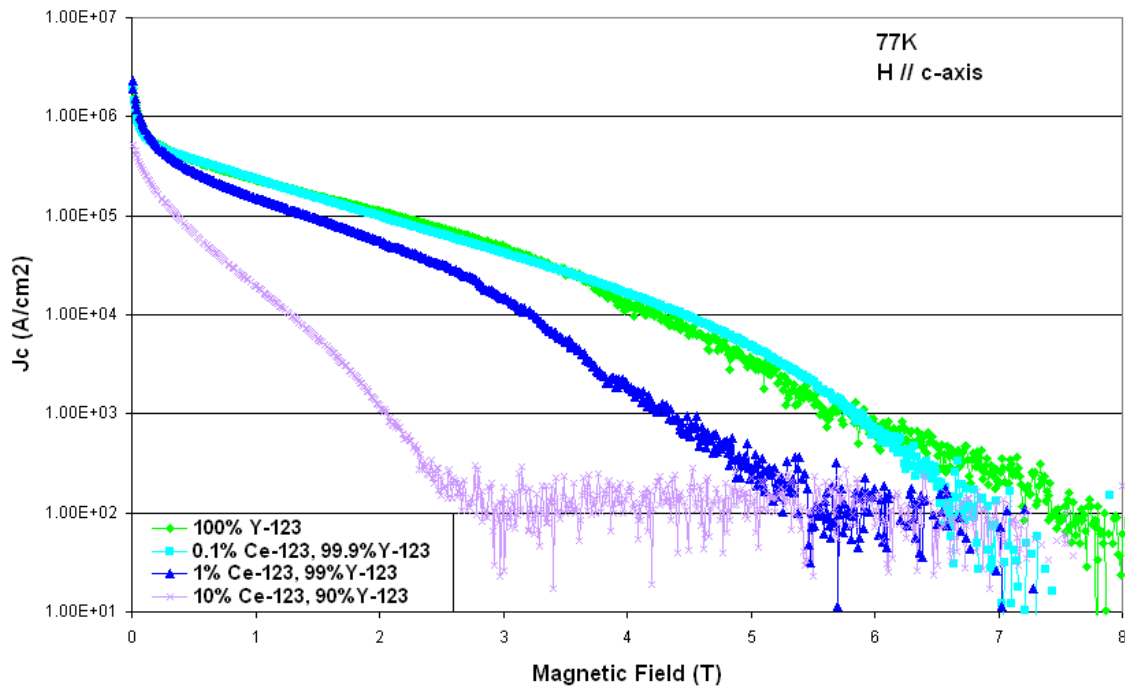


Figure 2c.2.7.1

Normalized Magnetic J_c 's of Ce doped Y-123 at 77K

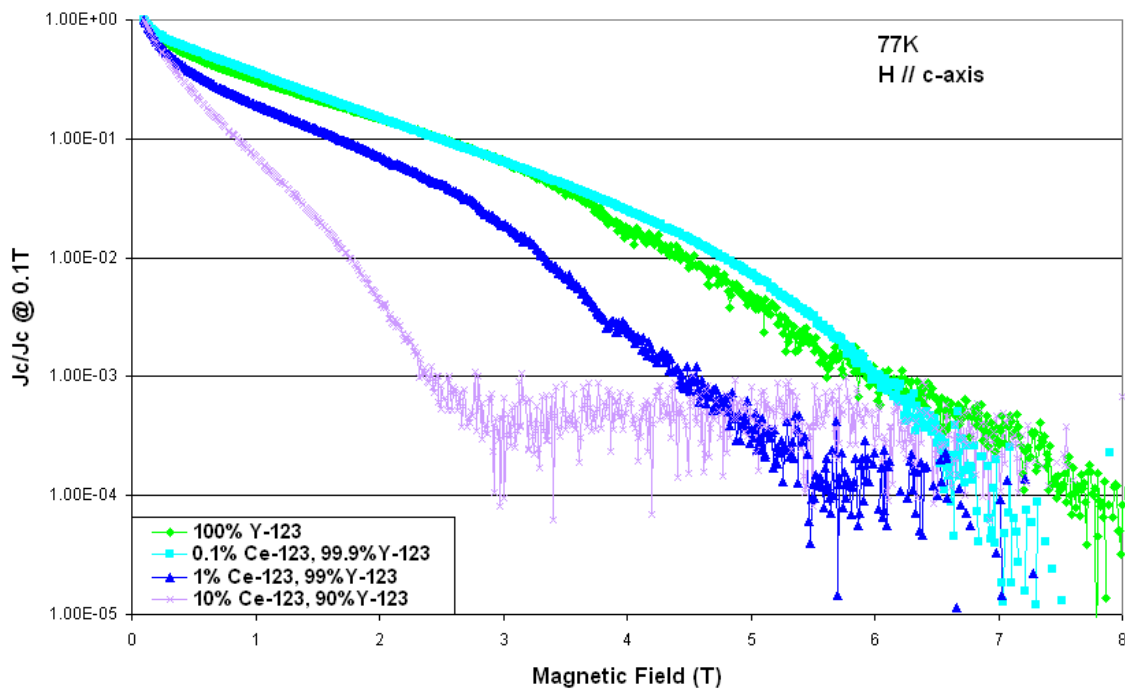


Figure 2c.2.7.2

2c.2.8 Magnetic J_c 's of Ce doped Y-123 at 65K

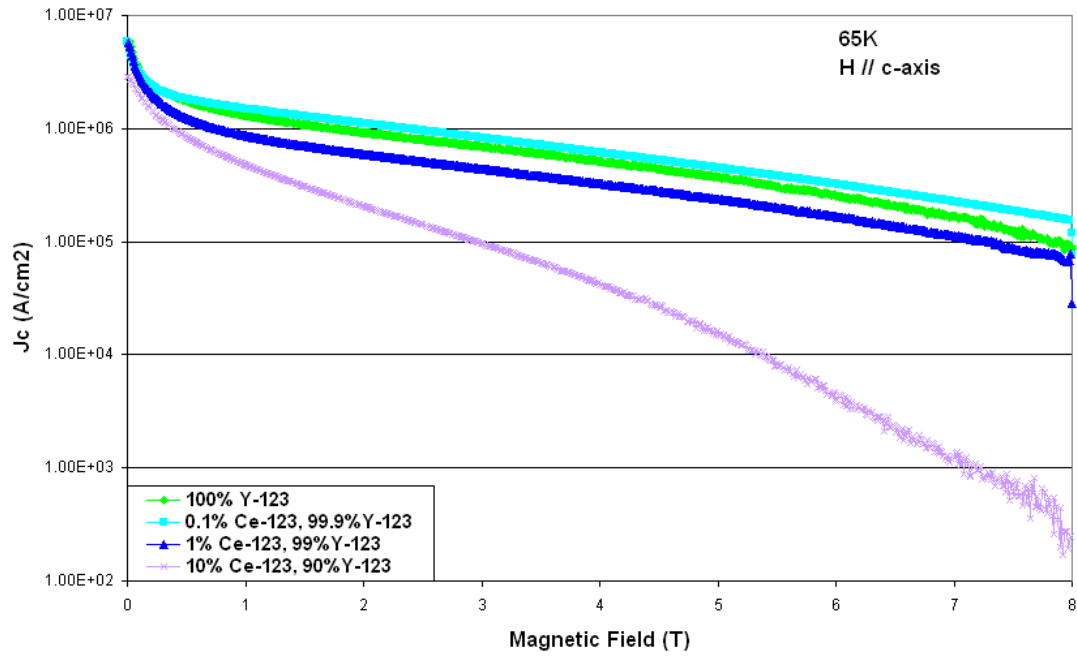


Figure 2c.2.8.1

Normalized Magnetic J_c 's of Ce doped Y-123 at 65K

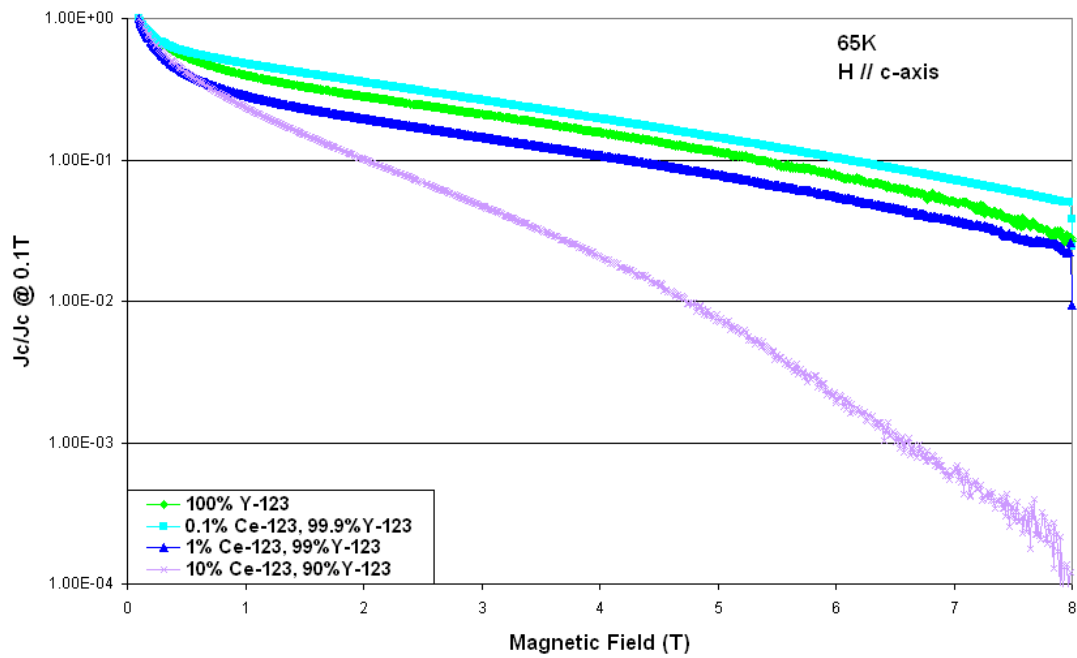


Figure 2c.2.8.2

2c.2.9 Summary of (Y,Ce)-123 Films

Film Composition	Y-123	(Y _{0.999} Ce _{0.001})-123	(Y _{0.99} Ce _{0.01})-123	(Y _{0.90} Ce _{0.10})-123
T _c (DC Magnetization)	89.2 K	88.9 K	88.5 K	84.8 K
J _c @ 77K and 0.01T Applied Field	2.23 MA/cm ²	1.65 MA/cm ²	2.10 MA/cm ²	0.523 MA/cm ²
J _c @ 65K and 0.01T Applied Field	5.87 MA/cm ²	5.66 MA/cm ²	5.44 MA/cm ²	2.86 MA/cm ²
J _c @ 77K and 2T Applied Field	0.140 MA/cm ²	0.0991 MA/cm ²	0.0555 MA/cm ²	0.00123 MA/cm ²
J _c @ 65K and 2T Applied Field	0.780 MA/cm ²	1.11 MA/cm ²	0.593 MA/cm ²	0.207 MA/cm ²

Figure 2c.2.9.1

2c.2.10 Conclusions

- Tb and Ce can be successfully substituted for Y in Y-123 superconducting thin films.
- Magnetic J_c's have been found to exceed 1 MA/cm² at 0.01T in Tb doped and in low percentage Ce doped Y-123
- At 77K, Y-123 composition of up to 10% Tb-123 can be produced that have similar properties to that of undoped Y-123.
- At 65K, Y-123 compositions of 0.1% and 1% Tb-123 exceed the J_c of undoped Y-123.
- At 77K, a Y-123 composition with 0.1% Ce-123 can be produced that has similar properties to that of undoped Y-123. However, even 1% Ce-123 can degrade film performance.
- At 65K, a Y-123 composition with 0.1% Ce-123 meets or exceeds the J_c of undoped Y-123.
- Overall, the addition of Tb-123 to Y-123, especially in small quantities, appears to improve the performance of the superconductor, especially when subjected to high fields at 65K.

2c.3 Nd doped $\text{YBa}_2\text{Cu}_3\text{O}_{7-x}$ Films Deposited by Pulsed Laser Ablation

References: 16

C. V. Varanasi¹, J.C. Tolliver,² T. J. Haugan,² K.W. Schmaeman,² S. Sathiraju,² L.B. Brunke¹, J.P. Murphy¹, I. Maartense,² Jack Burke,² Jason Carpenter,² and P. N. Barnes²

1. University of Dayton Research Institute, Dayton, OH 45469

2. Air Force Research Laboratory, Wright-Patterson AFB, OH 45433

Poster presented at ASC '04 Jacksonville, FL

2c.3.1 Introduction

Although YBCO coated conductors with high critical current density (J_c) ($\sim 10^6$ A/cm²) are being made, further enhancement in J_c is still desired for use in high magnetic field applications. These enhancements can be achieved by creating artificial flux pinning centers in YBCO films. These pinning centers can be

- A. nm sized non-superconducting particulates e.g. Y₂O₃ etc.
- B. chemical substitutions in YBCO crystal lattice e.g. Rare earth ion substitutions
- C. combination of both

Chemical Substitutions:

Chemical substitutions should help to create stress field induced pinning effects without adversely affecting the critical transitions temperatures (T_c). Partial rare earth ion substitutions for Y in YBCO films are of considerable interest from the point of view of pinning enhancements that are possible in these films.

In this study, pulsed laser ablation targets with different Nd substitutions for Y were made and Nd substituted films were grown in a standard procedure using oxygen during growth and the films were characterized to study the effects of Nd doping.

2c.3.2 Experimental

- All the targets used in this study were made in house using solid state sintering methods
- The following compositions targets were used
 - $\text{Nd}_{0.2}\text{Y}_{0.8}\text{Ba}_2\text{Cu}_3\text{O}_{7-x}$
 - $\text{Nd}_{0.4}\text{Y}_{0.6}\text{Ba}_2\text{Cu}_3\text{O}_{7-x}$
- $\text{NdBa}_2\text{Cu}_3\text{O}_{7-x}$
 - Pulsed Laser Deposition:
 - 248 nm KrF pulsed laser, 4 Hz, 4.2 J/cm²
 - 730°-750° C deposition temperature
 - 300 mTorr of oxygen pressure during growth
 - 20 min deposition on LaAlO₃ substrates
- Films were characterized by
 - Ac susceptibility

- X-ray photoelectron spectroscopy
- Raman spectroscopy
- Scanning electron microscopy
- X-ray diffraction
- Transport current measurements
- Magnetization measurements using a VSM

2c.3.3 AC susceptibility of $\text{Nd}_{0.2}\text{Y}_{0.8}\text{Ba}_2\text{Cu}_3\text{O}_{7-x}$ films

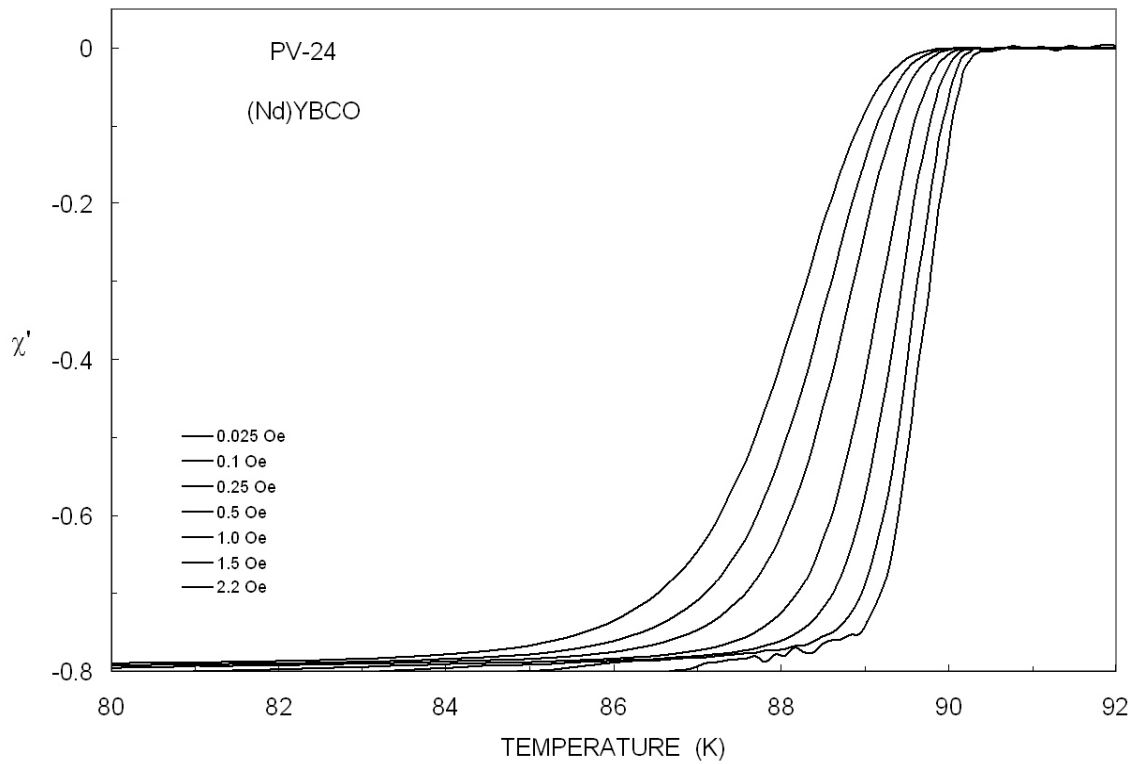


Figure 2c.3.3.1

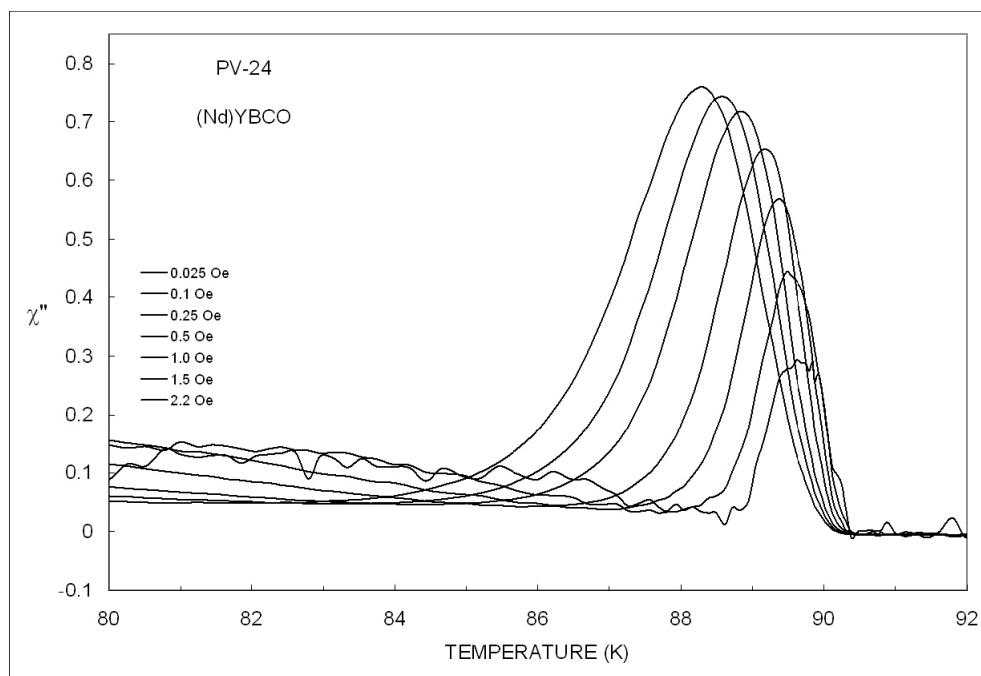


Figure 2c.3.3.2

2c.3.4 T_c comparison between different composition films (AC susceptibility curves)

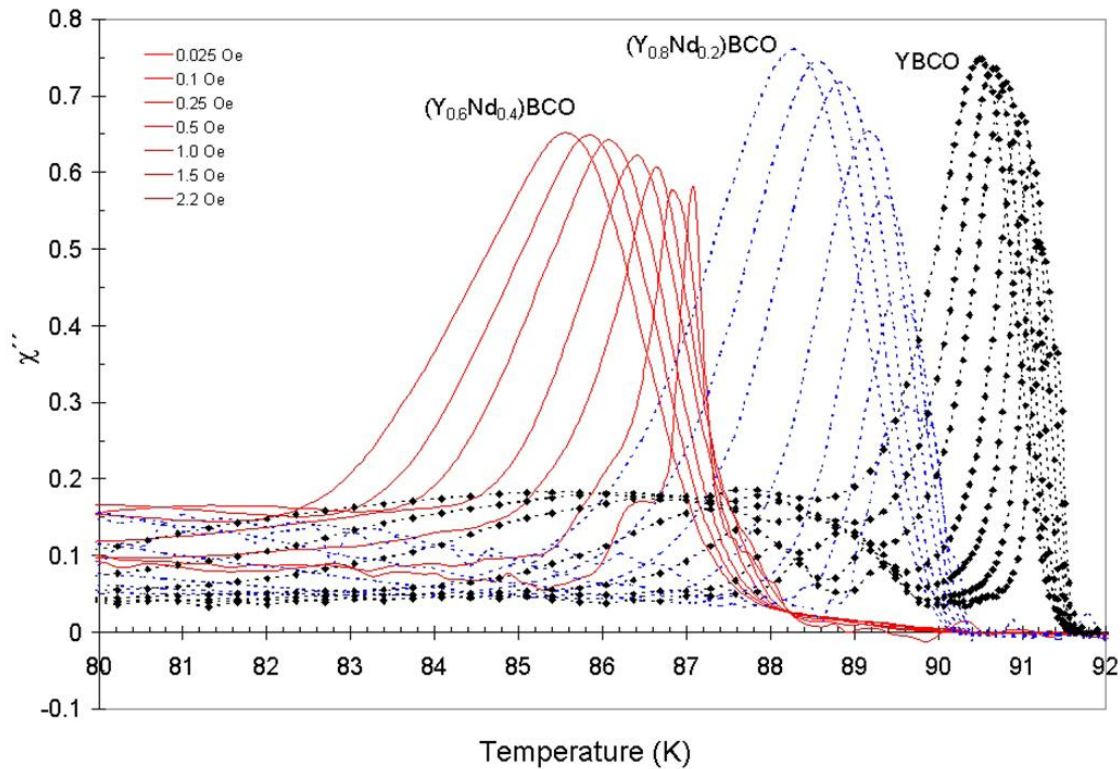


Figure 2c.3.4.1

2c.3.5 XPS data summary on films grown using $\text{Nd}_{0.6}\text{Y}_{0.4}\text{Ba}_2\text{Cu}_3\text{O}_{7-x}$ target

This table shows the relative atomic percentage of Y, Nd, Ba, Cu, and O present in the films as compared to a standard YBCO film. It can be seen that Nd content in the films is nearly same as that in the target.

	Sample 1	Sample 2
Y	58.26%	60.43%
Nd	41.74%	39.57%
Ba	99.15%	100.05%
Cu	95.21%	93.42%
O	97.46%	95.94%

Figure 2c.3.5.1

2c.3.6 Raman Spectra

Raman spectra from $\text{Nd}_{0.4}\text{Y}_{0.6}\text{Ba}_2\text{Cu}_3\text{O}_{7-x}$ film compared to the target

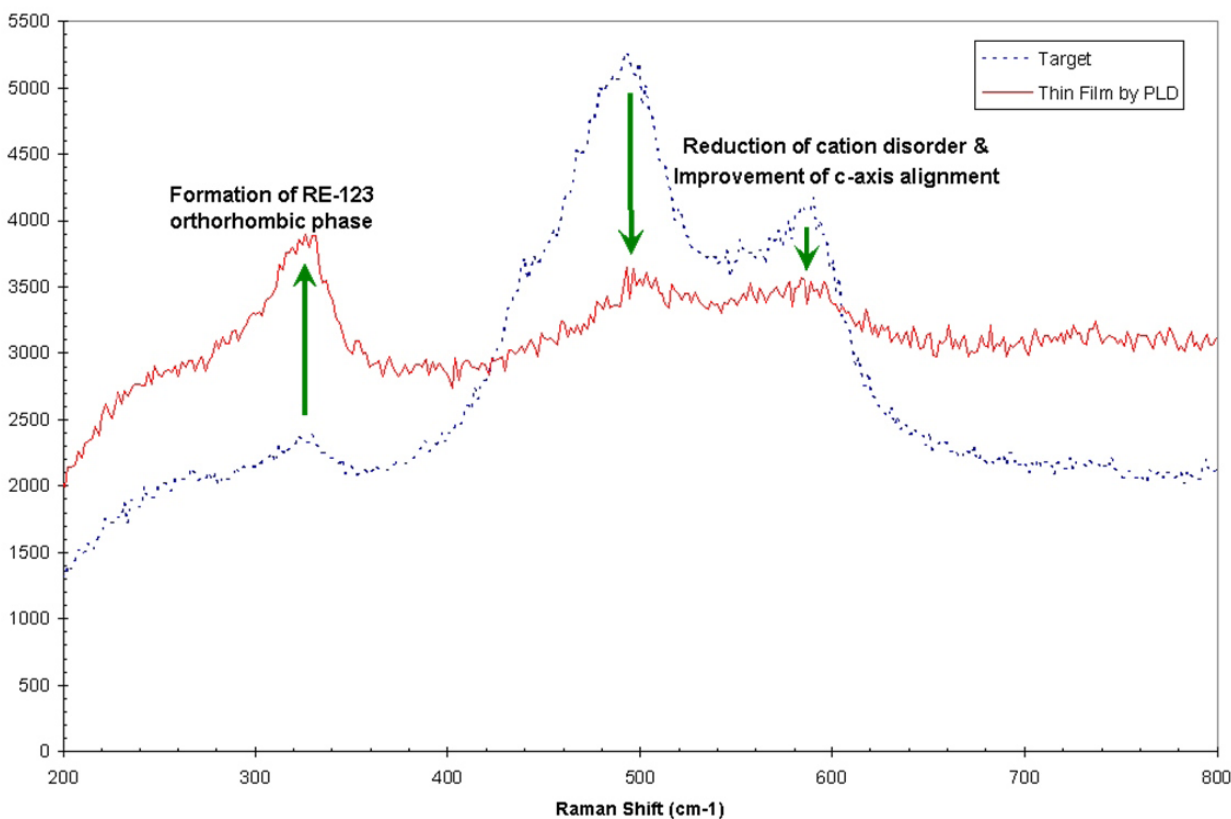


Figure 2c.3.6.1

Raman spectra taken from two different composition samples. NdCBO films show poor c-axis alignment (peaks around 500 cm^{-1}) and low T_c compared to $\text{Nd}_{0.2}\text{Y}_{0.8}\text{Ba}_2\text{Cu}_3\text{O}_{7-x}$.

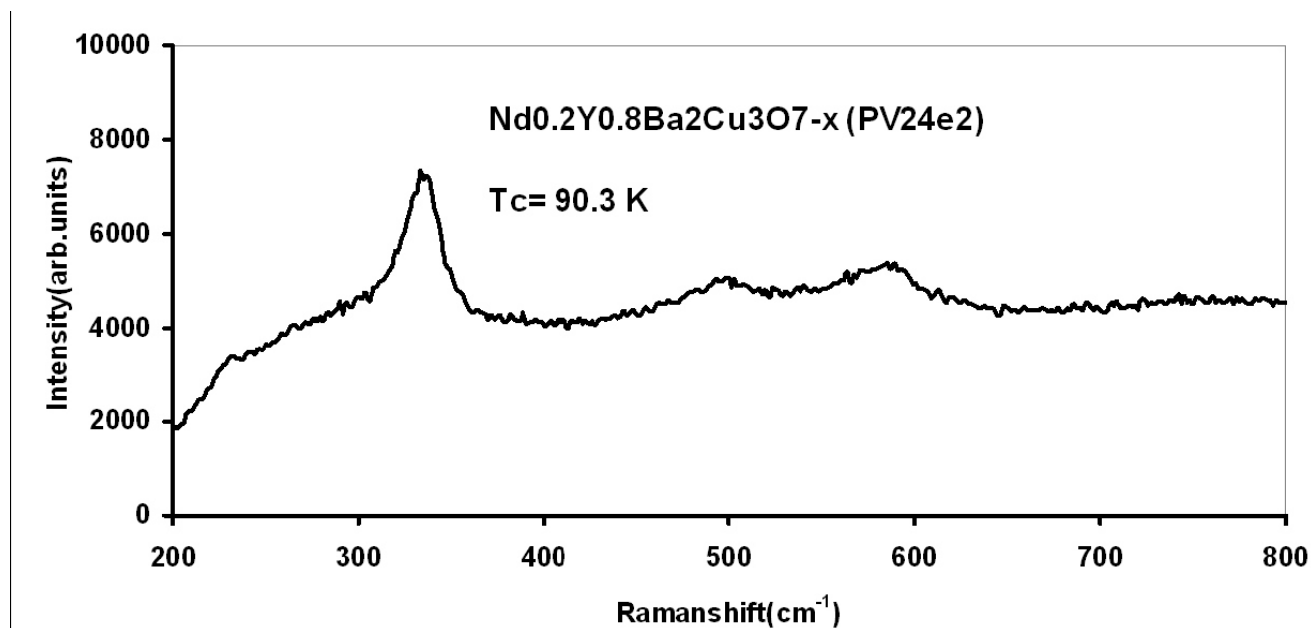


Figure 2c.3.6.2

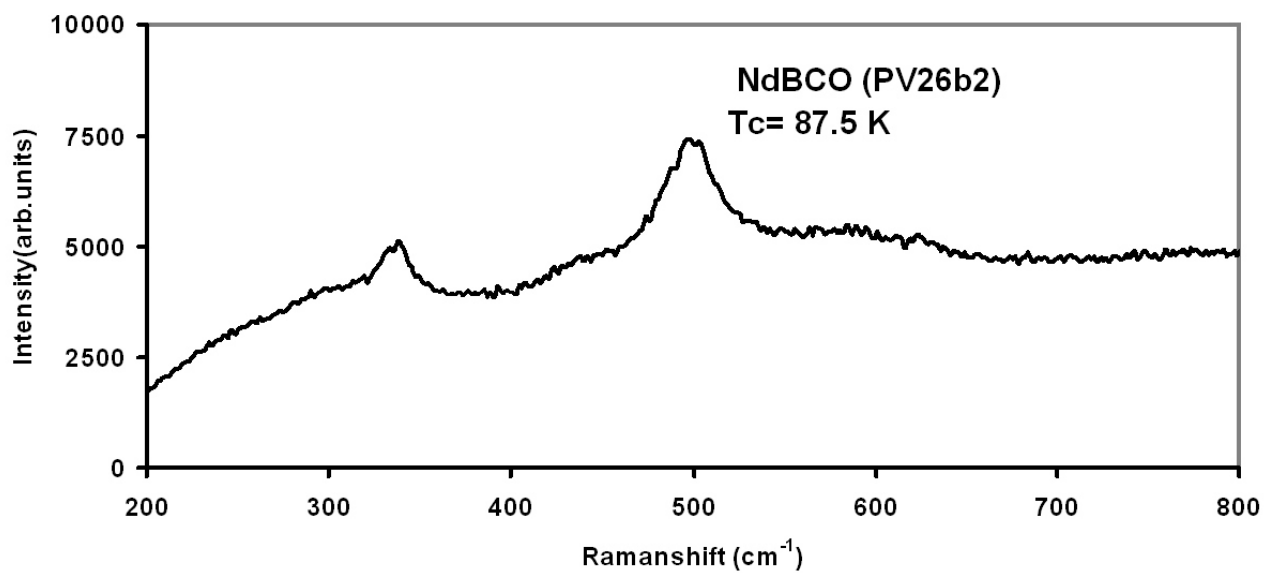


Figure 2c.3.6.3

Raman spectra from Nd_{0.4}Y_{0.6}Ba₂Cu₃O_{7-x} films with different T_c. In the poor T_c film there is evidence of poor c-axis alignment and cation disorder.

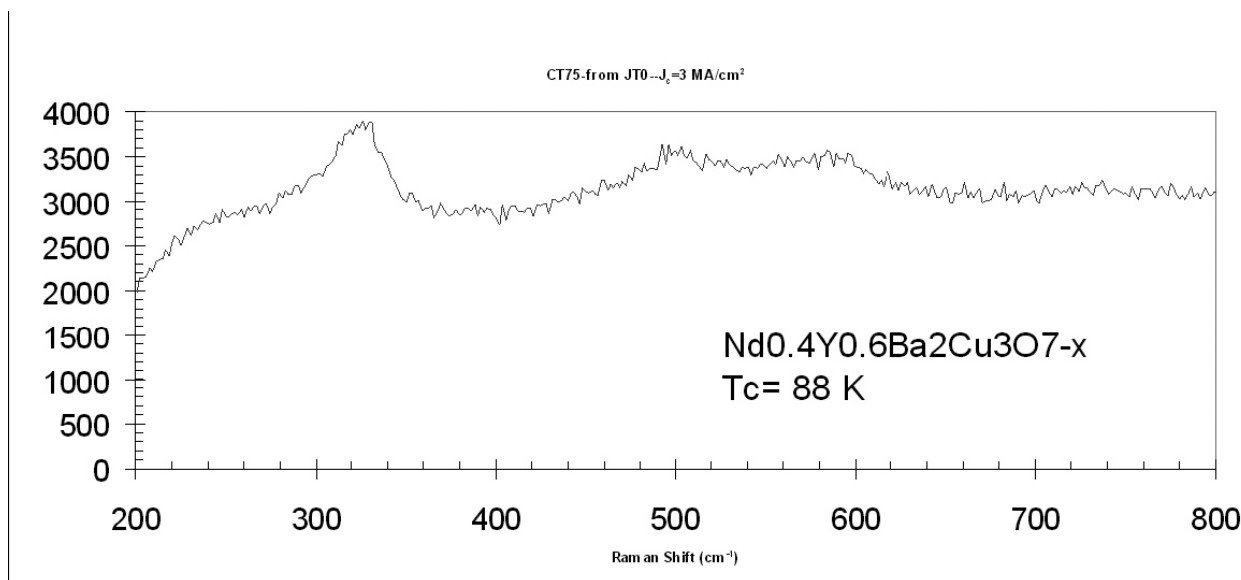


Figure 2c.3.6.4

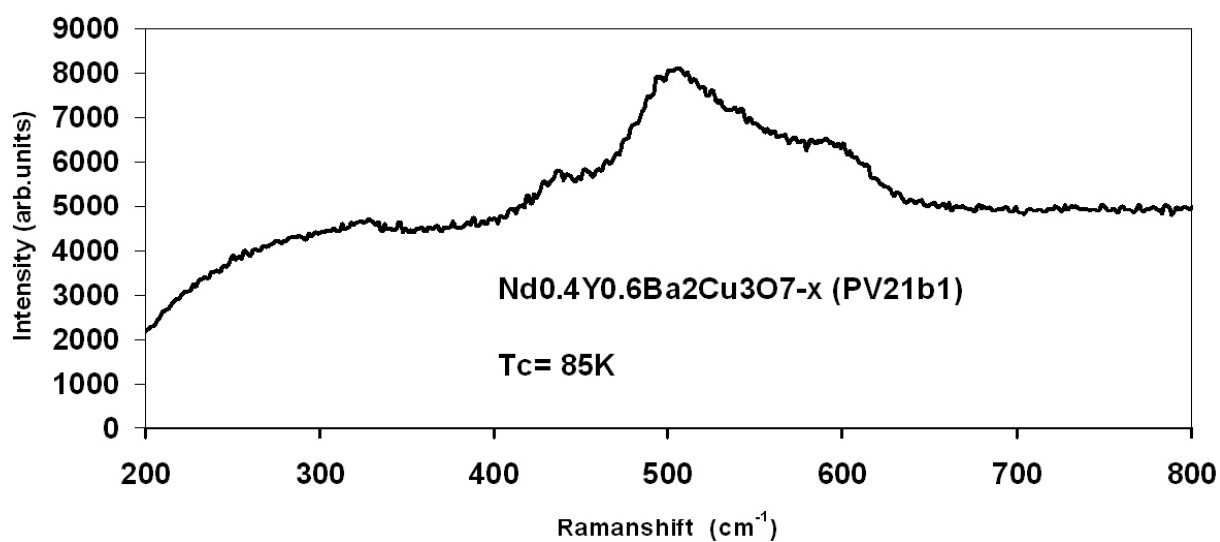


Figure 2c.3.6.5

2c.3.7 Scanning electron micrograph of a Nd_{0.4}Y_{0.6}Ba₂Cu₃O_{7-x} film on LAO substrate

Dense microstructure is observed with very small grain size (0.5 micron).

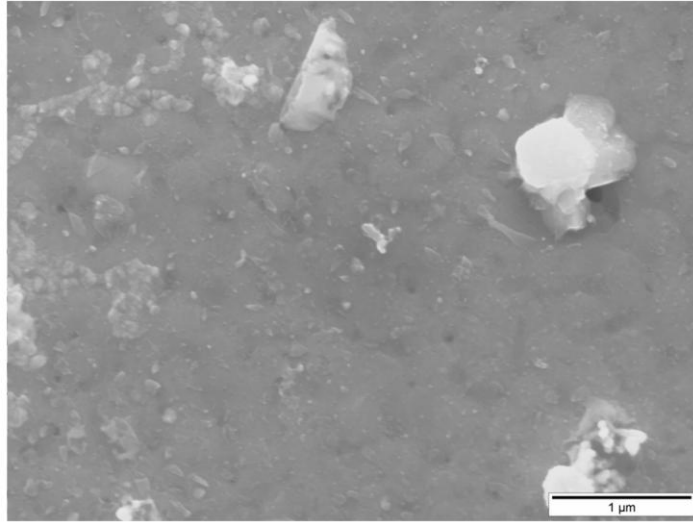


Figure 2c.3.7.1

2c.3.8 X-ray diffraction data on a Nd doped YBCO film

X-ray diffraction data shows the peak shift indicating the Nd substitution is possible in the lattice.

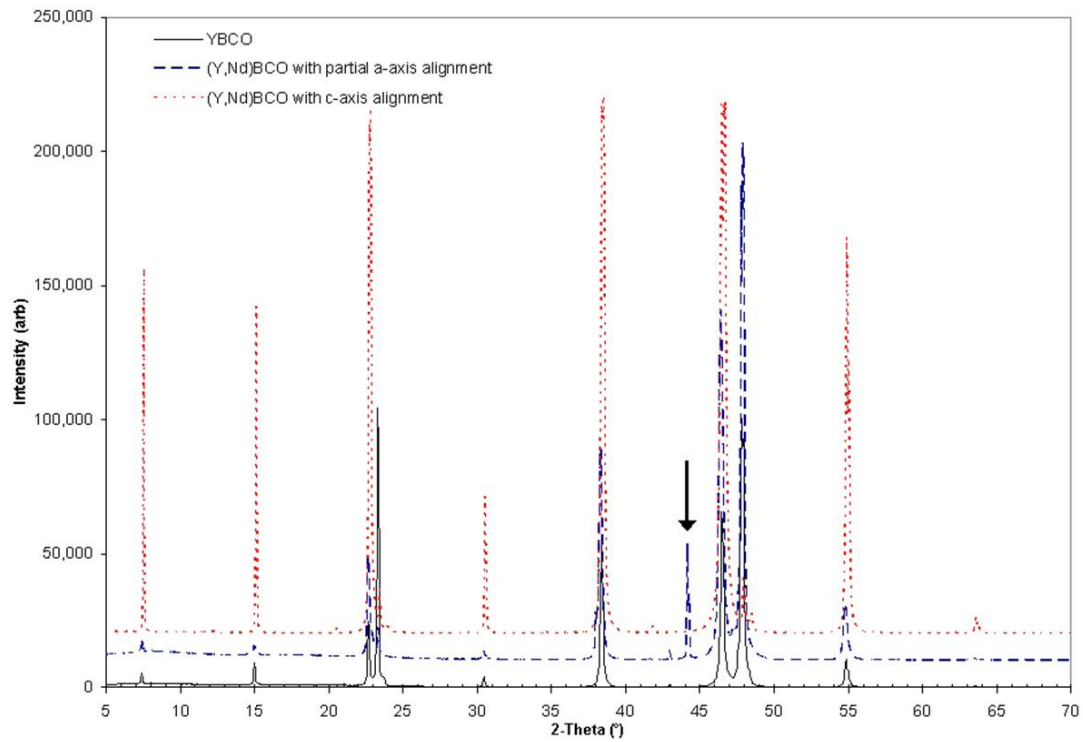


Figure 2c.3.8.1

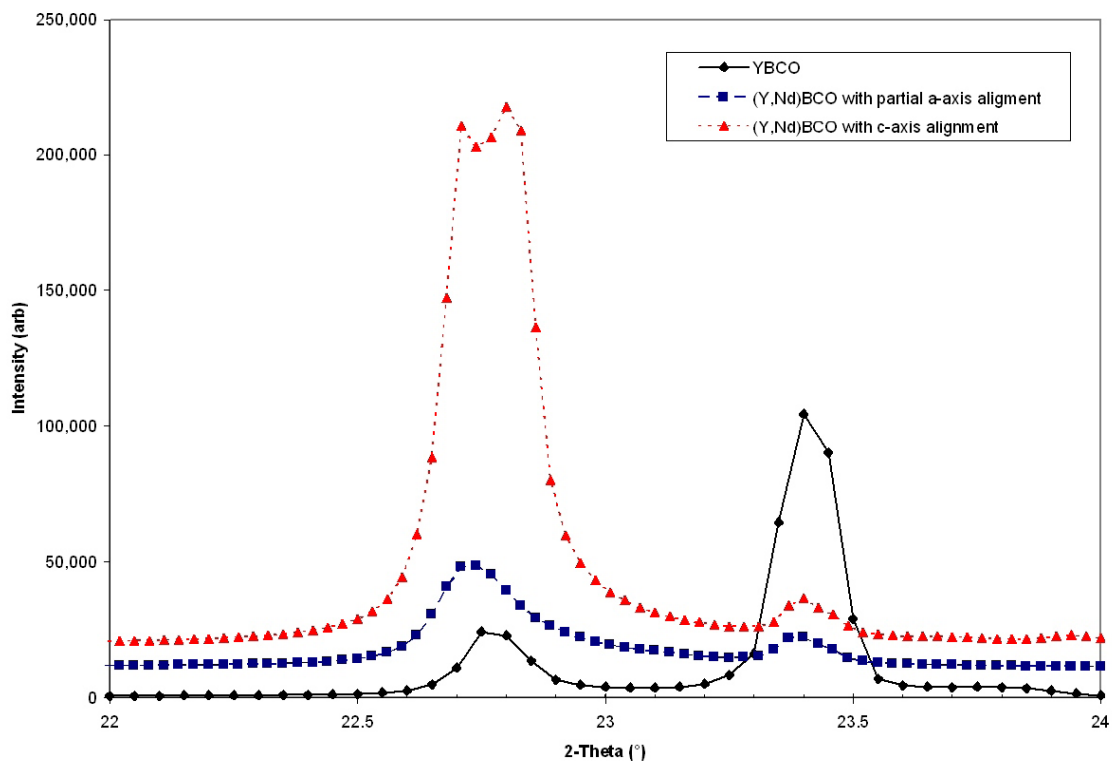


Figure 2c.3.8.2

2c.3.9 Transport current measurement on $\text{Nd}_{0.4}\text{Y}_{0.6}\text{Ba}_2\text{Cu}_3\text{O}_{7-x}$ film

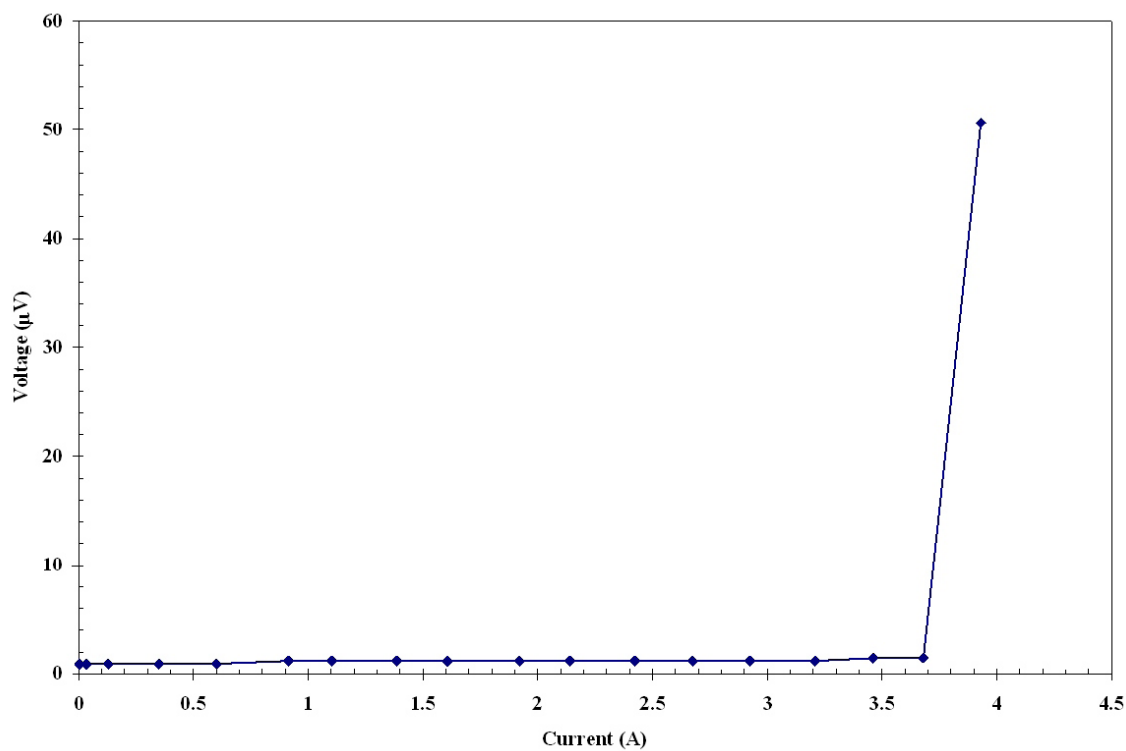


Figure 2c.3.9.1

2c.3.10 Magnetization J_c data of an $\text{Nd}_{0.2}\text{Y}_{0.8}\text{Ba}_2\text{Cu}_3\text{O}_{7-x}$ film at different temperatures

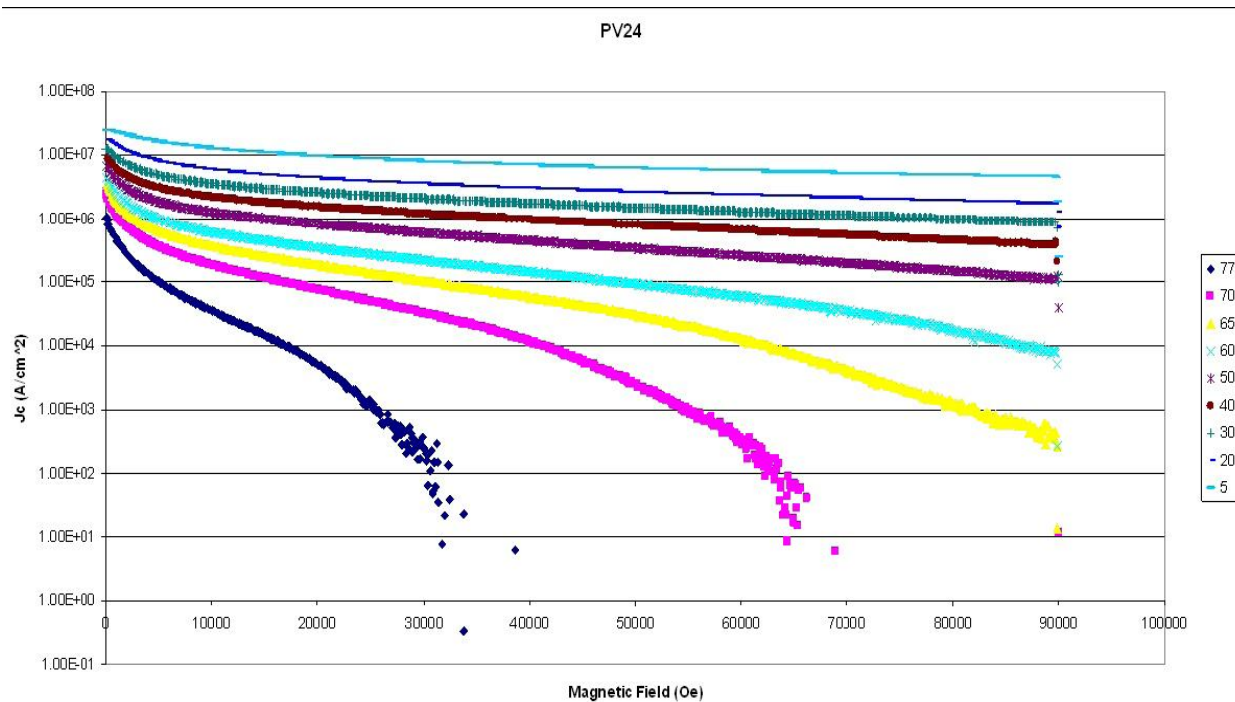


Figure 2c.3.10.1

2c.3.11 Conclusions

- Nd doped YBCO films at different doping levels were processed by PLD using appropriately doped targets
- Composition of the films were found to match the composition of the target very well as determined by XPS
- Nd substitutions into YBCO lattice appear to take place from the observation of the peak shifts in X-ray diffraction
- Nd doped films showed decrease in T_c as Nd content is increased when processed in oxygen. Process optimization may be required for each composition to improve the T_c further.
- Raman studies indicated poor c-axis alignment and cation disorder may be responsible for reduced T_c observed in some films
- Transport current density $3 \times 10^6 \text{ A/cm}^2$ was measure in $\text{Nd}_{0.4}\text{Y}_{0.6}\text{Ba}_2\text{Cu}_3\text{O}_{7-x}$ films grown in optimized conditions

2c.4 Flux Pinning of YBCO with Rare Earth Substitutions

References: 14, 16, 20, 21, 22, 23

Paul N. Barnes, Timothy J. Haugan, Julianna M. Evans, Justin C. Tolliver, and Iman Maartense,¹
Timothy L. Peterson and Srinivas Sathiraju²

Presented by Paul N. Barnes at AFOSR Review, January 2004

2c.4.1 Rare Earth Substitution $(Y,RE)_{1+x}Ba_{2-x}Cu_3O_{7-d}$

- Control physical properties (e.g. T_c , J_c , & flux pinning) by using rare earth solid solution substitution for Y in $YBa_2Cu_3O_{7-d}$ (YBCO)
- Mechanisms by which such substitutions increase flux pinning:
 - 2nd-phase defects by precipitation or composition changes
 - finely distributed lower T_c components (e.g mixed solubility of RE with Ba, intersolubility of RE, etc.)
 - randomly distributed oxygen-deficient zones with lower T_{cs}
- Why study composition changes in $(Y,RE)BCO$?
 - Powder compositions may have different properties than melt-processed or crystals due to non-equilibrium processes
 - eliminate formation of 2nd-phase defects such as RE211 which provide pinning other than the intrinsic properties
- Powders annealed in 1% O_2 atmosphere to sharpen & increase T_c
 - Annealing may decrease flux pinning by reducing the formation of lower T_c solid-solutions

2c.4.2 Experimental

- Powders prepared by solid-state reaction using RE_2O_3 , Y_2O_3 , $BaCO_3$, and CuO ($\geq 99.95\%$ purity).
 - dehydrated at $450^\circ C$ and weighed to ± 0.0001 g
 - mixed and ground with mortar and pestle, calcined by slow heating $\sim 600^\circ C$ to $\sim 850^\circ C$ at $\sim 25^\circ C/h$
 - annealed in air at $850 - 910^\circ C$ with intermediate grinding until phase equilibrium reached (3-4 annealings) by XRD
 - reacted in ~ 1 cm diameter pellets (0.5 g to 1 g batches), formed by lightly pressing ($5-10 \times 10^6$ Pa) in molds.
- After single-phase obtained, annealed in 1% O_2 (balance Ar); anneal temperature based on the melting point of the RE123
 - samples rechecked with XRD for single phase composition
 - A final anneal in 100% O_2 at $460^\circ C$ to $\sim 260^\circ C$, decreasing as RE content increased from 0 to 1.0 for optimized annealing
- Magnetic J_c estimated by extended Bean I_c model, $J_c = 15(\Delta M)/R$, where ΔM is the volume magnetization and R is the radius of the superconducting volume ($\sim 0.5 \mu m$ for finely reacted powders)



2c.4.3 J_c vs. H_{appl} – Air Anneal Only

- Max J_c vs. applied magnetic field of powders annealed in air
 - estimated from M-H loops for varying Nd content

- J_{cS} decreased with increasing Nd and decreasing Ba content

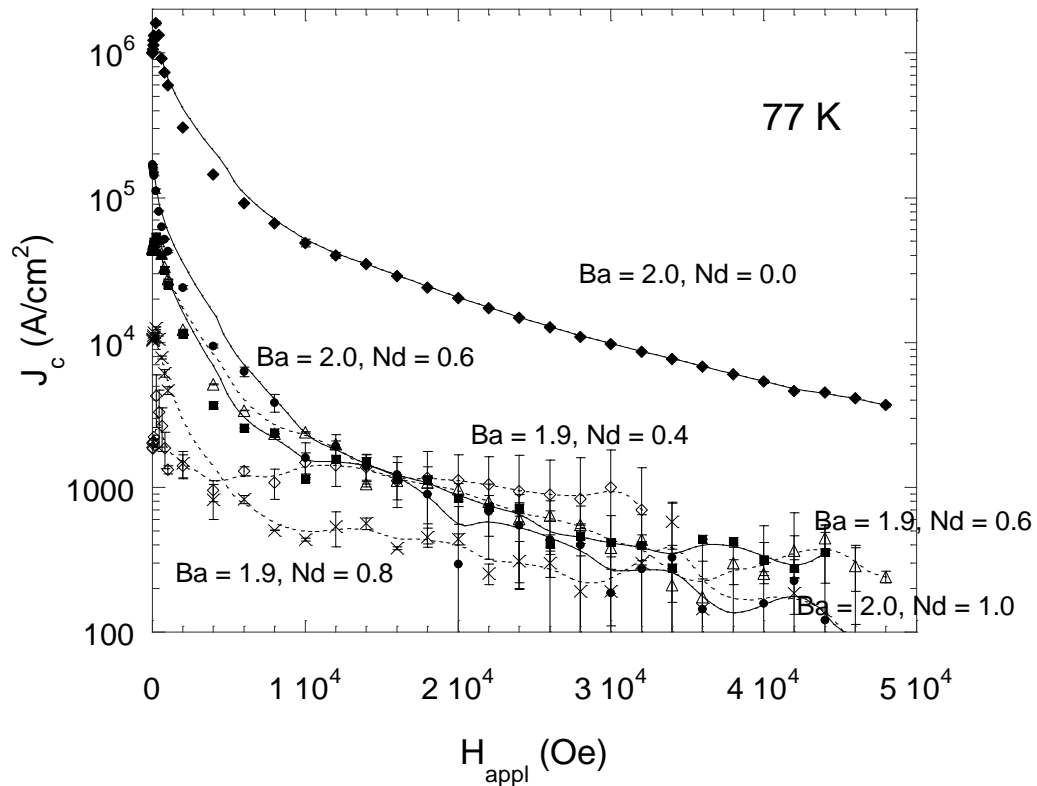


Figure 2.12.3.1

Ba = 1.9 (dashed lines)

Ba = 2.0 (solid lines)

Figure 2c.4.3

2c.4.4 J_c Norm. vs. H_{appl} – Air Anneal Only

- Normalized J_c as a function of H_{appl} for air annealed powders
 - maximum J_c (J_{c-max}) was measured for $H_{appl} \sim (0.06-0.1) T$
- Intrinsic differences in the pinning can be observed below

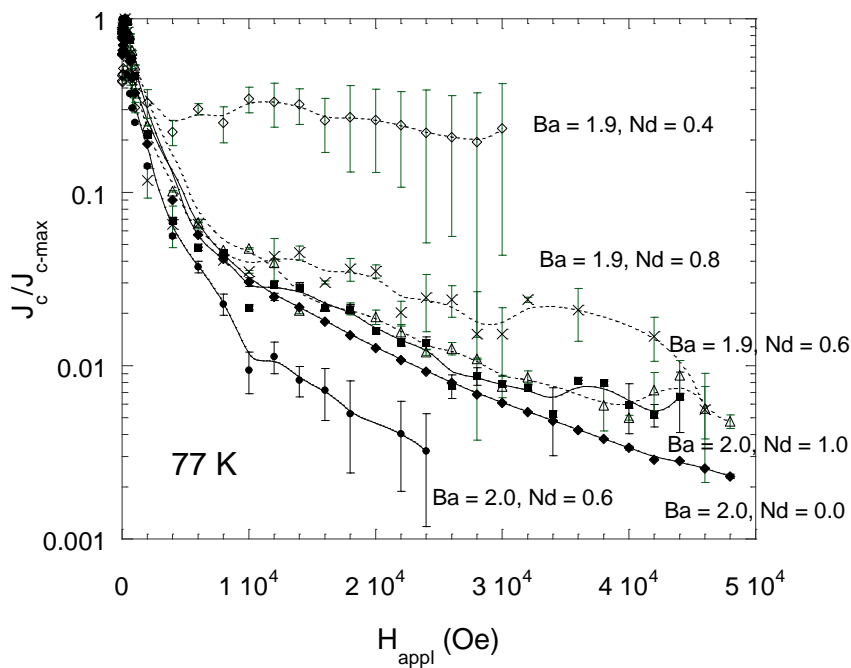


Figure 2c.4.4.1

2c.4.6 J_c vs. H_{appl} – 1% O₂ Anneal

- J_c as a function of H_{appl} for powders annealed with 1% O₂
 - J_c increased an order of magnitude for all compositions
 - J_{cs} of Ba=1.9 comp. almost equal to Y123 (Ba 2.0, Nd = 0)

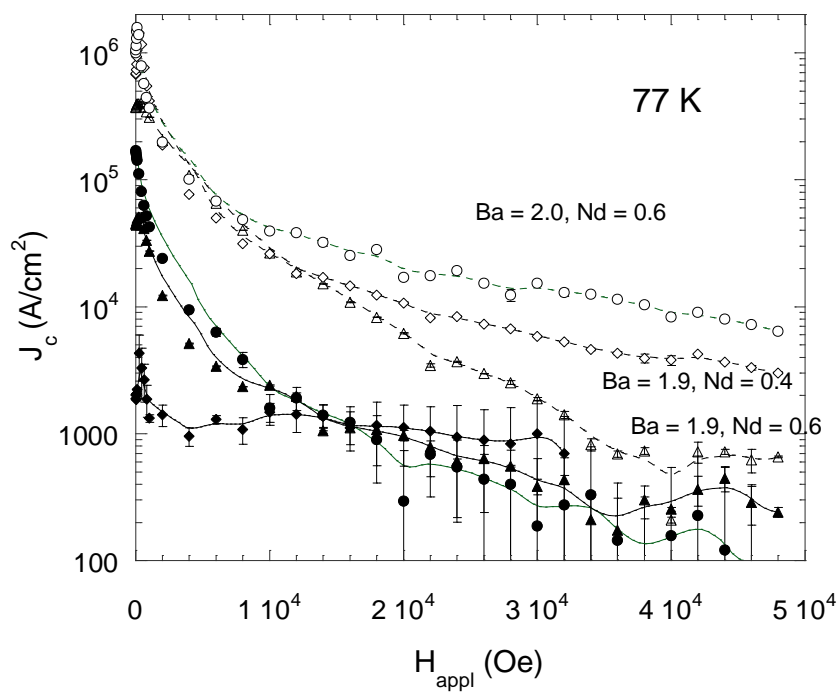


Figure 2c.4.6.1

1% O₂ anneal (open symbols)

Air only (closed symbols).

2c.4.7 J_c Norm. vs. H_{appl} – 1% O_2 Anneal

- Normalized J_c as a function of H_{appl} for 1% O_2 anneal
 - maximum J_c ($J_{c-\text{max}}$) was measured for $H_{\text{appl}} \sim (0.06-0.1)$ T
- (Ba = 1.9, Nd = 0.4) had best intrinsic pinning in both air only and 1% O_2 anneal

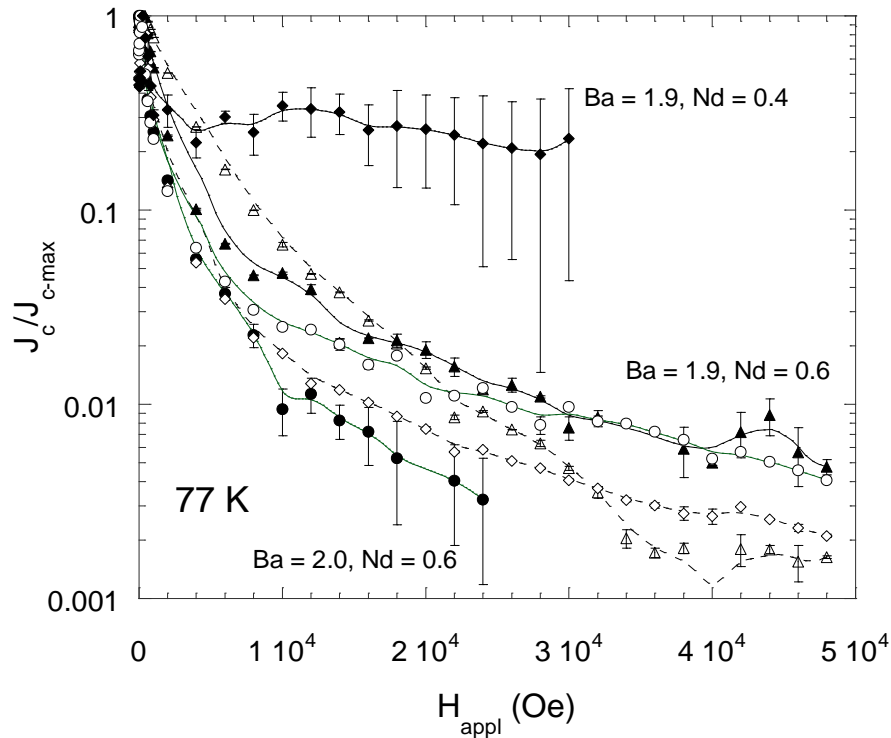


Figure 2c.4.7.1

2c.4.8 Primary Objective

- Chose a representative composition and create a PLD target
 - Deposit (Y,REmix)BCO thin films
 - Characterize the samples and compare with bulk properties

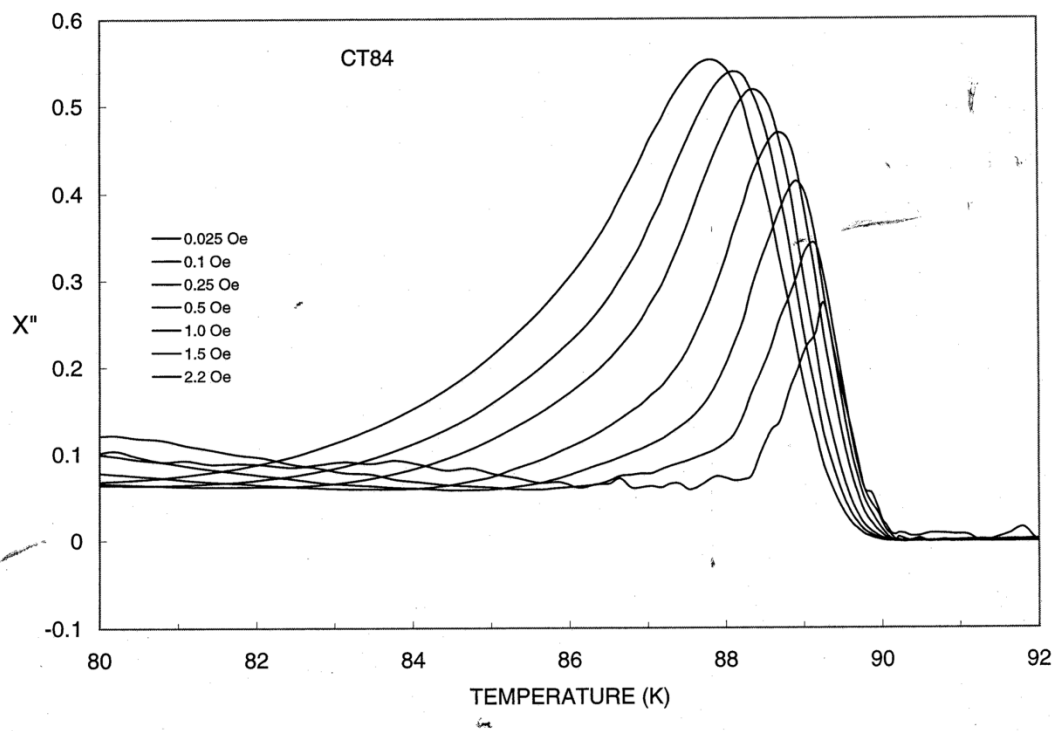


Figure 2c.4.8.1
 $(Y_{0.5}RE_{0.5+x})Ba_{2-x}Cu_3O_{7-\delta}$, RE = Eu, Sm, Ho, Er

2c.4.9 XRD of $(Y_{0.5},RE_{0.5})Ba_2Cu_3O_{7-d}$

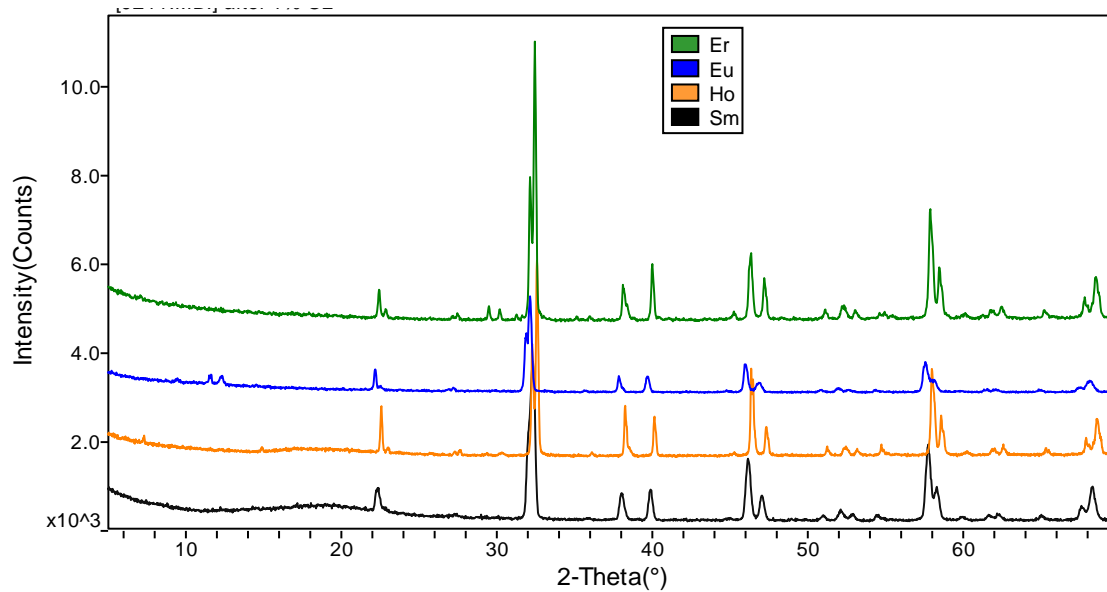


Figure 2c.4.9.1

2c.4.10 XRD of $(Y_{0.5},RE_{0.6})Ba_{1.9}Cu_3O_{7-d}$

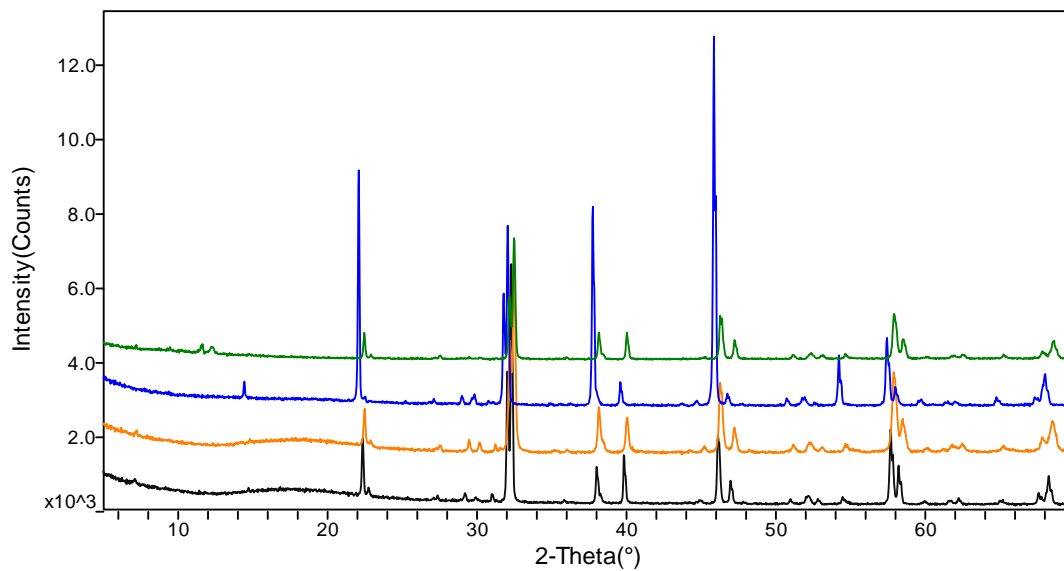


Figure 2c.4.10.1

2c.4.11 J_c/J_{c-max} , 65K, $(Y_{0.5},RE_{0.5})Ba_2Cu_3O_{7-d}$

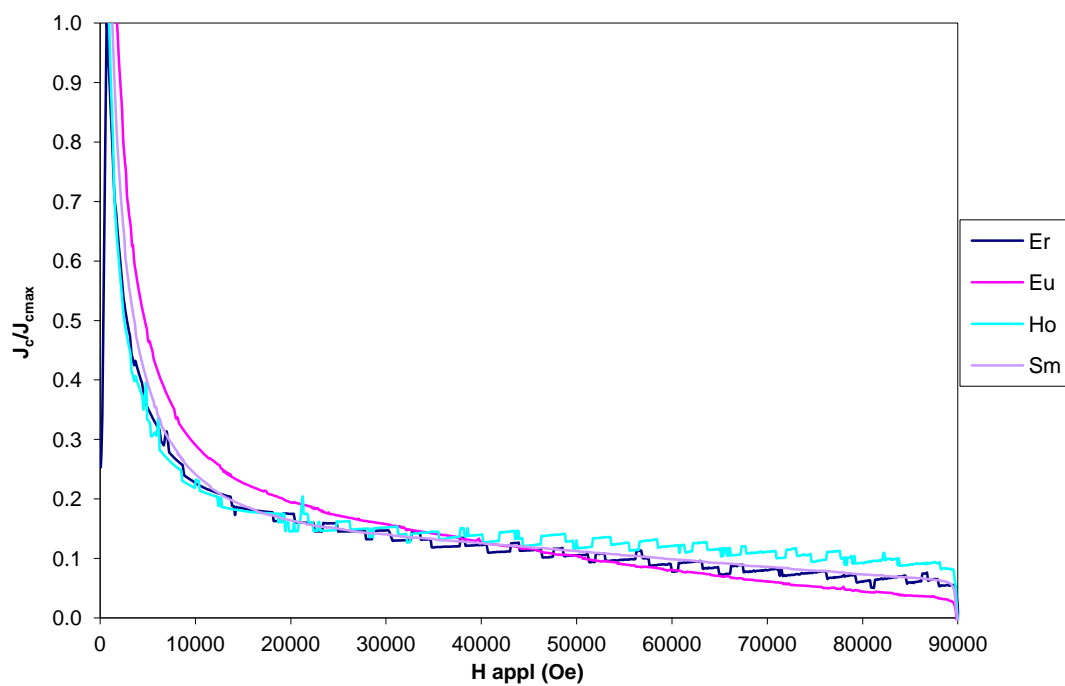


Figure 2c.4.11.1

2c.4.12 J_c/J_{c-max} , 65K, $(Y_{0.5},RE_{0.6})Ba_{1.9}Cu_3O_{7-d}$

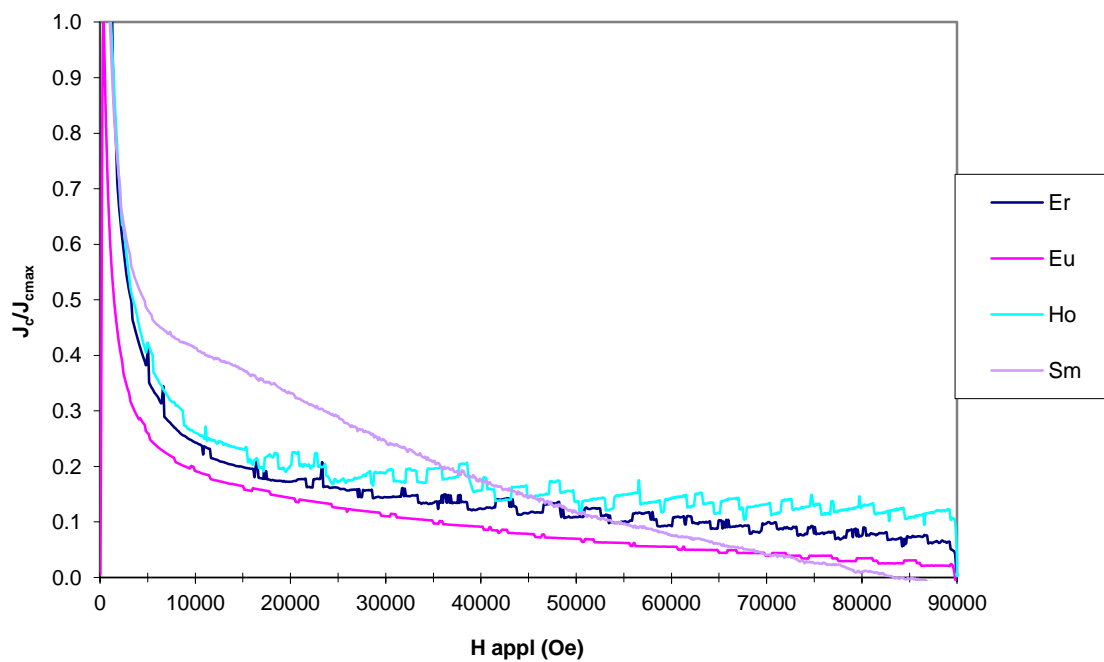


Figure 2c.4.12.1

2c.4.13 J_c vs. Ionic Radius

	Ionic Rad. (Å)
Y	1.019
Er	1.004
Ho	1.015
Eu	1.066
Sm	1.079

◇	Ba=2.0
□	Ba=1.9
■	65 K
■	70 K
■	77 K

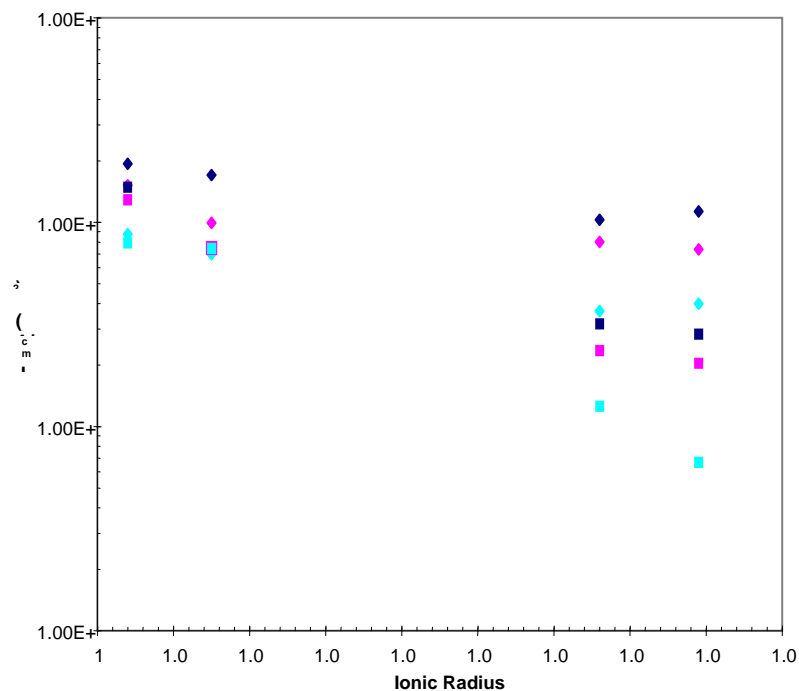


Figure 2c.4.13.1

Correlation to Magnetic Susceptibility Data

2c.4.14 Measurement Technique

- Desired for high temperature superconducting (HTS) films
 - A sharp transition in the resistivity vs. temperature curve at T_c
 - T_c close to the maximum value for the given HTS film
- Previously noted that the quality (J_c) of HTS film is lower as the temperature-dependent ac susceptibility curves spread
- A detailed study performed using available data of group
 - $\text{YBa}_2\text{Cu}_3\text{O}_{7-d}$ (YBCO) films
 - $\text{YBa}_2\text{Cu}_3\text{O}_{7-d}/\text{Y}_2\text{BaCuO}_5$ (Y123/Y211) composite films
- The superconducting transition temperature (T_c onset) was measured using ac susceptibility technique
 - The amplitude of the magnetic sensing field, h , varied from 0.025 Oe to 2.2 Oe at a frequency of approximately 4 kHz
- Samples were measured as the sample temperature increased through the transition region at very slow rate (~ 0.06 K/min)

2c.4.15 AC Susceptibility Data - χ'

- χ' is the imaginary or loss component of ac susceptibility data

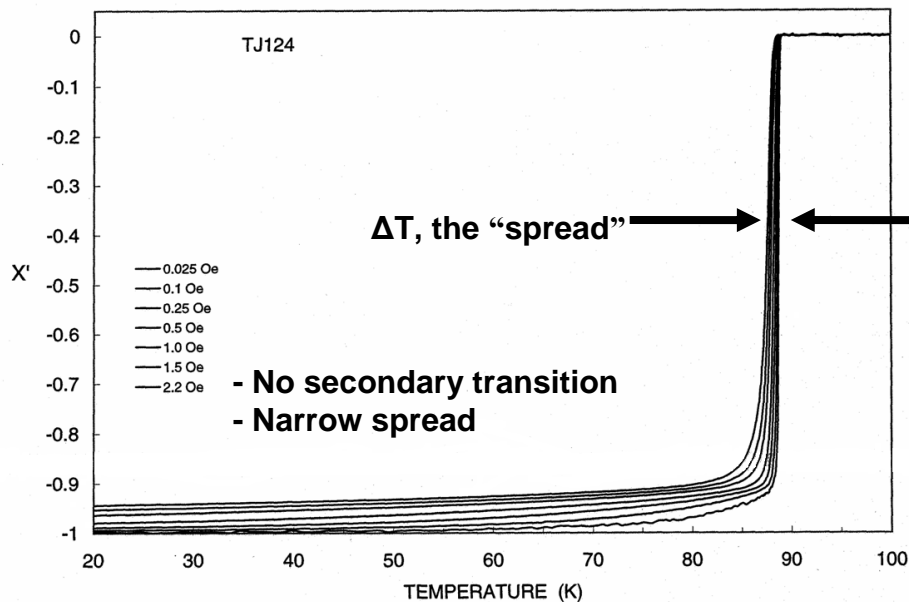


Figure 2c.4.15.1

2c.4.16 AC Susceptibility Data - χ''

- χ'' provides a better means to precisely determine the "spread"

- ΔT , or spread, defined as the difference between T_{\max} in the ac loss for the 0.025 & 2.2 Oe applied fields (peak to peak of χ'')
- FWHM of χ'' vs. T (ΔT) of the loss component also determined
 - 0.025 Oe and 2.2 Oe magnetic field data

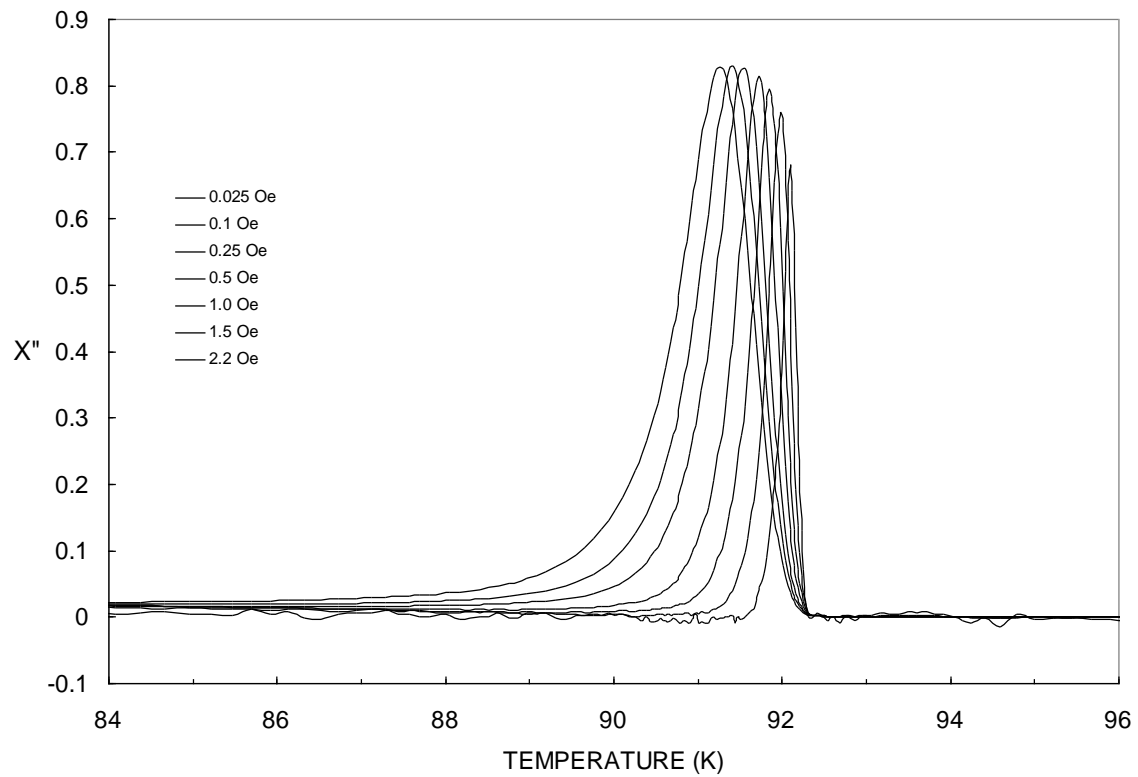


Figure 2c.4.16.1

2c.4.17 ΔT of AC Susceptibility Data

$\Delta T \equiv$ “spread” or peak to peak of 0.025 Oe

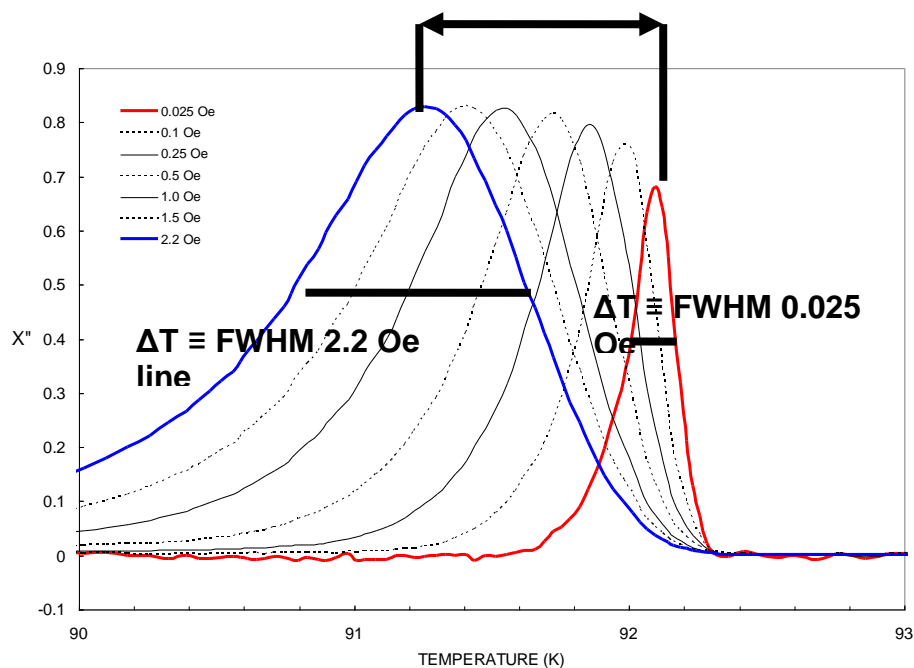


Figure 2c.4.17.1

2c.4.18 Critical Transition Temperature

- Measured onset T_c s of the PLD samples were generally
 - 90-92 K for the YBCO samples
 - 88-90 K for the Y123/Y211 composite films
- Thicknesses of the samples ranged from 0.2 – 1.0 microns

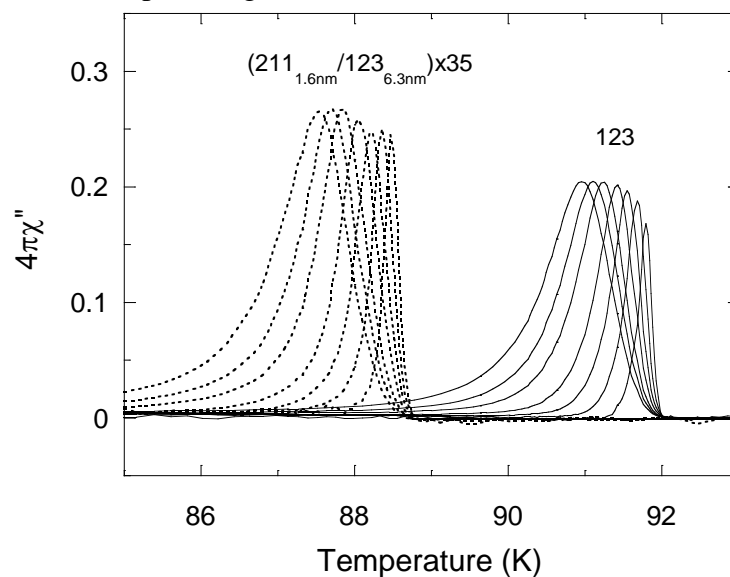


Figure 2c.4.18.1

2c.4.19 χ'' Peak to Peak Comparison

- J_c vs ΔT (peak to peak of χ'')
 - Better correlation than J_c vs ΔT (FWHM of the χ'' vs. T for the 2.2 Oe magnetic field line data)

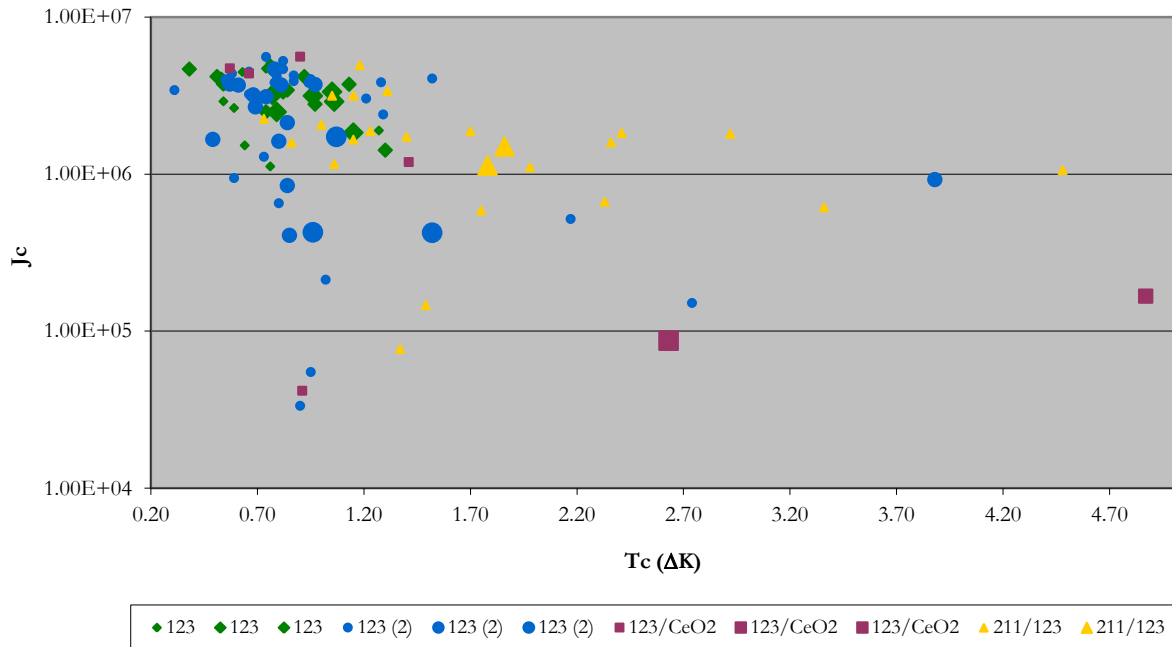


Figure 2c.4.19.1

2c.4.20 Results

- The temperature spread between the ac loss data for different magnetic fields increases as the J_c of the films decreases
 - The scatter of the data initially indicates that this is a general rule of thumb
 - Temperature spread slightly better than temperature FWHM at 2.2 Oe
- Of interest is that there are two “tails” in the figures
 - the data slowly degrades in J_c as the ΔT broadens
 - The data rapidly drops in J_c as the ΔT slightly increases

2c.4.21 χ'' Peak to Peak

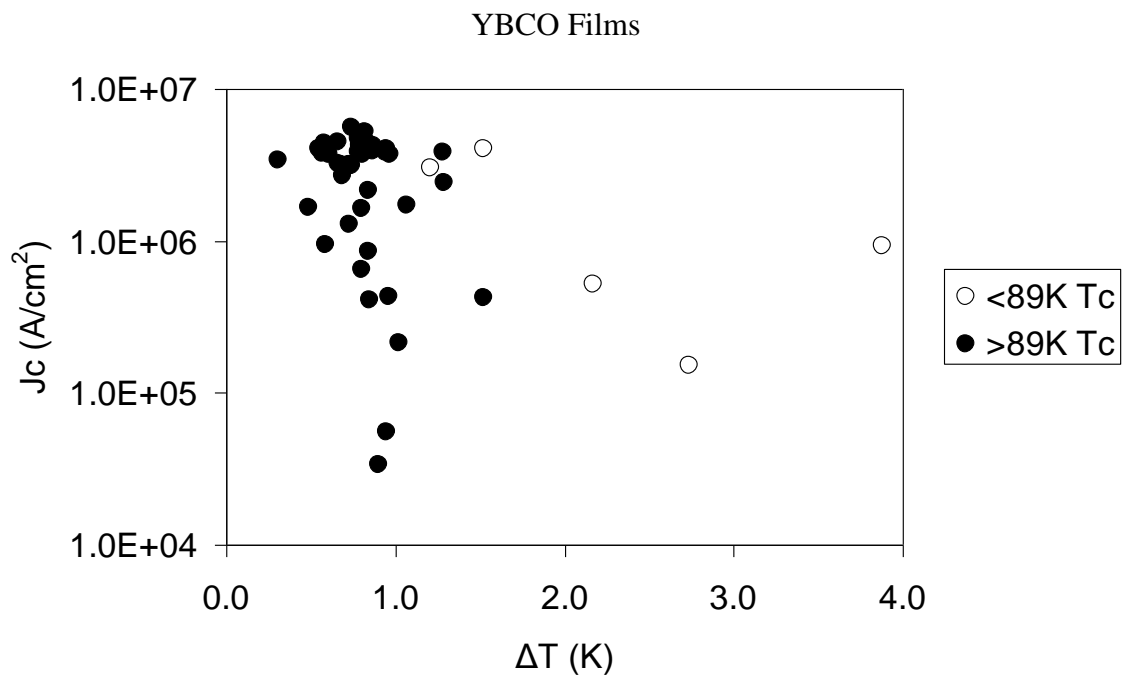


Figure 2c.4.21.1

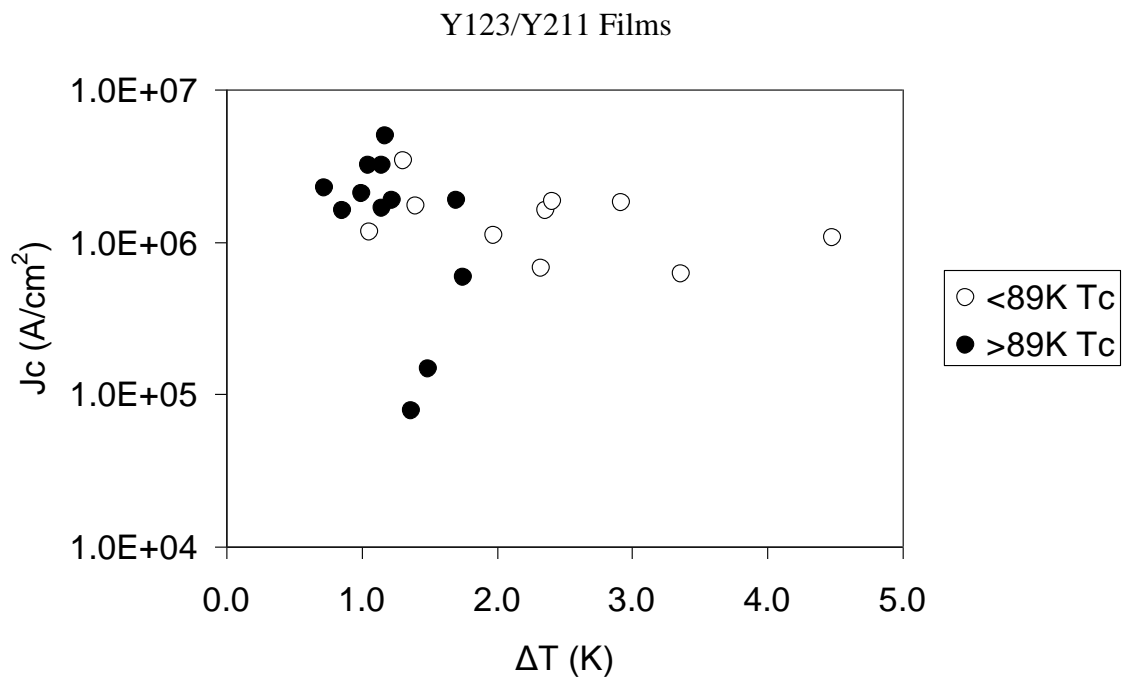


Figure 2c.4.21.2

2c.4.22 Results

- The two “tails” can be separated out by the T_c of the samples
 - A value of 89 K best separated the two
 - The relationship of the data to T_c may be influenced by the data being taken near the critical transition temperature.
- Data points with narrow ΔT and low J_c , the rapidly falling “tail,” may result from microstructural defects in the film
 - defects lower overall transport J_c yet remain high locally
 - One sample examined of this group had small cracks in the film providing some evidence to support this hypothesis
- J_{cs} of Y123/Y211 composite films (pinned) were higher for a given ΔT than YBCO
 - Possible indication of pinning strength within the sample

2c.4.23 Conclusions

- The superconducting properties of $(Y,Nd)_{1+x}Ba_{2-x}Cu_3O_{7-\delta}$ powders were studied for varying compositions
 - compared for different final high temperature processing steps in air or 1% O_2 atmosphere.
 - Subsequent processing in 1% O_2 increased and narrowed the T_c transitions and raised J_c values to the range of 106 A/cm^2
- For $(Y_{0.5},RE_{0.5+x})Ba_{2-x}Cu_3O_{7-d}$ compositions smaller ionic radii generally show less variation in J_c with differing temperatures
- The temperature spread between the ac loss data for different magnetic fields increases as the J_c of the films decreases
 - The scatter of the data indicates that this is a general rule of thumb

2c.5 Minute RE Doping for YBCO flux pinning

References: 18, 24

P. N. Barnes¹

1. Air Force Research Laboratory, Wright-Patterson AFB, OH 45433

Presented at AFOSR 2005, 24 Jan 05

2c.5.1 ($Y_{1-x}RE_x$)Ba₂Cu₃O_{7-z}

- Previous studies have focused on substituting quantities of RE for Y in YBCO ($x \geq 0.1$)
 - Focus on Y site substitution by RE as opposed to second phase precipitates
 - Done since Y123 and other RE123 materials have similar structures
- Alternate way to improve flux pinning characteristics is to introduce a high density of defects into the material
 - Defects are non-superconducting
 - Possibly introduce defects as a second phase into the YBCO
- Combine the two effects?

2c.5.2 ($Y_{1-x}RE_x$)Ba₂Cu₃O_{7-z}

- This study focuses on substituting small quantities ($x \leq 0.1$) of Tb and Ce for Y in Y123 thin films.
 - Tb and Ce do not form (or difficult to form) the RE123 phase
 - Potentially, an appropriate defect density of the inclusions can be produced if sufficiently dispersed
- Both of these elements are divalent, having both +3 and +4 valence states and possibly allow pinning by alternate chemical bonding
 - Pr??
- Terbium does not degrade the T_c of YBCO, but Ce significantly affects the T_cs of YBCO with increasing Ce content
- Small quantities of dopants potentially allows for the same deposition parameters as plain YBCO

2c.5.3 Experimental

- Powders dried and mixed (not necessarily simple)
 - calcined at 850 °C and 880 °C
 - Y₂O₃, BaCO₃, CuO, CeO₂, and Tb₄O₇ powders
 - all nominally 99.99+% pure
- Targets made from the powder
 - (Y_{1-x}Tb_x)Ba₂Cu₃O_{7-z}
 - (Y_{1-x}Ce_x)Ba₂Cu₃O_{7-z}

2c.5.4 Tb-doped, 77 K

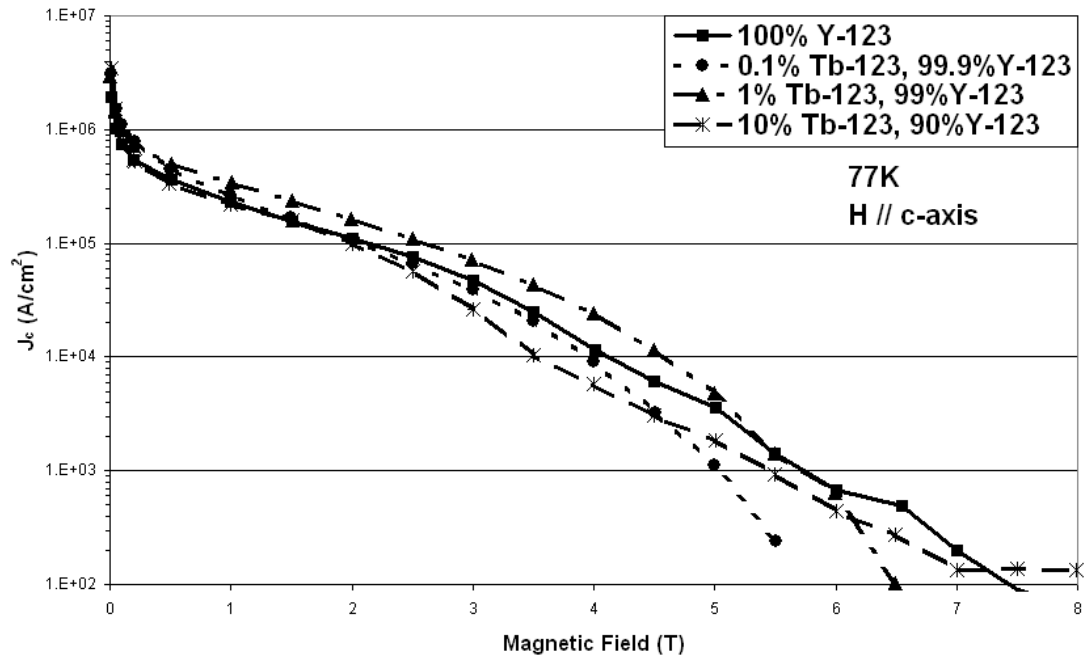


Figure 2c.5.4.1

2c.5.5 Tb-doped, 65 K

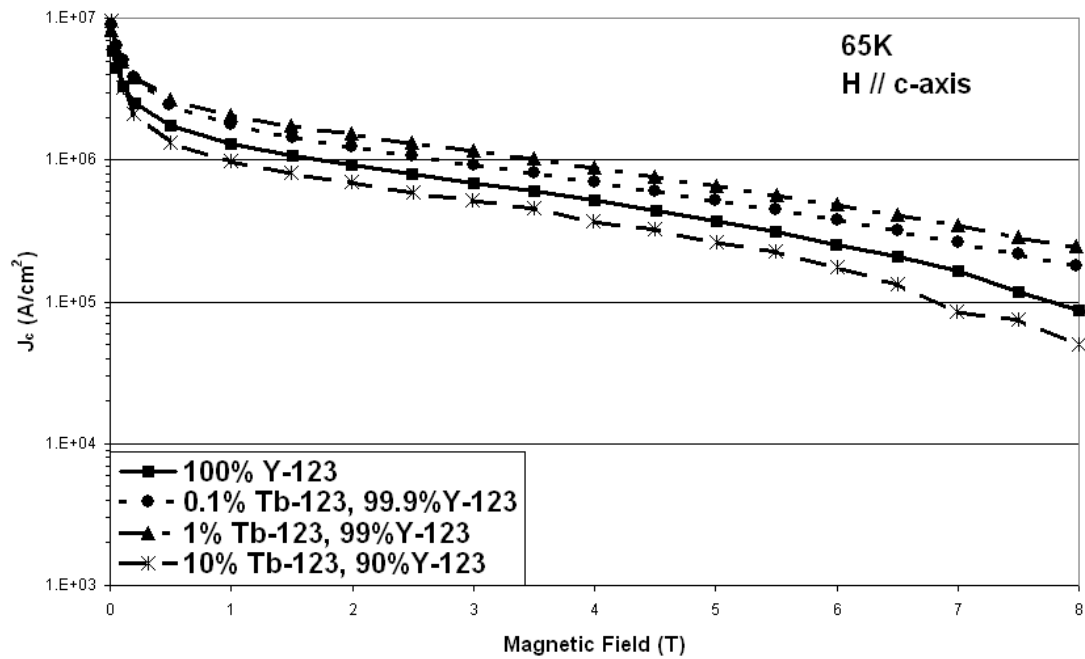


Figure 2c.5.5.1

2c.5.6 Ce-doped, 77 K

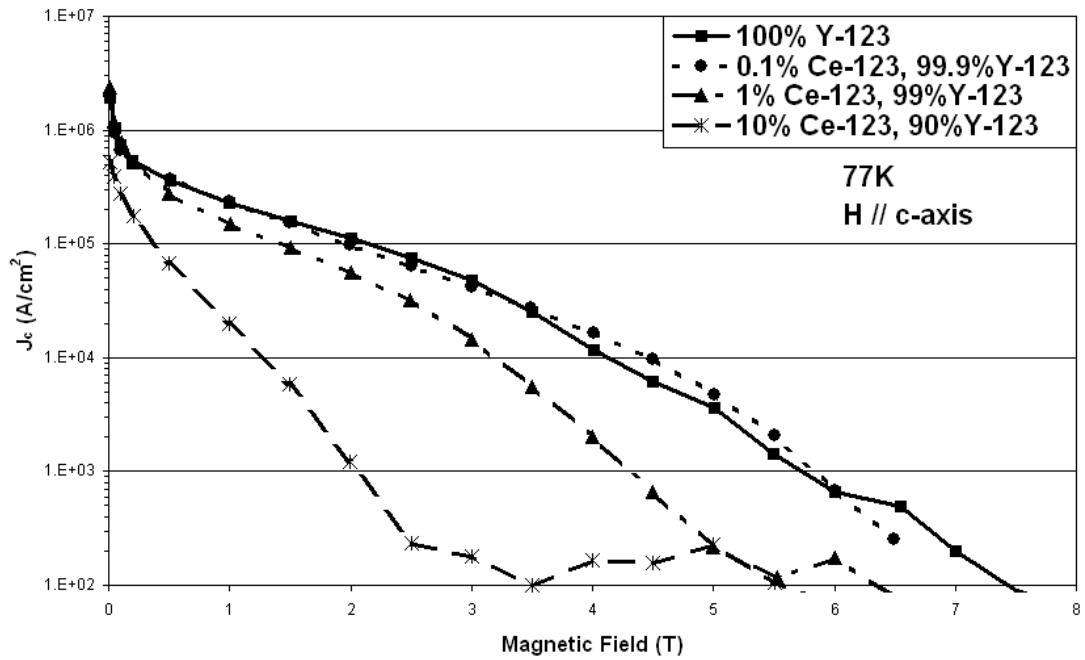


Figure 2c.5.6.1

2c.5.7 Ce-doped, 65 K

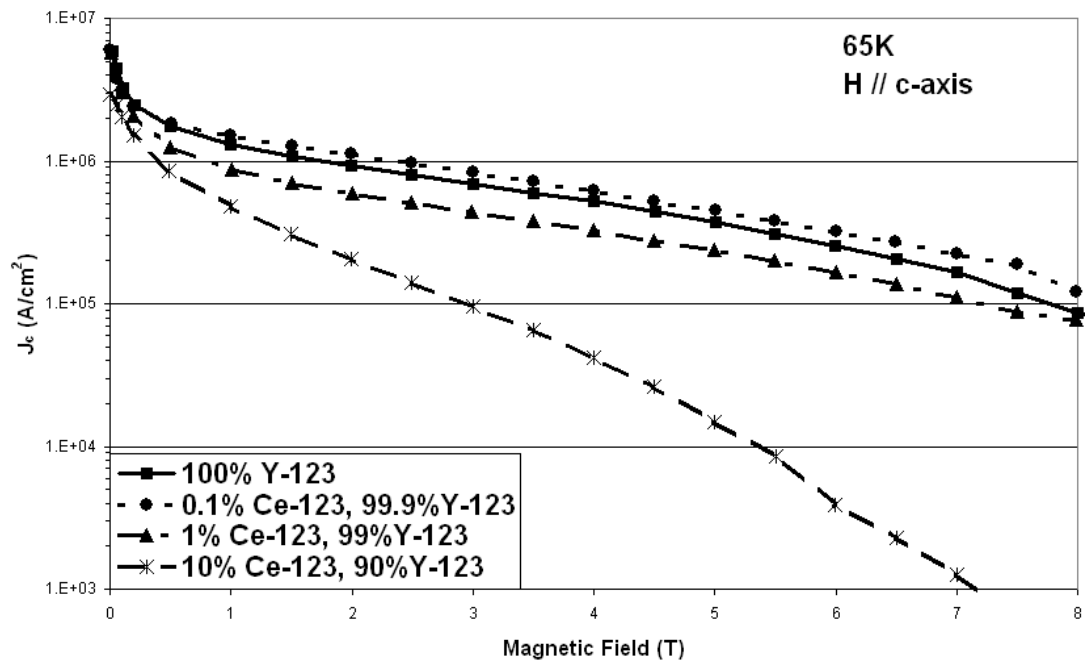


Figure 2c.5.7.1

2c.5.8 Nanoparticle Pinning

- The addition of nanoparticles significantly enhances J_c
- This is evident in the pinning force comparison

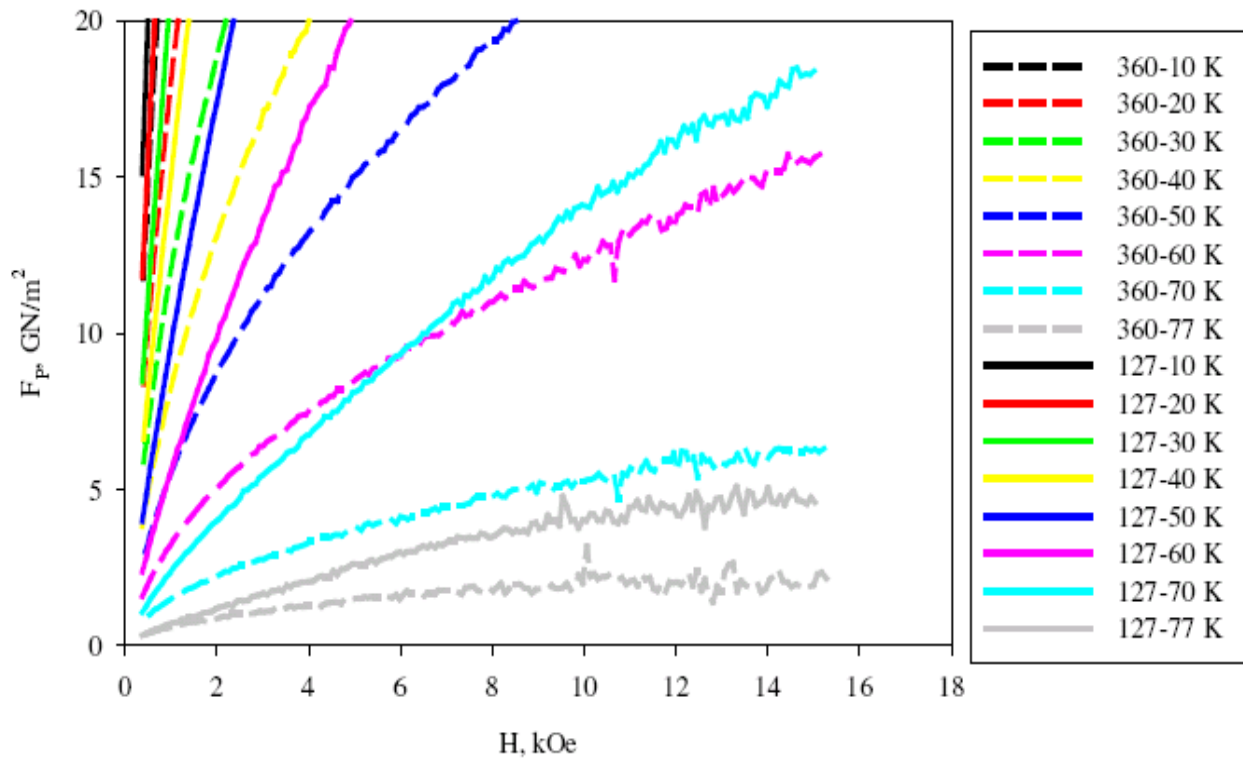


Figure 2c.5.8.1

2c.5.9 Nanoparticulate Pinning

- Why do the nanoparticles provide better pinning?
- Number of pinning sites and/or stronger sites (deeper wells)?

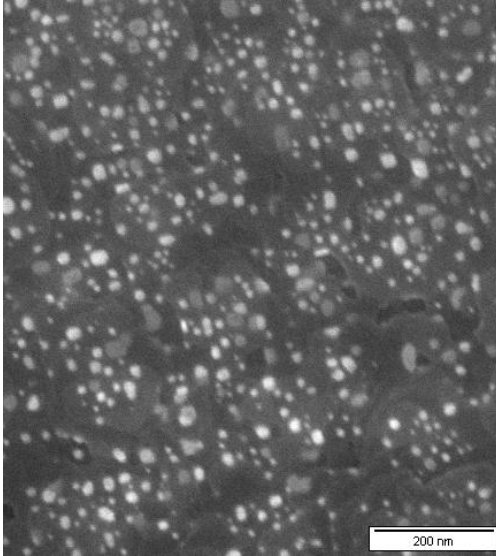


Figure 2c.5.9.1

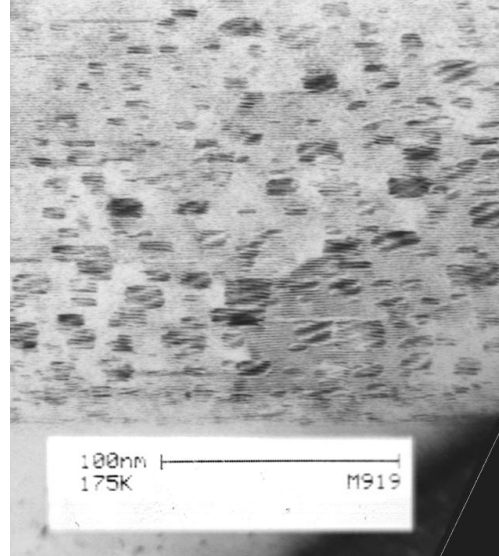


Figure 2c.5.9.2

2c.5.10 Y₂O₃ Nanoparticles

- 2nd number indicates spacing of the nanoparticulate layers
- 176 nm spacing still providing effective pinning (200 nm initial guess)

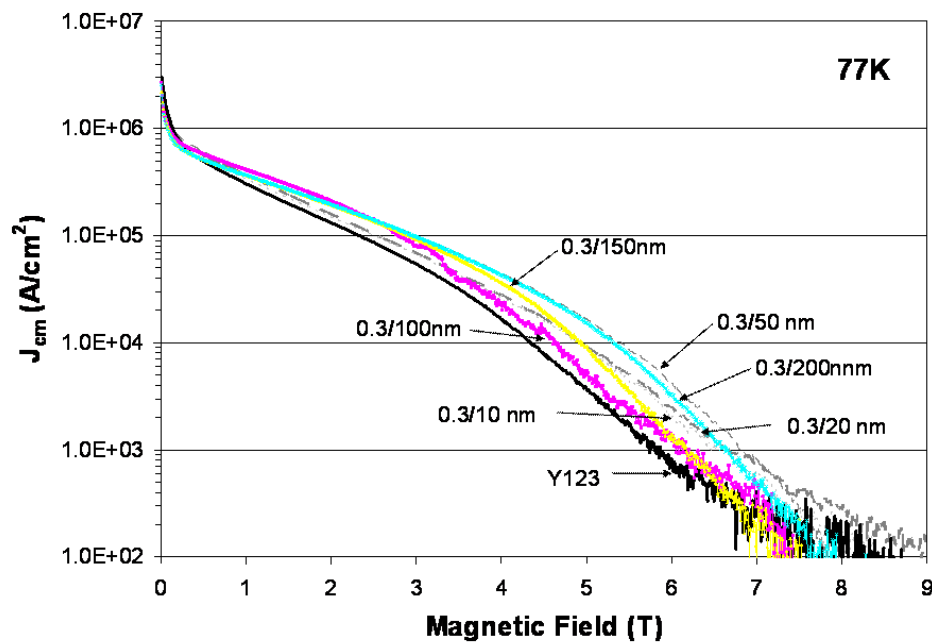


Figure 2c.5.10.1

2c.5.11 Defect Propagation

- 176 nm spacing suggests defect propagation, but this is not sufficient evidence

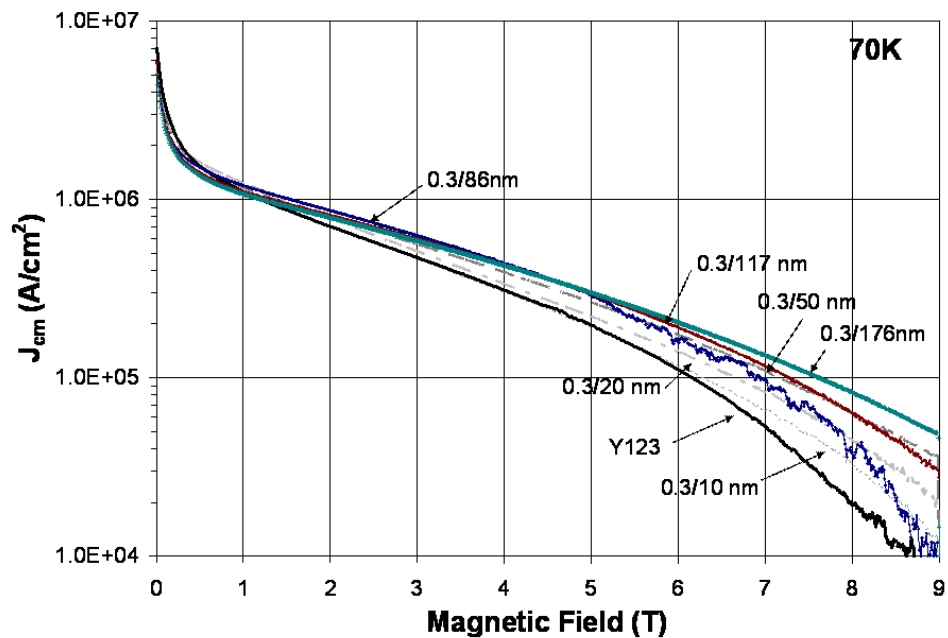


Figure 2c.5.11.1

2c.5.12 Ouch!

- My apology to Matt Feldman
- Why?
 - Because I am now going to be a hypocrite

2c.5.13 Pinning Potential

- Results of Mike Sumption (yes, I am not showing all the supporting data)
- Based on magnetization decay in vibrating sample magnetometry

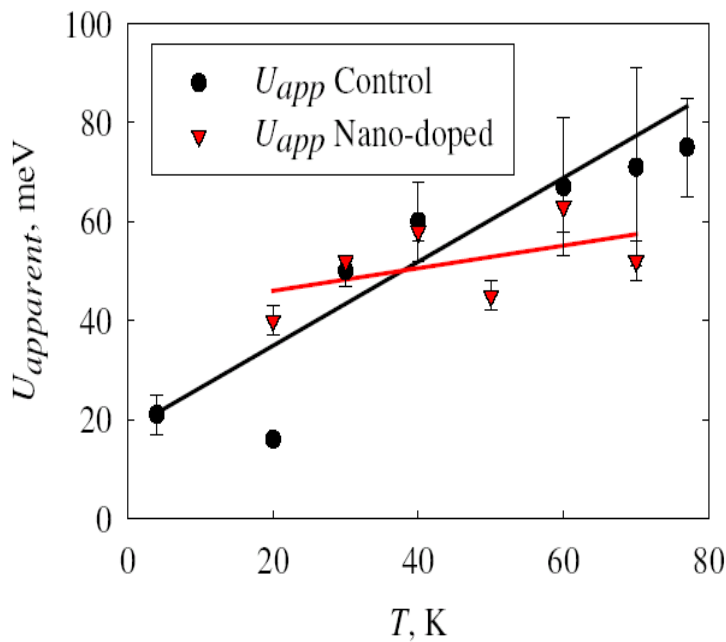
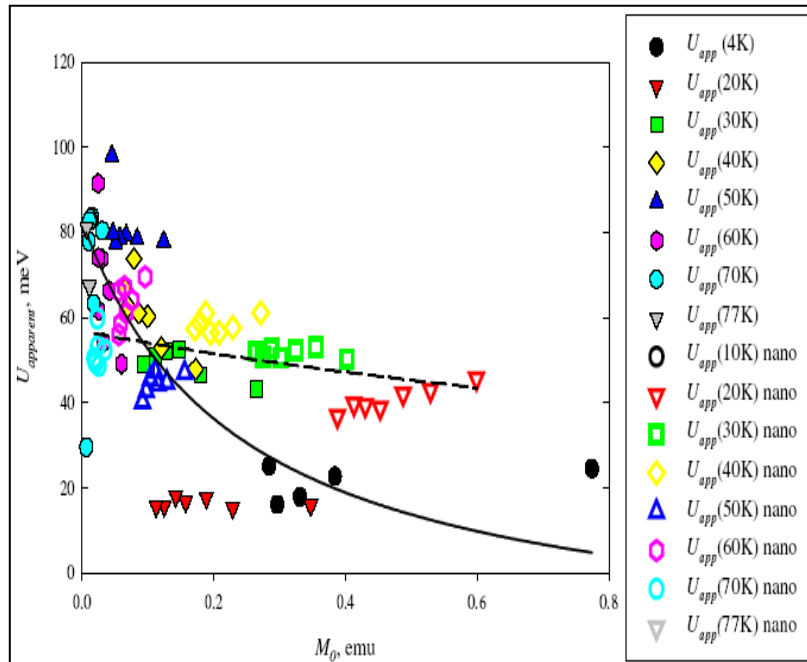


Figure 2c.5.13.1

2c.5.14 Nanoparticle Pinning

- Conclusions from data on nanoparticles
 - seem to increase F_p and J_c by increasing pinning sites rather than intrinsic U_0 values
 - Less influenced by flux gradients
 - effective at high flux gradients (low temperatures) equally as low flux gradients (high temperatures)

- Speculation – NANOPARTICLES ARE INDUCING DEFECTS
 - Same speculation as thickness data

2c.5.15 Summary

- Minute quantities of Tb and Ce dopants can provide pinning
 - Optimization may result in pinning as good as nanoparticulate pinning (Not shown yet)
- Nanoparticulate pinning can provide significant improvement in Jc and (at least in our case)
 - Pinning improvement due mainly to number of sites as opposed to stronger pinning centers
 - Nanoparticles cause defect propagation which aid in pinning (not confirmed, but speculated by two sets of data)
 - High Resolution TEM required (higher than currently used)

2c.6 Sm and Nd Substitutions in YBCO Films Produced Through Metal Organic Deposition

References: N/A

2d Lt Brandon Craig Harrison, PhD¹

1. Air Force Research Laboratory, Wright-Patterson AFB, OH 45433

Presented at CEC-ICMC August 29, 2005

2c.6.1

- Nanoparticle additions
 - AFRL by PLD: 211 or Y2O3
 - AMSC by MOD: (Ho,Y)O2
 - Superpower by MOCVD: (Sm-x)
 - ORNL+UWisc by MOD: Y2O3
- Nanoscale control or engineering\
- Irradiation
- Rare-earth or chemical substitution/additions

2c.6.2 Sample Compositions

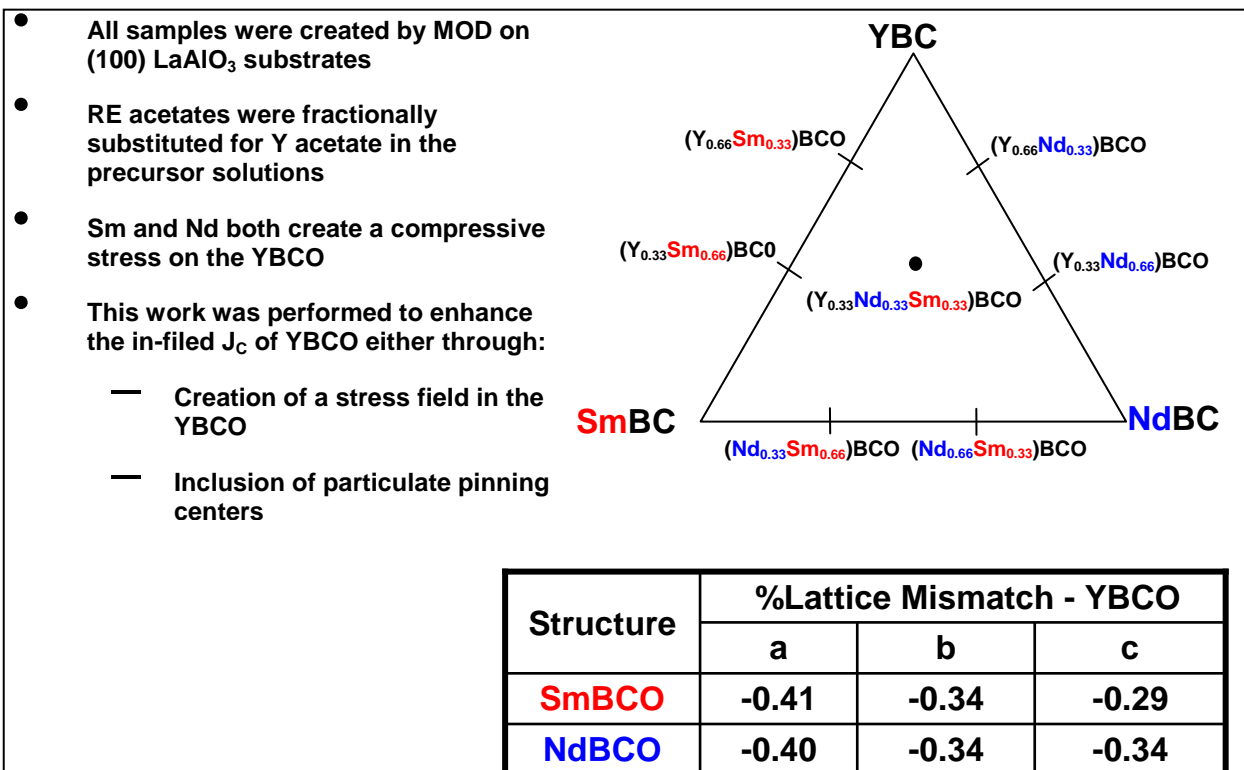


Figure 2c.6.2.1

2c.6.3 X-Ray Diffraction Data

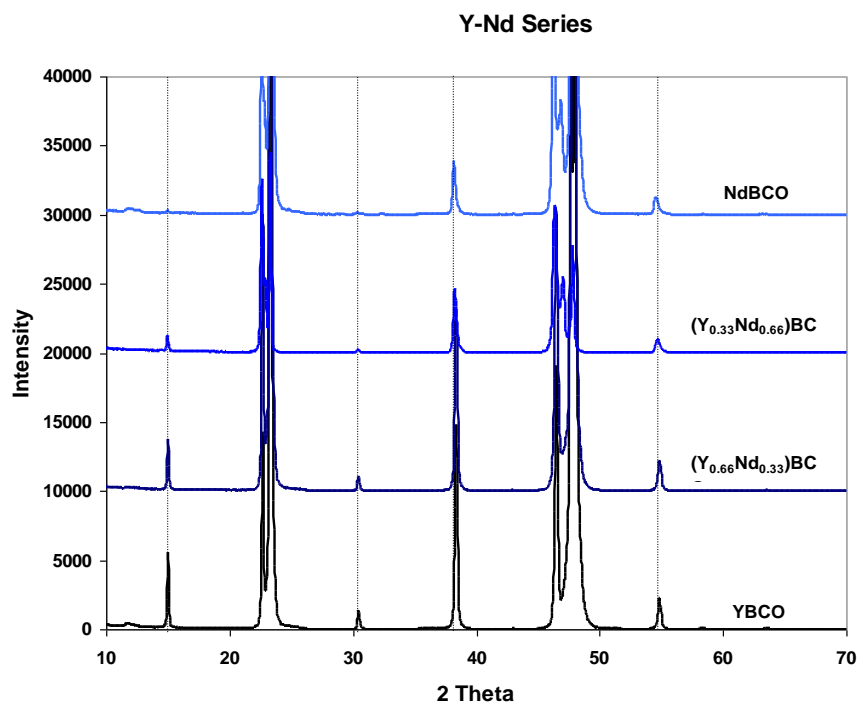


Figure 2c.6.3.1

2c.6.4 X-ray Diffraction Data

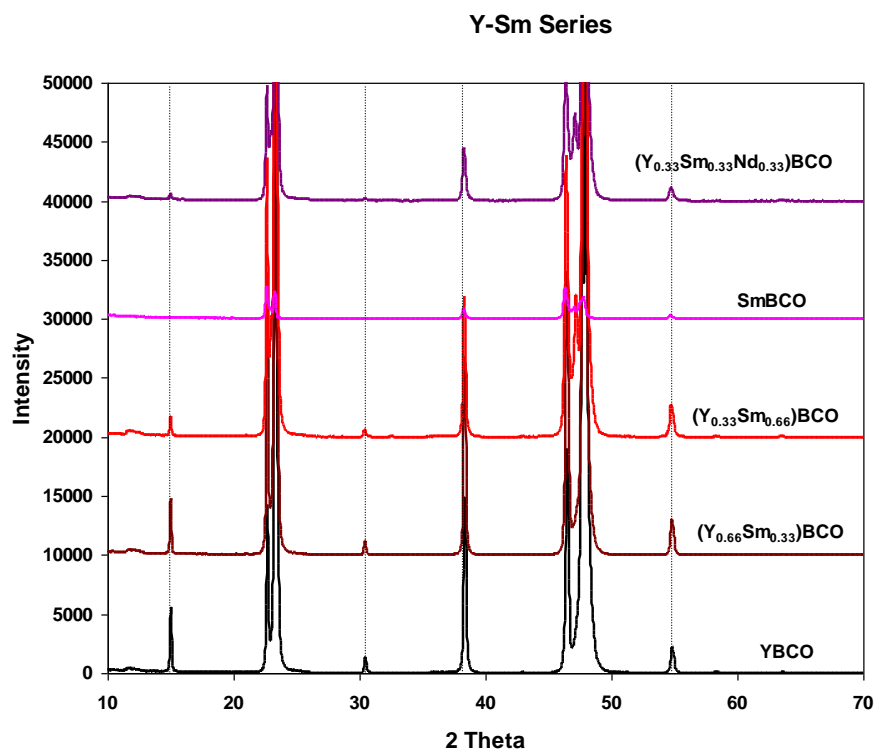


Figure 2c.6.4.1

2c.6.5 X-ray Diffraction Data

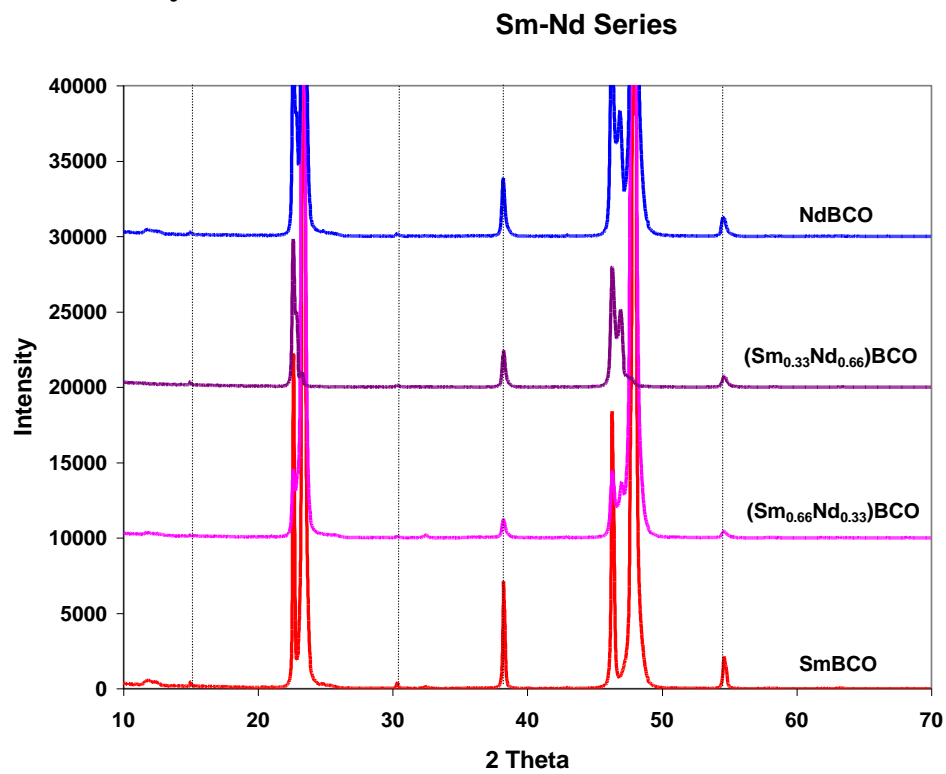


Figure 2c.6.5.1

2c.6.6 T_c by AC susceptibility

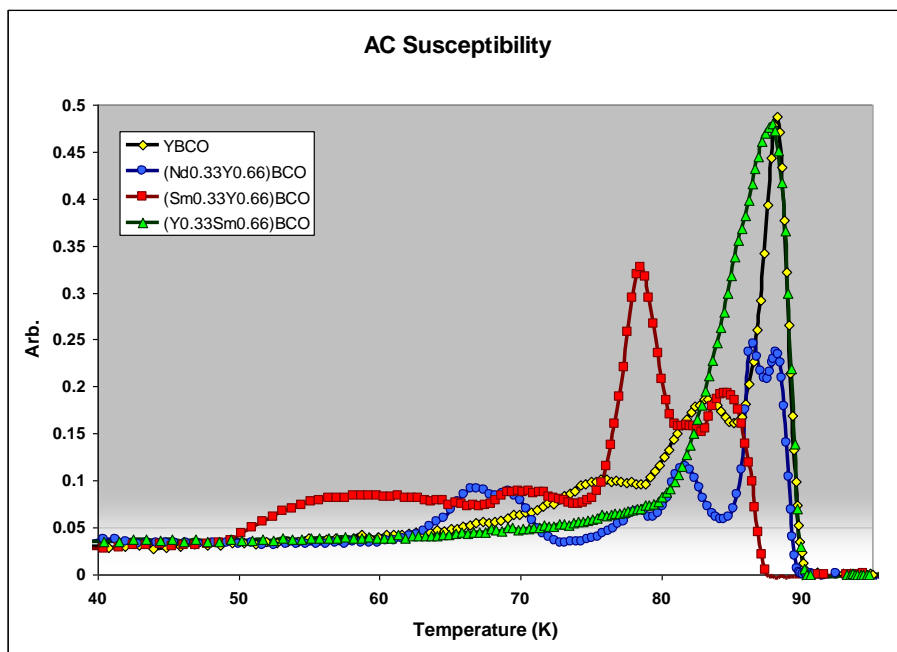


Figure 2c.6.6.1

2c.6.7 T_c by Transport

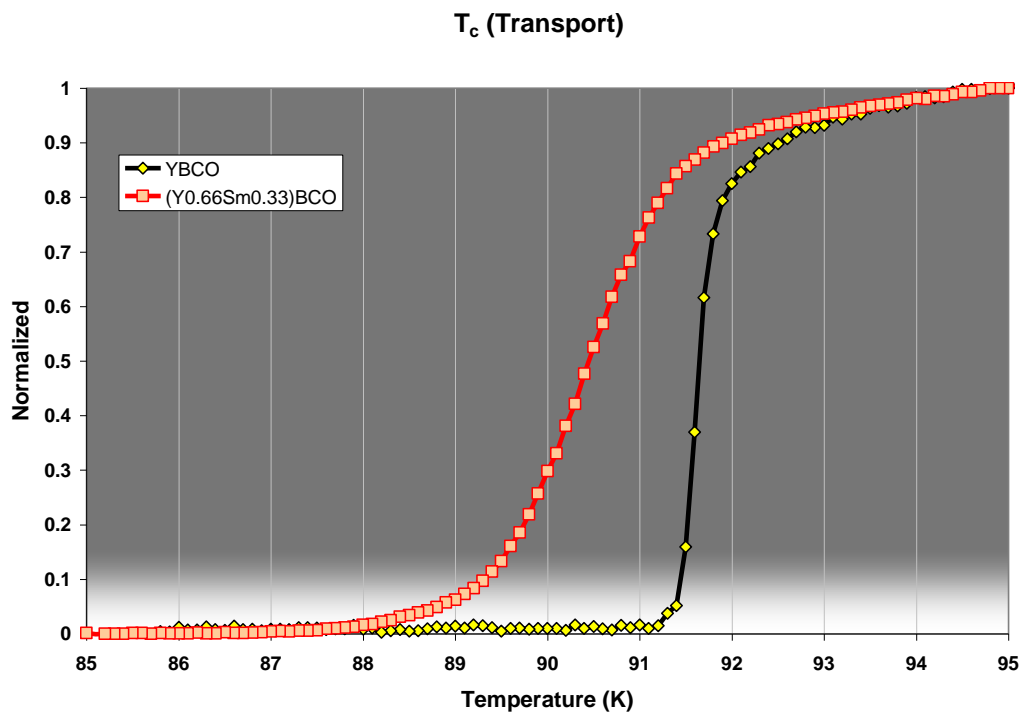


Figure 2c.6.7.1

2c.6.8 Jc by VSM

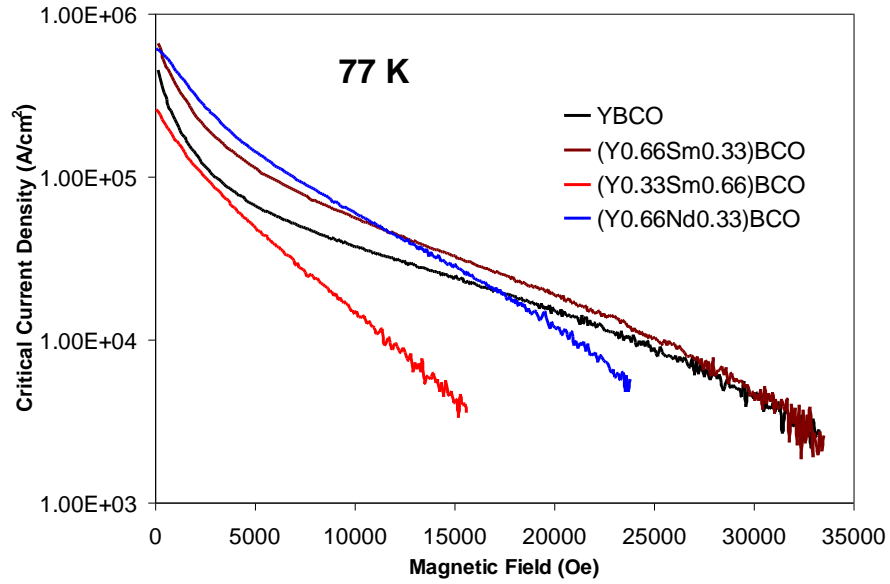


Figure 2c.6.8.1

2c.6.9 Jc by VSM

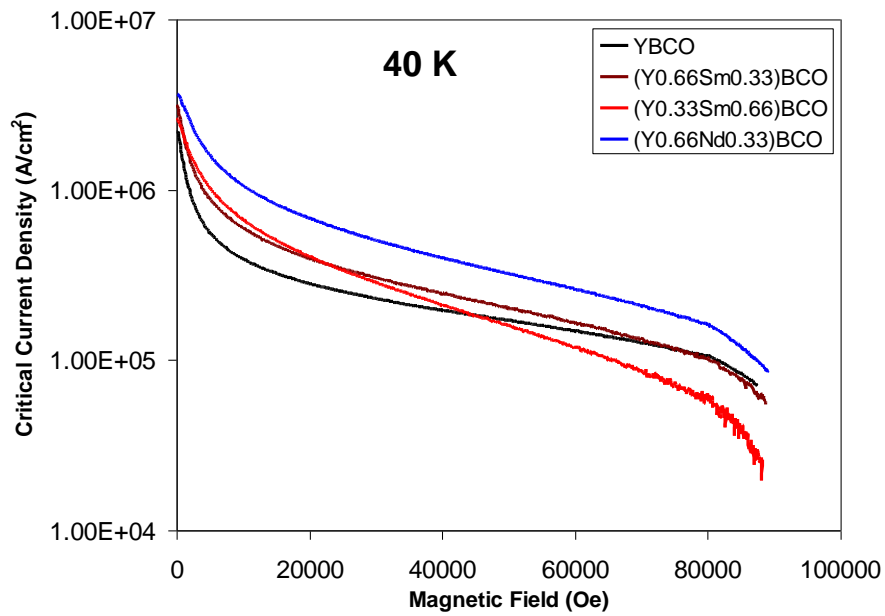


Figure 2c.6.9.1

2c.6.10 SEM Micrographs

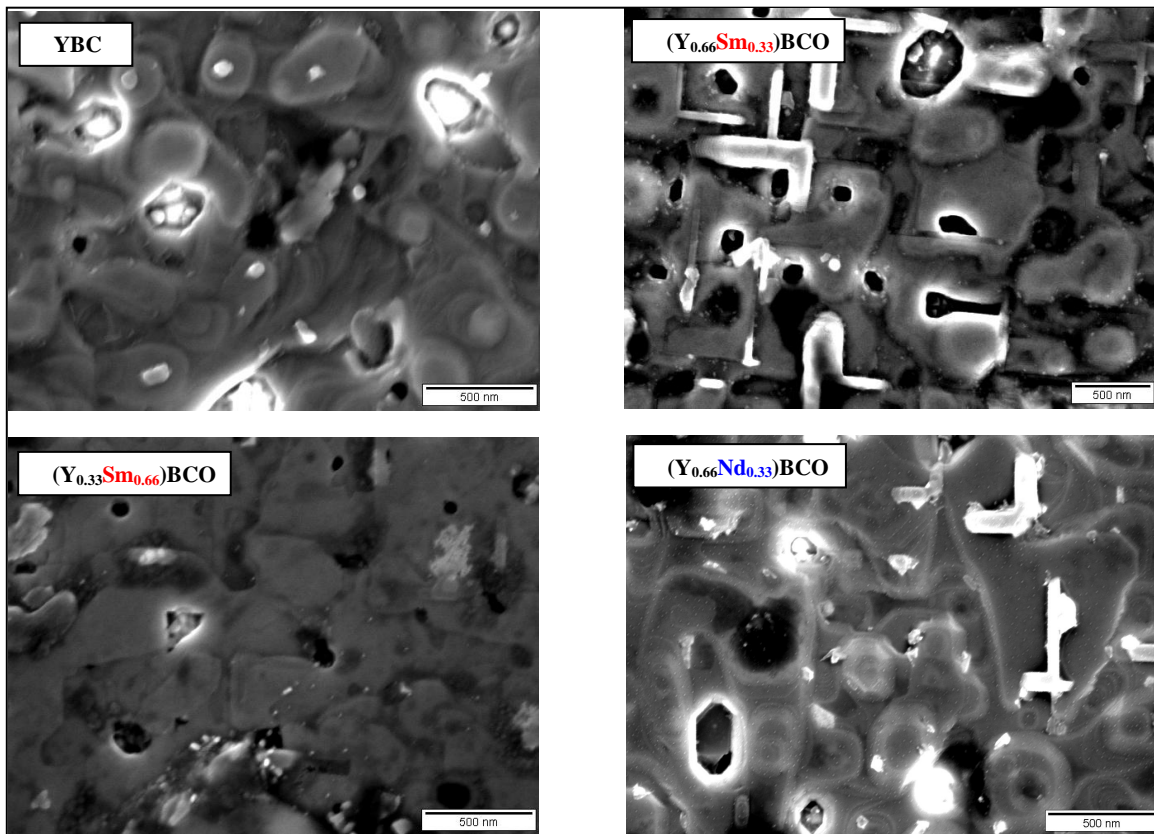


Figure 2c.6.10.1

2c.6.11 Surface Nanoparticles

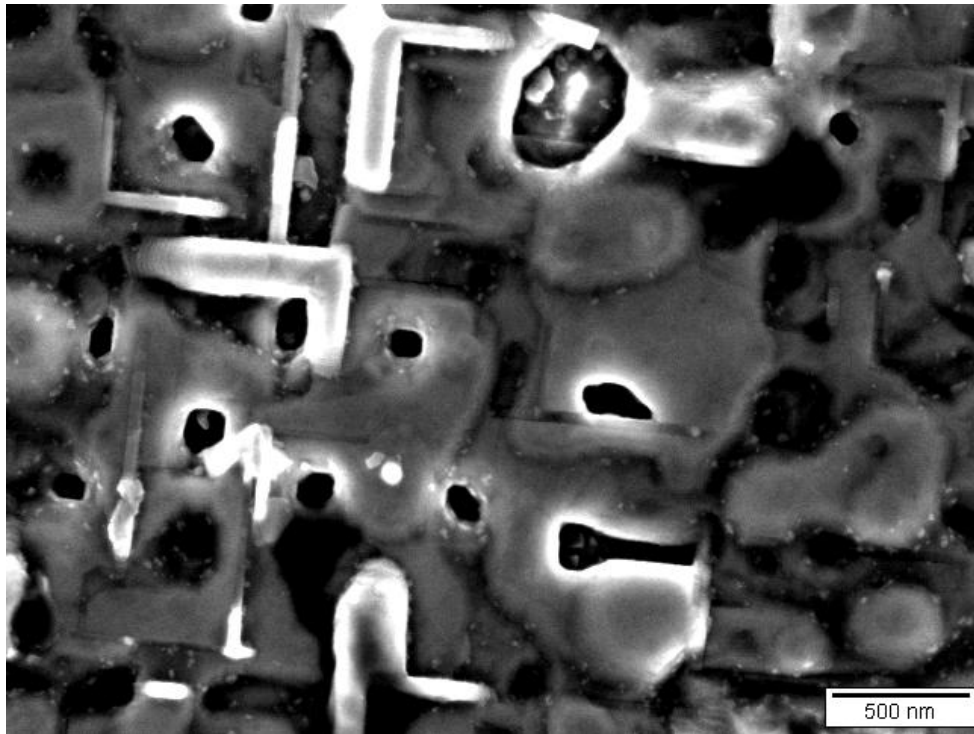


Figure 2c.6.11.1

2c.6.12 Surface Nanoparticles

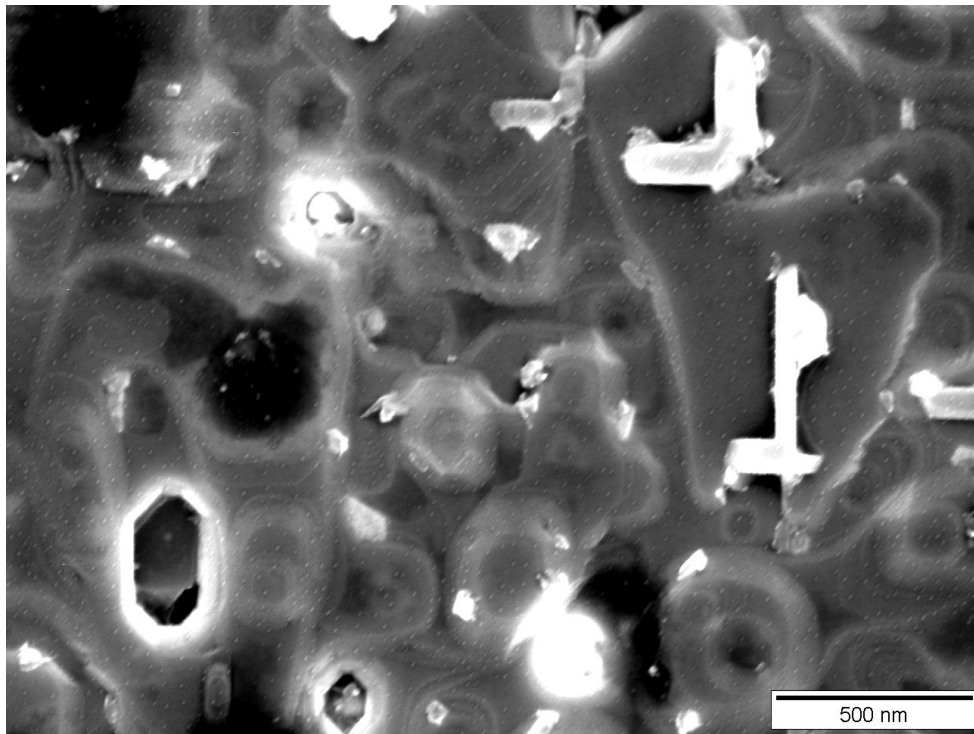
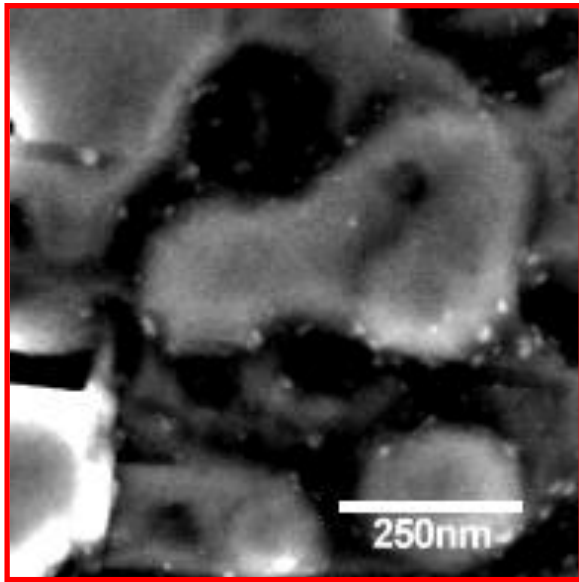


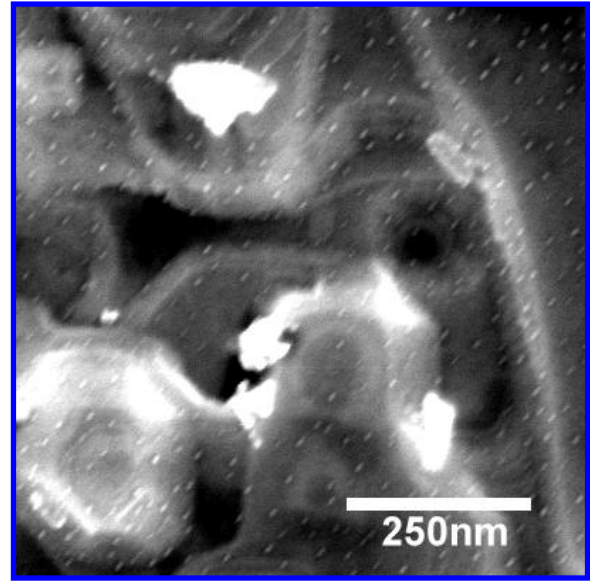
Figure 2c.6.12.1

2c.6.13 Nanoparticle Comparison



(Y_{0.66}Sm_{0.33})BCO

Figure 2c.6.13.1



(Y_{0.66}Nd_{0.33})BCO

Figure 2c.6.13.2

2c.6.14 CONCLUSIONS

- ~50%-150% improvement of JC up to 1T for 1/3 substituted films at 77K
- Both Sm_{0.33} and Nd_{0.33} films have surface nanoparticles
 - The particles have a diameter <10nm
 - In the case of Nd the particles are uniform across the entire surface, while for Sm the particles decorate the grain boundaries
- The in-field performance of the 1/3 substituted films are improved over pure YBCO at 77K and 40K
- The improvement in the in-field performance may be due to the presence of particular pinning centers created by phase separation

2c.7 Properties of $(Y_{1-x}RE_x)_{1+y}Ba_{2-y}Cu_3O_{7-z}$ Bulk Superconductors for Flux Pinning

References: N/A

J.M. Evans¹, B. C. Harrison, PhD¹, K.W. Schmaeman¹, M.F. Locke¹, T.J. Haugan¹, P.N. Barnes¹

1. Air Force Research Laboratory, Wright-Patterson AFB, OH 45433

Presented at CEC-ICMC August 29, 2005

2c.7.1 Objectives

- Investigate the effects of solid solution substitution on critical current densities (J_c) and flux pinning properties.
- Replace Y in $YBa_2Cu_3O_{7-\delta}$ (YBCO or Y123) with various rare earth elements (RE= Er, Eu, Ho, Sm, Gd, and Yb).
- Extend the survey to include the partial substitution of Ba with Y and RE.
- Investigate the influence of ionic radius on J_c and flux pinning properties.

2c.7.2 THEORY

- The high T_c and J_c of YBCO coated conductors enable their use at LN2 operating temperature (77K). However, the decrease of J_c as applied magnetic field increases limits their use for certain electronic applications.
- Flux flow through the superconductor increases with the increasing magnetic field strength, but flux pinning can improve the J_c in these fields by suppressing the flow.
- Pinning sites can be created by substituting rare earth elements into the solid solution YBCO.
 - The lattice mismatch between the substituted unit cell and the non-substituted unit cell creates a stress field that can act as a pinning center.
 - Substituting other RE elements that form 123 phases aid in the chemical compatibility of the two compositions

2c.7.3 EXPERIMENTAL

- Compositions were created using Y_2O_3 , $BaCO_3$, CuO , Er_2O_3 , Eu_2O_3 , Ho_2O_3 , Sm_2O_3 , Gd_2O_3 and Yb_2O_3 all with purity $\geq 99.99\%$
- All powders were dehydrated at 450oC prior to mixing
- The powders were then weighed to an accuracy of ± 0.0001 g before being mixed and ground using a mortar and pestle
- Calcined by slow heating from 600oC to 850oC at 25oC/H
- All compositions were annealed in air several times with intermediate grindings between 850oC and 910oC

2c.7.4 EXPERIMENTAL

- Compositions were annealed in a 1% O₂ (balanced Ar) atmosphere for 48 hr —annealing temperatures for the various RE compounds were based on the melting point of the RE123
- A final anneal in full a O₂ atmosphere was accomplished at varying temperatures (277oC-460oC)
- Unit cell volume were calculated by averaging the published unit cell volumes of Y123 and RE123 based on percent substitution of RE.
- The theoretical density was determined by using the mass and calculated volume of the unit cell. This was then used to determine the inferred J_c using the magnetization data.

2c.7.5 EXPERIMENTAL

	Ionic Radius (Å)	Melting Point of RE123 (oC)	1% O2 Temp (oC)	Final Annealing Temp (oC)
Yb	0.985	900	730	460
Er	1.004	980	810	405
Ho	1.015	990	820	389.5
Y	1.019	1000	830	460
Gd	1.053	1030	860	305
Eu	1.066	1050	880	279
Sm	1.079	1060	890	277.5

Figure 2c.7.5.1

2c.7.6 EXPERIMENTAL

	Ionic Radius (Å)	Unit Cell volume for (Y0.5,RE0.5)Ba2Cu3O7-δ (nm³)	Density of (Y0.5,RE0.5)Ba2Cu3O7-δ (g/cm³)	Density of (Y0.5,RE0.6)Ba1.9Cu3O7-δ (g/cm³)
Yb	0.985	0.17260	6.81305	6.84740
Er	1.004	0.17357	6.74725	6.77588
Ho	1.015	0.17379	6.72767	6.75404
Y	1.019	0.17380	6.36398	6.31772
Gd	1.053	0.17520	6.961	N/A
Eu	1.066	0.17517	6.61307	6.62694
Sm	1.079	0.17513	6.60704	6.61940

Figure 2c.7.6.1

2c.7.7 MEASUREMENTS

- X-ray diffraction (XRD) using CuK α was completed using a Rigaku Diffractometer with a coupled 2 θ scan and a step size of 0.03 $^{\circ}$
- Magnetic measurements were obtained using a Quantum Design Physical Property Measurement System (PPMS) with a Vibrating Sample Magnetometer (VSM)
 - Magnetic J_c was approximated using the extended Bean critical current method J_c=15 $\Delta M/R$, where ΔM is the difference in magnetic hysteresis in emu/cm⁵ and R is the radius of the superconducting volume estimated as 5x10⁻⁵ cm for finely ground powders.

2c.7.8

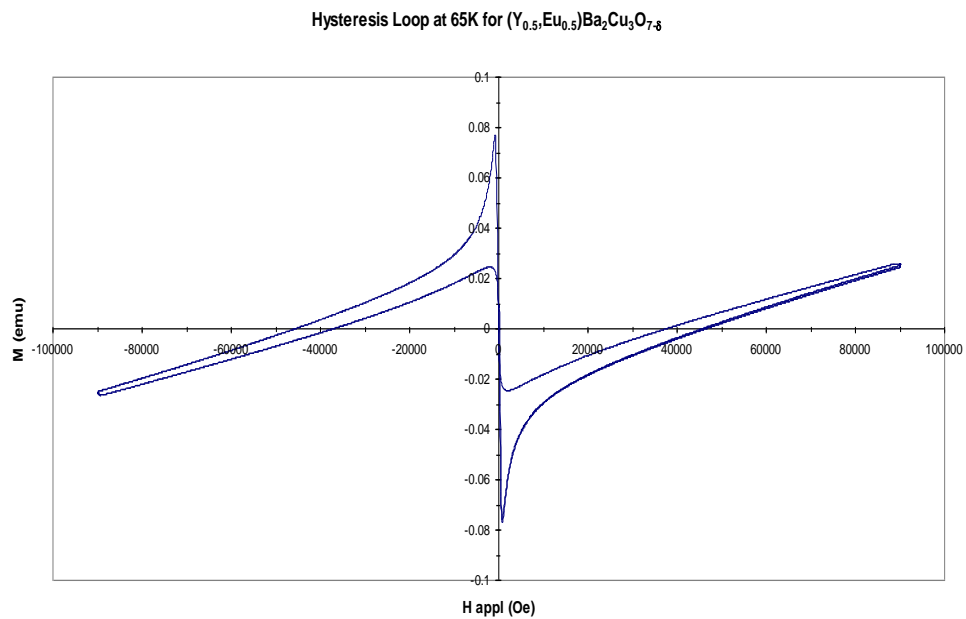


Figure 2c.7.8.1

2c.7.9

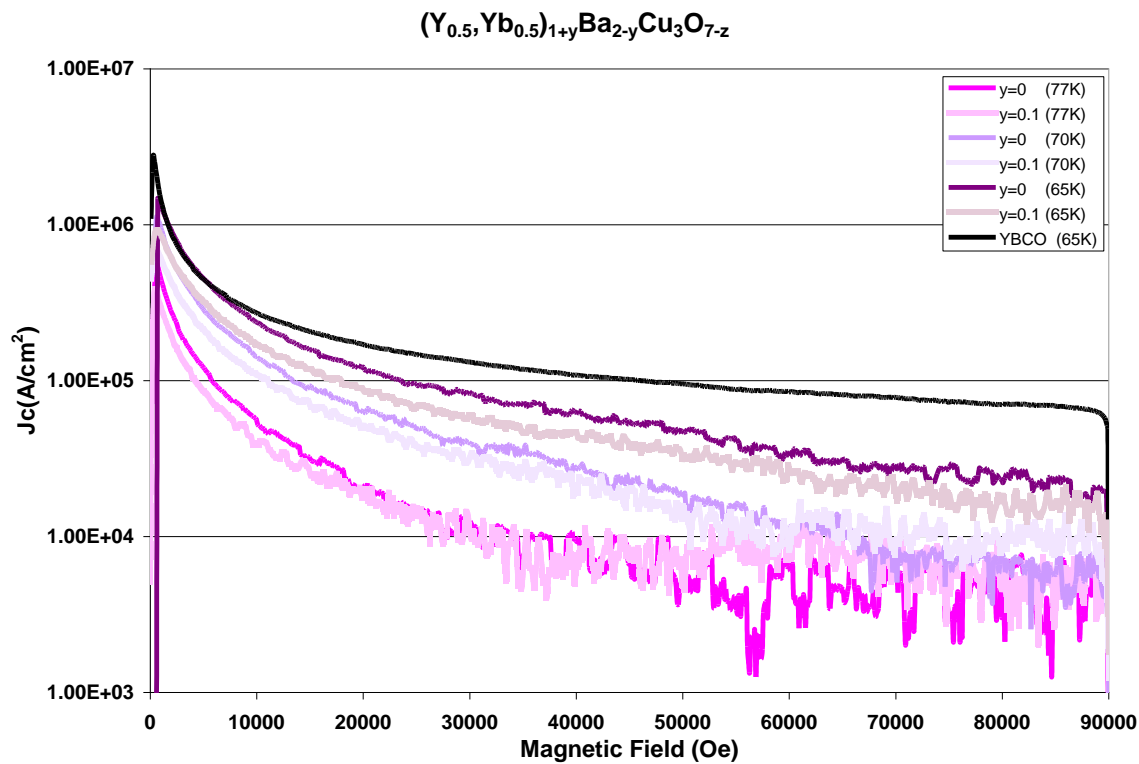


Figure 2c.7.9.1

2c.7.10

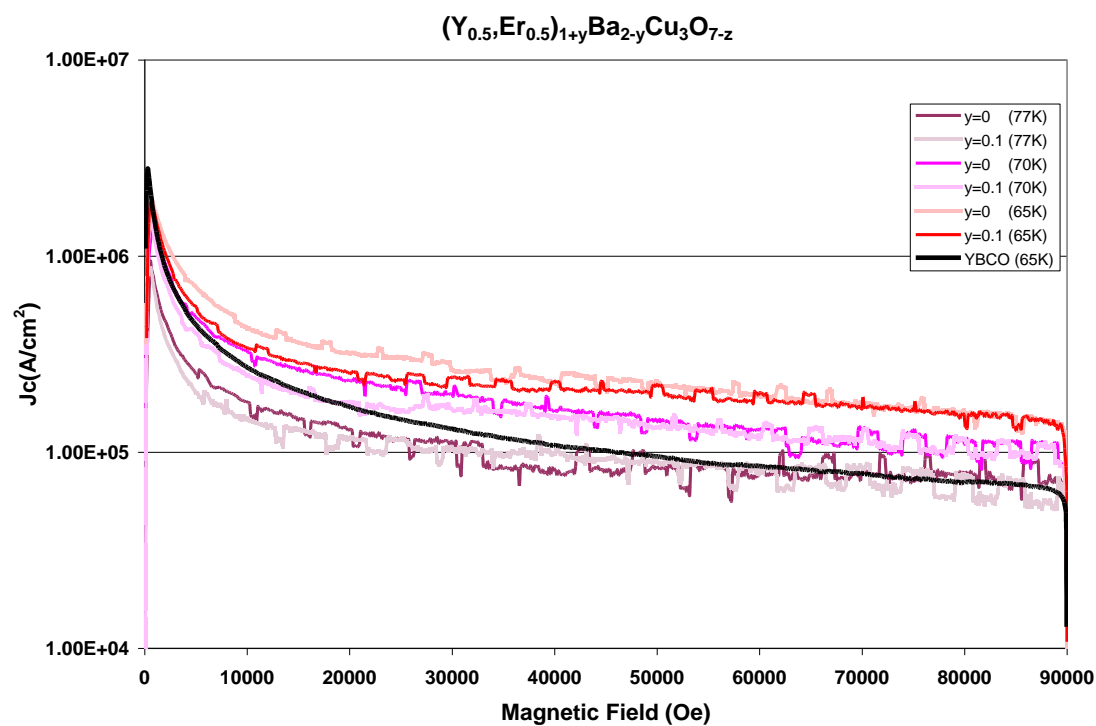


Figure 2c.7.10.1

2c.7.11

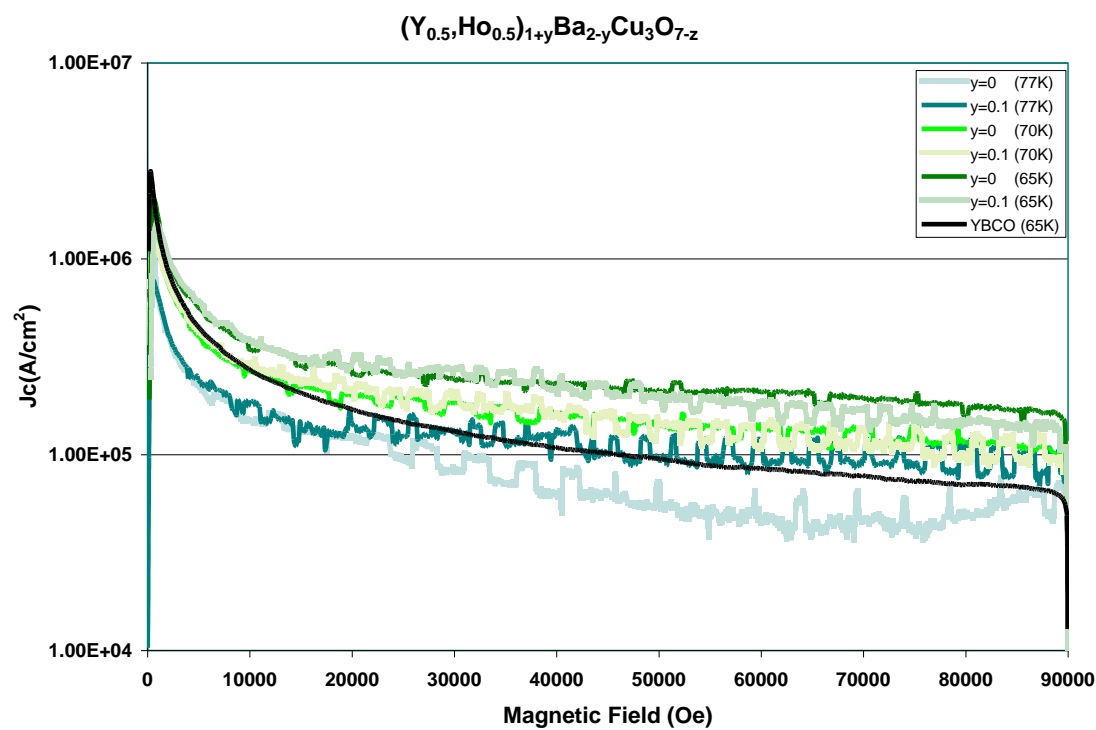
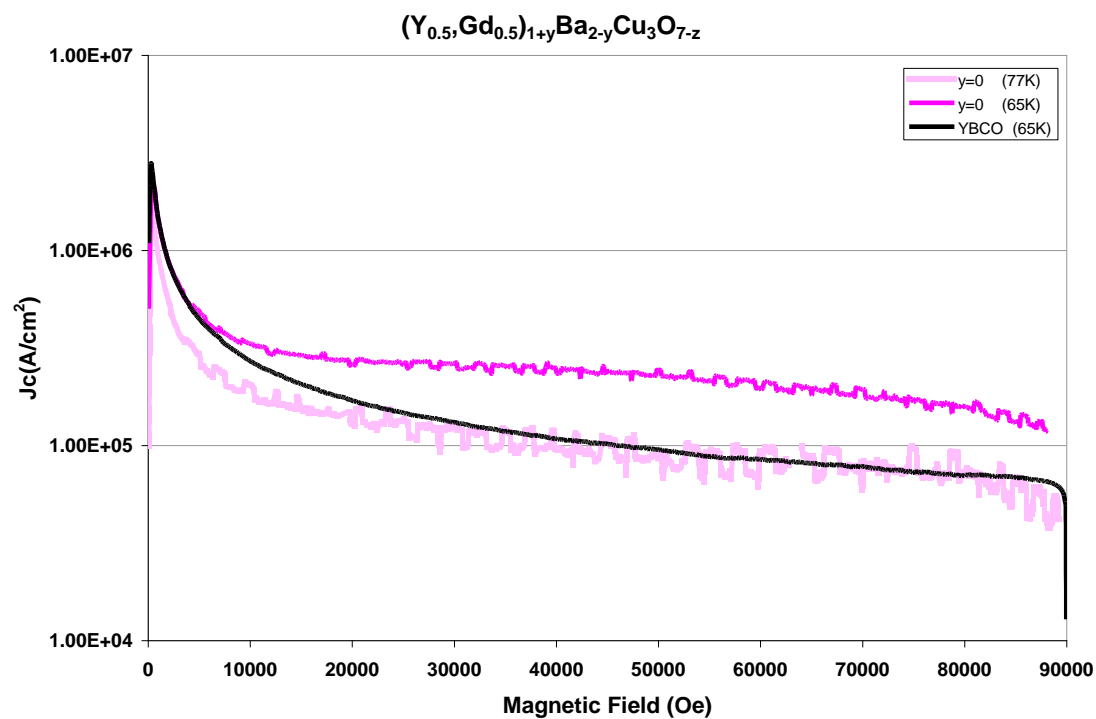
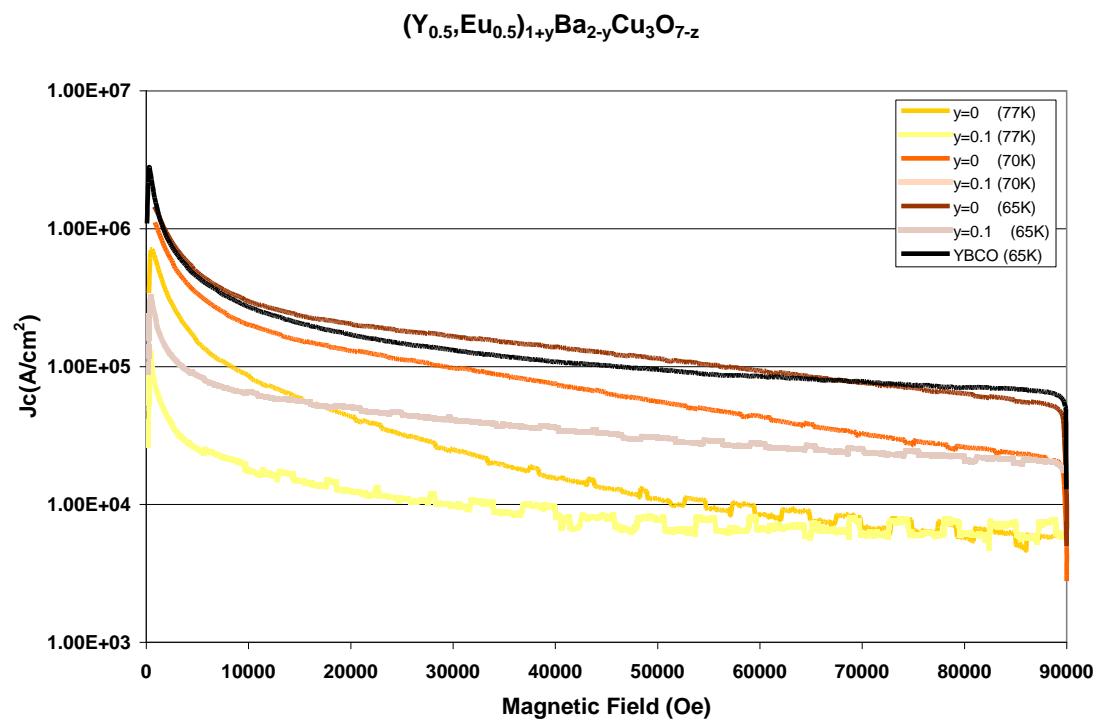


Figure 2c.7.11.1

2c.7.12



2c.7.13



2c.7.14

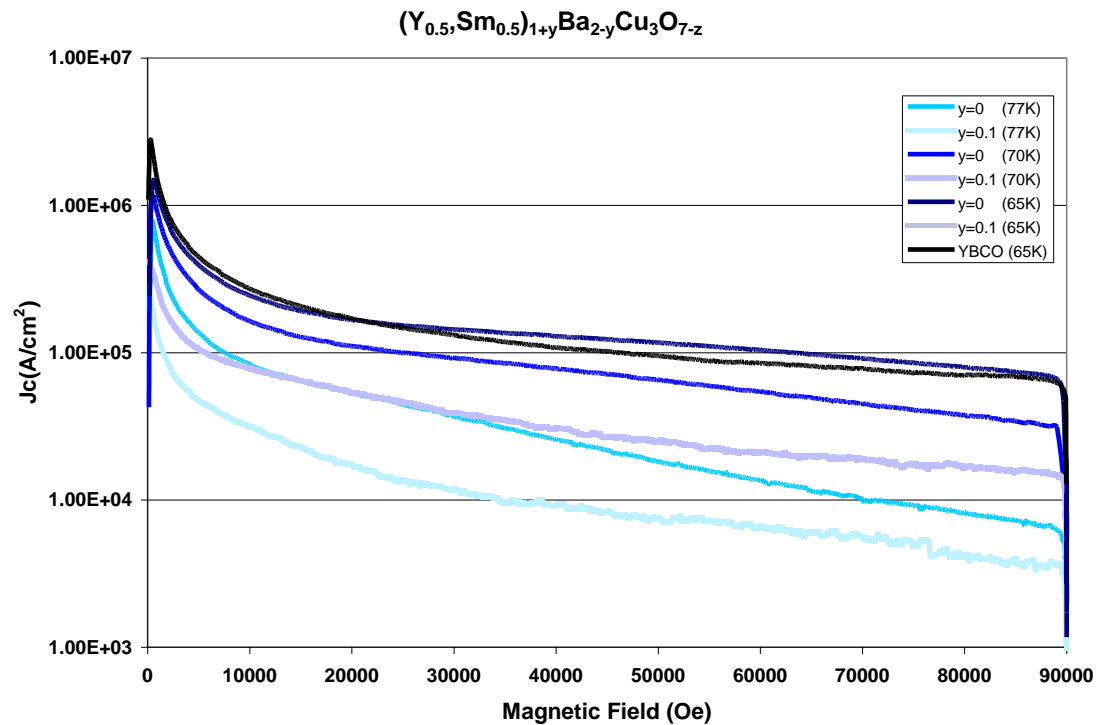


Figure 2c.7.14.1

2c.7.15

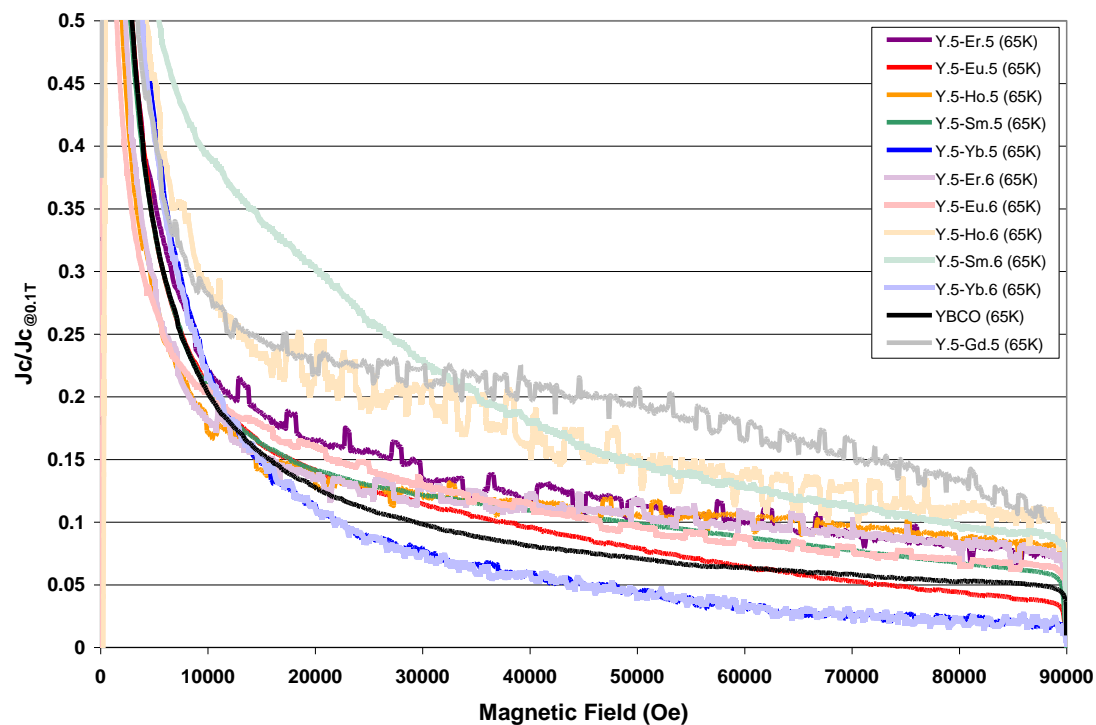


Figure 2c.7.15.1

2c.7.16

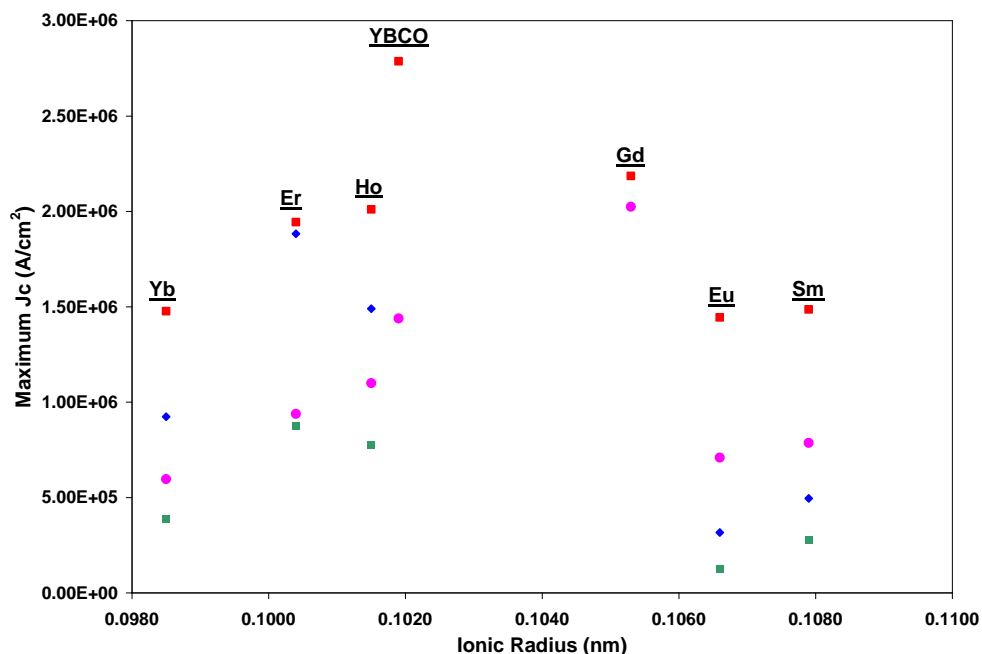


Figure 2c.7.16.1

2c.7.17 RESULTS

- Results show that substitution for only Y (Ba=2.0) generally produces higher J_c 's at all measured magnetic fields and temperatures as opposed to compositions with Ba=1.9.
- Ho was the only composition that showed some increase in J_c with Ba substitution.
- The reduction of J_c for Ba=1.9 vs. Ba=2 diminished as magnetic field strength increased.

2c.7. 18 CONCLUSIONS

- RE substitutions for Y were effective at increasing the J_c values versus Y123 bulk powder.
- For most compositions, replacing Ba did not improve the over-all J_c for the range of temperatures and magnetic fields investigated.
- There appears to be a parabolic relationship between the effectiveness of flux pinning by substitution of Y with RE elements and the difference in ionic radius between Y and the substitutionary element.

2c.7.19 COMMENTS

- Additional data needs to be collected on Yb substitutions into Y123.
- More information is necessary to verify an increase in J_c when substituting for Ba in the Y-Ho composition.
- Further investigation is needed to determine the relationship between atomic radii and increased flux pinning.

Chapter 3: AC Loss

3.1 Striated YBCO

References: 25, 26, 27, 28, 29, 30, 31, 32

3.1.1 Introduction

The design of lightweight superconducting generators requires a high speed rotor (6000 to 24,000 rpm), a high magnetic flux density (1 to 2T) and high frequency (200 to 1000 Hz). These conditions make it very difficult to minimize ac losses in a wide superconducting tape. Advances in YBCO coated thin film tape allows narrow filaments with very high current density on a thin metal alloy substrate that is separated from the superconductor by a dielectric buffer. These tapes can exhibit minimized ac loss by subdividing the YBCO layer with barriers which exhibit high electrical resistance. This configuration acts to decouple the filaments, unlike the metallic matrix of low temperature superconductors which permits significant coupled currents induced by perpendicular applied fields. The underlying alloy metal substrate can be non-magnetic with a very high resistivity to minimize eddy currents in the substrate. Twisting the conductor is necessary to minimize coupling loss even though the YBCO filaments are separated by high electrical resistance barriers. Research on this concept is initiated to explore the possibility. The following are the relevant sub-tasks:

3.1.2 Striated YBCO-VSM

This particular work was initiated with Dr. Ted Collings of OSU through the PR Summer faculty program and continued with Dr. Mike Sumption also from OSU. Magnetization vs. applied field measurements (M-H loops) were taken on short samples of $\text{YBa}_2\text{Cu}_3\text{O}_{7-\delta}$ (YBCO) thin films which were divided into narrow filaments. The YBCO was deposited using pulsed laser deposition onto single-crystal LaAlO_3 substrates, with a range of film thicknesses from 0.25 μm to 0.33 μm . Using a YAG laser, the thin films were patterned into linear striations by removing strips of the superconductor by laser ablation. The resulting striated filamentary structure serves to reduce the effective width of the YBCO films and hence the hysteresis loss in the superconducting samples. The magnetization measurements were taken over the temperature range of 4.2 - 77 K in applied fields of 0-3.7 T using a vibrating sample magnetometer. The measured hysteresis losses show a highly linear relationship between superconductor filament width and hysteresis loss as anticipated. However, the laser ablation process did result in the redeposition of YBCO along the edges of individual filaments. The laser ablation technique used was as an effective means of subdividing the filaments to reduce the high aspect ratio of the coated conductor although many other methods are possible. Even though susceptibility curves show a slightly sharper transition for the non-striated film, there is no evidence from the Q_h results that j_c is affected by the striations in any significant way. Additional measurements will be taken at higher magnetic fields in the VSM for verification of the linear relationship. Further variations in widths and the resulting ac losses will be examined to determine the relationships and properties of the material. Use of focused ion beam (FIB) will also be used as a precision way to make and investigate the striations.

3.1.3 Striated YBCO-Resistive Barriers

The Slovak Academy of Sciences (Polak) is using ion milling to make various width trenches in YBCO coatings which will be wide enough to prevent proximity coupling. Some samples will be subsequently coated with metal or CeO_2 to provide variable barrier resistance which will be measured by Polak with the intent of separating the barrier bulk resistance from the interface resistance at the two sides. When barrier resistances are known parametrically, suitable configurations will be selected and multiple, parallel barriers will be created in several samples with varying resistance for subsequent ac loss measurements. AC loss measurements will be conducted with a Hall probe technique. The University of Cambridge (Campbell) will alter the barrier resistance between adjacent filaments by using a magnetic material coating and will share samples with Polak for barrier resistance measurements. We will conduct high field (up to 9T) AC loss measurements at various temperatures in a vibrating sample magnetometer (VSM) on samples provided by both Campbell and Polak. We will provide the sample design configurations for Campbell and Polak based on models of prospective generator and transformer requirements. The team will then assess the best YBCO tape and barrier configurations for AC loss minimization. Sample exchange has been a significant problem with initiation of this effort and is being resolved by Dr. Oberly. The sample exchange agreement is almost resolved and work is expected to proceed in FY03. Once this is cleared, the first batch of samples will be made and sent (simple ones initially)—silver sputtered on LAO, silver on AlO_3 , silver on YBCO on LAO. We will send striped samples and longer samples when we get feedback from the Europeans based on initial samples.

3.1.4 Striated YBCO-Techniques

A variety of methods will be used to create the striated YBCO samples. A preliminary design for a low ac loss HTS tape patterned into a multifilamentary structure subdivided by electrically resistive barriers is only one possibility. However, there has been no effort to produce a HTS tape with a multifilamentary architecture suitable for ac applications, and methods for creating the multifilamentary structure have not been established. Submission for a patent is being initiated that provides a novel but simple method to create the filamentary structure without eliminating the possibility of current sharing. Hence there is not a complete resistive barrier separation as suggested by others. The approach used in this patent is to divide the HTS tape into superconducting filaments $\sim \mu\text{m}$'s – mm 's in width separated by lower critical current density barriers ~ 10 's nm – 100 's μm in width. The method used for creation of the filaments or divisions are by preparation of the substrate or buffered substrate upon which either the HTS material or the initial buffer layers of the HTS material will be applied. The material is physically affected to adversely affect initial epitaxial growth along long thin lengths whether by scratching, scribing, etching, specialized deposition of buffers to obtain the effect, initial formation of the substrate, etc. Subsequently, the final HTS layer is applied or subsequent buffers are applied for the HTS layer. In this case, the lower J_c barriers are naturally formed by the non-epitaxial growth of the final HTS layer (and/or subsequent buffers) along the long thin lengths. By whatever means, the final result is a multifilamentary structure in the HTS coated conductor that is superconducting up to a certain critical current (as determined by the affected striations) across the full width of the tape and superconducting along the filaments only above the critical current density determined by the affected striations. Since the ac loss is proportional to the current density as well as the width, a limiting factor is placed on the total ac loss of the HTS coated conductor. For further work, a variety of methods will be used to create the striated

YBCO samples. The techniques will allow us to examine various striations and the subsequent material response. After an understanding of the ac loss issues is assessed then methods more suitable to manufacturing to obtain the optimum conductor will be explored. Conductor design tradeoffs will be considered to allow ac loss minimization techniques compatible with realistic YBCO coated conductor processing.

3.1.5 Low Loss Substrates

There are presently two sub-tasks in this area which covers metallic, non-metallic as well as round versus flat conductor.

3.1.6 Low Loss Substrates-Non-magnetic

Evaluation of nickel-refractory metal alloys as metallic substrates for second generation coated conductors will be considered. Coated conductors based on textured substrate technology are in the forefront of developmental efforts towards long length manufacturing of conductor tapes for practical applications. Nickel and certain nickel alloys are shown to develop the necessary texture required for such applications. Even though substantial work has been done developing textured metallic substrates, pure Ni does not possess sufficient strength and stiffness to withstand processing steps in manufacturing and current Ni alloys still have developmental issues for immediate application as well as being magnetic (which results in greater losses in an ac magnetic field). The objective of the present investigation is to evaluate alternate nickel-refractory metal micro-alloys that can be used as metallic substrates for coated conductor fabrication. The affects of deformation parameters on rolling texture along with quality of recrystallization texture with different annealing conditions will be studied. The characterization of the materials will be done by microscopy, x-ray diffraction, orientation imaging microscopy and tensile testing. The effect of micro alloying of nickel on the quality of texture, thermal stability of texture and increased strength will be considered. As a note this work has largely suffered by lack of sufficient deformation in the final rolling. A collaboration has been struck with Oxford (Ken Marken) to do the final rolling of the material prior to treatment. This effort may be terminated this next FY pending outcome of the new collaboration.

3.1.7 Coil Testing

This task is on hold awaiting the delivery of YBCO placed in a coil configuration from the AF DUS&T program. It is possible that initial testing may commence in FY03. Work has commenced to prepare the Robicon power supply for ramping of the coil.

3.1.8 AC Loss Minimization

YBCO tapes can be adapted to minimize ac loss by subdividing the HTS layer. This creates barriers that exhibit high electrical resistance. Appropriate buffers and processing methods must be selected.

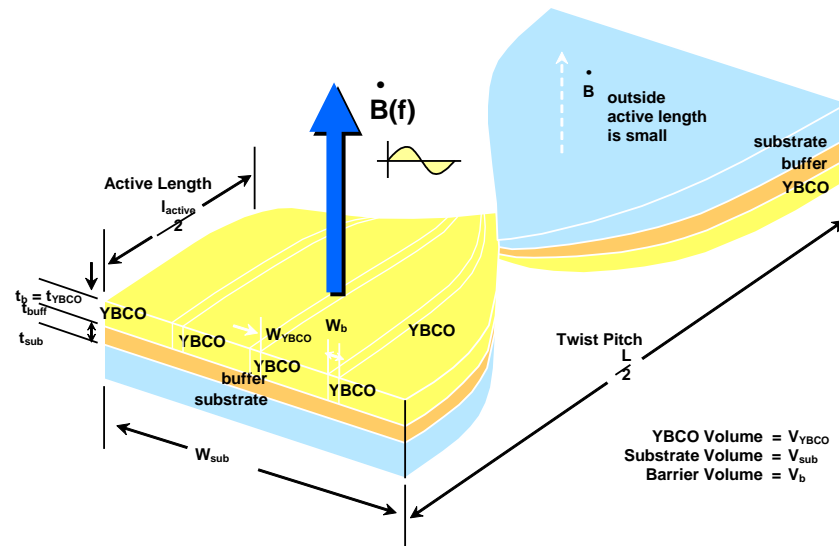


Figure 3.1.8.1

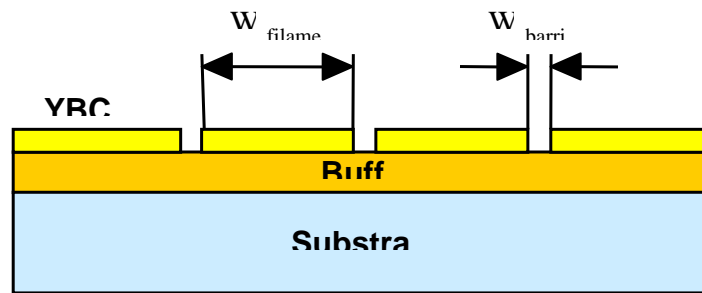


Figure 3.1.8.2

Striated filaments enable high J_c with low ac losses in high applied magnetic fields. It is possible to create filaments of varying width using ceramic masks and laser ablation.

Striated YBCO

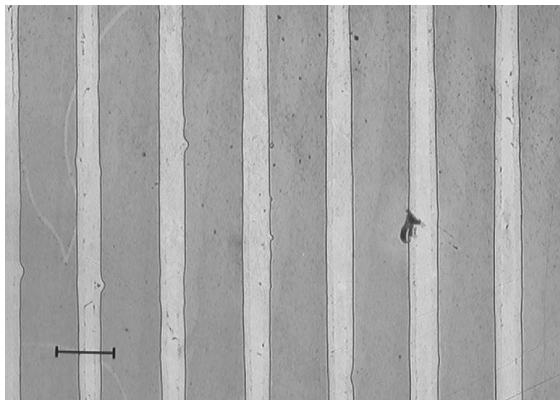


Figure 3.1.8.3

5 mil alumina mask
125  filament width



Figure 3.1.8.4

3.1.9 Susceptibility Data

The onset of the T_c transition is quite high at 92.3 K (0.3 μm thick YBCO on LaAlO_3), near the maximum T_c for $\text{YBa}_2\text{Cu}_3\text{O}_{7-\delta}$ of 92.6 K. The transition width from T_c onset to reach X'' maximum was ~ 0.2 K for 0.1 Oe applied field, and the overall transition was ~ 0.6 K.

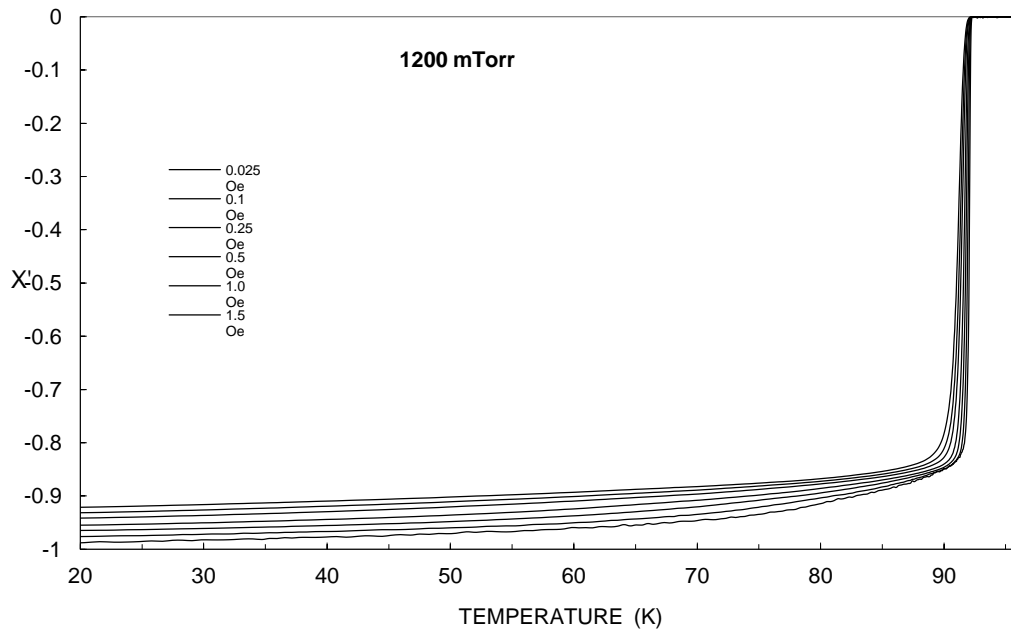


Figure 3.1.9.1

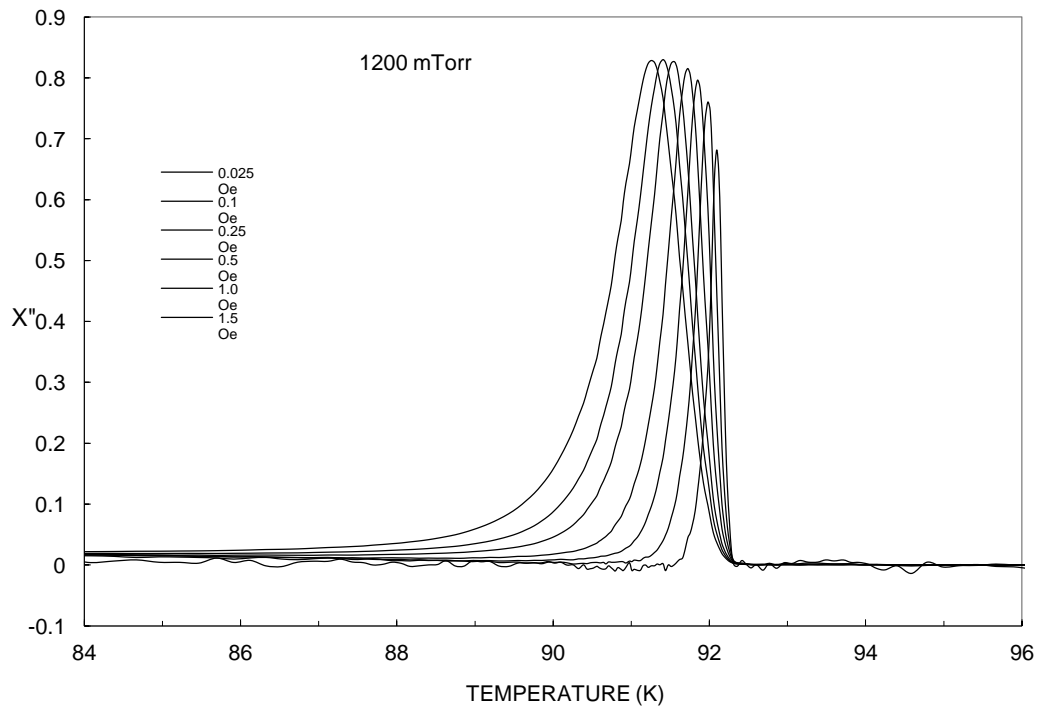


Figure 3.1.9.2

3.1.10 Hysteretic Loss

The loss per volume per cycle (no transport current) is:

$$\frac{Q}{V} \approx \frac{1}{10} d j_c H_0$$

where $d = 2a$ is the strip width, J_c is the current density, and H_0 is the field amplitude which is large compared to H_p , the full penetration field. [units are cgs-practical (A, cm, Oe)]

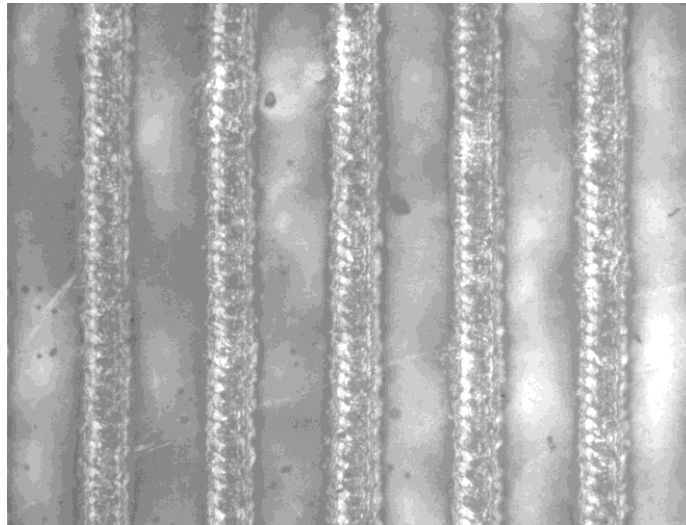


Figure 3.1.10.1

3.1.11 Loss Reduction

From magnetization measurements, the hysteretic loss is the area of the M-H loop:

$$Q_h = \int M dH$$

A significant reduction in hysteretic loss occurs.

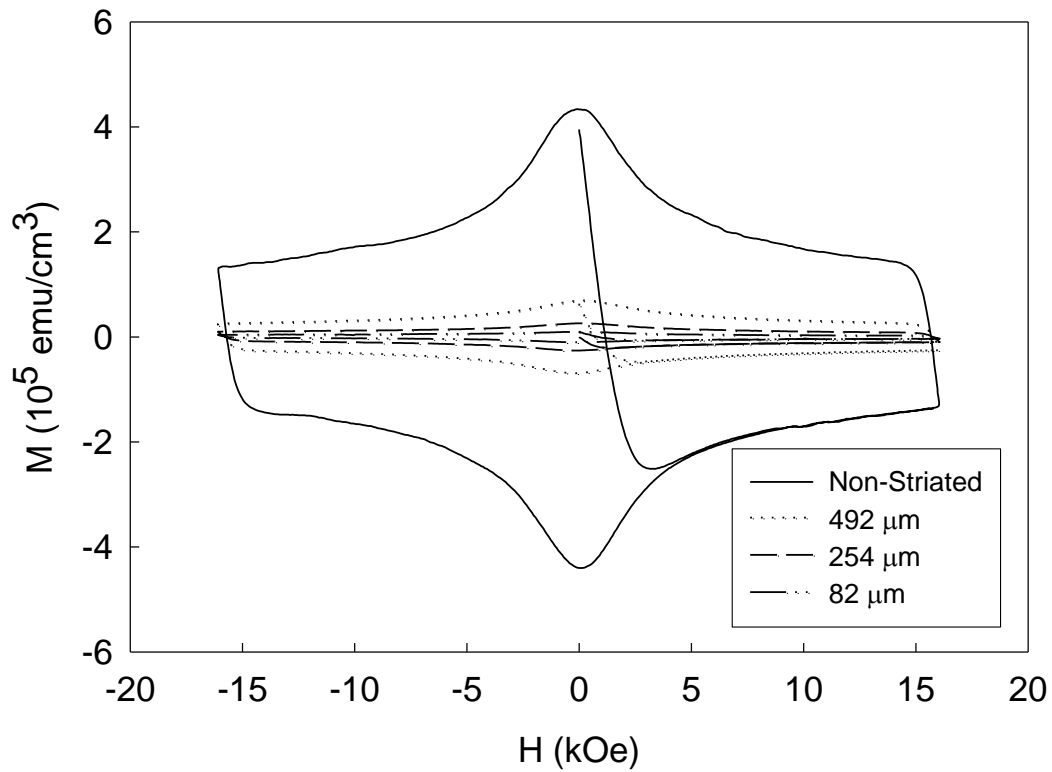


Figure 3.1.13.1

3.1.12 Effective Filament Width

Profilometry was used to determine nominal filament width, d_{nom} . The effective filament width, d_{eff} , can be defined by the loss ratio. If re-deposited conductor does not degrade (or enhance) the current-carrying capability of the filament, d_{nom} should equal d_{eff} .

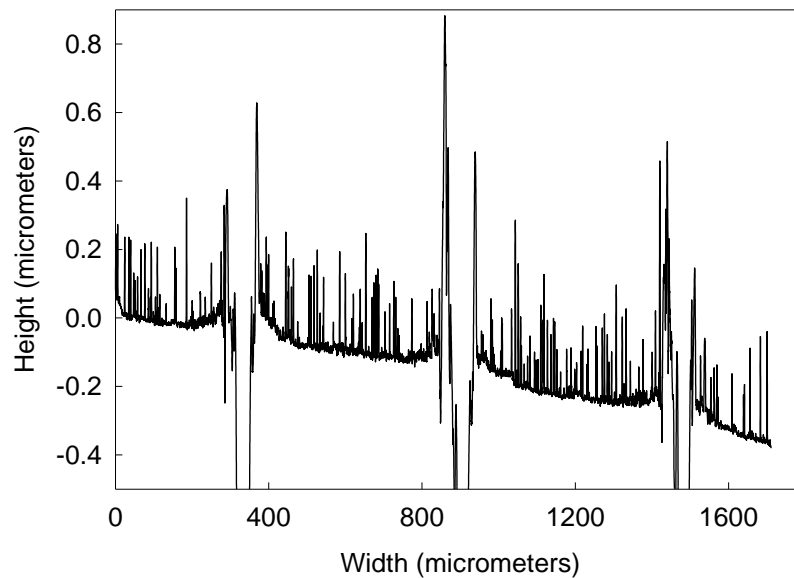


Figure 3.1.12.1

3.1.13 Validity of Hysteretic Loss Equation

The condition $H_0 \gg H_p$ is not really fulfilled.

- Even as low as $H_0 \approx 2 H_p$, equation (1) is roughly applicable with a prefactor

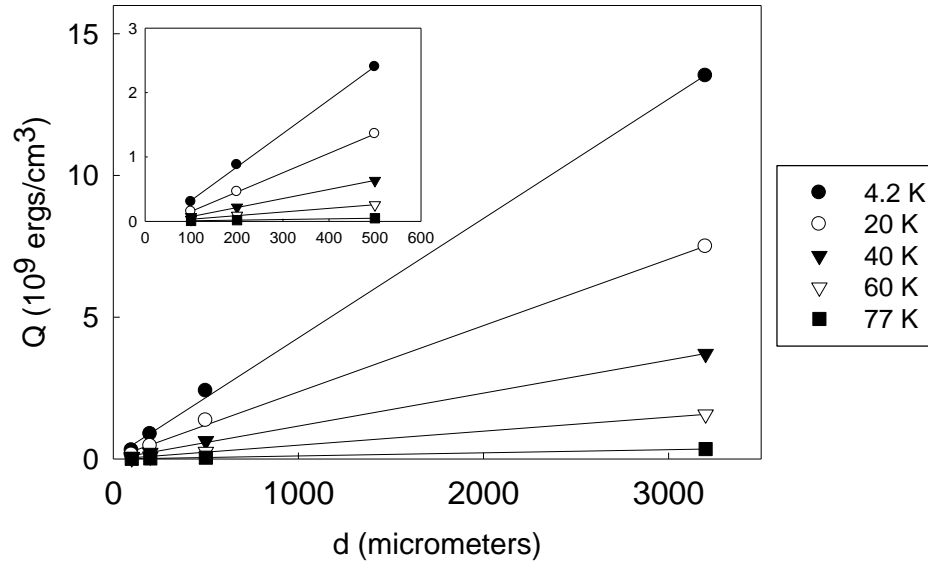


Figure 3.1.13.1

3.1.14 Hysteric Loss Normalized to Width

Normalizing the loss, Q_h , of each sample to filament width allows detection of even a small variation of loss with filament width. There is no clear evidence of deviation from linearity with d_{nom} of Eq. 1 -- variation in d_{nom} of individual filaments introduces sufficient noise that differences are not meaningful.

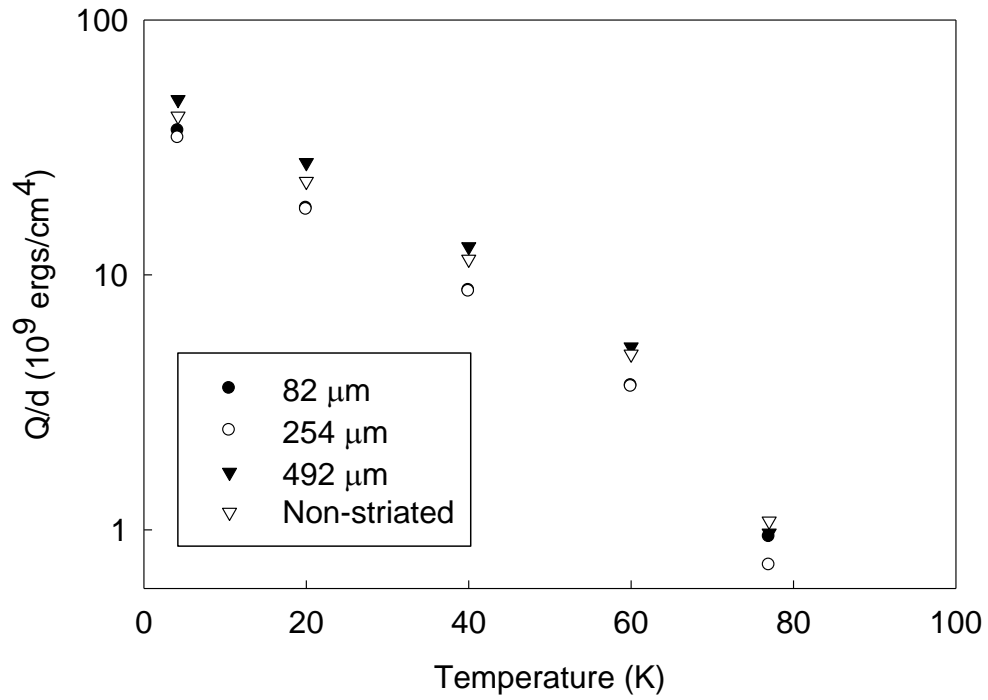


Figure 3.1.14.1

3.1.15 Effect of ablation on YBCO

The susceptibility curves for striated films are slightly shallower as compared to the transition of the non-striated film.

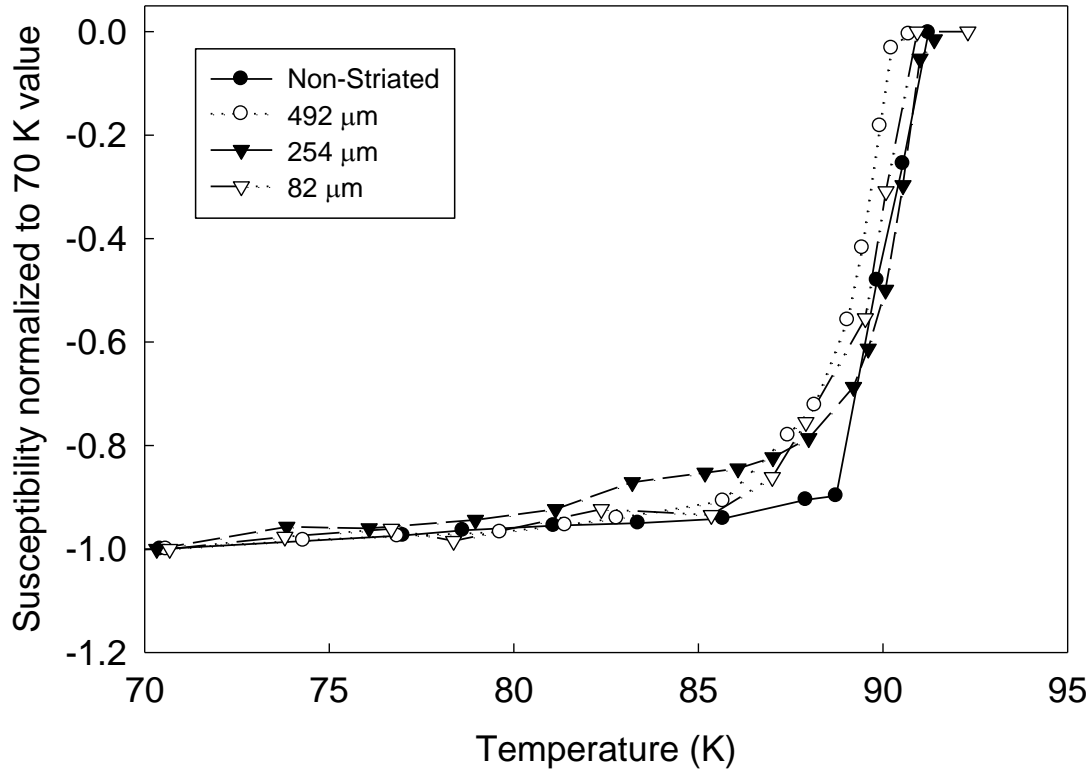


Figure 3.1.15.1

- Used VSM to measure DC susceptibility at a field of 2

3.1.16 Conclusions

Multifilamentary YBCO on LAO was created for reducing hysteretic loss. Upon testing, it was shown that the hysteretic losses decreased linearly with decreasing YBCO filament width. This *remained approximately true* even though the field amplitude was not always large compared to the full penetration field.

3.2 Magnetization losses in multiply connected coated superconductors

References: 25, 26, 27, 28, 29, 30, 31, 32

G. A. Levin and P. N. Barnes,

Superconductivity Group, Propulsion Directorate, Air Force Research Laboratory, Wright-Patterson AFB, Ohio USA

N. Amemiya, S. Kasai, K. Yoda and Z. Jiang

Faculty of Engineering, Yokohama National University, 79-5 Tokiwadai, Hodogaya, Yokohama 240-8501, Japan

Presented at Oak Ridge 2004

3.2.1 Motivation for introduction of multiply connected coated superconductors

- Wide (uniform) coated superconductors incurred large losses when subjected to time-varying magnetic field.
- Dividing the wide tape into many parallel stripes segregated by non-superconducting barriers allows reduction of losses.
- However, lack of current sharing between the superconducting filaments makes the conductor vulnerable to defects, so that a single blockage can impede the flow of transport current through the whole length of a given filament. This may lead to cumulative degradation of the current-carrying capacity of the long conductors.
- In multiply connected superconducting tapes a sparse network of superconducting bridges, which allows for current sharing, connects the filaments. The trade-off between the different types of losses and the connectivity requirement imposes restrictions on the properties of the network of bridges.

3.2.2 Objectives

Comparison of the magnetization losses in four samples of coated superconductors:

- 1) wide (uniform) tape
- 2) multifilament tape without current sharing, and
- 3) two different types of multiply connected superconducting tapes.

3.2.3 Experimental

- 10x1 cm uniform samples were cut from one 61 cm long tape with the "end-to-end" critical current of 173 A provided by Superpower Inc.
- 20-filament, simply- and multiply connected samples were made by laser ablation.
- A sample was placed inside the bore of a dipole magnet that generated time-varying magnetic field. The entire system was cooled in liquid nitrogen. The magnetization loss was measured using a linked pick-up coil. In the experiment, the frequency was varied from 13.1 to 171.0 Hz.

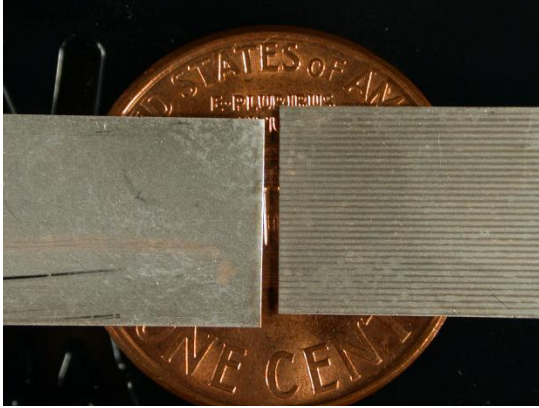


Figure 3.2.3.1

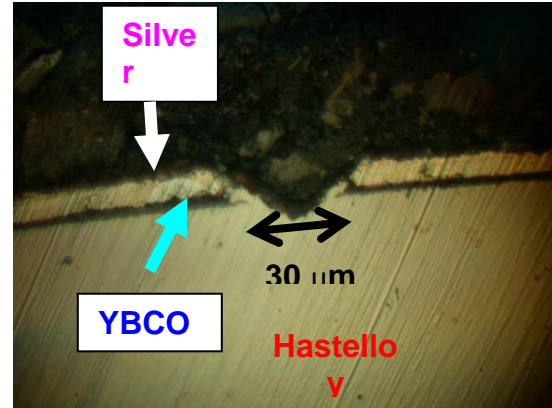


Figure 3.2.3.2

Left: One cm wide control (uniform) coated superconductor and 33-filament striated sample shown side by side. *Right:* Microphotograph of the cross-section of the striated sample in the groove area. The Hastelloy substrate, YBCO and silver layers are indicated.

3.2.4 Role of defects

The worst defect cluster is defined as a line of defects (misaligned grains perhaps) that maximally blocks the flow of transport current.

$$I_c(L) \approx I_c(0)(1 - \gamma \ln(LW/d_0^2))$$

Here $I_c(L)$ is an “end-to-end” critical current and its logarithmic decay with length is determined by the increasing probability of appearance of greater and greater worst defect cluster.

In the N-filament (striated) tape, Fig. 3.2.4.1 (b), the “end-to-end” critical current decays much more rapidly

$$I_c^{st}(L) = I_c(0)(1 - \gamma N \ln(LW/Nd_0^2))$$

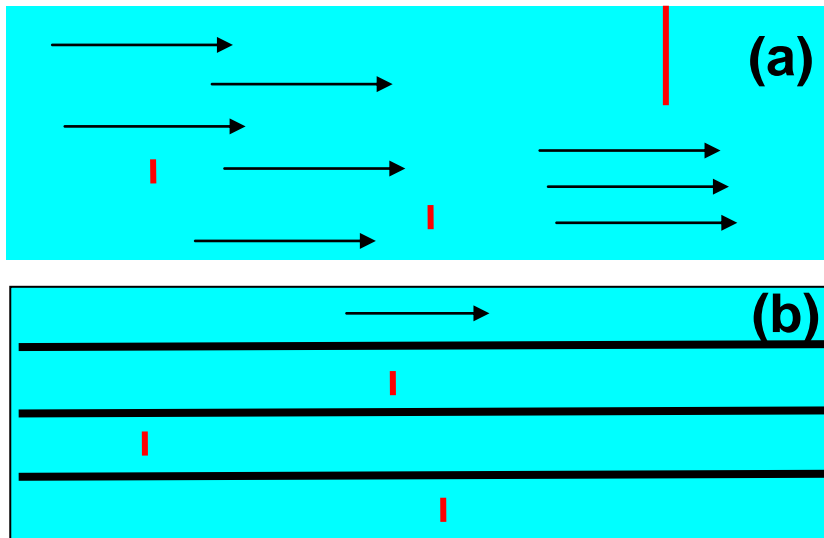


Figure 3.2.4.1

(a) Sketch of a uniform superconducting tape with the “worst-defect-clusters” (vertical red lines) blocking the flow of transport current.

(b) Sketch of a multifilament tape with worst-defect-clusters. The horizontal lines indicate non superconducting barriers.

3.2.5 Magnetization losses (L2,L3,L4,

Hysteresis loss in multifilament tape (power loss per meter length):

$$Q_h^{st} = I_c W_n (B - B'_c) f$$

$$\text{Coupling losses: } Q_n^{st} \propto \rho^{-1} |E_\perp|^2 d_n W = \kappa \frac{(BfL)^2}{\rho} d_n W$$

$$\text{Total loss: } Q = Q_h^{st} + Q_n^{st} \equiv \Lambda I_c (Bf)$$

Here Λ is defined as the power loss per unit length, per unit of the critical current, per unit of the sweep rate. It has the dimensionality of length, since $1 \text{ mJ}/(\text{A T m}) = 1 \text{ mm}$.

$$\Lambda = \lambda_1 + \lambda_2 (Bf)$$

$$\lambda_1 \approx W / N \quad \lambda_2 = 2 \frac{L^2}{\rho I_c} d_n W$$

3.2.6 Control sample

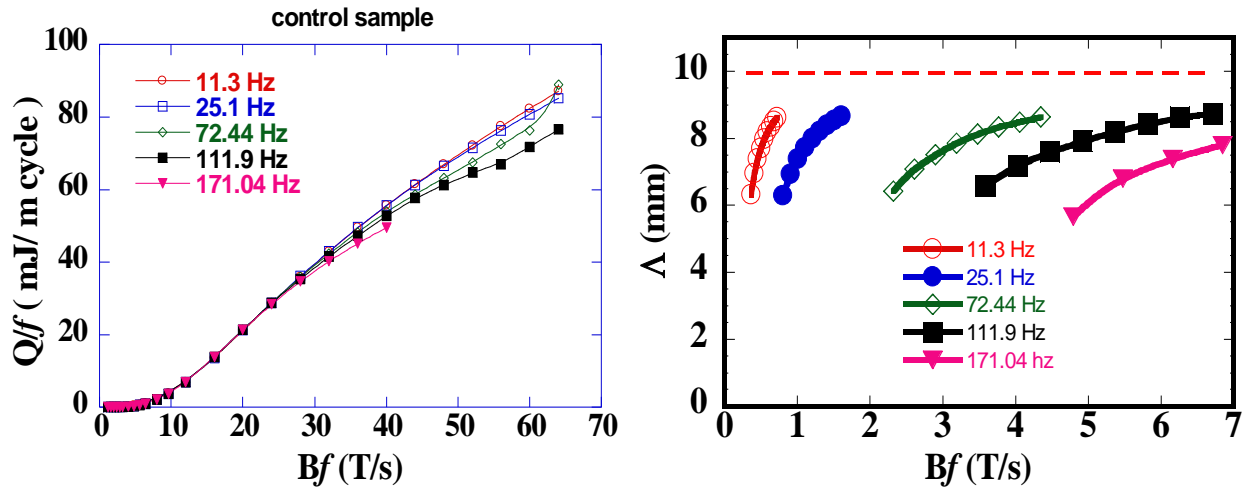
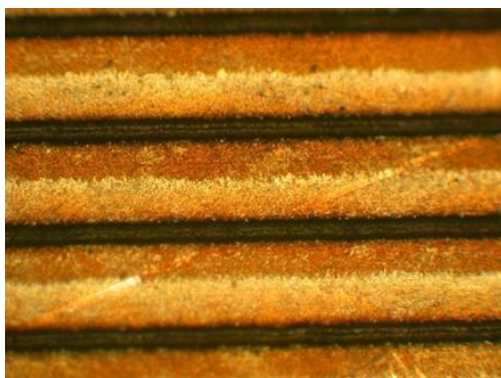


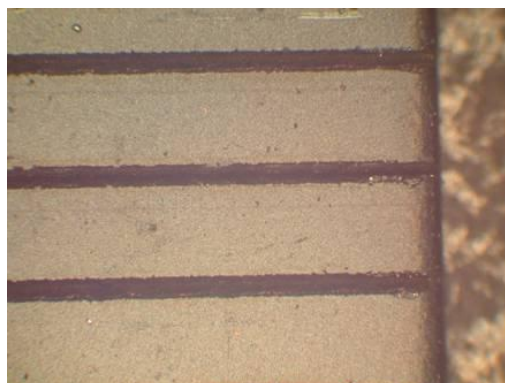
Figure 3.2.6.1

Left: Energy loss in the uniform sample per unit length, per cycle at five different frequencies, from 13.1 to 171 Hz, plotted vs amplitude of the applied magnetic field. *Right:* the specific loss vs sweep rate in a uniform tape.

3.2.7 20-filament without current sharing



20-filament sample;



20-filament sample; silver removed,
YBCO exposed.

Figure 3.2.7.1

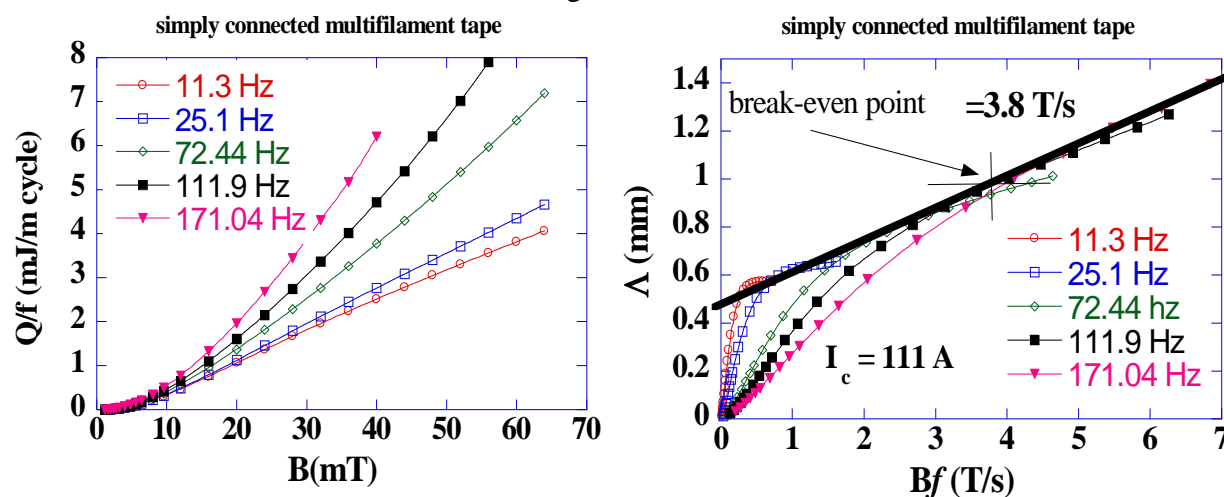


Figure 3.2.7.2

Left: The energy loss per cycle in the 20-filament sample, plotted vs field amplitude. *Right:* The specific loss L in mm vs sweep rate. The loss data were normalized by a constant value of transport current $I_c = 111$ A. Crossed lines in the center indicate the break-even point, where the coupling losses are equal to hysteresis loss.

3.2.8 Fishnet Pattern

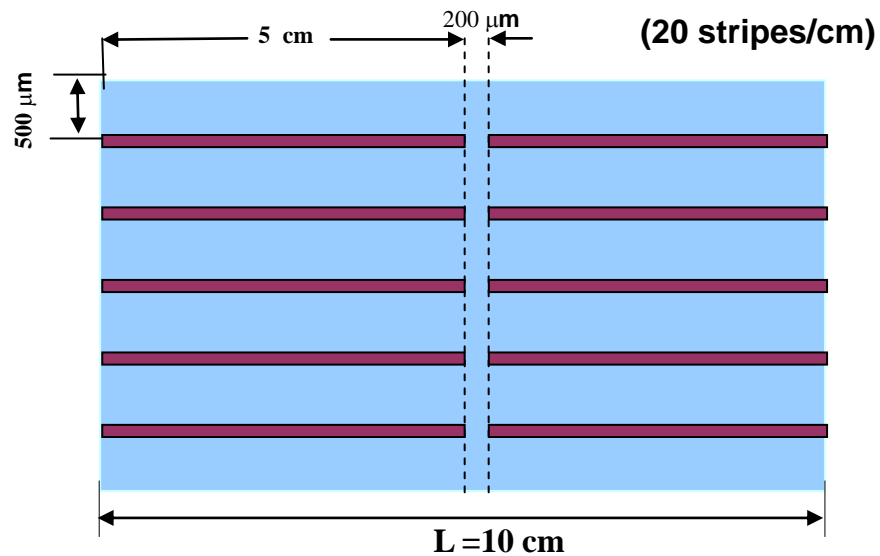


Figure 3.2.8.1

Sketch of a multiply connected 20-stripes sample ("fishnet" pattern). All superconducting stripes are connected by a single bridge in the center.

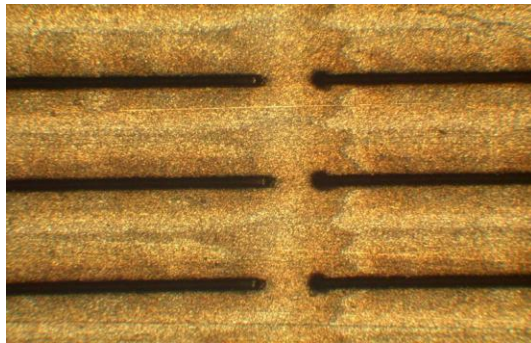


Figure 3.2.8.2

Area around the bridge in the actual sample. The grooves are made by laser ablation.

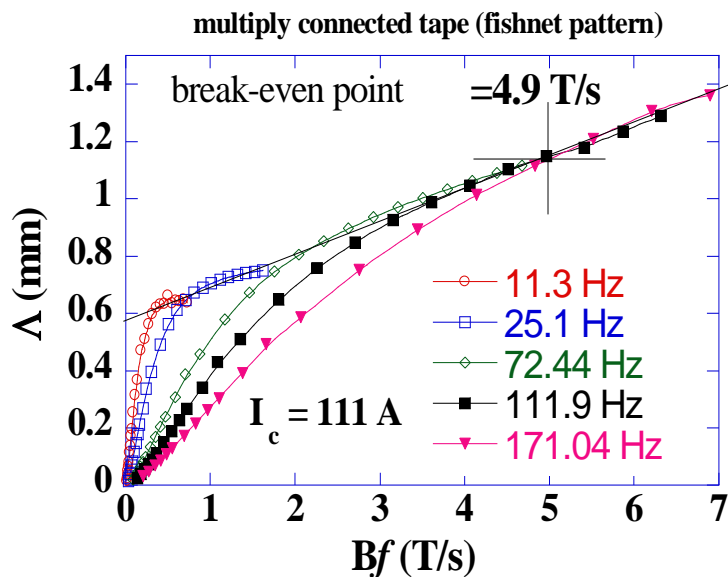


Figure 3.2.8.3

The specific loss L in mm vs sweep rate for multiply connected (fishnet) pattern. The loss data are normalized by a constant value of transport current $I_c=111$ A. Crossed lines in the center indicate the break-even point, where the coupling losses are equal to hysteresis loss.

3.2.9 Brickwall Pattern

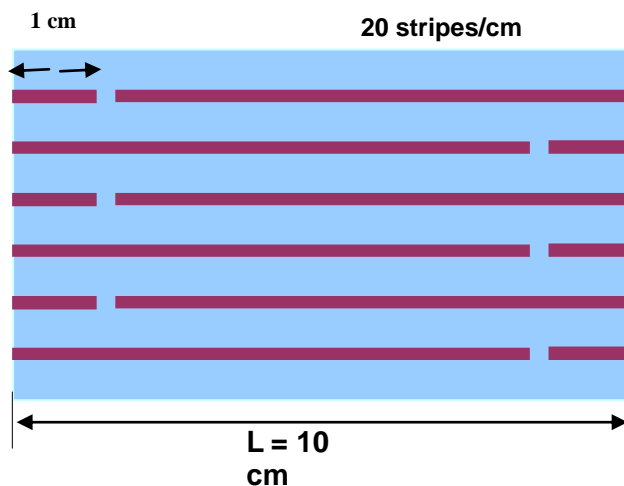


Figure 3.2.9.1

Sketch of a multiply connected 20-stripes sample (“brickwall” pattern). Each superconducting stripes is connected to the neighboring stripes by alternating bridges located near the ends of the sample.

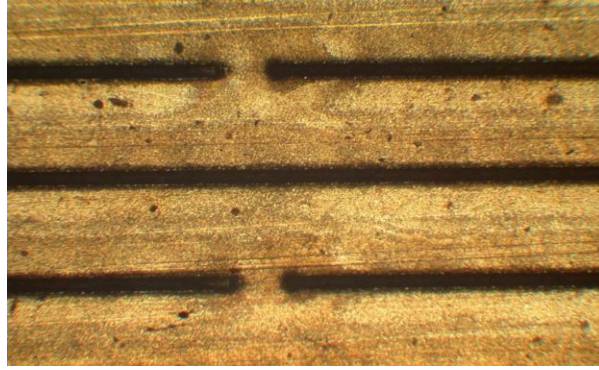


Figure 3.2.9.2

Area around the bridges in the actual sample. The grooves are made by laser ablation.

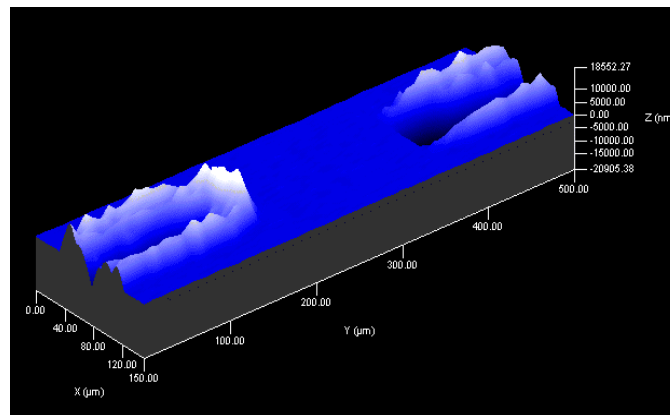


Figure 3.2.9.3

Profile of a bridge between two stripes.

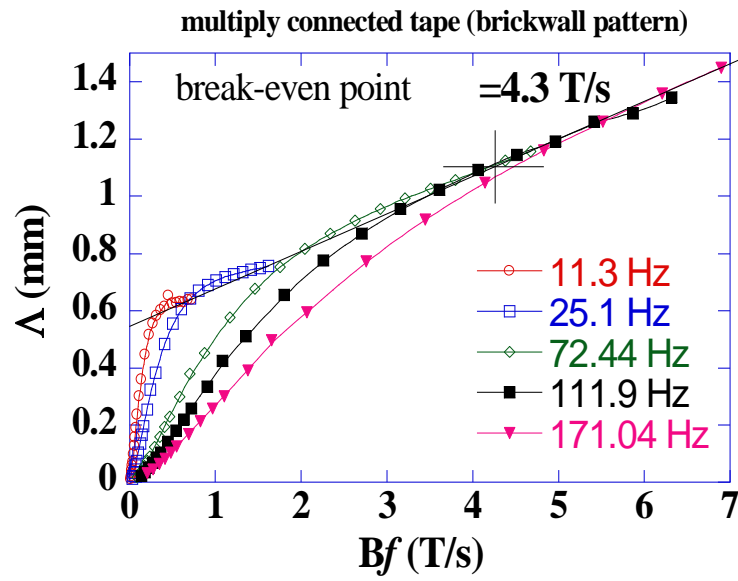


Figure 3.2.9.4

The specific loss L in mm vs sweep rate for multiply connected (brickwall) pattern. The loss data are normalized by a constant value of transport current $I_c=111$ A. Crossed lines in the center indicate the break-even point, where the coupling losses are equal to hysteresis loss.

3.2.10 Summary

- Multifilament tapes have substantially lower losses than the wide uniform tapes at sweep rates of several T/s.
- Multiply connected tapes can allow scale-up the manufacturing of long multifilament tapes without increasing substantially the level of losses.
- Scaling, L vs Bf , allows us to determine the intrinsic parameters l_1 and l_2 and predict what the losses will be outside the envelope of accessible values of the amplitude of applied field and frequency.

3.3 Reduction of Coupling Losses in Superconductor – Resistor – Superconductor (Hybrid) Wires

References: 25, 26, 27, 28, 29, 30, 31, 32

George A. Levin, P. N. Barnes, Srinivas Sathiraju

*National Research Council, Superconductivity Group/Power Systems, Propulsion Directorate,
Air Force Research Laboratory*

M. Sumption, Anjan Contractor, S. Kawabata*

Ohio State University, Columbus, Ohio

* *Kagoshima University, Kagoshima, Japan*

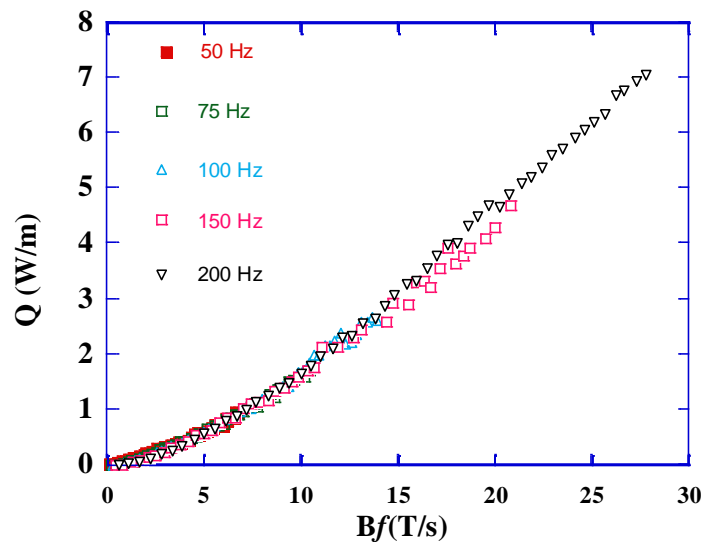
AFOSR 2005, January 24-26, 2005

3.3.1 Outline

- Losses in multifilament coated superconductors. Coupling losses as a major problem.
- Superconductor – Resistor – Superconductor hybrid: potential benefit - minimization of the total loss.
- Estimates of effectiveness of such contraptions.
- Toy model.

3.3.2 Sweep rate dependence of power loss

**Sample:
4 cm long
1 cm wide
20
filaments**



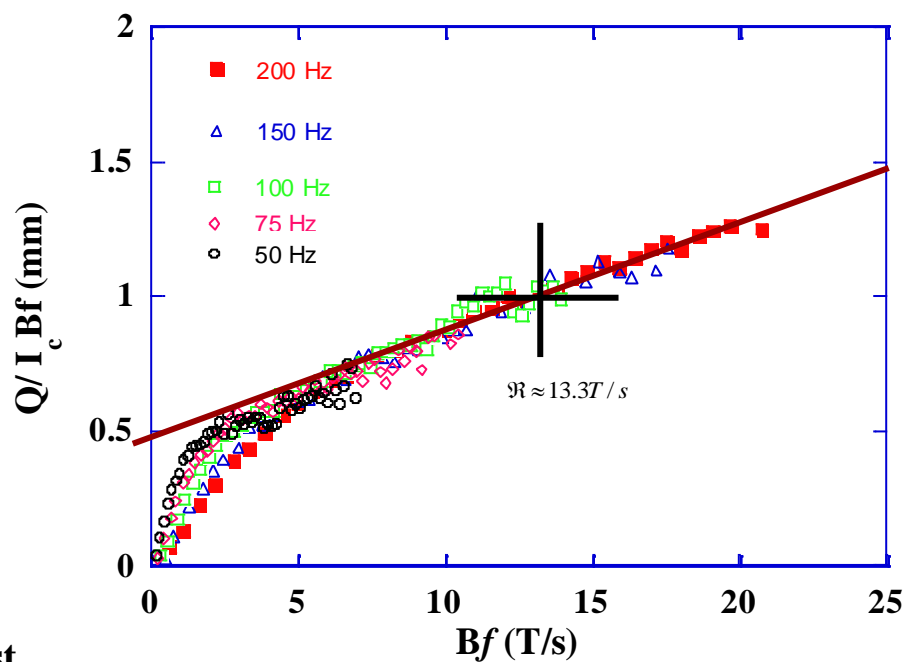
**B - amplitude of applied
field**

**Bf – sweep
rate**

Figure 3.3.2.1

3.3.3 Specific Loss

$I_c = 190 \text{ A}$
 $\lambda_1 = 0.5 \text{ mm}$
 $\mathcal{R} = 13.3 \text{ T/s}$
 for 8 cm twist
 pitch



$$\frac{Q}{I_c B f} = \lambda_1 \left(1 + \frac{B f}{\mathcal{R}} \right) \quad \lambda_1 \approx W_n$$

Figure 3.3.3.1

3.3.4 Coupling Loss

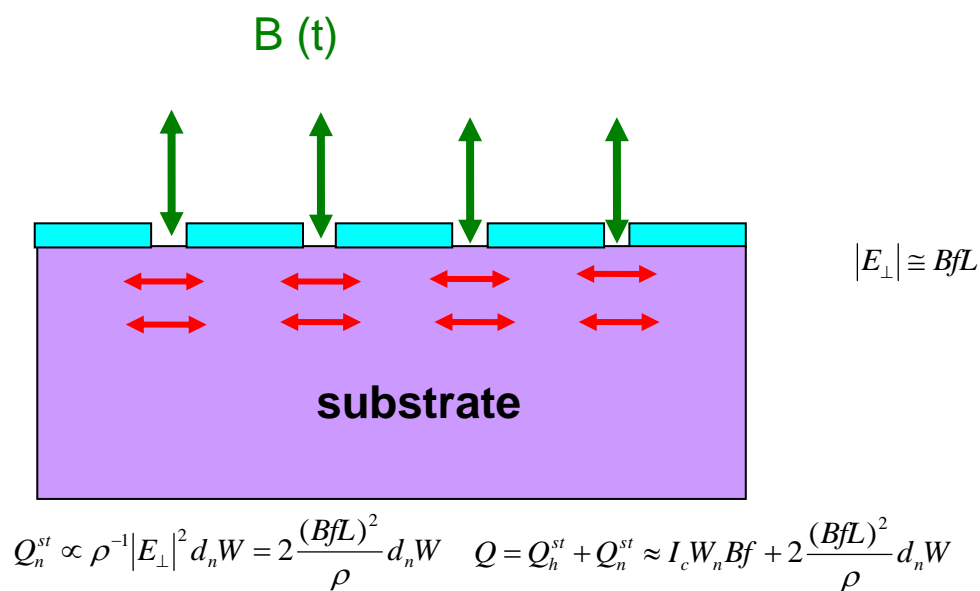


Figure 3.3.4.1

3.3.5 Break-even sweep rate and twist pitch

$$Q = Q_h^{st} + Q_n^{st} \approx I_c W_n Bf + 2 \frac{(BfL)^2}{\rho} d_n W$$

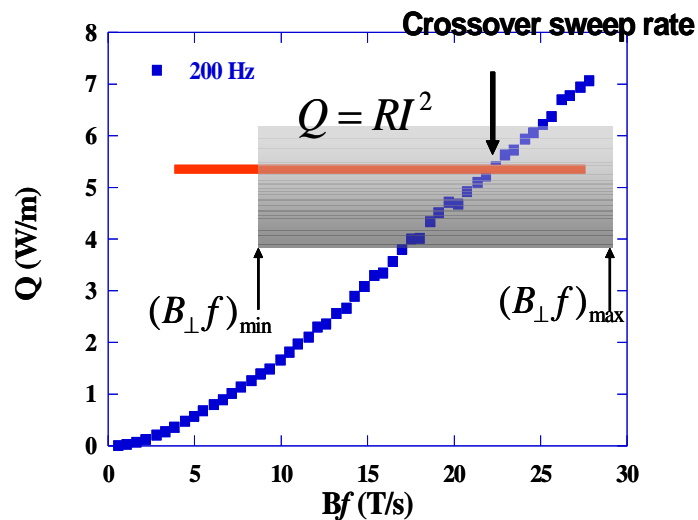
$$Q = W_n I_c \left(1 + \frac{Bf}{\Re} \right) Bf$$

$$\Re \propto \frac{w_n \rho I_c}{L^2 d_n W}$$

Operating sweep rate

$2L$ - twist pitch

3.3.6 Copper wire vs superconductor



At higher sweep rates copper (Litz) wire is more effective than superconductor.

Figure 3.3.6.1

3.3.7 Armature coil



Figure 3.3.7.1

3.3.8 Hyperconductor - superconductor hybrid

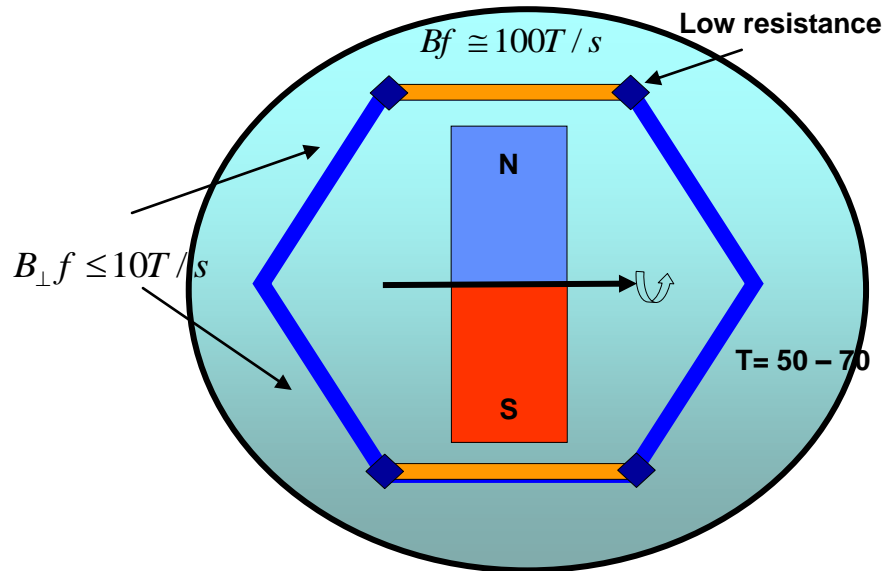


Figure 3.3.8.1

3.3.9 Goals

For the foreseeable future the Litz wire will remain superior to a superconductor in the magnetic environment characterized by the sweep rate of the order of 100 Tesla/s.

“Realistic” goal:

A superconductor that is superior, by a substantial margin, to copper wire at cryogenic temperature at the sweep rate of the order of 10 Tesla/s.

$JE > 10 \text{ kA/cm}^2$

$$\frac{Q}{I_{tr}} \leq 1 \frac{\text{mW}}{\text{A} \cdot \text{m}} \quad \text{at operating sweep rate } B_{\perp} f \leq 10 \text{ T/s}$$

3.3.10 Superconductor Parameters

$$Q = W_n I_c \left(1 + \frac{Bf}{\Re} \right) Bf$$

$$\frac{Q}{I_c} \leq 1 \frac{mW}{A \cdot m}$$

$$B_{\perp} f \leq 10 T/s$$

$$\left\{ \begin{array}{l} W_n = 50 \mu m \quad (200 \text{ stripes/cm}) \\ \Re \approx 10 T/s \end{array} \right.$$

$$\Re \propto \frac{w_n \rho I_c}{L^2 d_n W}$$

Twist will not allow us to reach $J_E > 10 \text{ kA/cm}^2$

Is it possible to preserve flat (2D) architecture of coated conductors and still limit the coupling losses?

3.3.11 Hybrid conductors

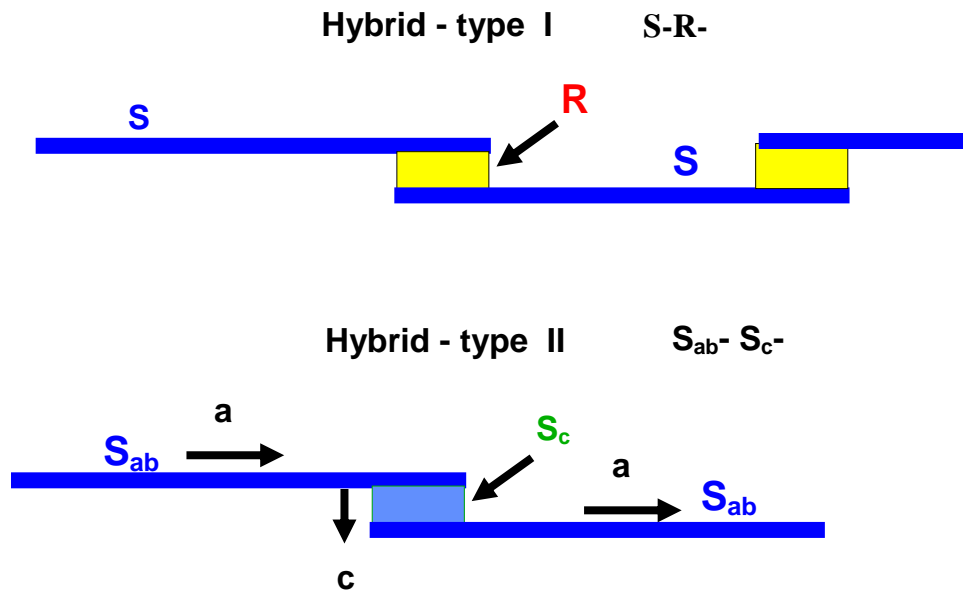


Figure 3.3.13.1

3.3.12 Toy Model

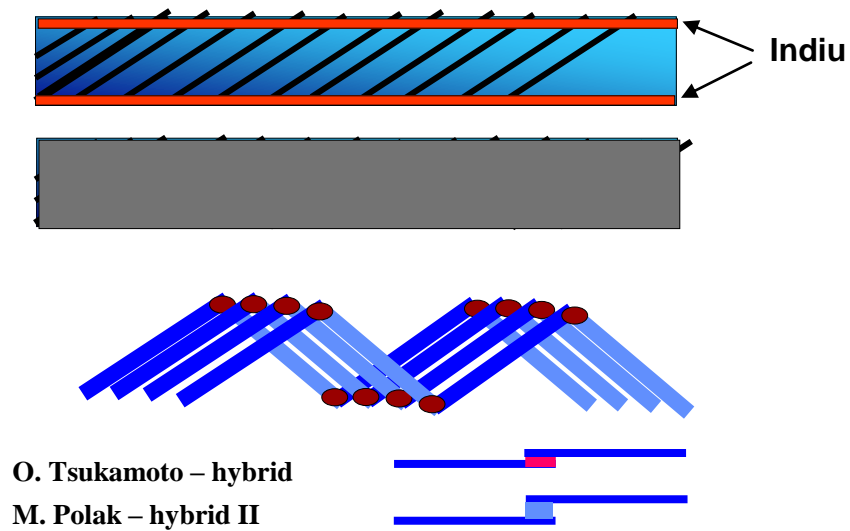


Figure 3.3.12.1

3.3.13 Conjugate conductors

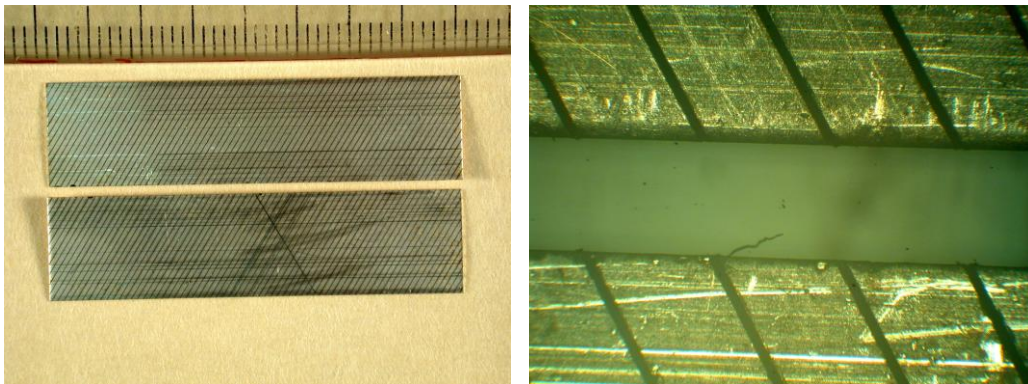


Figure 3.3.13.1

3.3.14 Power Losses

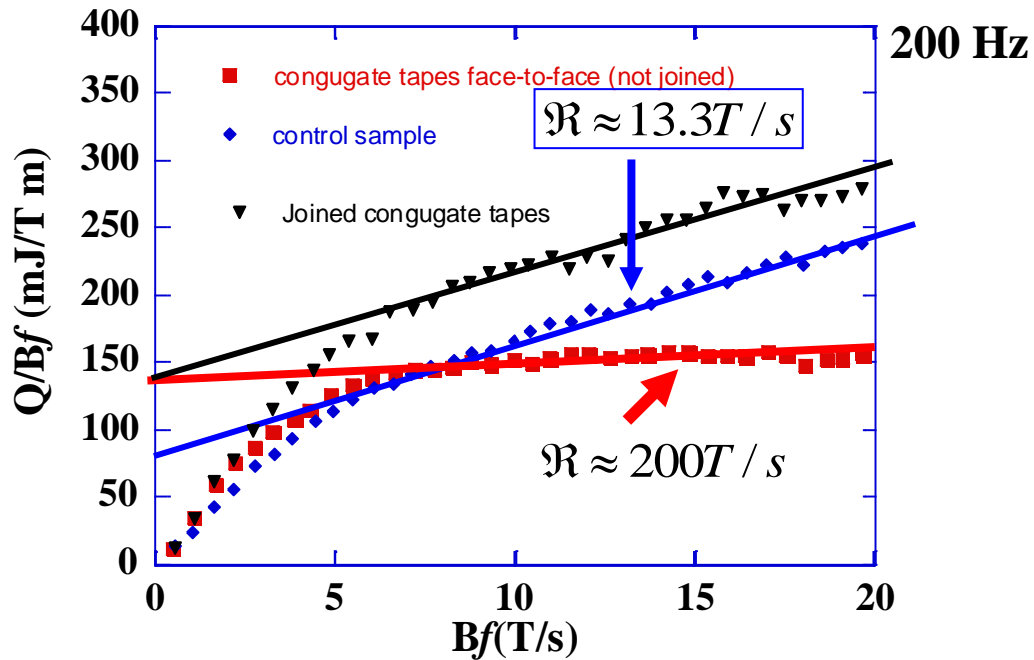


Figure 3.3.14.1

Disappointing but not unexpected outcome

Losses in the joints- To reduce the loss in the *Indium* layer, it should be as thin as possible and striated after it is deposited.

$$Q_n^{st} \propto 2 \frac{(BfL)^2}{\rho_s} d_n W + 2 \frac{(BfL)^2}{\rho_{ln}} d_{ln} \Delta$$

$$d_n \approx 75-100 \mu m;$$

$$W = 1cm$$

$$d_{ln} \approx 100 \mu m$$

$$\Delta = 1mm$$

$$\rho_{ln} \approx \frac{1}{100} \rho_s$$

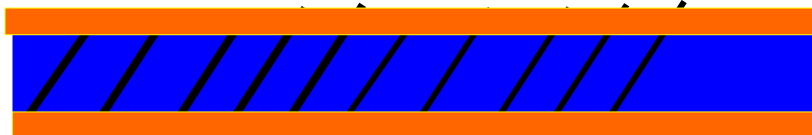


Figure 3.3.14.2

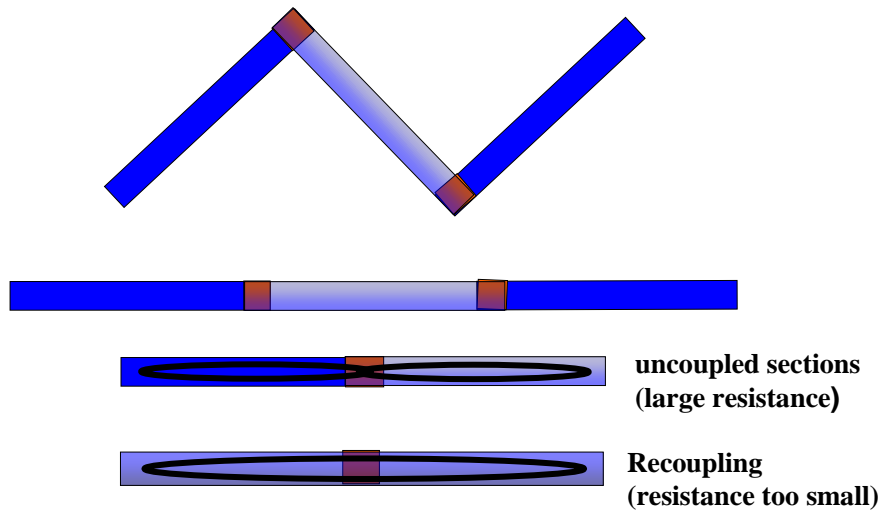


Figure 3.3.14.3

Stremlined version

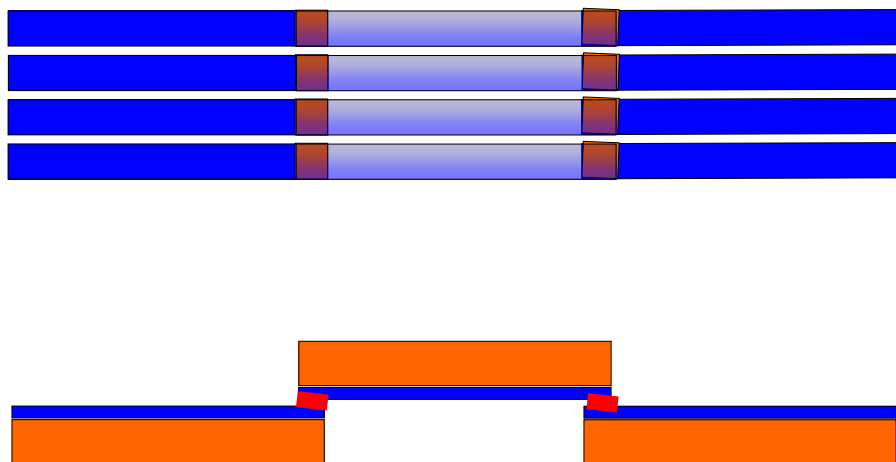


Figure 3.3.14.4

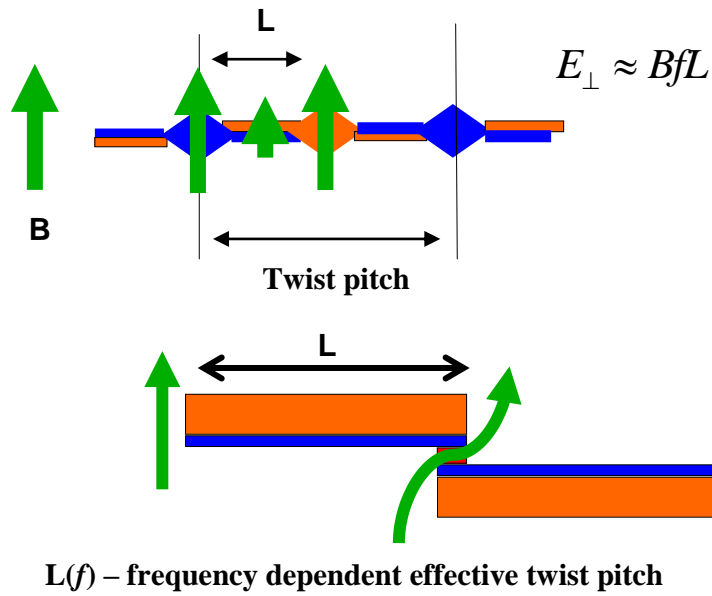


Figure 3.3.14.5

Another option

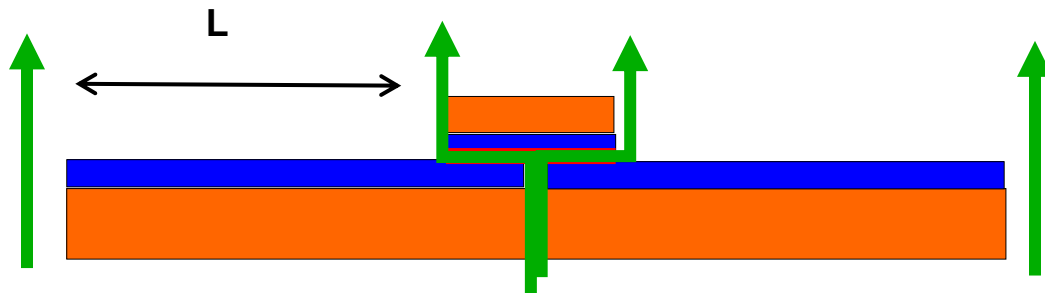


Figure 3.3.14.6

3.3.15 Conclusions

- Integration of copper and superconductor wires into a hybrid conductor may be successful in a number of applications.
- Additional work is needed to identify the promising options of hybrids and clarify the range of operational parameters.

3.4 AC losses in multifilament coated conductors; Hybrid conductor option

References: 25, 26, 27, 28, 29, 30, 31, 32

George A. Levin

*National Research Council, Superconductivity Group/Power Systems, Propulsion Directorate,
Air Force Research Laboratory*

P. N. Barnes, Srinivas Sathiraju

*Superconductivity Group, Propulsion Directorate, Air Force Research Laboratory, Wright-
Patterson AFB, Ohio*

M. Sumption, Anjan Contractor

Ohio State University, Columbus, Ohio

Wire Workshop January 2005

3.4.1 Outline

- Reduction of ac losses in multifilament coated superconductors (in external time-dependent magnetic field). Applications: transformers, armature windings for motors and generators.
- Generalization of the results of small scale experiments to practically important range of parameters.
- Superconductor – Resistor hybrid; potential benefit - minimization of the total power loss and weight reduction.

3.4.2 Reduction of Hysteresis Loss by Striation

Striation of superconducting tape allows to reduce the hysteresis loss. *W. J. Carr Jr. and C. E. Oberly (1999)*

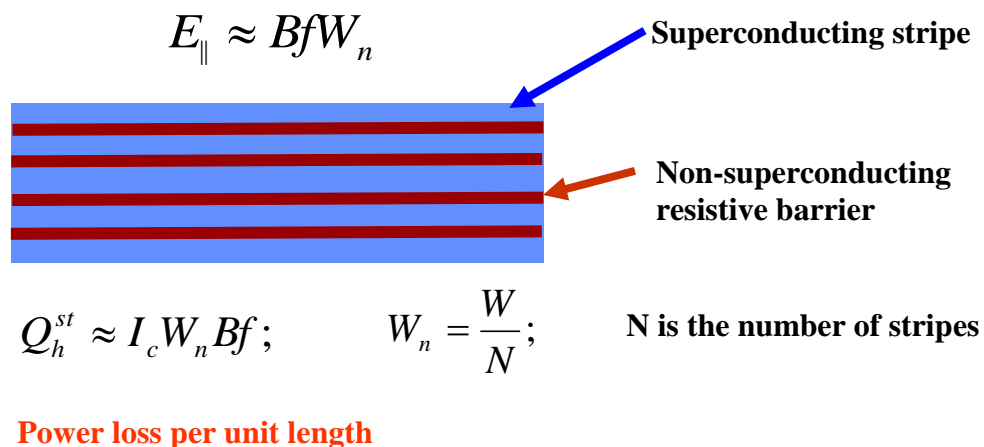


Figure 3.4.2.1

3.4.3 Power Loss

Power loss depends only on the sweep rate $B_{\perp}f$

Transformers: $B_{\perp} \approx 0.2T$; $f = 50 - 60Hz$

Low speed ship propulsion motors: $B_{\perp} \approx 1.5 - 2.5T$; $f = 4 - 5Hz$

$$B_{\perp}f \approx 10 - 12T/s$$

3.4.4 Summary

- In small scale, table-top experiments one can determine four parameters that determine ac losses in external field and reliably extrapolate the results to the practically important range of parameters inaccessible to the small scale tests.

3.4.5 Advantages of Hybrid Armature

- Total power loss can be lower than in either all-copper or all-superconductor armature.
- Armature coil weight can be about 1/3 of that of the all-copper coil.
- Resistivity of copper at 50 – 70 K is about an order of magnitude lower than at room temperature.
- The armature coil is assembled from relatively short pieces of superconductors and copper wires.
- An efficient process of making low resistance joints between copper wire and superconductor needs to be developed.

3.4.6 Conclusions

- Magnetization losses in multifilament superconductors can be measured in tabletop experiments and the results reliably extrapolated to practically important range of magnetic field - frequency.
- Reduction of the power loss in the armature coil might be possible with hyperconductor-superconductor hybrids.

3.5 Properties of Resistive Barriers Produced by Laser Micromachining in Coated Superconductors

G. A. Levin

Superconductivity Group, Propulsion Directorate, Air Force Research Laboratory, Wright-Patterson AFB

April 19, 2004

3.5.1 Architecture of Coated Superconductors

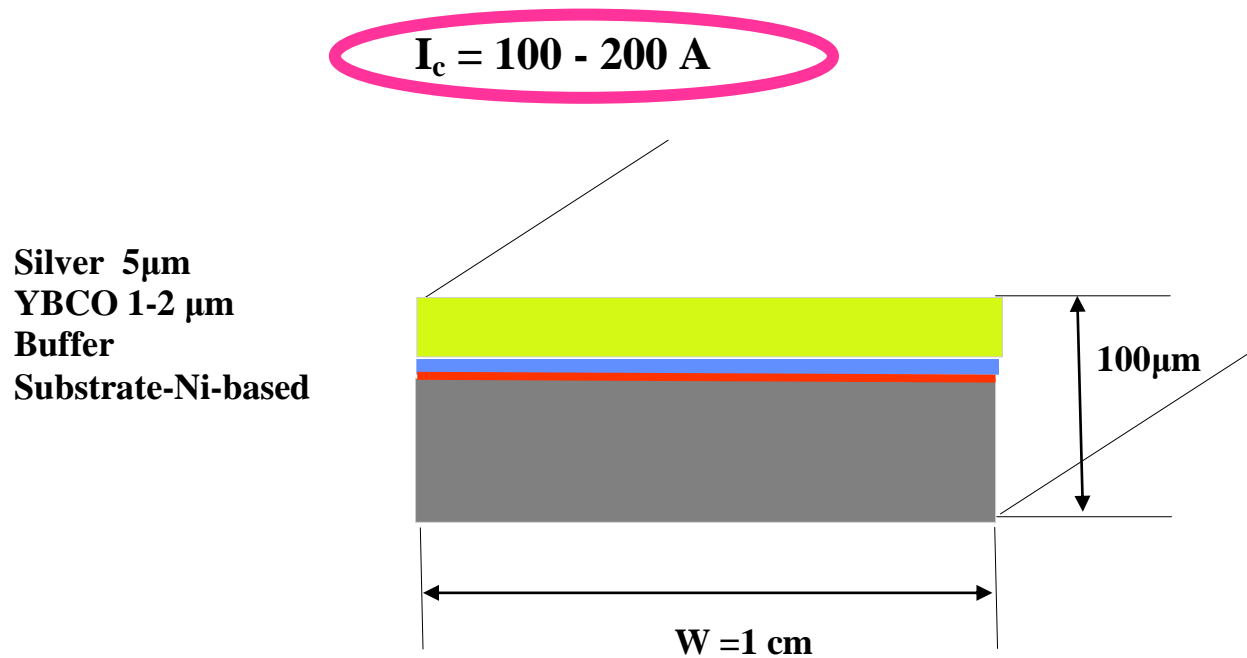


Figure 3.5.3.1

3.5.2 Hysteretic Losses in AC Magnetic Field

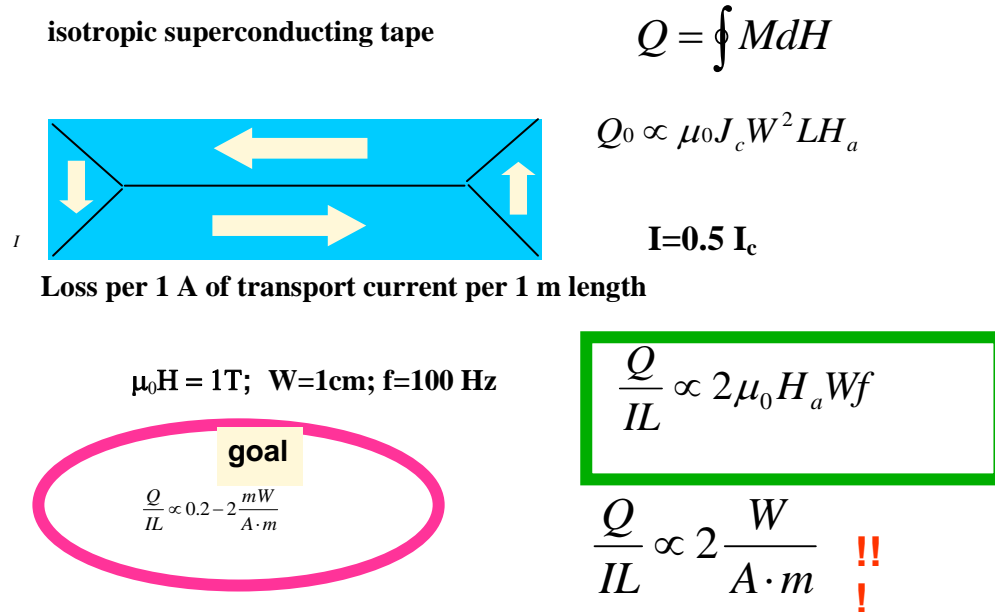
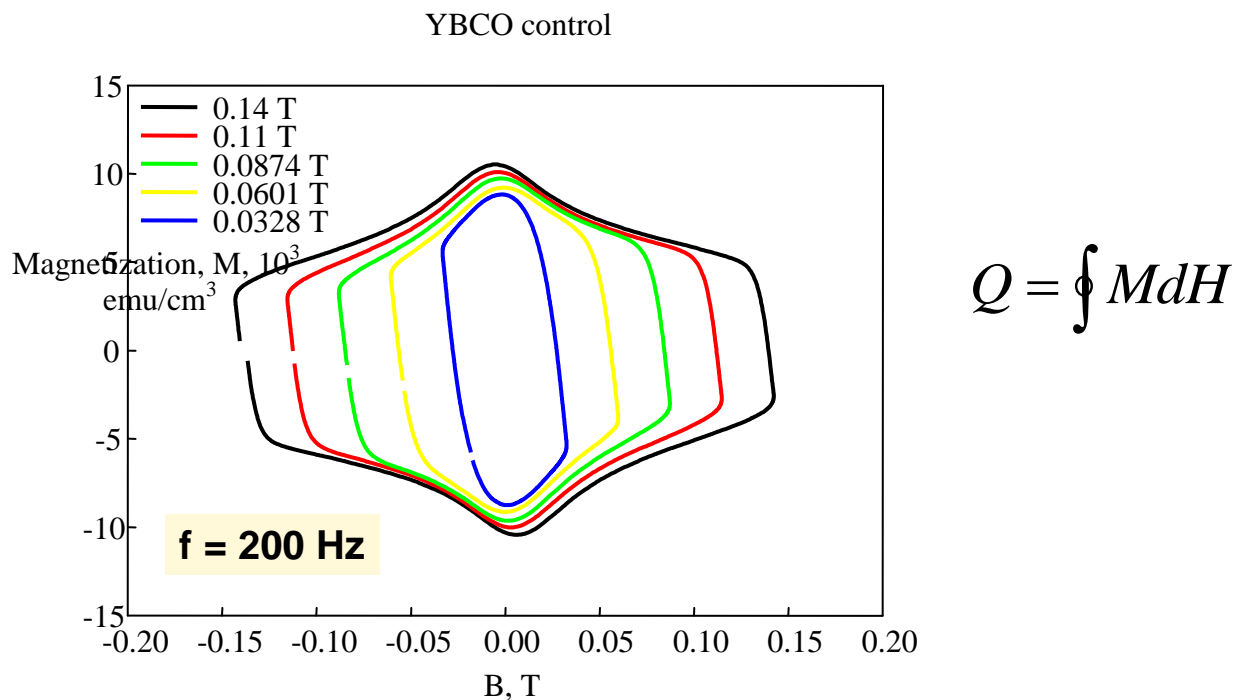


Figure 3.5.2.1

3.5.3 Hysteretic Losses in AC Magnetic Field



Hysteretic loops of 1x4 cm isotropic sample for different amplitude of ac magnetic field

Figure 3.5.3.1

3.5.4 Mechanism of Dissipation

Joule heating

$$Q = \oint M dH = \int_0^T dt \int (\vec{j} \cdot \vec{E}) dV$$

Normal metal $\vec{j} = \frac{\vec{E}}{\rho}$

superconductor $|\vec{j}| \approx j_c \approx 10^7 - 10^6 \text{ A/cm}^2$

Resistivity of copper at T=77 K:

$$\rho = 0.2 \times 10^{-6} \Omega \cdot \text{cm}$$

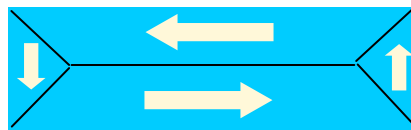
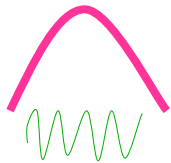
$$E \approx 10 \frac{\text{mV}}{\text{cm}} \quad j \approx \frac{10^{-2} \text{ V/cm}}{0.2 \times 10^{-6} \Omega \cdot \text{cm}} = 5 \times 10^4 \frac{\text{A}}{\text{cm}^2}$$

Figure 3.5.4.1

3.5.5 Origin of Electric Field

$$\nabla \times \vec{E} = -\dot{\vec{B}}$$

$$\left| \frac{\partial E_x}{\partial y} \right| \propto \dot{B}$$



$$E_x \propto \dot{B} w \approx B f w$$

$$E_x \propto \dot{B} w \approx B f \Delta l$$

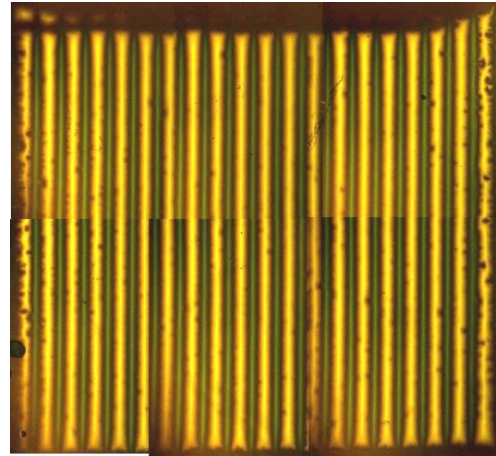
Figure 3.5.5.1

3.5.6 Magneto-optical images



$$E_x \propto \dot{B}W \approx BfW$$

$$Q_0 \propto j_c E$$



$$E_x \approx Bf\Delta l \approx Bf \frac{W}{N}$$

$$Q_{str} \propto j_c \frac{E}{N} \approx \frac{Q_0}{N}$$

Figure 3.5.6.1

3.5.7 Striated Samples

20 stripes/cm



40 stripes/cm

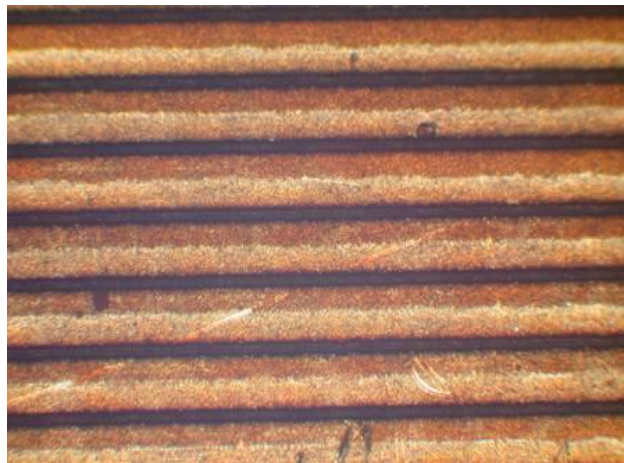


Figure 3.5.7.1

The top layer is silver. Its brown color is due to residue (Ni, YBCO) thrown out from the trenches by laser ablation.

3.5.8 Post-mortem images

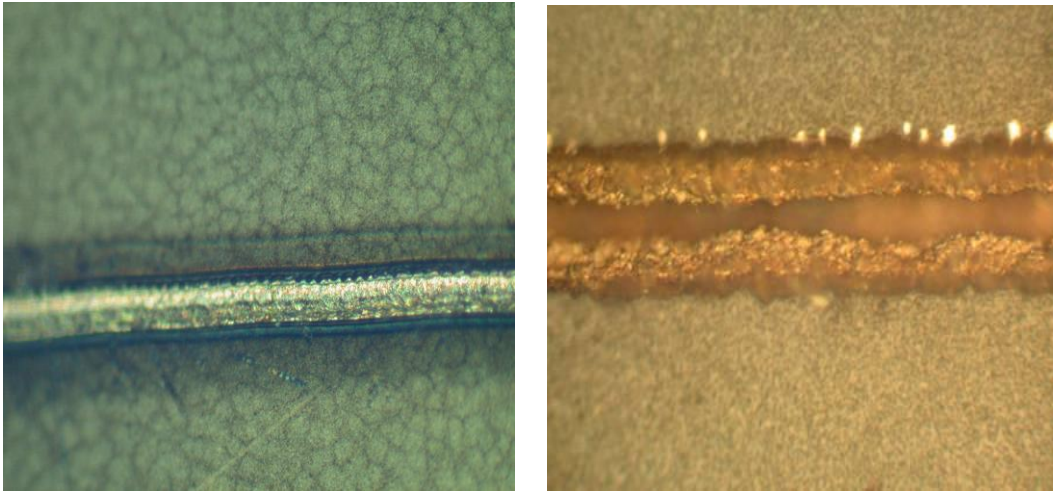
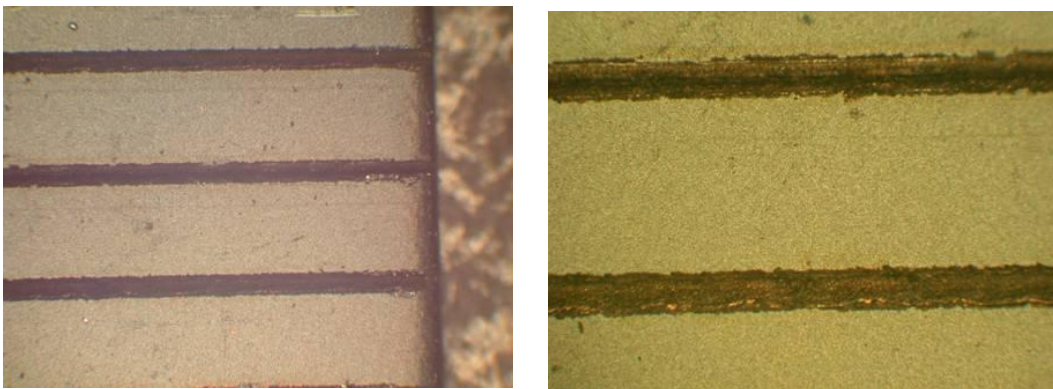


Figure 3.5.8.1

Silver is etched away, exposing the YBCO layer.



YBCO stripes

Figure 3.5.8.2

3.5.9 Barrier resistance

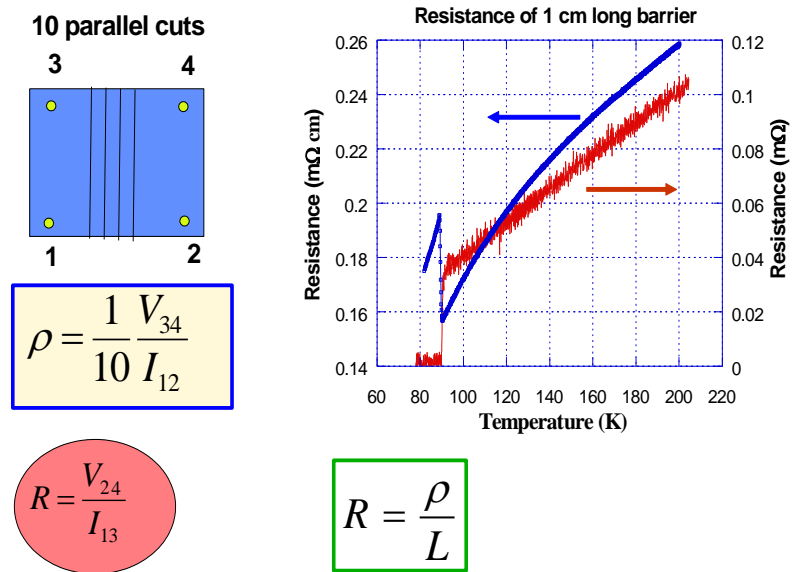


Figure 3.5.9.1

3.5.10 Profile of the barrier

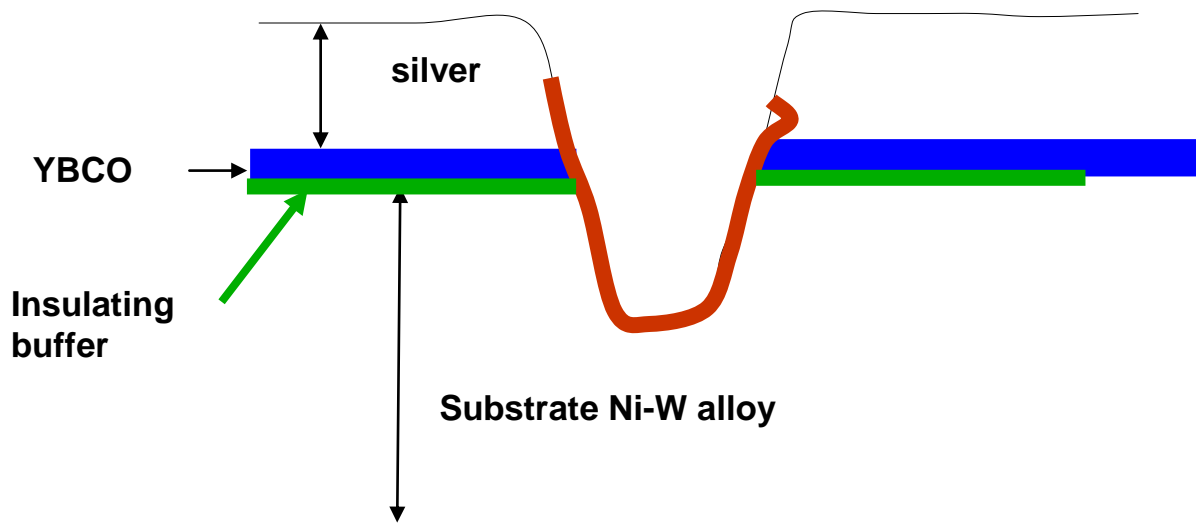


Figure 3.5.10.1

3.6 AC Loss Reduction: AFRL In-house Research

References: 25, 26, 27, 28, 29, 30, 31, 32

Paul N. Barnes, Rama Nekkanti, Timothy A. Campbell, C. Brent Cobb, George A. Levin, Michael D. Sumption¹

Air Force Research Laboratory

1. Ohio State University

Presented by Paul N. Barnes, PhD at AFOSR 2004, January 19-21, 2004

Superconductivity Team Leader, Propulsion Directorate, Air Force Research Laboratory

3.6.1 Substrate Induced Striations

- Induce striations into the HTS layer by affecting the substrate and destroying subsequent epitaxial growth
 - Will result in weakly linked YBCO filaments which increases hysteretic loss experienced
 - Enable current sharing between links to circumvent filament current blockages
- LAO substrate prepared for PLD YBCO deposition to test ability to induce low J_c striations
- Critical currents measured across control bridge and bridge over scratched substrate

3.6.2 Test Bridges

- $I_c = 1.8$ A across the unaffected bridge
- $I_c = 0.5$ A across the scratched substrate
 - Indicates I_c of weakest link; uniformity not considered

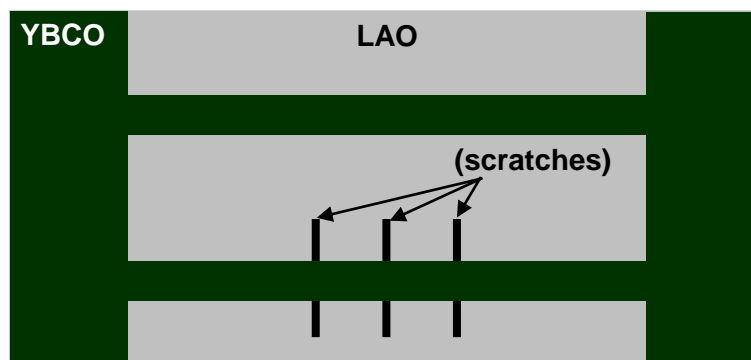


Figure 3.6.2.1

3.6.3 Weakly Linked Filaments

- Weak link superconducting connection may be achieved by
 - Continuous low J_c striations as displayed below
 - Discontinuous bridges linking filaments (refer to George Levin's talk)

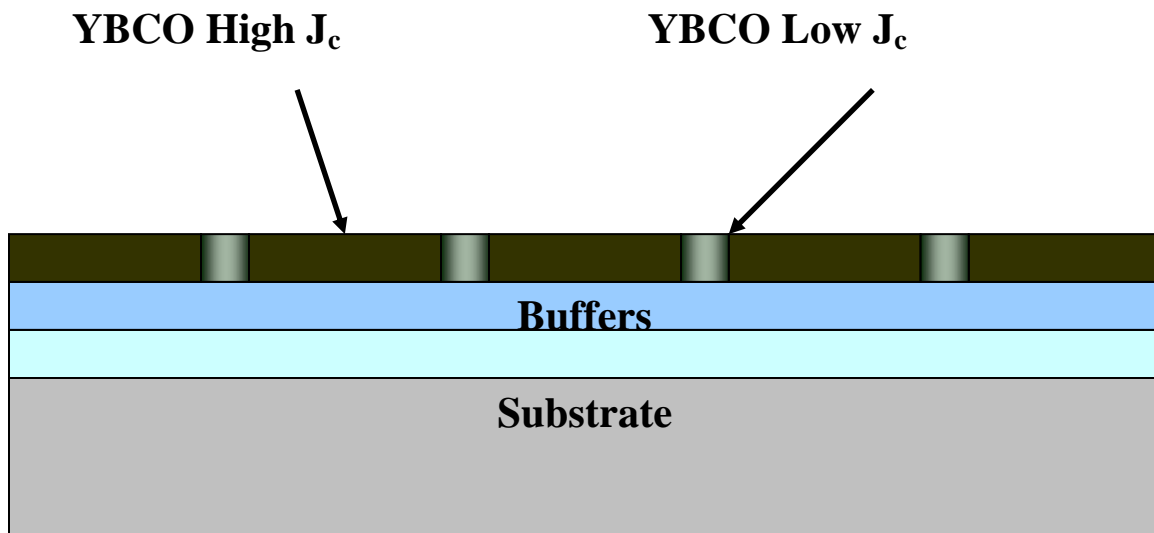


Figure 3.6.3.1

3.6.4 Scratched Substrate

- Can the weak J_c striations lower the hysteretic loss of the sample?
- Two samples were created using PLD
 - YBCO on LAO
 - YBCO on scratched LAO
 - Parallel scratches created by diamond tip scribe
 - Scratches divide the substrate into 10 filaments
- M-H loops were taken at OSU at different temperatures for the two samples
 - The third sample not relevant here

3.6.5 M-H loops at 20K

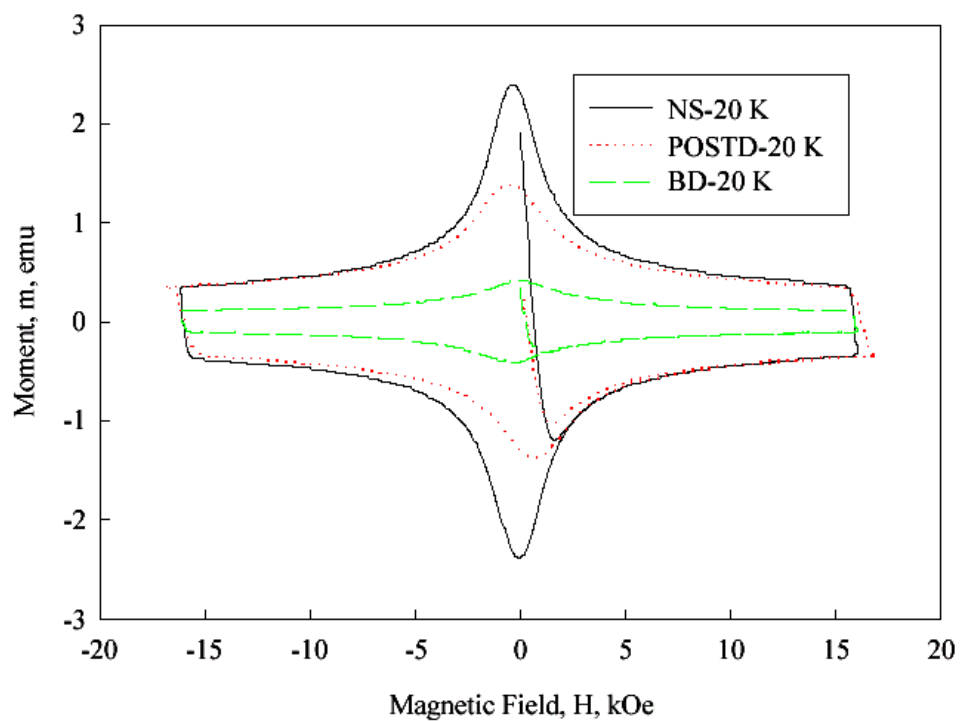


Figure 3.6.5.1

3.6.6 M-H loops at 77K

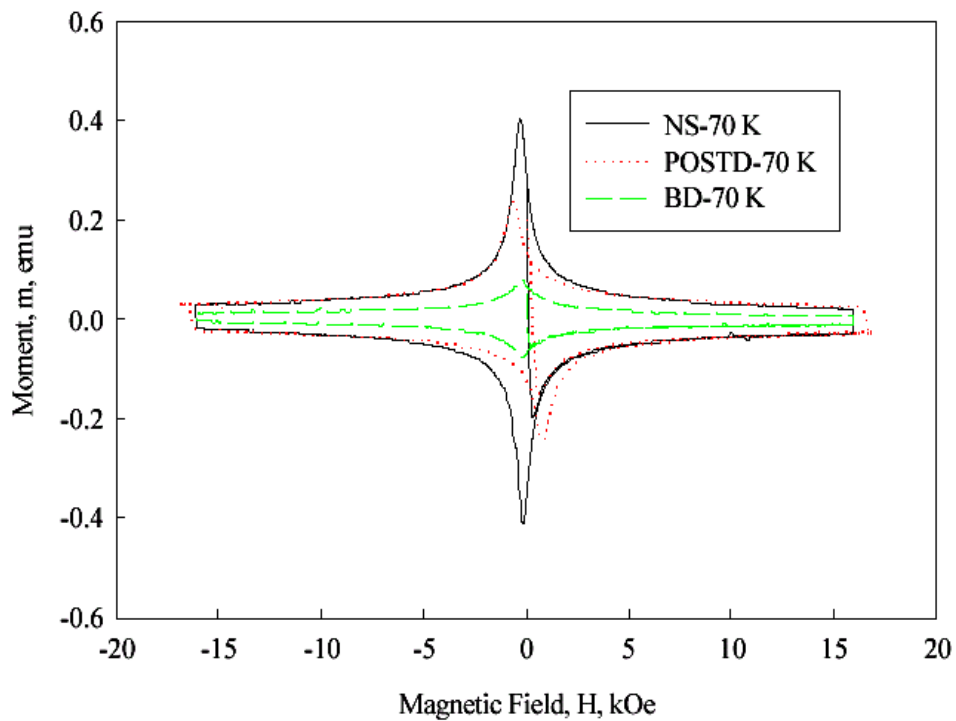


Figure 3.6.6.1

3.6.7 Current Sharing

Reasons for Current Sharing

- Allow current sharing between the filaments of HTS conductor, while not significantly degrading the loss benefit of filamentation.
- Blockage of the filament occurs if
 - some filament is defective in a small region
 - localized heating and a flux jump which does not propagate to neighboring filaments
- Coupling induced by normal metal connections will be frequency dependent
 - consider frequency independent SC alternative

Assumptions

- To have a useful current sharing scheme, several assumptions were made
 - The degraded regions to compensate are not localized
 - All of the filaments may have degraded regions, but these regions will occur occasionally and randomly
 - Defect separation is a length L_b
 - When current is re-routed around a given defect, it redistributes to all filaments in the cross section (not just a nearest neighbor)
 - Distance for current transfer to next strand is L_c
- Even if 100% of the filaments were degraded somewhere along their length, I_c would be only slightly degraded

3.6.8 SC Weakly Linked Relation

- Current sharing linkages must not substantially degrade the loss improvements
- If we require that the coupling currents add a magnetization no more than that of one of the filaments, then

$$J_{cw}L_c = J_{cf}d_f \quad \text{thus} \quad J_{cw} = \frac{J_{cf}d_f}{L_c}$$

- J_{cf} is the filamentary J_c along strand
- J_{cw} is the low-level J_c perpendicular to the filament
- d_f is the filamentary width
- If d_f is 100 microns and $L_c = L_p$ (twist pitch) = 20 cm, then J_{cw} is 2000 times smaller than J_{cf}
 - Note, the strand must be twisted
 - If L_p exceeds L_c , losses will increase (up to $L_p = nL_c$, where full magnetic filamentary recoupling will occur)

3.6.9 Metallic vs. SC Connection

- This scheme must be compared to using normal metal for current sharing between filaments
 - For this calculation, it must be determined what resistivity and cross section of normal metal is needed to allow for acceptable current sharing.
- After Mike's magic, the ratio of the magnetizations (losses) of the two cases is

$$\frac{M_{wc}}{M_e} = \frac{200}{H_m f w}$$

- Here H_m (max field sweep amplitude) is in Oe, f in Hz, and w (conductor width) in cm
- If $H_m = 10$ kOe (1 T), and $w = 1$ cm, then f must be sub-Hz in order for a better optimum with eddy current enabled current sharing

3.6.10 Conclusions

- For DC applications at any field and for low frequency applications
 - Eddy current enabled current sharing will always be superior
- For moderate and high frequency applications
 - SC-link enabled current sharing will have a better loss-sharing trade-off

3.7 Filamentary YBCO Coated Conductors

References: 25, 26, 27, 28, 29, 30, 31, 32

Paul N. Barnes, PhD

Propulsion Directorate, Air Force Research Laboratory

Presented at AFOSR Review, January 26, 2005

3.7.1 AC-Tolerant YBCO Conductor

- In generators, the YBCO coated conductor will be subjected to alternating magnetic fields
 - up to a few Tesla
 - Up to hundred Hz frequencies or even higher
- Improvements to the YBCO coated conductor can substantially reduce ac losses in the HTS wire
 - Can enable the all-cryogenic configuration for motors and generators with even greater weight and size reductions (both field and stator windings are superconducting)
 - This cannot be done to BSCCO, the first generation HTS wire
- Losses include hysteretic losses, coupling losses, eddy current losses, ferromagnetic losses, transport current losses, etc.

3.7.2 Substrate Induced Striations

- LEFT – Loss reduction by low J_c connection; accomplished by scribing the substrate and destroying epitaxial growth of YBCO
- RIGHT – Loss reduction by bridging
 - Enables current sharing to circumvent filament blockages
 - Only slight increase in hysteretic loss experienced

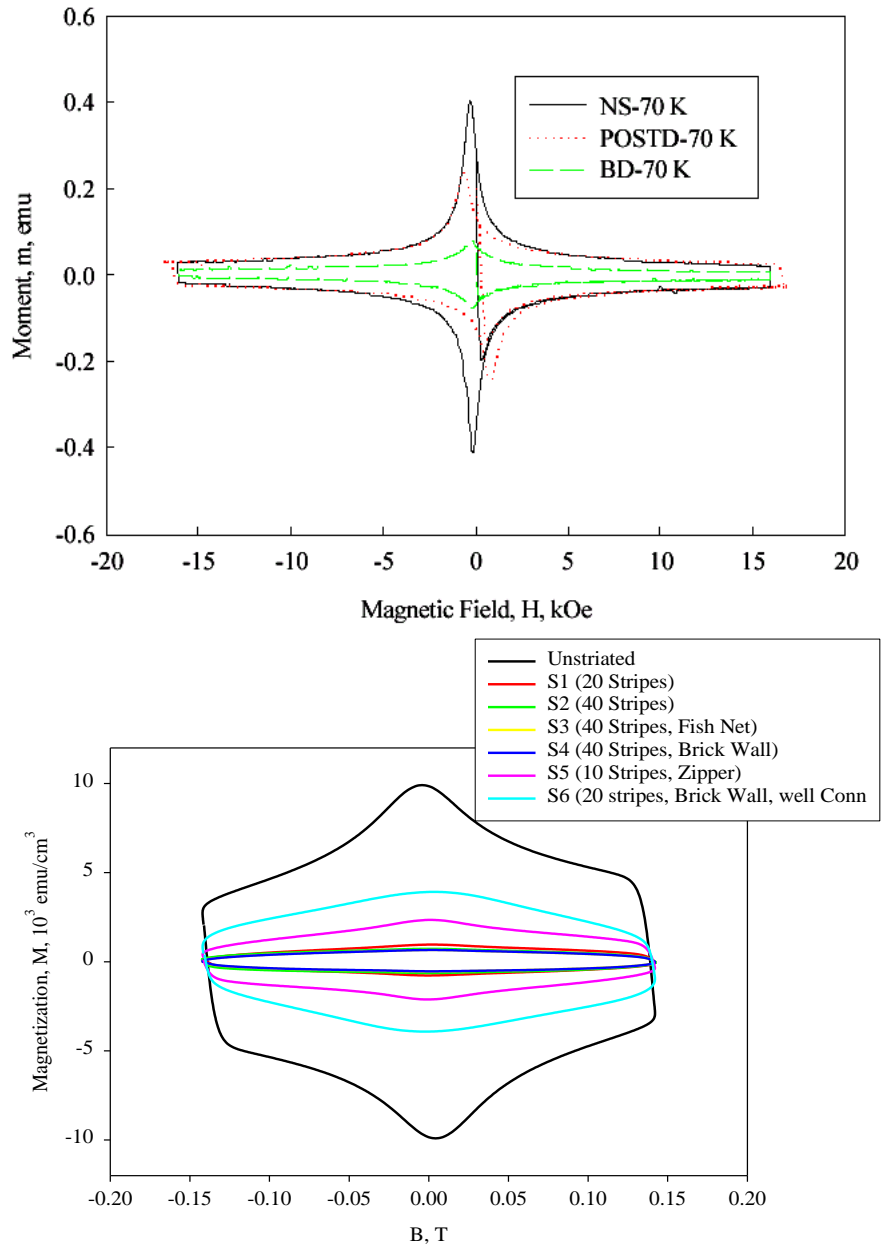


Figure 3.7.2.1

3.7.3 Metallic vs. SC Connection

- Not showing the calculations, the ratio of the losses of superconducting links to metallic is

$$\frac{M_{wc}}{M_e} = \frac{2 \times 10^{-4}}{B_m f w}$$

- Here B_m (magnetic field) is in Tesla
- f (frequency) in Hz and w (tape width) in meters
- For 1 Tesla and a width of 1 cm

- f must be sub-Hz in order for a better optimum to be possible with metallic (eddy current) enabled current sharing
- For DC and low field applications, eddy current enabled current sharing will always be superior
- For moderate and high frequency applications, superconducting enabled current sharing will have a better loss-sharing trade-off
 - Airborne generators are high frequency

3.7.4 Filamentary Samples

Sample B/0 (not striated), covered by silver layer



Sample B/1. The photograph shows only a part of the sample, which was used to measure I-V curves of individual filaments. There are no bridges between filaments.

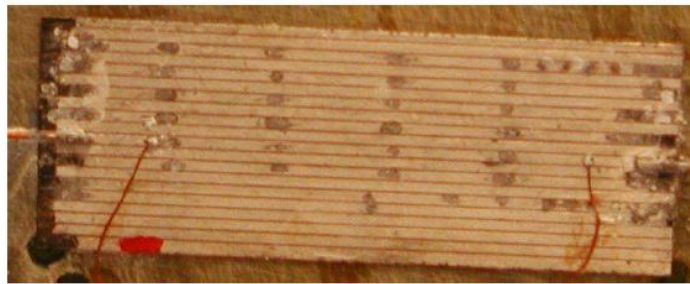


Figure 3.7.4.1

Sample B/2 with one central bridge (not well visible in the picture). Note that silver coating is separated from the filaments in the central part some parts of silver.



Sample B/3



Fig. 3.4 Sample B/3

Sample B/4



Fig. 3.5 Sample B/4

Figure 3.7.4.2

Sample B/5



Figure 3.7.4.3

3.7.5 List of measured samples

- NSa AFRL200310A 184 A @YNU non-striated
- ST20 AFRL200310B 110 A @YNU 400 mm, 20 filaments
 - ST20L: 100 mm, ST20S: 26.5 mm
- NSb AFRL2004A0 162 A @YNU non-striated
- ST40 AFRL2004A2 100 A @YNU 200 mm, 40 filaments
 - ST40L: 100 mm, ST40M: 50 mm, ST40S: ~25 mm
- A1 AFRL2004A1 70 A @YNU 400 mm, 20 filaments
- A3 AFRL2004A3 Not yet meas. 400 mm, 20 filaments
(bridges at center)
- A4 AFRL2004A4 Not yet meas. 400 mm, 20 filaments
(alternating bridges at ends)
- A5 AFRL2004A5 85 A @YNU Zipper

3.7.6 Q_m vs. $m_0 H_m$

A1

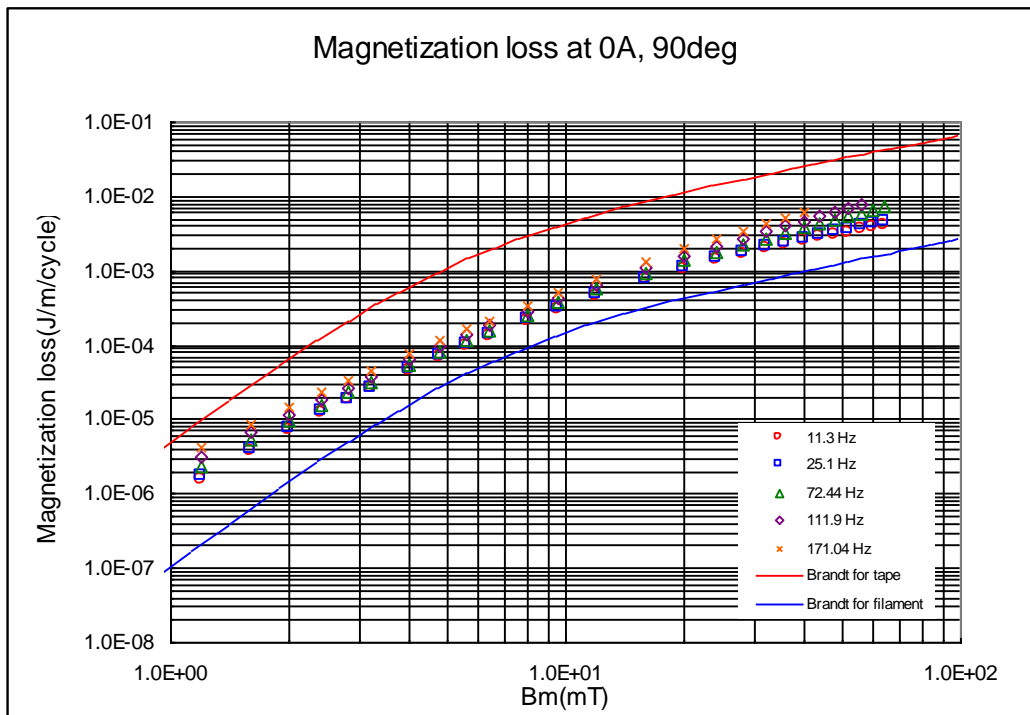


Figure 3.7.6.1

A3

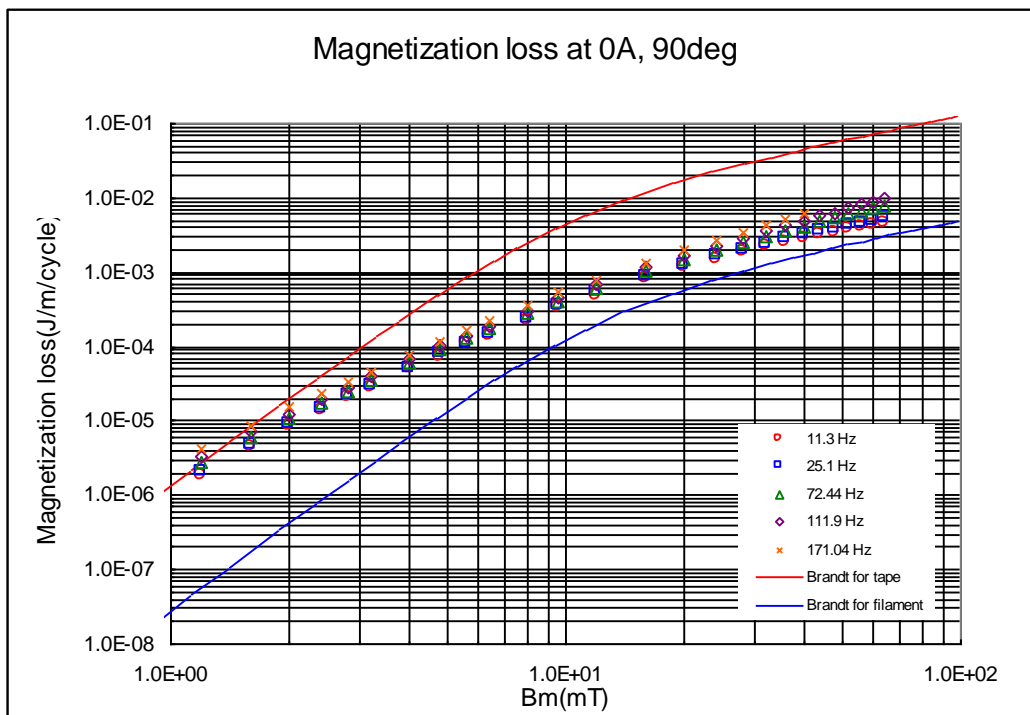


Figure 3.7.6.2

A4

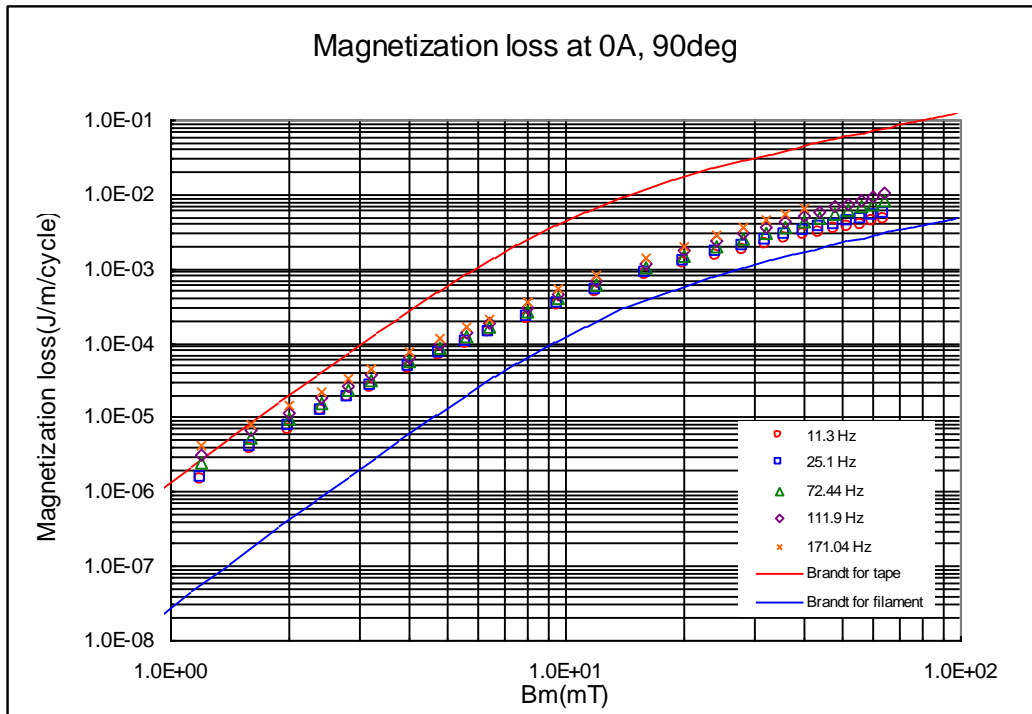


Figure 3.7.6.3

A5

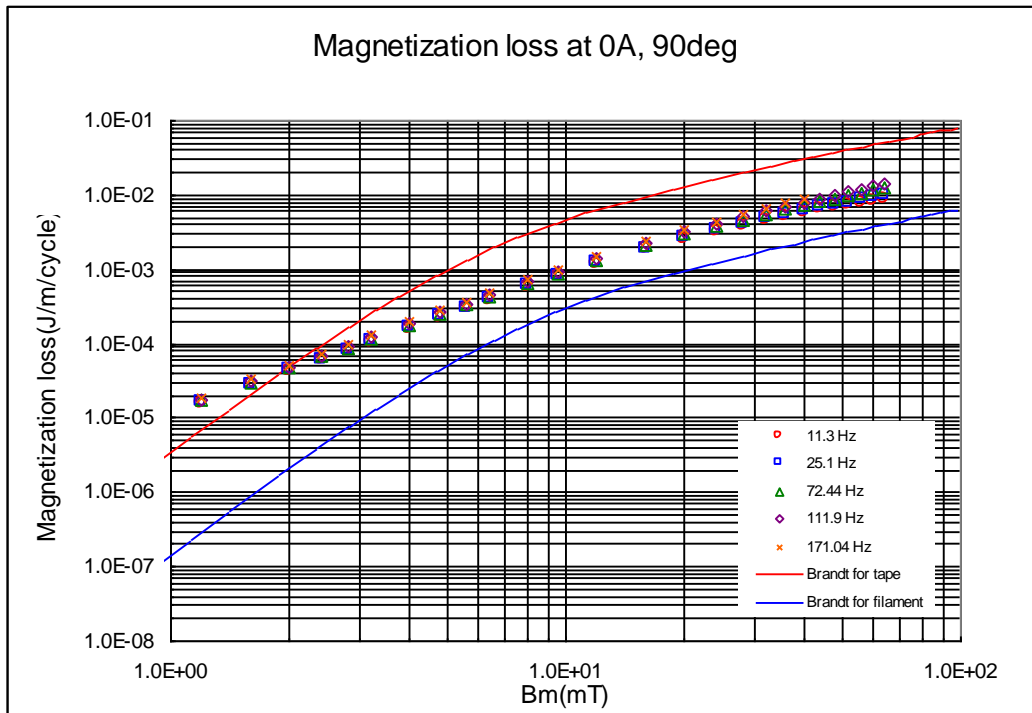


Figure 3.7.6.4

The substrate was prepared from sample B/1. The dimensions of the prepared sample are the following: thickness 0.10 mm, width 10 mm, distance between potential taps: 15.8 mm

Measurements at $T = 300\text{ K}$, $B = 0$

$I\text{ (A)}$	0.201	0.508	1.004
$V\text{ (mV)}$	3.86	9.76	19.31
$R\text{ (}\Omega\text{)}$	1.92×10^{-2}	1.92×10^{-2}	1.923×10^{-2}

$$\text{Resistivity } \rho(300\text{ K}) = 1.92 \times 10^{-2} \times (1 \times 10^{-6} / 15.8 \times 10^{-3}) = 1.215 \times 10^{-6} \Omega\text{m}$$

3.7.7 Filamentary Bridging

Frequency dependence of AC losses in B/0 and B/5 is very small, practically negligible. The losses can be defined as pure hysteresis losses. The ratio of losses measured at 500 Hz and 10 Hz at 20 mT is the following:

sample B/0 $A(500\text{ Hz})/A(10\text{ Hz}) = 1.05$

sample B/5 $A(500\text{ Hz})/A(10\text{ Hz}) = 1.25$

10. Using the results of electrical and thermometric loss measurements we determined the contribution of coupling losses to the total losses of the striated samples at 20 mT and 500 Hz:

sample B/2: $A_{\text{coupl}}/A_{\text{tot}} = 0.5$ ←

sample B/3: $A_{\text{coupl}}/A_{\text{tot}} = 0.68$ ←

sample B/4: $A_{\text{coupl}}/A_{\text{tot}} = 0.73$ ←

3.7.8 I-V Curves for Filaments

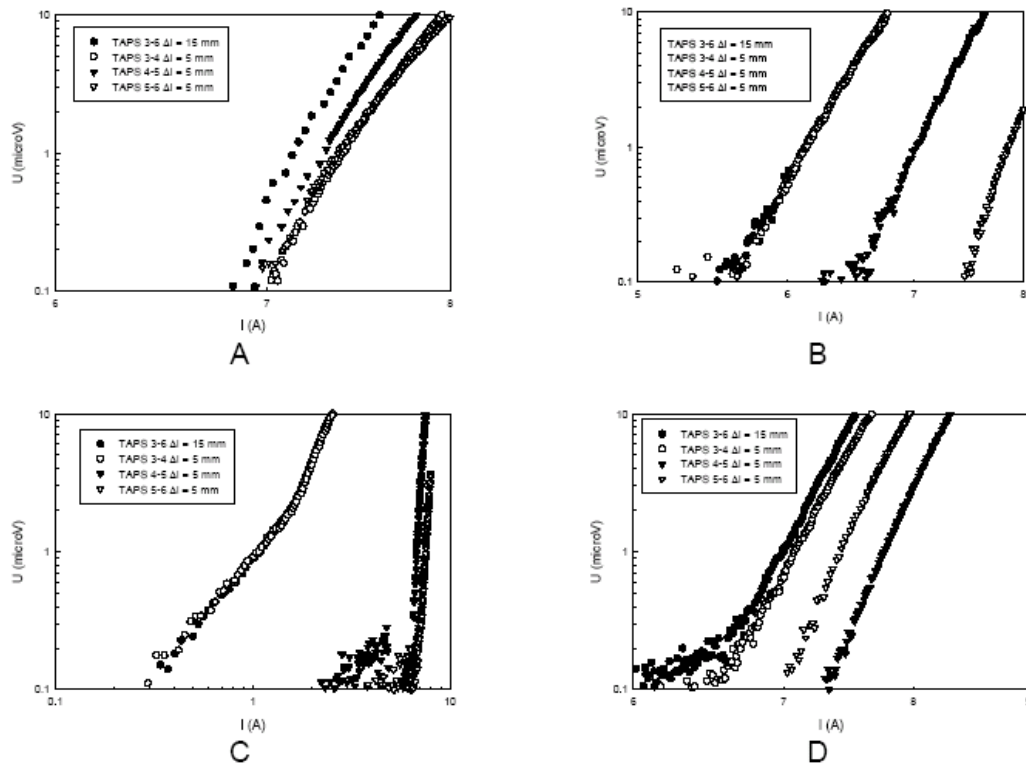


Figure 3.7.8.1

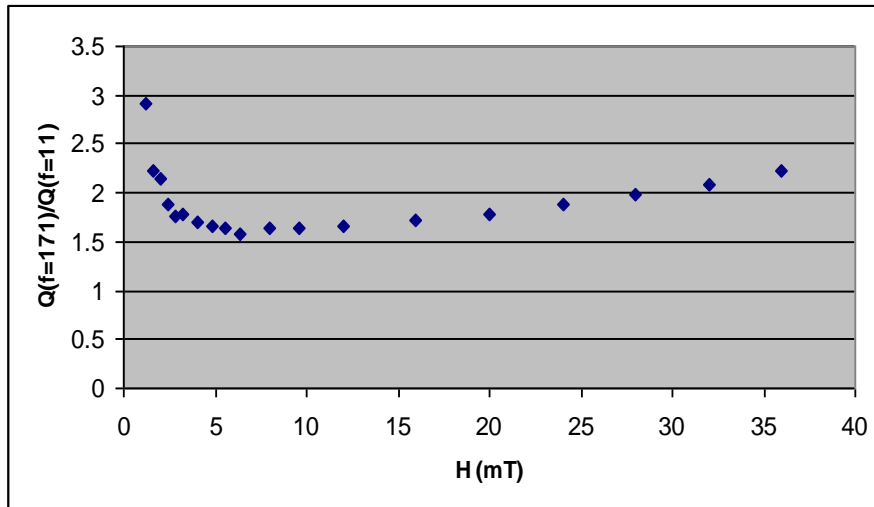


Figure 3.7.8.2

3.7.9 Summary

- Filamentary Current Sharing via superconducting connections is possible
 - Lower losses than metallic connections
 - Bridging must be adequately spaced
- Not all measurements are ideal
 - Comparison of the multiple systems/techniques necessary
 - New test apparatus

3.7.10 AC Losses

M.D. Sumption, E.W. Collings, and P.N. Barnes, Supercond Sci. Technol., vol. 18, pp.122-134 (2005).

- P_h = Superconductor hysteretic loss
 - YBCO layer, 2 μm thick
- $P_{e,sub}$ = Normal metal eddy current loss for substrate
 - Hastelloy-type alloy, 50 μm thick, $1 \times 10^{-6} \Omega\text{m}$
- $P_{e,over}$ = Normal metal eddy current loss for overlayer
 - Pure Ag, 3 μm thick, $2.9 \times 10^{-9} \Omega\text{m}$
 - The overlayer is assumed to be striped and values do not include the influence of the superconductor on the electric field
- P_c = Coupling eddy current loss
- P_{Fe} = Ferromagnetic substrate hysteretic loss
 - Ni-5%W here, but could be zero if nonmagnetic substrate used

3.7.11 Estimated AC Losses

Condition/ Loss in mW/m		500 Hz, 1 T	500 Hz, 0.2 T	200 Hz, 1 T
(1a)	P_{ha}	2500	500	1000
Face-on				
$w = 1$ cm	$P_{e,subb}$	20,000	800	3,200
$df = 50$ μ m				
	$P_{e,overc}$	5.3	0.212	0.85
	P_{cd}	--	--	--
	P_{Fee}	68	68	27

Note : $P_e = \frac{\pi^2}{6\rho_n} [(\mu_0 H_m) wf]^2$ $Q_h \approx \mu_0 w J_c H_m$

Figure 3.7.13.1

Condition/ Loss in mW/m		500 Hz, 1 T	500 Hz, 0.2 T	200 Hz, 1 T
(1c)	P_h	250	50	100
Face-on				
10 strips	$P_{e,sub}$	200	8	32
$w = 1$ mm				
$df = 5$ μ m	$P_{e,over}$	0.053	0.002	0.009
	P_c	--	--	--
	P_{Fe}	68	68	27

Figure 3.7.13.2

Condition/ Loss in mW/m		500 Hz, 1 T	500 Hz, 0.2 T	200 Hz, 1 T
(2) Edge-on	P_h	100	20	40
	$P_{e,sub}$	0.5	0.02	0.08
	$P_{e,over}$	0.019	0.001	0.003
	P_c	--	--	--
	P_{Fe}	68	68	27

Figure 3.7.13.3

3.8 The Integration of YBCO Coated Conductors into Magnets and Rotating Machinery

References: 25, 26, 27, 28, 29, 30, 31, 32

G. A. Levin and P.N. Barnes,
Superconductivity Group, Propulsion Directorate, Air Force Research Laboratory, Wright-Patterson AFB, Ohio USA

Presented at August 31, 2005

3.8.1 Outline

- Double pancake coil.
- Alternative way to twist coated conductor
- Examples:
 - A) Layered coil
 - B) Armature winding

3.8.2 DC application of YBCO coated conductors

- Double pancake coils

3.8.3 Double pancake field coil; YBCO coated conductor

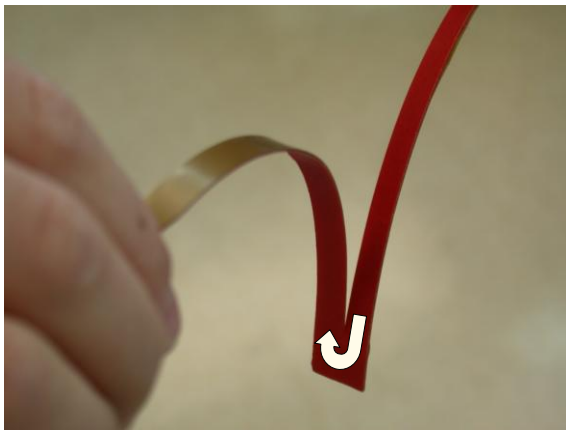
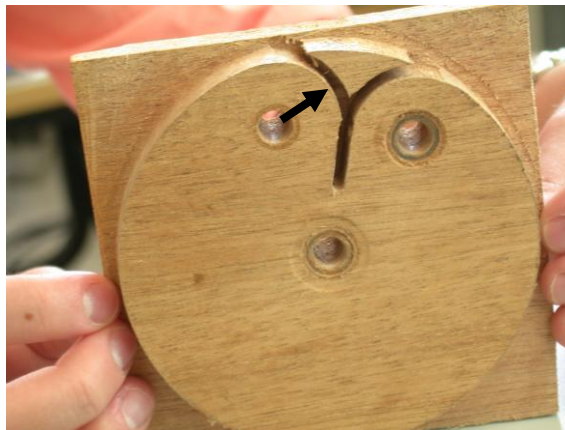


Figure 3.8.3.1



Coil former

Figure 3.8.3.2

3.8.4 Double pancake field coil; YBCO coated conductor

No sideways bending (hard)

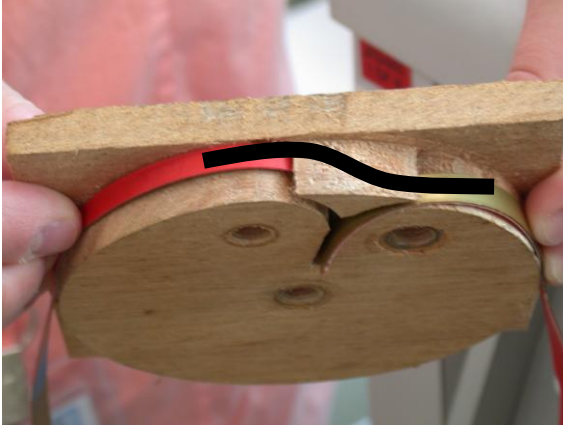


Figure 3.8.4.1

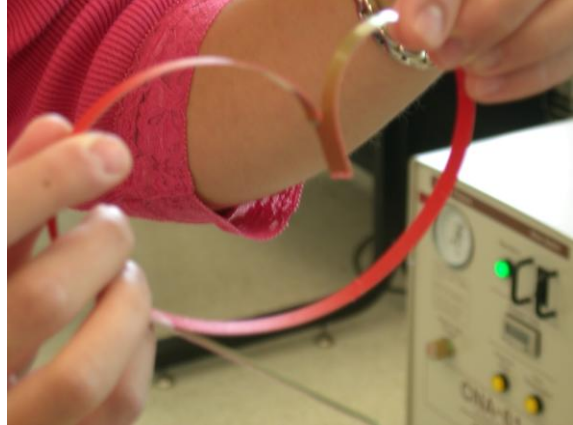


Figure 3.8.4.2

3.8.5 Double pancake field coil; YBCO coated conductor

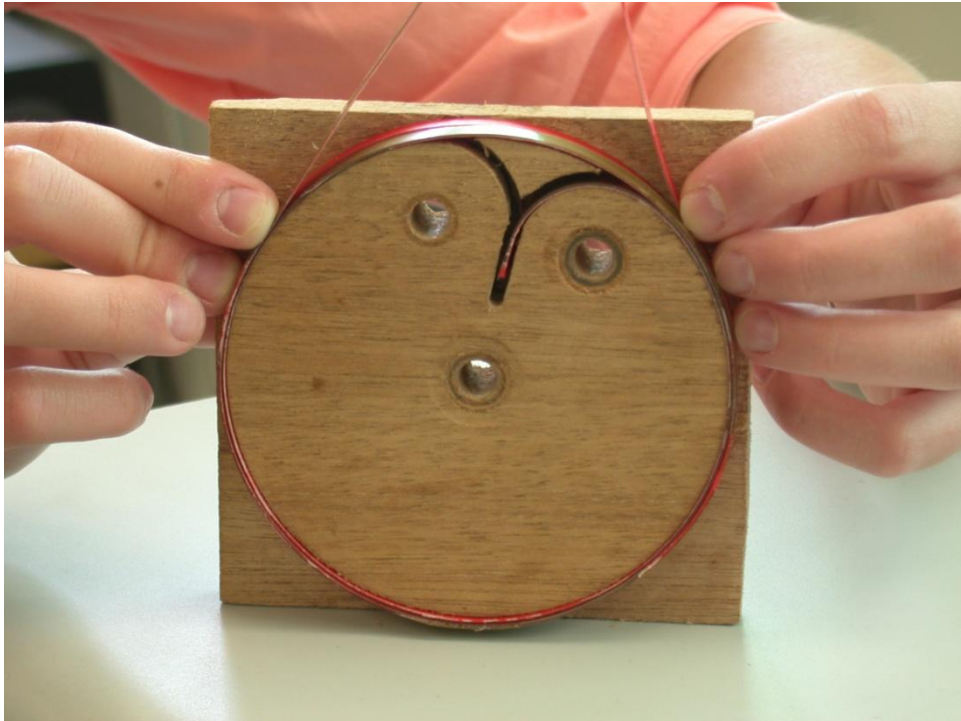


Figure 3.8.5.1

3.8.6 Double pancake field coil; YBCO coated conductor

Note that conductor is transposed (twisted)

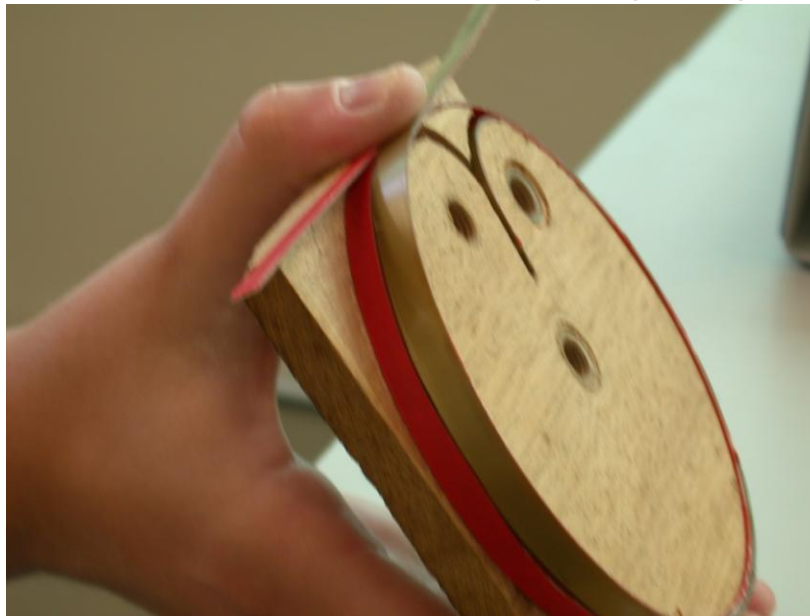
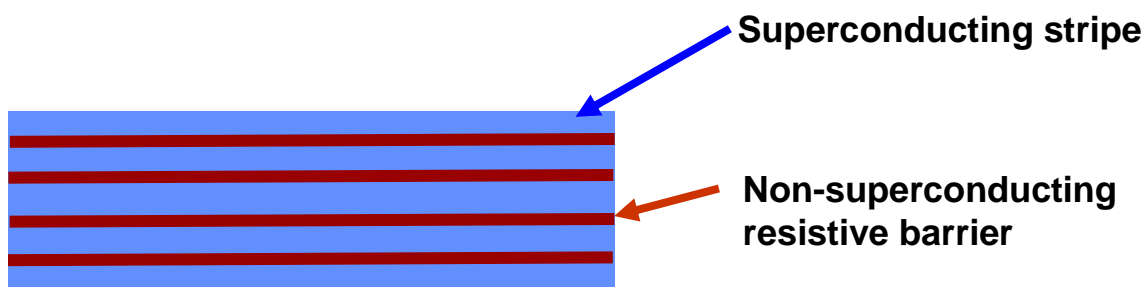


Figure 3.8.6.1

3.8.7 Reduction of ac losses in YBCO conductors

$$Q = Q_s + Q_n \approx I_c W_n Bf + k \frac{(BfL)^2}{\rho} d_n W$$



Conductor must be twisted in order to limit the coupling loss

Figure 3.8.7.1

3.8.8 Two types of twist

Axial

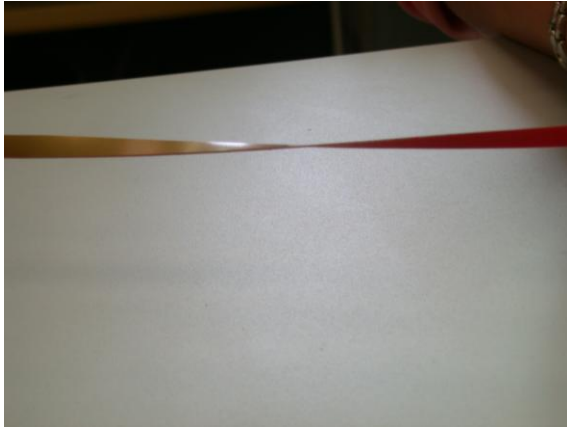


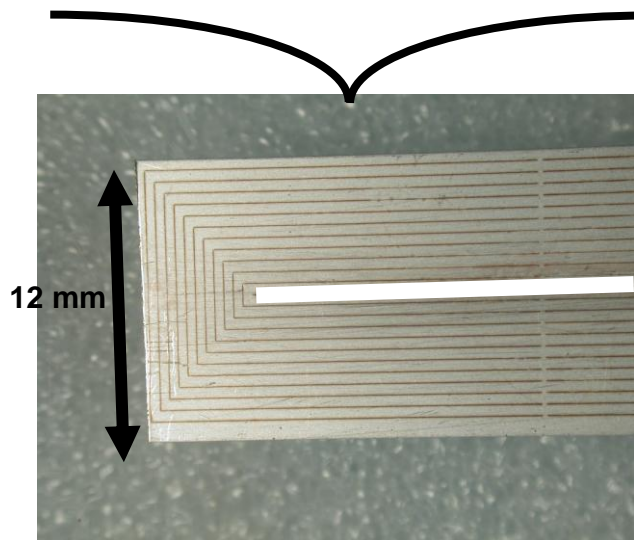
Figure 3.8.8.1

**Bending twist
(seagull twist)**



Figure 3.8.8.2

3.8.9 Race-track pattern (made by laser ablation)



Filament width – 500 μm

Figure 3.8.9.1

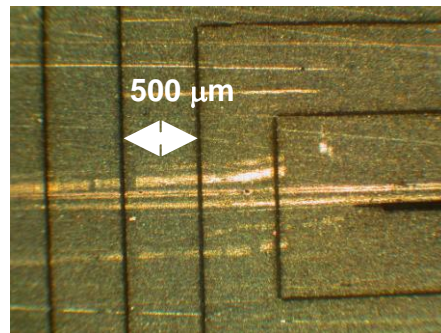
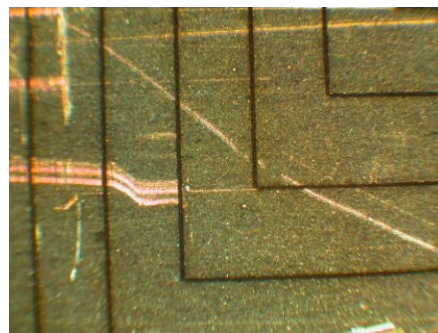
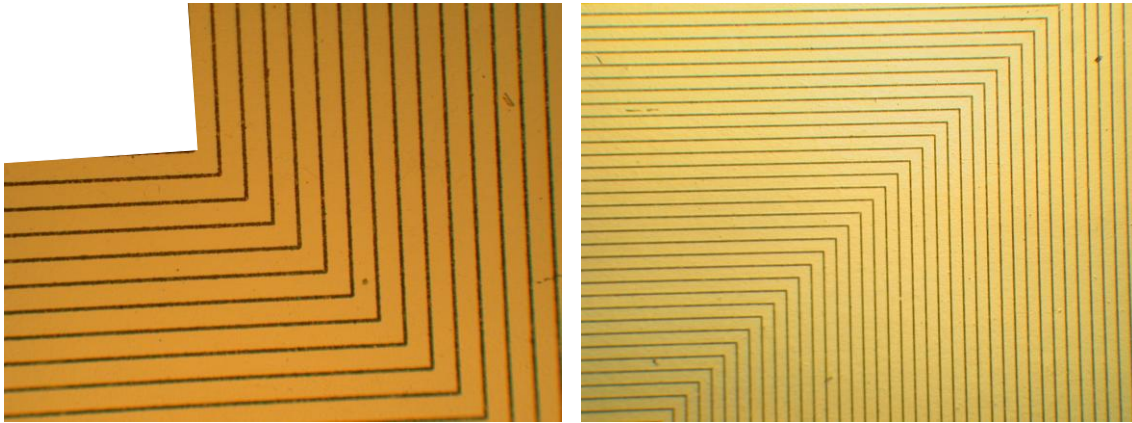


Figure 3.8.9.2
Figure 3.8.9.3



3.8.10 Patterned substrate (made by photolithography)

Collaboration with Albany



Filament width – 50

Figure 3.8.10.1

3.8.11 Making of twisted conductor

A sheet of YBCO coated conductor

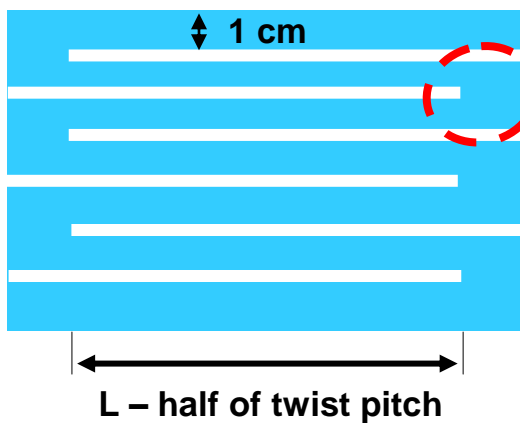


Figure 3.8.11.1

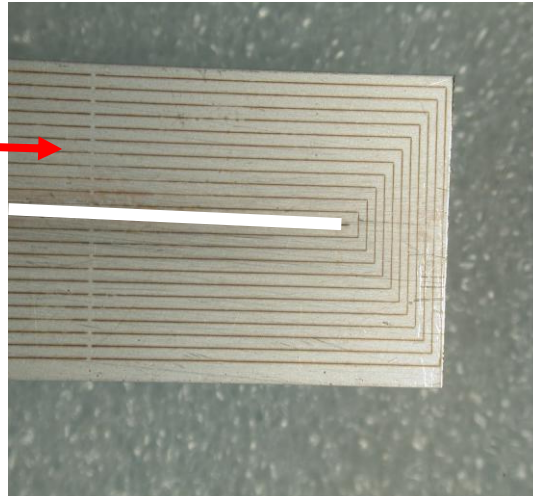


Figure 3.8.11.2

3.8.12 Demonstration model

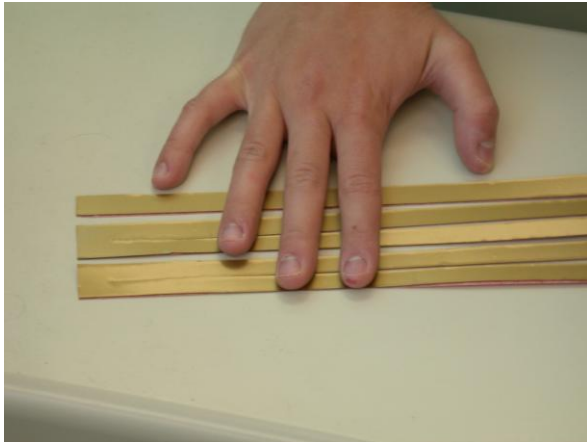


Figure 3.8.12.1



Figure 3.8.12.2

3.8.13 Layered coil

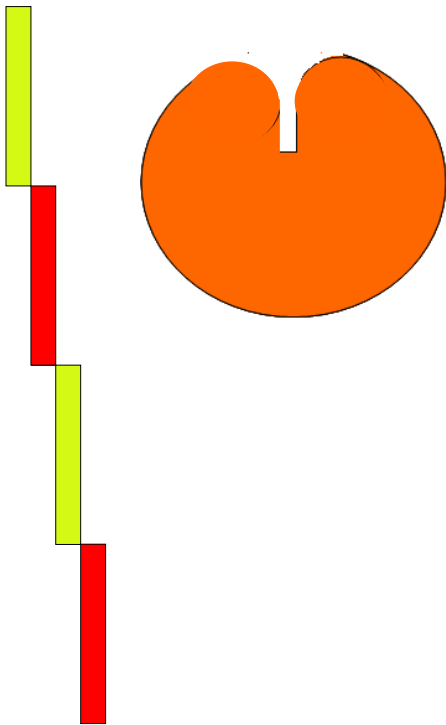


Figure 3.8.13.1

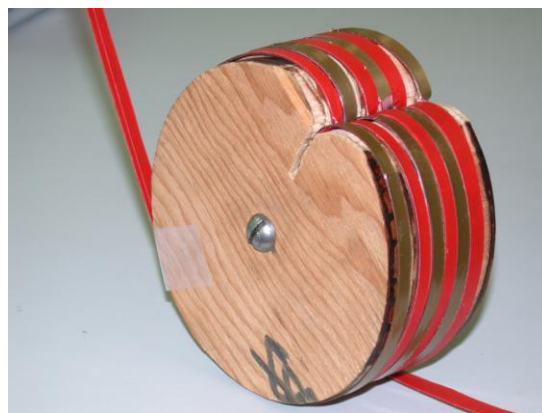


Figure 3.8.13.2

3.8.14 Layered coil



Figure 3.8.14.1

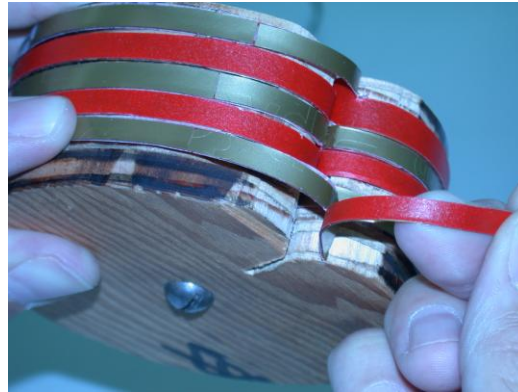


Figure 3.8.14.2

3.8.15 Layered coil



Figure 3.8.15.1



Figure 3.8.15.2

3.8.16 Layered coil

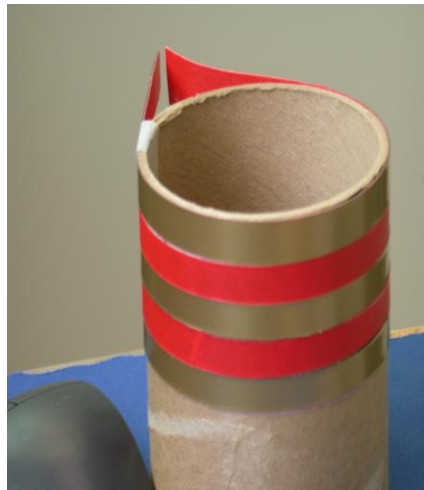


Figure 3.8.16.1

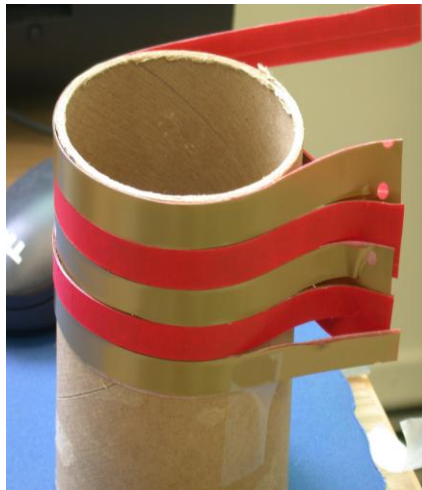


Figure 3.8.16.2

3.8.17 “Transformer”?

Coils can be placed over one another to minimize flux leakage.



Figure 3.8.17.1

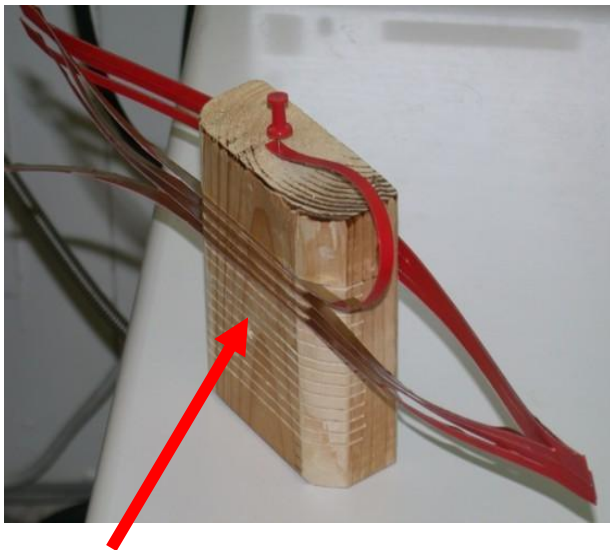


Figure 3.8.17.2

3.8.18 Armature winding

- Gramme ring
- Diamond coil

3.8.19 Gramme ring



Active length

Figure 3.8.19.1

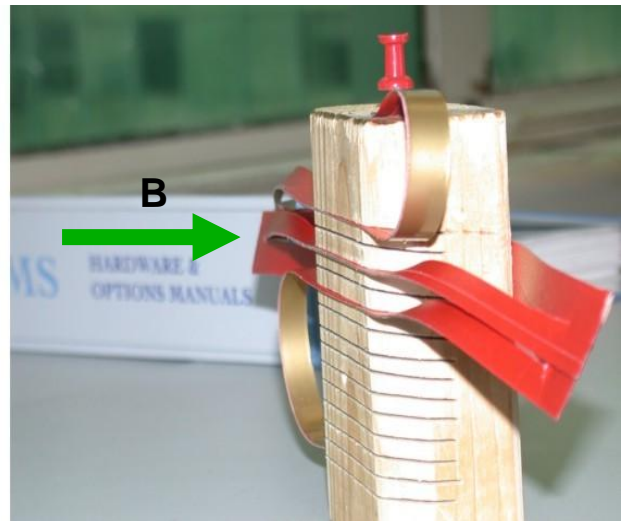


Figure 3.8.19.2

3.8.20 Diamond winding

5 MW ship propulsion motor

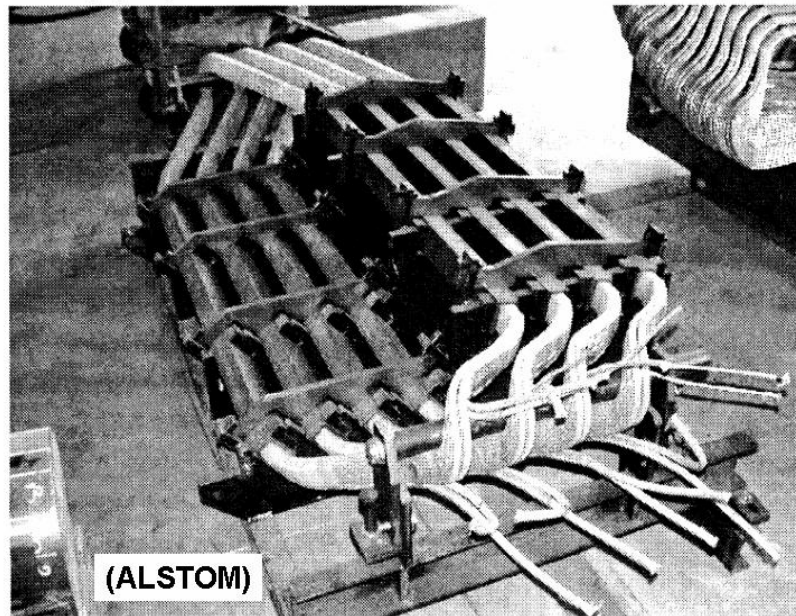


Figure 3.8.20.1

3.8.21 Diamond winding



Figure 3.8.21.1

3.8.22 Diamond winding

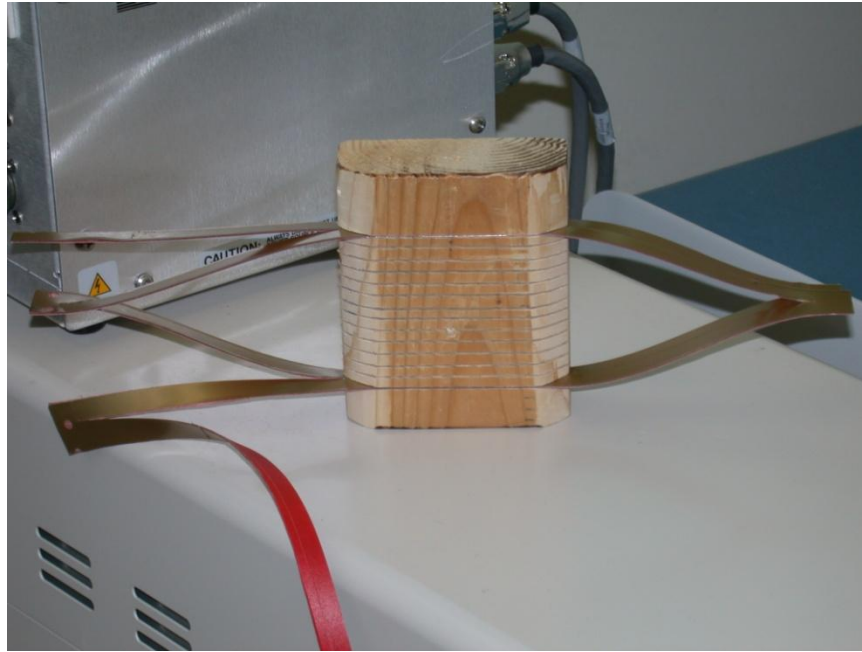
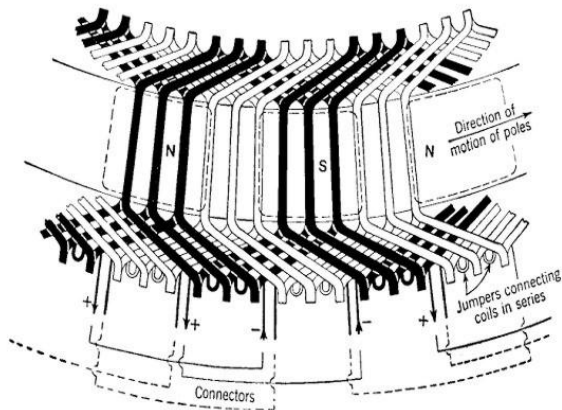


Figure 3.8.22.1

3.8.23 Sheep propulsion

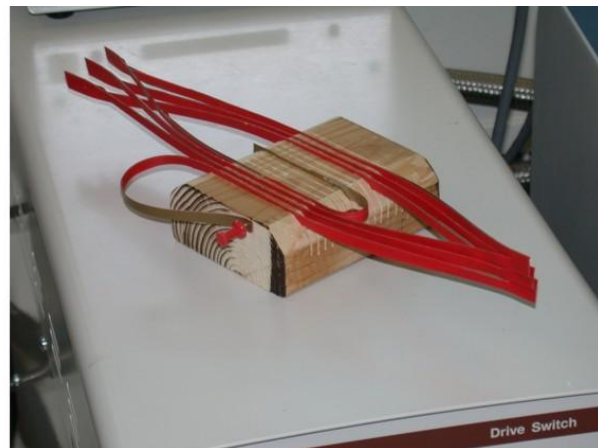
2-phase generator:

Three slots per phase per pole.



Black and white elements correspond to different phases

Figure 3.8.23.1



A model of three-turns group similar to a one-phase group on the left.

Figure 3.8.23.2

3.8.24 Diamond winding

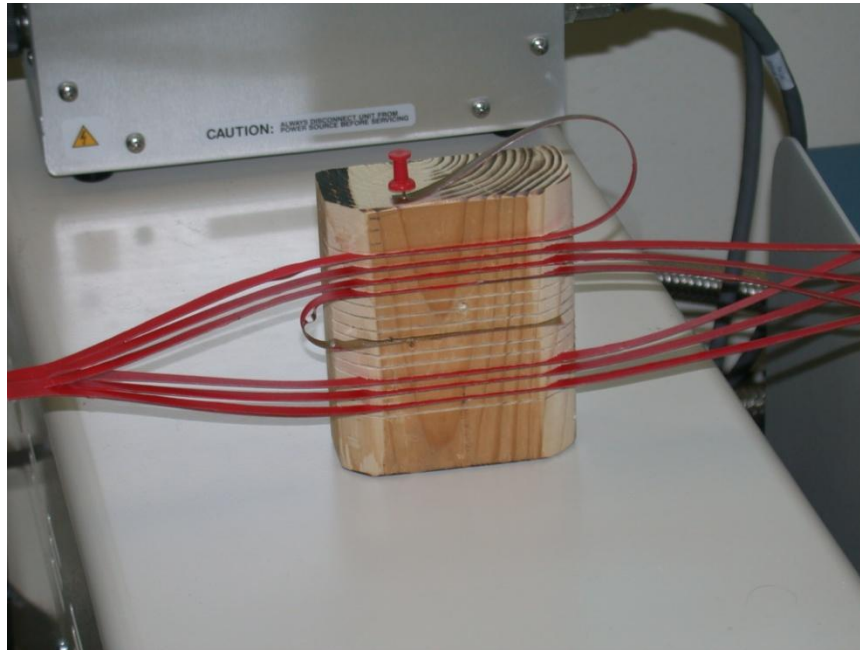


Figure 3.8.24.1

3.8.25 Summary

- Wider sheets of coated conductors can be cut into meander-like tapes and unfolded forming the bent-twisted tapes.
- Such conductors can have lower coupling losses (if striated) and offer much wider set of options for the design of ac machinery than simple linear tapes.

3.8.26 Double pancake field coil: 1st and 2nd generation hybrid

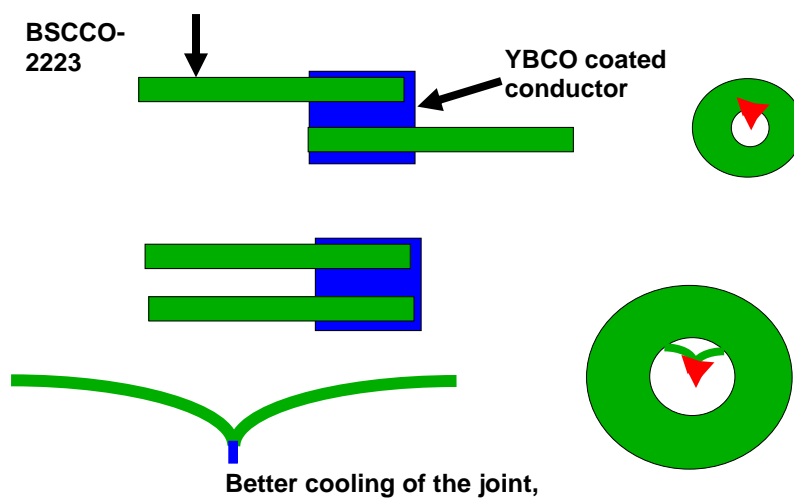


Figure 3.8.26.1

Chapter 4: XPS Study of YBCO Coated Conductors

This is a collaborative relationship with WSU that was initiated with the PR Summer Faculty Program. X-ray Photoelectron Spectroscopy (XPS) is used to investigate the compositional and chemical profile of a typical YBCO coated conductor architecture. The initial sample consisted of YBCO-CeO₂-YSZ-CeO₂-Ni layered substrate and current samples consists of YBCO on LaAlO₃ YBCO-CeO₂-YSZ(sc). Additional samples are being made as well as obtaining samples from AMSC and IGC SuperPower prepared in alternate ways for comparison. The chemical depth profiling involved bombarding a small area of the specimen surface with 3 KeV Ar⁺ ions and analyzing the freshly exposed surface after each bombardment. Results of the process show that the Y(3d) photo-electronic peak shape in these films is very different from YBCO superconductors made by other techniques (sintered, melt texturing, sputtering etc.) which may indicate a possible difference in the atomic co-ordination between PLD films and those grown differently. The correlation between chemical binding states of the ions and superconducting properties needs to be investigated in detail. The lower portion of the YBCO film showed distinct signs of contamination including Ce, Zr, and traces of Ni. We will explore the coated conductor for other issues, but the two current findings are: the peak shapes of the Y(3d) photoelectron peak are different in these films compared to bulk YBCO specimens and the presence of Zr in the YBCO (probable diffusion from the YSZ layer). The mechanisms behind these two observations and their implications (in terms of coated conductor quality) will be investigated in the upcoming year.

X-ray photoelectron spectroscopy (XPS) depth profiling was used to investigate the compositional and chemical profile of a typical YBCO coated conductor architecture. Dr. Sharmila Mukopadhyay, Wright State University, collaboratively supported the AFRL Power Division under the directorate's Summer faculty program using a unique, high resolution XPS system to examine a coated conductor sample from YBCO to buffers. Results of the process revealed that the Y(3d) photoelectronic peak shape in these films is very different from bulk YBCO. Initial results indicated a strong correlation between the Y(3d) XPS peak shape (full-width-half-maximum) of the YBCO and the film quality. A potential correlation may also exist with the Cu(2p)/Ba(3d) ratio indicating an interrelationship to the FWHM of the Y(3d) peak. Film quality was determined by current transport, resistive T_c, and AC magnetic susceptibility measurements.

4.1 Chemical Depth Profiling by XPS of YBCO Coated Conductor

References: 34

4.1.1 Introduction

XPS studies of a typical YBCO coated conductor architecture were conducted to investigate the chemical and microstructural profiles. The detailed XPS depth profiling study was performed on one sample (YBCO/CeO₂/YSZ/CeO₂/Ni) of coated conductor. The chemical depth profiling involved bombarding a small area of the specimen surface with 3 KeV Ar⁺ ions and analyzing the freshly exposed surface after each bombardment. Results of the process show that the Y(3d) photo-electronic peak shape in these films is very different from bulk (sintered and oxygen

annealed) YBCO superconductors and surface analysis of YBCO thin films. This may indicate a possible difference in the atomic co-ordination between some laser-ablated films and bulk sintered ones. The lower portion of the YBCO film showed distinct signs of contamination including Ce, and traces of Ni. A statement on Zr diffusion into this YBCO layer is also reported.

4.1.2 XPS Depth Profiling

The purpose of the profiling is to investigate the chemical and microstructural makeup of an YBCO coated conductor sample. A small area of the specimen's surface was bombarded with 3 KeV Ar^+ ions and the freshly exposed surface was analyzed. The sputtering was done in-situ to avoid surface contamination, since YBCO has chemical reactivity with air. This sputter-analysis cycle was repeated several times, which permitted the determination of the composition and chemistry at different depths of the conductor.

4.1.3 Sample Fabrication

A previously fabricated sample was used. The base was a nickel substrate with PLD deposited buffer layers on the order of on the order of 300 nm CeO_2 , 800 nm YSZ, and 300 nm CeO_2 . PLD was used to grow a thicker ($\sim 2 \mu\text{m}$) layer of YBCO.

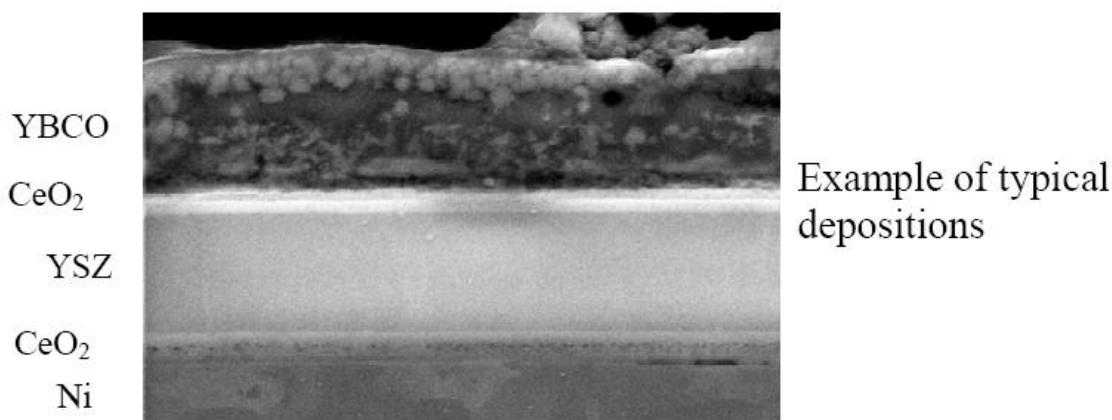
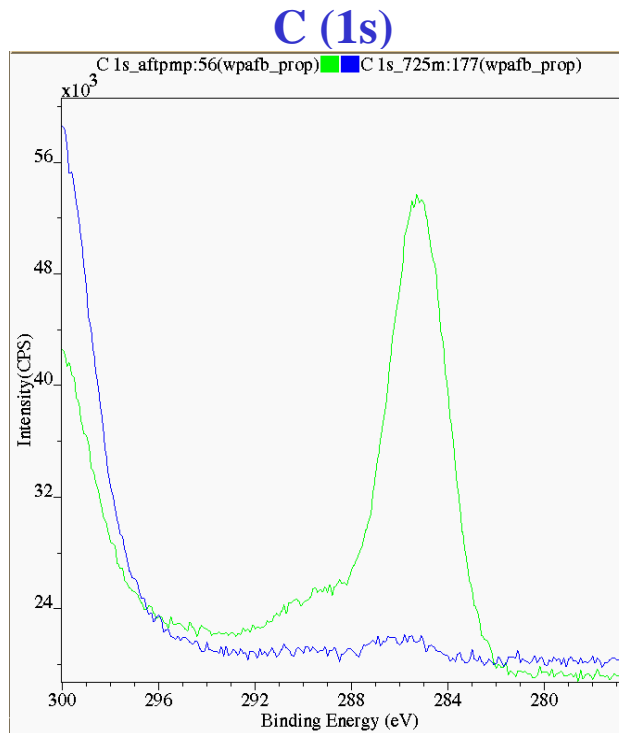


Figure 4.1.3.1

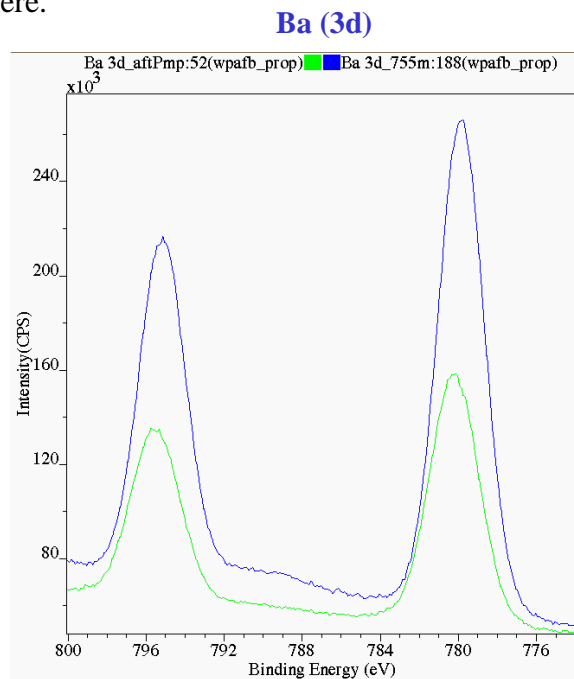
4.1.4 Surface of Conductor

The outer surface was coated with a carbon-containing layer. This layer was due to the sample being handled repeatedly. The thickness and durability of this layer with storage conditions may be an issue with regard to handling. For the current investigation this region was ignored.



4.1.5 YBCO Layer

The upper 1/3 of the YBCO layer had very uniform ionic concentrations ratio and peak shapes. This is a good indication of chemical homogeneity within this region and no detectable impurities were identified here.



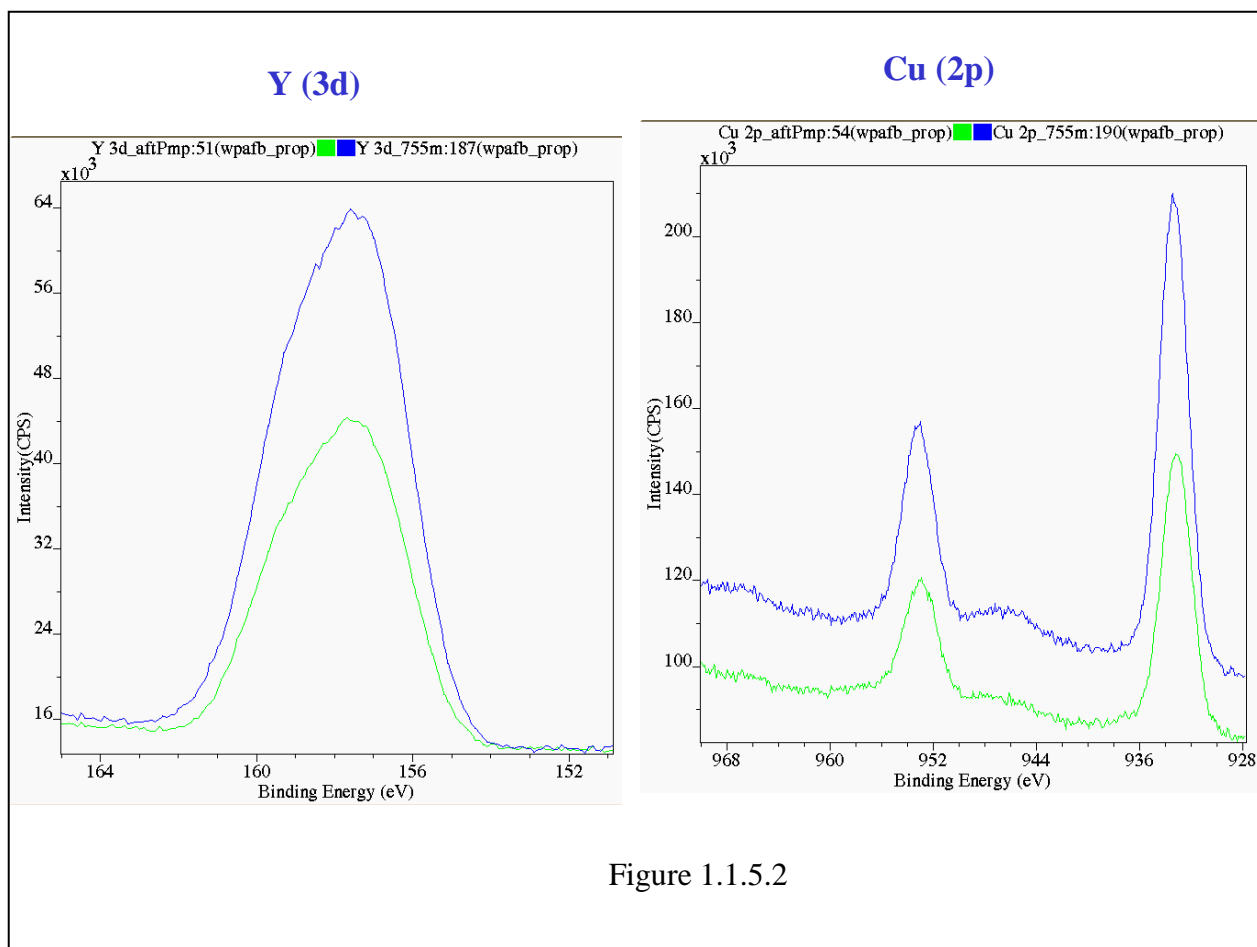


Figure 1.1.5.2

4.1.6 Yttrium Peaks

The two different Y(3d) peaks are from (a) bulk YBCO levitators made by melt growth and (b) thin film coated conductor made by laser ablation. The Y(3d) photo-electronic peak shape is different from bulk (sintered and oxygen annealed) YBCO superconductors that have been studied earlier using XPS for surface analysis.

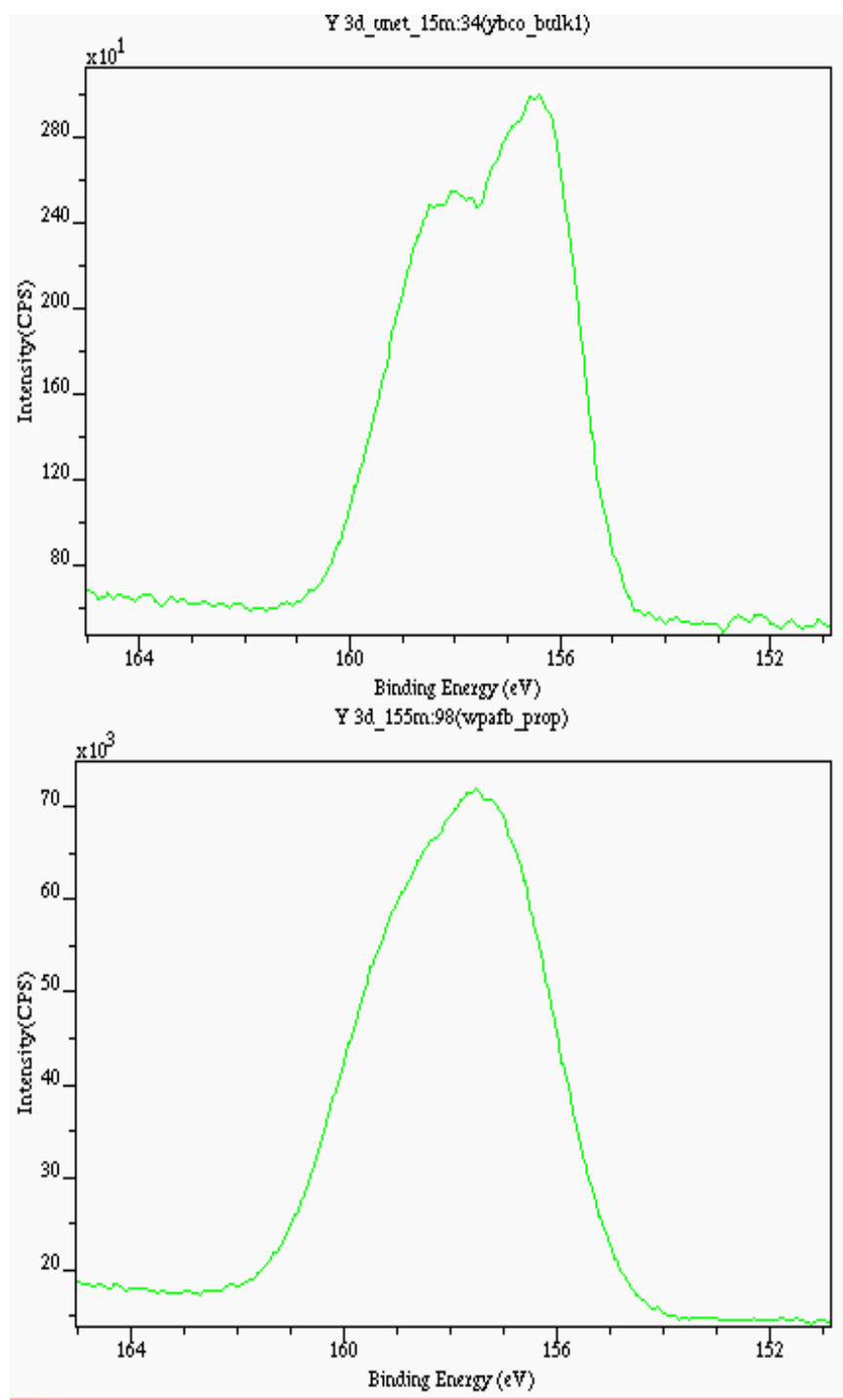


Figure 4.1.6.1

Both samples have been sputtered for some time, so surface contamination/degradation and ion-beam related artifacts could not have caused this difference. A difference in XPS shape might indicate that there may be some difference in the atomic co-ordination between these laser-ablated films and bulk samples made from melt solidification. If this difference can be linked to differences in current carrying capacity, photoelectron peak shapes can be used in monitoring film quality during film production.

4.1.7 YBCO Near Buffer Layer

The bottom 2/3 of the YBCO film showed signs of contamination. Some traces of Ni were seen, but the peaks were not strong enough to be quantifiable. Zr and Ce could also be seen. Averaged over the middle region, the Zr/Y atomic signal ratio is about 8-10%. The Ce/Y ratio is about 3-5%. The Ce concentration increases slowly indicating approach to the YBCO/CeO₂ interface. However, the Zr concentration remains steady.

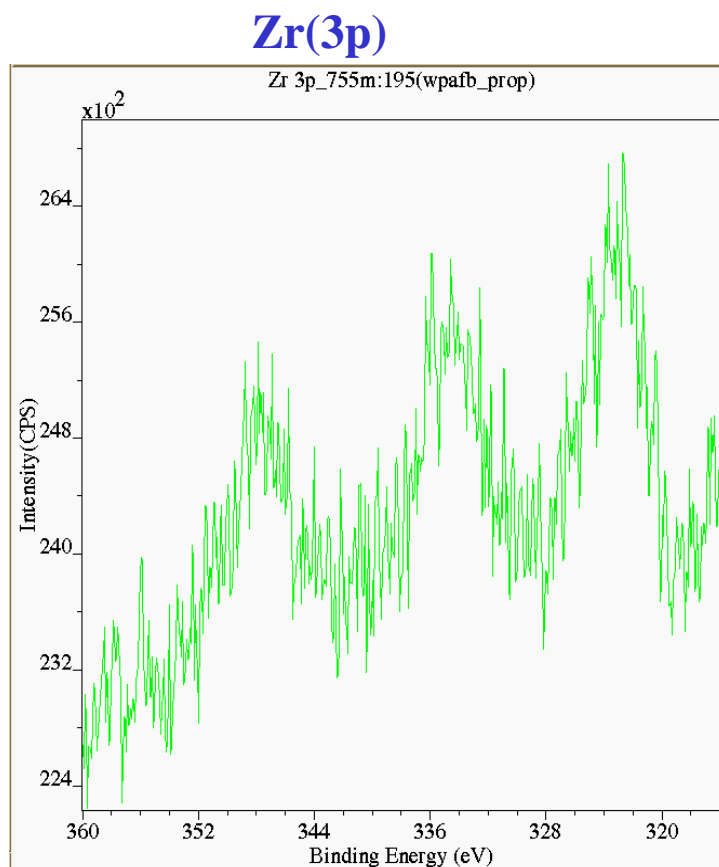


Figure 4.1.8.1

4.1.8 Zirconium Presence

The following figures show the presence of the Zr(2p) component. The top figure shows comparative rapid scans on top layers (no Zr) and deeper regions. The small additional peak from scans obtained deeper in the film is obvious. A careful (high resolution) scan of this region shows the Zr(3d) peak at 184.8 eV next to the Ba(4p) signal. Since the layer adjacent to YBCO is CeO₂, possible Zr diffusion occurs.

4.1.9 Possible Diffusion

The increase in Ce may be due to slightly uneven surface removal. However, the steady Zr concentration clearly indicates the potential diffusion of Zr into the YBCO region. Additional samples are currently being examined to verify this potential in the multi-layered specimen. What is not clear is whether this Zr presence is expected to slightly poison the YBCO, i.e. to

lower the expected J_c or T_c values, or if in fact it may act as pinning centers in the YBCO and possibly enhance its properties slightly. Future studies are needed to determine which the case is.

4.1.10 Conclusions

XPS depth profiling of YBCO coated conductor samples have been performed for the first time. Initial results reveal two important findings: the peak shapes of the Y(3d) photoelectron peak are different in these films compared to bulk YBCO, and the presence of Zr in the YBCO due to possible diffusion from the YSZ layer. The difference in photoelectron peak shapes can well be indicative of the difference in chemical binding that results in the differences in properties of the two.

4.2 Correlation Between the Y(3d) XPS Peak Shape of $\text{Y}_1\text{Ba}_2\text{Cu}_3\text{O}_{7-x}$ and Film Quality: XPS Depth Profiling Comparison

References: 34

4.2.1 Introduction

The purpose of the profiling is to investigate the chemical and microstructural makeup of several YBCO coated conductor samples to determine if a correlation exists between Y(3d) peak shapes and YBCO film quality. This was accomplished by performing detailed XPS depth profiling studies on several samples using an AXIS Ultra XPS Instrument made available by Wright State University. A small area of the specimen's surface was bombarded with 3 KeV Ar^+ ions and the freshly exposed surface was analyzed. The sputtering was done in-situ to avoid surface contamination, since YBCO has chemical reactivity with air. This sputter-analysis cycle was repeated several times, which permitted the determination of the composition and chemistry at different depths of the conductor.

4.2.2 Y(3d) Peak Comparison

The Y(3d) photo-electronic peak shape in films are very different from bulk. This may allow a possible correlation with the desired quality of the films. A difference in XPS peak shape can indicate that there may be some differences in the atomic co-ordination between the samples.

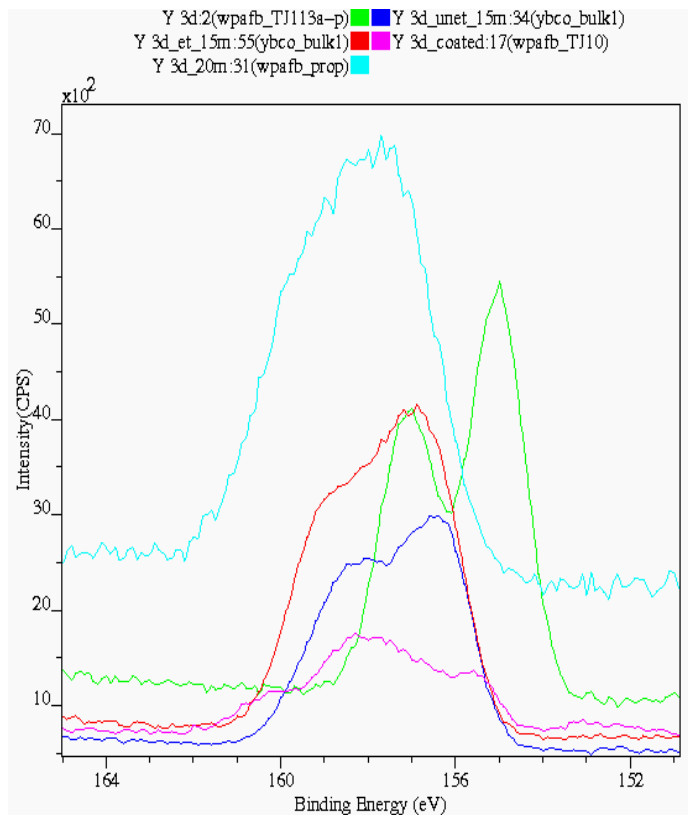


Figure 4.2.2.1

4.2.3 Transport J_c vs. Y(3d_{5/2}) FWHM

- A trend to higher FWHM of Y(3d_{5/2}) XPS peak for lower J_c samples
 - Transport J_c can be affected by physical discontinuities between contacts that will not affect XPS measurement
- Need more samples in 104 MA/cm² and 105 MA/cm² level for verification

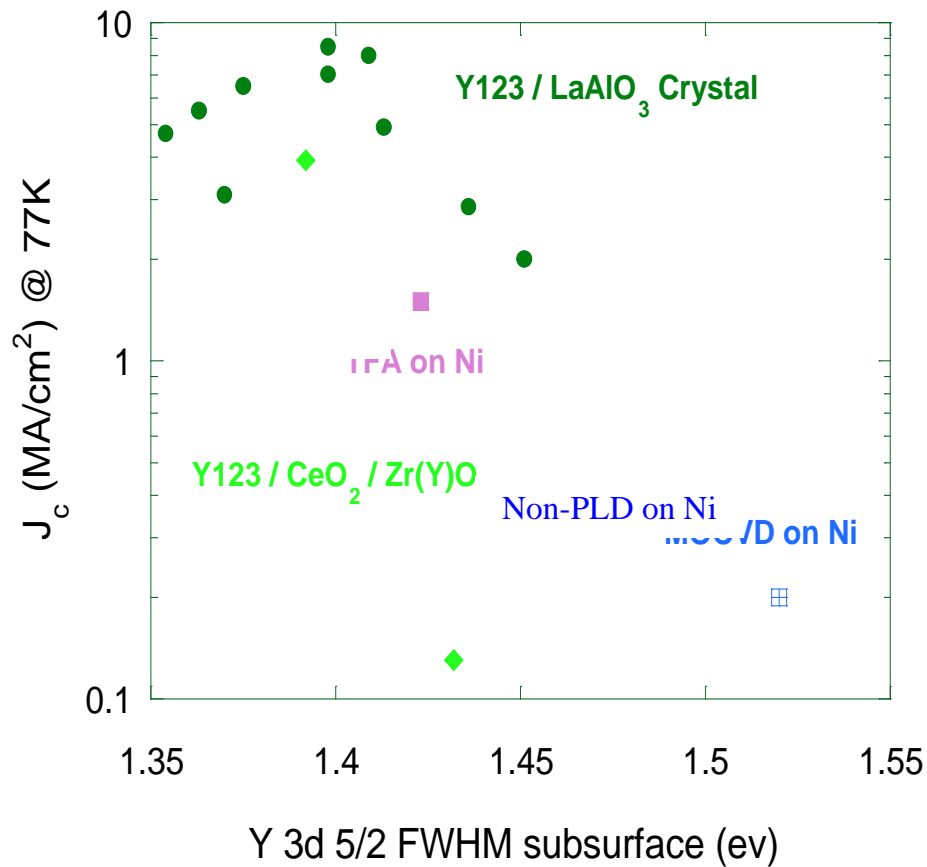


Figure 4.2.3.1

4.2.4 T_c FWHM χ'' vs. Y(3d_{5/2}) FWHM

This is not as clear, but a linearly increasing (log scale) ΔT_c χ'' (susceptibility) with higher FWHM of Y(3d_{5/2}) XPS peak

- Again need more lower quality samples for verification

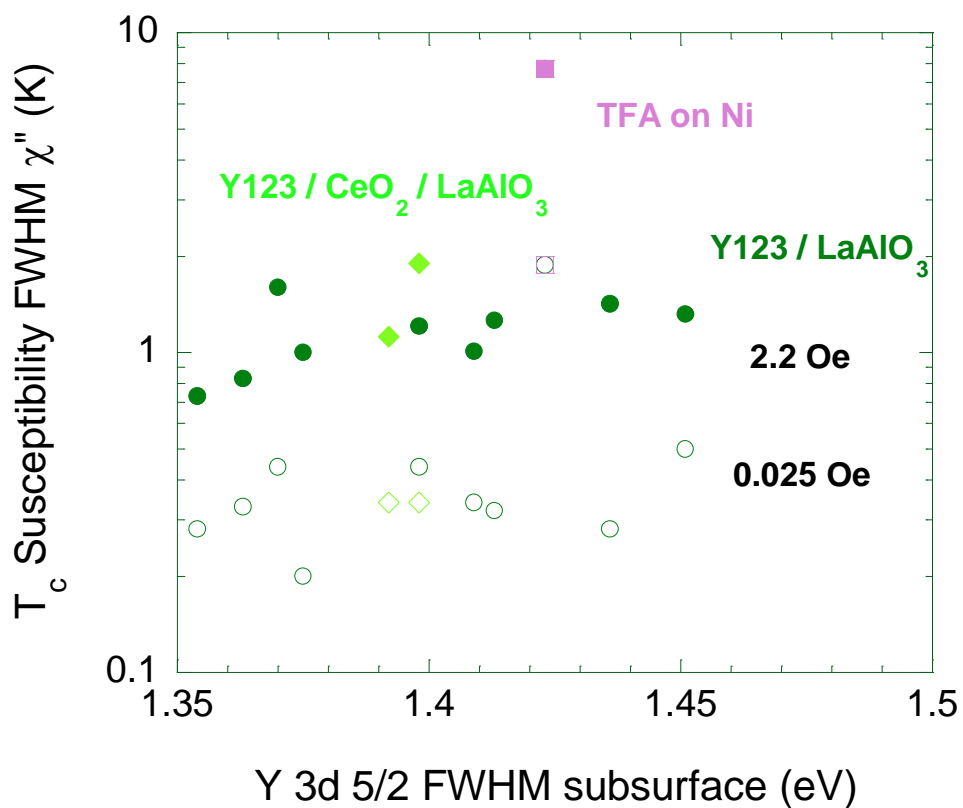


Figure 4.2.4.1

4.2.5 T_c vs. $Y(3d_{5/2})$ FWHM

- No relation seen with T_c

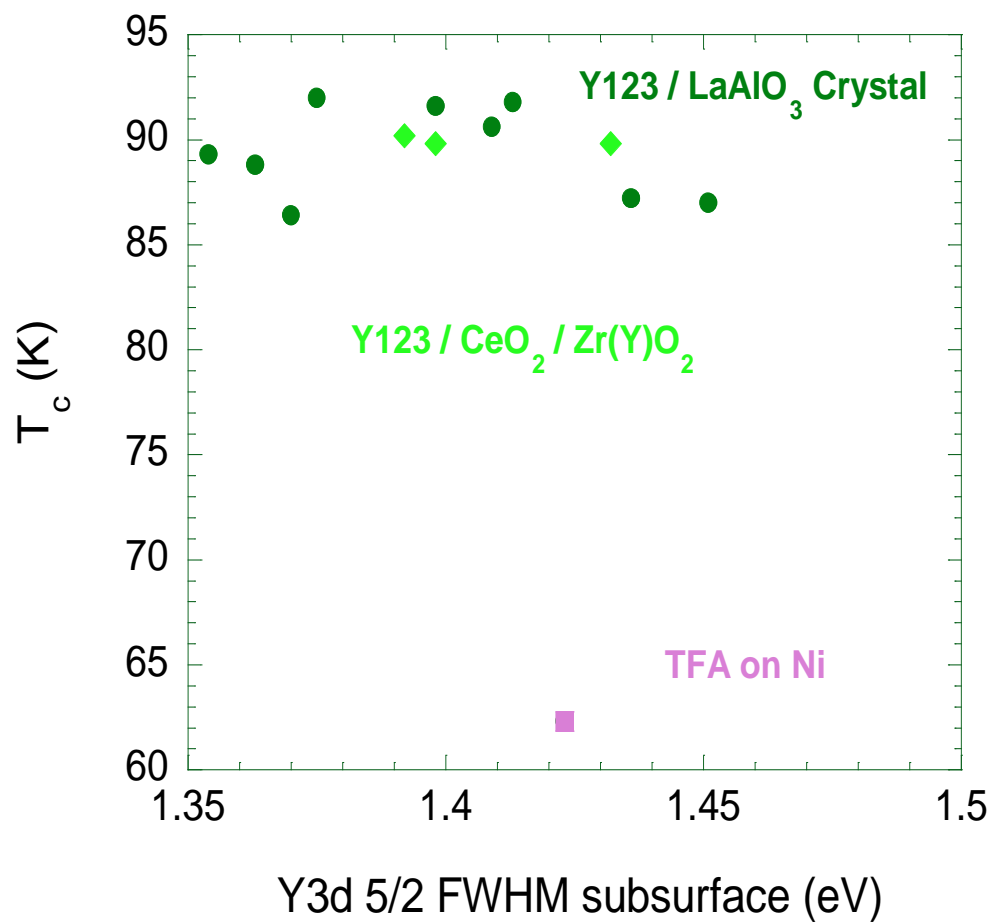


Figure 4.2.5.1

4.2.6 J_c vs. Cu(2p)/Ba(3d) Intensity Ratio

- Relationship is not clear for the given data
 - Transport J_c can be affected by physical discontinuities between contacts that will not affect XPS measurement
- Need more samples in 104 MA/cm^2 and 105 MA/cm^2 level for verification

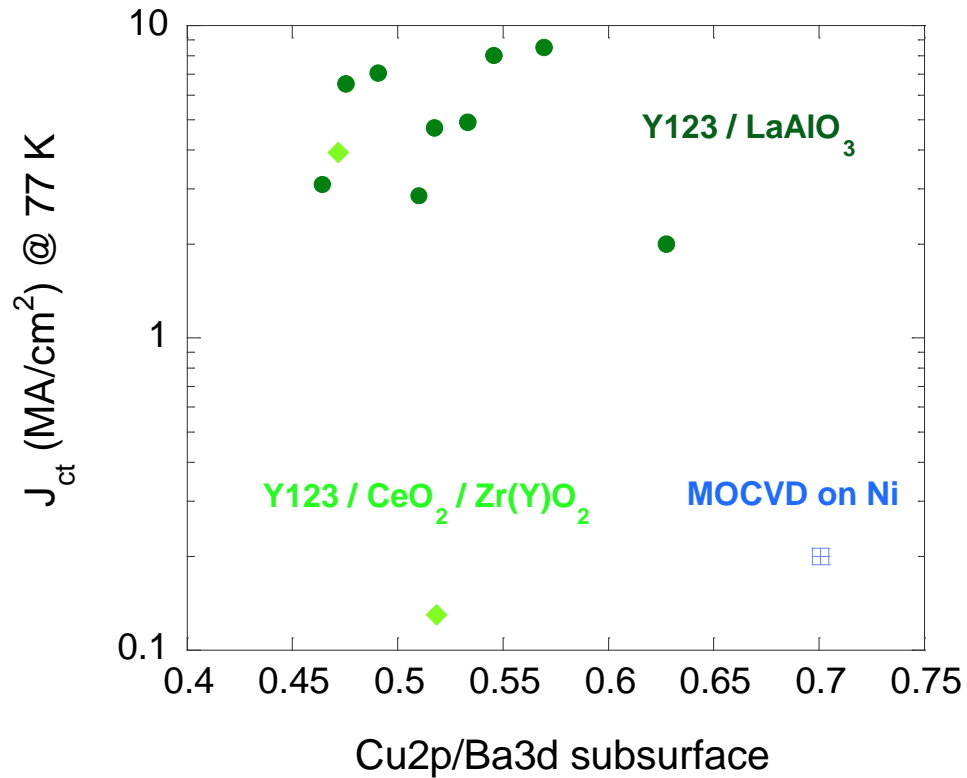
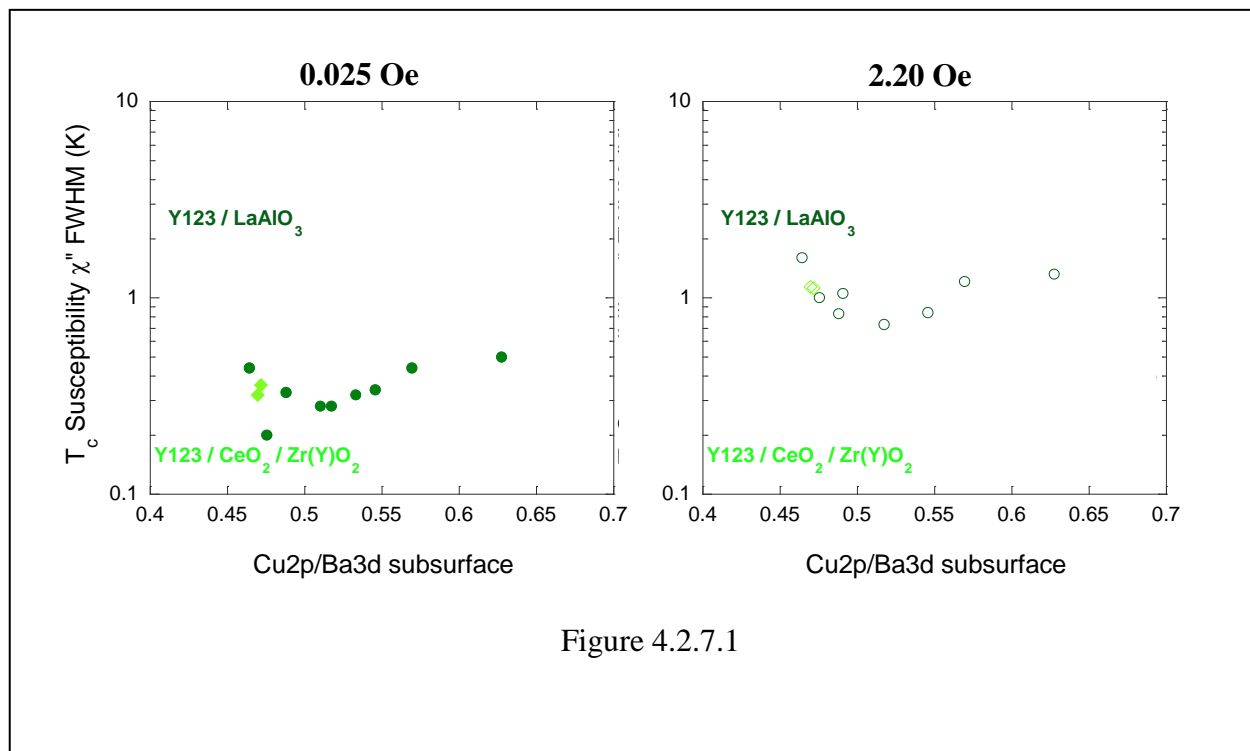


Figure 4.2.6.1

4.2.7 T_c FWHM χ'' vs. Cu(2p)/Ba(3d) Intensity Ratio

- This appears to be the best correlation for the given points
- This correlation is not directly the same as for the Y(3d5/2) FWHM



4.2.8 T_c vs. Cu(2p)/Ba(3d) Intensity Ratio

- Again no real relation seen with T_c

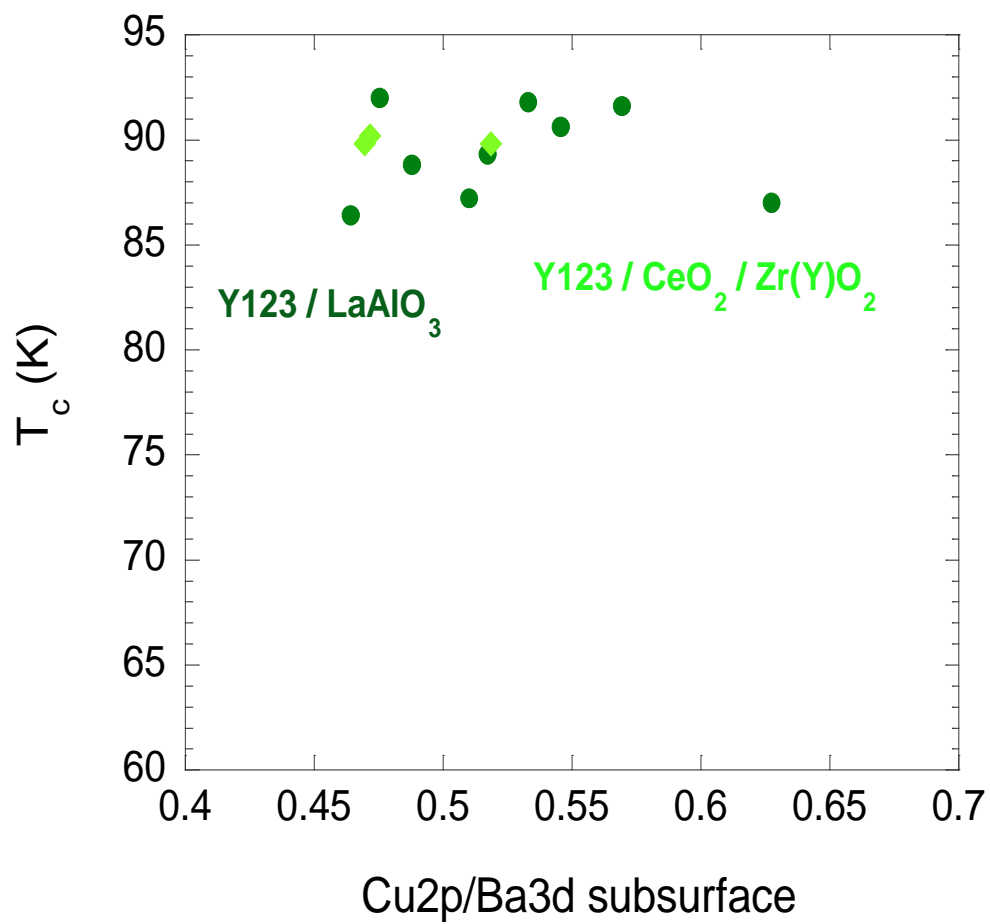


Figure 4.2.8.1

4.2.9 Zr Diffusion Issue

Textured Substrate (YBCO/CeO₂/YSZ/CeO₂/Ni)

- Ce concentration increases with sputter depth into the YBCO (indicating approach to YBCO/CeO₂ interface)
- Zr concentration remains steady in YBCO

Single Crystal (YBCO/CeO₂/YSZ-sc)

- Zr presence not detected in YBCO

• IBAD (YBCO/YSZ/Inconel)

- Zr presence in the YBCO

• Pinning or Poison?

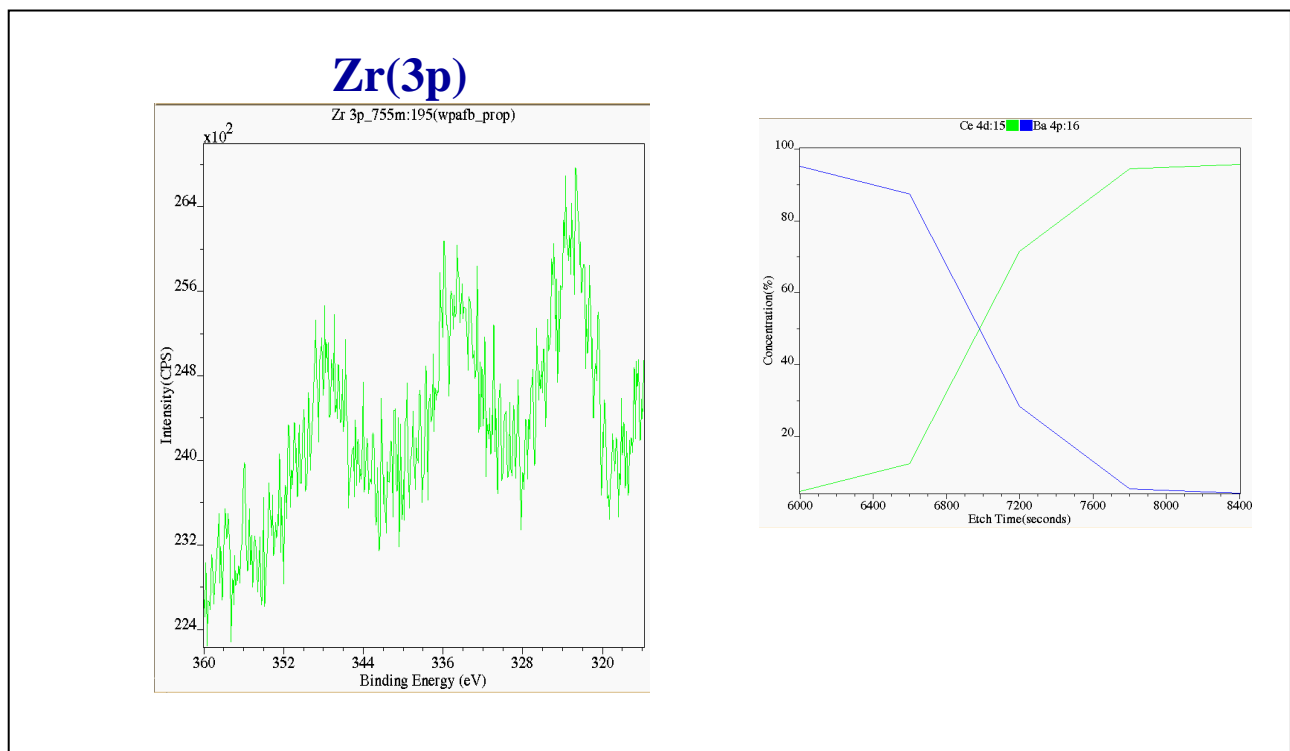


Figure 4.2.9.1

4.2.10 Summary

- Possible correlation of the FWHM of Y(3d_{5/2}) XPS peak of YBCO to the film quality: Transport J_c and ΔT_c χ''
 - Need more data in the 10⁴ MA/cm² and 10⁵ MA/cm² range to verify
- An apparent relationship between the T_c FWHM χ'' vs. Cu(2p)/Ba(3d) XPS peak intensity ratio
 - More data may indicate relationship of Cu(2p)/Ba(3d) intensity ratio with the transport J_c but very unclear at this point
- Not clear now if a direct relationship exists between the FWHM of Y(3d_{5/2}) XPS peak and Cu(2p)/Ba(3d) XPS peak intensity ratio
- Zr diffusion into lower layers of YBCO is evident but not clear how extensive without further samples

4.3 XPS Depth Profiling Comparison #2

References: 34

4.3.1 Sample Preparation

- Most samples by pulsed laser deposition on single crystal LaAlO_3
 - Two samples are PLD YBCO on $\text{CeO}_2/\text{sc-YSZ}$
 - One sample is MOCVD on buffered tape
 - One sample is PLD on buffered tape
- Sample quality variation not intentional except for 2 samples
 - Temperature was reduced by $\sim 100^\circ\text{C}$

4.3.2 Sputtering of Surface

- Since samples were exposed to air the top surface was removed by sputtering
- The before and after sputtering values are largely uncorrelated

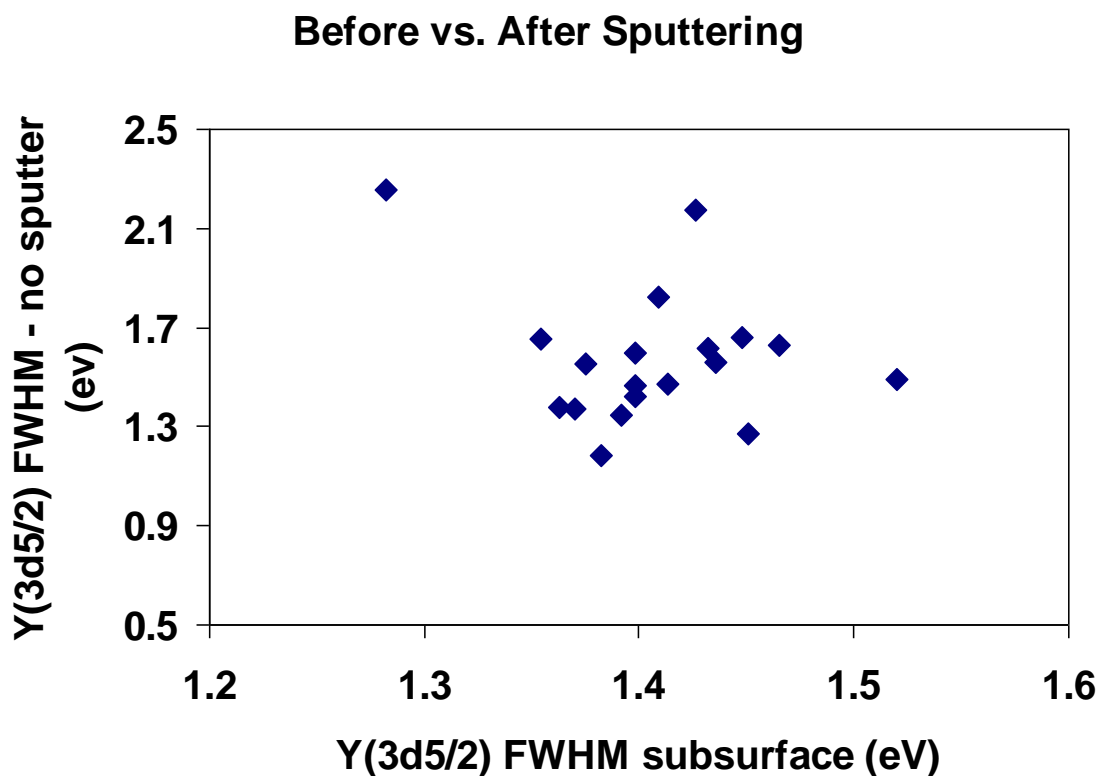


Figure 4.3.2.1

4.3.3 Parameters vs. $Y(3d_{5/2})$ FWHM

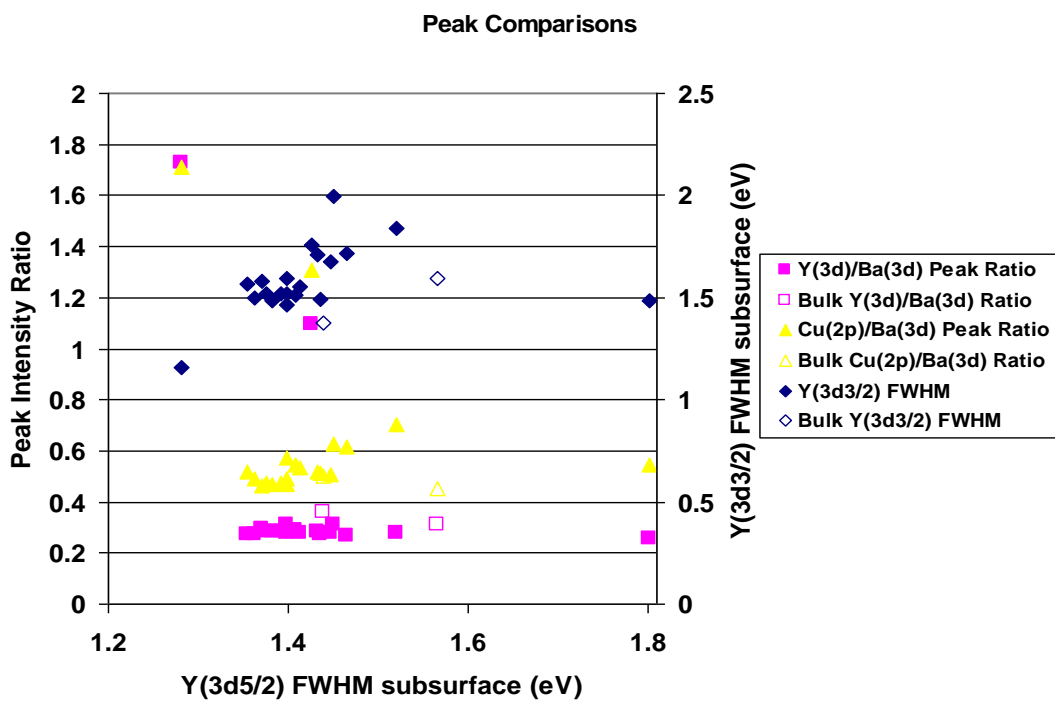


Figure 4.3.3.1

4.3.4 Comparison with $Y(3d_{3/2})$ FWHM

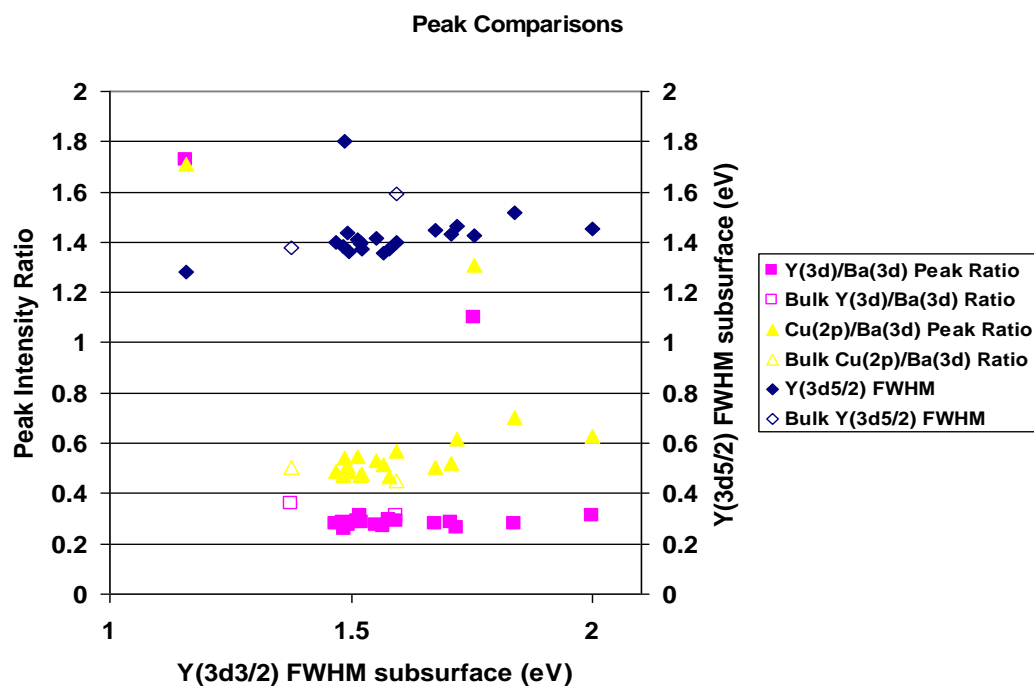


Figure 4.3.4.1

4.3.5 Cu(2p_{3/2}) vs. Y(3d_{5/2}) Intensity

- The two stray points as in previous charts were the two that were intentionally made bad by altering temperature
- Difference likely caused by film inclusions of alternate phases
- One film did have low J_c

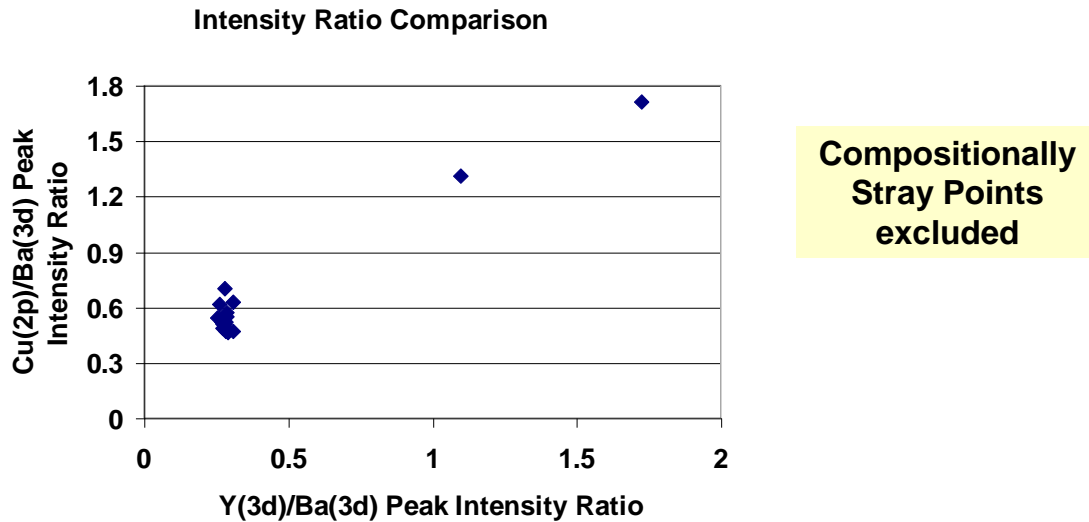


Figure 4.3.5.1

4.3.6 T_c vs. Y(3d_{5/2}) FWHM

- No correlation with T_c

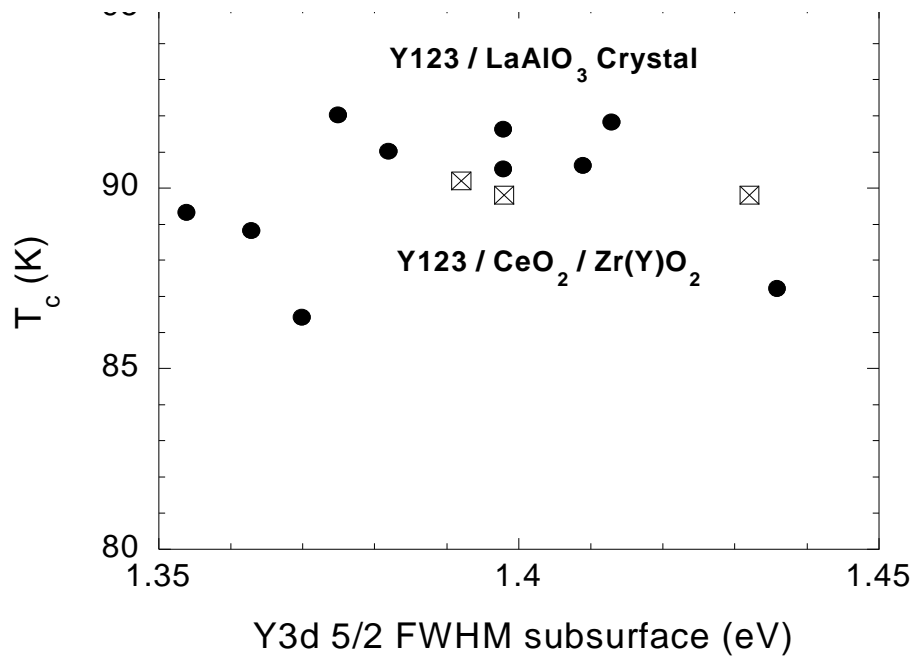


Figure 4.3.6.1

4.3.7 Transport J_c vs. $Y(3d_{5/2})$ FWHM

- Correlation of the FWHM for the $Y(3d_{5/2})$ peak and the critical transport current (four point resistive)
- The $Y(3d_{5/2})$ photoelectron peak shape FWHM correlates with the critical transport current of the YBCO films.
- Although scatter present, the trend is apparent.

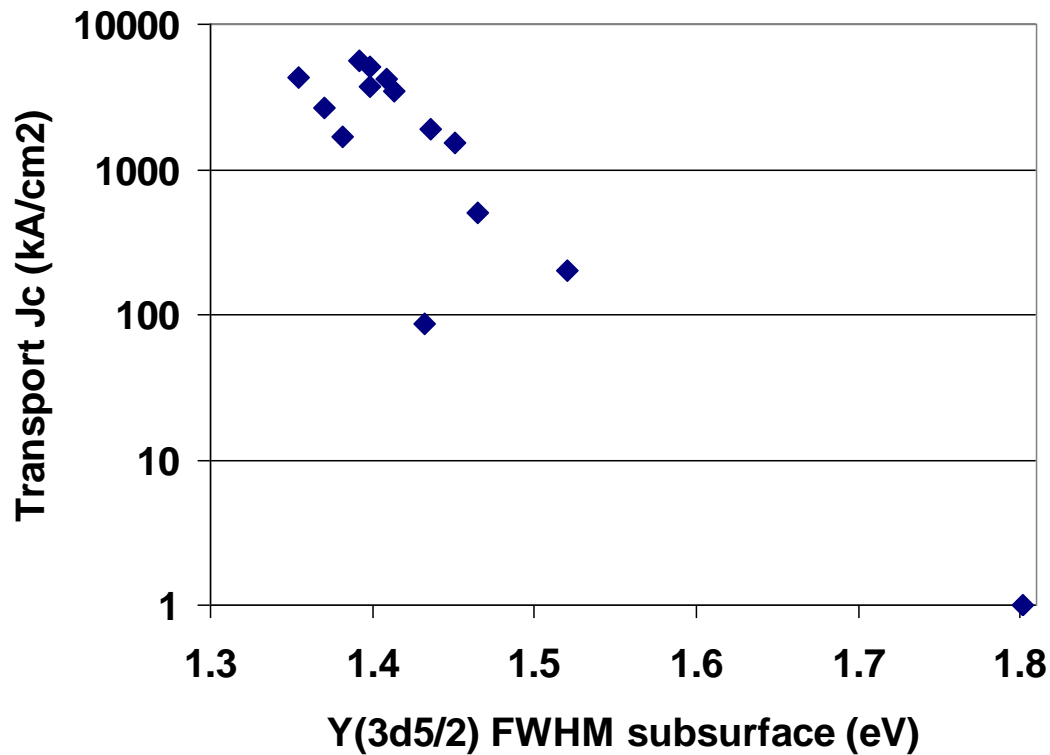


Figure 4.3.7.1

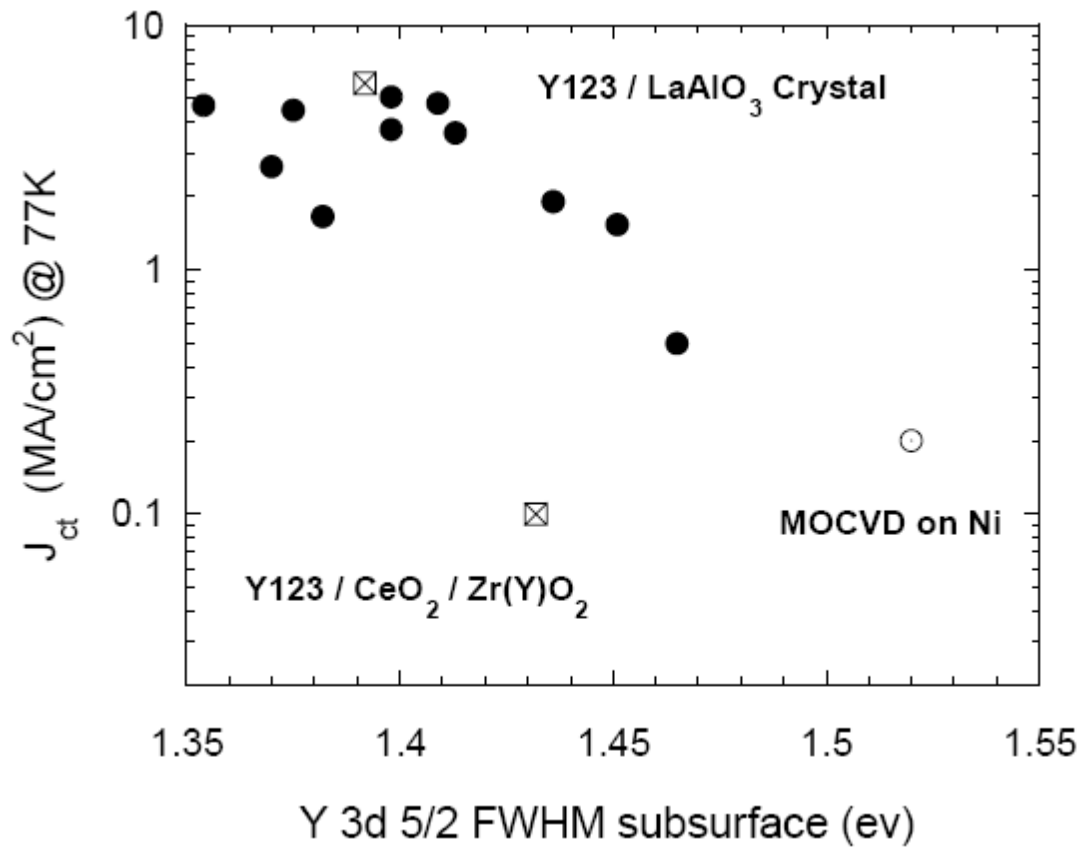


Figure 4.3.7.2

4.3.8 T_c FWHM χ'' vs. Y(3d_{5/2}) FWHM

- Correlation of the FWHM for the Y(3d_{5/2}) peak and the FWHM of the critical transition temperature by susceptibility measurement
- T_c FWHM data determined by comparison to 2.2 Oe magnetic field data.

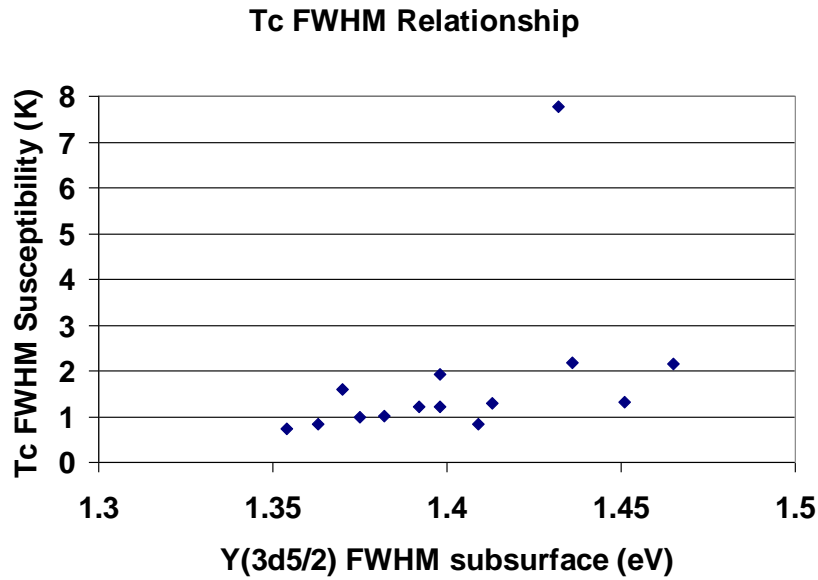


Figure 4.3.8.1

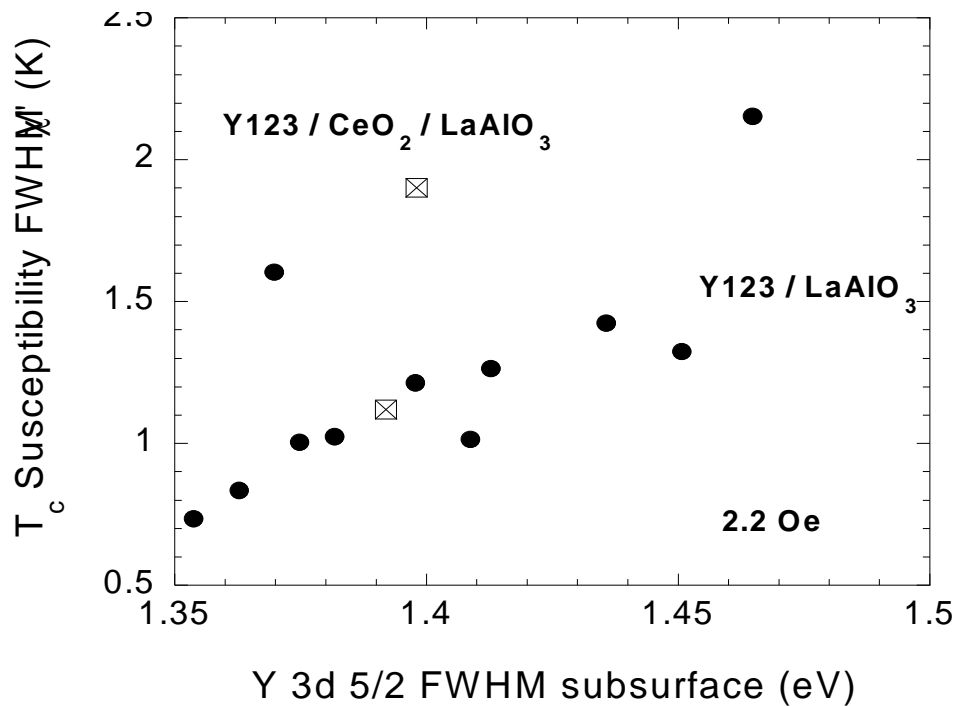


Figure 4.3.8.2

4.3.9 Transport J_c vs. Y(3d_{3/2}) FWHM

- Correlation of the FWHM for the Y(3d_{3/2}) peak and the critical transport current (four point resistive)
- Note the greater scatter in the plot with the Y(3d_{3/2}) peak as opposed to the Y(3d_{5/2})

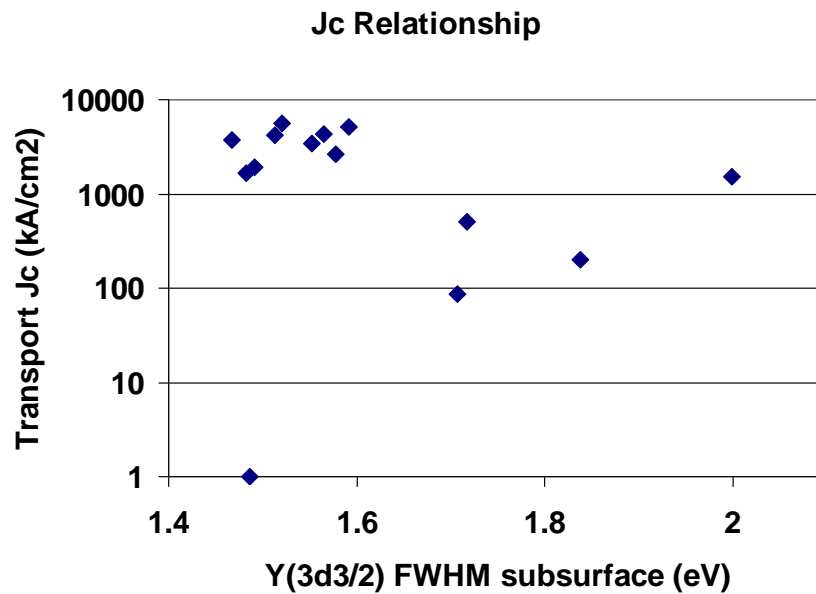


Figure 4.3.9.1

4.3.10 Transport J_c vs. $Y(3d_{3/2})$ FWHM

- Correlation of the FWHM for the $Y(3d_{5/2})$ peak and the FWHM of the critical transition temperature by susceptibility measurement
- T_c FWHM data determined by comparison to 2.2 Oe magnetic field data.
- Note the significant scatter in the plot with the $Y(3d_{3/2})$ peak as opposed to the $Y(3d_{5/2})$

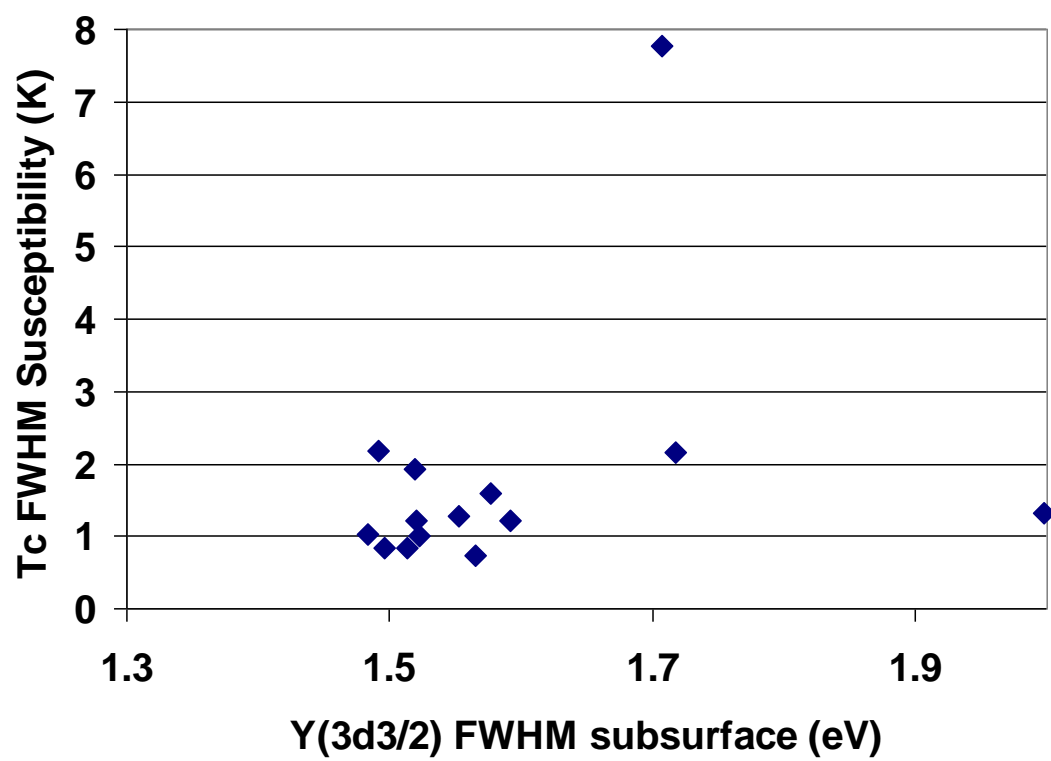


Figure 4.3.10.1

4.3.11 XPS Depth Profiling

- To investigate chemical and microstructural profiles of YBCO coated conductor samples.
- Performing detailed XPS depth profiling studies on several samples
- bombard small area of the specimen surface with 3 KeV Ar^+ ions and analyze the freshly exposed surface
- repeat sputter-analysis cycle
- determine composition and chemistry at different depths of the conductor

Ba (3d)

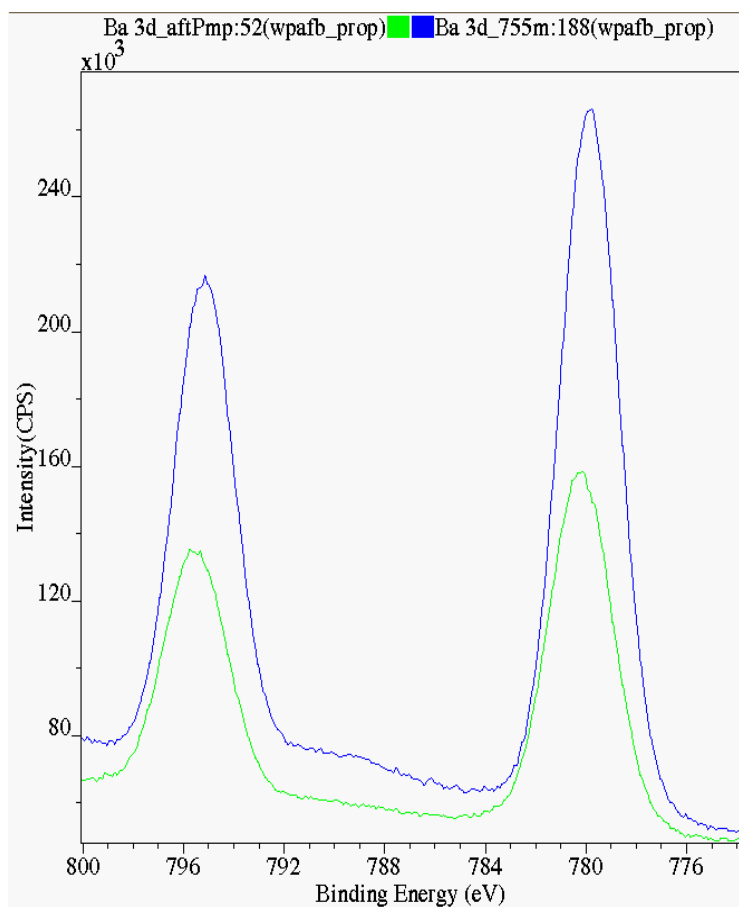


Figure 4.3.11.1

4.3.12 Zr Diffusion Issue

- Textured Substrate (YBCO/CeO₂/YSZ/CeO₂/Ni)
- Ce concentration increases with sputter depth into the YBCO (indicating approach to YBCO/CeO₂ interface)
- Zr concentration remains steady in YBCO
- Single Crystal (YBCO/CeO₂/YSZ-sc)
- Zr presence not detected in YBCO
- IBAD (YBCO/YSZ/Inconel)
- Zr presence in the YBCO

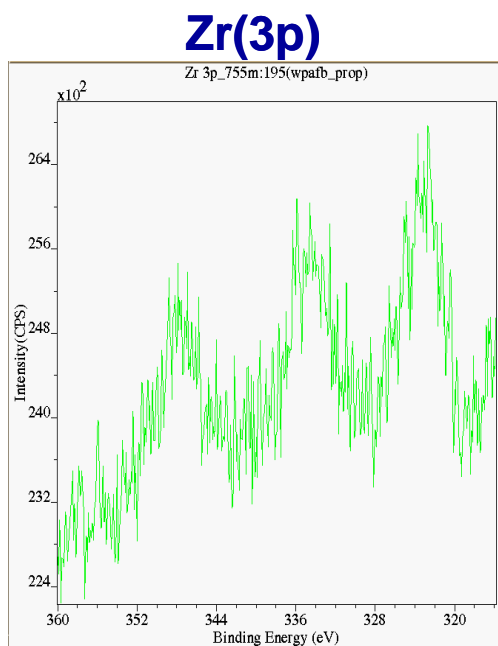


Figure 4.3.12.1

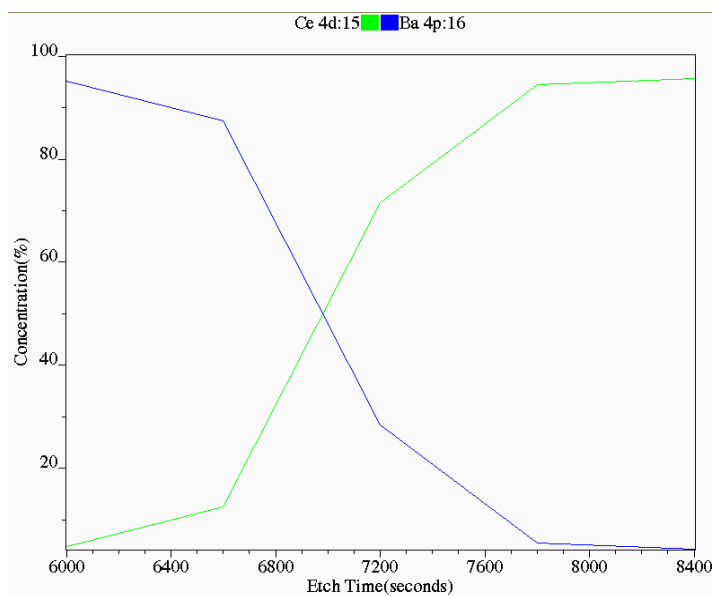


Figure 4.3.12.2

4.3.13 Summary

- It is seen that the FWHM of certain peaks as well as cationic peak ratios averaged over the analysis area can vary between differently grown samples.
- A possible correlation of the FWHM of the Y(3d5/2) XPS peak of YBCO to the thin film quality, specifically the critical transport current J_c , may exist.
- Broadening of the FWHM of the Y(3d5/2) XPS peak can indicate alternate undesirable bonding in the YBCO.
- More data is necessary to fully verify these relationships.

4.4 Photoelectron Spectroscopy of Superconducting Tapes

References: 34

¹S. Krishnaswami, ¹S. M. Mukhopadhyay, ²P. N. Barnes, ²T. J. Haugan, ²J. C. Tolliver, ²C. B. Cobb, ¹Pratik Joshi, and ¹Rajasekhar V. Pulikollu

¹*Wright State University, Dayton, OH 45432,*

²*Air Force Research Laboratory, Dayton, OH 45433*

The correlation between chemical properties and processing techniques of various thin films has been investigated. Coated conductors grown by PLD and MOCVD on single crystals and on metallic substrates have been compared. X-ray Photoelectron Spectroscopy (XPS) has been used in conjunction with ion beam sputtering to obtain composition and chemistry information at different depths into the film. It is seen that variations in overall composition such as average cationic ratios exist between films and may be used as possible indicators in monitoring film growth. It is also observed that films grown on metallic substrates (buffered with YSZ and CeO₂) have Zr diffusion into the YBCO region whereas those grown on single crystal zirconium (buffered with CeO₂) do not. These studies indicate that mechanisms of cationic diffusion from substrates and buffer layers into the superconducting region need to be investigated in carefully prepared specimens.

4.4.1 X-Ray Photoelectron Spectroscopy (XPS)

**XPS, Kratos
Analytical Inc.**



- Irradiation of the sample in vacuum with mono-energetic soft x-rays and sorting the emitted electrons by energy
- $KE = h\nu - BE$
KE = Kinetic Energy of the emitted electron
 $h\nu$ = Energy of the photon
BE = Binding Energy of the atomic orbital from which the electron originates
- BE is characteristic of the element present
- Mostly non-destructive

Figure 4.4.1.1

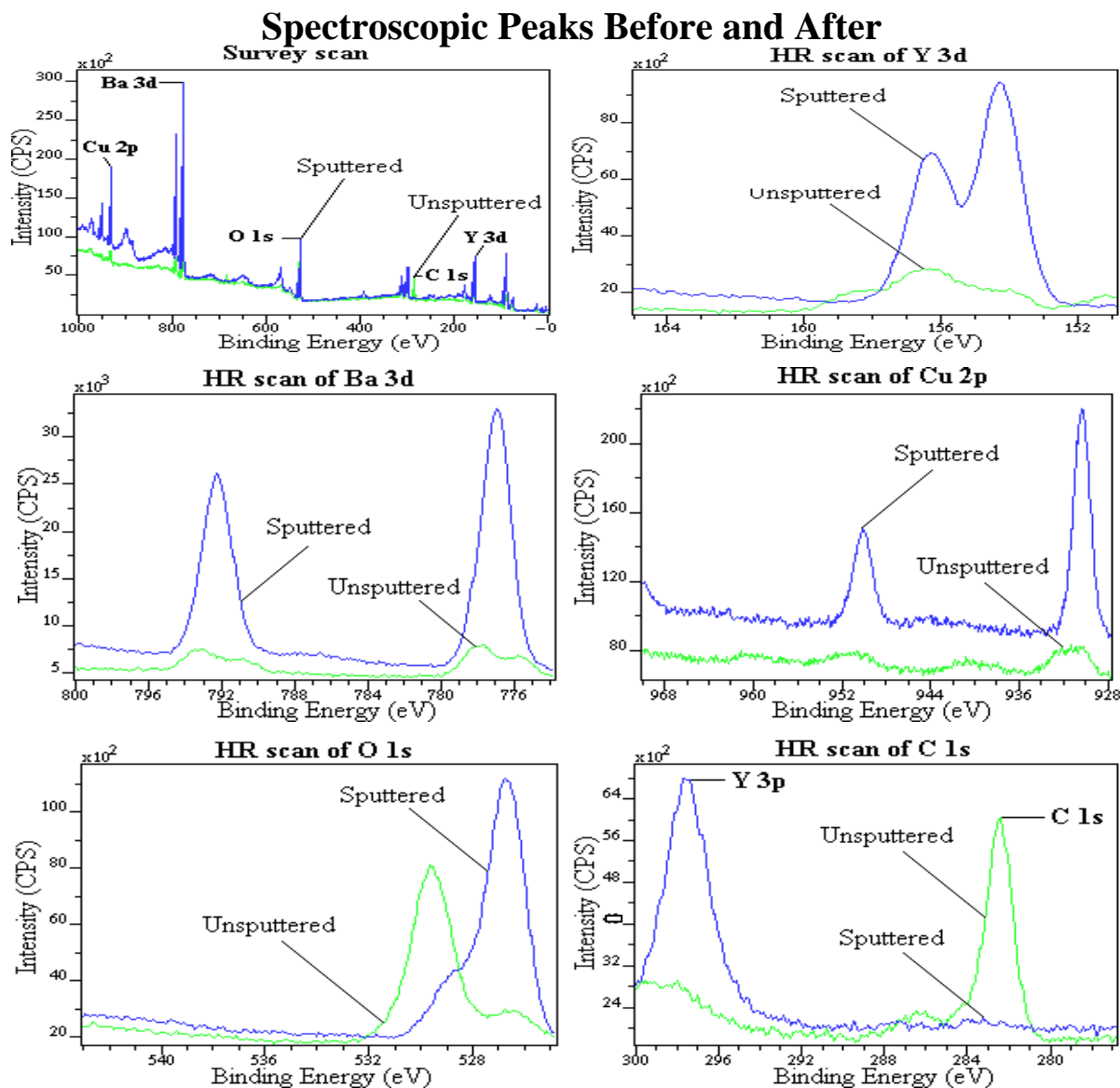


Figure 4.4.1.2

4.4.2 Spectroscopic Peaks Before and After Sputtering

- The outer surface is contaminated with carbonates, hydroxides and other phases due to the samples being exposed to atmosphere
- The intensity of Y, Ba, Cu and O increased considerably and the peaks became steady with 10-20 minutes of etching
- The bulk perovskite peak of O 1s at the lower binding energy region came up after sputtering, which is characteristic of the peaks obtained from the YBCO layer

4.4.3 Microstructural Study

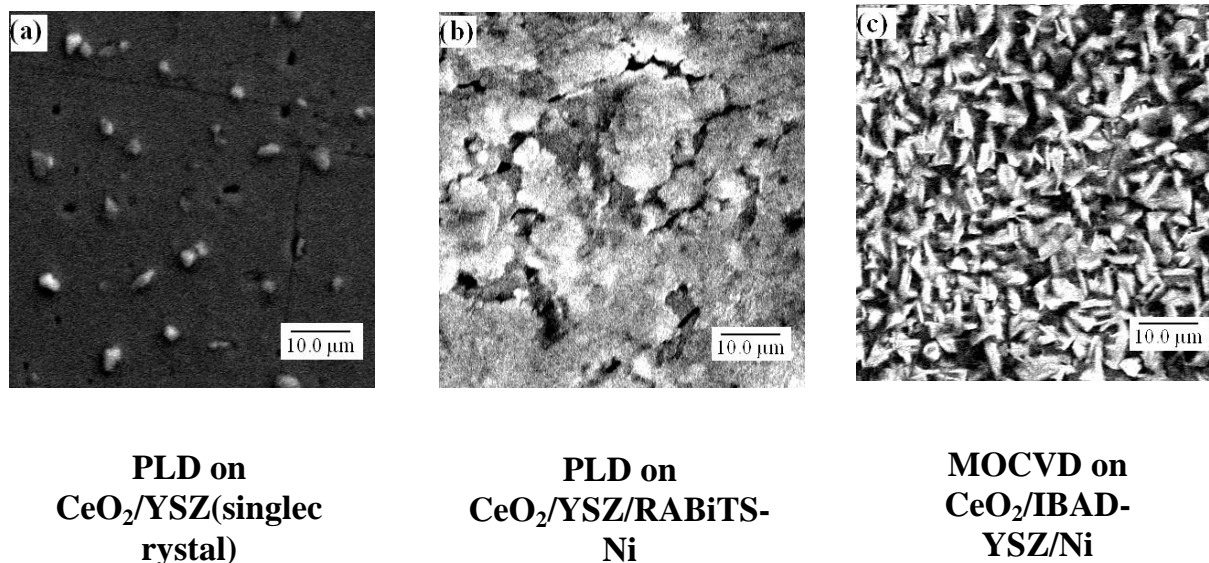


Figure 4.4.3.1

- The grain boundary texture of YBCO is driven by that of the buffer layers
- The grain boundary density (area of boundary per unit volume) is the lowest in sample (a) and highest in sample (c)

Zirconium Diffusion Into The YBCO Layer

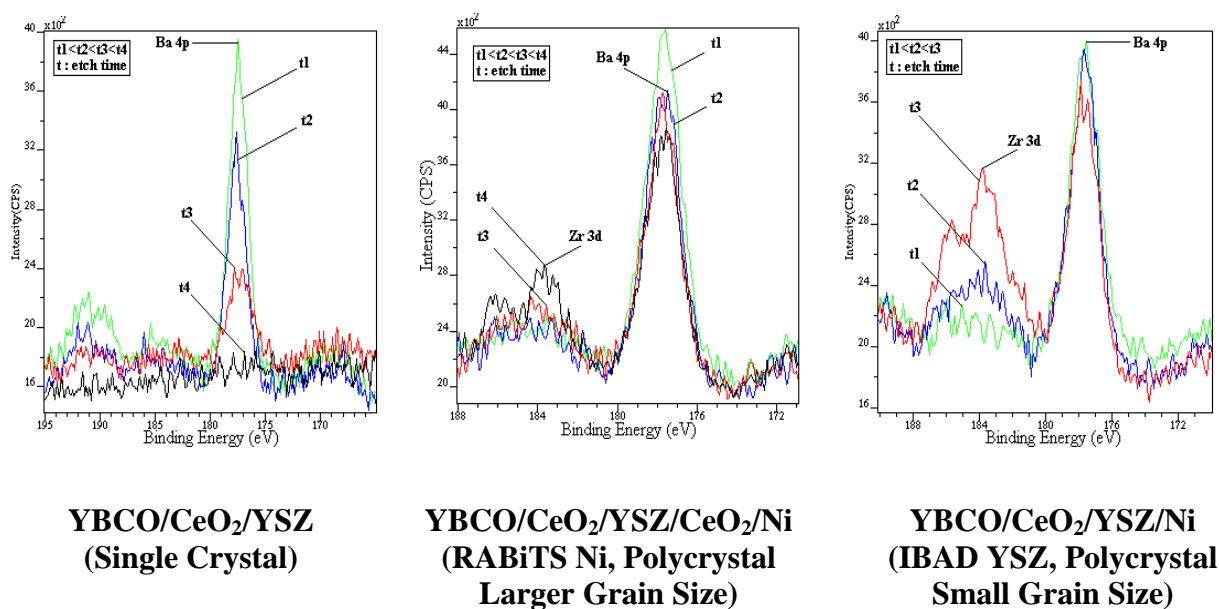


Figure 4.4.3.2

4.4.4 Films grown on Polycrystalline substrates show Zirconium diffusion from the buffer layers into the YBCO layer

- Such affects are lacking in single crystal films
- More detailed investigation in carefully prepared bi-crystals may be useful in analyzing the grain boundary diffusion mechanisms of cations through buffer layers

XPS Peaks of Different Samples

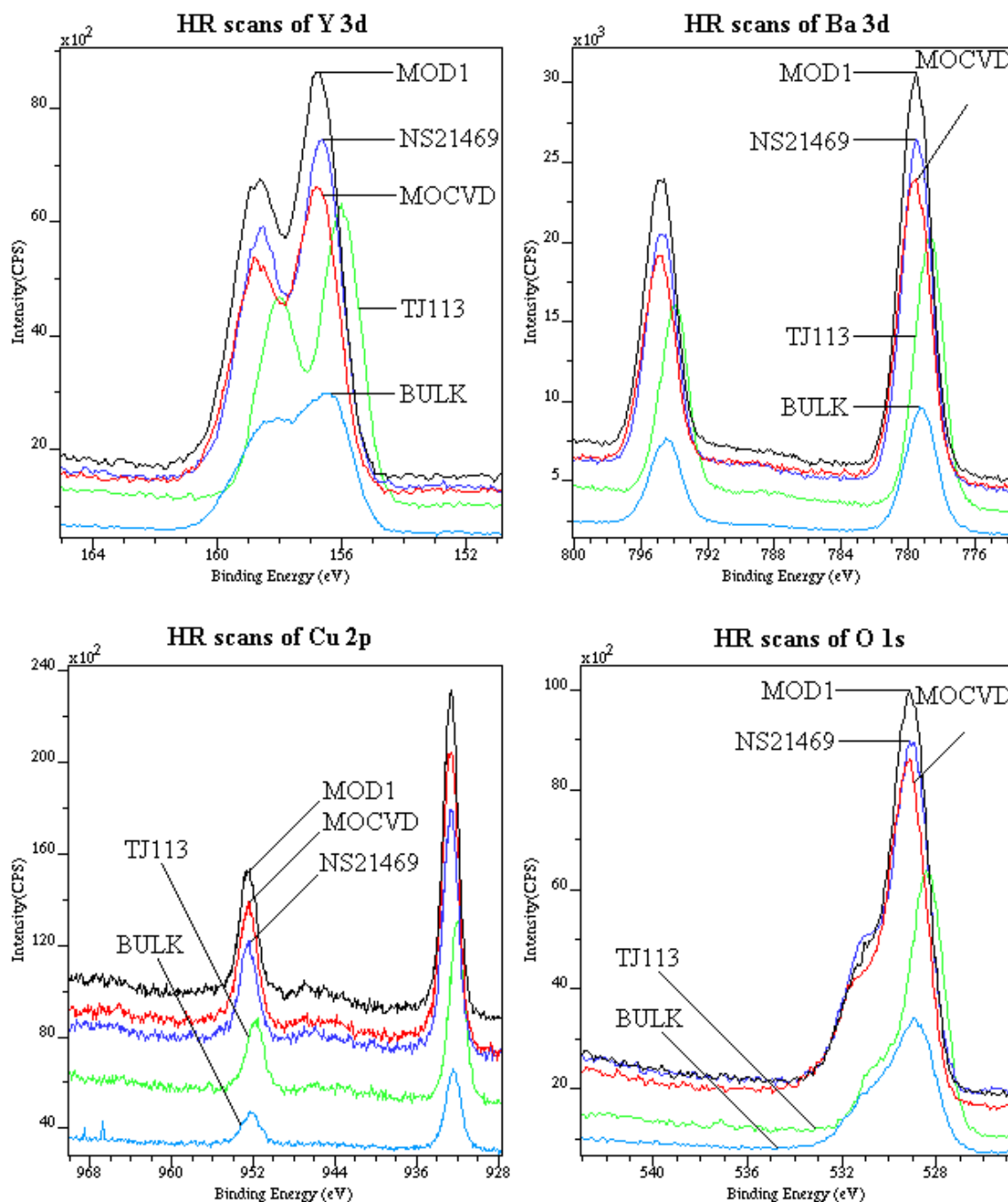


Figure 4.4.4.1

- The peaks obtained in all the samples are characteristic of Y-123
- The bulk material gives relatively broader and less resolved peaks compared to all thin film materials, which is possibly due to the presence of other phases and inclusions

4.4.5 XPS And Electrical Data For Different Samples

Sample	After sputtering		J_c @ 77K (MA/cm ²)	T_c onset (K)
	Y_{3d}/Ba_{3d}	Cu_{2p}/Ba_{3d}		
TJ113 (PLD on single crystal YSZ)	0.31	0.47	~ 2	89.8
NS21469 (PLD on Ni alloy)	0.28	0.51	<< 0.1	--
MOCVD (MOCVD on Ni alloy)	0.28	0.70	0.25	--
TJ10 (PLD on single crystal LaAlO ₃)	0.28	0.48	~ 6.5	92
MOD1 (TFA on Ni alloy)	0.28	0.57	Could not measure due to low T_c	62

Figure 4.4.5.1

4.4.6 The amount of copper present may be related to the grain boundary density in these films

Sample prepared using MOCVD has higher copper content and also higher grain boundary density

- Samples on single crystal substrates have the lowest copper content and correspondingly lower grain boundary density]
- XPS spectra are averaged over several grains and boundaries and hence it is not possible to detect the change in composition between grain interiors and boundaries
- Films grown on bi-crystals or other carefully prepared boundaries may be used for further investigation.

4.4.7 Summary

- The XPS photoelectron peaks and cationic concentration profiles of several thin film superconductors have been compared
- It is seen that overall cationic peak ratios averaged over the analysis area can vary between differently grown samples. This may possibly arise from differences in grain boundary composition and structure, and need to be monitored for film reliability
- Films grown on polycrystalline metallic substrates show Zr diffusion from the buffer layers into the YBCO, but those grown on single crystal substrates do not

Thin film studies involving a single grain boundary (films grown on a bi-crystal) or other carefully prepared boundaries may be needed to identify the atomistic mechanism of these changes.

Chapter 5: Substrates and Buffer Layers

5.1 Biaxially Textured Copper and Copper Alloy Substrates for use in HTS Coated Conductors

References: 33, 35

Chakrapani V. Varanasi*, Nicholas A. Yust, Jack Burke, Jason Carpenter, Lyle Brunke*, Srinivas Sathiraju, Paul N. Barnes, R. Srinivasan**

*University of Dayton Research Institute Dayton, OH

** Wright State University, Dayton, OH

Air Force Research Laboratory, Wright- Patterson Air Force Base, OH

Presented at ASM 2004

Biaxially Textured Copper Alloy Substrates and Buffer Layer Growth

Pani Varanasi*, Nick Yust, Paul N. Barnes

*University of Dayton Research Institute Dayton, OH

Air Force Research Laboratory, Wright- Patterson Air Force Base, OH

Presented at AFOSR 2005

5.1.1 High Temperature Superconductor Wire Architecture

- Yttrium barium copper oxide, $\text{YBa}_2\text{Cu}_3\text{O}_{7-x}$, or YBCO
- High temperature superconductor (HTS), $T_c = 92 \text{ K}$
- Coated conductors, $J_c > 1 \text{ MA/cm}^2$

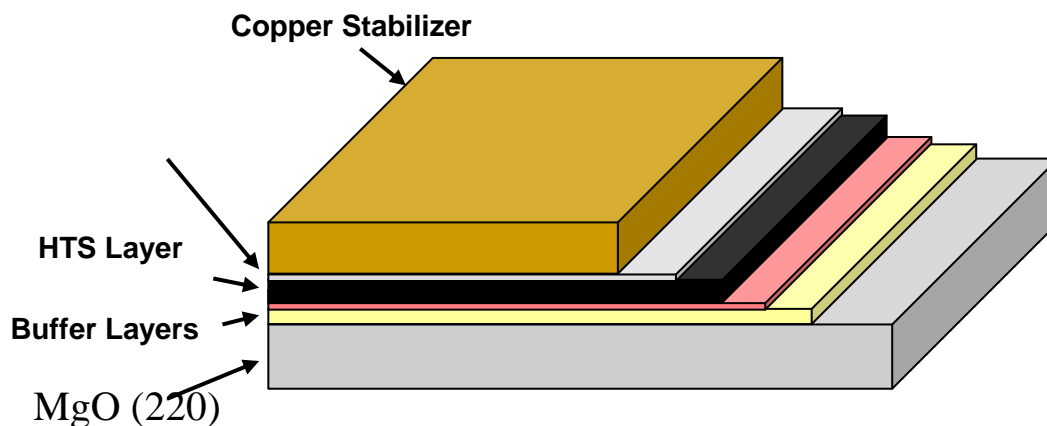


Figure 5.1.1.1

5.1.2 Biaxially Textured Metallic Substrates

- Heavily deformed fcc metals with medium to high stacking fault energy develop cube recrystallization textures $\{001\} < 100 >$ when properly annealed.
- The rolling-assisted biaxially textured substrate (RABiTS) process incorporates cube textured metallic substrates (e.g. Ni) to transfer texture into buffer layers and superconductor layers.
- Substrate grain misorientation influences the current density (J_c) of YBCO coated conductors.

5.1.3 Copper and Copper Alloy Substrates

Biaxially textured Copper and Copper alloy substrates are of great interest for the development of coated conductors intended for ac applications as they offer:

- Low ferromagnetic losses in ac applications
- High thermal and electrical conductivity (useful for thermal stabilization)
- Lower cost (5-6 times less than Ni alloys)
- Mechanical strength that can be improved by alloying

5.1.4 Experimental

- Pure copper (99.99%) and Cu 97.5% - Fe 2.5% alloys were used
- Reverse cold rolling was used to get more than 99% reduction in thickness with 10% reduction per pass
- Samples were annealed at 750°C - 1000°C in Ar/H₂ atmosphere
- Characterization :
 - Texture : Cube texture in the substrates was analyzed by XRD scans-viz., two theta, phi, psi, omega as well as orientation imaging microscopy (OIM)
 - Magnetic properties: Magnetization measurements to determine saturation magnetization (Msat) were taken in a vibrating sample magnetometer (VSM) at 5K and 77K
 - Mechanical Properties: Stress-strain curves were obtained on 3mm wide and 3 cm long annealed substrates using an Instron tensile testing machine
 - Electrical Properties: Resistivity data at 300K and 77K
 - Microstructures - SEM
- Buffer layers on these substrates
 - Ni-20wt%Cr
 - Pt (University of Cincinnati, Prof. Lin)
- In situ annealing experiment results with YSZ buffer layer

5.1.5 Results: Copper Substrate

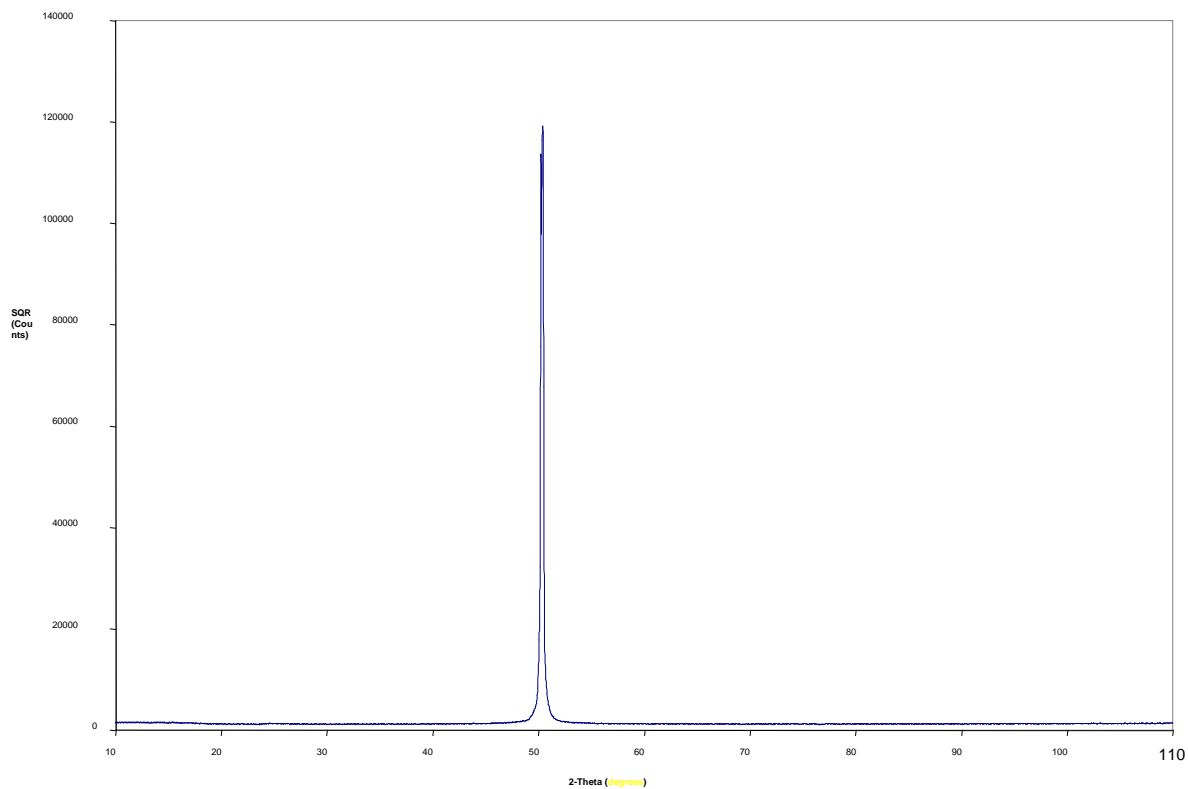


Figure 5.1.5.1 Two Theta scan of a textured Copper substrate

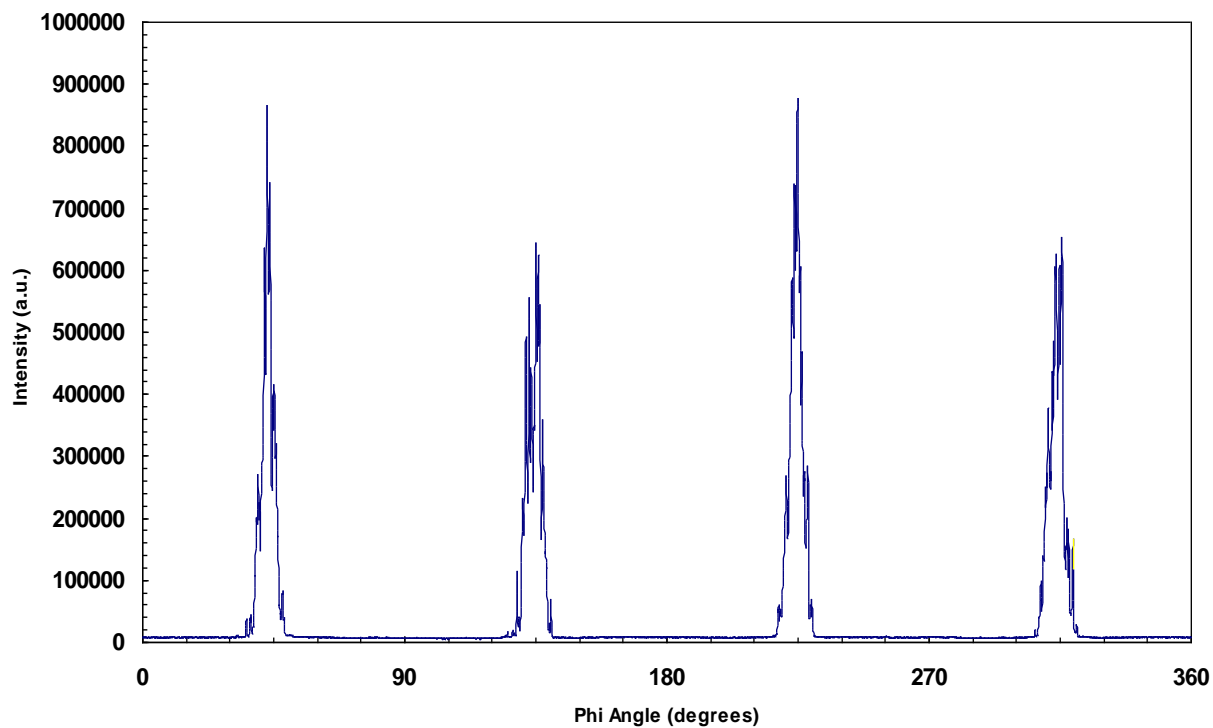


Figure 5.1.5.2 (111) PHI scan on a textured Copper substrate. FWHM 4.7°

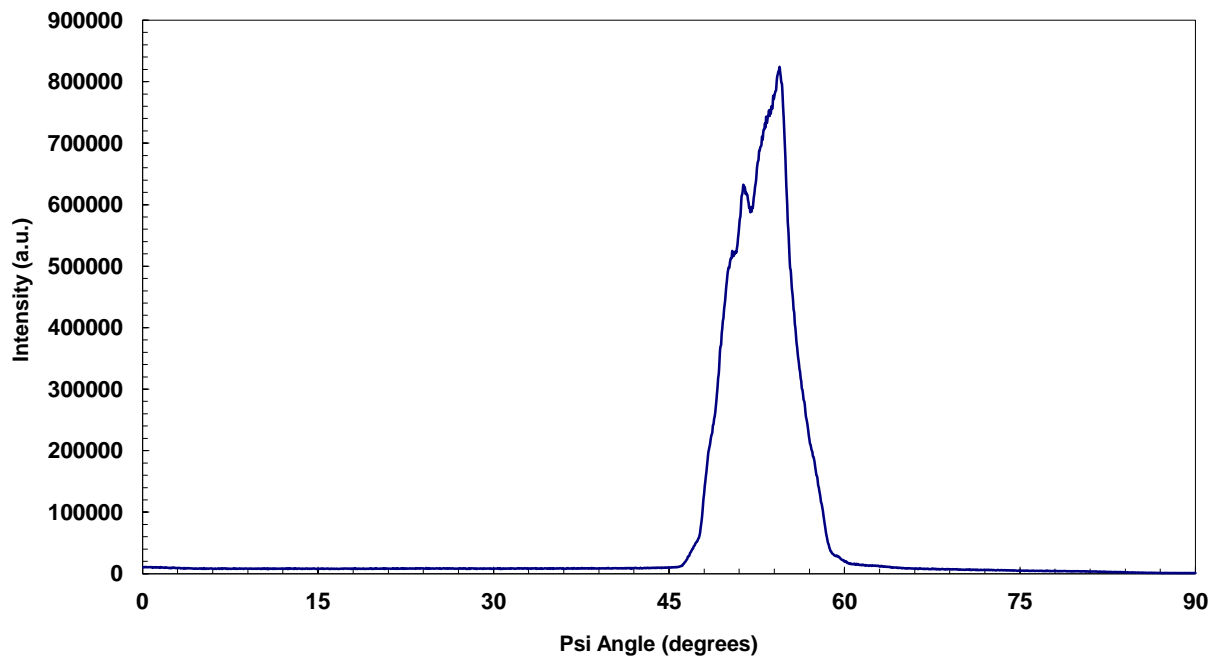


Figure 5.1.5.3 PSI scan on (111) peak of a textured copper substrate.
FWHM 6.2°

Omega Scan on CUPT5

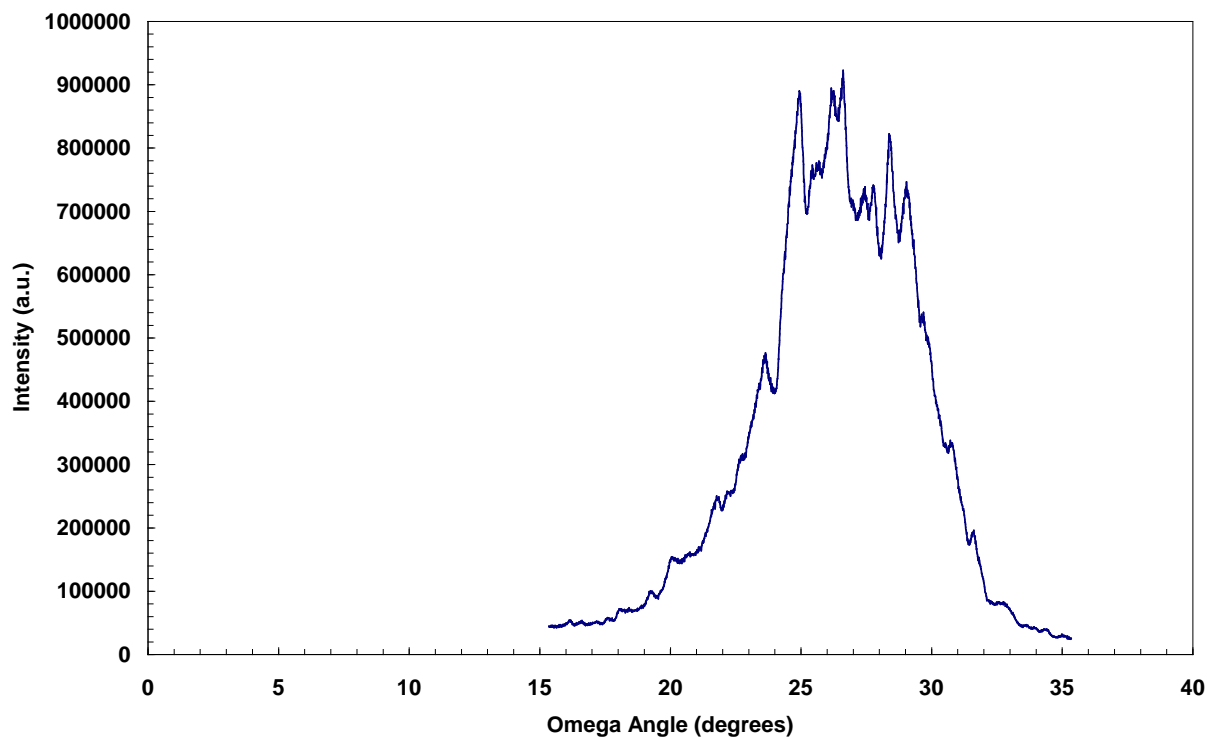


Figure 5.1.5.4 (200) Omega scan parallel to rolling FWHM 6.3°

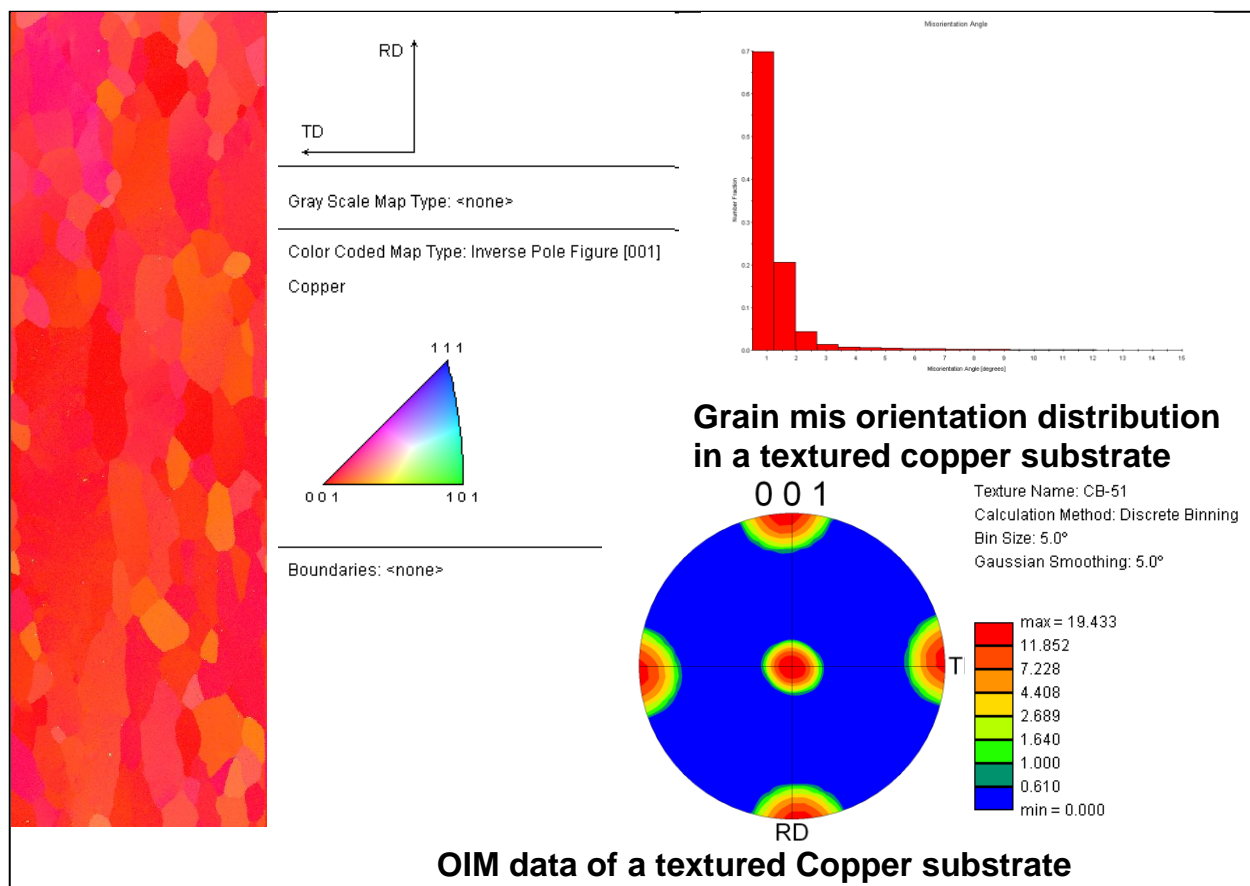


Figure 5.1.5.2

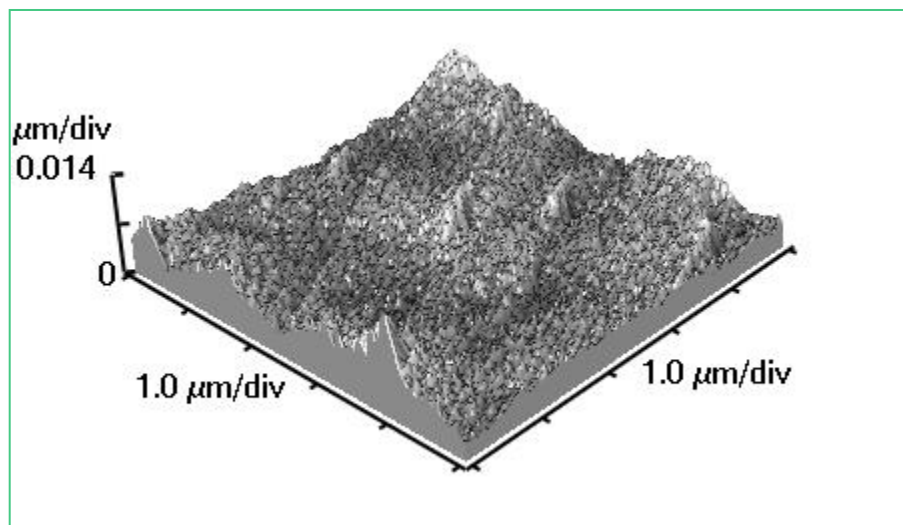


Figure 5.1.5.3

AFM scan on a textured Cu sample (rms roughness = 2.7 nm in this substrate)
(From Raghu Bhattacharya from NREL)

5.1.6 Results: Cu-Fe substrate

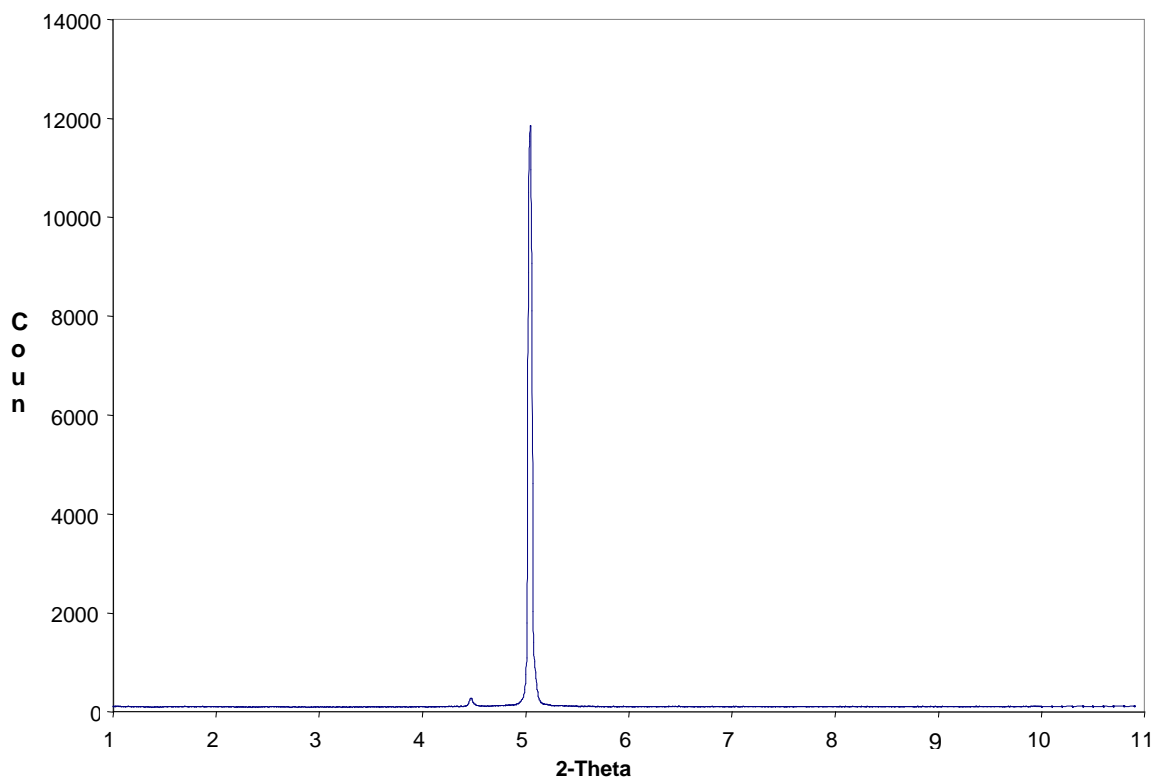


Figure 5.1.6.1 Two Theta scan of a textured Cu-Fe substrate

(111) Phi Scan on CD-09

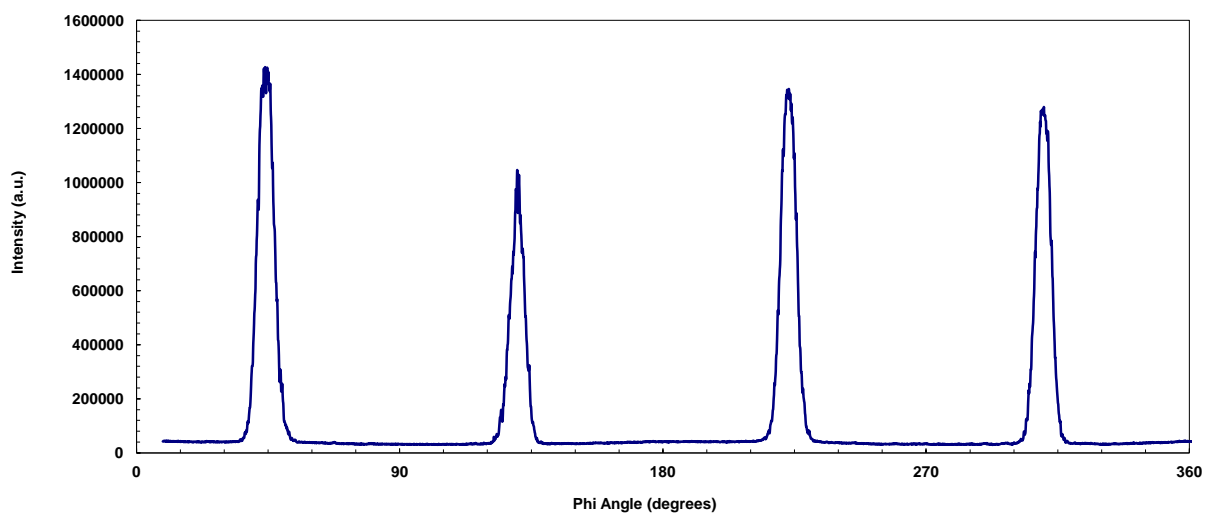


Figure 5.1.6.2 (111) Phi scan on a textured Cu-Fe alloy substrate FWHM is 5.1°

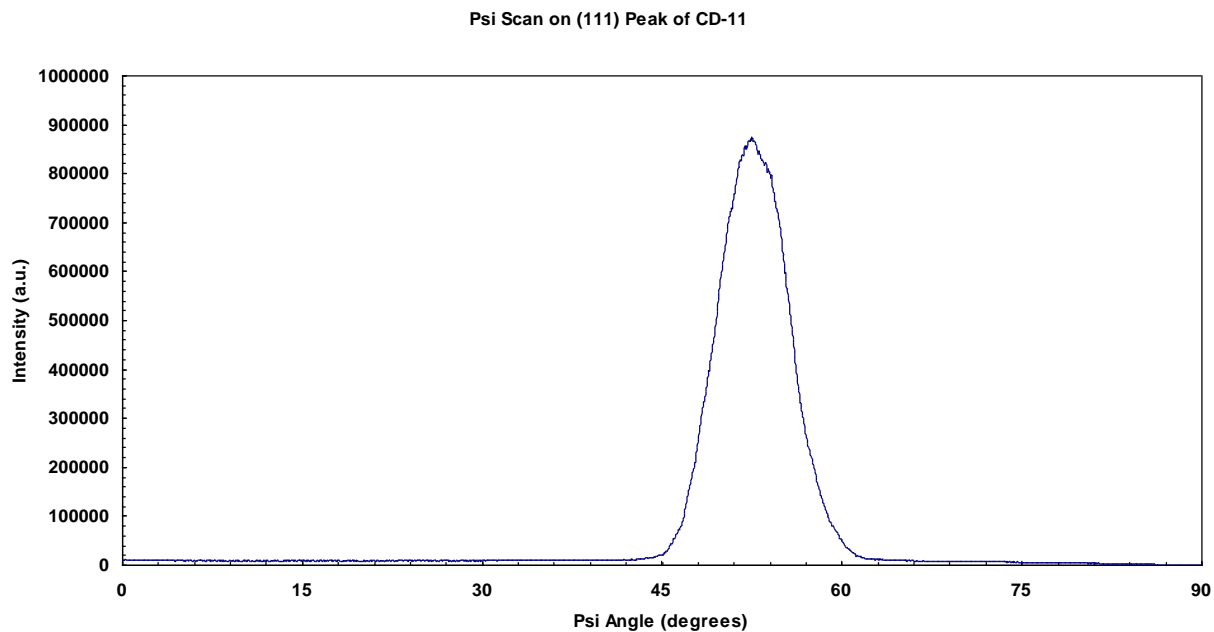


Figure 5.1.6.3 PSI scan on (111) peak of textured Cu-Fe substrate. Average FWHM 6.8°

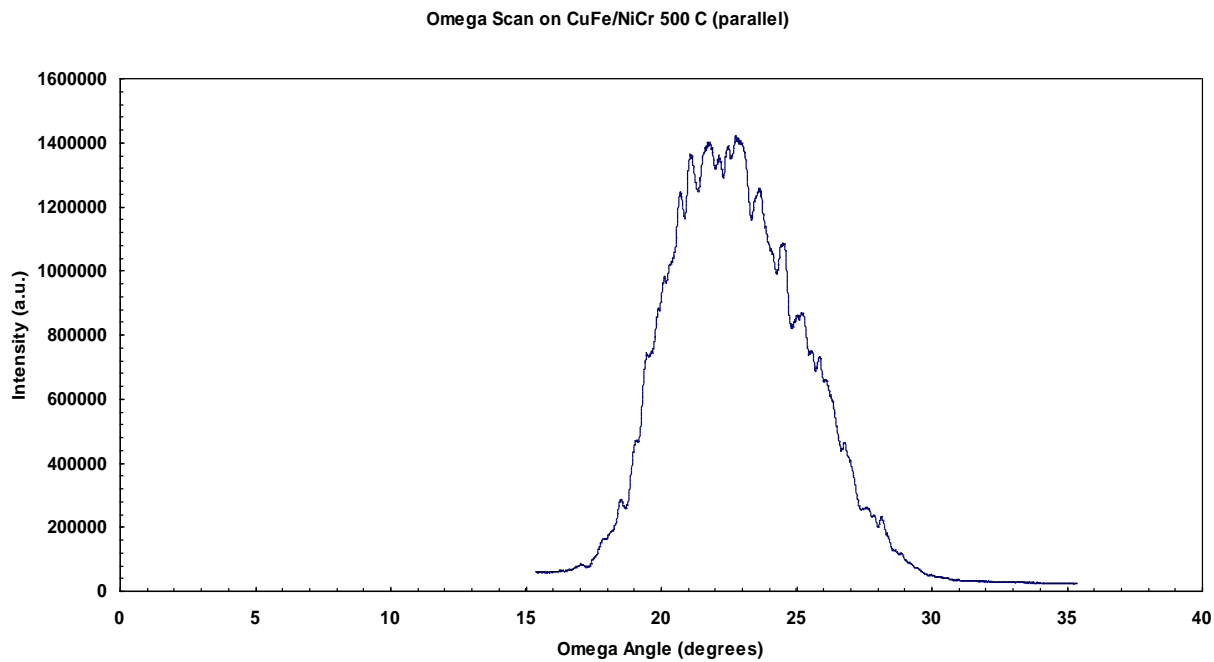


Figure 5.1.6.4 (200) Omega Scan. Parallel to rolling, FWHM=6.2o

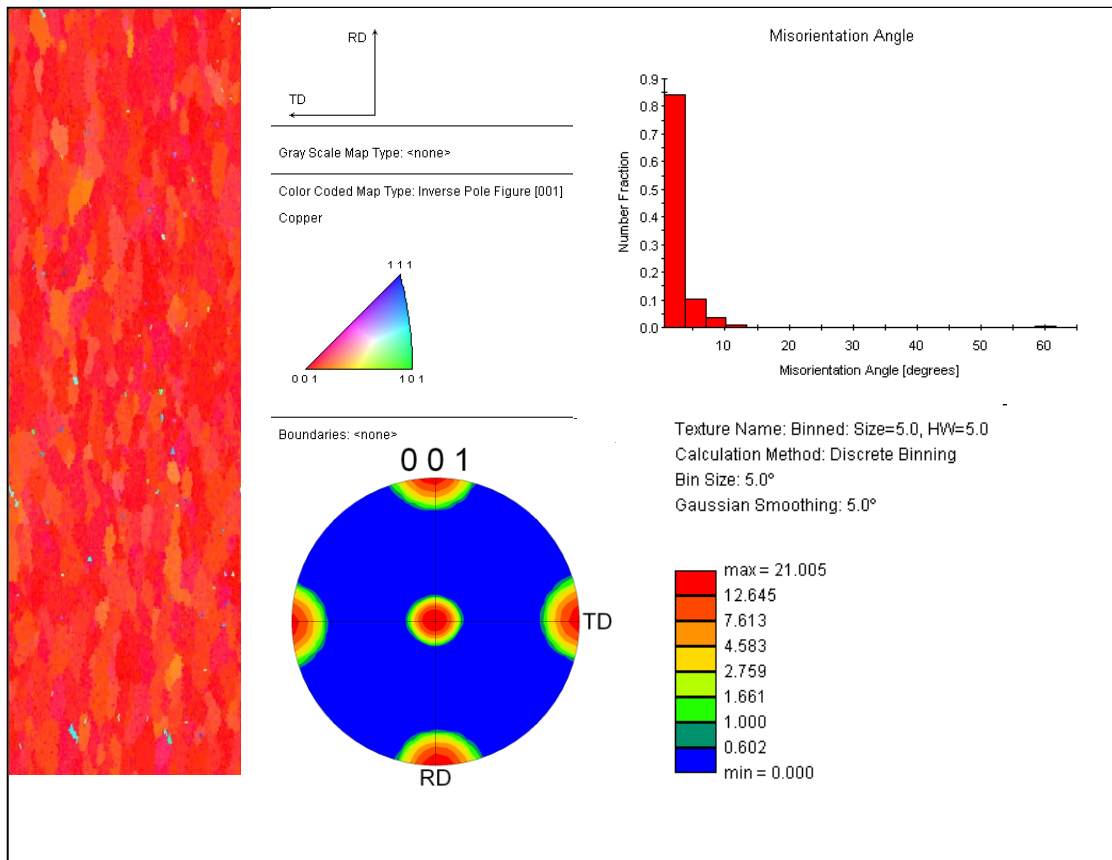


Figure 5.1.6.2

5.1.7 Mechanical Properties



Figure 5.1.7.1

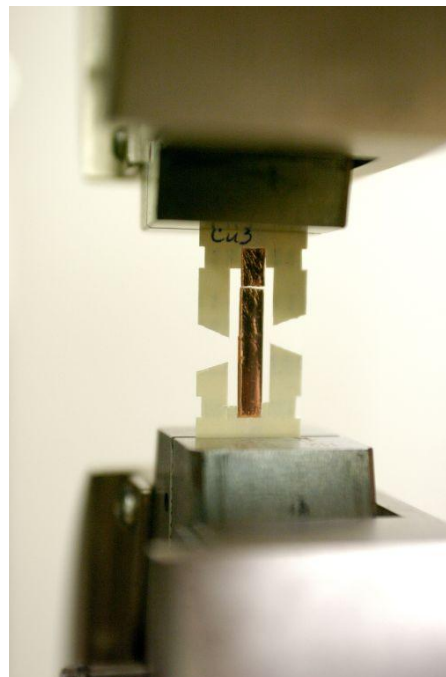
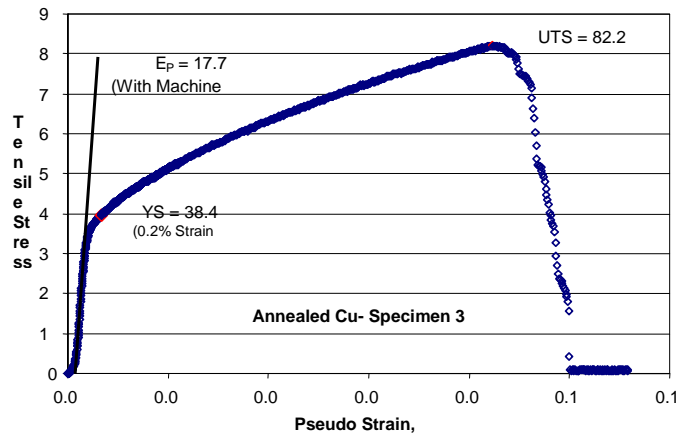
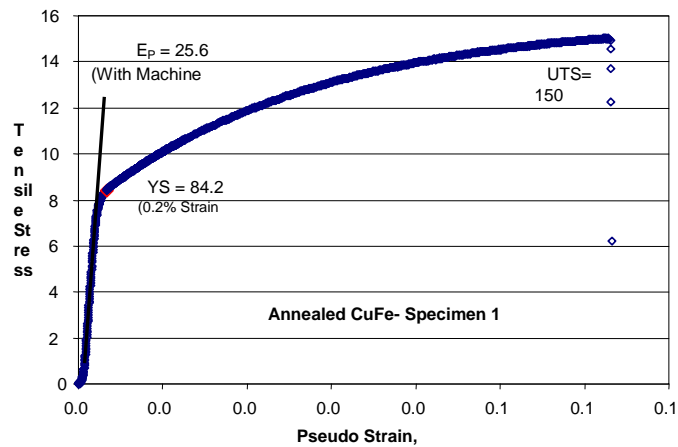


Figure 5.1.7.2



Cu
YS 38.4 MPa
UTS 82.2 MPa



Cu-Fe
YS 84.2 MPa
UTS 150 MPa

Figure 5.1.7.3

Stress-strain curves of Cu-Fe and Cu substrates

ID	Avg. W, mm	Avg. W, in	T, mm	T, in	A, in ²	Force, lbs	Failure Stress (psi)	Failure Stress (MPa)	Yield Strength (MPa)
CuFe-1	3.3956	0.1337	0.057	0.00224	0.000300	6.41	21369	147	82.4
CuFe-2	2.8398	0.1118	0.050	0.00197	0.000220	7.08	32170	222	
CuFe-3	3.6413	0.1434	0.050	0.00197	0.000282	6.89	24415	168	
				Average Strength =			25985	179MPa	82.4Mpa
Cu-1	3.1567	0.1243	0.052	0.0020	0.000254	3.40	13363	92	
Cu-2	4.0046	0.1577	0.052	0.0020	0.000323	3.80	11773	81	
Cu-3	3.6709	0.1445	0.052	0.0020	0.000296	3.39	11458	79	38.4
				Average Strength =			12198	84MPa	38.4MP

Crosshead rate (ipm) = 0.02 in/min

Figure 5.1.7.4

5.1.8 Magnetization Measurements

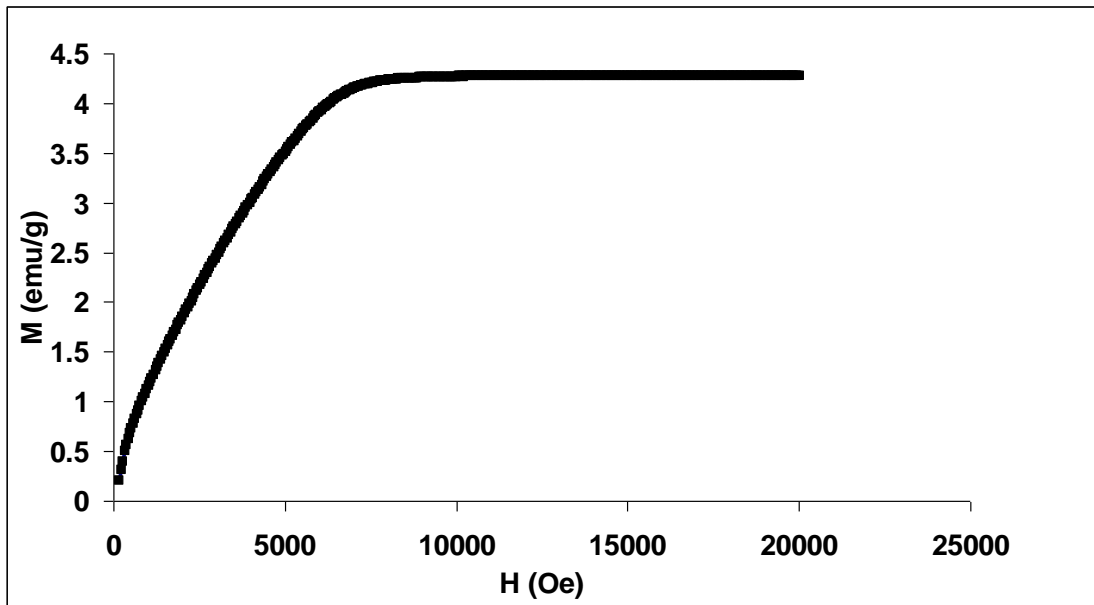


Figure 5.1.8.1

Material	M sat (emu/gm)
Nickel*	57.06
Ni- 3at% W*	36.4- 37.3
Ni-9 at% W*	4.36
Cu-Fe (This study)	3.6- 4.27

* A. O. Ijaduola et al. Physica C (2003)

Figure 5.1.8.2

5.1.9 Results: Resistivity Data

Temp	Annealed Cu-Fe (CD12) Ohm- m	Annealed Cu (CB69) Ohm- m
300K	3.8E-08	1.6E-08
77K	2.44E-08	1.85E-09

Figure 5.1.9.1

- Resistivity of Cu-Fe alloy at 77 K is higher than Cu at least by an order of magnitude
- Good for ac applications as eddy current losses will be low as resistivity is higher

5.1.10 Results: SEM of Annealed Cu- Fe Alloy Substrates

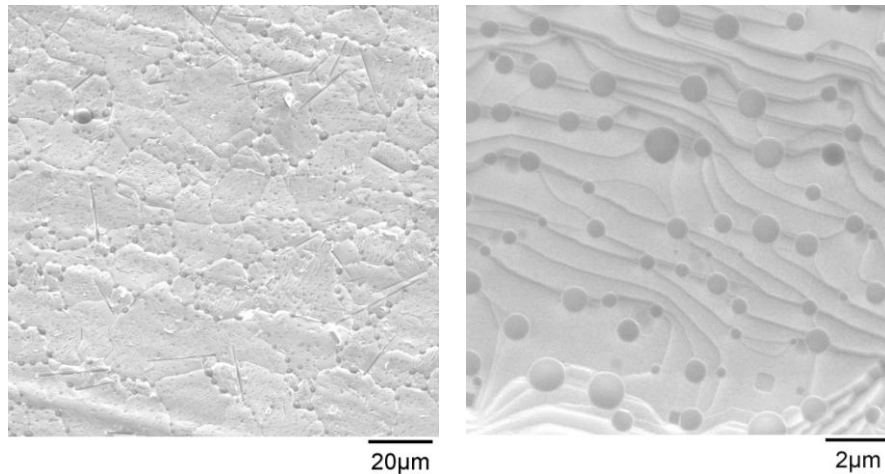


Figure 5.1.10.1

- Submicron sized precipitates (Fe rich) were observed
- Probably may be useful to create flux pinning defects in the subsequent YBCO layers?

5.1.11 Ni-Cr Buffer Layer

- Ni-20 wt% Cr non magnetic coatings by DC magnetron sputtering
- Deposition temperatures -300 °C, 400 °C, and 500 °C
- Thickness of the coatings 1 micron
- Both biaxially textured Cu and Cu-Fe substrates were used
- Analyzed for texture by x-ray diffraction

5.1.12 Ni-Cr coatings on Cu-Fe Substrates at different temperatures

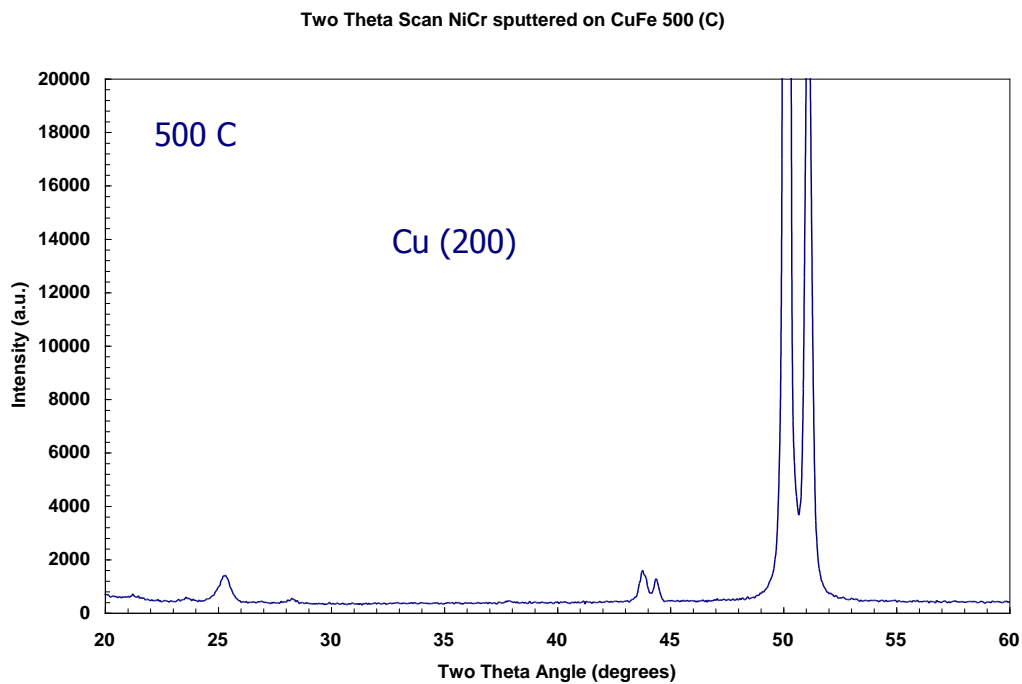


Figure 5.1.12.1

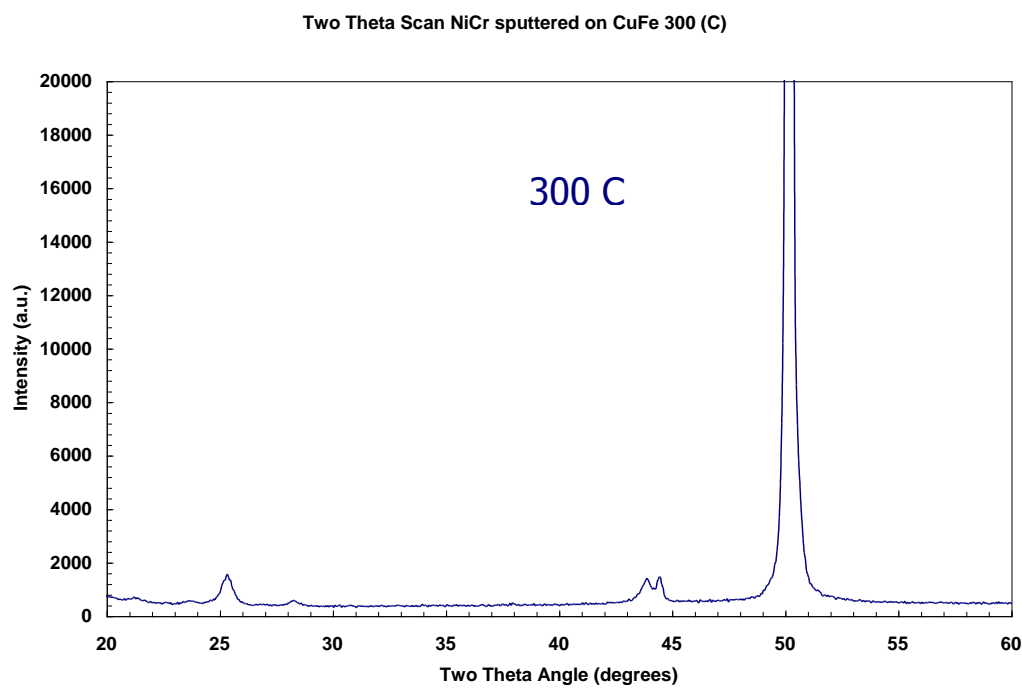


Figure 5.1.12.2

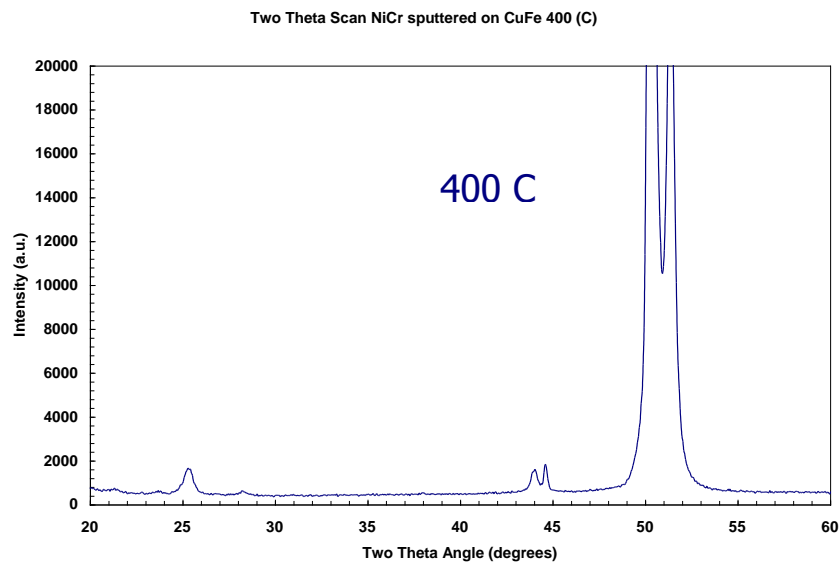


Figure 5.1.22.3

(111) Phi scans, Ni-Cr 500°C Deposition

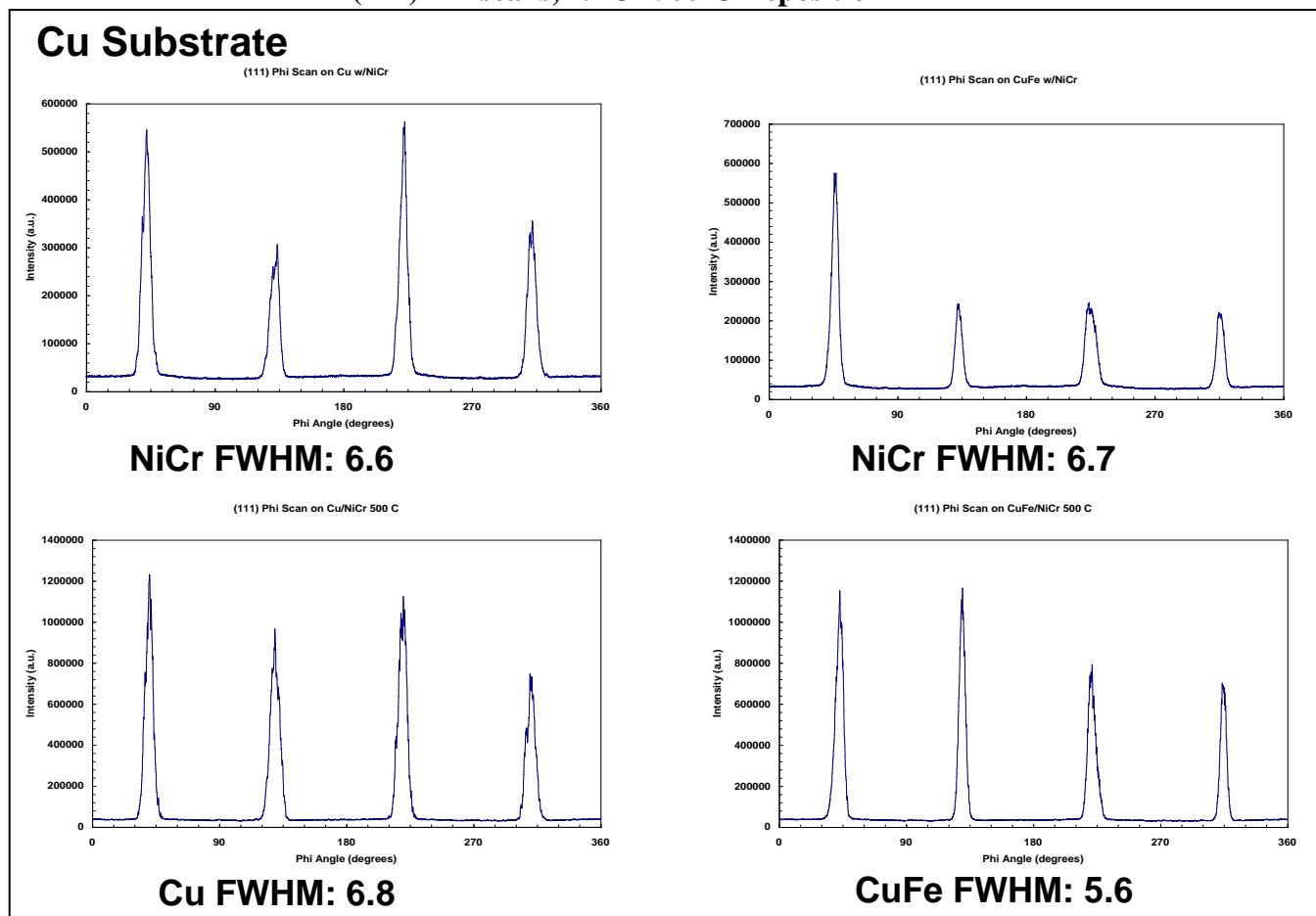


Figure 5.1.12.4

(200) Omega scans (parallel RD), 500° C Deposition

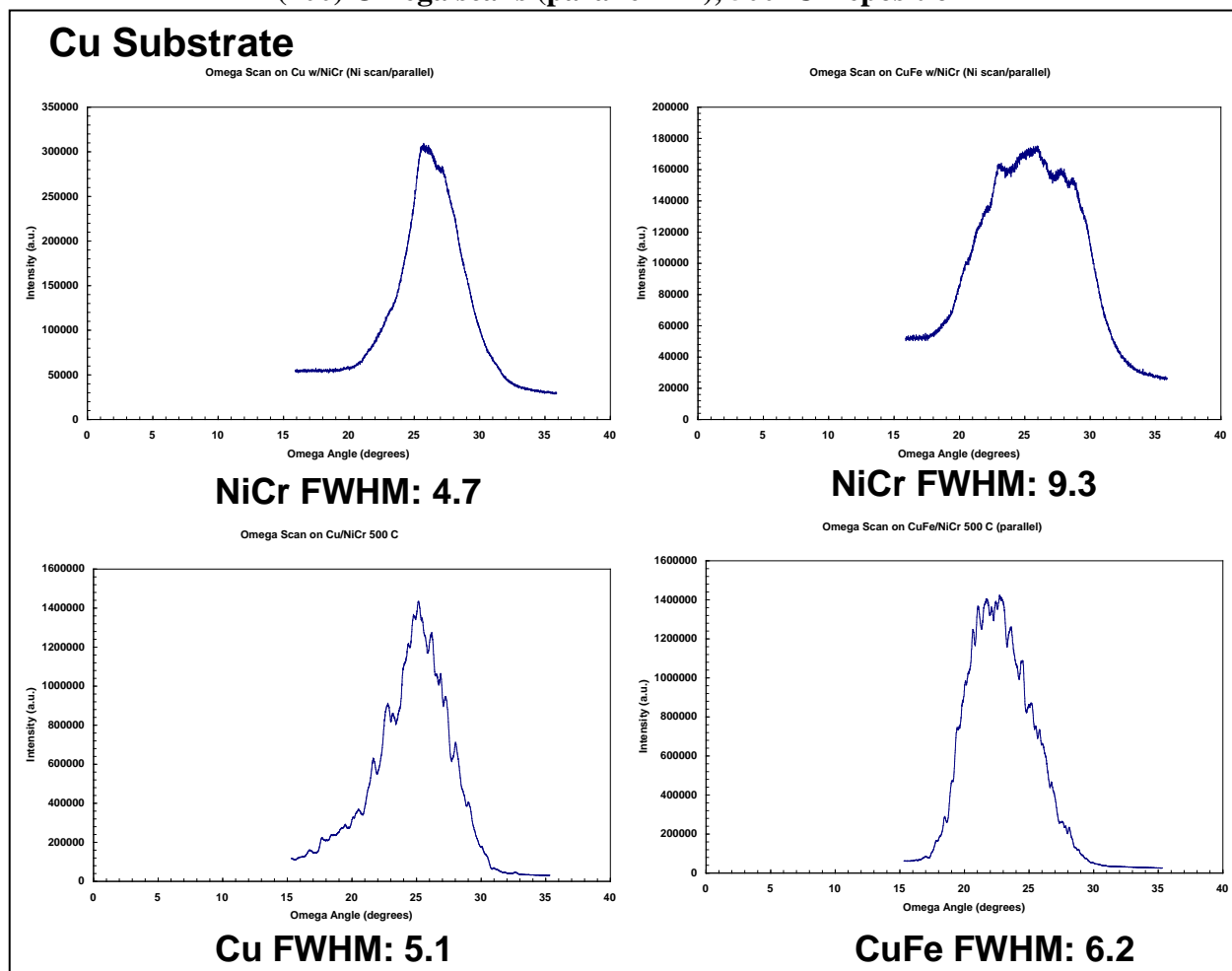


Figure 5.1.12.5

5.1.13 Buffer Layers: Pt coating

Substrate	Crystal Structure	Lattice Parameter Å
YBCO	Perovskite	3.825
Cu	FCC	3.615
Ni	FCC	3.524
Pt	FCC	3.924

Figure 5.1.13.1

- Pt was coated in a DC magnetron Sputtering unit at UC
- Deposition was done at 350°C for 10min, 30min, and 60 min.
- Texture was determined by using XRD

1.5.14 Pt buffer layers on Textured Cu

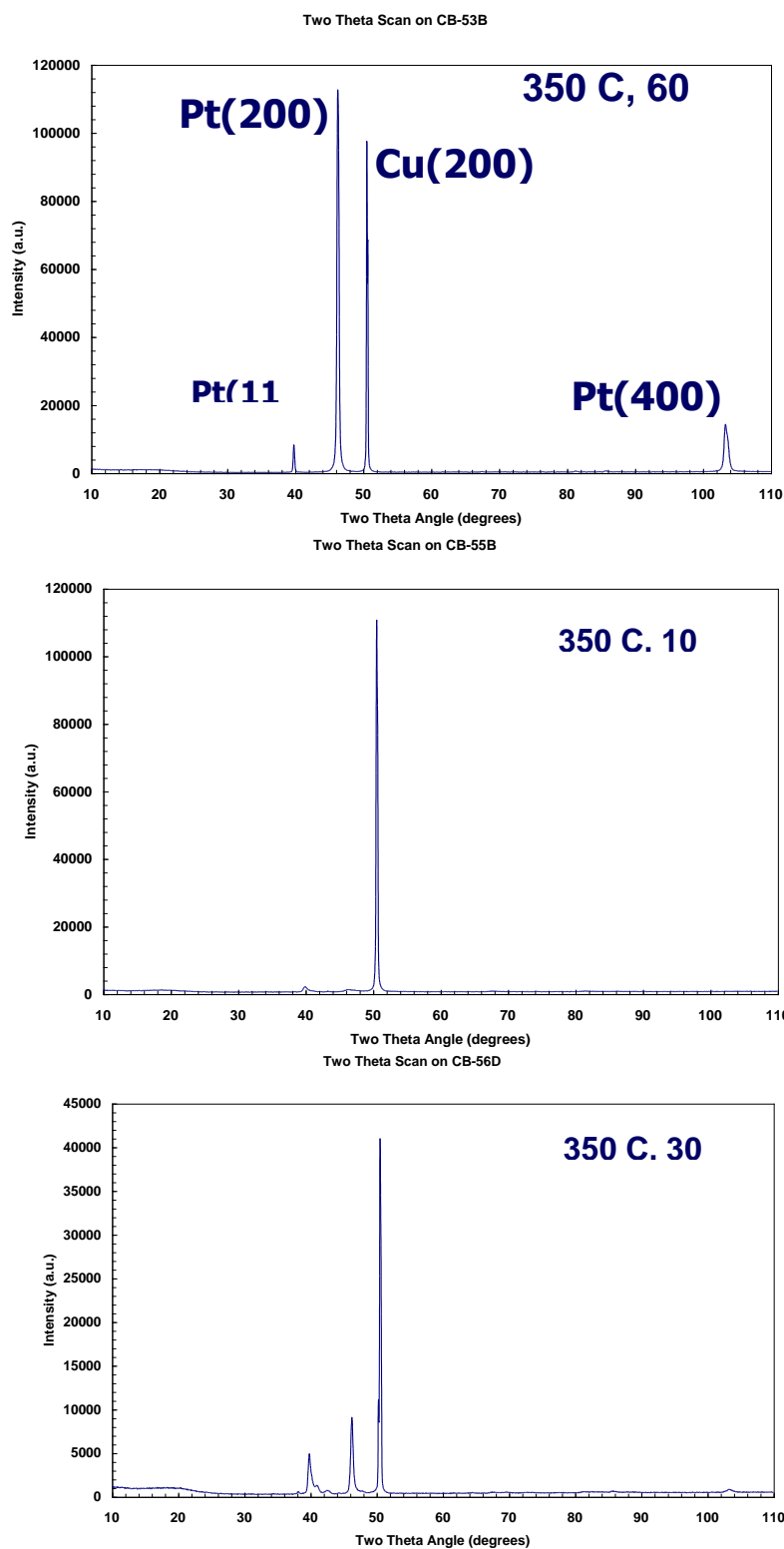


Figure 5.1.14.1

Pt Coating on Cu 350 C, 60 Min

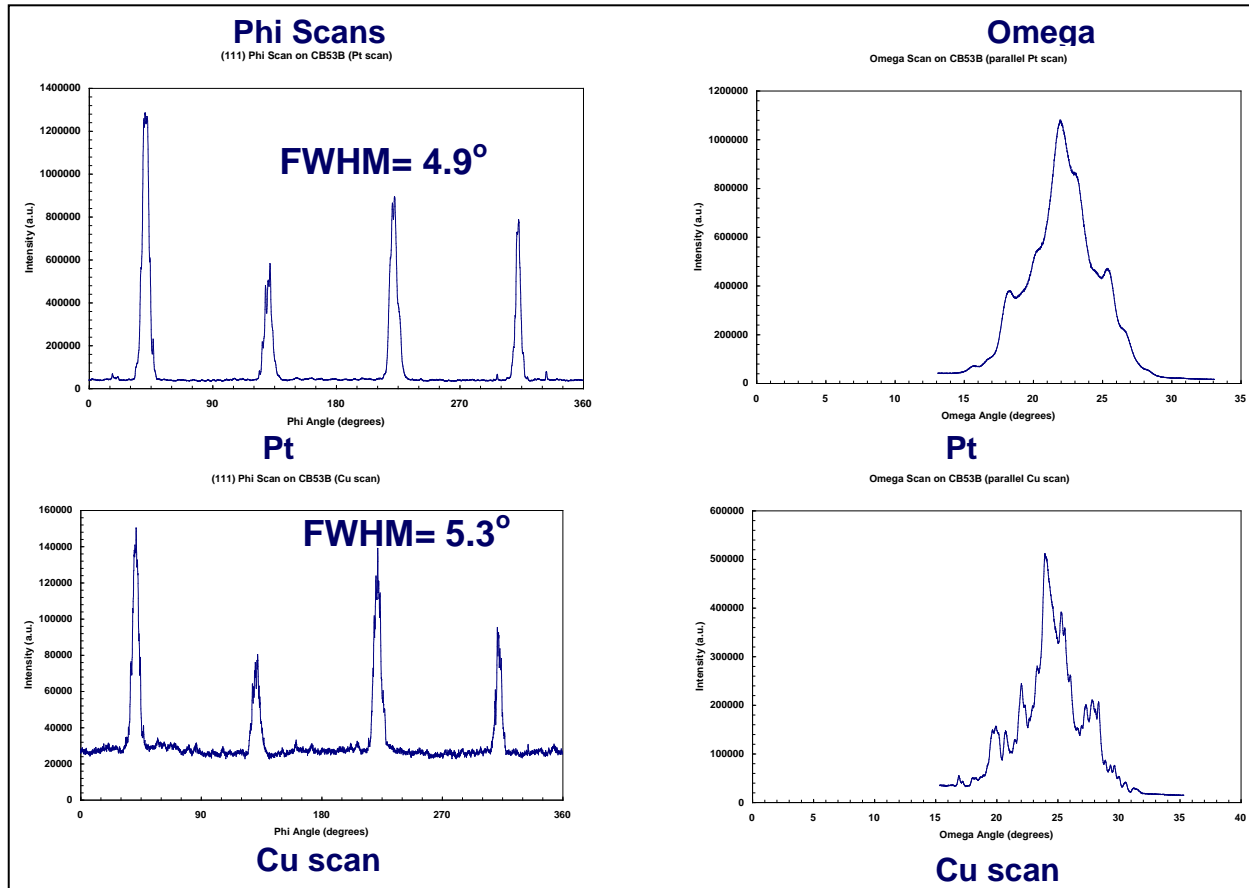


Figure 5.1.14.2

5.1.15 Buffer Layers: YSZ by Pulsed laser Ablation on Insitu Annealed Copper

Insitu annealing of substrates in a coating chamber provides these advantages:

- Ease of handling: substrates are stronger in the pre annealed condition
- Reduction of surface defects : surface is harder than annealed samples
- Clean surfaces : Reduced contamination and oxidation for buffer growth
- Suitable for Cu and Cu-Fe substrates: Annealing temperature lower than Ni

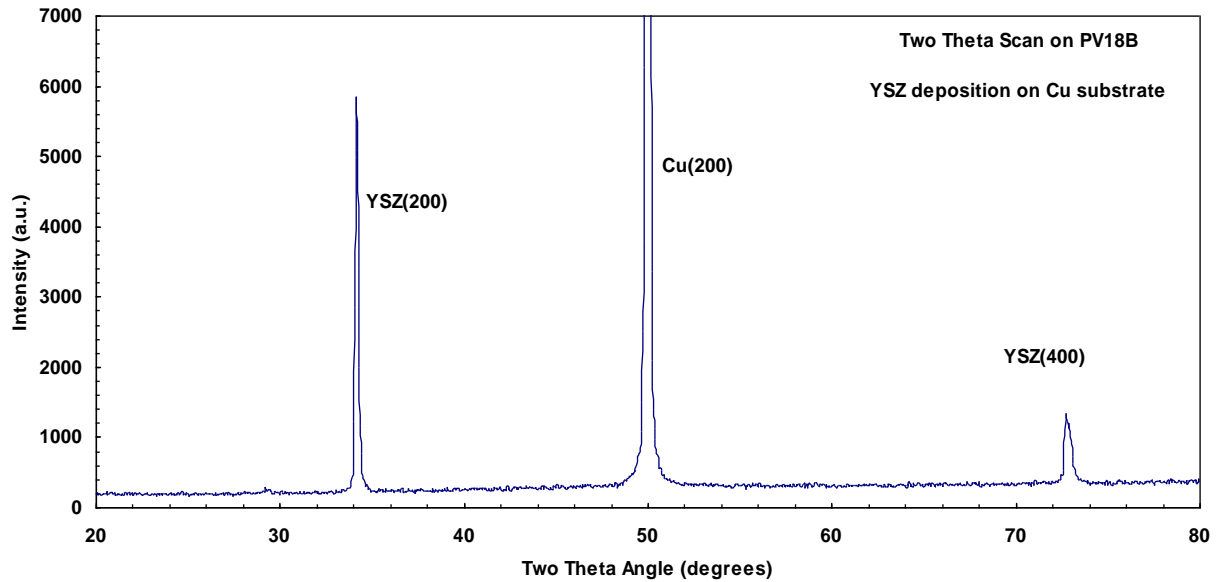


Figure 5.115.1

5.1.16 Conclusions

Substrates

- Biaxially textured Cu and Cu-Fe substrates were processed by optimizing the thermo mechanical processing schedules
- Cu-Fe substrates were found to be at least 2 times as strong as Cu substrates
- Saturation magnetization (M_{sat}) of Cu-Fe alloys is found to be similar to Ni- 9 at% W alloys but with better texture
- Resistivity of Cu-Fe alloy at 77 K is higher than Cu at least by an order of magnitude
- Precipitates found in Cu-Fe substrates may be engineered to create defects that can help flux pinning enhancements in YBCO layers subsequently grown on these (?)
- Biaxially textured Ni-20 wt % Cr non-magnetic buffer layers were successfully grown on both Cu and Cu-Fe textured substrates with biaxial texture by dc magnetron sputtering
- Biaxially textured Pt was also successfully grown on Copper and Cu- Fe alloy substrates
- C- axis oriented YSZ can be grown by PLD on copper substrates
- Insitu annealing of Cu- and Cu-Fe substrates can produce good textured substrates

5.2 Textured Copper Metallic Substrates for HTS Coated Conductors

References: 33, 35

Presented at AFOSR, January 19, 2004 by Nicolas A. Yust

Nicholas A. Yust, Rama Nekkanti,¹ Paul N. Barnes, Srinivas Sathiraju,² Timothy J. Haugan, Raghavan Srinivasan³

Air Force Research Laboratory, ¹UES, ²NRC, ³Wright State University

5.2.1 Objectives

- Optimization of Textured Copper Substrates
- Investigate the Deformation and Recrystallization Textures for a Copper Rod and Copper Foil
- Texturing of Copper Alloy Substrates
- Nickel plating of Copper Substrates

5.2.2 Ni vs. Cu Comparison

- Textured (200) nickel and nickel alloys
 - Successfully developed for YBCO coated conductors
 - Currently magnetic (increased ac losses)
- Textured (200) copper and copper alloys
 - Inexpensive (1/6 the cost of Ni)
 - Ease of cube texture development
 - Nonmagnetic
 - Highly conductive
 - Stability if electrically connected to HTS layer

5.2.3 Approach

- Goal: (200) <002> preferentially oriented Cu
- Reverse cold rolling (>95% deformation)
 - → (220) Deformation Texture
- Subsequent recrystallization (800°C > T > 300°C)
 - → (200) Recrystallization Texture

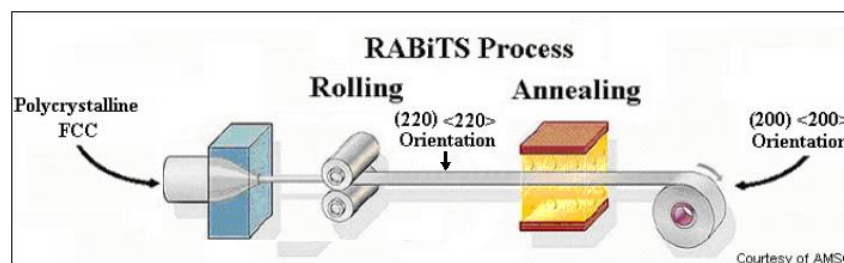


Figure 5.2.3.1

5.2.4 Starting Material

- Copper Rod

- ASTM 10100, 99.99% Pure
 - Diameter 9.5 mm, Length 100 mm
- Copper Foil
 - ASTM 10100, 99.99% Pure
 - Thickness 2.0 mm, Width 20 mm, Length 100 mm
- Copper Alloy
 - 97.5% Cu, 2.35% Fe, 0.12% Zn, 0.03% P
 - Width 20 mm, Length 100 mm

5.2.5 Material Processing

- Copper Rod
 - Flattened with uniaxial forge press
 - 7.5mm (roll opening)
 - 116 tons 2 faceted surface in axial direction
- Copper Rod & Copper Foil
 - Ground and polished to final thickness of 6.92mm
 - 120, 240, 400, 600 grit SiC paper
 - 6 μ m diamond paste on microcloth
 - Annealed
 - 1 hour at 450°C
 - (Ar + H₂) reducing atmosphere
 - 2 μ Torr back pressure, 200 mTorr partial pressure

5.2.6 Thermomechanical Processing

- Copper Rod & Copper Foil
 - Reverse cold rolled (ambient)
 - Cambered rolls with 6 μ m finish
 - 10% reduction per pass
 - Minimal dwell times
 - 5 final deformation levels
 - 50 passes total
 - Samples cut 1.0 mm x 0.5 mm
 - Long ways with rolling direction
 - Ultrasonically cleaned to remove lubricants

Rolling Schedule

- Copper Rod
 - 95.5% ~ (310μm)
 - 97.5% ~ (170μm)
 - 98.5% ~ (98μm)
 - 99.0% ~ (74μm)
 - 99.5% ~ (36μm)
- Copper Foil
 - 95.5% ~ (80μm)
 - 97.5% ~ (47μm)
 - 98.5% ~ (28μm)
 - 99.0% ~ (18μm)
 - 99.5% ~ (11μm)
- Copper Alloy
 - 99.5% ~ (35μm)

Annealing Schedule

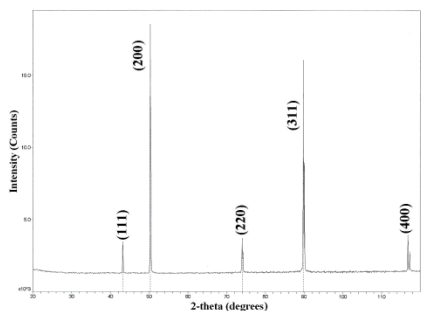
2μTorr Back Pressure/200mTorr Partial Pressure (Ar + H₂)

Reduction	95.5%	97.5%	98.5%	99.0%	99.5%	Duration (h)
Copper Rod	As Rolled	As Rolled	As Rolled	As Rolled	As Rolled	N/A
	300°C	300°C	300°C	300°C	300°C	6
	500°C	500°C	500°C	500°C	500°C	1
	550°C	550°C	550°C	550°C	550°C	1
	600°C	600°C	600°C	600°C	600°C	1
	650°C	650°C	650°C	650°C	650°C	1
	700°C	700°C	700°C	700°C	700°C	1
	750°C	750°C	750°C	750°C	750°C	1
	800°C	800°C	800°C	800°C	800°C	1
Copper Foil	As Rolled	As Rolled	As Rolled	As Rolled	As Rolled	N/A
	300°C	300°C	300°C	300°C	300°C	6
	500°C	500°C	500°C	500°C	500°C	1
	550°C	550°C	550°C	550°C	550°C	1
	600°C	600°C	600°C	600°C	600°C	1
	650°C	650°C	650°C	650°C	650°C	1
	700°C	700°C	700°C	700°C	700°C	1
	750°C	750°C	750°C	750°C	750°C	1
	800°C	800°C	800°C	800°C	800°C	1
Copper Alloy Foil					As Rolled	N/A
					300°C	6
					600°C	1
					800°C	1

5.2.7 Copper As-Received

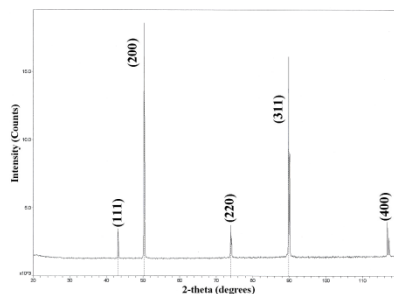
Copper Rod

- ASTM 10100
- 99.99% Pure
- Diameter 9.5mm
- Length 100mm
- 450°C Initial Anneal
- Dominant FCC



Copper Foil

- ASTM 10100
- 99.99% Pure
- Thickness 2.0mm
- Width 20mm
- Length 100mm
- 450°C Initial Anneal
- Dominant FCC



Copper Alloy

- 97.5% Cu
- 2.35% Fe
- 0.03% P
- 0.12% Zn
- 450°C Initial Anneal
- Dominant FCC

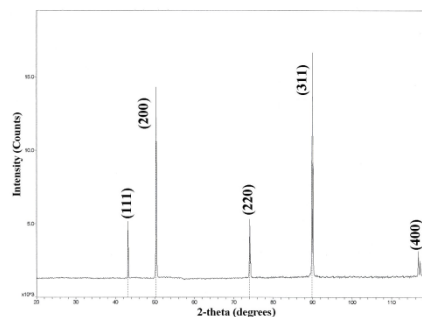


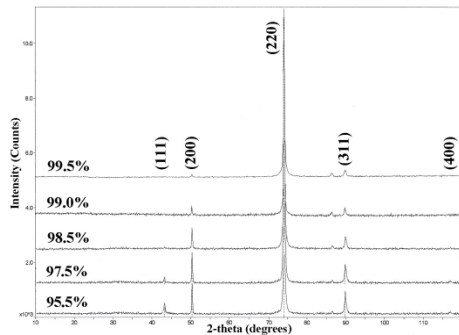
Figure 5.2.7.1

Initial Texture 2θ XRD

5.2.8 Copper After Rolling Deformation

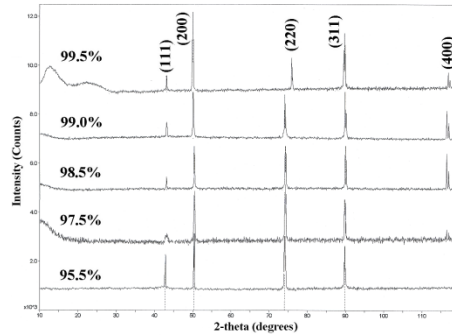
Copper Rod

- 5 deformation levels
- (220) Predominance
- Intensity trend



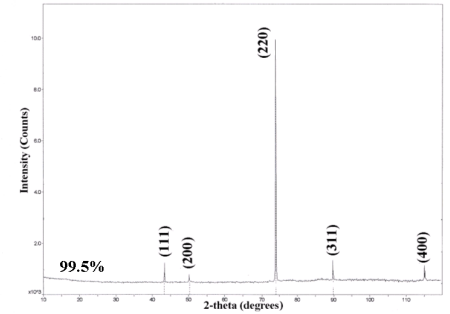
Copper Foil

- 5 deformation levels
- Dominant FCC
- No predominance
- No trends



Copper Alloy

- 1 deformation level
- (220) predominance



Deformation Texture 2θ XRD

5.2.9 Copper Rod After Annealing

Observations

- 5 deformation levels
- (200) predominance
- No deformation trend
- No temperature trend

Annealed Material XRD 2θ

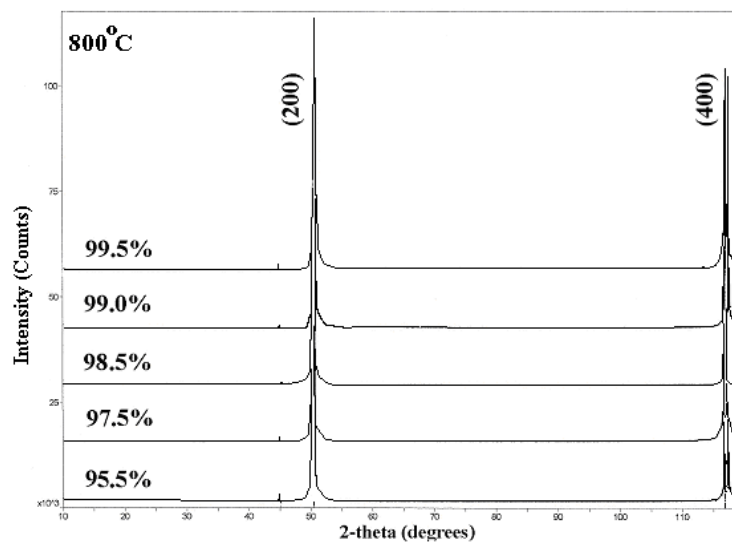


Figure 5.2.9.1

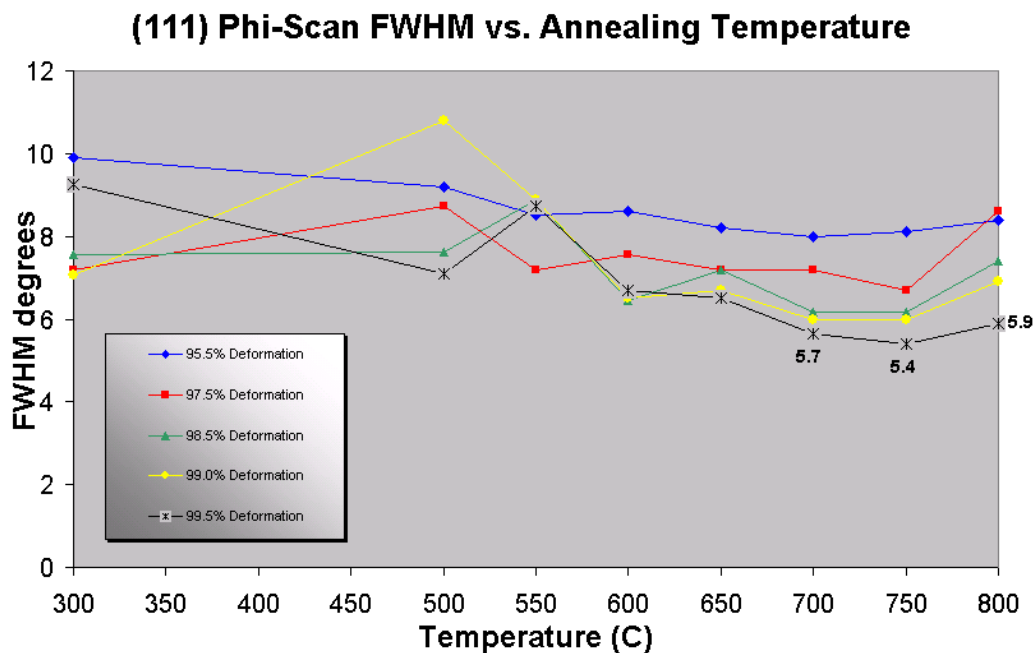


Figure 5.2.9.2

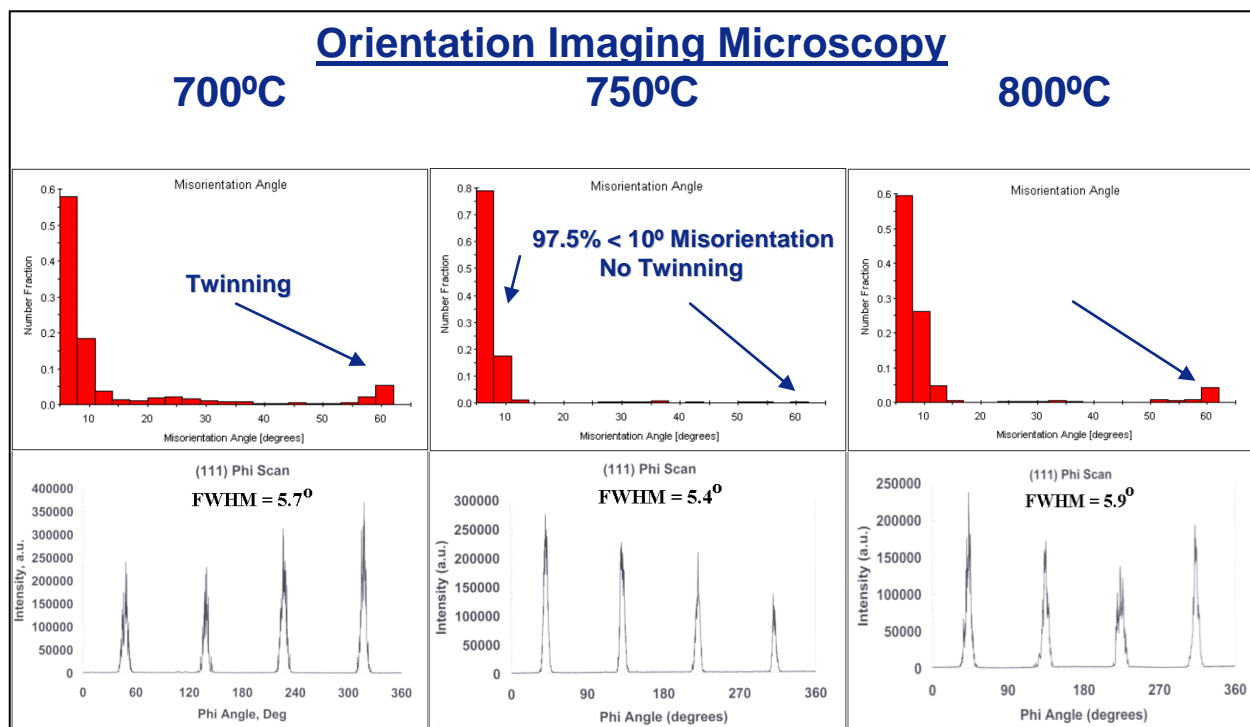


Figure 5.2.9.3

- **Copper Rod 750°C**
 - Grain Contrast ~ Constant
 - No Twinning Present

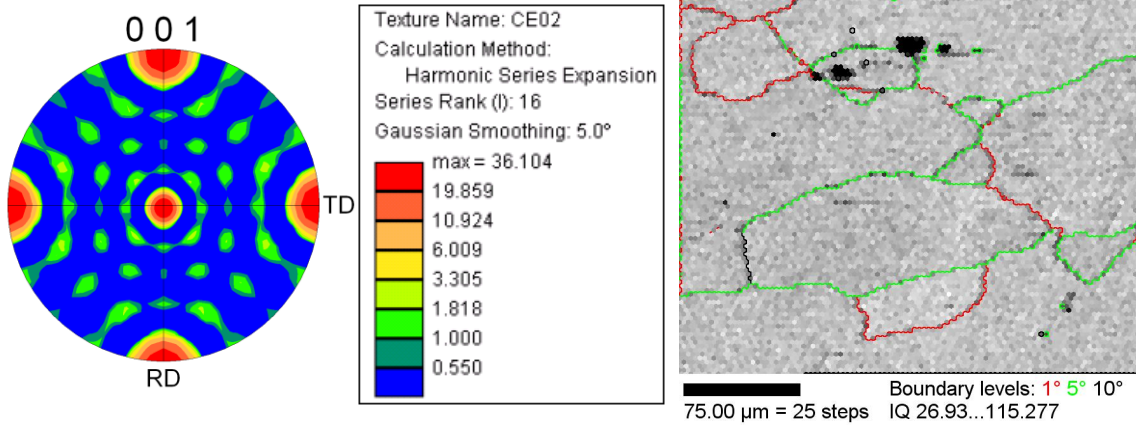


Figure 5.2.9.4

5.2.10 Copper Alloy After Annealing

Observations

1 deformation level

(200) peak predominance

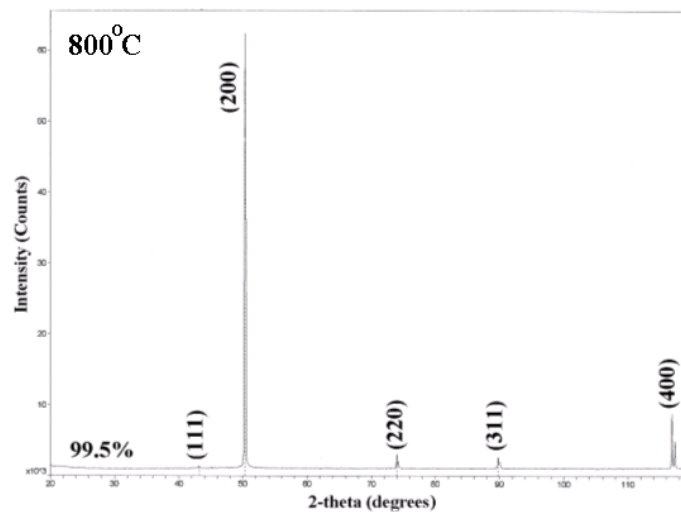


Figure 5.2.10.1

Annealed Material XRD 2θ Scans

Copper Alloy 800° C

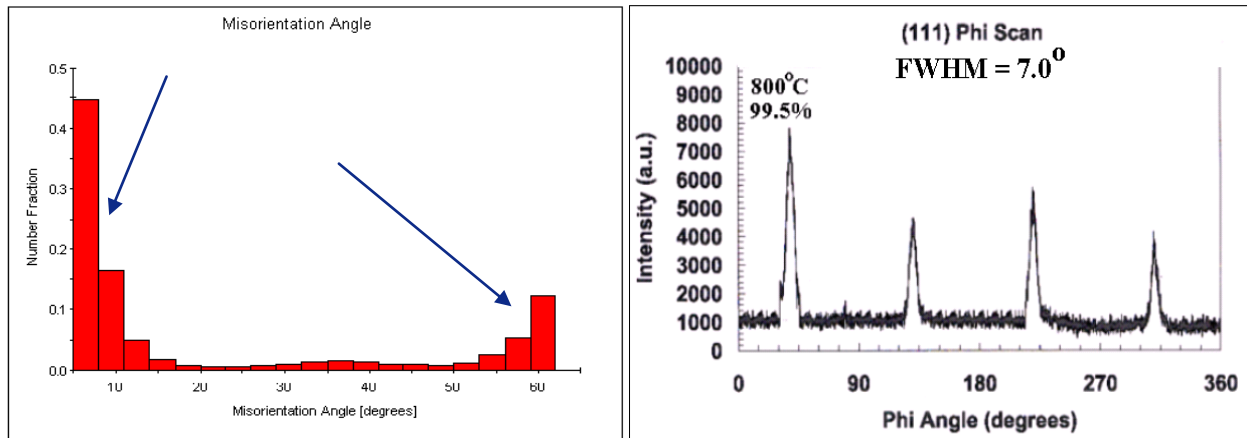


Figure 5.2.10.2

Orientation Imaging Microscopy

- Copper Alloy 800°C
 - Grain Contrast Varies
 - Minimal Twinning Present

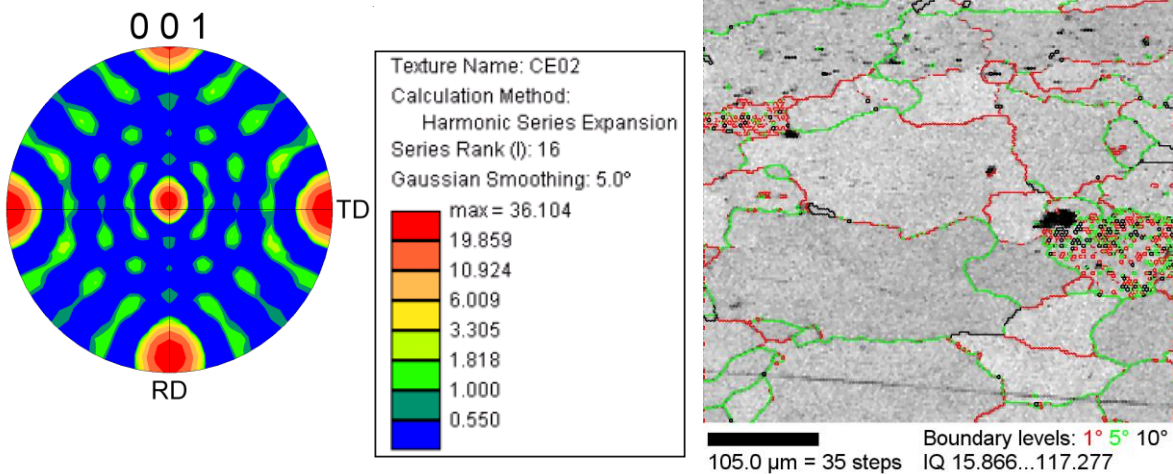


Figure 5.2.10.3

5.2.11 Discussion

Textured Copper Rod

- Optimization point at 750°C
- Sharp (200) cube texture
- Φ -Scan full-width-half-maximum value of 5.4°
- SEM/OIM showing 97.5% of grains with < 10° misorientation

Textured Copper Foil

- Showed no texture presence

Textured Copper Alloy

- Optimization at 800°C

Sharp (200) cube texture

Φ -Scan full-width-half-maximum value of 7.0°

SEM/OIM showing 60.0% of grains with $< 10^\circ$ misorientation

5.2.12 Conclusions

- The RABiTS Process
 - Successful for creating sharp (200) cube texture substrates for the copper rod and copper alloy
 - Unsuccessful for creating sharp (200) cube texture substrates for the copper foil.

5.3 Studies on YBa_2NbO_6 and $\text{YBa}_2\text{Cu}_{3-x}\text{Nb}_x\text{O}_y$ Buffer Layers

References: 17, 36, 37, 38, 39

S.Sathiraju, R. Wheeler, P.N. Barnes, T.L.Peterson, I. Maartense, A.L.Campbell, R. M. Nekkanti, L. Brunke, J.Murphy, T. A.Campbell, N. A. Yust, T. J. Haugan

Q. Jia and Paul Arendt
STC, Los Alamos National Laboratory, NM

S.Mukhopadya, S. Vemulakonda
Wright-State University, Dayton, OH

Presented at AFOSR REVIEW, January 19, 2004

Presented at ACERS 106 annual meeting, April 20, 2004

5.3.1 Objective

- YSZ, Y_2O_3 , LaMnO_3 , SrRuO_3 etc are perovskite buffers
- LANL, ORNL, SNL, AFRL actively working on this.
- FUJIKURA, Japan - $\text{Gd}_2\text{Zr}_2\text{O}_7$ Successful
- All buffers so far needs a CeO_2 cap layer
- SNL has projected \$1- \$3 per KA-m using solution based methods by 2010
- However, the search is on for an ideal buffer layer...!

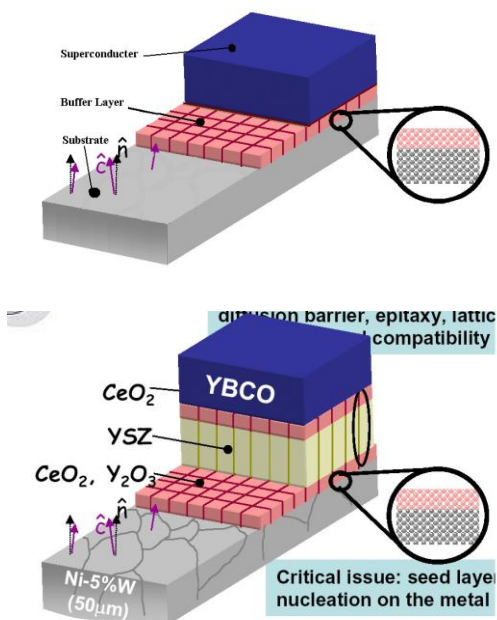


Figure 5.3.1.1

5.3.2 Present Work

- Ba_2YNbO_6 double perovskite
- 0.84 nm (Double the unit cell of MgO)
- No reaction up to 1200°C with Y123 or R-123 materials
- $\text{YBa}_2\text{Cu}_{3-x}\text{Nb}_x\text{O}_y$ $x = 0.25, 0.5, 0.75$ and 1.0
- $a_0 \sim 0.4$ nm
- Conducting as well as insulating buffers are possible

5.3.3 Experimental

Parameters	$\text{YBa}_2\text{Cu}_{3-x}\text{Nb}_x\text{O}_y$ $x = 0.25, 0.5, 0.75, 1$	Ba_2YNbO_6	$\text{YBa}_2\text{Cu}_3\text{O}_y$
Deposition Temp.	750 – 850 °C	RT – 850°C	750-820° C
Oxygen Pressure	250 mTorr	200 mTorr	230mTorr
Laser Energy	2.5 J/cm ²	2 J/Cm ²	2 J/Cm ²
Laser frequency	4- 10 Hz	10 Hz	4-10Hz
S-T distance	6 cm	6 cm	6 cm
Substrates	LAO, STO, MgO, Rabits Ni, I- MgO	MgO, IBAD MgO	All buffered substrates
Thickness	200nm – 500nm	200 nm	200-500 nm

Figure 5.3.3.1

5.3.4 $\text{YBa}_2\text{Cu}_{3-x}\text{Nb}_x\text{O}_y$ films deposited at 750 °C

- Highly *00l* oriented films were obtained for $x = 0.25$
- *00l* oriented peaks started broadening
- Mixed phases were obtained for $x = 1.0$
- Those phases may be YBNO, Y123 or YBCNO?
- No CuO peak observed

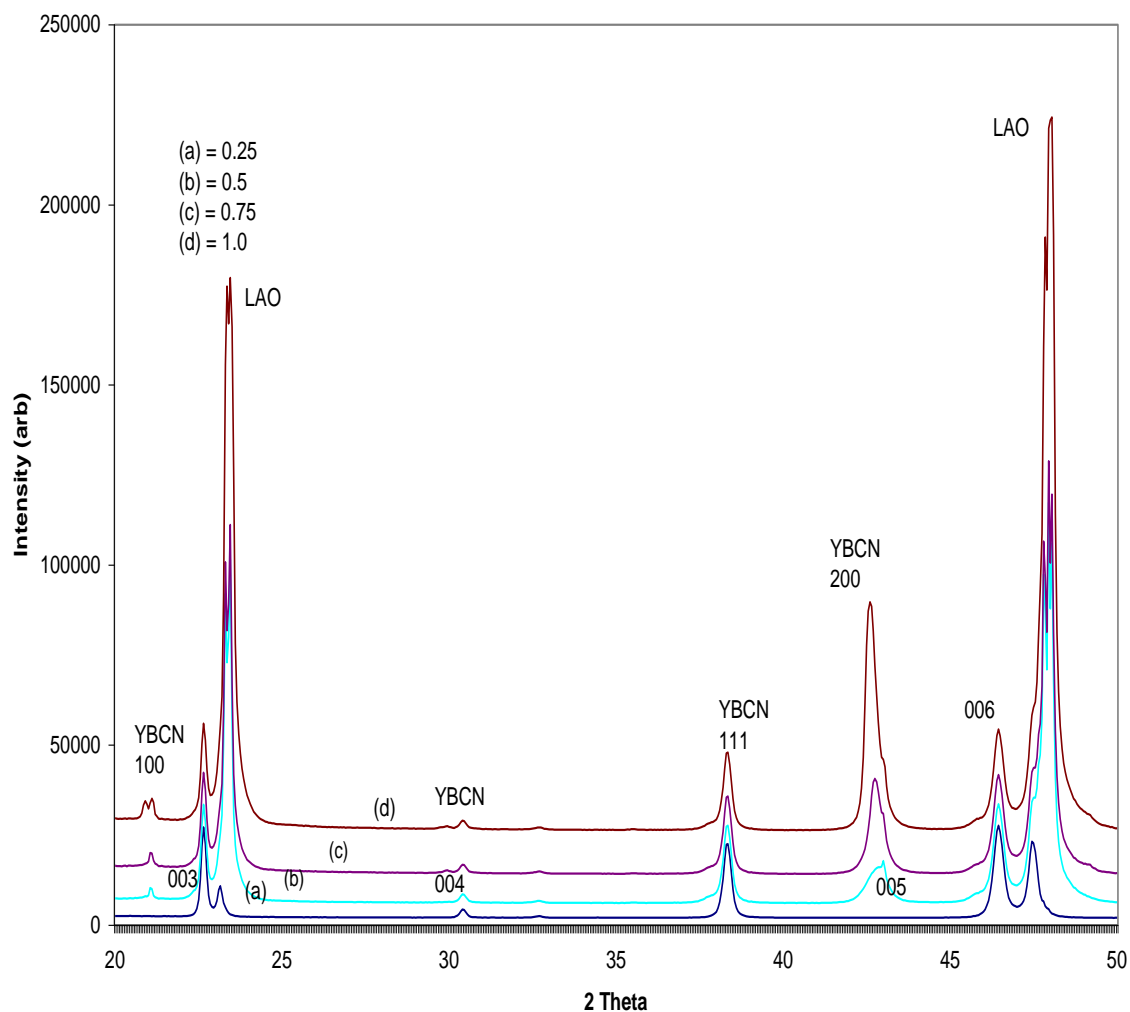


Figure 5.3.4.1

5.3.5 $\text{YBa}_2\text{Cu}_{3-x}\text{Nb}_x\text{O}_y$ films deposited at 800 °C

- The $h00$ oriented peak intensities increased with the increase of substrate temperature from 800 to 850 °C, and formation of single phase YBCNO was observed in films
- No CuO peak observed

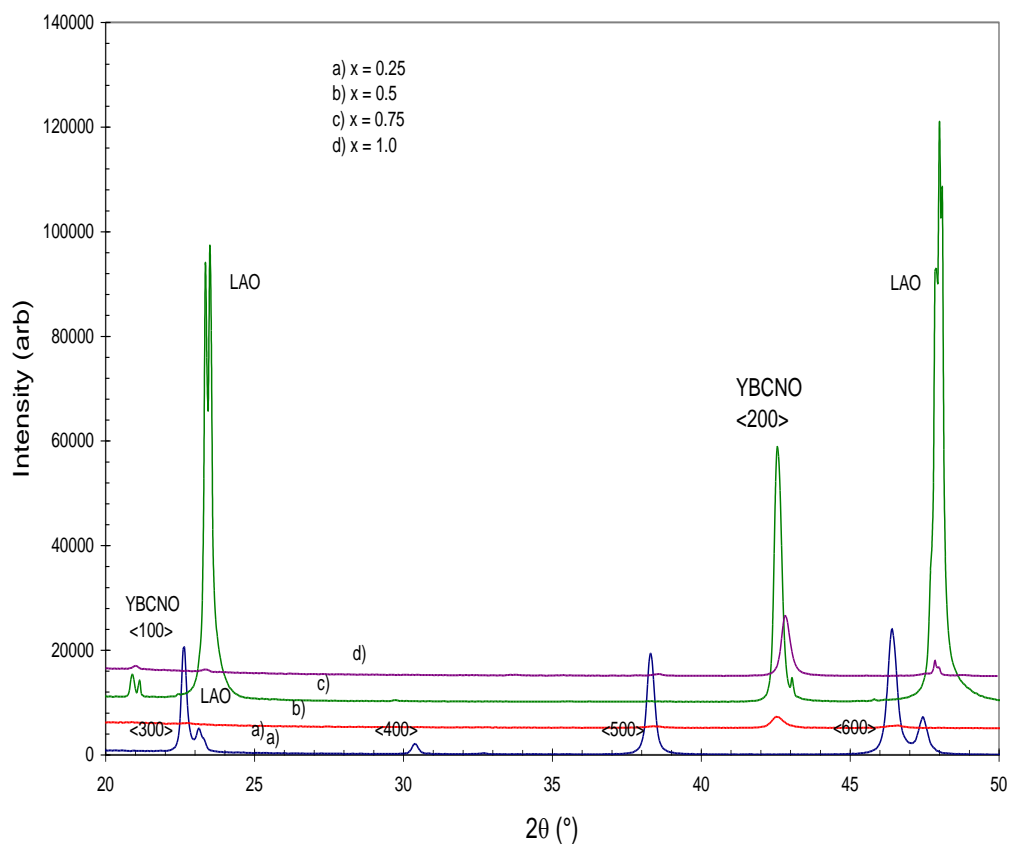


Figure 5.3.5.1

5.3.6 $\text{YBa}_2\text{Cu}_{3-x}\text{Nb}_x\text{O}_y$ films deposited at 850°C

- Using $\text{PrBa}_2\text{Cu}_2\text{NbO}_8$ (PBCNO) PDF file (#43-0176) the peaks present in our samples were indexed.
- The d values and peak positions are different from PBCNO compound.
- YBCNO may be tetragonal with lattice parameters $a = 0.409\text{nm}$ and $c = 1.16\text{nm}$

XRD of $\text{YBa}_2\text{Cu}_{(3-x)}\text{Nb}_x\text{O}_8$ Films Deposited at 850°C

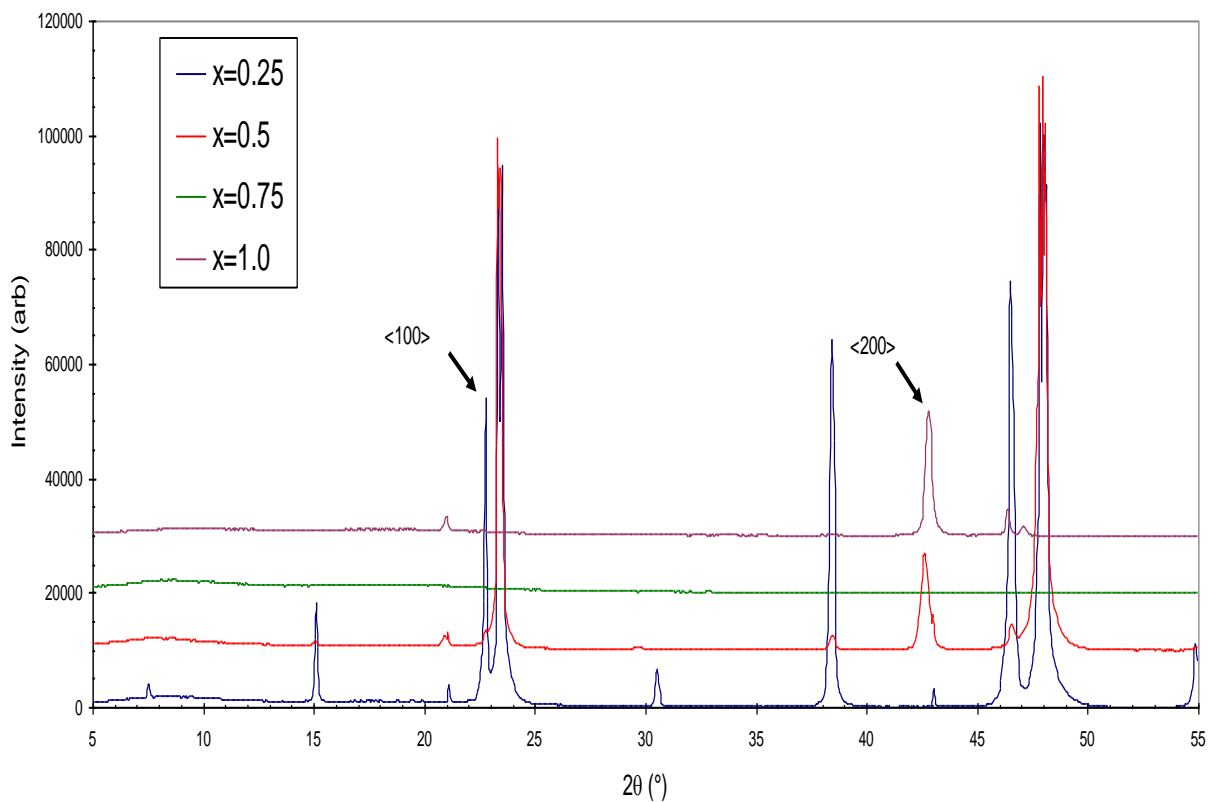


Figure 5.3.6.1

5.3.7 $\text{YBa}_2\text{Cu}_2\text{NbO}_y$ films on various substrates

- No CuO peak was observed in films deposited on any of these substrates
- Highly oriented films were observed on STO and MgO
- 113 peak growth becoming strong with the increase of temperature above 825°C

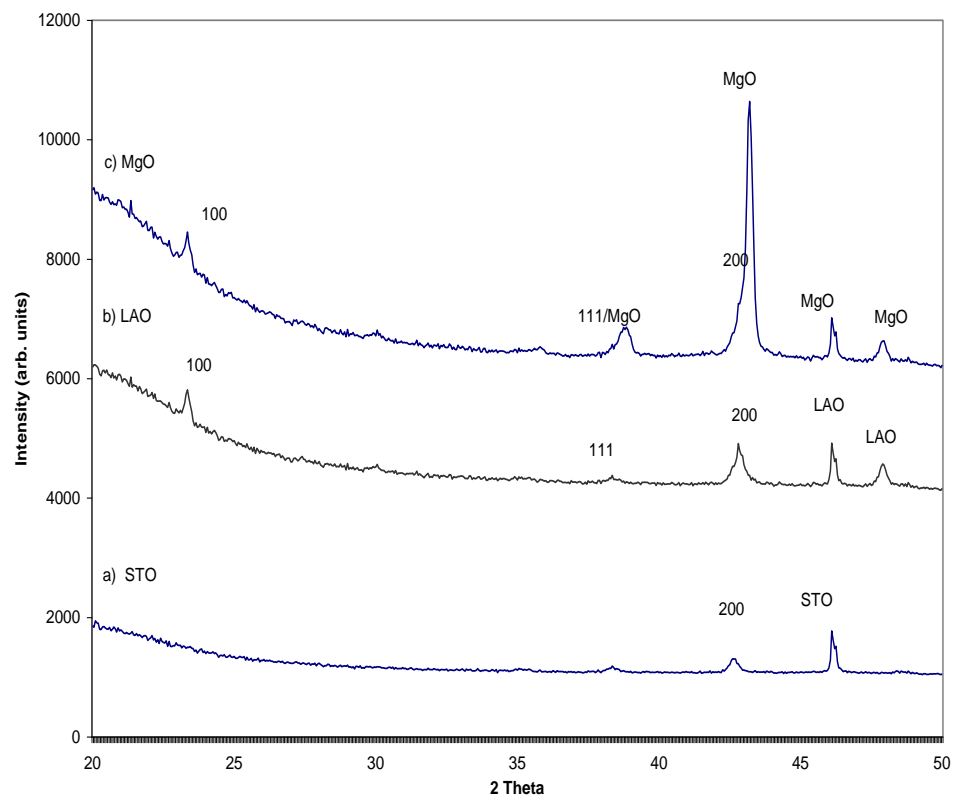


Figure 5.3.7.1

5.3.8 YBa₂Cu₂NbO₈ on MgO deposited at 850 °C

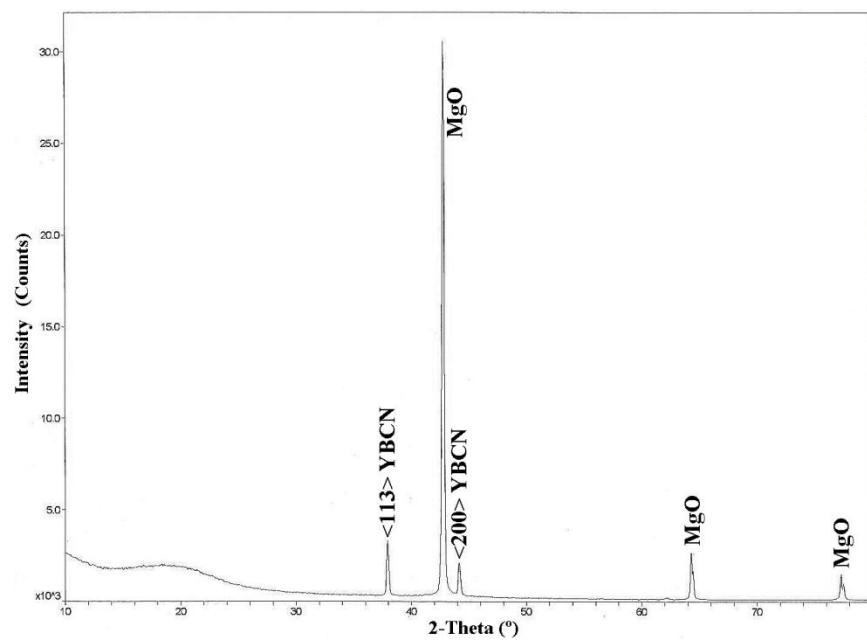


Figure 5.3.8.1

5.3.9 Highly C-axis oriented Y123 on YBCNO/IBADMgO/Inconel

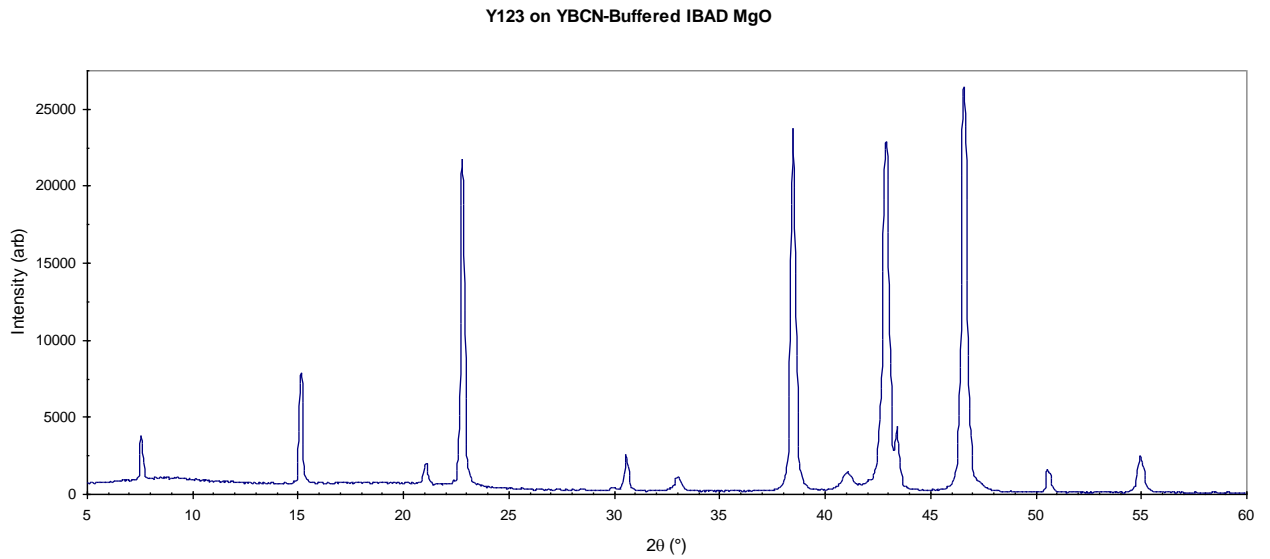


Figure 5.3.9.1

5.3.10 Texture of YBCNO films

- YBCNO in plane Texture is $10^\circ - 20^\circ$
- Y123 film in plane Texture is between $8 - 21^\circ$ on YBCNO buffer.
-

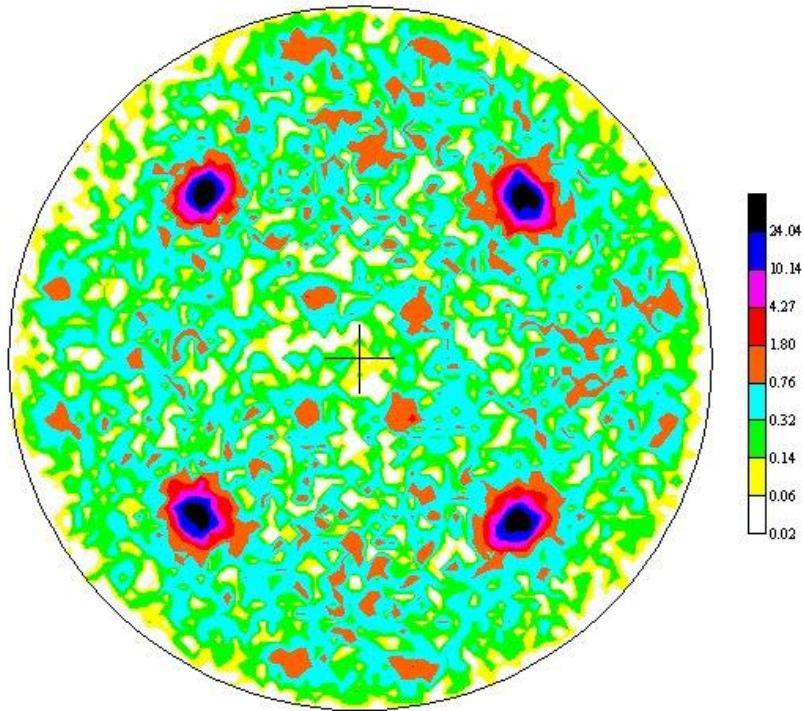


Figure 5.3.10.1

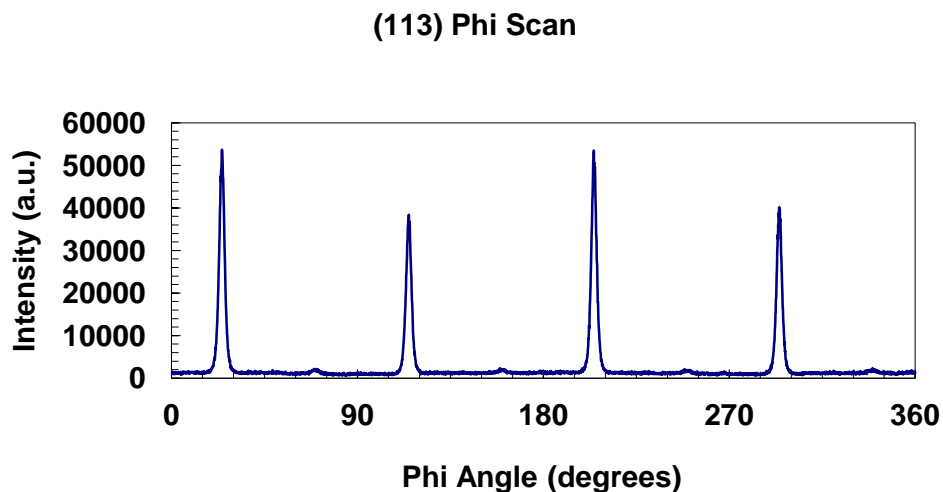


Figure 5.3.10.2

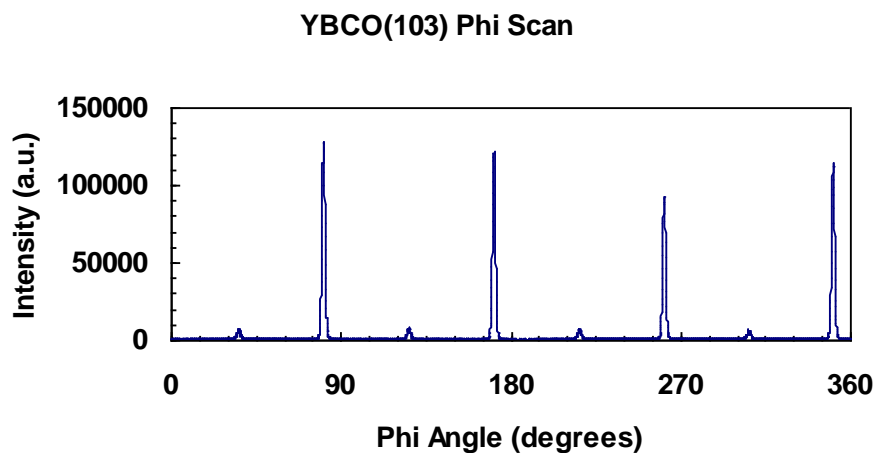


Figure 5.3.10.3

5.3.11 YBa_2NbO_6 thin films

- At 850 °C we have obtained highly epitaxial YBNO films on MgO single crystal
- Upto 600 °C films deposited are amorphous.
- 700- 800 °C highly a-axis oriented films were obtained on IBAD MgO. Above 800° C 220 orientation appears

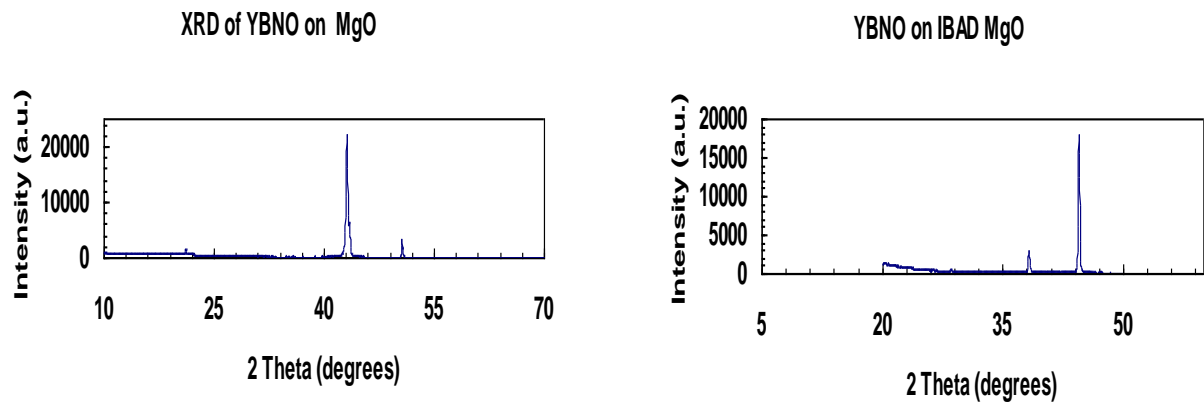


Figure 5.3.11.1

5.3.12 YBNO deposited on IBAD MgO/Inconel

Substrate	FWHM of YBNO 220 peak	FWHM of YBCO 103 peak
MgO	8°	6°
IBADMgO/Inconel	6°	5°
Inconel	28°	21°

Figure 5.3.12.1

(220) Phi Scan

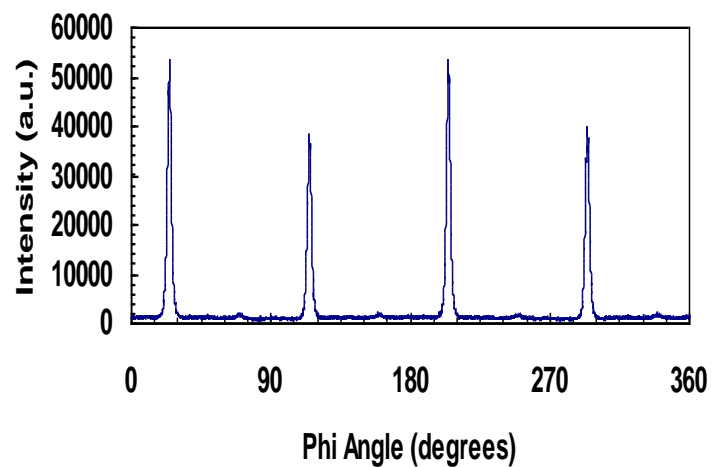


Figure 5.3.12.2

5.3.13 AC Susceptibility of Y123/YBCNO/INCONEL

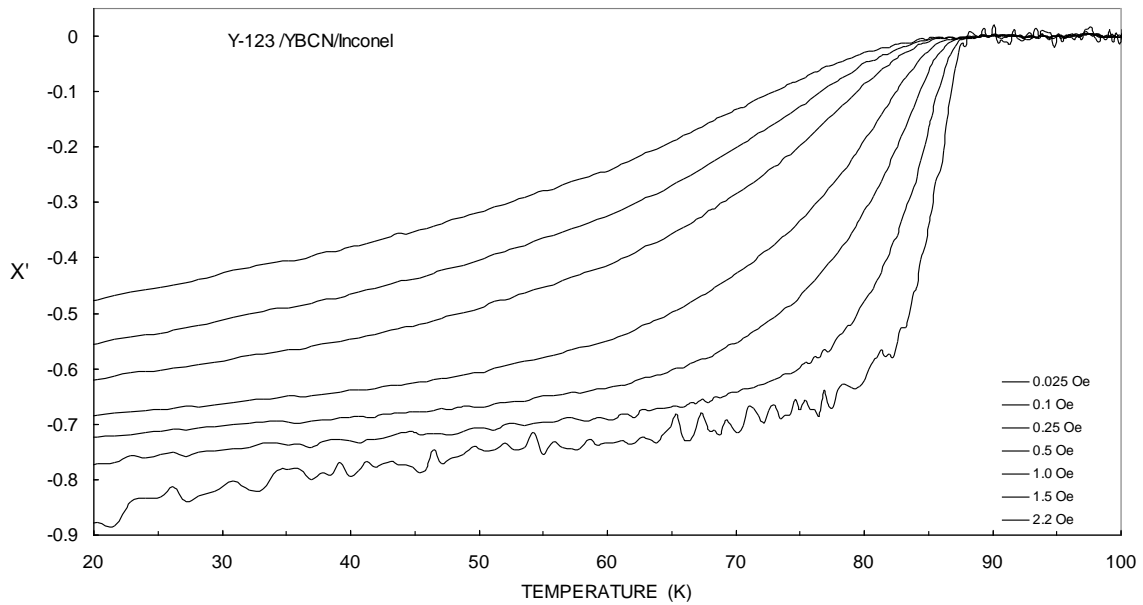


Figure 5.3.13.1

Y 123 on YBCNO buffered STO

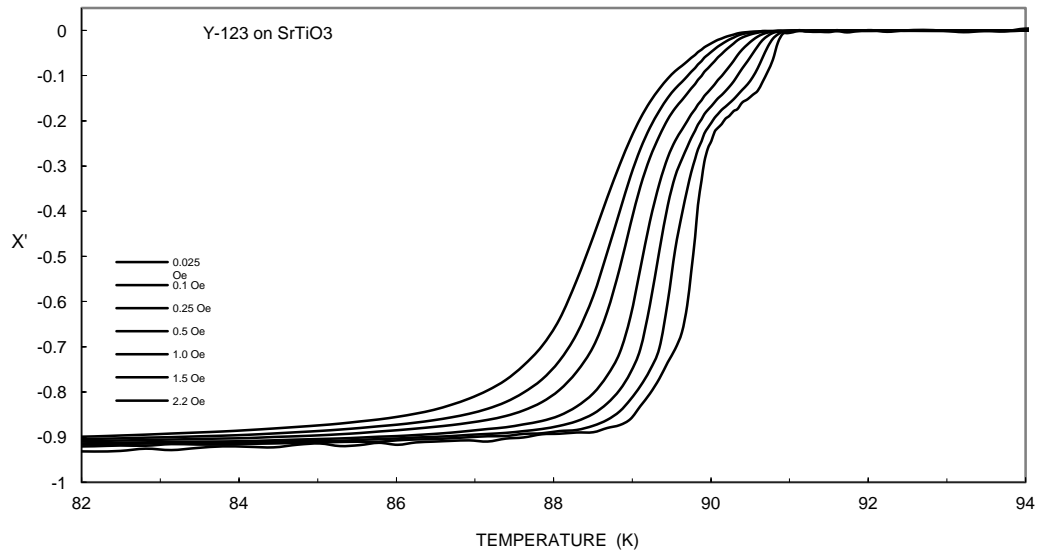


Figure 5.3.13.2

YBCNO ($x=0.25$) on LAO

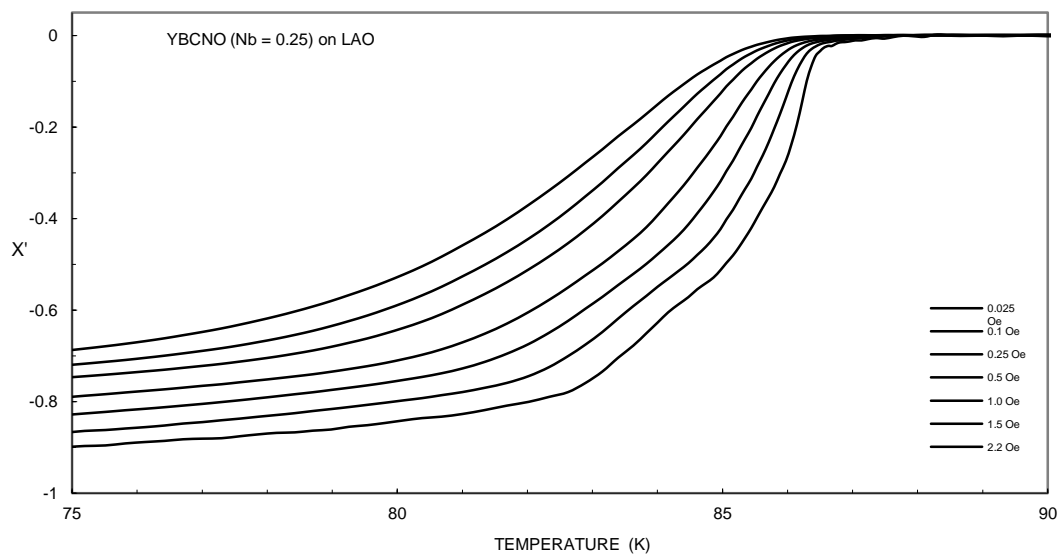


Figure 5.3.13.4

5.3.14 Transport results of Y-123 films

Y123 films on	T_c K	J_c 77K MA
YBCNO/LAO	85	0.005
YBCNO/MgO	87	0.09
YBCNO/STO	90	0.8
YBCNO(0.25)/STO	87	0.5
YBNO/MgO	87	0.1
YBNO/IBADMgO	86	0.2
CeO ₂ /YBNO/IMgO	87	0.5
YBNO/Inconel	85	0.001

Figure 5.3.14.1

T_c of YBCNO films and Y123 films deposited on these films

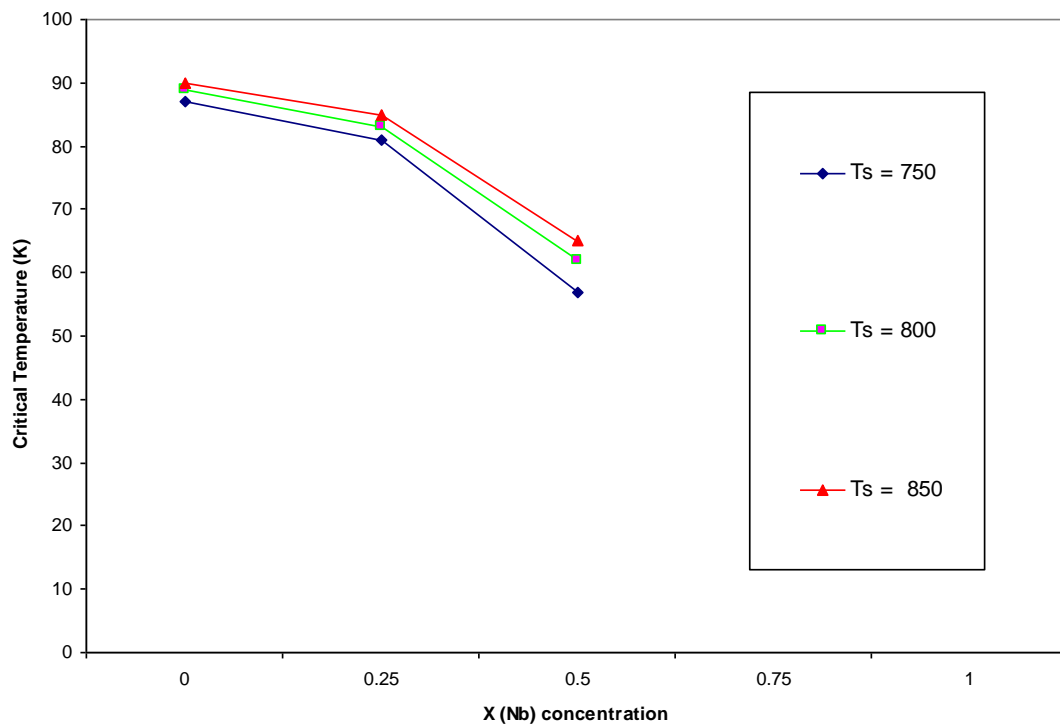
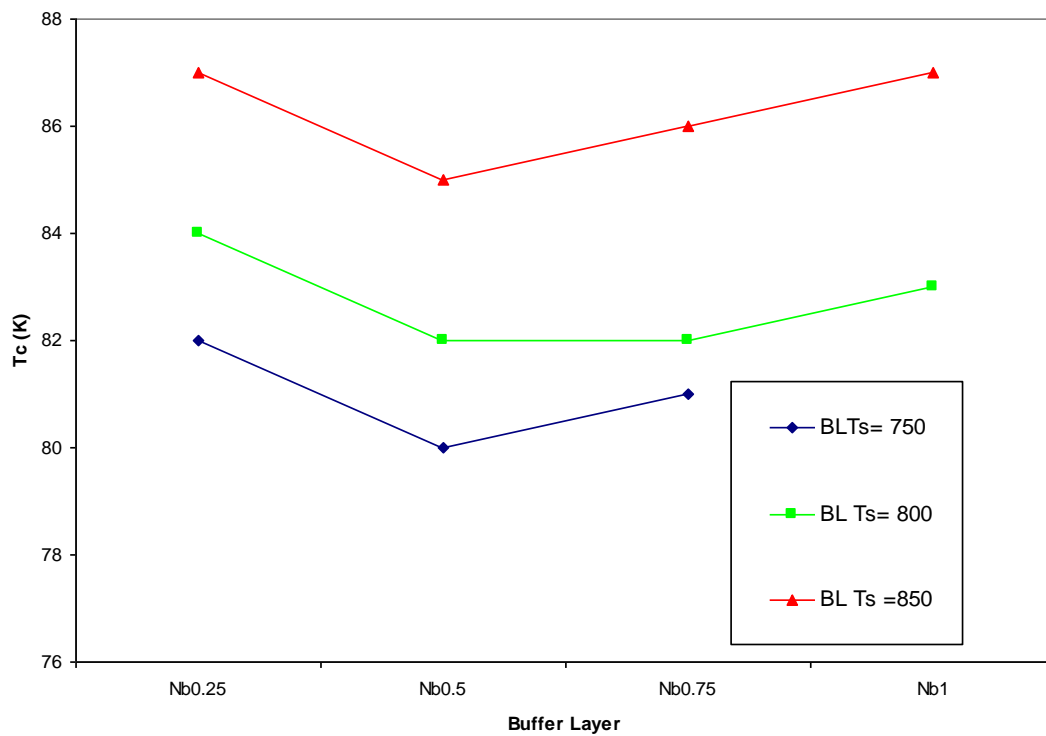


Figure 5.3.14.2



5.3.15 AFM micrographs of $\text{YBa}_2\text{Cu}_{3-x}\text{Nb}_x\text{O}_y$ and analysis

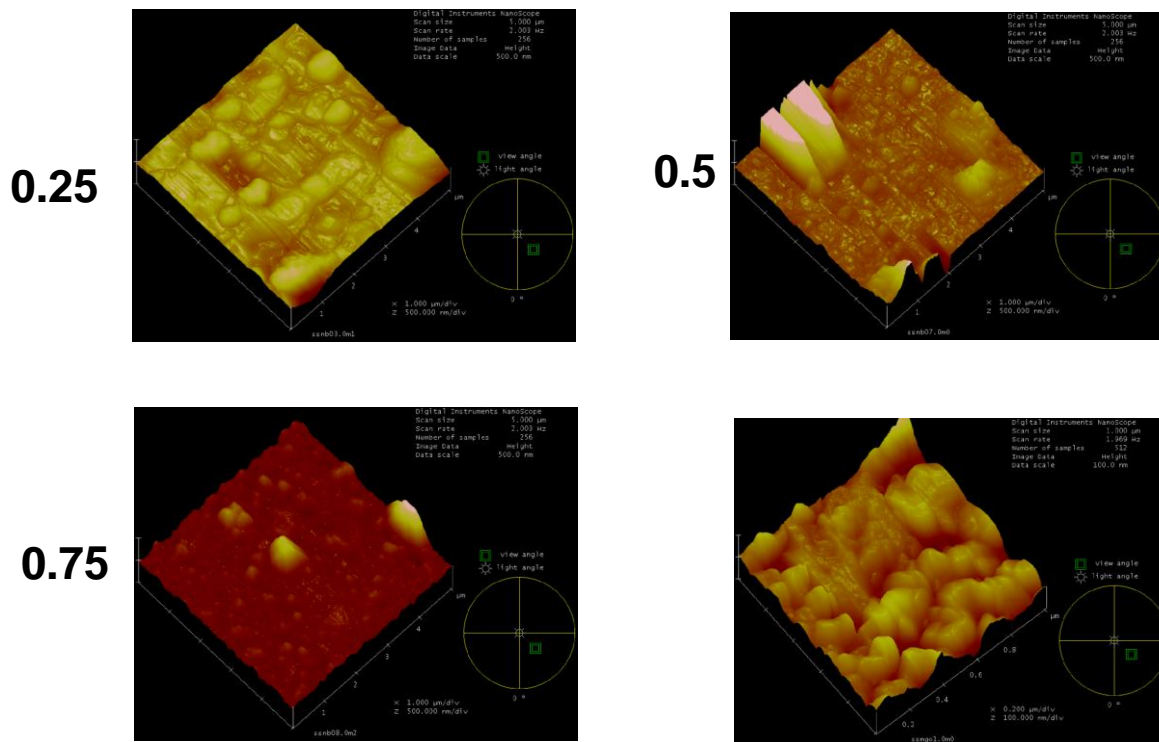
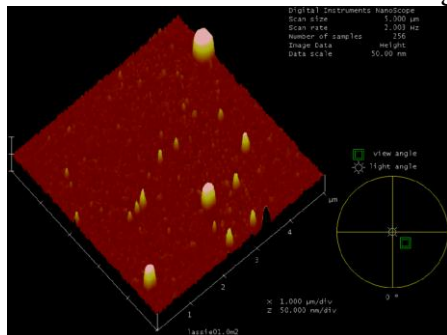
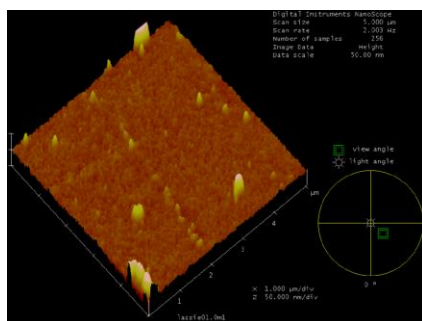


Figure 5.3.15.1



YBCNO/IBADMgO



YBNO/IBADMgO

Figure 5.3.15.2

Film	Average Ra nm
X = 0.25	25
X = 0.5	46
X = 0.75	76
X = 1.0	120
YBCNO/Inconel	170
YBCNO/I-MgO	3
YBNO/MgO	6
YBNO/I-MgO	1.5

Figure 5.3.15.3

5.3.16 XPS Studies of $\text{YBa}_2\text{Cu}_{3-x}\text{Nb}_x\text{O}_y$ ($x = 0.25, 0.5, 0.75, 1$) thin films

- A survey scan XPS spectrum was taken with binding energy varying from 0 to 1000 eV. It contains almost all the peaks from the elements present on the surface
- The surface was etched for 5 minutes using 3 KeV Ar^+ ions, the amount of carbon reduced to negligible amounts showing that the surface got cleaned up.

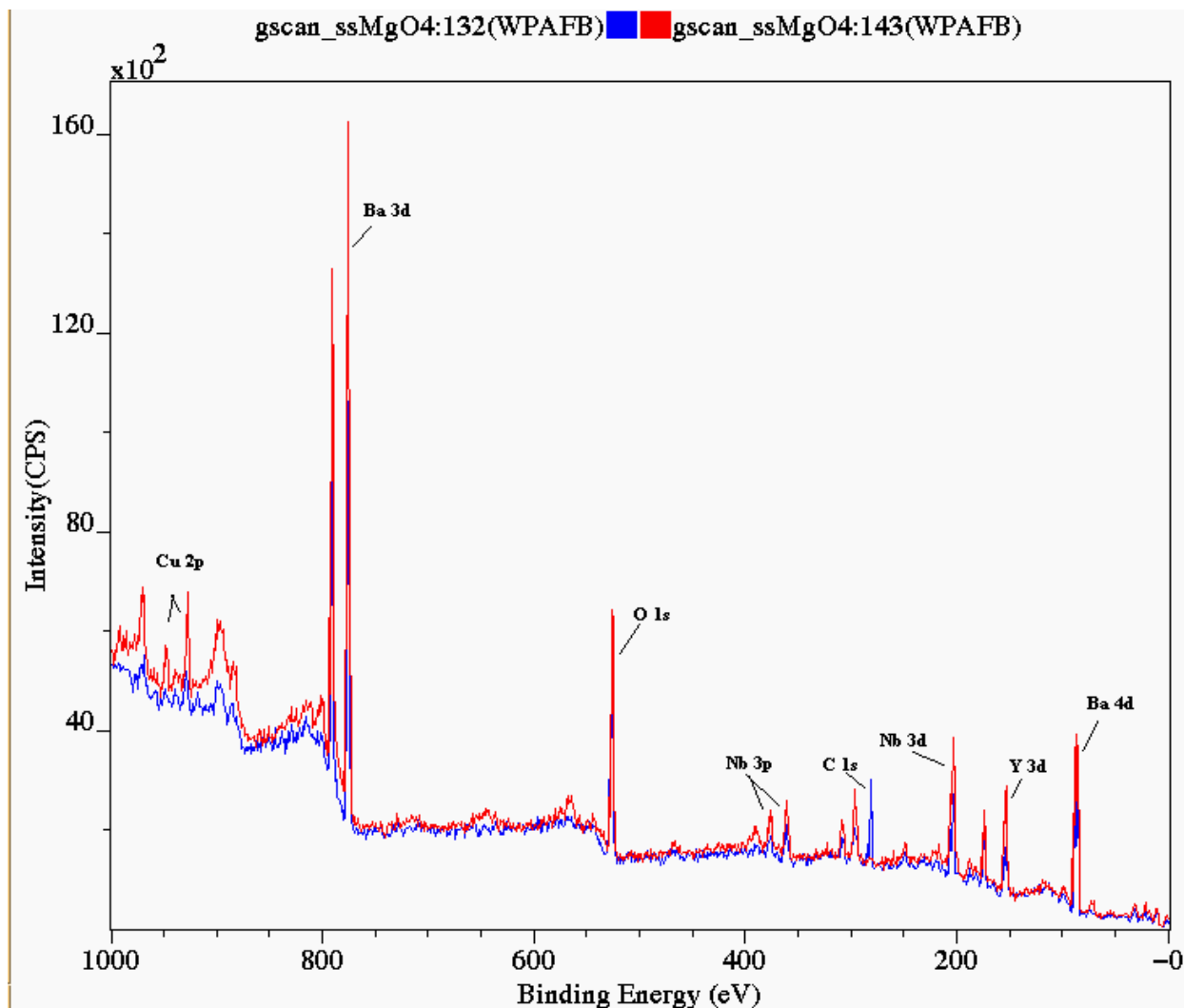


Figure 5.3.16.1

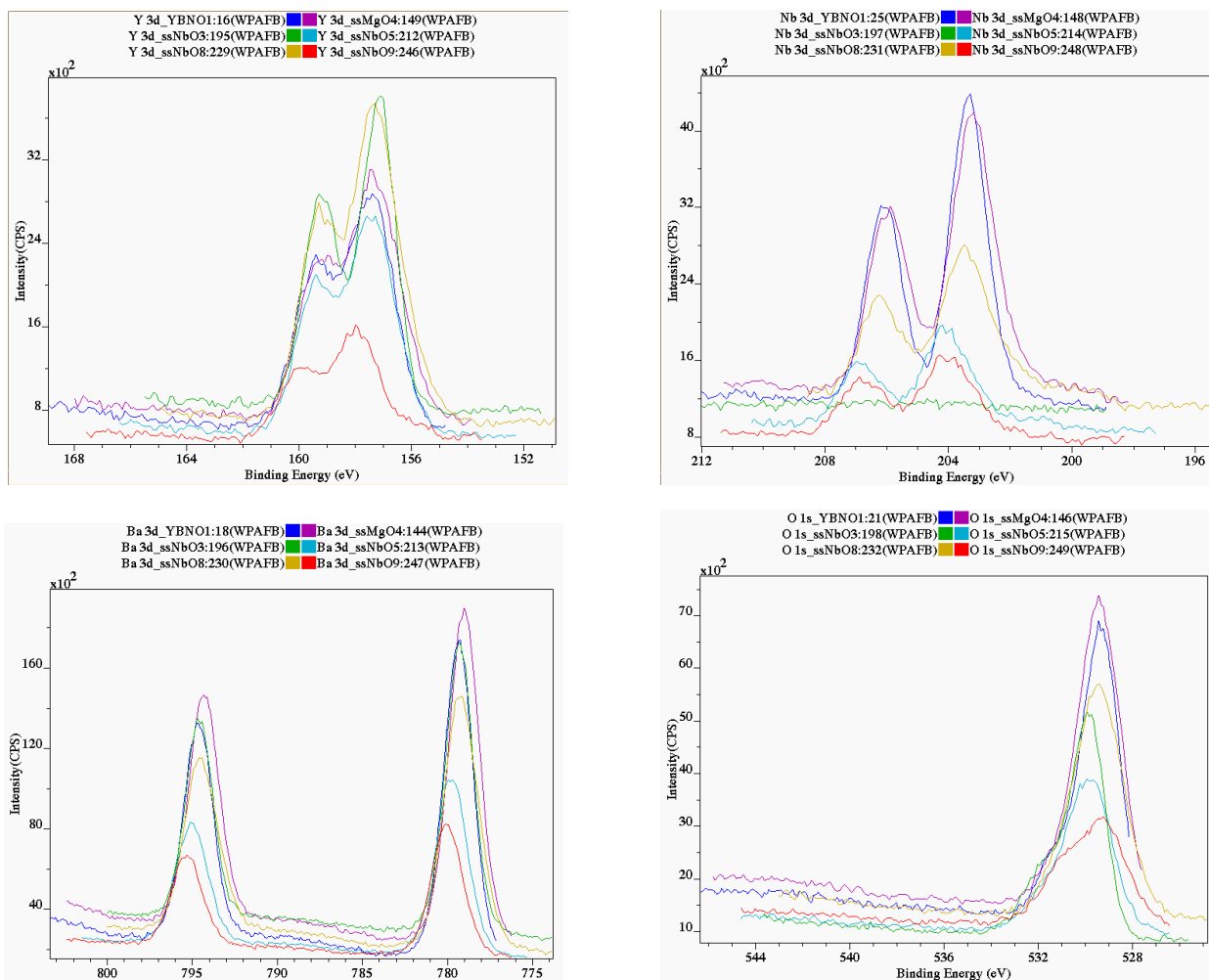


Figure 5.3.16.2

5.3.17 Cu-2p binding energy of YBCNO films

- Cu 2p binding energies does not corresponding to CuO
- Which confirms that Cu exists in +2 Valance state
- We expect that $\text{YBa}_2\text{Cu}_2\text{NbO}_8$ phase forms in thin films

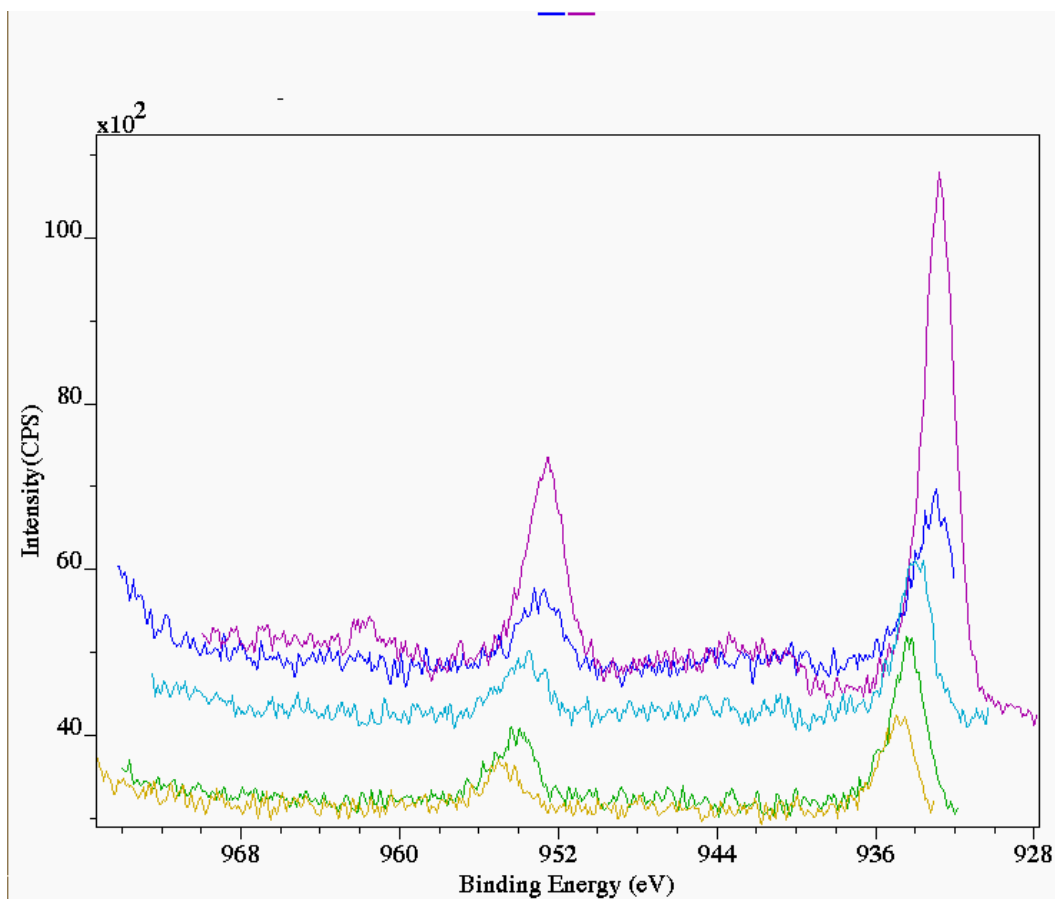


Figure 5.3.17.1

5.3.18 Raman Microscopy Studies

- 1 minute Raman spectra were collected on $\text{YBa}_2\text{Cu}_{3-x}\text{Nb}_x\text{O}_8$ films.
- $X=0.25$ retains ortho-rhombic nature and reflects in Raman orthorhombic modes of Y123 150, 230, 330, 500 and 575cm^{-1}
- Raman modes at 150, 230 and 500cm^{-1} started dissolving slowly for $x=0.5$ and 0.75
- For $x=1.0$ we have seen the complete absence of the orthorhombic peaks belong to Y-123 film structure.
- Shift in 334cm^{-1} to higher side (350cm^{-1}) and the Raman shift at 501cm^{-1} is completely absent for the film with $x=1.0$.
- No mode correspond to CuO has been observed.

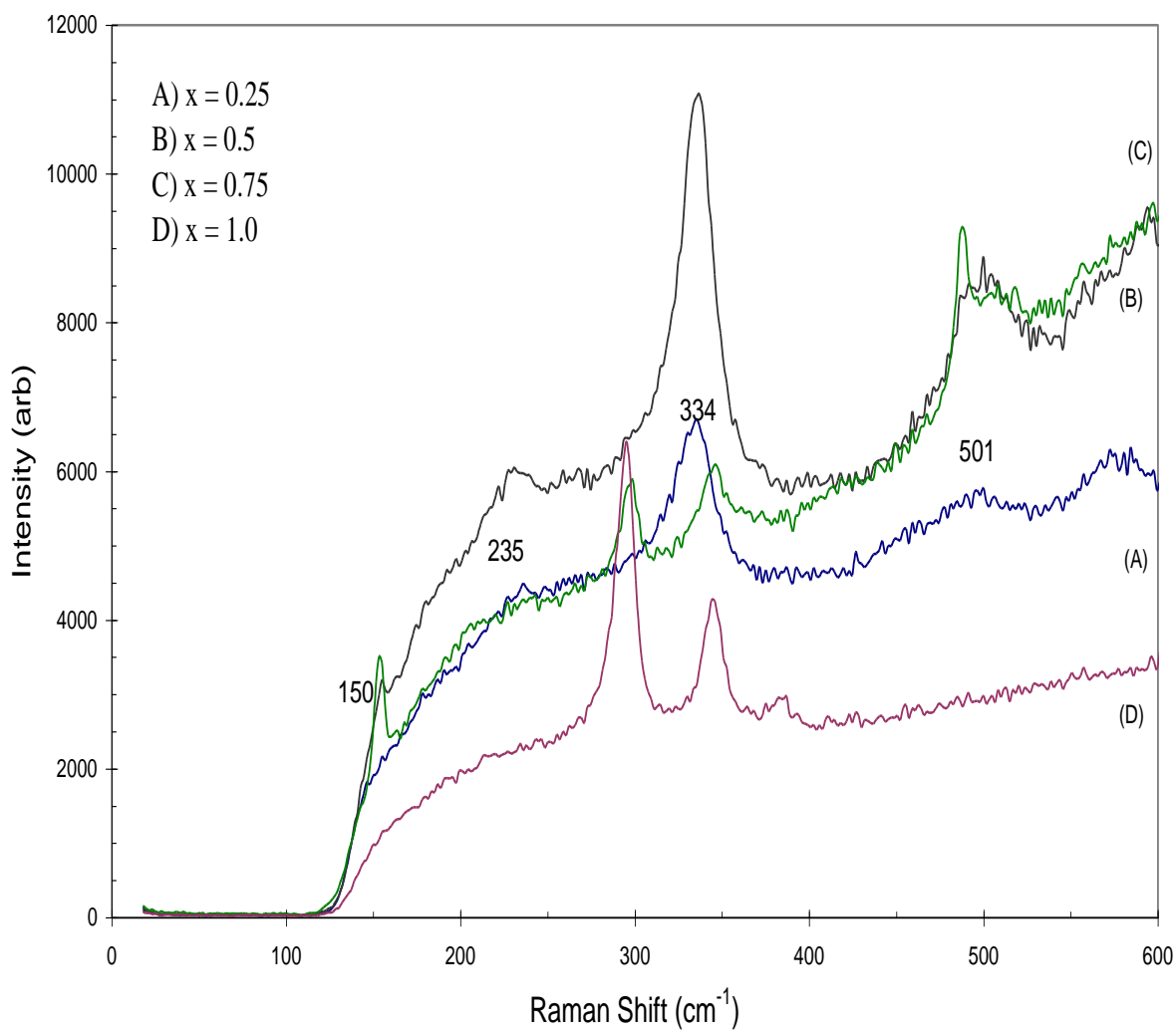


Figure 5.3.18.1

- By studying the raman shifts on three different substrates and identified the YBCNO modes
- Disappearance of peak at 500 cm^{-1} and decrease of 330 cm^{-1} mode clearly indicates that an existence of pronounced cation disorder in 123 crystal structure which confirms the transformation of orthorhombic phase to cubic phase
- YBa_2NbO_6 films are cubic and hence show no raman active mode.
- There is phase transformation from ortho to tetragonal in YBCNO films

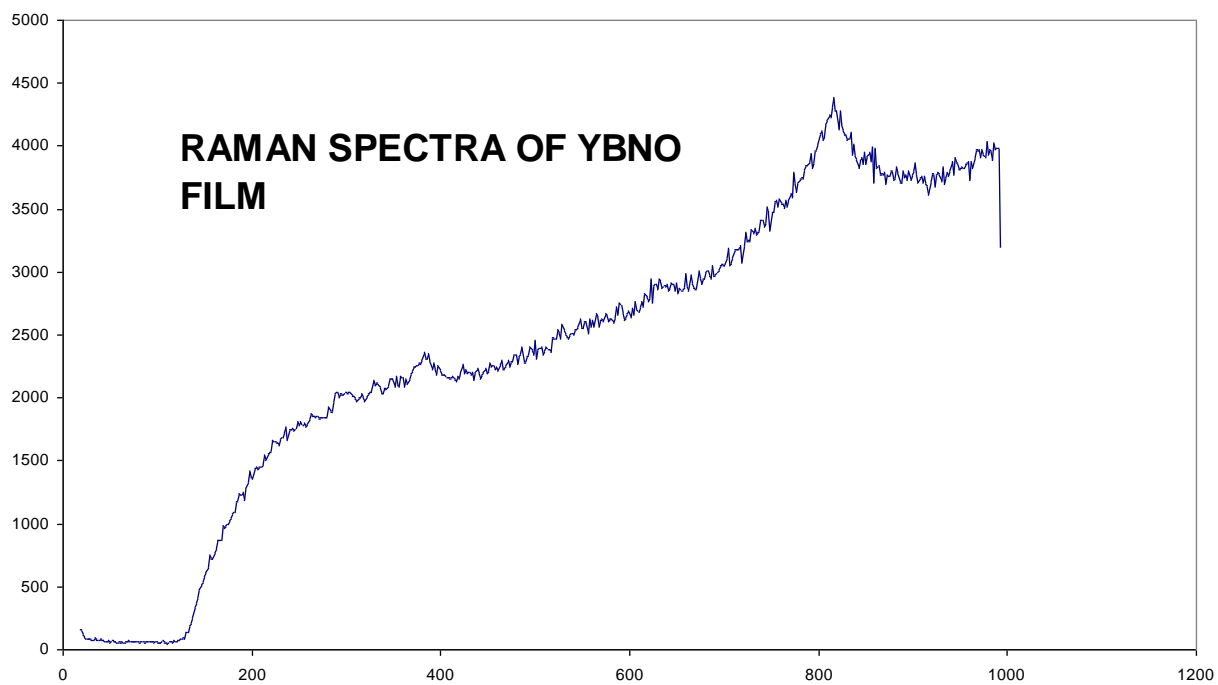
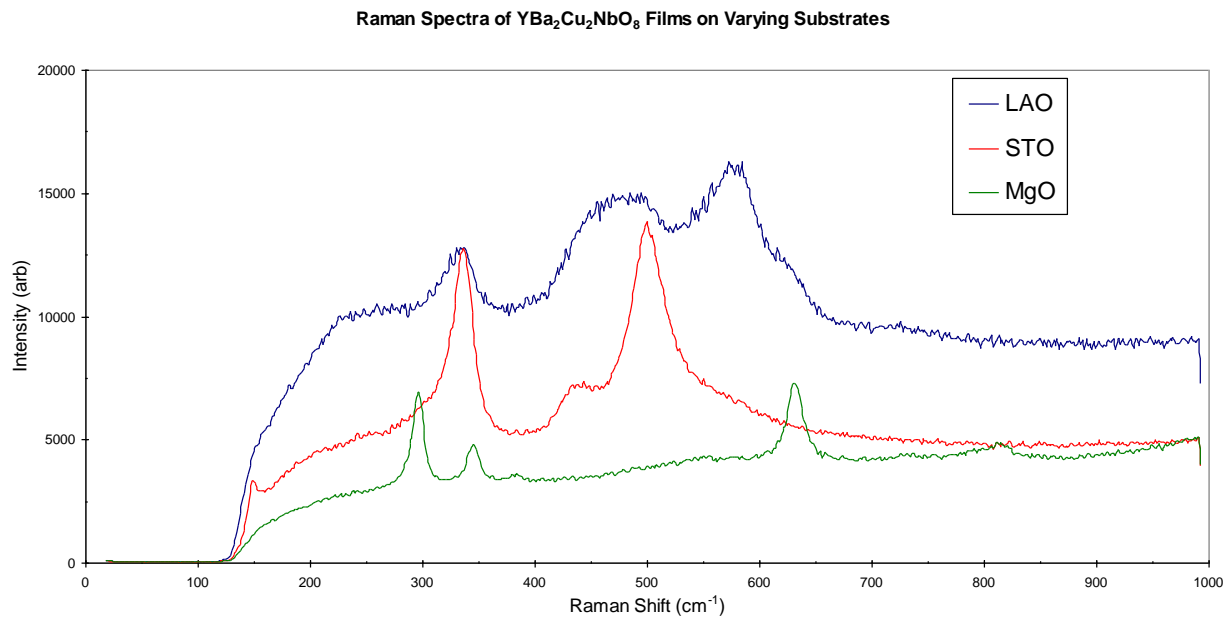
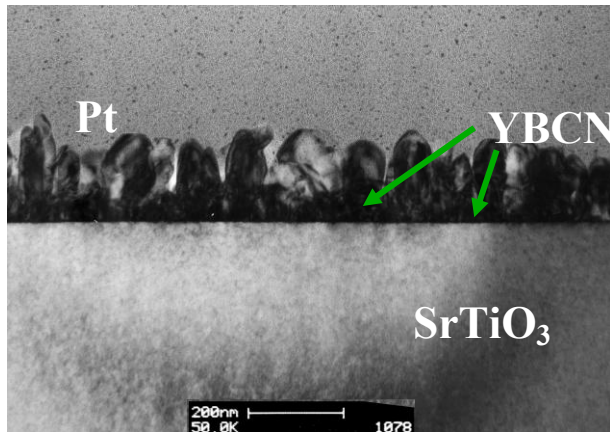


Figure 5.3.18.2

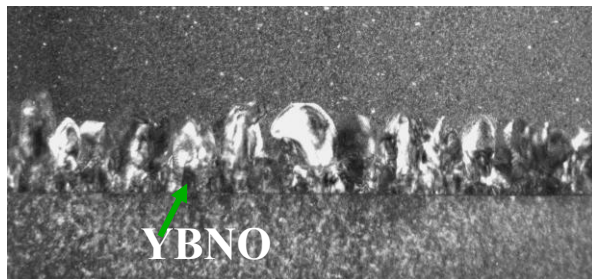
5.3.19 Cross sectional TEM of $\text{YBa}_2\text{Cu}_2\text{NbO}_8$ film on STO deposited at 800°C



TEM cross section prepared by FIB

- Pt protective layer
- Cut with Ga ion beam and lift out onto Cu grid bar
- Final thin with fine Ga beam (30 kV)

Figure 5.3.19.1



Dark Field

Figure 5.3.19.2

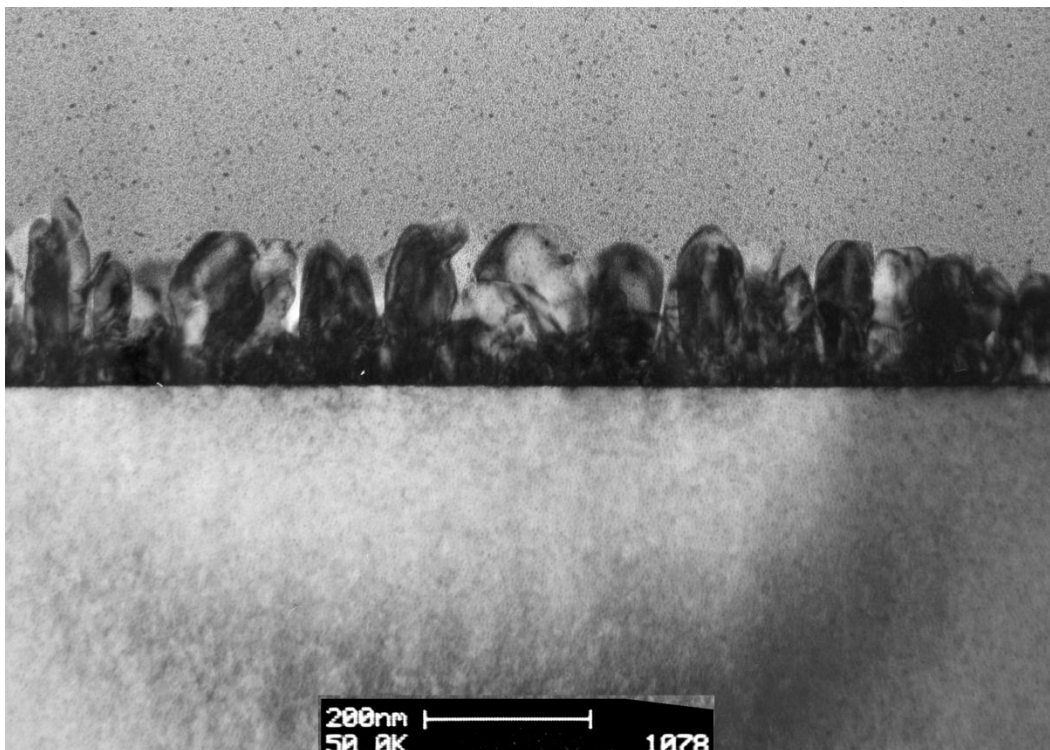


Figure 5.3.19.3

5.3.20 EDS SPECTRA OF YBCNO FILM

- It shows the Y and Nb Ka peaks with an intensity ratio of very nearly one.
- Excess Cu intensity is taken into account, the Ba L peak and Cu K peak intensity ratio is very close to unity and indicates a ratio of Ba or Cu with Y of 2:1.
- These observations suggest film has a compositional stoichiometry of approximately $\text{YBa}_2\text{Cu}_2\text{NbO}_8$.

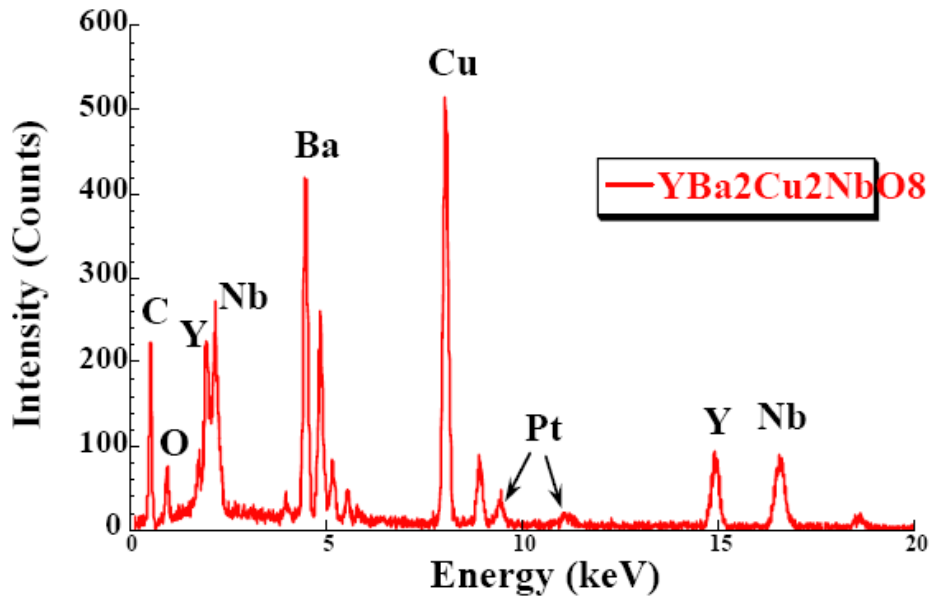


Figure 5.3.20.1

5.3.21 Stoichiometry of $\text{YBa}_2\text{Cu}_2\text{NbO}_y$

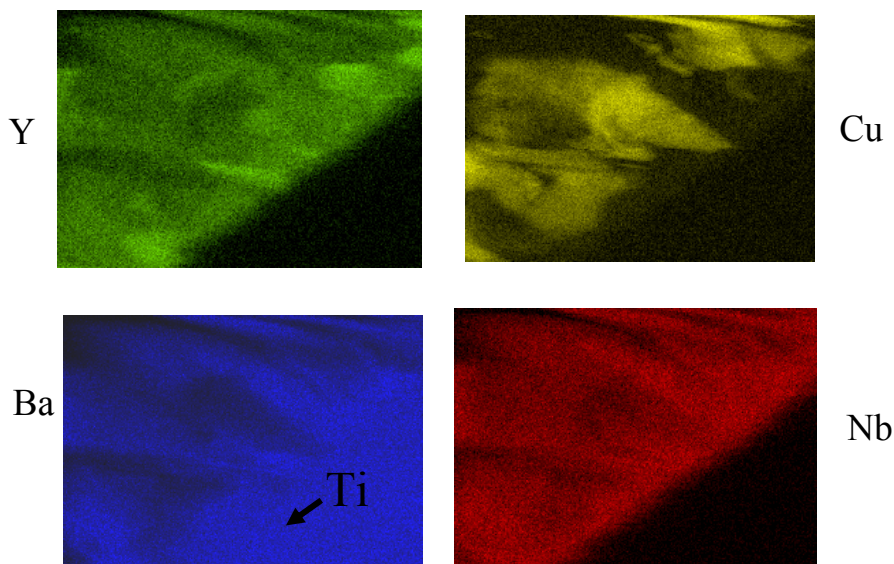


Figure 5.3.21.1

5.3.22 TEM S.A.D Micrograph of $\text{YBa}_2\text{Cu}_2\text{NbO}_x$

- Orientation images indicates that YBCNO film is epitaxial
- The pattern in this figure is oriented along the [001] axis of the cubic SrTiO_3 substrate and contains strong {200} and {110} type reflections.
- The STO phase was used to calibrate the lattice parameter of the new phase which has $a_0 \sim 0.41 \text{ nm}$. While this electron diffraction pattern suggests that the $\text{YBa}_2\text{Cu}_2\text{NbO}_x$ phase has one 4-fold axis of symmetry.

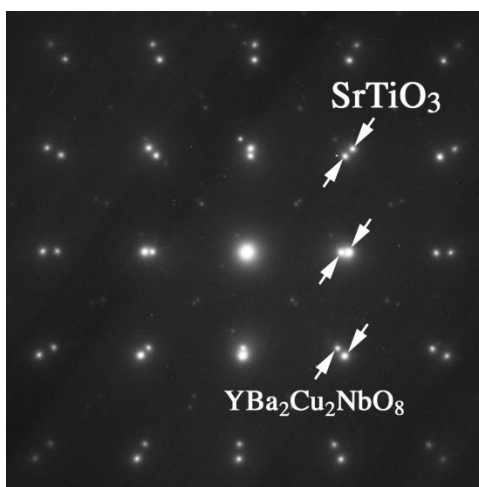


Figure 5.3.22.1

5.3.23 Summary Notes

- Substrate Temperature and Nature plays critical role in the Phase formation of YBCNO films
- At 800°C we have observed highly a – axis oriented $\text{YBa}_2\text{Cu}_2\text{NbO}_8$ films have grown on STO substrate
- Around 850°C single phase YBCNO has been observed in our studies.
- XPS, micro-raman results show no formation of CuO phase.
- TEM analysis has confirmed the growth of stoichiometric and highly a-axis oriented $\text{YBa}_2\text{Cu}_2\text{NbO}_8$ films.
- Raman Studies shows a systematic phase transformation in YBCNO films (from orthorhombic to tetragonal)
- Y-123 Films deposited directly on YBCNO buffered Inconel are poor in quality.
- $\text{YBa}_2\text{Cu}_2\text{NbO}_8$ Phase does forms on single crystal substrates and its $a \sim 0.41$ and $c \sim 1.18 \text{ nm}$.
- YBa_2NbO_6 a new double perovskite buffer with $a \sim 0.84 \text{ nm}$ appears to be promising for coated conductor applications. Further studies are in progress.

5.4 Growth of oxide and metal buffer layers for coated conductor applications

References: 17, 36, 37, 38, 39

Presented At
AFOSR REVIEW, January 24, 2005

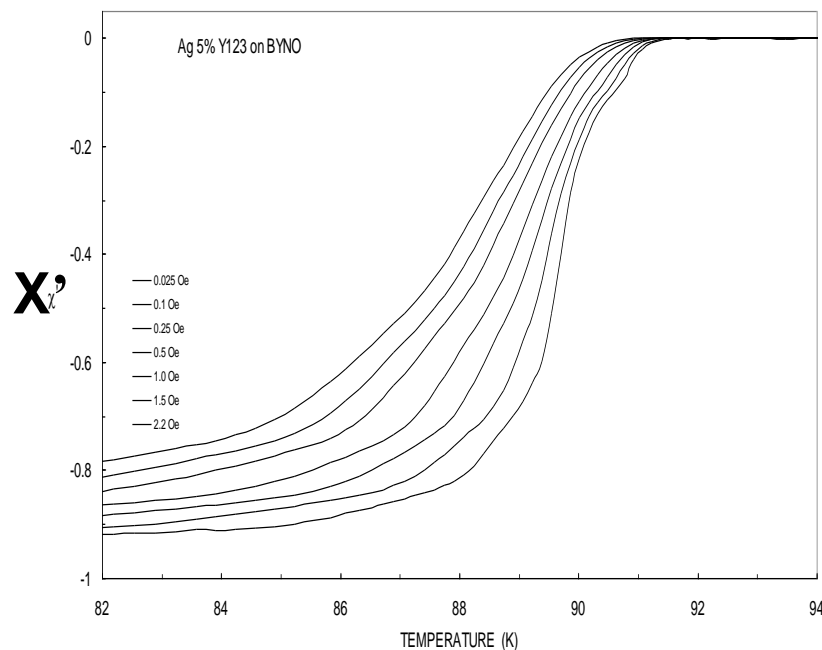
SRINIVAS SATHIRAJU
National Research Council
Propulsion Directorate
Air Force Research Laboratory

5.4.1 BYNO films

WHY BYNO ?

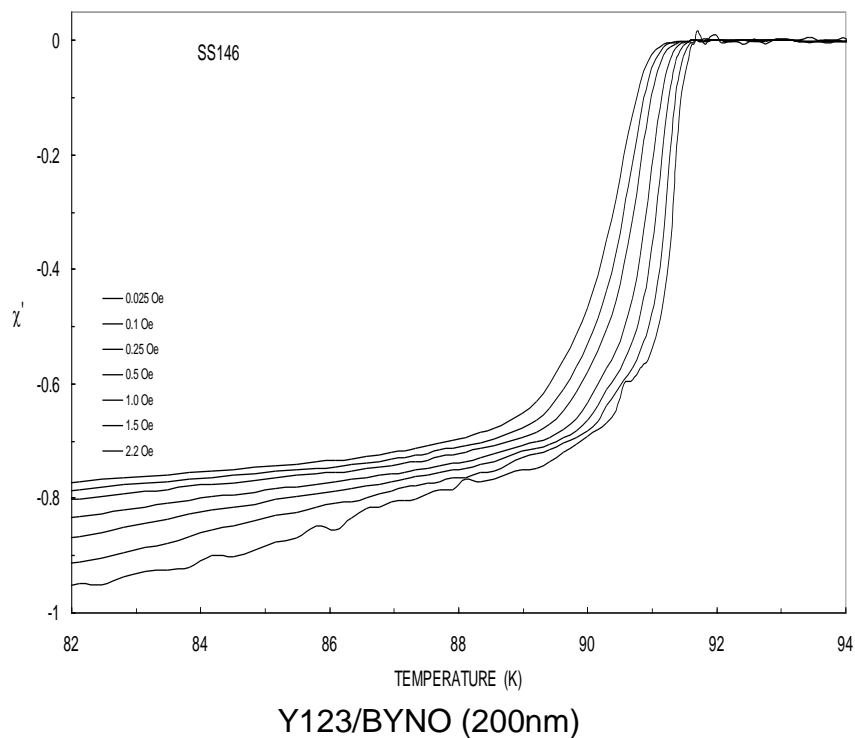
- Ba_2YNbO_6 double perovskite
- 0.84 nm (Double the unit cell of MgO)
- No reaction up to 1200 °C with Y123 or R-123 materials
- Last year we have achieved only 0.5 MA/cm² J_c at 77K on metallic substrates.
- 1MA/cm² J_c on single crystal substrates

5.4.2 AC susceptibility results



5%Ag+Y123/BYNO (100nm)

Figure 5.4.2.1



5.4.3 BYNO thickness variation on IMgO

THICKNESS OF BYNO (nm)	YBCO T_c (K)	YBCO J_c MA/cm ² @77K	Ag 5% YBCO T_c (K)	Ag 5% YBCO J_c (MA/cm ²) @77K
50	88	0.01		
100	89	0.5	89	1.09
200	89	0.9	91	3.2
250	91	1.2		
300	91	1.6		

Figure 5.4.3.1

5.4.4 Texture Analysis from Sandia National Lab

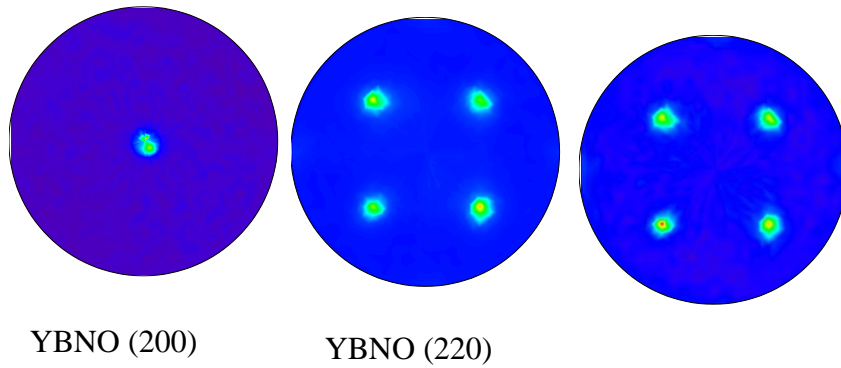
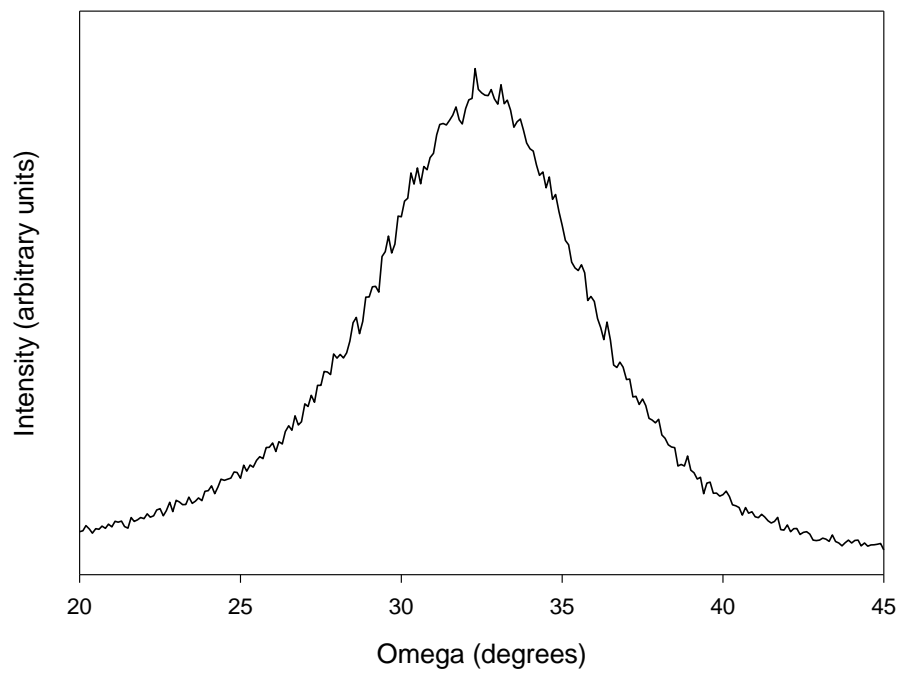


Figure 5.4.4.1

5.4.5 Rocking curve of MgO

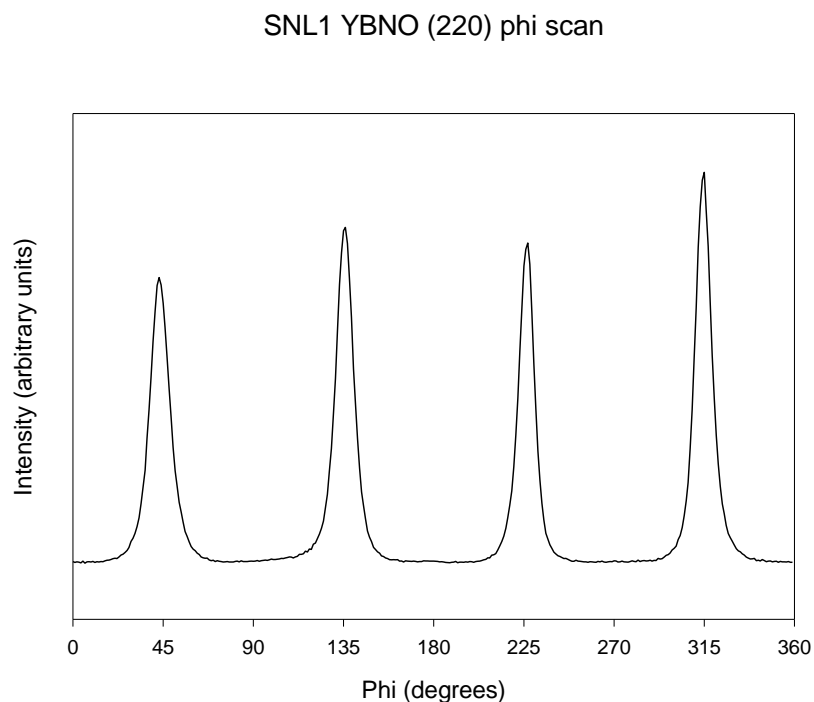
SNL1 MgO (220) omega scan



FWHM = 7.87 degrees

Figure 5.4.5.1

5.4.6 BYNO(220) Phi-scan



FWHM $\sim 7.7^\circ$

Figure 5.4.6.1

5.4.7 Sample information and summary

- Sample -1, UA-1: BYNO on single crystal MgO substrate
- Sample-2, UA-2: BYNO on single crystal MgO substrate, different deposition parameters
- Sample-3, UA-3: BYNO on metal substrate
- In sample-1 and -2, a thin layer of Au-Pd was deposited on the surface to prevent charging during FIB cross sectioning
- RBS was performed at 3.8 MeV using ^4He atoms

Sample	Composition from RBS	RBS thickness (nm) ± 10	FIB thickness (nm)
UA-1	YNbBa_2O_6	1100	608 ± 32
UA-2	YNbBa_2O_6	340	310 ± 25
UA-3	$\text{Y}_{1.1}\text{Nb}_{1.2}\text{Ba}_2\text{O}_6$	280	254 ± 10

Figure 5.4.7.1

Additional work is required to delineate the reason for discrepancy between the thickness from RBS and FIB for sample-1

5.4.8 FIB cross section- tilted at 45°

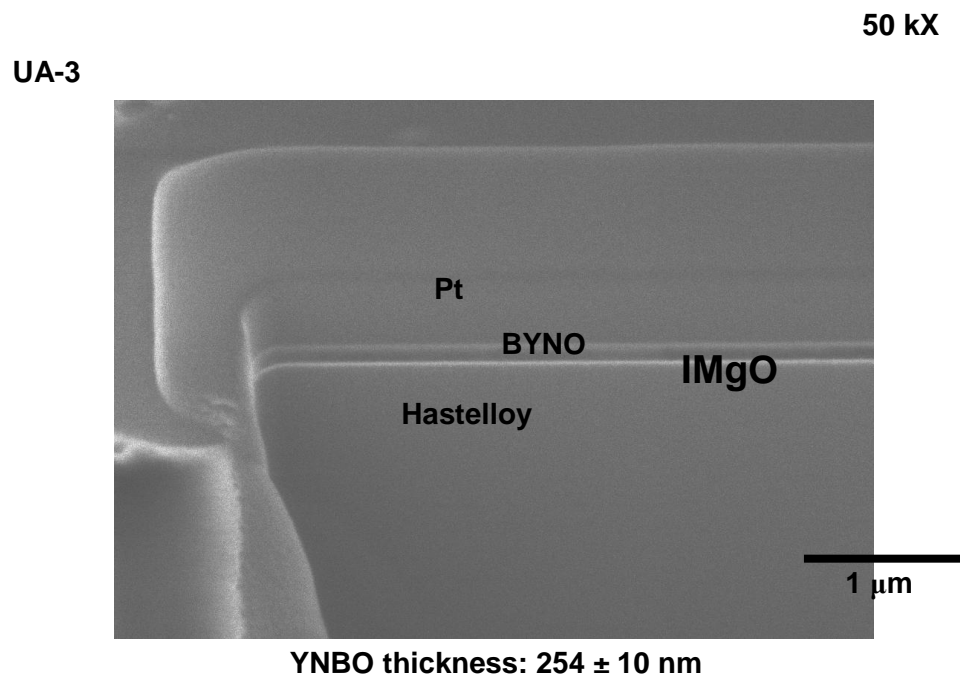


Figure 5.4.8.1

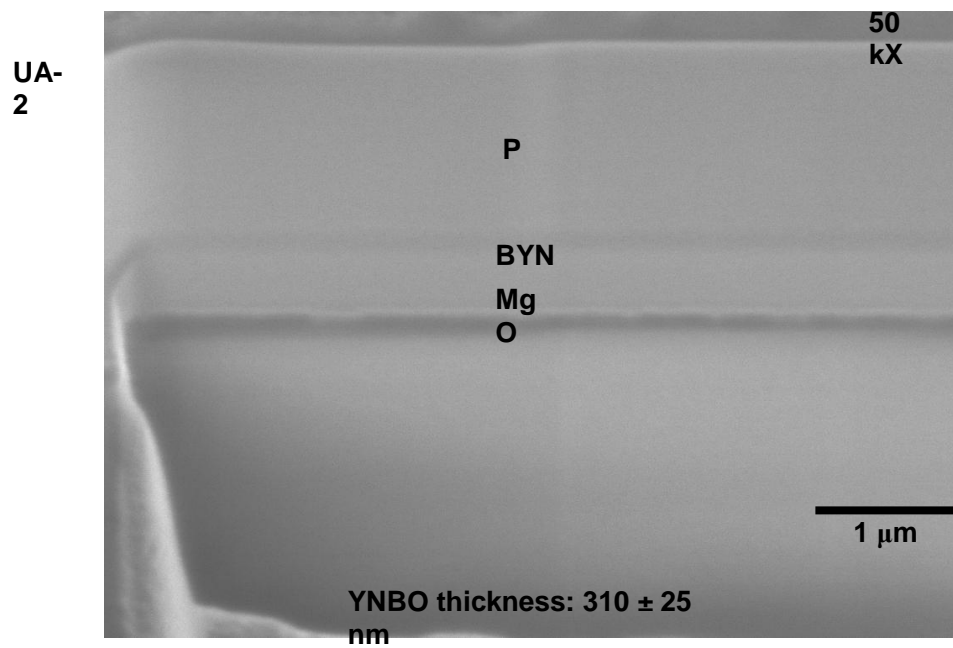


Figure 5.4.8.2

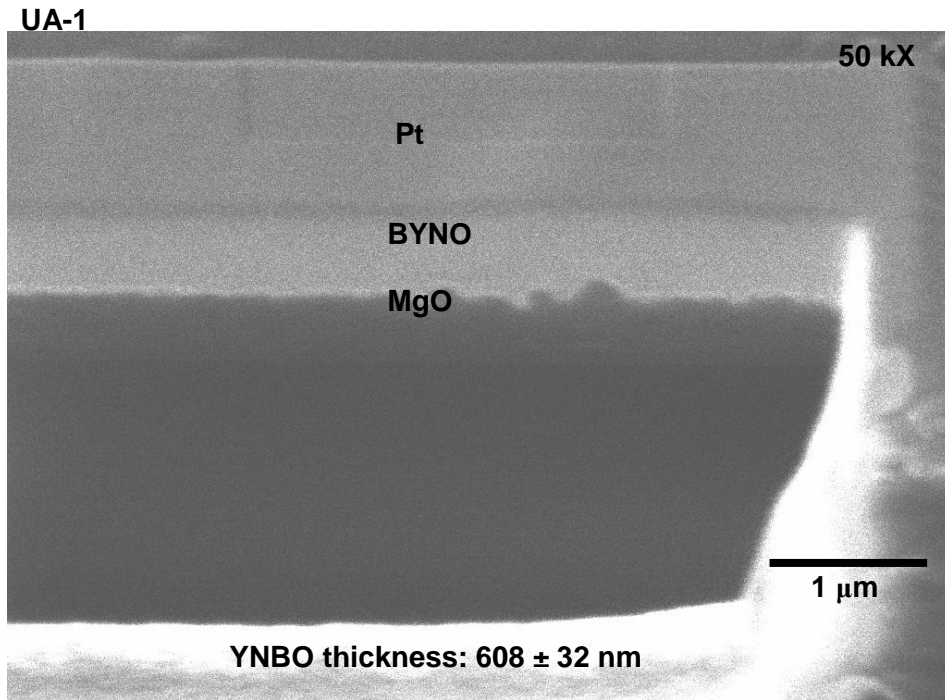


Figure 5.4.8.3

5.4.9 RBS Analysis of BYNO film

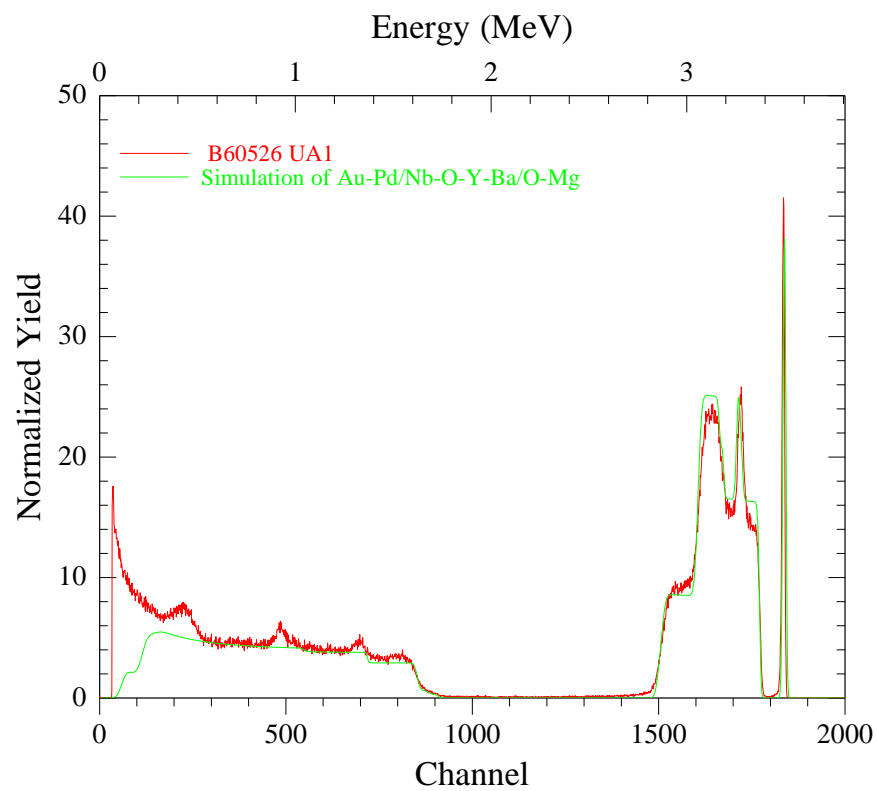


Figure 5.4.9.1

RBS spectrum at 3.8 MeV

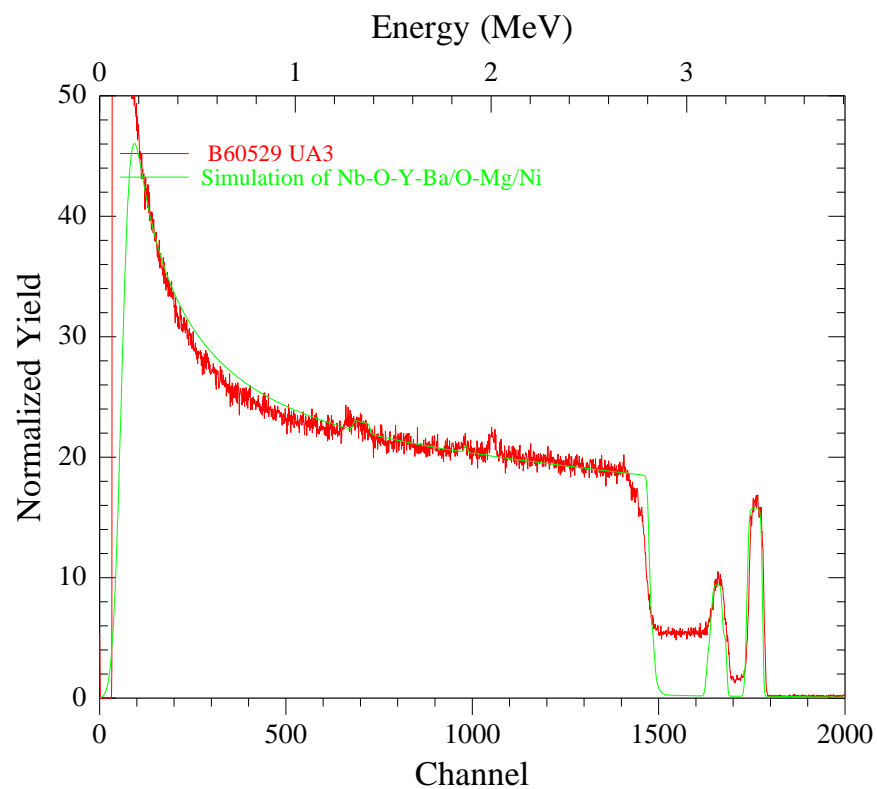


Figure 5.4.9.2

Peaks of Nb and Y are very close

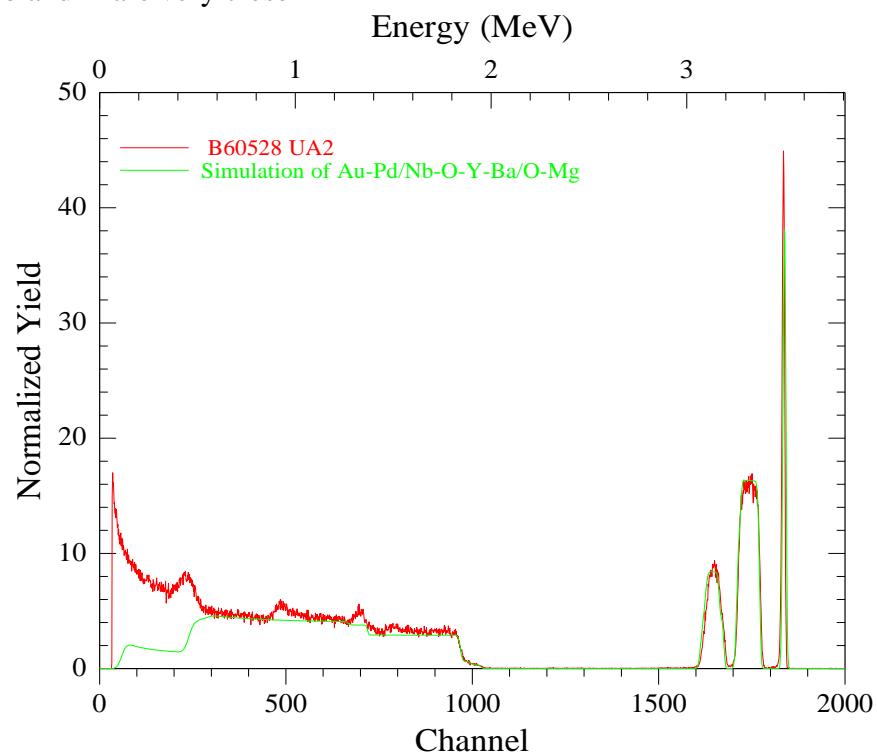


Figure 5.4.9.3

5.4.10 Cross sectional TEM Image of YBCO/BYNO/IMgO/Hastelloy

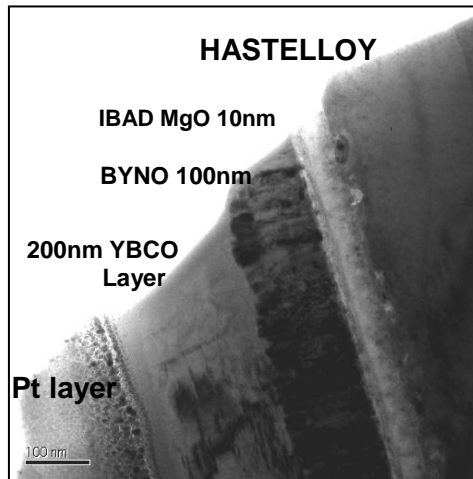


Figure 5.4.10.1

5.4.11 Ag and Ca doped YBCO films

- In order to overcome the oxygen deficiency in the YBCO films we have used Ag 5 wt% doped YBCO films
- Ag doped films carried $2-4 \text{ MA/cm}^2 J_c$ at 77 K.
- Thickness of BYNO buffer is 100nm and YBCO is 300nm.
- Very well oxygenated YBCO films have carried $1 \text{ MA/cm}^2 J_c$ at 77K.
- Ca doped Y-123 also have $1-3 \text{ MA/Cm}^2$ at 77K

5.4.12 Ba_2YNbO_6 film deposited on Textured Ni

- When deposited in vacuum we have seen oxidation of the substrate
- Reduced atmosphere we have improved the situation and highly a-axis oriented BYNO films were obtained
- No formation of NiO but difficult to confirm through X-ray as 400 peak of BYNO and NiO 100% peak 012 appears around 43°

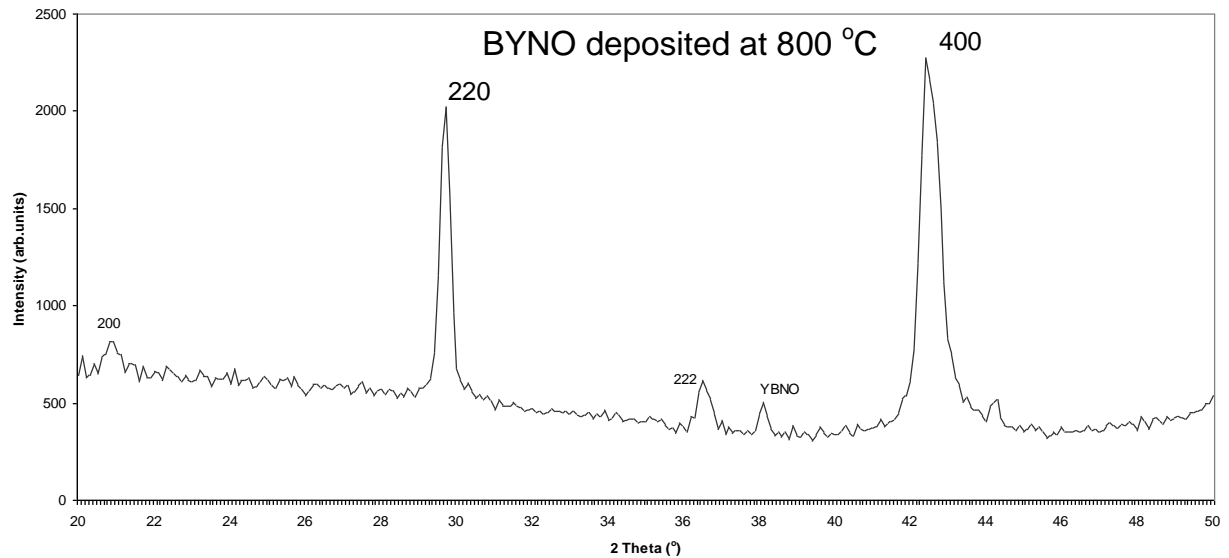


Figure 5.4.12.1

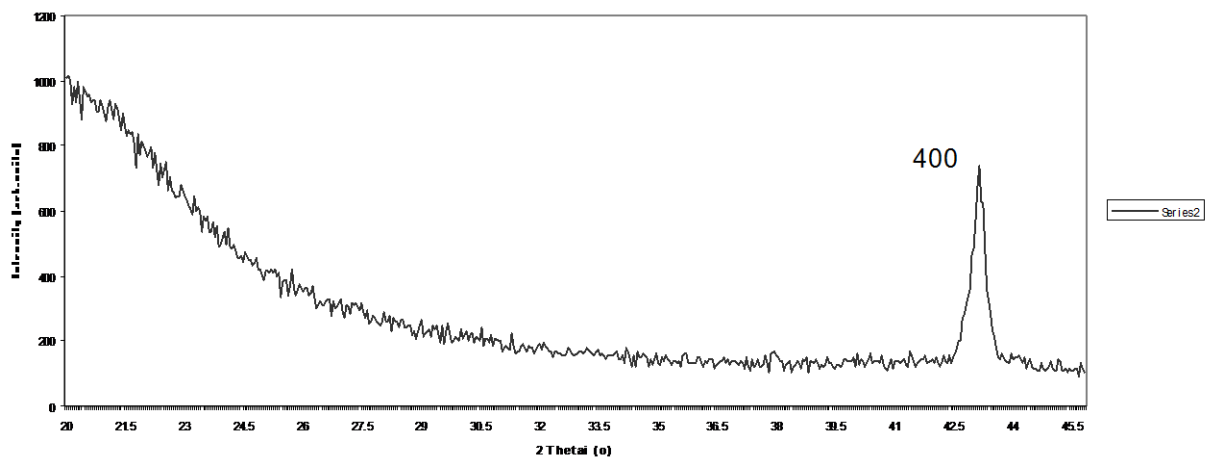
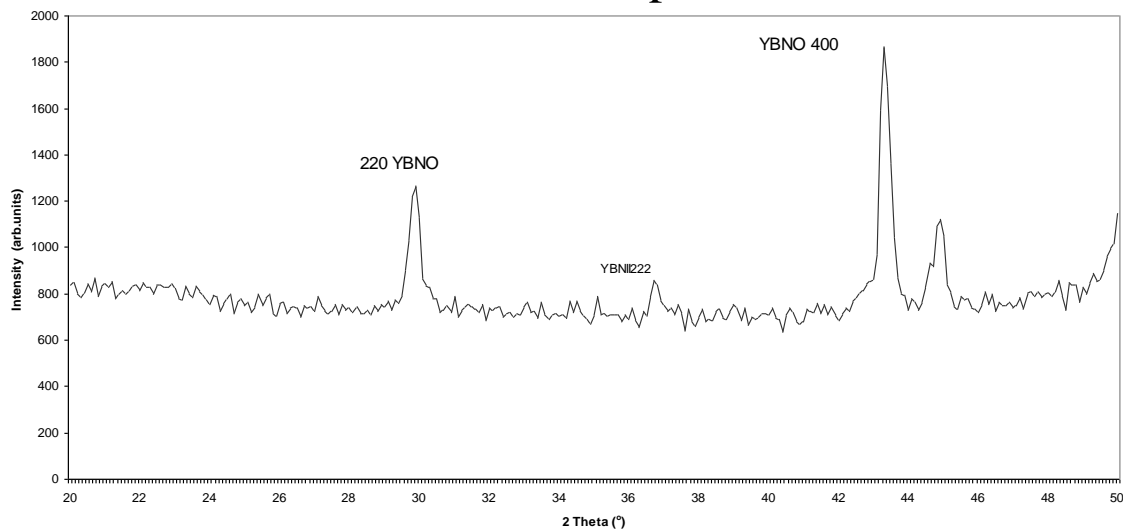


Figure 5.4.12.2

5.4.13 YBa_2NbO_6 films on RABiTS Cu-alloy

- Texturing of Cu –alloy : Attend Varanasi presentation for more details
- BYNO film deposited on textured Cu-alloy substrate shows strong 400 orientation along with 220(40%) and 222 (6%) orientations when deposited at 780 °C
- However, there is no CuO peak
- When BYNO deposited at 850 °C 400 orientation dominated the process.

YBNO film deposited at 680 °C



YBNO film deposited at 820 °C

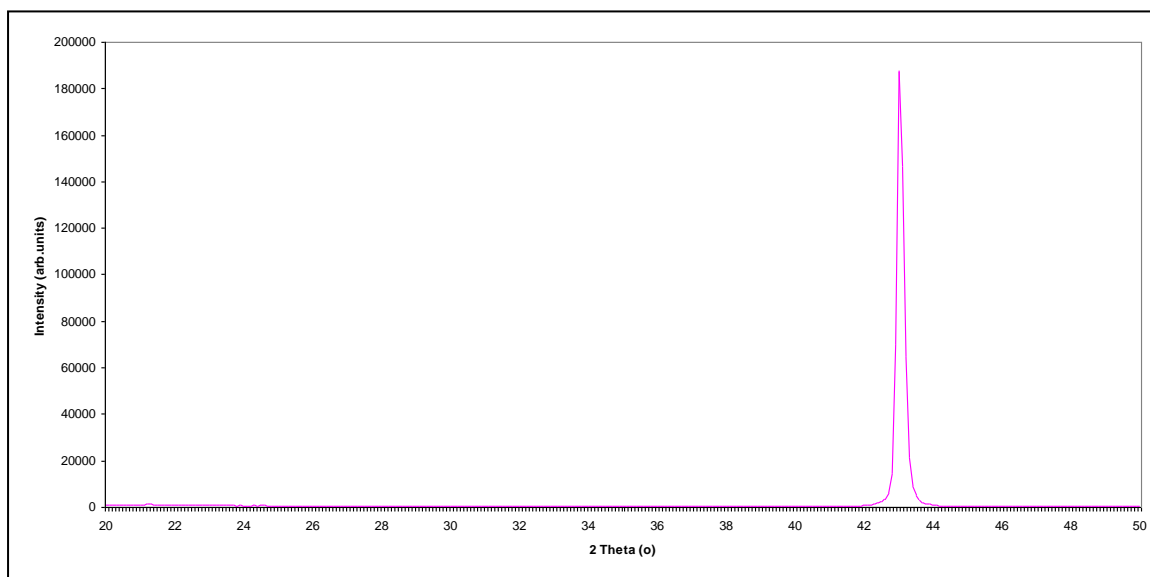
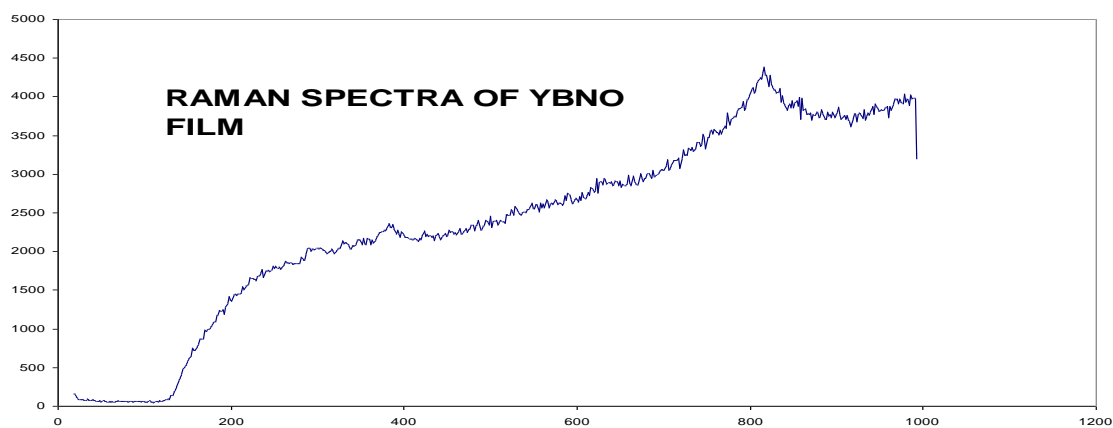


Figure 5.4.13.1

5.4.14 Micro-Raman Studies of YBNO films

- YBa_2NbO_6 films are cubic and hence show no raman active mode.
- There is no Raman mode of NiO observed
- There is no Raman active mode corresponding to CuO in YBNO films on Cu-alloy substrate

Raman spectra of YBNO film on Ni substrate



Raman spectra of YBNO film Cu-alloy substrate

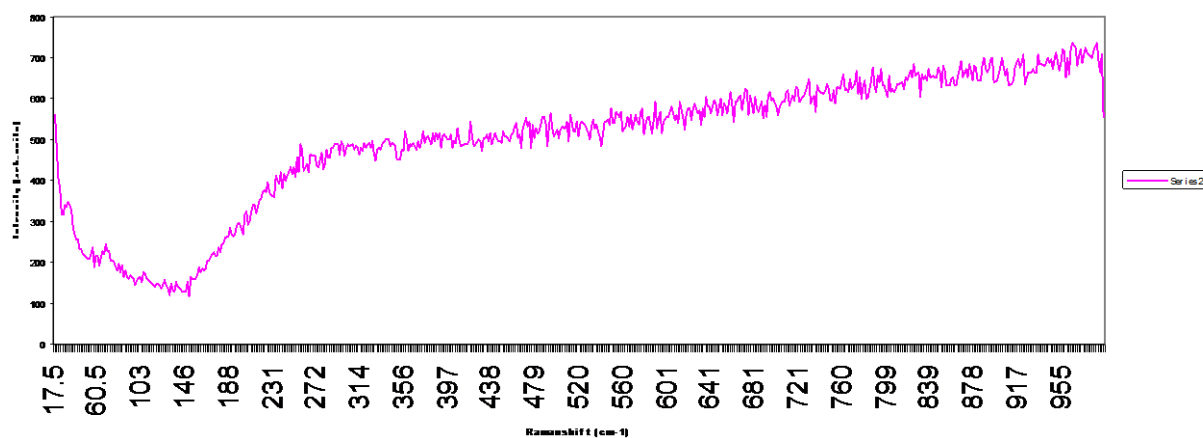


Figure 5.4.14.1

5.4.15 SEM images of YBa_2NbO_6 films on Ni substrate

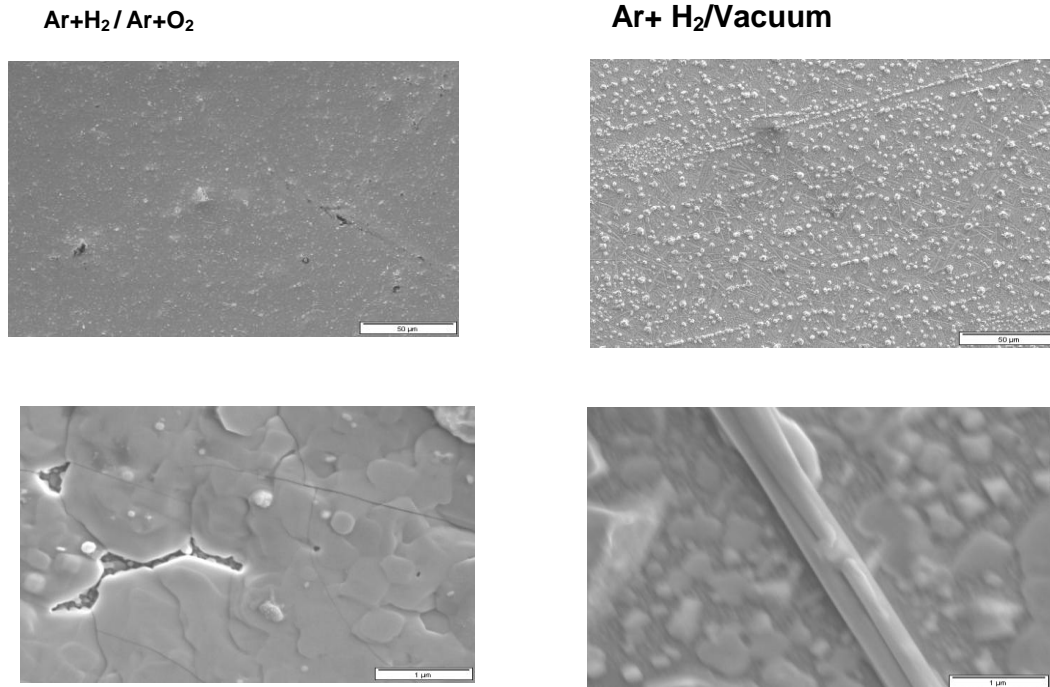
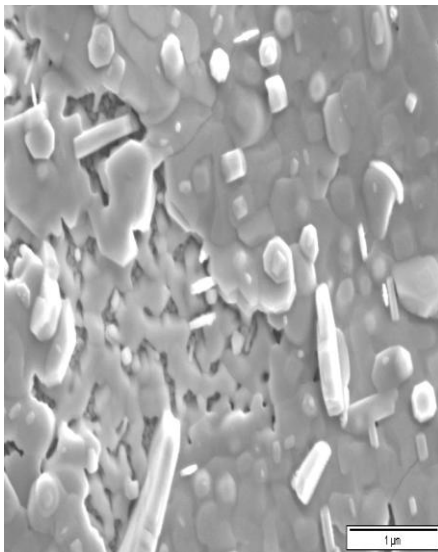


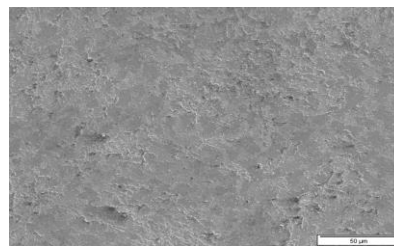
Figure 5.4.15.1

5.4.16 Oxidation of RABiTS Cu Substrates

**YBCO Film deposited
in O₂ atmosphere**



BYNO-In vacuum



BYNO in Ar+H₂

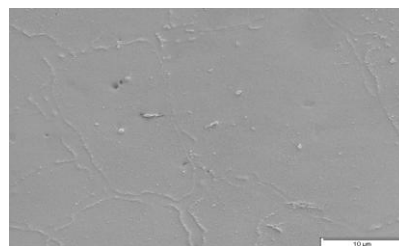


Figure 5.4.16.1

Possible solutions

1. IBAD process for oxide buffers on Metal Substrates
2. Deposit oxidation resistant metals using sputtering or ion beam sputtering methods in order to stop RABiTS substrate to get oxidized.
3. Possible metals: Pt, Ag, Au, Ru, Rh, Ir, Pd etc.

5.4.17 IBAD system for coated conductor applications

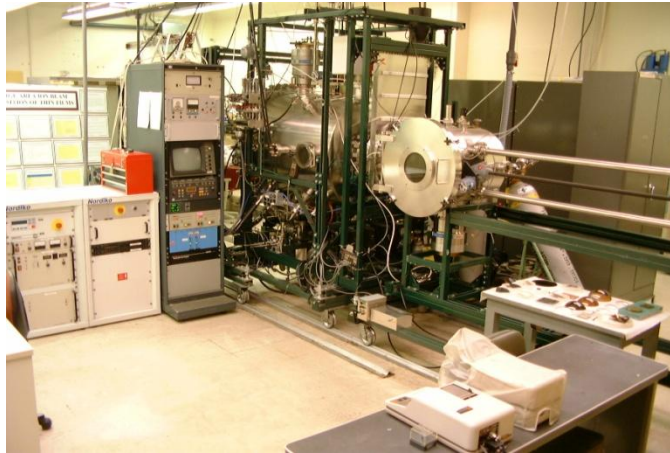


Figure 5.4.17.1

- ~900 liter UHV Chamber
- 4-Axis All Metal Sealed Scanner (X, Y, θY , θZ)
- 20 cm RF Ion Source (NORDIKO)
 - Hollow Cathode Neutralizers
- 3 cm Kaufman Ion Source (COMMON WEALTH)
- 2 Off-Axis Residual Gas Analyzers
- Substrate heater ~ 1000 °C
- 1x1 sq foot uniformity with double side reel to reel coating

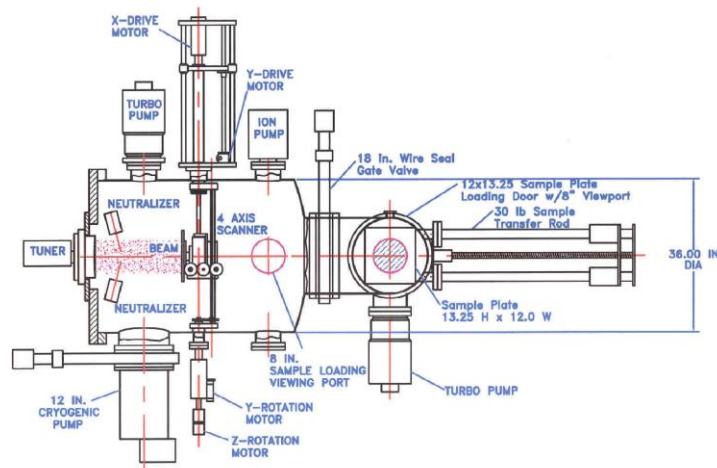


Figure 5.4.17.2

5.4.18 Schematic of the Experiment

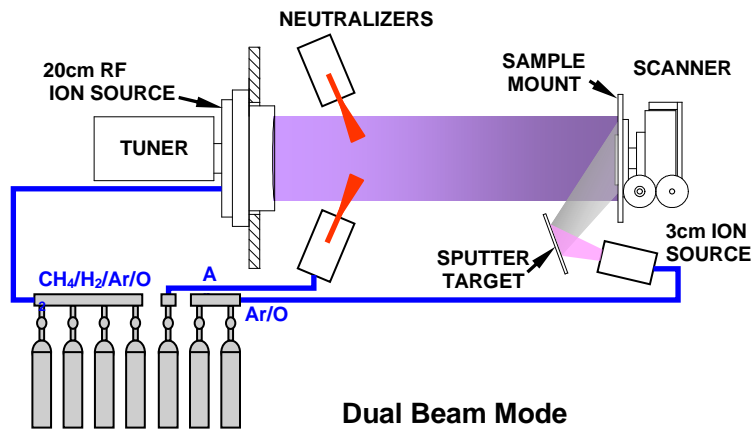


Figure 5.4.18.1

5.4.19 Substrate Holder

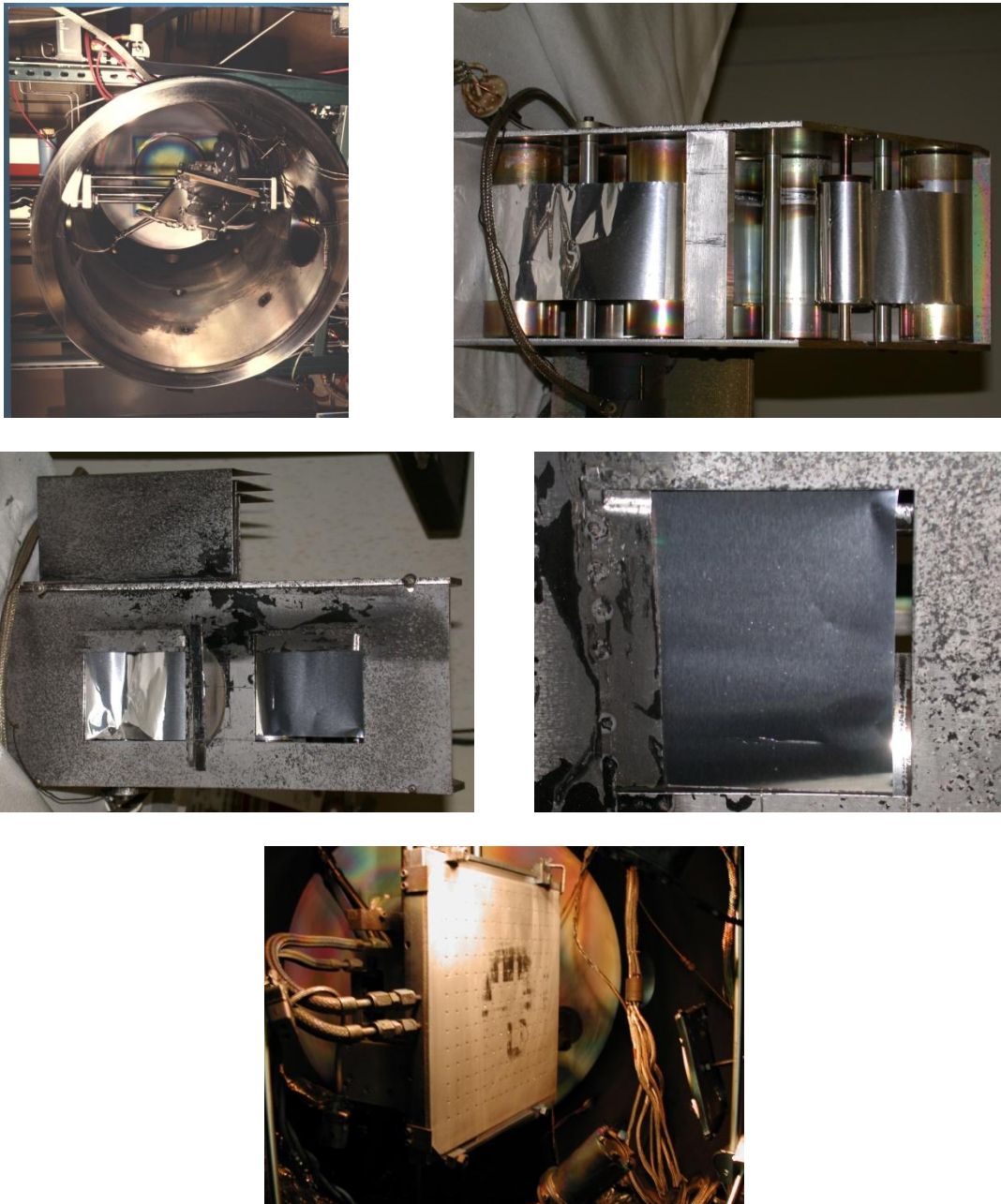


Figure 5.4.19.1

5.4.20 YSZ Film on Si (6" dia) Substrate

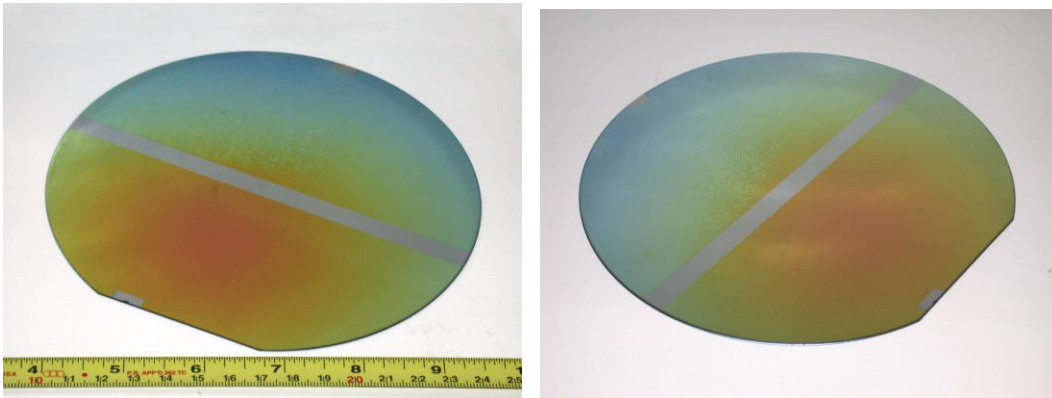


Figure 5.4.20.1

5.4.21 Ru film on Si substrate

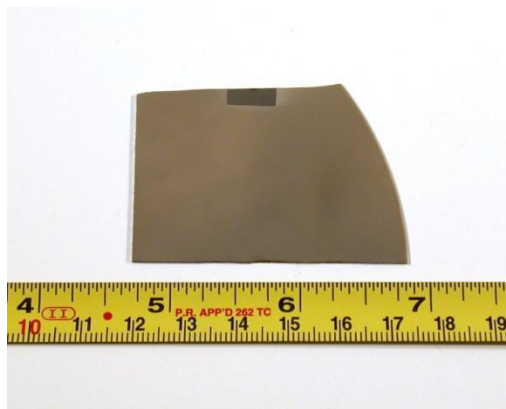


Figure 5.4.21.1

5.4.22 Mg Film using ISD

Mg on Si(100)



Mg on Cu substrate



Figure 5.4.22.1

5.4.23 Ru Film on Cu substrate

30nm film shows (100) orientation on poly copper

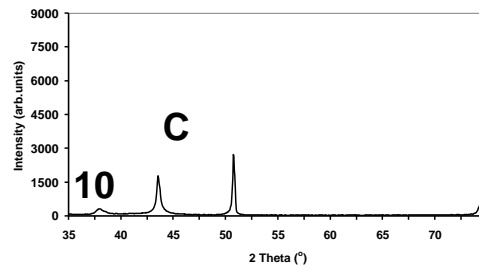


Figure 5.4.23.1

5.4.24 Work Progress on Cera-flex substrates

- Cera Flex is a flexible YSZ tape with different Yittria concentrations
- When Yittria is 3% then it is more flexible like metal
- As obtained Ceraflex samples are 10-50 nm rough.
- We are trying to polish them using different techniques to achieve 2 nm roughness to deposit IBAD YSZ and subsequent YBCO film
- WHY CERA FLEX? Our objective is to minimize AC Losses. If the substrate is a non-metal it is an interesting situation for lot of applications.

5.5 COATED CONDUCTORS ON FLEXIBLE SUBSTRATES

References: N/A

Srinivas Sathiraju,

Air Force Research Laboratory, Wright- Patterson Air Force Base, OH

Presented at CEC-ICMC 2005

5.5.1 Our Team

- GEORGE - Flexible Ceraflex Substrates
- WILLIAM C LANTER- IBAD
- PANI – Cu substrate
- SCOTT APT & ANDY- FIB, Cross sectional studies
- TIM HAUGAN - In filed measurements
- PAUL N BARNES – Program Manager

5.5.2 ACKNOWLEDGEMENTS

- Laraba Kendig – For XRD help
- Iman Maartense - AC susceptibility measurements
- Angela Campbell for AFM measurements
- Irene, John Murphy and Lyle Brunke
- AFOSR, PR, AFRL and NRC for the research support

5.5.3 Out Line of Talk

- Objectives
- Experimental
- Our efforts on Cera-Flex substrates (IBAD- PLD)
- Our efforts on Texturing of metals on polished metal substrates Using IBAD
- Our efforts on Texturing of metals (Rh) on RABITs Ni or Cu based substrates
- Status on YBCO film deposition
- Conclusions

5.5.4 What is the Present Status

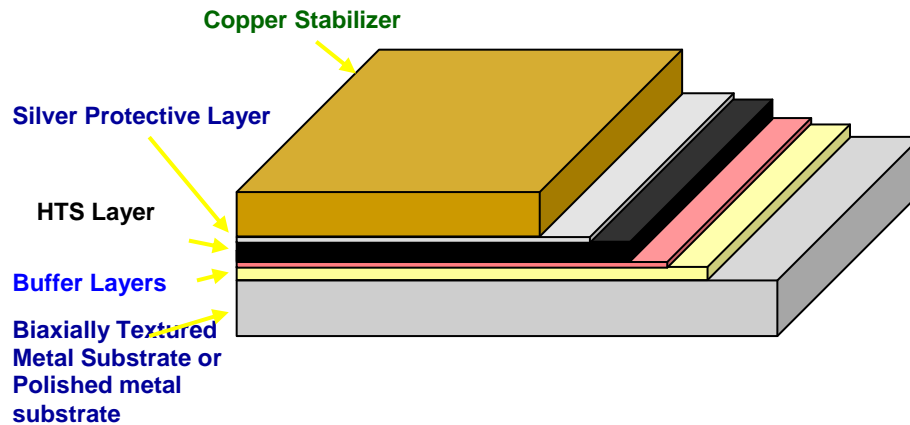


Figure 5.5.4.1

5.5.5 Objective of our Work

- Ceraflex work is mainly focused on minimizing Eddy Current losses in base substrate
- Metallic buffer path for thermally and electrically stable conductor
What is the need ??
- Engineering applications J_e Total thickness including the substrate and buffer layers is considered.
- At present stabilizing layer thickness is 75 microns.
- If we use Cu substrate or Cu-Fe bi-axially oriented substrate or stainless steel with a conducting path may eliminate the need for the stabilization layers

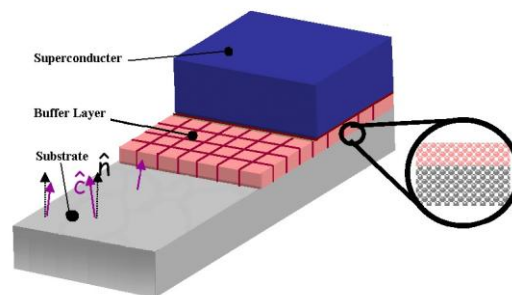


Figure 5.5.5.1

5.5.6 Why Copper Substrate???

- Low ferromagnetic losses in ac applications
- High thermal and electrical conductivity (useful for thermal stabilization) and Motor industry is comfortable in using Copper based technology

- Lower cost (5-6 times less than Ni alloys)
- Compatible to IBAD or RABITS methods

5.5.7 IBAD SYSTEM FOR CERAFLUX



Figure 5.5.7.1

5.5.8 Schematic of the Experiment

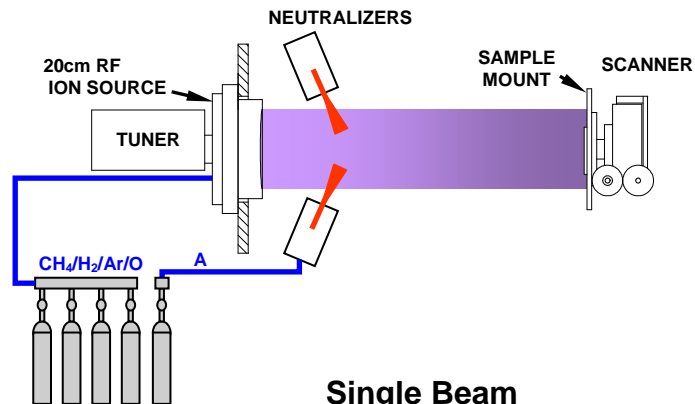


Figure 5.5.8.1

5.5.9 IBAD SYSTEM DETAILS

- ~900 liter UHV Chamber
- 4-Axis All Metal Sealed Scanner (X, Y, θY , θZ)
- 20 cm RF Ion Source (NORDIKO)
 - Hollow Cathode Neutralizers
- 3 cm Kaufman Ion Source (COMMON WEALTH)
- 2 Off-Axis Residual Gas Analyzers
- Substrate heater ~ 1000 oC
- 1x1 sq foot uniformity with double side reel to reel coating

5.5.10 Substrate Holder (stationary substrates)

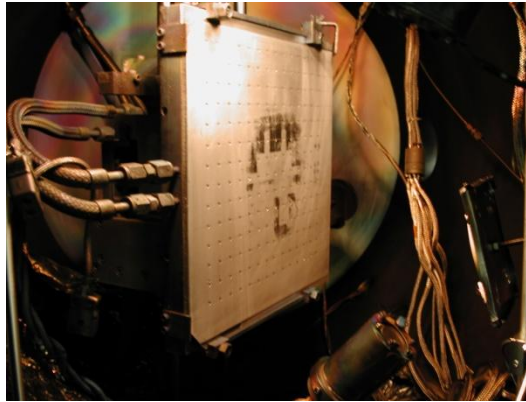


Figure 5.5.10.1

5.5.11 Reel to reel

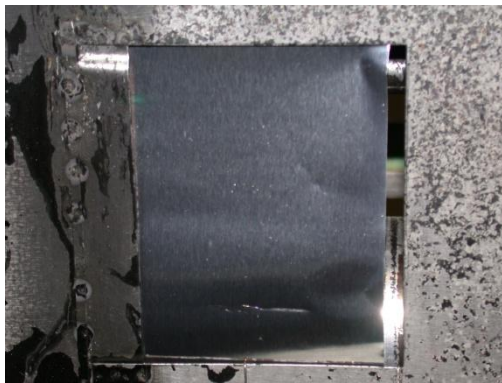


Figure 5.5.11.1

5.5.12 Double side coating



Figure 5.5.12.1

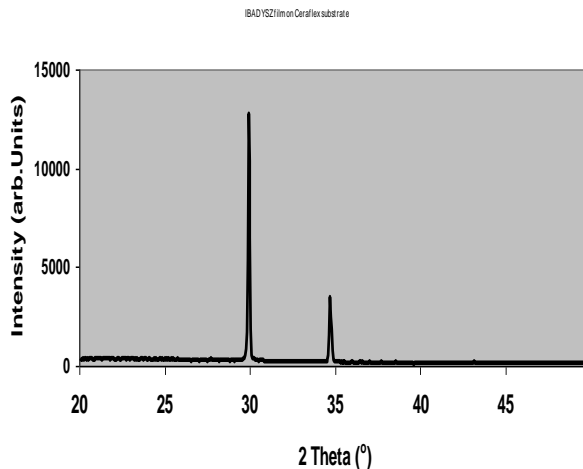
5.5.13 Work Progress on Cera-flex substrates

- Cera Flex is a flexible YSZ tape with different Yittria concentrations
- When Yittria is 3% then it is more flexible like metal

- WHY CERA FLEX?? : Our objective is to minimize eddy current Losses. Also for high sensitive SQUID
- As obtained Ceraflex samples are 50- 150 nm rough.
- We are trying to polish them using different techniques to achieve 2 nm roughness to deposit IBAD YSZ and subsequent CeO₂/ YBCO film

5.5.14 EFFORTS ON CERA FLEX

- We could achieve 10nm Ra with mechanical polishing
- YSZ films obtained till today are polycrystalline in nature



5.5.15 IBAD OF Mg Films

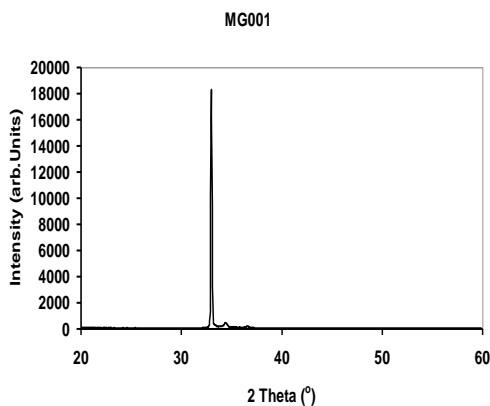


Figure 5.5.15.1

Figure 5.5.15.2



Figure 5.5.15.3

5.5.16 Ru Film on Cu substrate

- 300 nm film shows (100) orientation on polished copper



Figure 5.5.16.1

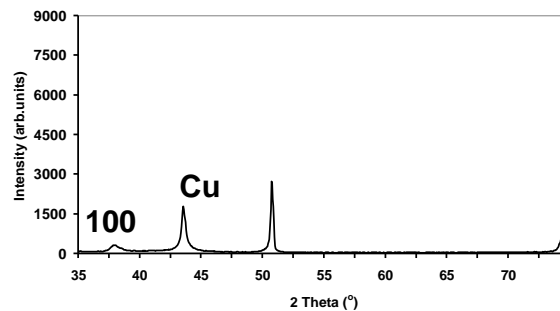


Figure 5.5.16.2

5.5.17 IBAD Ru Films on Cu substrate

No (100) growth

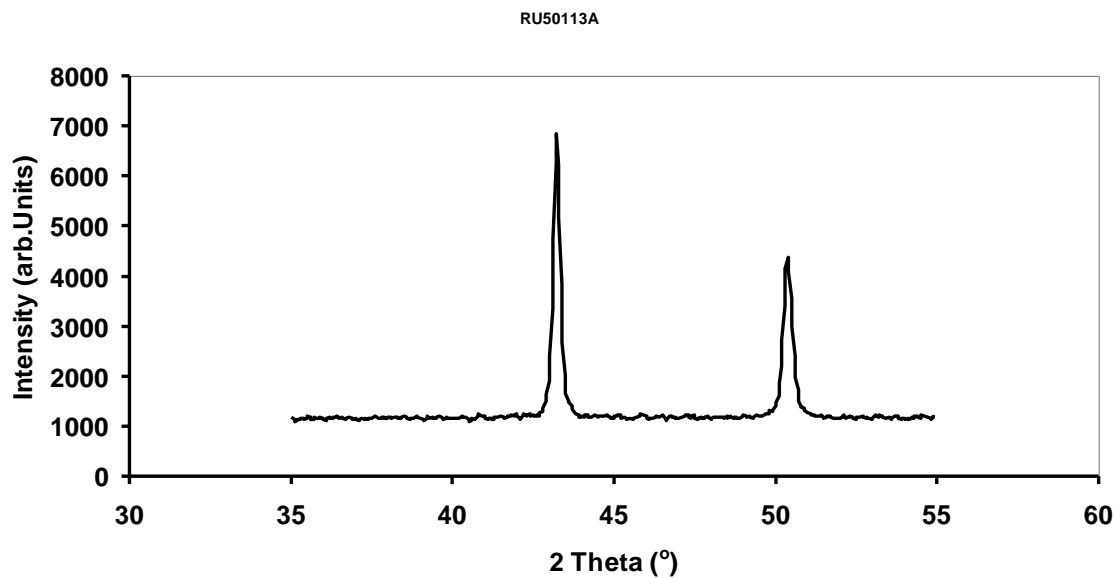


Figure 5.5.17.1

Growth in (100) direction

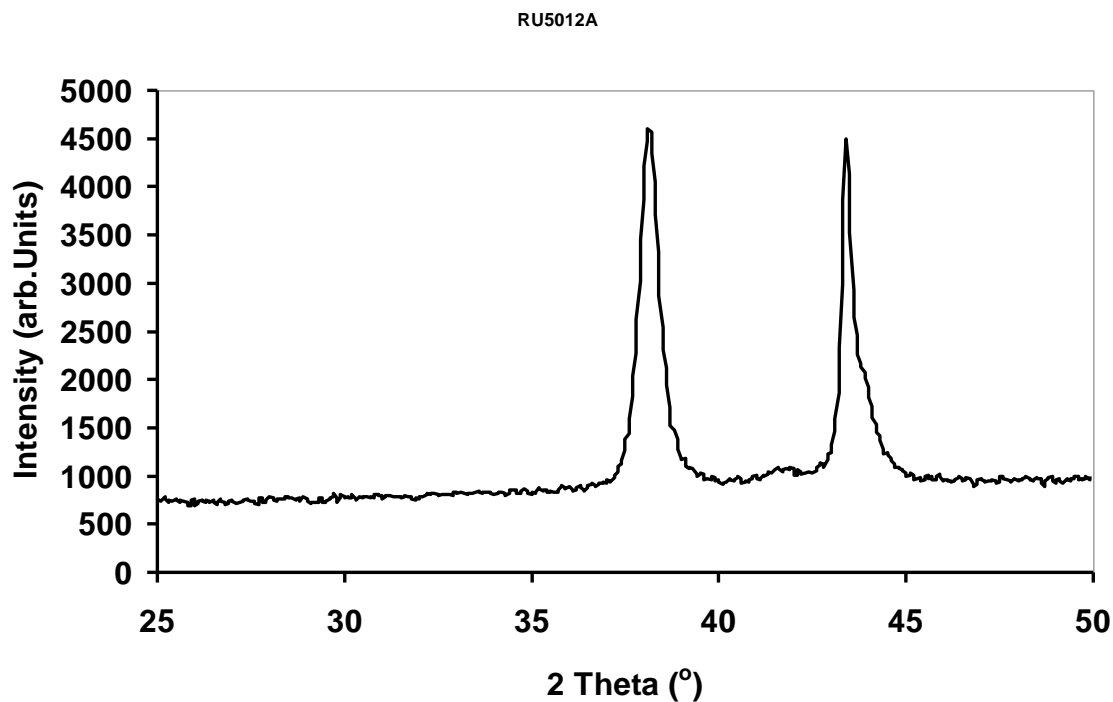


Figure 5.5.17.2

5.5.18 Pulsed Laser Deposition Parameters

Deposition Conditions	Rh Films
Deposition pressure	10 ⁻⁵ Torr
Deposition Temperature	RT -850 °C
Pulsed Laser Energy	2-3 J/cm ²
Repetition Rate	10 Hz
Thickness	200 – 2000nm
Substrates	STO,Cu-Fe, Ni-W, Cu

Figure 5.5.18.1

5.5.19 Rh films on Bi-axially textured Ni-W alloy deposited at RT

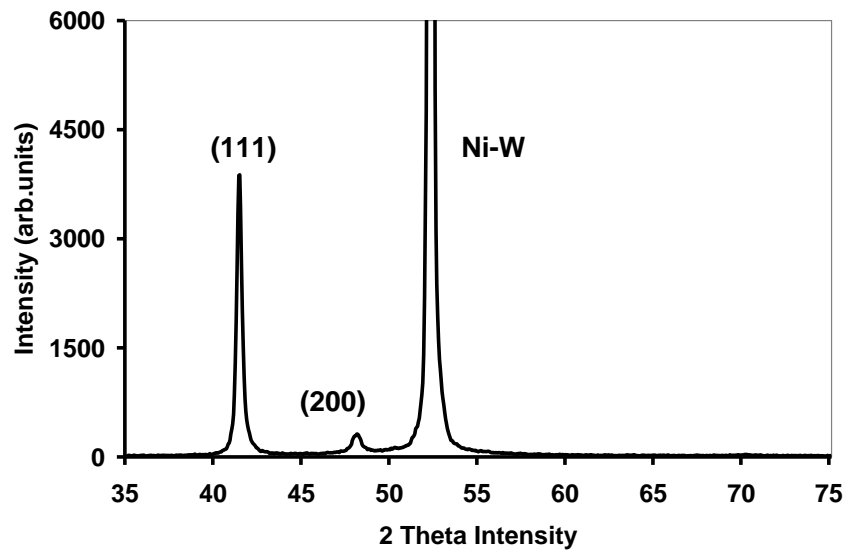


Figure 5.5.19.1

5.5.20 Rh films deposited at 700 °C

FWHM $\sim 6^\circ$

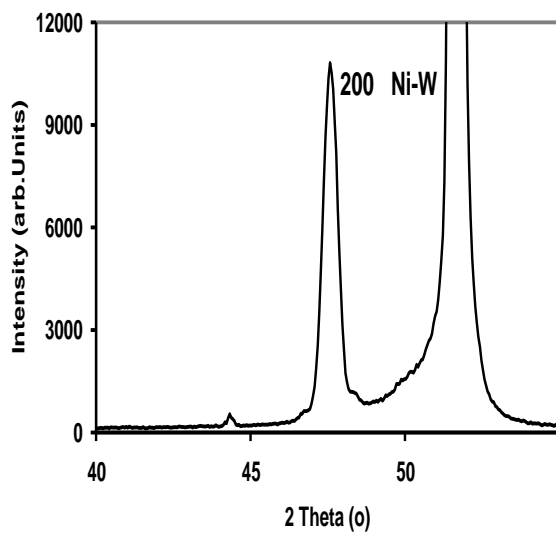


Figure 5.5.20.1

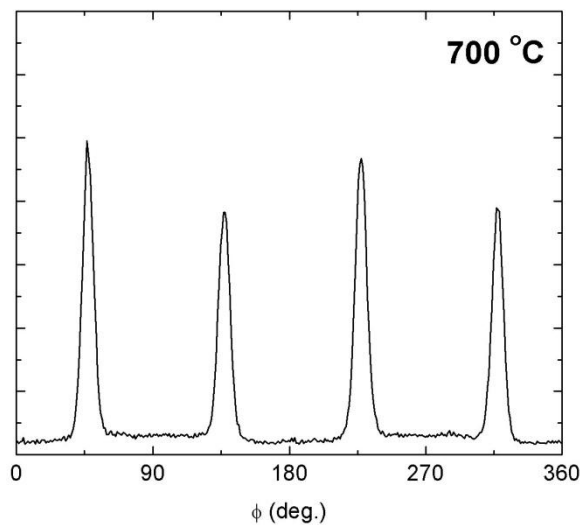


Figure 5.5.20.2

5.5.21 FIB X-section of Rh/Ni-W

Rh Films were deposited at 785 °C

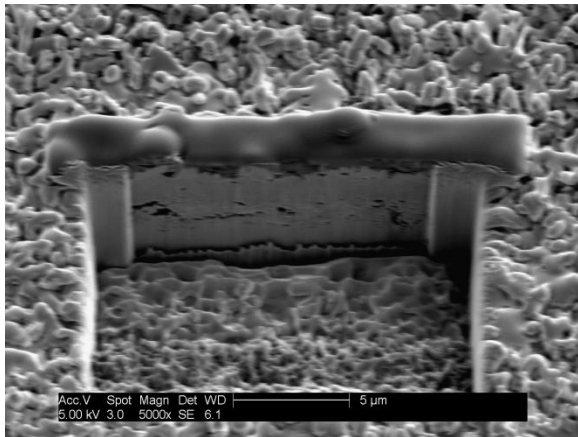


Figure 5.5.21.1

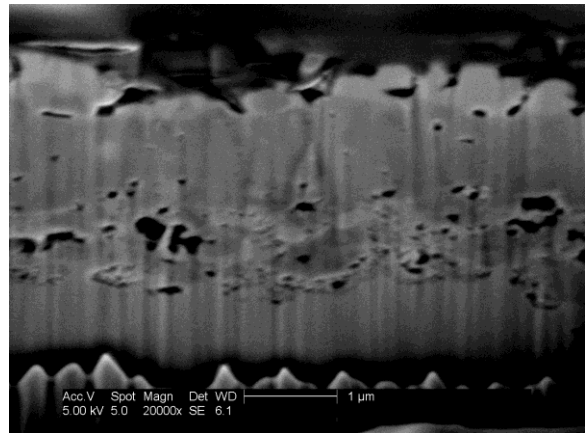
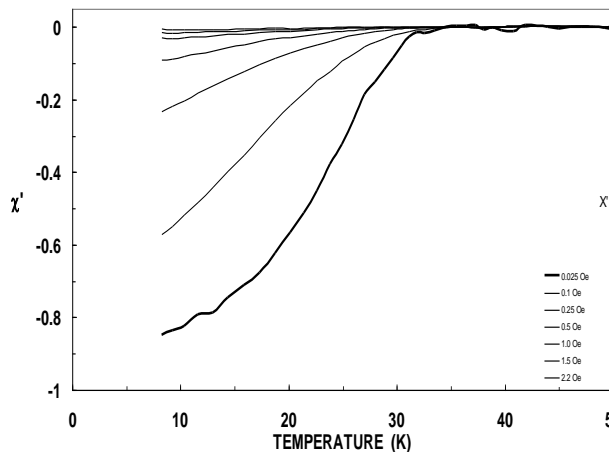


Figure 5.5.21.2

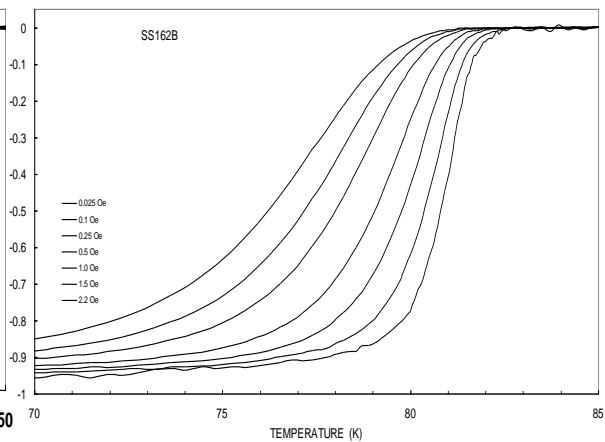
Efforts on YBCO growth

First YBCO film on 08/03



Ni-w/Rh/YBCO

Figure 5.5.22.1



Ni-W/Rh/5%Ag doped YBCO

Figure 5.5.22.2

What next???

- Further improving the properties YBCO films
- Biaxially textured Cu or Ni-alloy/Rh/m-ABO₃/Y123 (RABITS process)
- Polished Cu/ IBAD TiN/ IBAD Rh/ SrRuO₃/ Y123
- Polished Cu/IBAD Rh/ conducting ABO₃ /Y123

Summary

- Ceraflex substrates are attractive for certain applications but average surface roughness has to be improved in order to prove the concept.
- Metal buffers with another conducting oxide layer work is in progress
- Preliminary results are promising

Appendix

A.1 References

1. T. Haugan, P.N. Barnes, R. Wheeler, F. Meisenkothen, M. Sumption, *Addition of nanoparticles dispersion to enhance flux pinning of $YBa_2Cu_3O_{7-x}$ films*, Nature **430**, pp. 867 (2004).
2. T.J. Haugan, P.N. Barnes, I. Maartense, E.J. Lee, M. Sumption, and C.B. Cobb, *Island growth of Y_2BaCuO_5 nanoparticles in $(211\sim 1.5nm/123\sim 10nm)_xN$ composite multilayer structures to enhance flux pinning of $YBa_2Cu_3O_{7-d}$ films*, J. Mater. Res. **18**, 2618-2623 (2003).
3. T.A. Campbell, T.J. Haugan, P.N. Barnes, I. Maartense, J. Murphy, L. Brunke, J.M. Evans, J. Kell, N. Yust, S. Sathiraju, *Flux Pinning Effects of Y_2O_3 in YBCO Thin Films as Nanoparticulate Multilayered Dispersions*, J. Mater. Res., accepted.
4. T. Haugan, P. Barnes, I. Maartense, L. Brunke, and J. Murphy, *Effect of O_2 Partial Pressure on $YBa_2Cu_3O_{7-x}$ Thin Film Growth by Pulsed Laser Deposition*, Physica C, **397**, pp.47-57, (2003).
5. P. N. Barnes, P. T. Murray, T. Haugan, R. Rogow, G. P. Perram, *In situ creation of nanoparticles from YBCO by pulsed laser deposition*, Physica C, **377**, pp. 578, (2002).
6. P. N. Barnes, T. J. Haugan, C. V. Varanasi, T. A. Campbell, *Flux pinning behavior of incomplete multilayered lattice structures in $YBa_2Cu_3O_{7-d}$* , Appl. Phys. Lett., **85**, pp. 4088 (2004).
7. J.Z. Wu, R.L.S. Emergo, J.Z. Wu, T. Haugan, T. A. Campbell, and P. Barnes, *Tuning porosity of $YBa_2Cu_3O_{7-x}$ vicinal films by insertion of $Y_2BaCu_1O_5$ nanoparticles*, Appl. Phys. Lett., accepted.
8. T.J. Haugan, P.N. Barnes, T.A. Campbell, A. Goyal, A. Gapud, L. Heatherly, and S. Kang, *Deposition of $(Y_2BaCuO_5/YBa_2Cu_3O_{7-x})_xN$ multilayer coated conductors on Ni-based textured substrates*, Physica C, **425**, pp. 21 (2005).
9. T.J. Haugan, P.N. Barnes, T.A. Campbell, J.M. Evans, J.W. Kell, L.B. Brunke, J.P. Murphy, J.C. Tolliver, C.V. Varanasi, I. Maartense, L. Civale, B. Maiorov, W. Wong-Ng, L.P. Cook, *Addition of Alternate Phase Nanoparticle Dispersions to Enhance Flux Pinning of Y-Ba-Cu-O Thin Films*, **15**, pp. 3770 (2005).
10. P.N. Barnes, T.J. Haugan, M.D. Sumption, B.C. Harrison, *Pinning Enhancement of $YBa_2Cu_3O_{7-d}$ Thin Films with Y_2BaCuO_5 Nanoparticulates*, IEEE Trans. on Appl. Superconductivity, **15**, pp. 3766 (2005).

11. S. Sathiraju, P. T. Murray, T. J. Haugan, R. M. Nekkanti, L. Brunke, I. Maartense, A.L. Campbell, J. P. Murphy, J. C. Tolliver, and P. N. Barnes, *Studies on Nanoparticulate Inclusions in Y123 Thin Films*, Ceramic Transactions, Vol. **149**, pp. 177, (2004).
12. T. Haugan, P. Barnes, R. Nekkanti, J.M. Evans, L. Brunke, I. Maartense, J.P. Murphy, A. Goyal, A. Gapud, and L. Heatherly, *Deposition of (2111.0nm/12310nm)_xN Multilayer Coated Conductors on Ni-based Substrates, Functional Growth of Epitaxial Oxides*, pp. 359, (2003).
13. P.N. Barnes, T.J. Haugan, M.D. Sumption, S. Sathiraju, J.M. Evans, and J.C. Tolliver, *YBa₂Cu₃O_{7-d} Films with a Nanoparticulate Dispersion of Y₂BaCuO₅ for Enhanced Flux Pinning*, Trans. MRS-J, **29(4)**, pp. 1385, (2004).
14. T. Haugan, P. N. Barnes, J. M. Evans, J. C. Tolliver, L. Brunke, T. A. Campbell, I. Maartense, W. Wong-Ng, L. P. Cook, M. Sumption, *Flux pinning of YBa₂Cu₃O_{7-δ} by nanoparticle defect addition and RE substitution for Y and Ba*, in Extended Abstract: 2003 Japan-US Workshop on Superconductivity.
15. C. Varanasi, P.N. Barnes, J. Burke, J. Carpenter, T. J. Haugan, *Controlled Introduction of Flux Pinning Centers in YBa₂Cu₃O_{7-x} Films During Pulsed Laser Deposition*, Appl. Phys. Lett., accepted.
16. C.V. Varanasi, J. C. Tolliver, T. J. Haugan, K. W. Schmaeman, S. Sathiraju, L. B. Brunke, J. P. Murphy, I. Maartense, Jack Burke, Jason Carpenter, P. N. Barnes, *Nd doped YBa₂Cu₃O_{7-z} Films Deposited by Pulsed Laser Deposition*, IEEE Trans. on Appl. Superconductivity, **15**, pp. 3722 (2005).
17. S. Sathiraju, R. Wheeler, P. Barnes, T. Peterson, I. Maartense, A. Campbell, R. Nekkanti, L. Brunke, N. Yust, K. Fields, T. Campbell, T. Haugan, J. Tolliver, S. Velmulakonda, S. Mukhopadhyay, Q. Jia, P. Arendt, *Phase Formation of YBa₂Cu_{3-x}Nb_xO_y Thin Films*, *Functional Growth of Epitaxial Oxides*, pp. 367, (2005).
18. J.W. Kell, T.J. Haugan, P.N. Barnes, M.F. Locke, and T.A. Campbell C.V. Varanasi and L.B. Brunke, *Processing and Characterization of (Y_{1-x}Tb_x)Ba₂Cu₃O_{7-z} Superconducting Thin Films Prepared by Pulsed Laser Deposition*, Ceramic Transactions, **160**, pp. 15 (2005).
19. W. Wong-Ng, L.P. Cook, J. Suh, R. Feenstra, T. Haugan, and P. Barnes, *Phase Equilibria of Ba-R-Cu-O for Coated-Conductor Applications (R=lanthanides and Y)*, Physica C **408-410**, pp. 20, (2004).
20. T. Haugan, J.C. Tolliver, J.M. Evans, J.W. Kell, *Crystal Chemical Substitutions of YBa₂Cu₃O_{7-δ} to Enhance Flux Pinning*, in "Studies of High Temperature

- Superconductors", edited by A. Narlikar, Vol. 48, 49 (Nova Science Publishers, Inc., New York NY, 2004).
21. T. J. Haugan, T.A. Campbell, I. Maartense, P. N. Barnes, *Microstructural and Superconducting Properties of $(Y_{1-x}Eu_x)Ba_2Cu_3O_{7-x}$ Thin Films: $x = 0$ to 1*, J. Mater. Res., draft.
 22. T.J. Haugan, M.E. Fowler, J.C. Tolliver, P.N. Barnes, W. Wong-Ng, L.P. Cook, *Flux Pinning and Properties of Solid-Solution $(Y,Nd)_{1+x}Ba_{2-x}Cu_3O_{7-d}$ Superconductors*, Ceramic Trans. **140**, pp. 299 (2003).
 23. T.J. Haugan, J.M. Evans, J.C. Tolliver, I. Maartense, P.N. Barnes, W. Wong-Ng, L.P. Cook, R.D. Shull, *Flux Pinning and Properties of Solid-Solution $(Y,Nd)_{1+x}Ba_{2-x}Cu_3O_{7-d}$ Superconductors Processed in Air and Partial Oxygen Atmospheres*, in "Fabrication of High-Temperature Superconductors", Ceramic Transactions, **149**, pp.151-162 (2004).
 24. J.W. Kell, T.J. Haugan, J.M. Evans, P.N. Barnes, C.V. Varanasi, L.B. Brunke, J.P. Murphy, *Tb and Ce Doped $YBa_2Cu_3O_{7-x}$ Films Processed by Pulsed Laser Deposition*, IEEE Trans. on Appl. Superconductivity, **15**, 3726 (2005).
 25. G.A. Levin, P.N. Barnes, *Concept of Multiply Connected Superconducting Tapes*, IEEE Trans. on Appl. Superconductivity, **15**, 2158 (2005).
 26. G. A. Levin, P. N. Barnes, N. Amemiya, S. Kasai, K. Yoda, Z. Jiang, A. Polyanskii, *Magnetization Losses in Multiply Connected $YBa_2Cu_3O_{7-d}$ Coated Conductors*, J. Appl. Phys. accepted.
 27. G.A. Levin, P.N. Barnes, N. Amemiya, S. Kasai, K. Yoda, and Z. Jiang, *Magnetization Losses in Multifilament Coated Superconductors*, Appl. Phys. Lett., **86**, pp. 72509, (2005).
 28. N. Amemiya, S. Kasai, K. Yoda, Z. Jiang, G.A. Levin, P.N. Barnes, and C.E. Oberly, *AC loss reduction of YBCO coated conductors by multifilamentary structure*, Supercond. Sci. Technol., **17**, pp. 1464 (2004).
 29. Wang L. B. ; Selby P. ; Khanal C. ; Levin G. ; Haugan T. J. ; Barnes P. N. ; Kwon C., *The Distribution of Transport Current in YBCO Coated Conductor With Zipper Striations*, IEEE Trans. on Appl. Superconductivity, **15**, pp. 2950 (2005).
 30. Majoros M. ; Glowacki B. A. ; Campbell A. M. ; Levin G. A. ; Barnes P. N. ; Polak M., *AC Losses in Striated YBCO Coated Conductors*, IEEE Trans. on Appl. Superconductivity, **15**, pp. 2819 (2005).

31. N. Amemiya, K. Yoda, S. Kasai, Zhenan Jiang, G.A. Levin, P.N. Barnes, and C.E. Oberly, *AC Loss Characteristics of Multifilamentary YBCO Coated Conductors*, IEEE Trans. on Appl. Superconductivity, **15**, pp.1637 (2005).
32. M. Majoros, B. A. Glowacki, A. M. Campbell, G. A. Levin, P. N. Barnes, *Transport AC losses in striated YBCO coated conductors*, Proceedings of the European Conference of Applied Superconductivity, submitted.
33. C. V. Varanasi, N. Yust, P. N. Barnes, *Biaxially Textured Copper-Iron Alloy Substrates used in YBCO Coated Conductors*, J. Mater. Res., submitted.
34. P. N. Barnes, S. M. Mukhopadhyay, S. Krishnaswami, T.J. Haugan, J.C. Tolliver, and I. Maartense, *Correlation between the XPS peak shapes of $YBa_2Cu_3O_{7-x}$ and film quality*, IEEE Trans. on Appl. Superconductivity, **13**, pp. 3643, (2003).
35. C.V. Varanasi, G. Landis, P.N. Barnes, J. Burke, N. Yust, T. Haugan, *Ni-20%Cr Coatings on Biaxially Textured Copper and Copper-Iron Alloy Substrates for $YBa_2Cu_3O_{7-x}$ Coated Conductor Applications*, Ceramic Transactions, submitted.
36. S. Sathiraju, P.N. Barnes, Q.X. Jia, and P.N. Arendt, *Growth of $YBa_2Cu_3O_{7-x}$ films on Ba_2YNbO_6 dielectric buffer layer on a biaxially oriented MgO template for coated conductor applications*, Supercond. Sci. Technol., submitted.
37. S. Sathiraju, P. N. Barnes, C. V. Varanasi, R. Wheeler, *Studies on YBa_2NbO_6 buffer layers*, Ceramic Transactions, **15**, pp. 3009 (2005).
38. S. Sathiraju, N.A. Yust, R.N. Nekkanti, I. Martense, A.L. Campbell, T.L. Peterson, T.J. Haugan, J.C. Tolliver, and P.N. Barnes, *Growth Optimization of YBa_2NbO_6 Buffer Layers*, Mat. Res. Soc. Symp. Proc., **EXS-3**, pp. EE8.7.1-3 (2004).
39. S. Sathiraju, R.A. Wheeler, P.N. Barnes, *Pulsed Laser deposited $YBa_2Cu_2NbO_y$ thin films on $SrTiO_3$ Substrate*, Mat. Res. Soc. Symp. Proc., submitted.